PB92-205509

IC 9315

INFORMATION CIRCULAR/1992

Proceedings of the Workshop on Coal Pillar Mechanics and Design

Compiled by Anthony T. Iannacchione, Christopher Mark,
Richard C. Repsher, Robert J. Tuchman,
and Caddie C. Jones

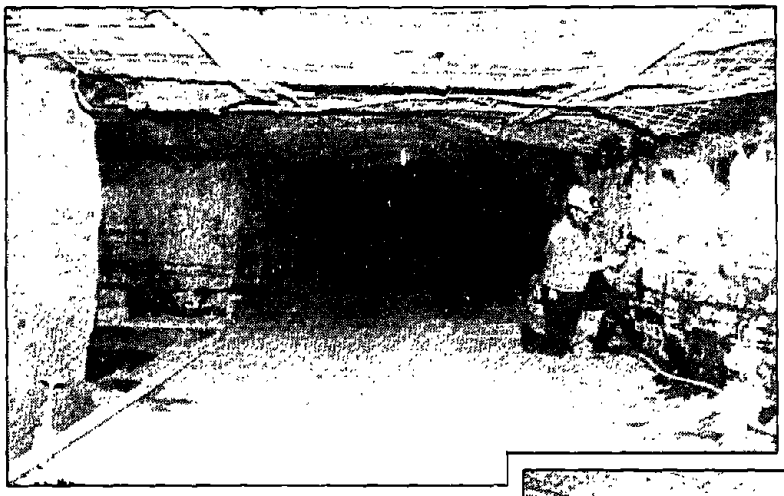

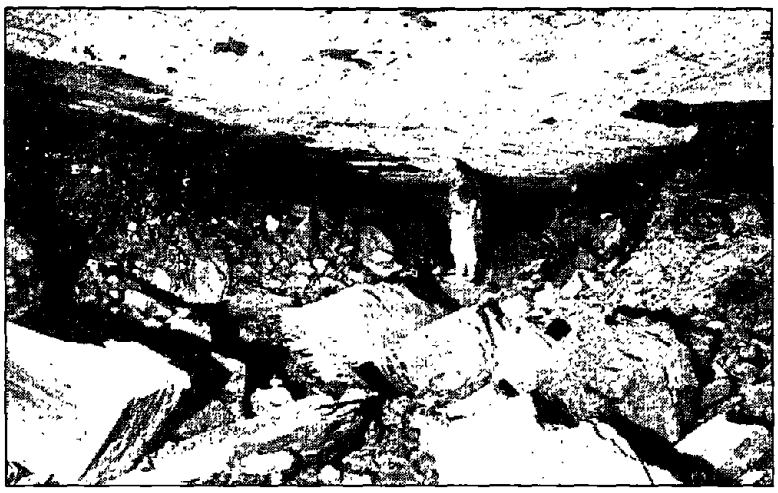

United States Department of the Interior

Bureau of Mines

REPRODUCED BY
U.S. DEPARTMENT OF COMMERCE
NATIONAL TECHNICAL INFORMATION SERVICE
SPRINGFIELD, VA 22161

Mission: As the Nation's principal conservation agency, the Department of the Interior has responsibility for most of our nationally-owned public lands and natural and cultural resources. This includes fostering wise use of our land and water resources, protecting our fish and wildlife, preserving the environmental and cultural values of our national parks and historical places, and providing for the enjoyment of life through outdoor recreation. The Department assesses our energy and mineral resources and works to assure that their development is in the best interests of all our people. The Department also promotes the goals of the Take Pride in America campaign by encouraging stewardship and citizen responsibility for the public lands and promoting citizen participation in their care. The Department also has a major responsibility for American Indian reservation communities and for people who live in Island Territories under U.S. Administration.

Cover Photographs: Top, Well Designed Pillars in the Pittsburgh Coalbed, Pennsylvania (By F. Chase); Bottom, Poorly Designed Pillars in the Harlan Coalbed, Kentucky (By A. Campoli)

PB92-205509

Information Circular 9315

Proceedings of the Workshop on Coal Pillar Mechanics and Design

Compiled by Anthony T. Iannacchione, Christopher Mark,
Richard C. Repsher, Robert J. Tuchman,
and Caddie C. Jones

UNITED STATES DEPARTMENT OF THE INTERIOR
Manuel Lujan, Jr., Secretary

BUREAU OF MINES
T S Ary, Director

REPRODUCED BY
U.S. DEPARTMENT OF COMMERCE
NATIONAL TECHNICAL
INFORMATION SERVICE
SPRINGFIELD, VA 22161

REPORT DOCUMENTATION PAGE

Form Approved
OMB No. 0704-0188

Public reporting burden for this collection of information is estimated to average 1 hour per response, including the time for reviewing instructions, searching existing data sources, gathering and maintaining the data needed, and completing and reviewing the collection of information. Send comments regarding this burden estimate or any other aspect of this collection of information, including suggestions for reducing this burden to Washington Headquarters Services, Directorate for Information Operations and Reports, 1215 Jefferson Davis Highway, Suite 1204, Arlington, VA 22202-4302, and to the Office of Management and Budget, Paperwork Reduction Project (0704-0188), Washington, DC 20503

1.	2. REPORT DATE	3. REPORT TYPE AND DATES COVERED
PB92-205509	6-15-92	IC 9315 1992

4. TITLE AND SUBTITLE

Proceedings of the Workshop on Coal Pillar Mechanics and Design

5. FUNDING NUMBERS

6. AUTHOR(S)

Anthony T. Iannacchione, Christopher Mark, Richard Repsher, Robert J. Tuchman and Caddie C. Jones

7. PERFORMING ORGANIZATION NAME(S) AND ADDRESS(ES)

Bureau of Mines
810 7th Street, NW
Washington, DC 20241

8. PERFORMING ORGANIZATION REPORT NUMBER

9. SPONSORING/MONITORING AGENCY NAME(S) AND ADDRESS(ES)

10. SPONSORING/MONITORING AGENCY REPORT NUMBER

11. SUPPLEMENTARY NOTES

12a. DISTRIBUTION/AVAILABILITY STATEMENT

12b. DISTRIBUTION CODE

13. ABSTRACT *(Maximum 200 words)*

IC 9315. Proceedings of the Workshop on Coal Pillar Mechanics and Design, compiled by Anthony T. Iannacchione, Christopher Mark, Richard Repsher, Robert J. Tuchman, and Caddie C. Jones. 1992. 302 pp. 271 figs. This publication contains papers prepared for the Workshop on Coal Pillar Mechanics and Design, Santa Fe, NM, June 7, 1992. The workshop was held in association with the 33rd U.S. Symposium on Rock Mechanics and was sponsored by the U.S. Bureau of Mines, the Mine Safety and Health Administration, CONSOL Inc., and Jim Walter Resources, Inc. The proceedings are divided into two broad topics: Coal Pillar Mechanics and the Design of Coal Pillars. The Mechanics Section focuses on recent insights into the behavior of coal pillars in situ as interpreted from field measurements, numerical models, and laboratory tests. Papers in the Design Section discuss practical aspects and field-proven techniques illustrated by the authors' own experiences. The authors of these papers are representatives of Government, industry, and academia from the United States, Canada, Australia, the United Kingdom, the Republic of South Africa, and India.

14. SUBJECT TERMS

15. NUMBER OF PAGES
302

16. PRICE CODE

17. SECURITY CLASSIFICATION OF REPORT	18. SECURITY CLASSIFICATION OF THIS PAGE	19. SECURITY CLASSIFICATION OF ABSTRACT	20. LIMITATION OF ABSTRACT
Unclassified	Unclassified	Unclassified	

GENERAL INSTRUCTIONS FOR COMPLETING SF 298

The Report Documentation Page (RDP) is used in announcing and cataloging reports. It is important that this information be consistent with the rest of the report, particularly the cover and title page. Instructions for filling in each block of the form follow. It is important to *stay within the lines* to meet *optical scanning requirements*.

Block 1. Agency Use Only (Leave blank).

Block 2. Report Date. Full publication date including day, month, and year, if available (e.g. 1 Jan 88). Must cite at least the year.

Block 3. Type of Report and Dates Covered. State whether report is interim, final, etc. If applicable, enter inclusive report dates (e.g. 10 Jun 87 - 30 Jun 88).

Block 4. Title and Subtitle. A title is taken from the part of the report that provides the most meaningful and complete information. When a report is prepared in more than one volume, repeat the primary title, add volume number, and include subtitle for the specific volume. On classified documents enter the title classification in parentheses.

Block 5. Funding Numbers. To include contract and grant numbers; may include program element number(s), project number(s), task number(s), and work unit number(s). Use the following labels:

C	- Contract	PR	- Project
G	- Grant	TA	- Task
PE	- Program Element	WU	- Work Unit Accession No.

Block 6. Author(s). Name(s) of person(s) responsible for writing the report, performing the research, or credited with the content of the report. If editor or compiler, this should follow the name(s).

Block 7. Performing Organization Name(s) and Address(es). Self-explanatory.

Block 8. Performing Organization Report Number. Enter the unique alphanumeric report number(s) assigned by the organization performing the report.

Block 9. Sponsoring/Monitoring Agency Name(s) and Address(es). Self-explanatory.

Block 10. Sponsoring/Monitoring Agency Report Number. *(If known)*

Block 11. Supplementary Notes. Enter information not included elsewhere such as: Prepared in cooperation with...; Trans. of...; To be published in.... When a report is revised, include a statement whether the new report supersedes or supplements the older report.

Block 12a. Distribution/Availability Statement. Denotes public availability or limitations. Cite any availability to the public. Enter additional limitations or special markings in all capitals (e.g. NOFORN, REL, ITAR).

DOD	-	See DoDD 5230.24, "Distribution Statements on Technical Documents."
DOE	-	See authorities.
NASA	-	See Handbook NHB 2200.2.
NTIS	-	Leave blank.

Block 12b. Distribution Code.

DOD	-	Leave blank.
DOE	-	Enter DOE distribution categories from the Standard Distribution for Unclassified Scientific and Technical Reports.
NASA	-	Leave blank.
NTIS	-	Leave blank.

Block 13. Abstract. Include a brief *(Maximum 200 words)* factual summary of the most significant information contained in the report.

Block 14. Subject Terms. Keywords or phrases identifying major subjects in the report.

Block 15. Number of Pages. Enter the total number of pages.

Block 16. Price Code. Enter appropriate price code *(NTIS only)*.

Blocks 17. - 19. Security Classifications. Self-explanatory. Enter U.S. Security Classification in accordance with U.S. Security Regulations (i.e., UNCLASSIFIED). If form contains classified information, stamp classification on the top and bottom of the page.

Block 20. Limitation of Abstract. This block must be completed to assign a limitation to the abstract. Enter either UL (unlimited) or SAR (same as report). An entry in this block is necessary if the abstract is to be limited. If blank, the abstract is assumed to be unlimited.

Bureau of Mines
Information Circular 9315

PROCEEDINGS OF THE WORKSHOP ON COAL PILLAR MECHANICS AND DESIGN

Compiled by Anthony T. Iannacchione, Christopher Mark, Richard Repsher, Robert J. Tuchman, and Caddie C. Jones

---

ERRATA

Page 123:

The note to table 1 should read as follows:

NOTE.–In the case of rectangular pillars, the equivalent square pillar width was obtained from

$$w = \frac{2 w_1 w_2}{w_1 + w_2},$$

where w_1, w_2 are the two sides of a rectangular pillar.

Page 253, column 1, lines 10-11, should read:

σ_{tn} = normalized tensile strength, expressed

$$\frac{1}{2} m - (m^2 + 4s)^{1/2}.$$

Page 253, column 2, equation 7 should read:

$$\tau_{xy,allowable} = A\sigma_c \left(\frac{\sigma_z}{\sigma_c} + \sigma_{tn}\right)^B \qquad (7)$$

where $\tau_{xy,allowable}$ is allowable shear stress, and σ_z is normal stress in z-axis.

Page 295, figure 15:

On the y-axis of the graph, ".1" should read as "1".

CONTENTS

Page

Abstract 1
Introduction 2

COAL PILLAR MECHANICS SESSION

Influence of Specimen Size and Shape on Strength of Coal, by K. Barron and T. Yang (University of Alberta), Canada 5
Study of Pillar Behavior in the Parkgate Seam at Asfordby Colliery, by J. W. Cassie (British Coal Corp.), United Kingdom, and K. W. Mills (Strata Control Technology Pty. Ltd.), Australia 25
Design of Partial Extraction Coal Mine Layouts for Weak Floor Strata Conditions, by Y. P. Chugh and W. M. Pytel (Southern Illinois University), U.S.A. 32
Pillar Design in Bump-Prone Ground Using Numerical Models With Energy Calculations, by K. A. Heasley and J. C. Zelanko (Bureau of Mines), U.S.A. 50
MSHA's Simple Technique for Predicting Stress Distribution in a Mine Panel, by M. T. Hoch, G. J. Karabin, and J. M. Kramer (Mine Safety and Health Administration), U.S.A. 61
In Situ Pillar Strength and Failure Mechanisms for U.S. Coal Seams, by H. Maleki (Bureau of Mines), U.S.A. 73
Coal Pillar Mechanics: Theoretical Models and Field Measurements Compared, by C. Mark and A. T. Iannacchione (Bureau of Mines), U.S.A. 78
Strength and Stability of Coal Pillars, by M. D. G. Salamon (Colorado School of Mines), U.S.A. 94
Pillar Strength Considering In Situ Stresses, by P. R. Sheorey (Central Mining Research Station), India 122
Analysis of Stable and Unstable Pillar Failure Using a Local Mine Stiffness Method, by R. K. Zipf, Jr. (Bureau of Mines), U.S.A. 128

COAL PILLAR DESIGN SESSION

A Revised Model for Coal Pillars, by K. Barron and Y. Pen (University of Alberta), Canada 144
A Method Revisited: Coal Pillar Strength Formula Based on Field Investigations, by Z. T. Bieniawski (The Pennsylvania State University), U.S.A. 158
Ten Years' Experience of the Wilson/Carr Pillar Sizing Method at Jim Walter Resources, Inc., by F. Carr (Jim Walter Resources, Inc.), U.S.A. 166
Coal Pillar Design for Longwalls Under the Ocean, by D. J. Forrester, D. A. Payne (Cape Breton Coal Research Laboratory, CANMET), and J. Kochhar (Cape Breton Development Corp.), Canada 180
A Pillar Design Approach, by W. Gale (Strata Control Technology Pty. Ltd.), Australia 188
A Review of Coal Pillar Design in Australia, by J. Galvin (Angus Place Colliery), Australia 196
Coal Pillar Design for Deep Conditions: An Operational Approach, by M. Gauna (Island Creek Coal Co.), U.S.A. 214
A Comprehensive Integrated Approach for Longwall Development Design, by G. J. Hasenfus and D. W. H. Su (CONSOL Inc.), U.S.A. 225
Analysis of Longwall Pillar Stability (ALPS): An Update, by C. Mark (Bureau of Mines), U.S.A. 238
Numerical Modeling as a Tool for Mine Design, by D.-W. Park (The University of Alabama), U.S.A. 250
Evaluation of Various Pillar Design Methods: A Case Study, by S. S. Peng and D. Dutta (West Virginia University), U.S.A. 269
A Practitioner's Approach to Pillar Design, by V. A. Scovazzo (John T. Boyd Co.), U.S.A. 277
Pillar Design in South African Collieries, by H. Wagner (South African Chamber of Mines), Republic of South Africa 283

Appendix.—Abbreviations used in this report 302

UNIT OF MEASURE ABBREVIATIONS USED IN THIS REPORT

°C	degree Celsius	MJ/kg	megajoule per kilogram
C/m	degree Celsius per meter	mm	millimeter
cm	centimeter	mm/m	millimeter per meter
cm/yr	centimeter per year	MPa	megapascal
deg	degree	MPa/m	megapascal per meter
ft	foot	mt	metric ton
ft^2	square foot	mtpa	metric tons per annual
ft^3	cubic foot	pcf	pound per cubic foot
h	hour	pct	percent
in	inch	psi	pound (force) per square inch
in/in	inch per inch	psi/ft	pound (force) per square inch per foot
in/lb	inch per pound	st	short ton
in/yr	inch per year	st/ft^2	short ton per square foot
km	kilometer	st/ft^3	short ton per cubic foot
km^2	square kilometer	t/ft^2	ton per square foot
lb/ft^3	pound per cubic foot	yd	yard
m	meter	μin/in	microinch per inch
m^2	square meter		

The views expressed by non-Bureau authors in these proceedings are not necessarily those of the U.S. Bureau of Mines.

Reference to specific products does not imply endorsement by the U.S. Bureau of Mines.

PROCEEDINGS OF THE WORKSHOP ON COAL PILLAR MECHANICS AND DESIGN

Compiled by Anthony T. Iannacchione,[1] Christopher Mark,[2] Richard Repsher,[3] Robert J. Tuchman, [4] and Caddie C. Jones[5]

ABSTRACT

This publication contains papers prepared for the Workshop on Coal Pillar Mechanics and Design, Santa Fe, NM, June 7, 1992. The workshop was held in association with the 33rd U.S. Symposium on Rock Mechanics and was sponsored by the U.S. Bureau of Mines, the Mine Safety and Health Administration, CONSOL Inc., and Jim Walter Resources, Inc. The proceedings are divided into two broad topics: Coal Pillar Mechanics and the Design of Coal Pillars. The Mechanics Section focuses on recent insights into the behavior of coal pillars in situ as interpreted from field measurements, numerical models, and laboratory tests. Papers in the Design Section discuss practical aspects and field-proven techniques illustrated by the authors' own experiences. The authors of these papers are representatives of government, industry, and academia from the United States, Canada, Australia, the United Kingdom, the Republic of South Africa, and India.

[1]Supervisory geologist.
[2]Mining engineer.
Pittsburgh Research Center, U.S. Bureau of Mines, Pittsburgh, PA.
[3]Staff engineer, Div. of Health, Safety, and Mining Technology, Research Directorate, Washington, DC.
[4]Technical writer/editor, Pittsburgh Research Center, U.S. Bureau of Mines, Pittsburgh, PA.
[5]Editor, Office of Technology Transfer, Research Directorate, Washington, DC.

INTRODUCTION

By Anthony T. Iannacchione[1]

A sound understanding of coal pillar behavior has long been needed by the mining industry. Despite decades of research, much controversy still exists concerning pillar stress distribution; coal deformation in reaction to these stresses; and the best empirical, analytical, and/or numerical approaches to predict pillar behavior. Because these concerns are so central to the safe and efficient operation of coal mines worldwide, a state-of-the-art review of current design philosophies and methodologies was deemed necessary.

Undoubtedly, pillar failures still represent a significant health and safety problem throughout the world, especially in conjunction with full-extraction mining. In the United States alone, Mark (*1*)[2] found 45 cases of unsuccessful longwall pillar designs and an additional 18 examples of pillar failure associated with room-and-pillar mining. Recently, a section within the Emaswati Colliery in Swaziland collapsed, temporarily trapping 26 miners (*2*). Certainly, this event must have rekindled memories of the Coalbrook Colliery disaster in January 1960 in neighboring South Africa, wherein 437 miners perished in a vast pillar collapse event (*3*). In Australia, several recent accidents associated with pillar failures have prompted the industry to execute an extensive pillar design research effort funded by the Joint Coal Board.

Although problems persist, great advancements in mine designs based on ground control considerations have been made in recent years. There now exists a wealth of design methods capable of fulfilling many of the industry's needs. While no single design approach has been universally accepted as the most reliable one, particular design methods have proved to be quite successful for certain site-specific conditions. However, the strengths and weaknesses of these approaches are not always readily apparent to the user. It is therefore not surprising to find that problems associated with inadequate pillar designs still trouble the industry.

To solve these design problems, many issues must be addressed and eventually overcome. Certain issues are more important than others, depending on the design approach used. In general, the approaches taken by the authors in these proceedings are divided among empirical, analytical, and numerical techniques, with heavy emphasis placed on either laboratory or field measurements (see table 1). Of the 22 design approaches presented, 9 are primarily empirical, 5 are analytical, and 8 are based on numerical models.

One of the key issues in pillar design is the determination of material properties. Approaches that depend on laboratory data have difficulty in scaling of these data to represent in situ strengths. Methods involving the use of field measurements suffer from an inability to accurately measure stresses contained within coal. Purely empirical techniques, derived from case histories, often do not consider site-specific material properties at all.

Another key issue in pillar design is the performance of squat (width-to-height > 10) pillars under heavy overburdens (> 1,500 ft) and difficult geology. Empirical approaches are often inappropriate due to the lack of appropriate case studies in this range. Most analytical and numerical approaches consider the core to behave in an elastic fashion with a surrounding inelastic yield zone. Unfortunately, at considerable overburden, elastic theories predict that a pillar core can achieve unrealistic stress states, giving the pillars extremely high-calculated strength. Clearly, some other behavior besides elasticity must be involved, and indeed several explanations are considered within these papers.

Understanding the interaction between the coal pillar and the surrounding strata is another key issue. Many attempts have been made to determine the influence of geology on pillar behavior, with varying degrees of success. An even more difficult pillar design problem has been to forecast the appropriate mode of failure (quasistatic yield versus dynamic violent failure). Several papers discuss attempts to develop a stability index by which the mode of failure can be considered. This could represent a major breakthrough in the design process.

In an effort to draw from the wealth of knowledge already developed concerning pillar design issues, a Workshop on Coal Pillar Mechanics and Design was organized in conjunction with the 33rd U.S. Symposium on Rock Mechanics, June 7, 1992, in Santa Fe, NM. The aim of this workshop was to assemble the world's leading experts on coal mine structures and to discuss the significant scientific and technical strides that have occurred in this realm over the past decade. Six of the world's major coal-producing countries are represented at this workshop, with authors evenly distributed among government, industry, and academia. The assemblage of 23 papers herein presents the ideas of these coal pillar design experts and certainly fulfills the original goals of the workshop. The compilation of these papers represents a truly unique publication in the annals of coal mine design, with a decidedly international flavor.

---

[1]Supervisory geologist, Pittsburgh Research Center, U.S. Bureau of Mines, Pittsburgh, PA.

[2]Italic numbers in parentheses refer to items in the list of references at the end of this introduction.

The proceedings are divided into two basic themes: Coal Pillar Mechanics and the Design of Coal Pillars. The Mechanics Section focuses on recent insights into the behavior of coal pillars in situ as interpreted from field measurements, numerical models, and laboratory tests. Papers in the Design Section discuss practical aspects and field-proven techniques illustrated by the authors' own experiences. It is hoped that practitioners will be able to draw from this wealth of knowledge to find better solutions to their own difficult pillar design problems.

REFERENCES

1. Mark, C. Analysis of Longwall Pillar Stability (ALPS): An Update. Paper in these proceedings.

2. Maher, S. The Day the Earth Fell In. MAE, 1991, pp. 21-29.

3. Bryan, A., J. G. Bryan, and J. Fouche. Some Problems of Strata Control and Support in Pillar Workings. Min. Eng., London, Feb. 1964, pp. 238-254.

Table 1.—Summary of papers for the Workshop on Coal Pillar Mechanics and Design

Author(s)	Approach	Input	Remarks
Barron and Pen	Analytical	Laboratory	Expands upon prior work by Wilson and considers dual failure criteria.
Barron and Yang	NAp	do	Evaluates coal triaxial strength in new ways and determines the effect of rank on strength.
Bieniawski	Empirical	do	Summarizes a method for determining pillar strength that has been used successfully for more than 20 years.
Carr	Analytical	Field	Describes a method for Alabama longwall conditions and presents data from more than 30 longwall panels.
Cassie and Mills	Numerical	Field and laboratory.	Uses field measurements, laboratory testing, and numerical modeling to provide site-specific design guidelines at British Coal operations.
Chugh and Pytel	Analytical	Laboratory	Approaches pillar design for weak floor strata conditions based on the ultimate bearing capacity as well as pillar settlement.
Forrester, Payne, and Kochhar.	Empirical	Field	Presents a strategy for undersea mine layout in Canada, utilizing pillar load formula and maximum allowable tensile strain on the seabed.
Gale	Numerical	do	Discusses a design method utilizing numerical models in conjuction with the deformational characteristics of the roof rock, coal, floor rock, and their interfaces.
Galvin	Empirical	do	Provides a broad perspective of the conditions and statutory requirements governing pillar design in Australia.
Gauna	do	do	Suggests a design method for overburdens exceeding 1,500 ft by calculating a pillar resistance/load ratio that relies heavily upon monitoring entry deformations.
Hasenfus and Su	Numerical	do	Identifies a design technique based on the use of finite-element modeling that accounts for pillar stability, floor heave, rib sloughing, overburden caving and deformation.
Heasley and Zelanko	do	do	Previews a new design technique for mining in bump-prone strata utilizing a boundary element code that calculates dissipated energy as a measure of bump potential.
Hoch, Karabin, and Kramer.	Analytical	NAp	Describes a simple approach for predicting stress distribution in coal mine pillars based on analysis of stresses around cracks in rocks.
Maleki	Numerical	Field	Identifies maximum average stress levels, depending on geologic condition, beyond which stability problems occur as a result of failure in the roof, coalbed, and/or floor strata.
Mark	Empirical	do	Reports on the practical applications of the longwall pillar sizing program called ALPS after 5 years of field experience.
Mark and Iannacchione.	do	do	Evaluates current pillar strength theories using a comprehensive data base of stress measurements from coal pillars.
Park	Numerical	Laboratory	Uses an iterative finite-element technique run on a supercomputer for simulating the progressive failure of coal and applies this method to size pillars in a new longwall mine.
Peng and Dutta	do	Field	Illustrates the use of both empirical and finite-element methods in evaluating the interaction between roof, coal, and floor strata.
Salamon	Analytical	Laboratory	Defines a mechanics-based pillar strength approach, removes some theoretical shortcomings of Wilson's formula, and proposes a method for analyzing the stability of pillars.
Scovazzo	Empirical	Laboratory and field.	Suggests a design method based on the mine-specific characteristic of coal as defined by laboratory rock testing and in-mine observation.
Sheorey	do	Laboratory	Discusses a successful empirical design method used in India formulated by large-scale strength tests and statistical evaluation of case histories, which gives considerable weight to overburden in determining pillar strength.
Wagner	do	do	Provides an extensive review of pillar design practices in South African collieries.
Zipf	Numerical	do	Presents a stability criterion based on comparing numerically calculated roof and local mine stiffness values, which has the capability of distinguishing the mode of pillar failure (stable to violent).

NAp Not applicable.

INFLUENCE OF SPECIMEN SIZE AND SHAPE ON STRENGTH OF COAL

By K. Barron[1] and Tao Yang[2]

PART 1: SIZE EFFECTS OF UNIAXIAL STRENGTH OF COAL

INTRODUCTION

If computer modeling techniques are to be successfully applied to the analysis of the stability of excavations in coal, it is essential that correct coal strength parameters be used in these models. It is well known that the strength of laboratory-size coal specimens is very size-dependent, and the coal mass strength properties needed for input into such models are difficult to estimate.

The uniaxial strength of coal has been studied by numerous workers since the turn of the century and has resulted in the derivation of a number of empirically based formulas to describe the strength variation with specimen size. In contrast, virtually no work has been done to quantify these size effects under triaxial stress conditions. In part 1 of this paper, the past work[4] investigating the uniaxial strength/size effects is reviewed, and a new empirical relationship is derived and tested. In part 2, a semiempirical/theoretical approach is developed whereby both the intact and the coal mass strength properties (in Hoek/Brown form) can be estimated from laboratory tests on coal specimens of known size and shape. In part 3, the results of laboratory triaxial testing on suites of different size coal specimens are reported in an attempt to validate the concepts developed in part 2. Finally, in part 4, the influence of coal rank on these properties is examined.

SIZE/STRENGTH RELATIONSHIPS FOR CUBICAL SPECIMENS

Many studies of the variation in the strength of coal cubes with edge dimension have been carried out (*1-15*)[3]. From a review of these studies, it may be concluded that the bulk of the uniaxial coal cube strength data may be expressed in the form:

$$\sigma_c = k\, D^{-1/2}, \qquad (1)$$

where k is a constant for the coal (and is numerically, but not dimensionally, equal to the strength of a 1-in cube), D is in inches and σ_c is given in pounds per square inch.

There is some doubt (*9*) as to whether this equation applies to specimens of edge dimension much less than 1 in. However, this is not seen to be of a major practical consideration since usually k is derived from convenient size coal cubes in the 1- to 4-in size range.

Logically, there should be an upper size limit to this equation since, clearly, the strength will not reduce ad infinitum with increasing edge dimension. There appears to be some minor disagreement between the various authors on the upper limit beyond which the cube strength is, for all practical purposes, a constant. Hustrulid (*9*) suggests 36 in, Bieniawski (*10-14*) suggests 60 in, while Gaddy (*7*) indicates a continuing small strength reduction even beyond this size.

---

[1]Professor.

[2]Graduate student.

Department of Mining, Metallurgical and Petroleum Engineering, University of Alberta, Edmonton, Alberta, Canada.

[3]Italic numbers in parentheses refer to items in the list of references at the end of each part of this paper.

[4]In part 1 of this paper, virtually all the data derived from the literature were presented in imperial units. For this reason, the analysis in this part has been carried through in these same units, and it is only after the analysis that the resulting equations are also expressed in SI units.

STRENGTH/SHAPE RELATIONSHIPS FOR PRISMATIC SPECIMENS

TEST RESULTS

In this section, the effect of varying the width/height ratio, B/H, on specimen strength will be considered. For the most part, prismatic specimens having a square cross section are considered, but some data from specimens having rectangular and circular cross sections are also included. For specimens with a rectangular cross section, the width, B, will be considered to be the minimum lateral dimension.

In a number of cases, the results of previous work have been expressed in normalized form to assist in comparison with other data, i.e., the prism strengths, σ_p, have been divided by a cube strength, σ_c, to produce an equation in dimensionless form. However, it should be pointed out that previous investigators have been inconsistent in their choice of sample dimension (height or width) used to specify the comparative cube strength. That is, some workers have divided the prism strength by the strength of a cube of edge dimension equal to the prism height, while others have divided the prism strength by the strength of a cube of edge dimension equal to the prism width. This has resulted in some inconsistencies between the reported results when the specimen height is varied and the width is kept constant and vice versa. Care should be taken to bear this in mind when reviewing previous work.

Again, a large number of studies of the strength/shape relationships have been carried out (*1-23*) and have resulted in the derivation of a number of different empirical relationships. In summary, the results of past work investigating the coal prism strength/shape relationships have been expressed in one of three different basic forms:

1. The power form:

$$\sigma_p = k\left\{\frac{B}{H}\right\}^{1/2}. \qquad (2)$$

(Salamon and Munro's relationship (*23*), given by $\sigma_p = k\ B^{0.46}H^{-0.66}$, can be regarded as a variation of this power form)

2. The "linear" form:

$$\sigma_p = a + b\left\{\frac{B}{H}\right\}, \qquad (3)$$

and,

3. The "general" form:

$$\sigma_p = k\left\{\frac{B^{1/2}}{H}\right\}. \qquad (4)$$

The power curve form of Salamon and Munro has been criticized by Bieniawski (*11*) on the grounds that, for constant height, the strength of the pillar increases as the pillar width increases, and further, for a constant width, the strength of the pillar decreases with increasing height, both trends continuing to infinity. Bieniawski argues, with good justification, that there must be some limits to these trends. This same criticism is equally applicable to the other forms given above unless some limits are set. Bieniawski and Hustrulid introduce such limits by limiting the maximum cube strength—in Bieniawski's case to a 60-in cube, in Hustrulid's case to a 36-in cube.

Much emphasis has been placed by Hustrulid and others on the fact that the normalized linear form is dimensionally correct. Hustrulid states, when comparing this form with the power form of Salamon and Munro, that "the attractiveness of this equation is that it is dimensionally correct and provides the opportunity to introduce the various coal cube strengths." In the authors' opinion, this is a fallacious statement since, although this equation is dimensionally correct, the introduction of the "various coal cube strengths" by the relationship:

$$\sigma_c = k\left\{\frac{1}{D^{1/2}}\right\},$$

defeats this alleged advantage. The constant k cannot have the dimensions of strength and therefore is no better than or worse than the direct use of k in the Salamon/Munro equation, which is criticized as being dimensionally incorrect.

Hustrulid (*9*) concludes that the size/shape effects from all data may be expressed by two equations, one for the size effect and the other for the shape effect:

1. A cube size/compressive strength relationship given by:

$$\sigma_c = \left\{\frac{k}{D^{1/2}}\right\}, \quad \text{when } D < 36 \text{ in}, \qquad (5)$$

and,

$$\sigma_c = \left\{\frac{k}{36^{1/2}}\right\}, \quad \text{when } D > 36 \text{ in}. \qquad (6)$$

This is in general agreement with all other work, except that he puts an upper size limit of 36 in, whereas Bieniawski uses an upper size limit of 60 in. Other authors stated no limits, due primarily to a lack of data in the upper size range.

2. A compressive strength/shape relationship given by:

$$\frac{\sigma_p}{\sigma_c} = 0.778 + 0.222 \left\{\frac{B}{H}\right\}, \qquad (7)$$

where the normalizing cube strength, σ_c, is the strength of a cube of edge dimension equal to the prism height.

There is no doubt that these equations compiled by Hustrulid give a reasonable fit to most of the experimental data reported in the literature. However, the authors are uneasy with the conclusion that it requires two separate equations to define the combined size/shape effects and with the consequent difference in the shape effects when B is varied and H kept constant or vice versa. After all, a cube is only a special case of a prism and thus, intuitively, it would be expected that the combined size/shape effects ought to be able to be expressed in a single relationship which reduces to the cube equation for that specific case. The general form of equation developed by Holland and Gaddy (*21*), based on Steart's rules (*5*), does in fact satisfy these requirements:

$$\sigma_p = k \left\{\frac{B^{1/2}}{H}\right\}. \qquad (8)$$

Consequently, in the authors' opinion, a relationship in this form has a much greater basic appeal. However, a comprehensive reevaluation of all the data with respect to this form needs to be carried out if it is to be accepted.

STATISTICAL REEVALUATION OF ALL DATA IN STEART'S GENERAL FORM

Barron and Das (*24*) undertook to reevaluate the available strength/size/shape data with the objective of assessing whether a single equation in this general form could adequately express all of these data. They developed some limits of applicability for this equation, and these limits were further refined by Tao Yang (*25*). In addition to the experimental data taken from the references already cited, data were also drawn from a number of other sources (*26-30*). This mass of data was then statistically analyzed as follows:

1. For each set of results for any one coal, a linear correlation between σ_p and$\{B^{1/2}/H\}$ was carried out giving an equation in the form

$$\frac{\sigma_p}{k} = a_o + b_o \left\{\frac{B^{1/2}}{H}\right\} \qquad (9)$$

together with the correlation coefficient, where B and H were expressed in inches and σ_p in pound per square inch. From this equation the uniaxial cube strength, $\sigma_c = k$, for a 1-in cube was determined and the data were normalized by dividing each individual σ_p value by the k value for that coal.

2. A linear correlation was then performed on all these normalized data taken together. The results are shown in figure 1 and yielded the following equation

$$\frac{\sigma_p}{k} = 0.220 + 0.695 \left\{\frac{B^{1/2}}{H}\right\}, \qquad (10)$$

with a correlation coefficient r = 0.82 for the 219 data pairs. Considering the wide range of coals, the variance in the testing techniques, etc., this correlation was deemed to be relatively good.

3. Because the $1/D^{1/2}$ form is fairly well established for cubes, and because cube strength data dominated the total number of measurements available (145 of the 219 data pairs), it was decided to investigate the applicability of this general equation to the noncubic (prism) data only. The following result was obtained:

$$\frac{\sigma_p}{k} = 0.229 + 0.639 \left\{\frac{B^{1/2}}{H}\right\}, \qquad (11)$$

with a correlation coefficient of r = 0.76. Statistical testing showed that there was no significant difference between these equations at the 0.05 level. It follows therefore that the general form of equation appears to fit all of the data, both prisms and cubes, quite well and thus it is not necessary to use the two expressions of Hustrulid to describe size/shape effects.

4. On examining figure 1, a disproportionate number of points at high $\{B^{1/2}/H\}$ values appeared to deviate from this correlation line. Further examination showed that most of these points were associated with tests where $\{B^{1/2}/H\} > 1.4$. Above this value the normalized strength was approximately constant.

For cubes, when B=H=D, this breakdown of the relationship occurs when:

$$D^{1/2} = 1.4D \quad \text{i.e., } D = \left\{\frac{1}{1.4}\right\}^{1/2} = 0.51 \text{ in.}$$

This is in accordance with Hustrulid's comments (*9*) on the doubtfulness of the application of his equations to Evans' results (*8*) for cube specimens of an edge dimension less than 1 in. The correlation was then reperformed,

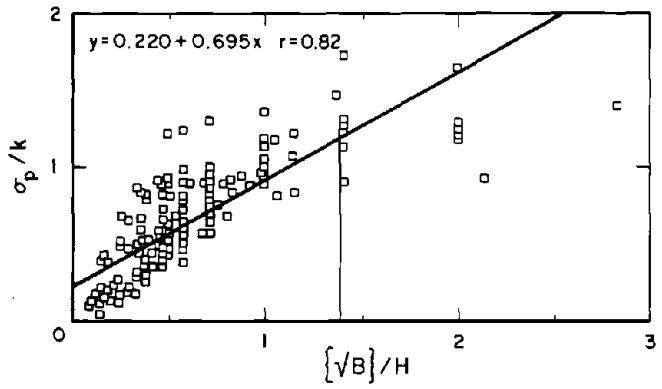

Figure 1.—Correlatin of σ_p/k versus $\{\sqrt{B}\}/H$ - all coal data.

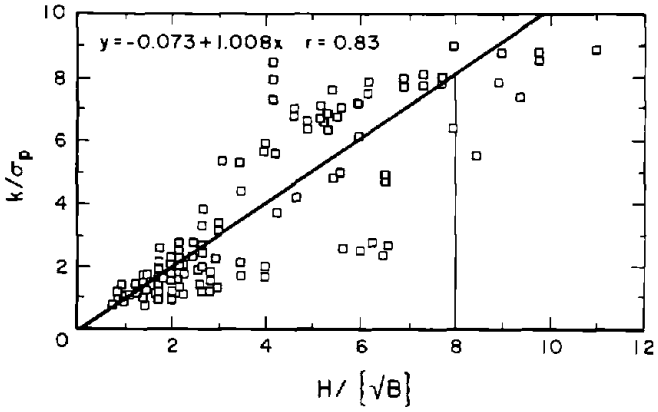

Figure 2.—Inverse correlation of k/σ_p versus $H/\{\sqrt{B}\}$.

eliminating all data where $\{B^{1/2}/H\} > 1.4$. This yielded the relationship:

$$\frac{\sigma_p}{k} = 0.094 + 0.947 \left\{\frac{B^{1/2}}{H}\right\}, \qquad (12)$$

with an improved correlation coefficient r = 0.86.

5. It was then decided to examine the data to see if there was a lower limit to the value of $\{B^{1/2}/H\}$ for which the general form of relationship applies. In figure 1, all the points for the small values of $\{B^{1/2}/H\}$ are clustered close to the origin and it is difficult to see whether or not there is a deviation from the correlation line. Consequently, the inverse correlation of k/σ_p was plotted against $\{H/B^{1/2}\}$. This correlation is shown in figure 2 and is given by:

$$\frac{k}{\sigma_p} = -0.073 + 1.008 \left\{\frac{H}{B^{1/2}}\right\} \qquad (13)$$

with a correlation coefficient r= 0.83. Examination of this figure shows that all data points for $\{H/B^{1/2}\} > 8$ fall on one side of the curve only and that above this value k/σ_p is approximately constant. That is, it appears that this general form of relationship again breaks down when $\{B^{1/2}/H\} < 1/8 = 0.125$.

For cubes, where B=H=D, this breakdown occurs when

$$D^{1/2} = 0.125D \quad \text{i.e., } D = \{8\}^2 = 64 \text{ in.}$$

This is in close agreement with Bieniawski's maximum cube size of 60 in beyond which the cube has a constant strength.

6. Finally, following the same procedure as before, all the data points where $\{B^{1/2}/H\} < 0.125$ were eliminated and the correlation was repeated. This yielded, for all specimens where $1.4 > \{B^{1/2}/H\} > 0.125$, the following relationship

$$\frac{\sigma_p}{k} = 0.107 + 0.929 \left\{\frac{B^{1/2}}{H}\right\} \qquad (14)$$

with a correlation coefficient r = 0.85.

7. Further examination of these limits on this general form of relationship were carried out by Tao Yang (*25*) and he was able to place some additional restrictions on these limits as follows:

(a) when $1.4 > \{B^{1/2}/H\} > 0.125$, then B must lie between 0.5 and 64 in, and the normalized strength equation is given by equation 14.

(b) when $\{B^{1/2}/H\} > 1.4$, then B must be <0.5 in and the normalized strength is given by putting $\{B^{1/2}/H\} = 1.4$ in equation 14, i.e.,

$$\frac{\sigma_p}{k} = \text{constant} = 1.41. \qquad (15)$$

(c) when $\{B^{1/2}/H\} < 0.125$ or B >64 in, then the normalized strength equation is given by putting $\{B^{1/2}/H\} = 0.125$ in equation 14, i.e.,

$$\frac{\sigma_p}{k} = \text{constant} = 0.22. \qquad (16)$$

Figure 3 shows these relationships and the comparison with all the data points used. Table 1 summarizes these relationships when expressed in imperial units (as given above) and when expressed in SI units.

Table 1.—Summary of size/shape strength relationships for coal

Category	√B/H limits	Normalized strength equation
Imperial units:		
1	{√B}/H <0.125 or B >64 inches	σ_p/k = constant = 0.22
2	0.125 <{√B}/H <1.4 and 0.5 <B <64 inches	σ_p/k = 0.107 + 0.929 {√B}/H
3	{√B}/H >1.4 and B <0.5 inches	σ_p/k = constant = 1.41
where B and H are in inches, σ_p is in pounds per square inch, and k is numerically (but not dimensionally) equal to the uniaxial compressive strength of a 1-in cube given in pounds per square inch.		
SI units:		
1	{√B}/H <0.784 or B >1.626 m	σ_p/K = constant = 0.88
2	0.784 <{√B}/H <8.784 and 0.013 <B <1.626 m	σ_p/K = 0.452 + 0.548 {√B}/H
3	{√B}/H >8.784 and B <0.013 m	σ_p/K = constant = 5.226
where B and H are in meters, σ_p is in MPa and K is numerically (but not dimensinally) equal to the uniaxial compressive strength of a 1-m cube given in MPa.		

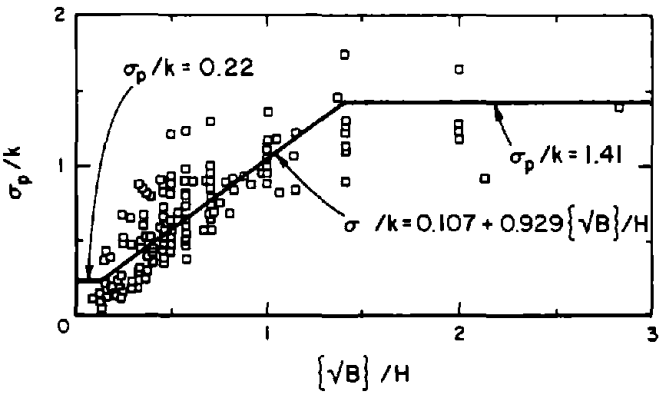

Figure 3.—Summary of uniaxial compressive strength versus size/shape relationships.

CONCLUSIONS

1. Reexamination of all the uniaxial compressive strength data for coal taken from the literature has shown that the general form of relationship for the size and shape effects on coal strength proposed originally by Steart, and by Holland, gives a relatively good fit to the data provided that upper and lower limits are placed on this relationship. Above and below these limits, the coal strength can be considered as constant. The equations are summarized in table 1.

2. Hustrulid's analysis requires two equations, one to describe the size effects and one to describe the shape effects. The general form equation established here does not give a significantly better fit to the data than Hustrulid's equations. However, the use of a single relationship is intrinsically more satisfying since a cube is, after all, only a special case of a prism. Further, the use of this general form eliminates the need for concern about the differences between tests where the width, B, is varied and the height, H, kept constant and vice versa; the general form allows data from either set of tests to be lumped together.

REFERENCES

1. Daniels, J., and L. D. Moore. The Ultimate Crushing Strength of Coal. Eng. Min. J., 1907, pp. 263-268.

2. Rice, G. S. Test of the Strength of Roof Supports Used in Anthracite Mines of Pennsylvania, BuMines B 303, 1929, pp. 1-44.

3. Lowall, C. E., and C. T. Holland. Some Physical Characteristics of West Virginia Coal, Res. Bull. Eng. Experimental Station, WV Univ., Bull. 17, 1937.

4. Greenwald, H. P., H. C. Howarth, and I. Hartmann. Experiments on the Strength of Small Pillars of Coal in the Pittsburgh Bed. BuMines TP 605, 1939, 22 pp.

5. Steart, F. A. Strength and Stability of Pillars in Coal Mines. J. Chem. Metall. Min. Soc. S. Africa, 1954, pp. 309-325.

6. Millard, D. J., P. C. Newman, and J. W. Phillips. The Apparent Strength of Extensively Cracked Materials. Proc. Phys. Soc., B, v. 68, 1955, pp. 723-728.

7. Gaddy, F. L. A Study of the Ultimate Strength of Coal as Related to the Absolute Size of the Cubical Specimens Tested. Bull. 112, Va. Exp. Stn., VA Polytechnic Inst., 1956, pp. 1-27.

8. Evans, I., C. D. Pommeroy, and R. Berenbaum. The Compressive Strength of Coal. Colliery Eng., v. 38, 1961, Feb. pp. 75-80, Mar. pp. 123-127, and Apr. pp. 172-178.

9. Hustrulid, W. A. A Review of Coal Pillar Strength Formulae. Rock Mech., v. 8, 1976, pp. 115-145.

10. Bieniawski, Z. T. Contribution to the Discussion of A Study of the Strength of Coal Pillars and to A Method of Design of Bord and Pillar Workings. J., S. Afr. Inst. Min. and Metall., 1967, pp 187-192.

11. ____. In-Situ Strength and Deformation Characteristics of Coal. Eng. Geol., v. 2, No. 5, 1968, pp. 325-340.

12. Bieniawski, Z. T. The Effect of Specimen Size on the Compressive Strength of Coal. Int. J. Rock Mech. and Min. Sci., v. 5, No. 4, 1968, pp. 325-335.

13. ____. In-Situ Large Scale Testing of Coal. Paper in Proc. Conf. on In-Situ Investigations of Rock and Soils, British Geotech. Soc., 1969, pp. 44-49.

14. ____. Note on the In-Situ Testing of the Strength of Coal Pillars. J., S. Afr. Inst. Min. and Metall., 1968, pp. 445-465.

15. Evans, I. Discussion on The Effect of Specimen Size on the Compressive Strength of Coal. Int. J., Rock Mech. and Min. Sci., v. 7, No. 2, 1970, p. 230.

16. Griffith, W., and E. T. Conner. Mining Conditions Under the City of Scranton, Pa. BuMines B25, 1912, pp. 77-82.

17. Holland, C. T. The Physical Properties of Coal and Associated Rock as Related to the Causes of Bumps in Mines. Trans. AIME, v. 149, 1942, pp. 75-93.

18. Bauschinger, J. Communication of the Mechanical-Technical Laboratories of the Technical University in Munich, v. 6, 1876.

19. Withey, M. O., and J. Aston. Johnson's Materials of Construction. 7th ed., Wiley, 1930, pp. 112-114.

20. Bunting, D. Chamber Pillars in Deep Anthracite Mines. Trans. AIME, 1911, pp. 739-748.

21. Holland, C. T., and F. L. Gaddy. Some Aspects of the Permanent Support of Overburden in Coal Beds. Paper in Proc., WV Coal Min. Inst., 1957, pp. 43-66.

22. Holland, C. T. The Strength of Coal Mine Pillars. Paper in Proc., 6th Symp. on Rock Mech., Univ. MO, Rolla, MO, 1964, pp. 450-466.

23. Salamon, M. D. G., and A. H. Munro. A Study of the Strength of Coal Pillars. J., S. Afr. Inst. Min. and Metall., 1967, pp. 55-67.

24. Barron, K., and M. Das. Empirically Derived Formulae for Coal Pillar Strength. CIM Workshop on The Role of Pillars in Soft Rock Mining, Saskatoon, Nov. 13-14, 1986, 28 pp.

25. Yang, T. Influence of Specimen Size and Shape on the Strength of Coal. M. Sc. Thesis, Univ. Alberta, 1991.

26. Hobbs, D. W. The Strength and Stress Characteristics of Oakdale Coal Under Triaxial Compression. Geol. Mag., v. 97, 1960, pp. 422-435.

27. ____. The Strength and Stress-Strain Characteristics of Coal Under Triaxial Compression. J., Geol., v. 72, 1964, pp. 214-231.

28. Hazen, G., and L. Alder. Practical Coal Pillar Design Problems. Min. Congr. J., 1976, pp. 86-92.

29. Greenwald, H. P., H. C. Howarth, and I. Hartmann. Progress Report: Experiments on Strength of Small Pillars of Coal in the Pittsburgh Bed. BuMines RI 3575, 1941, 6 pp.

30. Jeramec, M. L., and D. M. Cruden. Strength of Coal From the Star-Key Mine Near Edmonton. Alberta, CIM Bull., 1979, 802 pp. 94-99.

PART 2: AN APPROACH TO EVALUATION OF INTACT AND MASS STRENGTHS OF COAL FROM TRIAXIAL TESTS ON LABORATORY-SIZE SPECIMENS

INTRODUCTION

Hoek and Brown (*1-2*) developed an empirical strength criterion for both intact and heavily jointed rock masses given by:

$$\sigma_1 = \sigma_3 + \{m\sigma_3\sigma_c + s\sigma_c^2\}^{1/2} \qquad (1)$$

where σ_1 and σ_3 are the major and minor principal stresses at failure, σ_c is the intact uniaxial compressive strength of the rock, and m and s are parameters that depend on the properties of the rock and the degree to which the rock had been broken prior to the application of the failure stresses σ_1 and σ_3. This equation is valid for the brittle failure of rocks at stresses below the brittle/ductile transition point. Hoek and Brown used Mogi's criterion (*3*) to define this point, i.e., the equation is valid provided that $\sigma_1 > 3.4\ \sigma_3$.

These workers showed that for tests on intact rocks (s=1), the parameter m can be determined from laboratory triaxial strength tests on intact rock specimens and, further, that for any particular rock type the value of m is approximately constant.

For heavily jointed rock masses (four or more discontinuity sets), Hoek and Brown (*1-2*) showed that the rock mass is approximately isotropic. They then examined empirically the manner in which the values of m and s varied with the rock mass characteristics. The presence of discontinuities in the rock mass results in a decrease in both m and s below the intact values. Hoek and Brown were able to relate the variation in the m and s parameters to both the Council for Scientific and Industrial Research (C.S.I.R.) and the Norwegian Geotechnical Institute (N.G.I.) rock mass classification ratings. From these results, they were able to prepare their well-known table describing the approximate failure criteria for intact and jointed rock masses of various rock types. This table has been well accepted and is probably the best approach to date that allows the estimation of rock mass properties for preliminary design purposes. Hence, if the rock type is known, a value of the uniaxial compressive strength can be estimated or determined, and the rock mass rating can be evaluated, then their equation gives an approximate empirical strength criterion for the rock. This has proved to be exceedingly useful in preliminary design considerations since it requires no testing other than the determination of the uniaxial compressive strength and an estimate of the rock mass rating.

Bieniawski and Bauer (*4*) believed that such an empirical strength criterion would also be of major practical importance in coal mining for estimating the in situ strength of coal pillars. Since Hoek and Brown had not studied coal as one of their rock types, Bieniawski and Bauer attempted to extend this work to cover coal by considering a range of triaxial strength data obtained for eight different U.S. coals. They showed that, contrary to Hoek

and Brown's experience, for coal the m value could not be regarded as constant, but covered a very wide range for these intact coal specimens. Commenting on these results, Hoek and Brown (*5*) noted that:

1. The coals were of various ranks, and
2. The most likely explanation for this wide range in m values was that the specimens were not truly intact and that the assumption s=1 was not justified.

Expanding on this latter statement, it is well established that the uniaxial compressive strength of laboratory-size coal specimens is very sensitive to the size and shape of the specimen tested. This sensitivity to specimen size and shape is a clear, but indirect indication that the specimens contain discontinuities causing the strength variations. Consequently, in the size range represented by the usual laboratory size test specimens, the coal cannot be regarded as "intact" and thus s cannot be unity.

The following questions can therefore be posed:

1. How can the intact m values for coal be determined from triaxial strength tests on nonintact specimens?
2. Can the coal mass strength be estimated from the results of tests on laboratory size specimens?

If this can be done, then it should be possible to examine the variation of m and s with degree of fracturing and with coal type (rank) to define coal mass failure criteria.

APPROACH TO EVALUATION OF INTACT m VALUES FROM TRIAXIAL STRENGTH TESTS ON NONINTACT SPECIMENS

Let σ_{pi} be the intact uniaxial prism strength, let M be the intact m value and S=1 be the intact s value for a particular coal. Assume that the failure criterion for intact coal is given in the form derived by Hoek and Brown (*1-2*) as:

$$\sigma_{1i} = \sigma_{3i} + \{M\sigma_{3i}\sigma_{pi} + S\sigma_{pi}^2\}^{1/2} \qquad (2)$$

where S=1, σ_{1i} and σ_{3i} are the principal stresses at failure for the intact coal.

Assume that triaxial tests are carried out on a suite of laboratory-size specimens of height H, and diameter (width), B. Further, it is assumed that these specimens cannot be regarded as being intact. Assume that the results of these strength tests can also be expressed in Hoek/Brown form

$$\sigma_1 = \sigma_3 + \{m\sigma_3\sigma_{pi} + s\sigma_{pi}^2\}^{1/2}; \qquad (3)$$

hence, the uniaxial prism strength, σ_p, of this nonintact coal of this size is given by:

$$\sigma_p = \{s\sigma_{pi}^2\}^{1/2} \qquad (4)$$

where s is not equal to unity.

The problem then arises as to whether the intact M and σ_{pi} values can be estimated from the test results on these nonintact specimens. To do this, some additional information is required, namely a functional relationship describing how the uniaxial compressive strength varies with specimen size.

VARIATION OF UNIAXIAL COMPRESSIVE STRENGTH WITH SPECIMEN DIMENSIONS

It was shown in part 1 of this paper that the effect of specimen size and shape on the uniaxial strength of coal can be expressed in normalized form by the following equations and limits:

Category 1: $\{B\}^{1/2}/H < 0.784$, or $B > 1.626$ m, then σ_p = constant given by:

$$\sigma_p = \text{constant} = 0.88\ K \qquad (5)$$

Category 2: $0.784 < \{B\}^{1/2}/H < 8.784$, and $0.013\ m < B < 1.626$ m, then:

$$\sigma_p = K[0.452 + 0.548\ \{B\}^{1/2}/H] \qquad (6)$$

Category 3: $\{B\}^{1/2}/H > 8.784$, and $B < 0.013$ m, then σ_p = constant given by:

$$\sigma_p = \text{constant} = 5.266\ K \qquad (7)$$

where B and H are the specimen width and height respectively and are given in meters, σ_p is the uniaxial prism strength in megapascals, and K is numerically (but not dimensionally) equal to the uniaxial cube strength of a 1-m cube given in megapascals.

IMPLICATIONS WITH RESPECT TO INTACT COAL STRENGTH

Consider the limit $\{B\}^{1/2}/H = 8.784$, then for a cube in which B=H=D, at this limit $\{D\}^{1/2} = 1/8.784$, i.e., D = 0.013 m. That is, this limit implies that the uniaxial

prism strength becomes a constant for small specimens. Hence, beyond this limit the strength is no longer affected by the specimen size or shape. It follows, therefore, that this value can be regarded as the intact uniaxial prism strength. Therefore, from equation 7:

$$K = \sigma_{pi}/5.266. \quad (8)$$

Hence, substituting from equation 8 into equation 6, the following expression is obtained:

$$\sigma_p = K\{0.452 + 0.548\ \{B\}^{1/2}/H\}$$

$$= \{\sigma_{pi}/5.266\}\{0.452 + 0.548\ \{B\}^{1/2}/H\}$$

$$= \sigma_{pi}\ \{0.086 + 0.104\ \{B\}^{1/2}/H\}, \quad (9)$$

but now equations 4 and 9 can be equated, hence:

$$\sigma_p = \sigma_{pi}\ \{0.086 + 0.104\ \{B\}^{1/2}/H\} = \{s\sigma_{pi}^2\}^{1/2},$$

which gives $s = \{0.086 + 0.104\ \{B\}^{1/2}/H\}^2$. (10)

Thus, substituting from equation 10 for s into equation 3 gives:

$$\sigma_1 = \sigma_3 + \{m\sigma_3\sigma_{pi} + s\sigma_{pi}^2\}^{1/2},$$

$$\sigma_1 = \sigma_3$$

$$+ \{m\sigma_3\sigma_{pi} + [\{0.086 + 0.104\{B\}^{1/2}/H\}^2]\sigma_{pi}^2\}^{1/2}. \quad (11)$$

Dividing this equation by s and rearranging, the following expression is obtained:

$$\{\sigma_1 - \sigma_3\}^2/s = \{(m/s)\sigma_3\sigma_{pi} + 1\,\sigma_{pi}^2\} \quad (12)$$

and comparing equation 12 with equation 2 it is seen that

$$\{\sigma_{1i} - \sigma_{3i}\}^2 = \{\sigma_1 - \sigma_3\}^2/s \qquad \text{and } M = m/s$$

where s is given by equation 10, i.e.,

$$\{\sigma_1 - \sigma_3\}^2/s = \{M\,\sigma_3\,\sigma_{pi} + \sigma_{pi}^2\}. \quad (13)$$

Hence, following the procedure of Hoek and Brown (*2*, appendix 5), put

$$\{\sigma_1 - \sigma_3\}^2/s = y, \quad \text{and } \sigma_3 = x$$

then equation 13 becomes:

$$y = M\,\sigma_{pi}\,x + \sigma_{pi}^2$$

and M and σ_{pi} can be evaluated from:

$$\sigma_{pi}^2 = \frac{\Sigma y_i}{n} - \left\{\frac{\Sigma x_i y_1 - \frac{\Sigma x_i \Sigma y_i}{n}}{\left[\Sigma x_i^2 - \frac{(\Sigma x_i)^2}{n}\right]}\right\}\frac{\Sigma x_i}{n} \quad (14)$$

$$M = \frac{1}{\sigma_{pi}}\left\{\frac{\Sigma x_i y_i - \frac{\Sigma x_i \Sigma y_i}{n}}{\left[\Sigma x_i^2 - \frac{(\Sigma x_i)^2}{n}\right]}\right\} \quad (15)$$

and the correlation coefficient, r, is given by:

$$r^2 = \left\{\frac{\left[\Sigma x_i y_i - \frac{\Sigma x_i \Sigma y_i}{n}\right]^2}{\left[\Sigma x_i^2 - \frac{(\Sigma x_i)^2}{n}\right]\left[\Sigma y_i^2 - \frac{(\Sigma y_i)^2}{n}\right]}\right\}. \quad (16)$$

Thus, M and σ_{pi} for the intact coal can be evaluated, and also for this particular size of specimen tested

$$s = \{0.086 + 0.104\ \{B\}^{1/2}/H\}^2 \quad \text{and} \quad m = s\,M, \quad (17)$$

i.e., given n sets of triaxial test data (σ_1, σ_3) at failure for a suite of specimens of height, H, and width, B, such that $0.784 < B^{1/2}/H < 8.784$, the intact uniaxial prism strength, σ_{pi}, the intact M value, the intact s value (= 1, by definition), and the m and s value for this particular size specimen can all be determined.

LIMITATIONS

Hoek and Brown (*1*) placed practical limitations on the use of their equation due to the change from brittle to ductile behavior for most rocks. They used Mogi's definition (*3*) of the transition point given by

$$\sigma_1 = 3.4\ \sigma_3. \quad (18)$$

At high-confining pressures, when σ_1 is less than the value given by equation 18, the curve bends over more severely due to ductile behavior and departs from the relationship given by equation 2.

Consequently, in their determination of m values for intact rocks, Hoek and Brown only used data where $\sigma_1 > 3.4\sigma_3$. Other work (*6-8*) suggests that this brittle/ductile transition point occurs due to pseudoductile behavior and may be expressed in terms of the sliding coefficient of friction of the failed rock, as

$$\sigma_1 = \alpha\ \sigma_3 \quad (19)$$

where $\alpha = (1 + \sin\phi)/(1 - \sin\phi)$ (20)

where ϕ is the angle of sliding friction of the failed rock. (NOTE: If α = 3.4, as suggested by Mogi, then this corresponds to a ϕ value of 33°.) For coal, ϕ appears to lie in the range of about 23° to 42°, giving a range of α from about 2.3 to 5.0.

Thus, when evaluating M, m and s from triaxial test data, care should be taken to try to distinguish at what stress level brittle/ductile transition occurs, and the data above this transition point should not be used in the evaluation of these parameters.

IMPLICATIONS WITH RESPECT TO COAL MASS STRENGTH

In the above analysis, use has been made of the empirically derived lower size limit, $B^{1/2}/H = 8.784$, to assist in evaluating the M value for intact coal. However, this empirical work also indicated an upper size limit beyond which the uniaxial strength can again be regarded as constant and given by equation 5, i.e., if $\{B\}^{1/2}/H < 0.784$, then

$$\sigma_p = \text{constant} = 0.88\ K. \quad (5)$$

For a cube (B=H=D), then the critical cube dimension at this limit is given by $D^{1/2} = 1/0.784$. That is, D = 1.626 m. This corresponds very closely to the upper limit of size beyond which cubes tested by Bieniawski (*9*) were shown to have a constant strength, i.e., above this limit the coal strength is again constant and hence it follows that this can be regarded as the coal mass uniaxial compressive strength.

Thus, from equation 8, putting $K = \sigma_{pi}/5.266$, the uniaxial compressive strength at this upper limit, σ_{pu}, can be expressed as

$$\sigma_{pu} = 0.88\ K = \{\sigma_{pi}/5.266\}\ 0.88 = 0.167\ \sigma_{pi} \quad (21)$$

and equating equations 21 and 4 gives

if $\{B\}^{1/2}/H < 0.784$, then

$$\sigma_{pu} = 0.167\ \sigma_{pi} - \{s\sigma_{pi}^2\}^{1/2}$$

i.e., $$s = \{0.167\}^2 = 0.028 \quad (22)$$

i.e., for large specimens, there is a minimum value of s = 0.028 beyond which, for all practical purposes, s remains constant and the strength also remains constant.

This also implies that the strength of a large coal mass (large enough that $\{B\}^{1/2}/H < 0.784$) is given by putting s = 0.028 in equation 3, i.e., for the coal mass

$$\sigma_{1m} = \sigma_{3m} + \{m_m\ \sigma_{3m}\ \sigma_{pi} + s\sigma_{pi}^2\}^{1/2} \quad (23)$$

where $$m_m = 0.028\ M. \quad (24)$$

Hence, the rock mass m and s values can also be estimated from tests on laboratory-size specimens.

CONCLUSIONS

1. In part 1 of this paper, a relationship was established that described the size and shape effects on the uniaxial strength of coal. There are upper and lower limits to this relationship above and below which the uniaxial compressive strength can be regarded as a constant. It has been shown here that these limits can be regarded as defining the uniaxial compressive strength of the coal mass and of the intact coal respectively.

2. Most laboratory tests on coal specimens are carried out in the regime in which the strength is varying rapidly with the size and shape of the specimen. However, by making use of the upper and lower limits of the uniaxial compressive strength relationship, equations have been developed that allow the estimation of the triaxial strength of both the intact coal and the coal mass from tests on laboratory-size specimens. To verify the applicability or otherwise of these equations, it will be necessary to carry out a comprehensive triaxial testing program on laboratory specimens of different sizes and shapes. This has been done for one coal, and the results are presented in part 3 of this paper.

REFERENCES

1. Hoek, E., and E. T. Brown. Empirical Strength Criterion for Rock Masses. J., Geotech. Eng. Div., A.S.C.E., 1980, pp. 1013-1035.

2. ___. Underground Excavations in Rock. Inst. Min. and Metall., London, 1980, pp. 137-140.

3. Mogi, K. Pressure Dependence of Rock Strength and Transition From Brittle to Ductile Flow. Bull. Earthquake Res. Inst., Japan, v. 44, 1966, pp. 215-232.

4. Bieniawski, Z. T., and J. Bauer. Discussion of Empirical Strength Criterion for Rock Masses. J., Geotech. Eng. Div., A.S.C.E., 1982, pp. 670-672.

5. Hoek, E., and E. T. Brown. Discussion of Empirical Strength Criterion for Rock Masses - Closure. J., Geotech. Eng. Div., A.S.C.E., 1982, pp. 672-673.

6. Orawin, E. Mechanism of Seismic Faulting. Rock Deformation. Geol. Soc. Am. Memor. 79, 1960, pp. 323-345.

7. Maurer, W. C. Shear Failure of Rock Under Compression. Soc. Petrol. Engrs., J., No. 5, 1965, pp. 167-175.

8. Barron, K. An Analytical Approach to the Design of Coal Pillars. CIM. Bull., v. 77, 1984, No. 8, pp. 37-44.

9. Bieniawski, Z. T. In-Situ Strength and Deformation Characteristics of Coal. Eng. Geol., v. 2, No. 5, 1968, pp. 325-340.

PART 3: LABORATORY TEST RESULTS

INTRODUCTION

In part 2 of this paper, a semitheoretical/empirical approach was taken to develop equations that would allow the intact coal and the coal mass strength parameters, m and s, to be estimated from the results of triaxial tests on laboratory-size specimens. To verify the applicability of these equations, it is necessary to carry out a comprehensive laboratory triaxial testing program on coal specimens of different sizes and shapes. This has been done for one coal, and the results are reported and discussed here.

TEST PROGRAM AND PROCEDURES

The coal chosen for testing was obtained from the Whitewood Mine in Alberta, a subbituminous C coal (ECE rank No. 12). Difficulty was experienced in drilling small-diameter specimens from blocks of this coal, and only two diameters were successfully cored. Three different specimen heights were chosen. Table 1 summarizes the five size/shape groups tested, giving their dimensions, the value of s as calculated from equation 10 in part 2 of this paper, and the number of specimens tested in each of these size groups.

Table 1.—Summary of test specimens

Size group	B-m	H-m	B/H	$\{B\}^{1/2}/H$	s	No. specimens tested
A . . .	0.056	0.12	0.47	1.97	0.085	3
B . . .	.068	.12	.57	2.17	.097	2
C . . .	.056	.09	.62	2.63	.129	4
D . . .	.056	.08	.70	2.95	.155	4
E . . .	.068	.08	.85	3.26	.181	5

Multistage triaxial strength tests following the procedure of Kovari and Tisa (*1*) were carried out for each of the these specimens. This allowed four peak strengths and three residual strengths at different confining pressures to be determined from each specimen.

To minimize test biased error and to allow for statistical analysis of the results, the specimens were tested in random order and the four confining pressures for each peak strength were randomly selected in ascending order from a preselected range of 20 confining pressures every 3.45 MPa over the range 0 to 69 MPa. The three confining pressures for the residual strength tests were those corresponding to the first three confining pressures used for peak strength determination with that specimen. The detailed results of all these tests are reported and tabulated elsewhere (*2*).

TEST RESULTS

ANALYSIS OF RESIDUAL STRENGTH DATA

Graphs of the residual strength, σ_r, versus the confining pressure, σ_3, for each size group were plotted and a linear correlation performed. This yielded the equations and correlation coefficients given in table 2 for each of the size groups, and for all the data points taken together.

The significance of these regressions and the resulting parameters were then statistically tested and the equations for each individual size group were statistically compared

Table 2.—Residual strength data correlations

Size group	s	No. data points	Equation MPa	r
A	0.085	9	$\sigma_r = 14.2 + 1.15\,\sigma_3$	0.92
B	.097	6	$\sigma_r = 19.5 + 1.27\,\sigma_3$	.95
C	.129	12	$\sigma_r = 16.7 + 1.21\,\sigma_3$	.95
D	.155	12	$\sigma_r = 12.5 + 1.75\,\sigma_3$	.98
E	.181	15	$\sigma_r = 14.4 + 1.37\,\sigma_3$	.94
All data together	-	54	$\sigma_r = 15.4 + 1.32\,\sigma_3$	.93

with the equation derived from taking the data from all the size groups together. These tests showed:

1. There is a 95% degree of confidence that the assumed regression model is appropriate for each size group and for all the data taken together.
2. Comparing each individual size group with the total group in which all the data have been considered together, it was shown that there is no statistical difference between them at a 5% significance level.
3. It can therefore be concluded that the specimen size and shape has no significant influence on the residual strength results and these can be expressed by the relationship

$$\sigma_r = 15.4 + 1.32\,\sigma_3 \qquad (1)$$

with a correlation coefficient r = 0.93, as shown in figure 1.

It will be convenient later to express this relationship in normalized form. To derive the normalized relationship, each value of σ_r and σ_3 was divided by the intact uniaxial compressive strength, σ_{pi}, calculated from the peak strength results for that specific specimen (this calculation assumes that the specimens are not intact and the expressions developed in part 2 are correct). A linear correlation was then carried out on this normalized data and yielded the following equation:

$$\frac{\sigma_r}{\sigma_{pi}} = 0.25 + 1.27\,\frac{\sigma_3}{\sigma_{pi}} \qquad (2)$$

with a slightly improved correlation coefficient of r = 0.97. The results in this form are shown in figure 2.

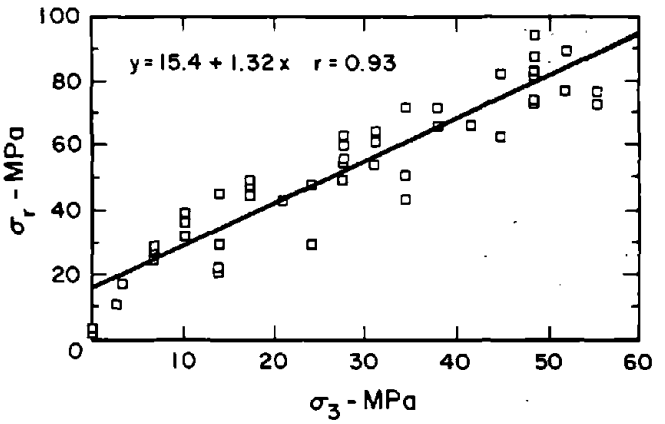

Figure 1.—Residual strength, σ_r, versus confining pressure, σ_3, for all data.

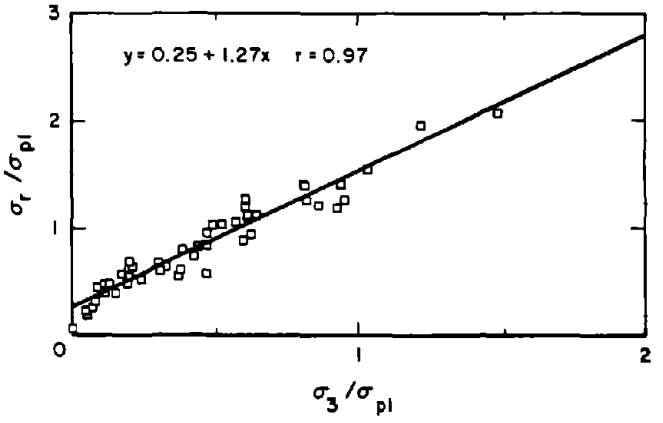

Figure 2.—Normalized residual strength, σ_r/σ_{pi}, versus normalized confining pressure, σ_3/σ_{pi}, for all data.

ANALYSIS OF PEAK STRENGTH DATA, TREATING SPECIMENS AS IF THEY WERE INTACT

The original premise of this work was based on the assumption that laboratory-size coal specimens cannot be regarded as intact and therefore s cannot be equal to 1. It is therefore important to verify that this assumption is correct. This was done by treating the peak strength data as if the specimens were intact and calculating m and the uniaxial compressive strength, σ_p, assuming that s = 1, and then statistically testing whether or not these values were significantly affected by the change in specimen height, the change in specimen diameter and, finally, by the change in height-diameter combinations. The details of these calculations and the statistical tests are reported elsewhere (*2*), and the conclusion will only be summarized here. It was shown, with an error of probability of 5%, that:

1. Tests on the three different specimen height groups with the same diameter gave significantly different m values. However, the σ_p values were not significantly affected by the height.
2. Tests on the two different diameter groups with the same height also gave significantly different m values, but the difference in σ_p values was not significant at this level.
3. Tests on the combined effect of height and diameter on the m values showed that there was a significant difference in the results at the 5% error of probability level. Again, the differences in the uniaxial compressive strengths were not significant at this level.

It was therefore concluded that specimen size/shape does have a significant effect on the m values when the specimens were treated as if they were intact. Therefore, the assumption that the specimens could not be considered to be intact was justified.

A similar result had been anticipated for the uniaxial compressive strength when treated in this manner. However, this was not confirmed by the statistical tests. That is, the uniaxial compressive strength results were not significantly affected by the size/shape. The mean uniaxial compressive strength was 24.0 MPa with a coefficient of variation of 32.9%. This large variation in the uniaxial compressive strength, coupled with the fact that the range of size/shape variation was small, leads to the speculation that perhaps any influence of the size/shape on the compressive strength was masked by this large natural variation in the compresive strength.

ANALYSIS OF PEAK STRENGTH DATA, TREATING SPECIMENS AS IF THEY WERE NOT INTACT

The peak strength data were then analyzed assuming that the specimens were not intact and that the relationships developed in part 2 of this report were correct. That is, it was assumed that s was given by $s = \{0.086 + 0.104\{B\}^{1/2}/H\}^2$. The steps in this analysis were as follows:

1. For each individual specimen a linear correlation between $(\sigma_1 - \sigma_3)^2/s = y$ and $\sigma_3 = x$ was carried out and the intact M and intact uniaxial compressive strength σ_{pi} were calculated. Table 3 summarizes the results of these correlations together with the correlation coefficents, r.

Table 3.—Summary of uncorrected values for M and σ_{pi} for each individual specimen

Size group	Specimen No.	s	σ_{pi}-MPa	M	r
A	9-1	0.085	57.9	0.41	0.97
	7-2	.085	89.3	.60	.97
	6-3	.085	52.1	.81	.99
B	1-D	.097	77.3	.51	.79
	5-B	.097	114.3	.61	.90
C	5-3	.129	58.5	.56	.97
	6-2	.129	49.9	.94	.99
	6-4	.129	86.1	.66	.82
	7-4	.129	36.5	.67	.99
D	1-4	.155	92.5	1.31	.88
	3-1	.155	51.3	2.09	.78
	5-2	.155	70.4	1.62	.82
E	1-C	.181	33.9	1.79	.95
	2-A	.181	59.0	1.41	.99
	2-B	.181	80.2	.83	.95
	4-B	.181	78.7	.99	.98
	4-E	.181	58.6	.99	.98
	5-A	.181	37.1	.68	.91
Mean	-	-	65.8	.97	-
Standard deviation	-	-	21.9	.48	-

2. Each individual data point (σ_1, σ_3) was then normalized by dividing by σ_{pi} for that individual specimen. A linear correlation between $(\sigma_1 - \sigma_3)^2/s\ \sigma_{pi}^2 = y$ and $\sigma_3/\sigma_{pi} = x$ was carried out for all the data in each size group and all the data taken together. These results are given in table 4. Figure 3 shows this normalized correlation for all the data taken together. The significance of these regressions and the resulting parameters for each size group were statistically compared with the correlation using all the data taken together. The tests showed that:

(a) There is a 95% degree of confidence that the assumed regression model is appropriate for each size group and for all the data taken together.

(b) Comparing each individual size group with that in which all the data have been considered together, it was shown that there was no significant difference between groups A,B,D,E and the total group at 5% significance level. For group C, there was a difference at the 5% significance level but not at the 2% level.

(c) The preliminary conclusion was therefore drawn that all the data could be lumped together and could be expressed as:

$$\frac{(\sigma_1 - \sigma_3)^2}{s\sigma_{pi}^2} = a_o + M\frac{\sigma_3}{\sigma_{pi}} = 0.97 + 1.02\frac{\sigma_3}{\sigma_{pi}} \qquad (3)$$

with a correlation coefficient of r = 0.74.

However, it must be borne in mind that these data may include data points lying above the brittle/ductile transition point, above which the Hoek/Brown form of equation is inapplicable.

3. The normalized brittle/ductile transition point $(\sigma_{1NT}, \sigma_{3NT})$ is given by the intersection of the two curves for the residual and peak strengths

$$\frac{\sigma_{1r}}{\sigma_{pi}} = \alpha + \beta\frac{\sigma_{3r}}{\sigma_{pi}} \qquad (4)$$

and

$$\frac{(\sigma_{1p} - \sigma_{3p})^2}{s\sigma_{pi}^2} = a_o + M\frac{\sigma_{3p}}{\sigma_{pi}} \qquad (5)$$

which occurs when $\sigma_{1p}/\sigma_{pi} = \sigma_{1r}/\sigma_{pi} = \sigma_{1T}/\sigma_{pi} = \sigma_{1NT}$ and $\sigma_{3p}/\sigma_{pi} = \sigma_{3r}/\sigma_{pi} = \sigma_{3T}/\sigma_{pi} = \sigma_{3NT}$ where σ_{1T}, σ_{3T} are the stresses at the brittle/ductile transition point, and the subscript N indicates normalized values. From these two

equations, the normalized confining pressure is related to s by:

$$\sigma_{3NT} = \frac{\{Ms - 2\alpha(\beta - 1)\} + \{[Ms - 2\alpha(\beta - 1)]^2 - 4(\beta - 1)^2(\alpha^2 - a_o s)\}^{1/2}}{2(\beta - 1)^2} \quad (6)$$

and, for this case where $\alpha = 0.25$, $\beta = 1.27$, $a_o = 0.97$, $M = 1.02$, gives:

$$\sigma_{3NT} = \frac{\{1.02s - 0.135)\} + \{[1.02s - 0.135]^2 - 0.292(0.625 - 0.97s)\}^{1/2}}{0.146} \quad (7)$$

Table 5 gives the values of σ_{3NT} and σ_{1NT} calculated from this equation for each of the size groups tested.

Table 4.—Normalized data correlations, $(\sigma_1 - \sigma_3)^2/s\sigma_{pi}^2$ versus σ_3/σ_{pi} (no data eliminated)

Size group	s	No. data points	a_o	M	r
A	0.085	12	0.986	0.625	0.87
B	.097	8	1.016	.508	.81
C	.129	16	.983	.752	.93
D	.155	12	.945	1.826	.77
E	.181	24	.936	1.206	.81
All data together	-	72	.966	1.023	.74

Table 5.—Normalized brittle/ductile transition point for each size group

Size group	A	B	C	D	E
s ...	0.085	0.097	0.129	0.155	0.181
σ_{3NT}	.288	.456	.904	1.268	1.631
σ_{1NT}	.616	.829	1.400	1.860	2.321

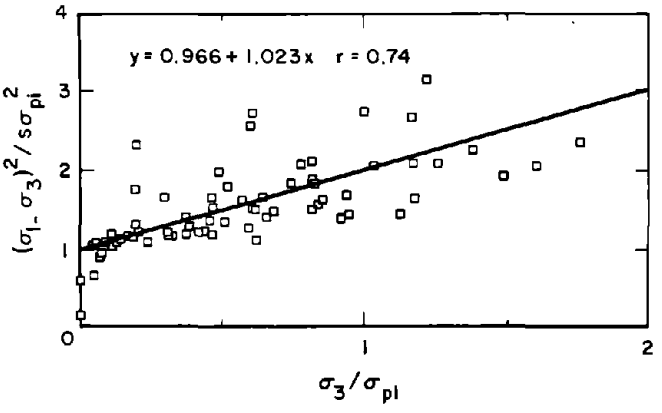

Figure 3.—Normalized peak strength correlation, $(\sigma_1 - \sigma_3)^2/s\sigma_{pi}^2$, versus normalized confining pressure, σ_3/σ_{pi}, for all data.

4. Using the σ_{pi} value for each individual specimen the brittle/ductile transition point was then calculated for that specimen, any data points above this transition point were eliminated and the analysis steps 1 and 2 were repeated using the revised data. Thus, revised M and σ_{pi} values were determined for each individual specimen, a revised normalized equation similar to equation 3 was determined, as were revised normalized brittle/ductile transition points. A second similar revision was needed before it was unnecessary to eliminate (or add back in) data points.

For all the specimens in size group A, at least two of the four peak strength values were eliminated during this exercise. Consequently, there were insufficient data from which to calculate M and σ_{pi} values. For the other size groups, there were always at least three valid data points remaining.

The revised mean M and σ_{pi} values and their standard deviations were 1.05 (s.d. = 0.48) and 65.6 MPa (s.d. = 23.0 MPa), respectively.

Table 6 shows the final revised normalized correlations for each size group and for all the data taken together. The final revised correlation for all the data taken together is shown in figure 4 and is given by:

$$\frac{(\sigma_1 - \sigma_3)^2}{s\sigma_{pi}^2} = 0.947 + 1.21\frac{\sigma_3}{\sigma_{pi}} \quad (8)$$

with a correlation coefficient r = 0.78. That is, using all the remaining data, the best estimate of M is 1.21 compared to the mean value of 1.05.

It was then shown that:

(a) There is a 95% degree of confidence that the assumed regression model is appropriate for each size group and for all the data taken together.

(b) Comparing groups B, C, D, and E with all the revised data taken together, it was shown that there was no significant difference at the 5% level.

(c) It was therefore concluded that all the data could be lumped together and expressed by equation 8.

Table 6.—Final normalized data correlations, $(\sigma_1 - \sigma_3)^2/s\,\sigma_{pi}^2$ versus σ_3/σ_{pi} (data eliminated)

Size group	s	No. data points	a_o	M	r
A	0.085	1	insufficient data remaining		
B	.097	6	0.996	0.61	0.94
C	.129	13	.965	.84	.90
D	.155	12	.945	1.827	.77
E	.181	24	.936	1.206	.81
All data together	-	56	.947	1.21	.78

Table 7 shows the revised normalized brittle/ductile transition point calculated, using equation 6, for each of the size groups tested and for the intact coal putting s = 1. The approximate magnitudes of the stresses at the brittle/ductile transition point, using the mean value of σ_{pi} = 65.6 MPa, are also shown in this table. This shows clearly the sensitivity of the brittle/ductile transition point to the specimen size/shape.

Table 7.—Final normalized brittle/ductile transition point for each size group

Size group	A	B	C	D	E	Intact
s	0.085	0.097	0.129	0.155	0.181	1
σ_{3NT} ..	.323	.525	1.061	1.494	1.927	15.53
σ_{1NT} ..	.660	.917	1.597	2.148	2.6981	19.97
and assuming the mean σ_{pi} value of 65.6 MPa gives:						
σ_{3T} - MPa	21.2	34.4	69.6	98	126.4	1020
σ_{1T} - MPa	43.2	60.2	104.8	140.9	177	1310

STATISTICAL TESTS WHEN DATA ARE TREATED AS IF SPECIMENS WERE NOT INTACT

It has been assumed that the specimens cannot be treated as intact, but that the intact M and σ_{pi} values can be estimated assuming that $s = \{0.086 + 0.104\{B\}^{1/2}/H\}^2$. If this is correct, then these derived values should not be significantly affected by specimen height, diameter, or by combinations of these two parameters. Statistical tests, similar to those reported previously, were therefore carried out to examine the influence or otherwise of these parameters.

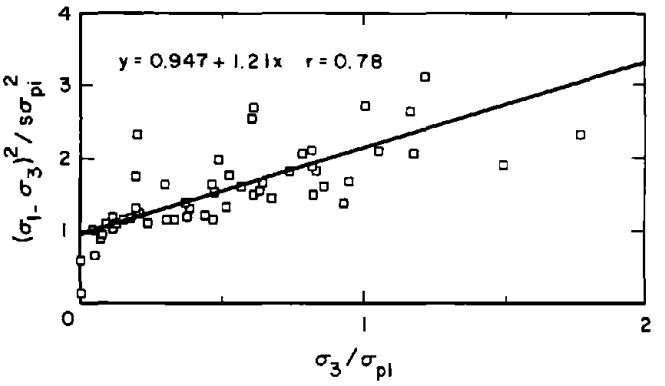

Figure 4.—Final revised normalized peak strength correlation, $(\sigma_1 - \sigma_3)^2/s\sigma_{pi}^2$, versus normalized confining pressure, σ_3/σ_{pi}, for all data.

It was shown, with an error of probability of 5%, that:

1. There was no significant influence of height, diameter, or combinations thereof, on the σ_{pi} values. However, since the same conclusion was drawn from the statistical tests when the specimens were treated as if they were intact, no general conclusion can be drawn with respect to the validity of the size/shape correction factor when applied to σ_{pi}.
2. There was no significant influence of either the diameter or of the height/diameter combinations on the M values. However, the height still showed a significant influence at this level of error of probability (although the F statistic was somewhat reduced below that calculated when the specimens were treated as if they were intact).

It was therefore concluded that the approach proposed in part 2 of this paper successfully eliminates the influence of diameter and height-diameter combinations but does not totally eliminate the influence of specimen height. It is thus believed that this approach is valid but that some refinement to the expression for s is probably required before size/shape effects can be totally eliminated and the intact M values can be reliably determined from tests on laboratory-size specimens.

ESTIMATE OF COAL MASS STRENGTH

According to part 2 of this paper, the coal mass m and s values are given by putting s = 0.028 and m_m = Ms and the uniaxial coal mass strength is given by σ_{pu} = $\{s\ \sigma_{pi}^2\}^{1/2}$. That is, m_m = 1.21(0.028) = 0.034 and σ_{pu} = $\{0.028\ (65.6)^2\}^{1/2}$ = 10.98 MPa.

If s = 0.028 is substituted into equation 6 to derive the brittle/ductile transition point for the coal mass, it is found that σ_{3NT} is negative. Clearly this cannot be correct, again indicating that some refinement to the expression for s is needed. However, it is clear that the brittle/ductile transition point for this coal mass must occur at a low-confining pressure level.

Figure 5 shows the σ_1 / σ_3 relationship at failure for the coal mass, for each size group and for the intact rock derived from these test results for this particular coal. The residual curve is also shown on this figure.

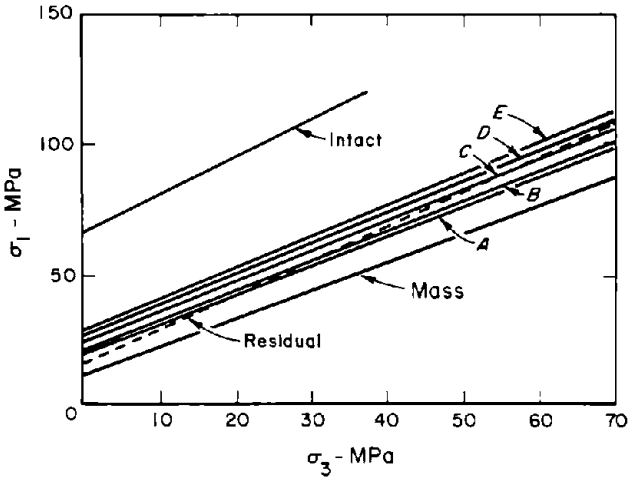

Figure 5.—σ_1 versus σ_3 relationships for failure for all size groups, and estimated intact and coal mass failure criteria.

CONCLUSIONS

Coal is a highly variable material, specimens are difficult to prepare and strength results are scattered. Consequently, when carrying out a test program such as this, it is important to randomize the specimens to minimize the test biased error and to allow for careful statistical analysis of the results. It is also helpful to normalize the results for better comparison between different specimen groups.

Analysis of the strength tests carried out on this coal showed that:

1. The residual strength was uninfluenced by the specimen size/shape and could be expressed as a linear relationship with the confining pressure.

If the peak strength data are treated as if the specimens could be considered as being intact, then it was shown that:

2. The resulting Hoek/Brown parameter m was significantly affected (at a 5% level of error of probability) by the specimen height, diameter, and combinations thereof. However the uniaxial compressive strength, σ_p, was not affected by the size/shape of the specimens. It was speculated that this latter result was due to the wide natural variation in the uniaxial compressive strength masking any effect of size/shape.

It was therefore concluded that specimen size/shape does have a significant influence on the strength of coal and, hence, the specimens cannot be considered to be intact.

If the peak strength data are treated as if the specimens were not intact, following the concepts developed in part 2 of this paper, then it was shown that:

3. The intact M parameter derived from the data was not significantly influenced by the specimen diameter or by height/diameter combinations. However, at a 5% level of error of probability, there was still a significant influence of specimen height on the results (albeit this effect was reduced relative to the results when the specimens were treated as if they were intact).

4. There was no significant influence of the specimen size/shape on the intact compressive strength, σ_{pi}. Since the same conclusion was drawn from the results when the specimens were treated as intact, no general conclusion can be drawn with respect to the validity of these concepts when applied to σ_{pi}.

It was therefore tentatively concluded that the approach developed in part 2 of this paper to account for size/shape effects under triaxial conditions is probably valid, but some refinement of the expression relating s to the specimen dimensions is needed before the effects of height variation can be totally eliminated.

When attempting to use the concepts to estimate the coal mass strength for this coal, it was found that the predicted brittle/ductile transition point would occur at a negative confining pressure. Clearly this is incorrect, again indicating that the expression for s probably requires some modification. Nonetheless, the results did indicate that the

brittle/ductile transition point for coal reduces rapidly as the specimen size increases, so that it could be expected that the coal mass would behave in a ductile manner at a relatively low-confining pressure.

It is therefore believed that the approach presented here is promising, but that further testing is required to refine the developed expressions before this approach can be said to have been fully validated.

REFERENCES

1. Kovari, K., and A. Tisa. Multiple Failure State and Strain Controlled Triaxial Tests. Rock Mech. 7, 1975, pp. 17-33.

2. Yang, T. Influence of Specimen Size and Shape on the Strength of Coal. M. Sc. Thesis, Univ. Alberta, 1991.

PART 4: INFLUENCE OF COAL RANK

INTRODUCTION

An approach has been developed in the previous parts of this paper to estimate the intact M values for coal based on tests on laboratory size nonintact specimens. Ideally, the intact M value so determined should be independent of the specimen size and shape. In fact, it was shown in part 3 that these size effects were not totally eliminated by the expressions developed in part 2 of the paper. However, the size/shape effects were much reduced, and for the purposes of this part of the paper, it will be assumed that these size/shape effects are totally eliminated by using the developed expressions. If indeed the intact M value is independent of size/shape, then it is possible to investigate how M varies with the rank of the coal.

This is done in this part of the paper, using as much of the triaxial test data on coal that could be found in the literature in which the authors had reported both the specimen size and the coal rank. Unfortunately, many authors report neither their specimen size nor the coal rank; thus, the amount of data obtainable was rather limited (*1-7*).

Data were drawn from both European and North American sources, consequently the rank of the coals was reported according to different coal classification systems. All coal ranks were therefore transformed to the common base of the Economic Commission for Europe (ECE) International Class Number, using the conversion tables given by Williamson (*8*). This base was chosen because it is purely numerical and is therefore more amenable for correlation purposes.

DATA ANALYSIS

The σ_1 and σ_3 values at failure for each of the suites of triaxial specimens of given dimensions and known coal rank were derived from the literature sources and s was calculated from the dimensions. The intact σ_{pi} and M values were then calculated, as were the correlation coefficients. Appendix A at the end of this paper summarizes these results and gives the source references.

Little or no information was available on the residual strengths of these specimens; consequently, the brittle/ductile transition point could not be determined. As a result, it is not known whether this analysis includes data that lie above the brittle/ductile transition point.

Each individual data pair (σ_1, σ_3) was then normalized by dividing by the σ_{pi} value for that particular suite of specimens. Normalized correlations between $(\sigma_1 - \sigma_3)^2/s\sigma_{pi}^2$ and σ_3 / σ_{pi} for all the data in each rank group were then carried out and group M values and the group correlation coefficients were determined. These results are also tabulated in appendix A. Figure 1 shows one such correlation, that for ECE rank 6.

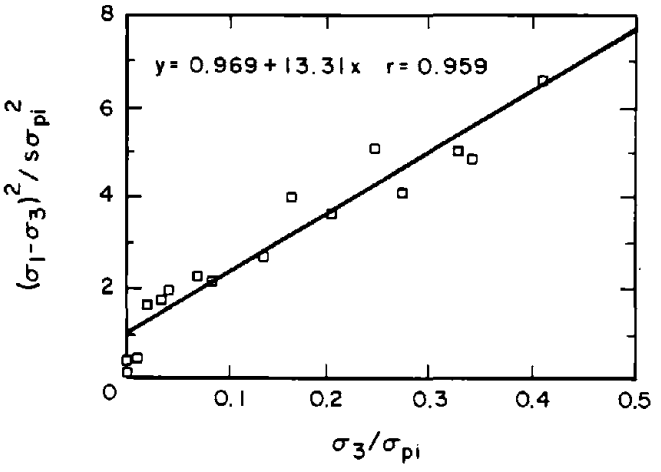

Figure 1.—Correlation for ECE Rank No. 6 coal.

Figure 2 shows a graph of $\log_e M$ for each suite of specimens versus the ECE coal rank number, R. This yields a correlation given by

$$\log_e M = 5.38 - 0.4\,R, \qquad (1)$$

with a correlation coefficient of r = 0.87. It was shown that there is a 95% level of confidence that this assumed regression model is appropriate. Figure 3 shows a graph of this equation (as the solid line) together with the group M values.

Equation 1 can also be expressed as:

$$M = e^{5.38 - 0.4\,R}. \qquad (2)$$

Hence, taking into account both specimen size and coal rank, a linear correlation should exist for all data given by:

$$\frac{(\sigma_1 - \sigma_3)^2}{s\,\sigma_{pi}^2} = a + b\left\{\frac{\sigma_3}{\sigma_{pi}}\right\} e^{5.38 - 0.4R}. \qquad (3)$$

Figure 4 shows this correlation for all the data points from all the sources for all the coal ranks. The resulting equation is given by:

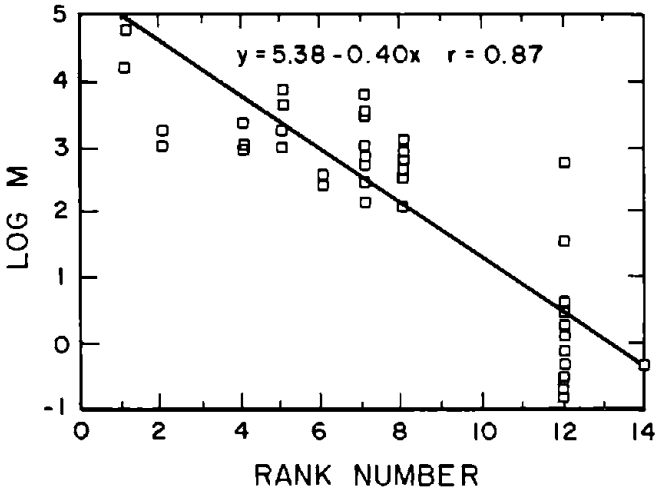

Figure 2.—$\text{Log}_e M$ versus ECE rank number.

$$\frac{(\sigma_1 - \sigma_3)^2}{s\,\sigma_{pi}^2} = 1.43 + 0.738\left\{\frac{\sigma_3}{\sigma_{pi}}\right\} e^{5.38 - 0.4R}, \qquad (4)$$

with a correlation coefficient of r = 0.93. This correlation is surprisingly good considering the large range of data sources, test methods, etc., from which the data were gathered.

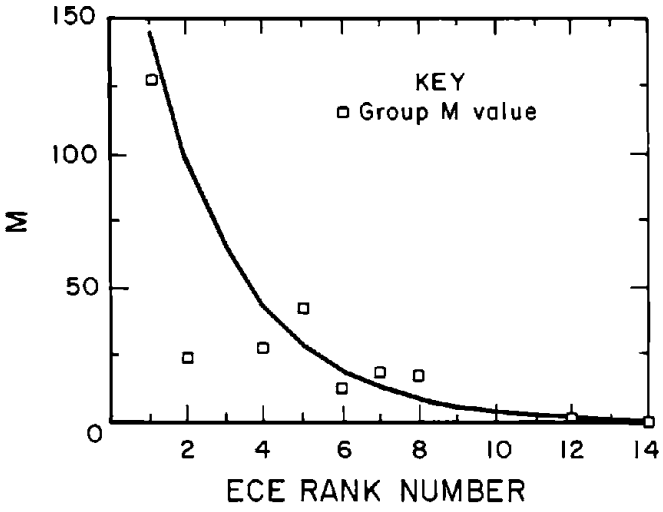

Figure 3.—Correlation of M with ECE rank number.

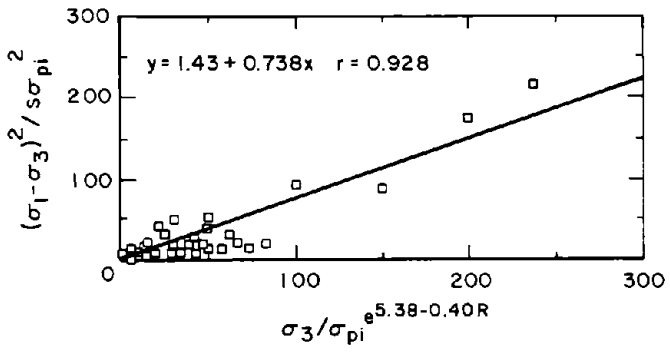

Figure 4.—$(\sigma_1 - \sigma_3)^2 / s\sigma_{pi}^2$ versus $(\sigma_3/\sigma_{pi})\, e^{5.38-0.40R}$.

DISCUSSION AND CONCLUSIONS

Despite the fact that the expressions developed in part 2 of this paper do not totally eliminate the size effects from the data analysis, there would nonetheless appear to be a significant correlation between the intact M values and the coal rank.

It had originally been hoped to attempt a similar correlation with the moisture content of the coal. However, the moisture content was not reported in any of the data sources and this was not possible. Intuitively, it is believed that the intact M values are probably influenced by moisture content, and if this had been recorded then, perhaps, some of the variation in the data might have been able to be eliminated. This remains an area for further study.

It is unfortunate that many authors do not report their specimen sizes, the coal rank, or the moisture content. It is recommended that, in future, these parameters should be recorded for all laboratory tests on the triaxial coal strength. In addition, such tests should include the determination of the residual coal strength so that the brittle/ductile transition point can be estimated. This would require that the laboratory tests be carried out up to confining pressures higher than has been the general practice to date. It is suggested that confining pressures up to about 70 MPa should be used.

Conceptually, from the work reported in this paper, it is possible to estimate the intact M values, the m and s values for specimens of known dimensions, and the coal mass m and s values, given only the coal rank and the uniaxial compressive strength. (This is analogous to the Hoek/Brown approach (*9*) to the estimation of rock mass properties from the intact rock strength and a rock mass rating.) However, it would indeed be an optimist who regarded the correlations given in this paper as defining these parameters with any great degree of accuracy. Nonetheless, it is believed that this approach has been shown to be very promising and, as the data bank is increased by future testing, it will be possible to refine and improve the expressions and correlations so that better estimates of the coal mass strength under triaxial conditions can be made. In the authors' opinion, such coal mass strength properties must be better defined if full advantage is to be taken of the current numerical techniques for assessing the stability of excavations in coal.

REFERENCES

1. Hobbs, D. W. The Stress and Strain Characteristics of Coal in Triaxial Compression. J., Geol., v. 72, 1964, pp. 214-231.

2. Murrell, S. F. The Strength of Coal Under Triaxial Compression. Mechanical Properties of Non-Metallic Materials, Butterworths, London, 1958, pp. 123-145.

3. Atkinson, R. H., and H. Ko. Strength Characteristics of U.S. Coals. Paper in Proceedings, 18th Symposium on Rock Mechanics, Kestone, CO, pp. 2B3-1 to 2B3-6, 1977.

4. Pomeroy, C. D., D. W. Hobbs, and A. Mahmoud. The Effect of Weakness Plane Orientation on the Fracture of Barnsley Hards by Triaxial Compression. Int. J., Rock Mech. Min. Sci., v. 8, 1971, pp. 227-238.

5. Barron, K. An Analytical Approach to the Design of Coal Pillars. Part 3: Coal Testing and Size Effects, D.S.S. contract report 24ST-23440-3-9234 (for Energy, Mines and Resources, Canada), June 1985.

6. Yang, T. Influence of Specimen Size and Shape on the Strength of Coal. M. Sc. Thesis, Univ. of Alberta, 1991.

7. Thompson, T. W., J. J. Menzies, and K. E. Gray. The Engineering Properties of Texas Lignite and Associated Rocks in Relation to the Stability of an In Situ Gassification Chamber. In-Situ, v. 1, 1977, pp. 171-190.

8. Williamson, I. A. Coal Mining Geology. Oxford Univ. Press, London, 1967, pp. 236-256. .

9. Hoek, E., and E. T. Brown. Empirical Strength Criteria for Rock, Masses. J., Geotech. Eng. Div., A.S.C.E., 1980, pp. 1013-1035.

APPENDIX A.—ANALYSIS OF COAL FRACTURE DATA WITH RANK

Coal rank ECE No.	Name/location	Ref	σ_{pi} MPa	s	M	r	Group M	Group r
1	Pentremahr, bedding parallel, cleats parallel	1	20.1	0.17	123.2	0.97	127.0	0.98
1	Pentremahr, bedding perp., cleats parallel	1	65.3	.17	67.4	.99		
2	Deep Duffryn, bedding parallel, cleats parallel	1	40.6	.17	26.3	.99	24.2	.976
2	Deep Duffryn, bedding perp., cleats parallel	1	46.6	.17	20.9	.99		
4	Oakdale, bedding parallel, cleats parallel	1	21.8	.17	21.3	.98	27.6	.94
4	Oakdale, bedding perp., cleats parallel	1	31.1	.17	30.3	.95		
4	Oakdale, bedding parallel, cleats perp.	1	32.1	.17	20.3	.95		
5	Cwmtillery, bedding parallel, cleats parallel	1	39.5	.17	39.5	.99	43.0	.94
5	Cwmtillery, bedding perp., cleats parallel	1	60.8	.17	21.8	.99		
5	Cwmtillery, bedding parallel, cleats parallel	2	27.3	.17	50.7	.99		
5	Cwmtillery, bedding perp., cleats parallel	2	59.3	.17	26.9	.98		
5	Cwmtillery, bedding parallel, cleats perp.	2	48.0	.17	27.1	.98		
6	Markham, bedding parallel, cleats parallel	1	100.5	.17	11.8	.96	13.3	.96
6	Markham, bedding perp., cleats parallel	1	83.9	.17	14.2	.97		
7	Blind Canyon seam, Beehive mine	3	70.3	.095	34.3	.66	19.1	.79
7	Pittsburgh seam, Federal No. 2 Mine	3	78.0	.095	36.3	.60		
7	Pittsburgh seam, Bruceton Experimental Mine	3	102.8	.095	34.3	.65		
7	York Canyon bed, York Canyon No. 1. Mine	3	44.8	.095	48.3	.53		
7	Barnsley Top Hards, bedding parallel, cleats parallel	1	92.9	.17	18.4	.97		
7	Barnsley Top Hards, bedding perp., cleats perp.	1	145.5	.17	9.13	.91		
7	Barnsley Top Hards, bedding parallel, cleats parallel	2	85.6	.17	20.0	.92		
7	Barnsley Top Hards, bedding perp., cleats parallel	2	128.4	.17	12.4	.93		
7	Barnsley Top Hards, bedding parallel, cleats perp.	2	101.9	.17	20.6	.99		
7	Barnsley Top Hards, bedding parallel, cleats perp.	4	68.4	.17	20.3	.98		
7	Barnsley Top Hards, bedding 15 degrees, cleats 75 degrees	4	43.7	.17	35.1	.99		
7	Barnsley Top Hards, bedding 30 degrees, cleats 60 degrees	4	26.0	.17	16.9	.98		
7	Barnsley Top Hards, bedding 45 degrees, cleats 45 degrees	4	53.5	.17	19.3	.98		

Coal Rank ECE No.	Name/location	Ref	σ_{pi} MPa	s	M	r	Group M	Group r
7	Barnsley Top Hards, bedding 60 degrees, cleats 30 degrees	4	76.2	0.17	18.6	0.99		
7	Barnsley Top Hards, bedding 75 degrees, cleats 15 degrees	4	127.4	.17	12.6	.93		
7	Barnsley Top Hards, bedding perp., cleats parallel	4	116.5	.17	22.4	.99		
8	Barnsley Brights, bedding parallel, cleats parallel	1	100.6	.17	14.7	.98	18.4	0.96
8	Barnsley Brights, bedding perp., cleats parallel	1	96.3	.17	15.6	.98		
8	Dunsil Seam, Teversal bedding parallel, cleats parallel	1	80.6	.17	23.8	.99		
8	Dunsil Seam, Teversal bedding perp., cleats parallel	1	76.3	.17	19.9	.98		
8	High Main Seam, Linby bedding parallel, cleats parallel	1	65.5	.17	16.0	.97		
8	High Main Seam, Linby bedding perp., cleats parallel	1	105.3	.17	18.5	.98		
8	Dietz No. 1, Decker Coal Co., bedding perp.	3	53.0	.191	8.86	.72		
12	Highvale Mine, Alberta, bedding perp.	5	47.1	.097	18.0	.79	1.66	.30
12	Whitewood Mine, Alberta, bedding perp.	6	78.4	.097	.52	.99		
12	Whitewood Mine, Alberta, bedding perp.	6	114.3	.097	.61	.90		
12	Highvale Mine, Alberta, bedding perp.	5	60.5	.101	5.3	.82		
12	Whitewood Mine, Alberta, bedding perp.	6	58.4	.129	.57	.94		
12	Whitewood Mine, Alberta, bedding perp.	6	49.1	.129	1.02	.98		
12	Whitewood Mine, Alberta, bedding perp.	6	86.1	.129	.66	.82		
12	Whitewood Mine, Alberta, bedding perp.	6	36.2	.129	.72	.98		
12	Whitewood Mine, Alberta, bedding perp.	6	92.5	.155	1.31	.88		
12	Whitewood Mine, Alberta, bedding perp.	6	51.3	.155	2.09	.77		
12	Whitewood Mine, Alberta, bedding perp.	6	70.4	.155	1.63	.82		
12	Whitewood Mine, Alberta, bedding perp.	6	33.9	.181	1.79	.96		
12	Whitewood Mine, Alberta, bedding perp.	6	59.0	.181	1.41	.99		
12	Whitewood Mine, Alberta, bedding perp.	6	80.2	.181	.83	.96		
12	Whitewood Mine, Alberta, bedding perp.	6	78.7	.181	.99	.98		
12	Whitewood Mine, Alberta, bedding perp.	6	58.6	.181	.99	.98		
12	Whitewood Mine, Alberta, bedding perp.	6	37.1	.181	.68	.91		
12	Highvale Mine, Alberta, bedding perp.	5	46.4	.276	1.56	.72		
14	Texas Lignite	7	28.8	.109	.82	.61	.82	.61

STUDY OF PILLAR BEHAVIOR IN THE PARKGATE SEAM AT ASFORDBY COLLIERY

By J. W. Cassie[1] and K. W. Mills[2]

INTRODUCTION

The Parkgate Seam at Asfordby Mine is currently being developed by driving a network of in-seam ladder roadways to provide access to future longwall panels. Correct dimensioning of the intermediate pillars is important to ensure the long-term stability of these drivages. Barrier pillars must also be sufficient to provide protection against the additional loading imposed by future longwall operations.

Previous work on the design of pillars in mines operated by British Coal has generally been based on the methods developed by Wilson (*1*).[3] As a result of the progress being made in computational modeling and underground monitoring techniques, a more sophisticated approach is now becoming feasible. More detailed characterization of material behavior is now possible, and this level of detail can be incorporated into the computational model to accurately reflect real material behavior.

The increase in modeling detail is matched by an improvement in underground monitoring capability. For instance, the feasibility of measuring stress levels within pillars allows verification of pillar behavior that was not previously possible.

The approach to pillar design described in this paper is described in detail by Gale (*2*). In general, the approach involves:

1. Observation of underground pillar behavior, including measurement of rib stress and displacement profiles.
2. Detailed measurement of rock properties, including the properties of horizontal bedding plane contacts.
3. Computational modeling using these properties to provide insight into the mechanisms that characterize pillar behavior.
4. Development of site-specific pillar design guidelines based on the behavior indicated by computational modeling. Ongoing monitoring to provide confirmation and further refinement as more data become available.

Pillar design requires that estimates be made of pillar strength, stress-strain behavior, and loads that will be imposed during various stages of extraction. Work described in this paper concentrates primarily on modeling pillar behavior. Work to determine pillar loading characteristics is ongoing.

ACKNOWLEDGMENTS

The authors would like to acknowledge the contribution of several colleagues to the work described here. In particular, thanks are due to the team who carried out the difficult task of obtaining the stress measurement results.

The first-named author wishes to thank Mr. A. J. Wardle for his permission to publish this paper. The views expressed are those of the author and not necessarily British Coal.

SITE DESCRIPTION

GEOLOGICAL SECTION

A generalized geological section of the strata about the Parkgate Seam is shown in figure 1. The Parkgate Seam is approximately 3 m thick and lies at a depth of 500-600 m.

Immediately above the coal is a 0.8-m-thick weak mudstone, referred to locally as "clod," that is highly sheared with many listric surfaces. This is overlain by a sequence of muddy siltstones that extend almost to the next seam. At approximately 5 m above the seam, there is a stiff sandstone band that is 0.3-0.5 m thick. The coal is

[1]Engineer, British Coal, Burton-on-Trent, United Kingdom.
[2]Senior geotechnical engineer, Strata Control Technology, Wollongong, Australia.
[3]Italic numbers in parentheses refer to items in the list of references at the end of this paper.

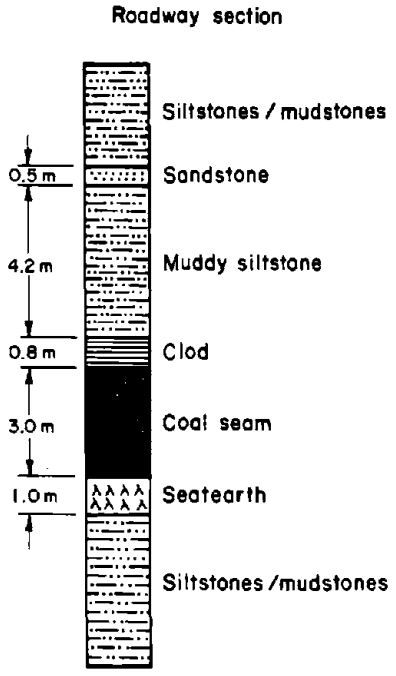

Figure 1.—Geological section.

underlain by 1 m of mudstone "seatearth" below which are further muddy siltstones.

PILLAR MONITORING SITE

A plan of workings in the Parkgate Seam at Asfordby Mine is shown in figure 2. Ladder headings are currently being developed with 30-m-wide pillars separating each pair of roadways. Roadways are being developed using primary roof bolt support and are rectangular in profile. The current mining horizon works to a parting above the clod and leaves a coal floor.

Observation of roadway behavior indicates that the rib and floor yield extensively with significant amounts of both rib displacement and floor heave. A 200-mm step at the contact between the clod and siltstone, with the clod extending beyond the siltstone, indicates significant slip across this interface.

At the first pillar monitoring site, pillar width was reduced to 20 m to investigate the possibility of obtaining improved conditions in a second driven roadway as a result of horizontal stress relief from the first driven roadway. Conditions in both roadways deteriorated with increased rib movement and floor heave observed.

The Deep Main Seam lies 20-25 m above the Parkgate Seam and is also being developed. Because no panels have yet been extracted, the Deep Main workings are not considered to influence pillar or roadway behavior in the Parkgate Seam.

UNDERGROUND MONITORING

Underground measurements were made at the two pillar sites shown in figure 2. The pillar at the first site was 20 m wide. A vertical stress profile and horizontal displacements were measured at this site. At the second site, the pillar was 30 m wide and only the vertical stress profile was measured.

Horizontal displacements were measured right across the 20-m pillar as it was formed. A 20-m-long extensometer was installed as close as practical to the face of the first driven roadway and ahead of the second driven roadway. The displacements that occurred as the pillar was formed are shown in figure 3.

Measurable displacements extend into the center of the pillar. There is a slight asymmetry, greatest nearest the ribsides, with displacements lower adjacent to the ribside of the first driven roadway. It is considered that this asymmetry is caused primarily by displacements that occurred prior to installation of the extensometer and were therefore missed.

Vertical stress profiles across the pillars were measured by overcoring hollow inclusion stress cells at various distances from the ribside. The instruments were installed in a stiff sandstone band in the roof strata to facilitate core recovery. Four successful measurements were made at each site.

The vertical stress components measured are plotted against distance from the pillar edge in figure 4. The vertical stress profile measured in the 30-m pillar is essentially the same as that measured in the 20-m pillar.

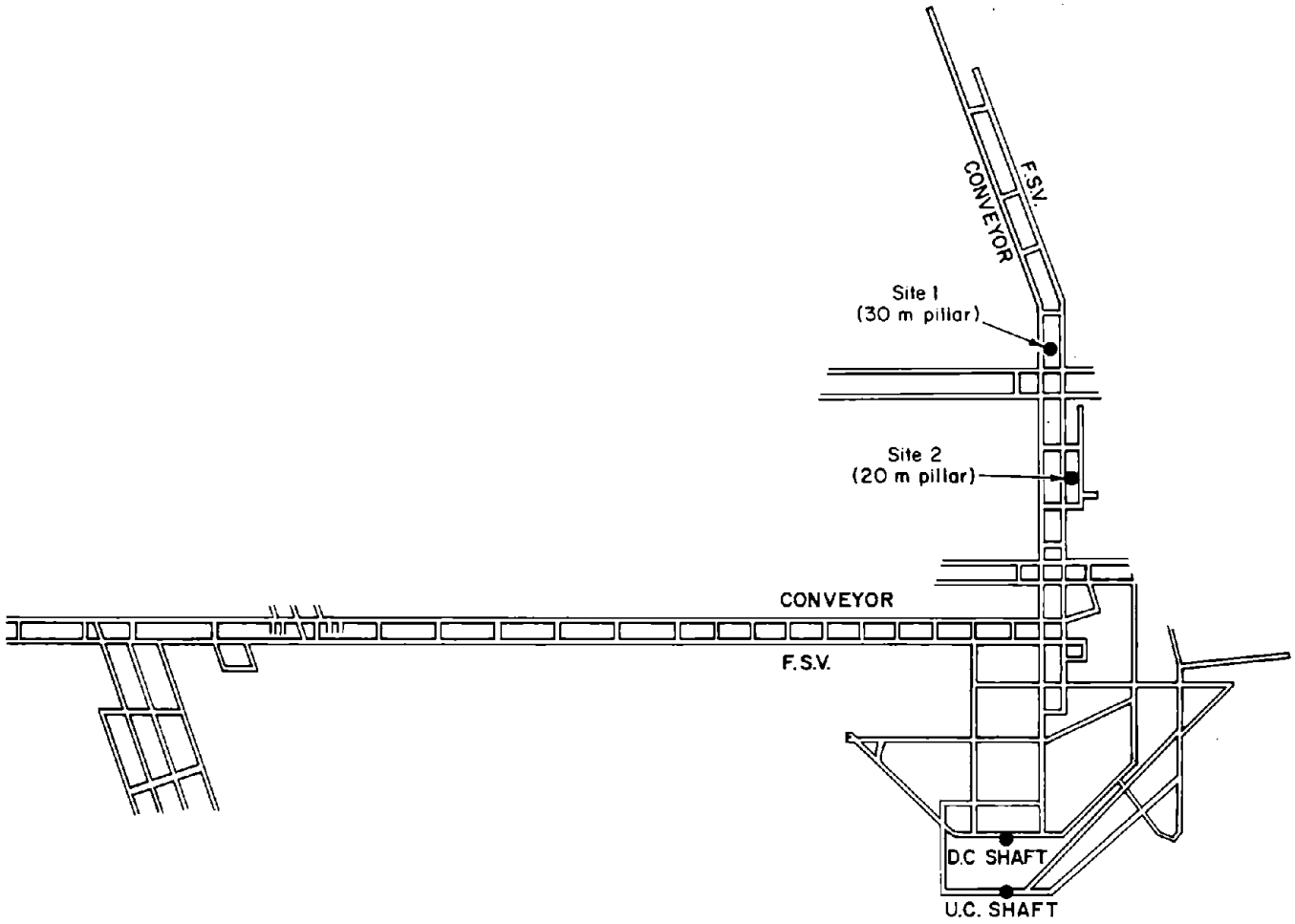

Figure 2.—Plan of workings.

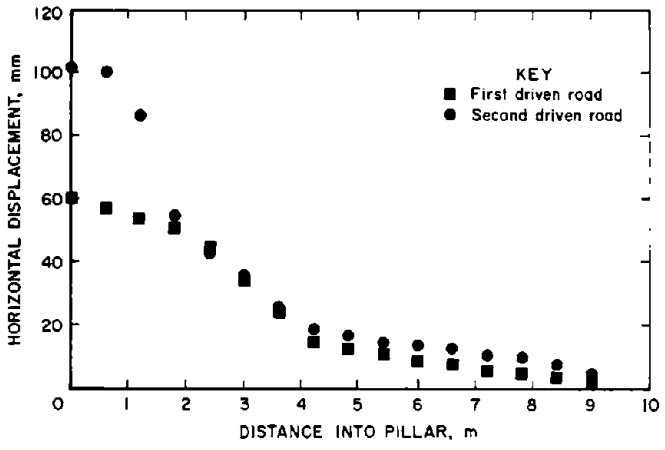

Figure 3.—Measured rib displacements in 20-m pillar.

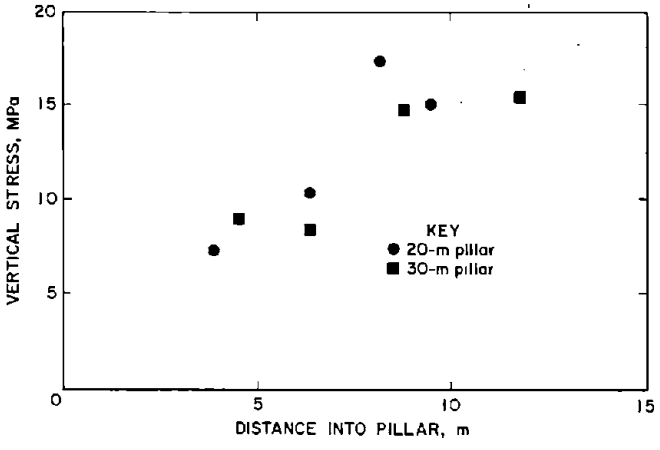

Figure 4.—Measured vertical stresses.

MATERIAL PROPERTIES

The elastic mechanical properties of each of the strata units were determined by unconfined compression testing with measurement of elastic modulus and Poisson's ratio. The intact and residual confined strength properties were determined by single-stage and multistage triaxial testing. The properties of the horizontal bedding contacts were measured in multistage shear tests. These results were supplemented by test results available from other collieries mining the same seam.

The confined triaxial strengths for Parkgate Seam coal are shown in figure 5. Triaxial strength increases with confining pressure as expected. At low-confining pressures, the rate of increase in strength is high and this rate decreases with further confinement. As a result, the failure envelope is nonlinear.

The residual strength properties of the coal have been determined by triaxial tests on granulated material. The residual failure envelope is similar in shape to the intact failure envelope, but of lower strength.

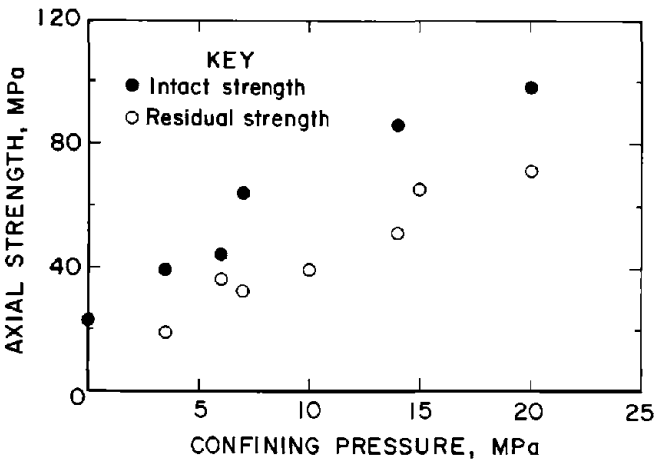

Figure 5.—Triaxial test results for coal.

COMPUTATIONAL MODELING

The deformational characteristics of pillars of several widths were studied using computational models that allowed them to be loaded from zero to failure. Sensitivity to key material properties was also studied. Once these characteristics were understood, another model was used to simulate formation of a pillar in rock that was subjected to measured in situ stress levels to confirm the observed pillar behavior.

MODELING DETAILS

Pillar behavior was modeled using an explicit finite difference solution scheme that effectively follows material deformations and stresses through time by solving the equations of motion at each step. The major benefits of this scheme are that equilibrium is not a prerequisite for solution and complex material behavior, such as nonlinear and postfailure behavior, can be modeled with relative ease.

The overall structure of the model is shown in figure 6. Each pillar was modeled with the center line of the roadway and the center line of the pillar taken to be vertical axes of symmetry. The model extended approximately 10 m above and below the roadway.

The stratigraphy observed at the pillar sites was represented in the model. Bedding plane contacts were also included at the boundaries between materials and at several horizons in the siltstone.

Pillar loading was applied in stages. Each stage involved moving the top and bottom boundaries of the model together by a small amount and then allowing the model to reach equilibrium. Because the roadway was excavated

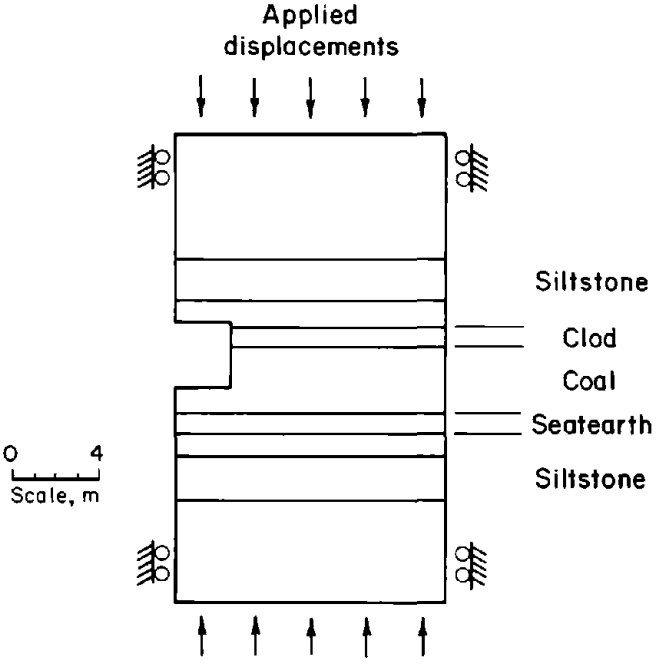

Figure 6.—Structure of model.

before loading began, this convergence of the top and bottom boundaries had the effect of increasing the vertical load carried by the pillar.

The materials in and around the pillar were modeled as following a nonlinear failure criterion that reduced to a lower residual strength after failure. Both intact and residual failure envelopes were represented as having a decreasing friction angle with increasing confining pressure to approximate the curvature of the strength envelopes measured in laboratory tests.

The intact strength of rock at low-confining pressures was reduced in the model from that measured in laboratory tests to account for the effect of specimen size on unconfined strength reported by Bieniawski (*3*) and others.

RESULTS OF MODELING

Figure 7 shows the pillar deformation mechanism indicated by modeling. The clod, seatearth, and weak interfaces yield at an early stage of loading with yield in the coal developing later and progressing toward the pillar center more slowly. The largest movements occur along the interfaces above the clod and below the seatearth allowing the rib and floor to extrude into the roadway. This is also observed at the pillar sites.

The mechanisms controlling behavior are essentially similar to those proposed by Wilson (*1*). A zone of yielded rock forms at the pillar edge. Within this zone, horizontal confinement is generated. This confinement increases the strength of the remaining intact core.

In the geological environment that was modeled, low-strength materials and bedding plane contacts above and below the coal seam limit the rate at which horizontal confinement can be generated to less than that which could be generated by the coal alone. Analysis of the sensitivity of pillar behavior to material property variations confirms this.

The load deformation characteristics of pillars of various widths ranging 15 to 40 m have been determined. These are shown in figure 8. A 15-m-wide pillar shows a strength reduction after reaching peak load. The 20-m pillar maintains its peak load as it continues to deform. The larger pillars continue to increase in strength over the range of deformations modeled.

Theoretically, these large pillars would also reach a strength plateau if loading continued. Practically, however, closure of adjacent roadways would at some point prevent further failure and the pillars would continue to gain strength.

COMPARISON WITH FIELD MEASUREMENTS

The results of the modeling presented in this section are taken from the load stage that corresponds to the loading conditions measured underground to allow comparison of measured and modeled results. Because of the similarity between the stress profiles measured in the 20- and 30-m-wide pillars, the vertical stress measurements have been combined for comparison purposes.

The modeled vertical stress profile are plotted together with the values measured at each site in figure 9. The vertical stress profile indicated by the model closely approximates the values measured. This indicates that the vertical

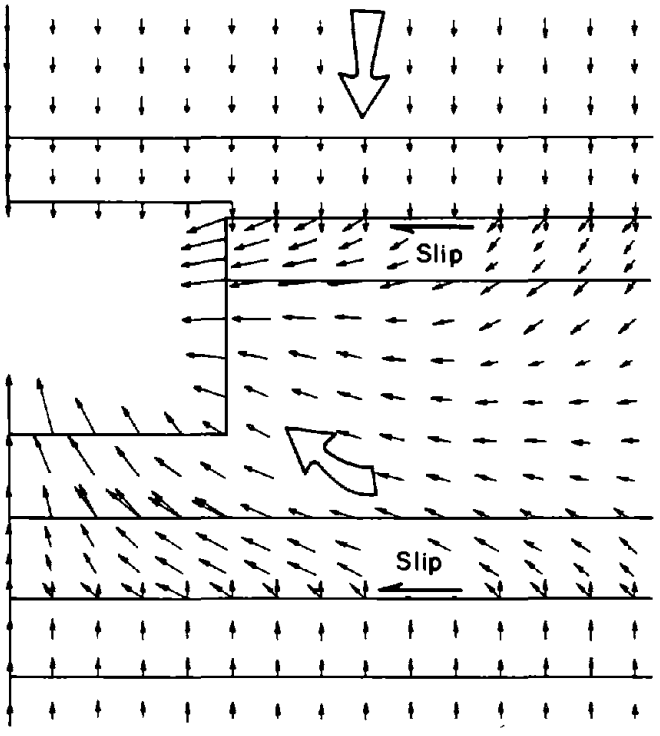

Figure 7.—Pillar deformation mechanism.

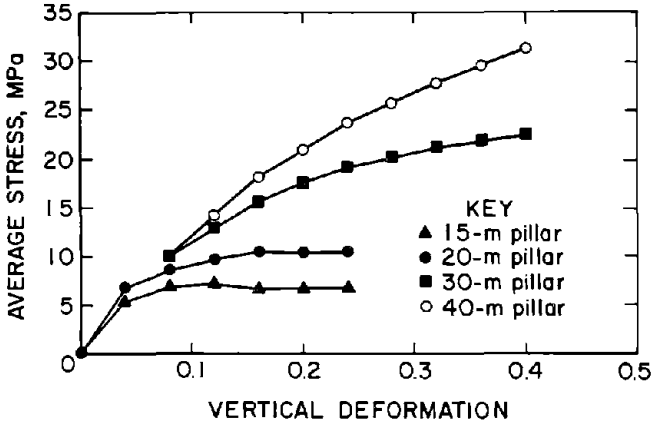

Figure 8.—Load deformation characteristics of pillars.

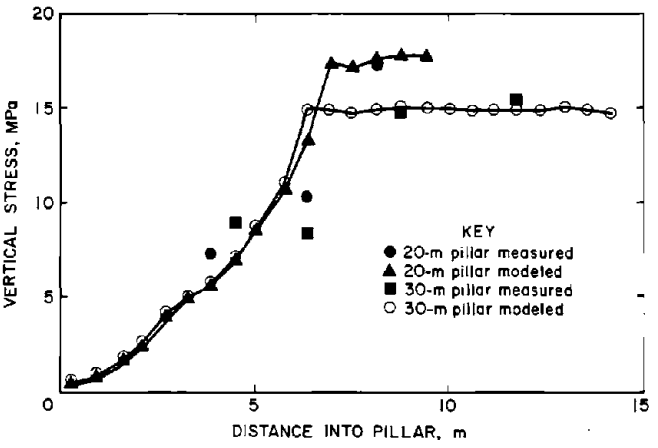

Figure 9.—Measured and modeled vertical stress profiles.

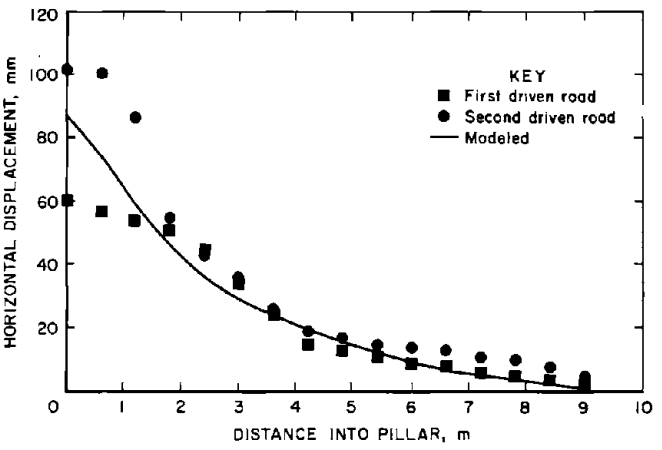

Figure 10.—Measured and modeled rib displacements.

stresses increase relatively slowly with distance from the ribside and that yield extends 6-7 m into the pillar.

The model profile can also be matched using the equations developed by Wilson (*1*) for yielding roof and floor strata. The parameters required to achieve this fit fall within the range that would normally be considered realistic under these geological conditions.

Horizontal displacements measured across the 20-m pillar are compared with the model in figure 10. The two are consistent in the center of the pillar, but the model underestimates displacements near the ribsides. This is considered to be a consequence of dilatancy not being modeled.

APPLICATION TO PILLAR DESIGN

Computational modeling provides an understanding of the mechanisms involved in pillar behavior which confirmed by field measurement. It also provides an indication of the likely stress-strain characteristics of pillars of various sizes.

The modeling indicates that the vertical stress profile over the yielded ribside is highly dependent on material properties, but independent of pillar width. In effect, it is characteristic of the geological setting, but not of pillar geometry.

For the particular geological setting at Asfordby Mine and the horizon being mined, pillars can be designed using this vertical stress profile and an understanding of their stress-strain characteristics.

The condition of pillars at the test sites is assessed using this approach. Cover depth is approximately 500 m giving an estimated cover load of 12.5 MPa. The imposed loads are estimated on the basis of tributary area assuming 5-m-wide roadways.

The modeled stress-strain characteristics of 20- and 30-m pillars indicate that the ultimate strength of both occurs when the coal has yielded across its entire width.

For the 20- by 60-m pillar at site 1, the vertical stress profile indicates an ultimate load of 10 MPa. Tributary area load is estimated to be 17 MPa, which indicates that a significant portion of the cover load has to be carried elsewhere.

Measurements and modeling show that the average pillar stress is close to ultimate and that the cover load has been redistributed.

The ultimate load of the 30- by 60-m pillar at site 2 is estimated to be 19 MPa. Tributary area load is estimated to be 16 MPa, which indicates that the pillar is able to carry all the tributary area load if it were required to do

so. Measurements indicate that the average pillar stress is approximately 12 MPa so that some of the tributary load has been redistributed anyway. This is thought to be a result of pillar deformation.

In the above calculation, pillar load has been compared with ultimate pillar strength without regard for the condition of adjacent roadways. The modeling provides an indication of roadway condition by estimating the amount of rib displacement that could be expected for any given pillar load. Rib displacement indicated by modeling for different width pillars is shown in figure 11. Although larger pillars are able to carry more load, they can only do so at the expense of increased rib displacement.

It is thought that, although the model would underestimate rib displacements because dilatancy effects have not been included, the indicated trends would be representative. Using this approach, pillars could be designed on the basis of roadway condition instead of simply ultimate load considerations. Monitoring and more detailed modeling is continuing to further refine these guidelines.

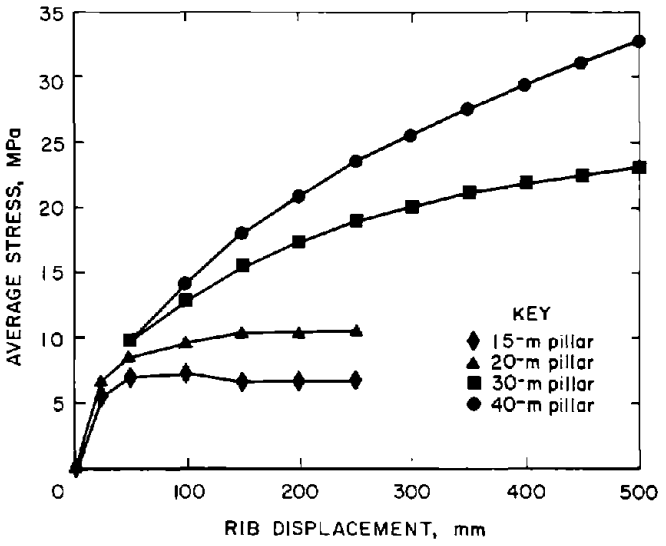

Figure 11.—Average stress versus rib displacements.

CONCLUSIONS

1. The approach described has been successfully used to provide initial characterization of the behavior of coal pillars at Asfordby Mine.

2. Properties of rock, coal, and bedding contacts measured in laboratory tests on material recovered from the site provided a model of pillar behavior consistent with that observed in the field.

3. In the geological environment that was modeled, low-strength materials and bedding plane contacts above and below the coal seam significantly influence pillar strength and deformational characteristics.

4. Computational modeling provided insight into the stress-strain characteristics and mechanisms controlling the behavior of different sized pillars, allowing detailed site-specific design guidelines to be developed.

REFERENCES

1. Wilson, A. H. The Stability of Underground Workings in the Soft Rock of the Coal Measures. Int. J. Min. Eng., v. 1, 1983, pp. 91-187.

2. Gale, W. A Pillar Design Approach. Paper in these Proceedings.

3. Bieniawski Z. T. An Analysis of Underground Tests Aimed at Determining the In Situ Strength of Coal Pillars. CSIR Report MEG 569, Pretoria, Republic of South Africa, 1967.

DESIGN OF PARTIAL EXTRACTION COAL MINE LAYOUTS FOR WEAK FLOOR STRATA CONDITIONS

By Yoginder P. Chugh[1] and Witold M. Pytel[2]

INTRODUCTION

Partial extraction mining systems such as room-and-pillar mining with or without pillar recovery currently account for about 70 pct of underground coal production in the United States. These systems will continue to play a dominant role in the United States in areas involving shallow mining depths, prime agricultural lands, prime ground water resources, and high-population density. Effective design of partial extraction mine layouts must consider in-mine stability of mine workings as well as their remote effects, such as surface and subsurface subsidence and ground water alterations.

The design practice until the mid-1970's for partial extraction mining systems typically involved design of coal pillars based on coal strength only and, in some cases, mine opening spans (opening width and intersection size). The coal seam floor characteristics and interaction between roof, pillar, and floor elements were generally not considered in analyzing stability of mine workings. Furthermore, remote effects of partial extraction were rarely considered since it was assumed that such effects were negligible. Several in-mine studies of roof-pillar-floor interaction in room-and-pillar mining layouts in Illinois Basin coal mines [Chandrashekhar, 1990 (*6*); Chugh, 1988, 1991 (*10, 14*)][3] and associated surface subsidence effects have indicated the need for more in-depth and scientific design of partial extraction mining systems. These studies were undertaken since actively mined coal seams in the Illinois coal basin are generally associated with relatively thick (3 to 8 ft, or 0.9 to 2.4 m) and weak (300 to 700 psi, or 2.07 to 4.83 MPa of UBC) floor strata that seem to govern the design of mine layouts down to a mining depth of about 450 ft (≈137 m). Slow settlement of coal pillars on weak floor strata generally lead to time-dependent surface subsidence at rates varying from 0.5 to 1.0 in/y_r (1.3 to 2.5 cm/y_r) [Chugh, 1991 (*14*)]. Inadequate pillar designs result in pillar sloughing, floor heave, roof falls underground, and localized and/or trough subsidence movements on the surface.

Over the past 5 years, the authors have been engaged in extensive research related to design of partial extraction mine layouts for weak floor strata conditions. This paper presents the theoretical background for design approaches which were developed, their application for mine design, and the validation of the developed approaches. The main goal of the analysis is to design mine layouts that would maximize coal recovery in different sections of the panel while maintaining pillar, floor, and roof stability. Overriding considerations may include factors such as equipment size, panel geometry, etc.

In the authors' opinion, the design problem requires calculation of stable opening widths, including intersections and size of coal pillars to ensure stability against foundation failure and/or limiting pillar settlements. The relative importance of the possible failure modes may also vary over the panel geometry. Thus, theoretically the pillar and opening sizes may be varied in different areas of the panel to maximize extraction ratio with optimum structure stability and associated surface effects. A design procedure should consider: (1) bearing capacity of coal pillars (pillar strength), (2) bearing capacity of immediate floor strata, (3) differential settlement of adjacent pillars based on strength of roof strata, (4) absolute pillar settlement based on floor heave in mine openings, (5) roof-pillar-floor interaction, and (6) surface subsidence characteristics such as strains, tilt, settlement particularly where sensitive surface structures are located. Item 1 above has been researched to a large degree and will not be discussed within this paper. The authors have been developing items (2) to (6) above for the past 5 years. Discussion of items (2) to (5) will be presented in the following sections.

[1]Professor.

[2]Senior scientist.

Department of Mining Engineering, Southern Illinois University at Carbondale, Carbondale, IL.

[3]Italic numbers refer to items in the list of references at the end of this paper.

ACKNOWLEDGMENTS

The authors sincerely acknowledge the financial support of the Illinois Mine Subsidence Research Program funded by the Illinois Department of Energy and Natural Resources, the U.S. Bureau of Mines, the Mine Systems Design and Ground Control Generic Center at Virginia Polytechnic Institute and State University, and several coal companies in the Illinois coal basin. Without the active support of the Illinois basin coal industry, this research would not have been possible.

DESIGN OF COAL PILLARS FOR WEAK FLOOR STRATA CONDITIONS: CURRENT PRACTICE

Design of coal pillars for weak floor strata conditions in the United States is presently based on ultimate bearing capacity (UBC) of weak floor strata without a consideration of pillar settlement. Current design techniques typically estimate UBC underneath full-size pillars using the Vesic [1970 (*45*)] analysis, which considers weak floor strata as a two-layer nonhomogenous cohesive soil or rock system with a weak layer overlying the stiffer layer, and an angle of internal friction, which is equal to zero for both layers. The cohesion c of the weak layer may be estimated from its moisture content [Speck, 1981 (*39*)] rather than from laboratory compressive strength data. This technique (Vesic-Speck approach) is most commonly used for mining applications today. The validity of this analysis technique has never been checked for shallow foundations on layered rock strata involving weak layer(s) overlying a competent rock layer. Furthermore, the effect of adjacent pillars on estimate UBC of a single pillar has never been considered in the analysis. Furthermore, foundation failure of coal pillars is most likely to occur during pillar extraction in room-and-pillar mining or for chain pillars in longwall mining. In a partial extraction room-and-pillar mining system, pillar settlements on weak floor strata may result in changed geometry of the mine roadways, in failure of roof, coal pillar, and/or floor strata, and in surface and subsurface movements. It is therefore important that pillar design techniques for weak floor strata conditions consider the UBC as well as the deformability of weak floor strata.

PROBLEM DEFINITION

U.S. coal seams may be associated with weak floor strata whose thickness typically ranges from 0.5 to 8 ft (0.15 to 2.4 m). These weak strata are underlain by relatively competent beds, which may have an order of magnitude of higher strength and lower deformability as compared with the weak floor strata. The coal seam is generally overlain by relatively stiff layers varying in thickness from 1 to 6 ft (0.3 to 1.8 m), which may cause significant interaction between roof, pillar, and floor strata where weak floor conditions exist.

The design problem requires calculation of stable opening widths including intersections and size of coal pillars to ensure stability against foundation failure and/or limiting pillar settlements. Prior to mine development, data available for design typically include lithologic cross sections from boreholes and strength-deformation geotechnical data on rock cores obtained during exploration. After mine development, plate load tests may be conducted in entries to obtain UBC and deformability of immediate floor strata, and boreholes may be drilled in-mine to obtain variability of weak floor strata thickness and its properties. Furthermore, studies related to in-mine performance of opening and pillars may be conducted to alter the design as needed. The following elements of design must be developed in order to design a stable mining system for weak floor strata conditions:

1. Estimation of UBC and deformability underneath a square plate (6 to 12 in, or 15.2 to 30.5 cm in size) from engineering index properties and strength-deformation properties on rock cores of immediate floor strata.
2. Estimation of UBC and deformability underneath a full-size pillar from UBC and deformability values determined from small-scale plate-loading tests or estimated in item 1 above.
3. Influence of adjacent pillars on estimated UBC and deformability in item 2 above.
4. Calculation of loads acting on pillars.
5. Interaction between roof, pillar, and floor strata.
6. Definition of failure criterion for immediate roof and floor strata and coal pillar.

These design elements are developed and discussed in this paper.

ESTIMATION OF UBC AND DEFORMABILITY OF WEAK FLOOR STRATA UNDERNEATH A SMALL PLATE

Over the past 5 years, the Southern Illinois University, Department of Mining Engineering, has conducted plate-loading tests, borehole shear tests, and laboratory geotechnical studies on immediate floor strata at seven mines in Illinois [Chugh, 1988 (*8*); Chugh, 1989 (*9*)]. Based on statistical analyses, the authors (Pula, 1990 (*27*)] have developed the nonlinear regression equations below to estimate UBC and modulus of deformation at 50 pct of the UBC (DM_{50}) underneath a square test plate varying in size from 6 to 12 in (15.2 to 30.5 cm). These equations can be used with data developed during the premining exploration stage, or in lieu of plate load tests.

$$UBC = 1{,}274.1 \exp(-0.112\ MC)\ \text{(claystone), psi,}$$

$$UBC = 2{,}416.3 \exp(-0.209\ MC)\ \text{(siltstone), psi,}$$

$$UBC = 1{,}603.5 \exp(-0.145\ MC)\ \text{(weak floor strata), psi,} \quad (1)$$

$$DM_{50} = 54{,}176/(MC)^{0.60}\ \text{(claystone), psi,}$$

$$DM_{50} = 105{,}873/(MC)^{0.88}\ \text{(siltstone), psi,}$$

$$DM_{50} = 53{,}103/(MC)^{0.47}\ \text{(weak floor strata), psi,} \quad (2)$$

where MC is the average moisture content (percent) for weak floor strata down to a depth of 12 in (30.5 cm) below the coal seam. The weak floor strata category includes all types of rocks, i.e., claystone, mudstone, and siltstone.

ESTIMATION OF UBC AND DEFORMABILITY OF INFINITELY THICK WEAK FLOOR STRATA UNDERNEATH FULL-SIZE PILLAR FROM PLATE-LOADING TESTS

The UBC and DM_{50} should be determined for as large a plate size as possible to minimize plate size effect on these parameters; a minimum 8 by 8 in square plate is recommended. The maximum plate size that can be used, however, is limited by the size of the loading device and the nature of the immediate roof strata. Therefore, the relationships between plate size B, UBC, and DM_{50}) (assuming infinite thickness of immediate weak floor strata) were developed using multilinear regression analysis. The relationships for UBC, obtained for claystone, siltstone, and all weak floor strata, are as follows:

$$UBC = 1{,}018.8 - 67.29\ MC + 907.88/B\ \text{(claystone), psi,}$$

$$UBC = 1{,}509.6 - 156.34\ MC + 2{,}518.1/B\ \text{(siltstone), psi,}$$

$$UBC = 1{,}207.7 - 103.12\ MC + 1{,}678.7/B\ \text{(weak floor strata), psi,} \quad (3)$$

where UBC is the plate ultimate bearing capacity, MC (percent) is the natural moisture content, and B (inches) is the plate size. These relationships are shown in figure 1. They indicate that weak floor strata underneath a small plate is in shear phase and is being subjected to significant lateral deformations in addition to axial compression. For larger plate sizes, deformations predicted by the linear theory of elasticity may be expected.

Equation 3 was used to estimate the mean value of the reduction factor F_r (UBC) due to effect of plate size. Plots of reduction factors for claystone, siltstone, and weak floor strata for different natural moisture content are shown in figure 2 (top). For moisture content range between 5 and 8 pct and plate size ranging from 4 to 10 in (0.10 to 0.25 m), the mean value of the F_r (UBC) reduction factor ranges from 0.675 to 0.881 for claystone, 0.288 to 0.740 for siltstone, and 0.473 to 0.802 for all weak floor strata.

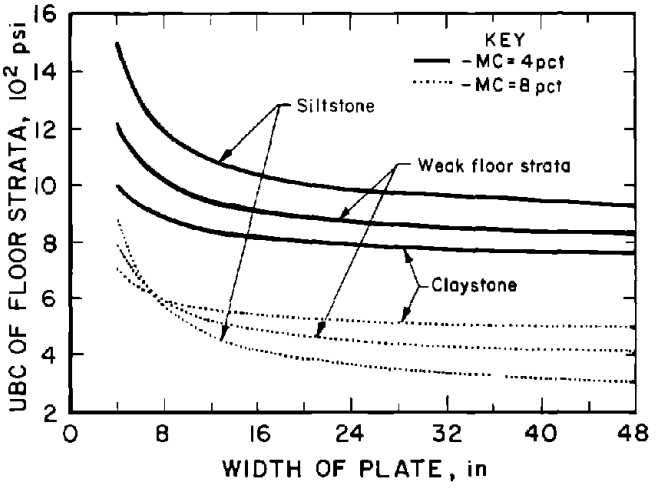

Figure 1.—Effect of plate size on UBC, and DM_{50}.

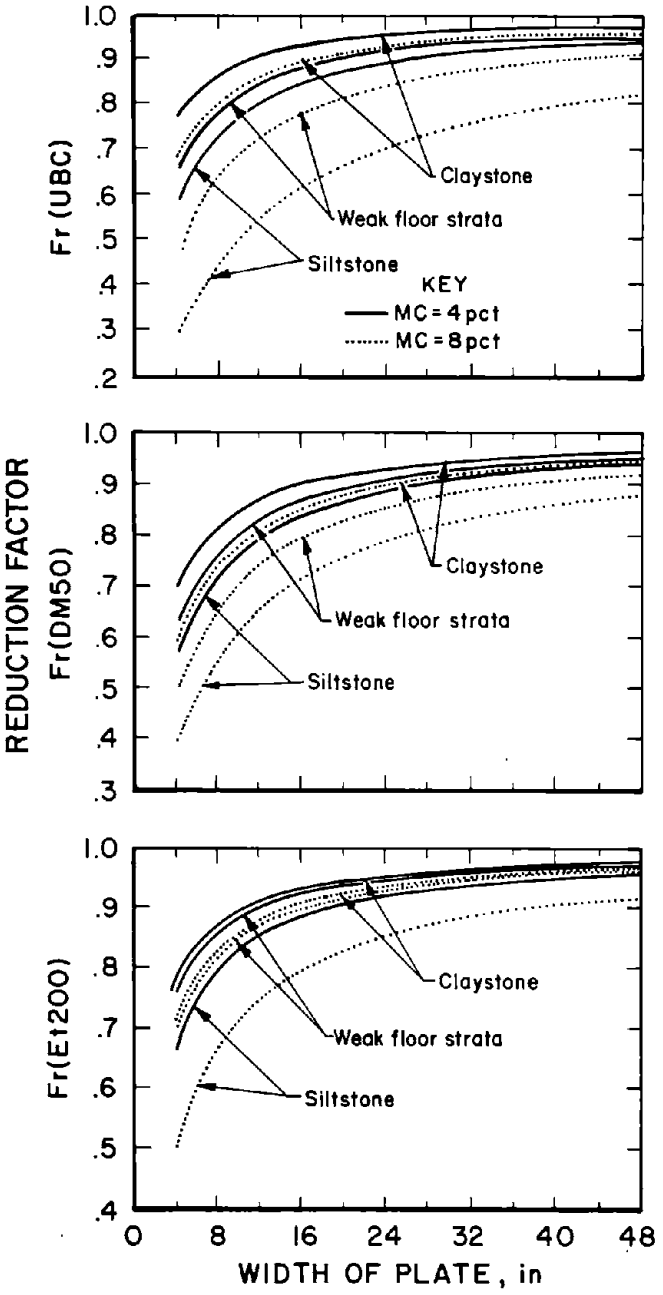

Figure 2.—Reduction factors due to plate size.

These relations are similar to Gaddy's equation for size effect on coal strength.

The above analysis approach was also used for estimation of deformability underneath a test plate and/or full-size pillars (B→∞), and the relevant equations are given below:

DM_{50} = 34,996.3 - 2,298.8 MC + 44,309.1/B (claystone), psi,

DM_{50} = 43,002.2 - 3,799.8 MC + 78,511.6/B (siltstone), psi,

DM_{50} = 35,997.1 - 2,600.4 MC + 60,582.4/B (weak floor strata), psi, (4)

Et200 = 39,028.3 - 1,840.5 MC + 38,998.8/B (claystone), psi,

Et200 = 71,124.0 - 5,895.6 MC + 95,984.0/B (siltstone), psi,

Et200 = 42,015.9 - 2,078.3 MC + 43,966.5/B (weak floor strata), psi, (5)

where DM_{50} is the tangent modulus of floor deformation (measure of deformability) at 50 pct of the plate UBC and Et200 is the secant modulus of floor deformation at 200 psi (1.38 MPa) of applied pressure. For the range of plate size between 4 and 10 in (0.10 to 0.25 m) and moisture content of 5-8 pct, the reduction factor F_r (DM_{50}) ranges from 0.596 to 0.839 for claystone, from 0.387 to 0.750 for siltstone, and from 0.497 to 0.788 for all weak floor strata, while F_r (Et200) ranges from 1.194 to 1.497 for claystone, 1.209 to 1.650 for siltstone, and 1.213 to 1.546 for all weak floor strata (see fig. 2, center and bottom). Since the regression correlations for equations 3 through 5 developed using the multi-linear regression have substantially less confidence level than for equations 1 and 2 (single, nonlinear regression), the former equations cannot replace the latter equations. Therefore, reduction factors must be introduced. These factors may be used to determine the suitable parameter X, (UBC, DM_{50}, Et200), underneath a full-size pillar of size B (inches), from the plate load test results X_{pl} (or equations 1 and 2) as shown below:

$$X = F_r (X) X_{pl}. \quad (6)$$

The size reduction factor of F_r (UBC) determined in this study corresponds to a reduction in c and ϕ due to the size as proposed by Terzaghi [1943 (*43*)]:

$$c^* = 0.67c, \ \phi^* = \arctan (0.67\tan\phi), \quad (7)$$

where c^* and ϕ^* represent reduced values of c and ϕ due to size effect. Field data on UBC and DM_{50} for different size pillars is currently being collected at several mines in Illinois to validate equations 1 through 4.

ESTIMATION OF BEARING CAPACITY OF HETEROGENEOUS FLOOR STRATA UNDERNEATH COAL PILLARS

VESIC-SPECK APPROACH FOR UBC ESTIMATION

A brief discussion of the approach proposed by Speck [1981 (*39*)] (so called Vesic-Speck approach) and its modification by Chugh [1990 (*12*)] is given below.

Vesic-Speck analysis approach for a single pillar, which considers weak floor strata as a two-layer cohesive soil/rock (weak layer overlying stiff layer) with $\phi = 0$ for both layers, is the most common approach utilized by coal companies for analyzing stability of coal pillars against floor failure. The laboratory compressive strength of the weak layer is estimated from its natural moisture content [Speck, 1981 (*39*)]. The appropriateness of this design technique, as well as the adequacy of safety factors currently utilized, has not been established to date through field observations.

VESIC-CHUGH-HAQ-CHANDRASHEKHAR (VESIC-CHC) PILLAR DESIGN APPROACH FOR WEAK FLOOR STRATA CONDITIONS

This is a modification of the Vesic [1970 (*45*)] approach. In the Vesic-CHC approach, the bearing capacity of the upper weak floor stratum and the lower competent bed are determined as in the Pytel-Chugh approach and then used to calculate factor N_m from the Vesic equation. This approach assumes angle of internal friction to be zero for both layers and neglects the effect of adjacent pillars. The main advantage of this approach over the Vesic-Speck approach is that realistic estimates of the bearing capacities of the upper and lower beds are used in the analysis.

DEVELOPMENT OF THE PYTEL-CHUGH APPROXIMATE APPROACH

Effect of Nonhomogeneous (Layered) Floor Strata

Bearing capacity of coal pillars on floor strata may be analyzed as a shallow foundation problem [Rockaway, 1979 (*36*); Pytel, 1988 (*29*)]. These analyses assume the validity of the general bearing capacity equation given by Brinch Hansen [1968 (*2*)] with appropriate shape, inclination, and surcharge depth factors. Several analytical techniques have been developed to estimate UBC of shallow foundations on layered soil/rock. These may be subdivided into the following groups:

1. Foundation on two-layer cohesive soils with angle of internal friction for both layers $\phi_1 = \phi_2 = 0$ [Button, 1953 (*5*); Brown, 1969 (*3*); Vesic, 1970 (*45*); Shield, 1955 (*38*); Suklje, 1954 (*42*)].

2. Foundation on two-layer cohesionless soils with $\phi_1 \neq \phi_2 \neq 0$ [Meyerhof, 1974 (*24*); Herdy, 1982 (*18*); Hanna, 1982 (*17*)].

3. Foundation on two-layer soil foundation with c and ϕ for both layers not equal to zero [Myslivec, 1978 (*25*) (experimental work for H/B>0.2); Wilun, 1972 (*47*) (only for lower layer)].

4. Foundation on weak deformable layer on bedrock [Livneh, 1965 (*20*); Mandel, 1969 (*23*)].

5. Foundation on nonhomogeneous soil exhibiting variation of cohesion with depth and $\phi \neq 0$ [Livneh, 1973 (*21*); Salencon, 1973 (*37*)].

The results of the above applicable methods for calculation of bearing capacity of a plate or pillar on weak floor strata are compared in figure 3. Methods applicable for cohesionless soils and for a stiff layer overlying a weak layer were not considered in this comparison. For the case where cohesion and the angle of internal friction for weak floor strata are assumed *not* equal to 0, there is only one applicable technique [Mandel, 1969 (*23*)]. This

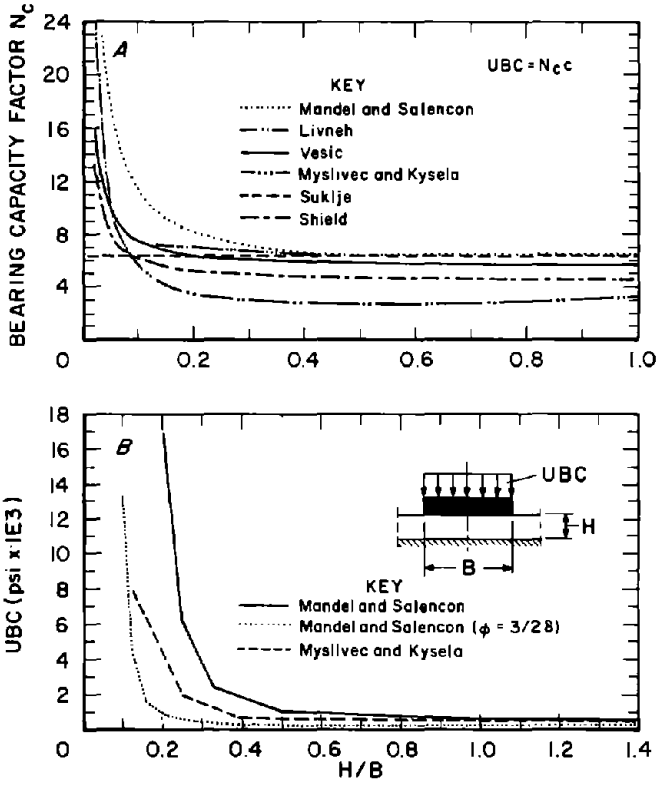

Figure 3.—*A*, Bearing capacity factors $\bar{N}_c$ for selected analysis methods involving ϕ=0°. *B*, Calculated UBC for B=60 ft (18 m), γ=149 pcf (23.8 kN/m^3), c=75 psi (0.5 MN/m^2), and ϕ=27° (δ is the angle of friction at the footing-subsoil interface).

technique is based on a slip-line method with Coulomb criterion of failure (fig. 4). By combining the yield criterion with the equations of equilibrium (set of differential equations of plastic equilibrium), the problem was transformed to curvilinear coordinates whose directions at every point in the yielded region coincided with the directions of slip plane. The solution, i.e., UBC obtained using this technique is given by [Mandel, 1969 (*23*)]:

$$UBC = c N_c s_c F_c + q N_q s_q F_q + \frac{1}{2} B\gamma N_\gamma s_\gamma F_\gamma \quad (8)$$

where c is cohesion, q is a surcharge load, γ is soil or rock unit weight; N_c, N_q, N_γ are bearing capacity factors; $s_c = 1 + 0.2\ (B/L)$, $s_q = 1 + 0.3\ (B/L)$, $s_\gamma = 1 - 0.4\ (B/L)$ are shape factors (B and L are width and length of the foundation/pillar, respectively) [Brinch Hansen, 1968 (*2*)], and F_c, F_q, and F_γ are Mandel-Salencon coefficients. The values of F_c, for the angle of friction at the pillar-floor interface $\delta = 2/3\phi$, are given in figure 5. F_q and F_γ values, available elsewhere [Mandel, 1969 (*23*)], are not presented in this paper, since that coefficients were not found to be important through later analyses. This is because (1) pillars are assumed to be shallow footings, i.e., surcharge q = 0, and therefore F_q value is insignificant, and (2) the contribution of $1/2\ \gamma B N_\gamma$ to equation 8 is very low, and therefore F_γ may be also neglected. Therefore, all analyses from hereon will consider pillars as a shallow footing resting on a weightless rock material.

Based on the Mandel-Salencon technique, the theoretical minimum distance between two pillars (s_o) beyond which UBC for each pillar is independent of the other pillar may be estimated from:

$$\frac{s_o}{B} = 2\cos\left(\frac{\pi}{4}\frac{\phi}{2}\right)\frac{H}{B}\exp\left[\left(\frac{\Pi}{4}\frac{\phi}{2}\right)\tan\phi\right]/\cos\phi, \quad (9)$$

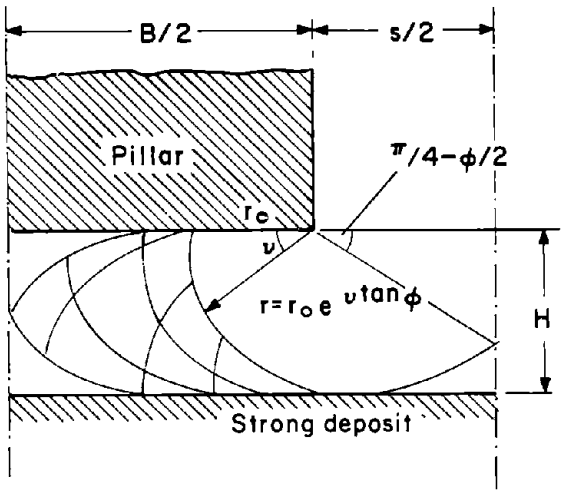

Figure 4.—Mandel and Salencon analysis approach.

where H is the thickness of weak floor stratum and B is the pillar width.

Influence of Adjacent Pillars

Studies of the effect of adjacent foundations/pillars on change in bearing capacity of a single pillar are very limited [Stuart, 1962 (*41*); Mandel, 1965 (*22*); West, 1965 (*46*); Pula, 1981 (*28*); Graham, 1984 (*16*)]. At present, Mandel's method is the only one that can account for both cohesion and angle of internal friction and effect of adjacent foundations. This is achieved by replacing bearing capacity factors, N_c, N_q, and N_γ by N_c^*, N_q^*, and N_γ^* defined below:

$$N_c^* = \xi N_c, N_q^* = \left[(\xi - 1)\left[1 - \frac{1}{N_q}\right] + 1\right]N_q,$$

$$N_\gamma^* = G N_\gamma, \quad (10)$$

where ξ is the "factor of majoration," i.e., multiplication factor greater than or equal to unity representing increase in UBC due to presence of adjacent foundations, and its values for several values of angle ϕ are shown in figure 6. Factor G may be neglected since contribution of N_γ to pillar UBC is insignificant.

All theoretical investigations generally prove that the effect of adjacent foundations on UBC is small for low values of ϕ (less than 10 deg), but it may be significant for high values. Laboratory investigations [Graham, 1984 (*16*)] found the effect of adjacent foundations to be smaller than indicated by theoretical investigations. Assuming infinite thickness of weak floor strata with $\phi = 20°$, for typical partial extraction room-and-pillar mining operations in the United States (s/B = 0.25-0.5), the UBC of a full-size pillar may be expected to increase 1.3 to 2.5 times the UBC of a single pillar due to presence of adjacent pillars. It

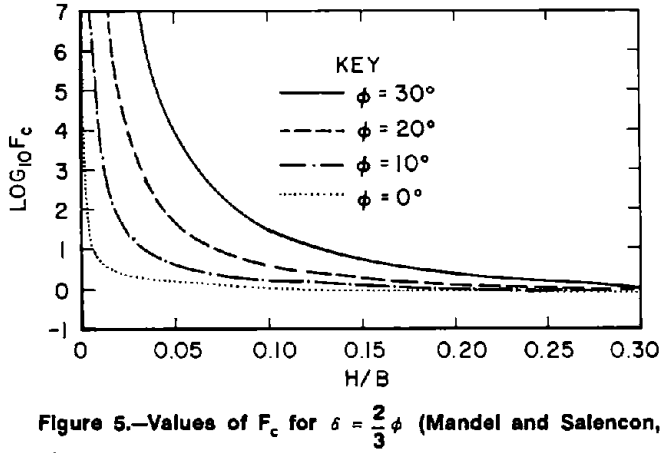

Figure 5.—Values of F_c for $\delta = \frac{2}{3}\phi$ (Mandel and Salencon, 1969).

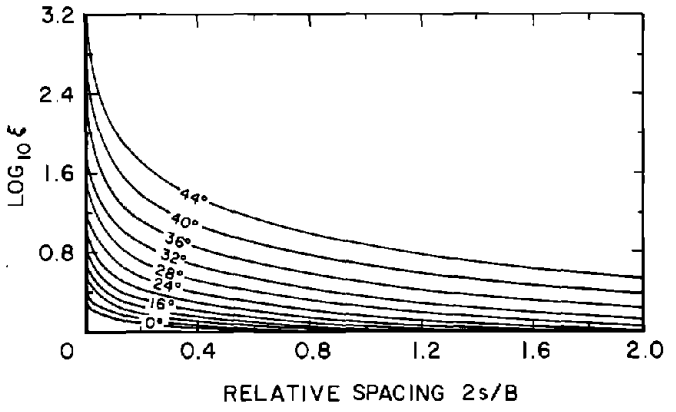

Figure 6.—Factor of majoration ξ for different values of ϕ (Mandel, 1965).

should be emphasized, however, that these are theoretical values based on figure 6.

Proposed Approach

Discussion in the previous sections has indicated that currently there are no analytical techniques that can consider effect of adjacent pillars as well as two deformable layers with varying strength properties. An approximate analytical technique is developed here which overcomes both these limitations (fig. 7). Figure 7 (top) depicts the problem where multiple pillars of width B spaced s apart are resting on a finite layer of weak floor stratum (c_1, ϕ_1, γ_1) of thickness H underlain by another deformable layer (c_2, ϕ_2, γ_2). The estimate of UBC is given by:

$$q = \frac{q_1 q_2}{q_1 + q_2} + E_\gamma \frac{\bar{q}_1}{\bar{q}_2}, \tag{11}$$

where $\bar{q}_1$, $\bar{q}_2$ are the ultimate bearing capacities of the pillar on layers 1 and 2 separately, assuming homogeneous soil conditions:

$$\bar{q}_1 = c_1 N_{c_1} s_c \bar{F}_{c_1} + \frac{1}{2}\gamma_1 B N_{\gamma_1} s_\gamma \bar{F}_{\gamma_1},$$

$$\bar{q}_2 = c_2 N_{c_2} s_c \bar{F}_{c_2} + \frac{1}{2}\gamma_2 B N_{\gamma_2} s_\gamma \bar{F}_{\gamma_2}, \tag{12}$$

where $\bar{F}_c$ and $\bar{F}_\gamma$ are Mandel and Salencon coefficients for homogeneous conditions for a given ϕ value (for $\phi = 10°$, $\bar{F}_c = 0.691$ and $\bar{F}_\gamma = 0.816$, for $\phi = 20°$, $\bar{F}_c = 0.585$ and $\bar{F}_\gamma = 0.650$, and for $\phi = 30°$, $\bar{F}_c = 0.460$ and $\bar{F}_\gamma = 0.489$).

In equation 11, q_1 (fig. 7, top) represents the UBC of the pillar, assuming the lower layer to be infinitely rigid (Mandel and Salencon solution) and spacing s between pillars is greater than s_o) (equation 9). The q_2 (fig. 7, bottom) represents bearing capacity of the lower layer including factor of majoration: $\xi\left(\frac{2s_1}{B_1}, \phi_2\right)$, where $B_1 = \frac{B}{\eta}$ and $s_1 = s - B\left(\frac{1}{\eta} - 1\right)$ (see fig. 7, bottom).

The calculation assumes foundation load distribution over a larger area on the lower layer with coefficient $\alpha = 1/\eta^2$, where η is the coefficient of stress distribution below the center of the uniformly loaded area. The term $E\gamma$ is the maximum error of the calculation in the following equation:

$$\frac{1}{q} = \frac{1}{q_1} + \frac{1}{q_2} \tag{13}$$

which occurs when $\bar{q}_1 = \bar{q}_2$. It was also assumed that $q_1 = q_1^* + \bar{q}_1$, and $q_2 = q_2^* + \bar{q}_2$, where

$$q_1^* = c_1 N_{c_1} s_c (F_{c_1} - \bar{F}_{c_1}) + \frac{1}{2}\gamma_1 B N_{\gamma_1} s_\gamma (F_{\gamma_1} - \bar{F}_{\gamma_1}),$$

$$q_2^* = c_2 N_{c_2} s_c \bar{F}_{c_2} (\alpha\xi - 1) + \frac{1}{2} N_{\gamma_2}\gamma_2 s_B \bar{F}_{\gamma_2} (B_1 G\alpha - B)$$

$$+ \gamma_1 H s_q \bar{F}_{q_2} N_{q_2}\alpha. \tag{14}$$

Finally, the UBC estimate given by equation 11 seems to be reasonable and justified provided the maximum error of estimation is expressed by:

$$E_\gamma = q_{1s}\frac{q_1 q_2}{q_1 + q_2}, \tag{15}$$

where q_{1s} is the bearing capacity of the homogeneous infinite layer composed of the upper layer material, including effect of adjacent pillars.

A major simplification can be made in equation 11 assuming that the influence of soil/rock weight underneath the shallow pillar is small and is therefore negligible ($\gamma_1 = 0$, $\gamma_2 = 0$). For such cases, equation 11 transforms into the following relationship:

$$q = \bar{q}_1\left[\frac{1}{\frac{\bar{q}_1}{\bar{q}_2}\frac{1}{\alpha\xi} + \frac{1}{F_c^*}} + \frac{\bar{q}_1}{\bar{q}_2}\left\{\xi_1 - \frac{1}{\frac{1}{\xi\alpha} + \frac{1}{F_c^*}}\right\}\right], \text{ or}$$

$$q = \bar{q}_1 N_t, \tag{16}$$

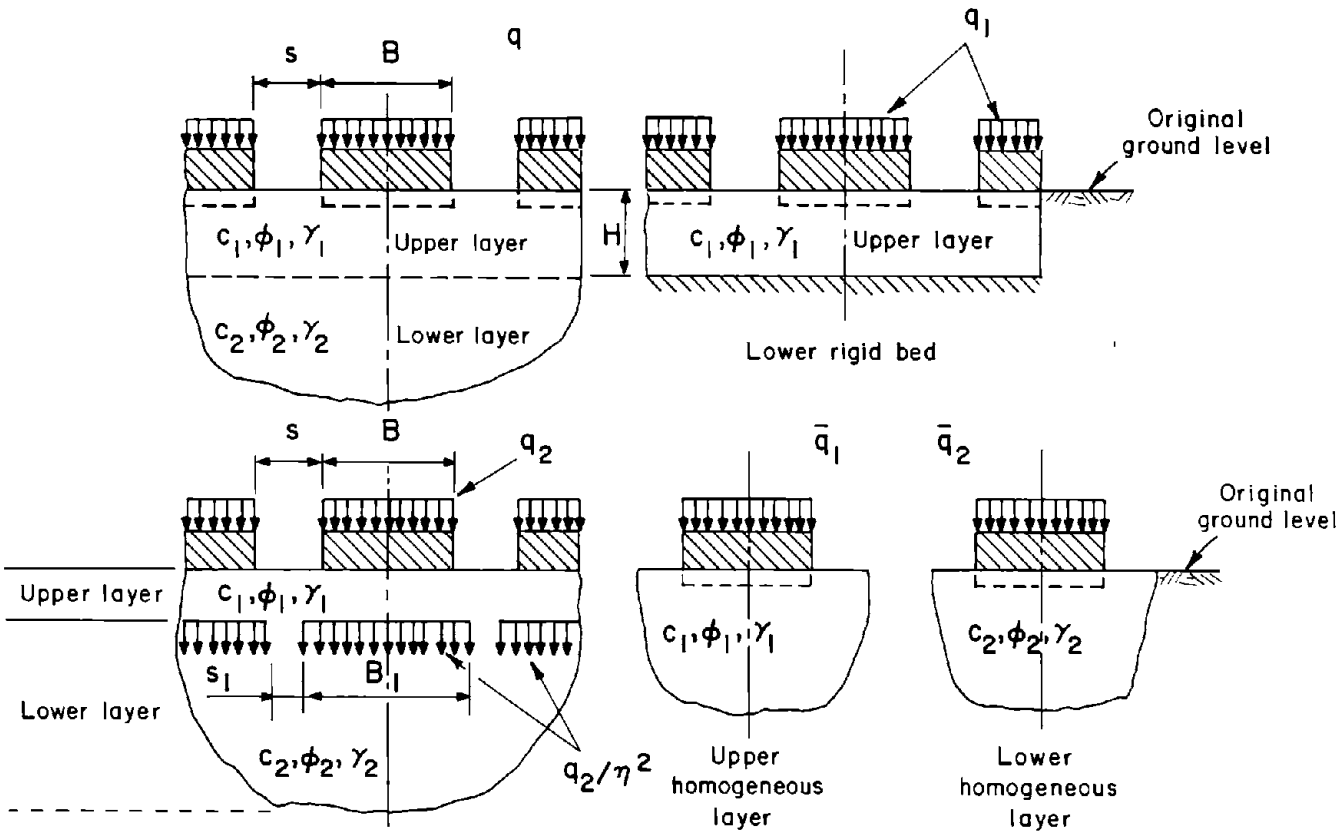

Figure 7.—Authors' approach for calculation of pillar-bearing capacity.

where ξ_1 is calculated using angle ϕ_2 and $F_c^* = F_{c_1}/\bar{F}_{c_1}$. If plate bearing capacity data are available, the term $\bar{q}_1$ in equation 16 may be expressed as:

$$\bar{q}_1 = UBC\, F_r(UBC) \qquad (17a)$$

and it represents the normalized plate load test-bearing capacity (large H/B ratio). If the analysis is carried out using material parameters only, then

$$\bar{q} = c_1 N_{c_1} \bar{F}_{c_1}. \qquad (17b)$$

Equation 16 has been plotted in figure 8 for the value $\bar{q}_1/\bar{q}_2 = 0.3$ (for $\bar{q}_1/\bar{q}_2 = 0$, $N_t = F_c^*$, and for $\bar{q}_1/\bar{q}_2 = 1$, $N_t = \xi_1$). This approach for pillar design by the authors has been called Pytel-Chugh approach and may be summarized as follows:

1. This approach considers the foundation to consist of two layers with weak floor layer overlying the stiff layer.
2. It can consider the effect of adjacent pillars and nonzero values of the angle of internal friction for both layers.

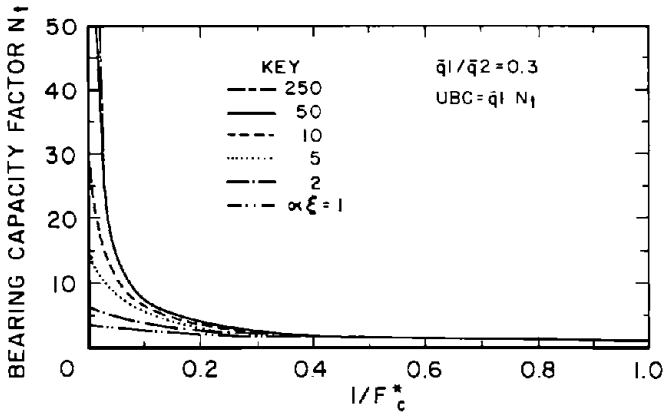

Figure 8.—Modified bearing capacity factor N_t for two-layered weak floor strata.

3. A new modified bearing capacity factor N_t is calculated based on the Mandel-Salencon bearing capacity estimation approach.
4. The bearing capacity of the weak floor strata underneath a pillar is estimated from measured or estimated

plate load test values using natural moisture content of the weak floor strata (equation 1) [Pula, 1990 (*27*)].

5. The bearing capacity of the underlying competent bed is calculated from the bearing capacity equations.

6. The reduction factors are based on equations developed by Pula [1990 (*27*)] (see fig. 2).

The use of this approach is illustrated with an example below.

Numerical Example

The design approach developed in this paper is illustrated with step-by-step solution for a physical problem. For this case, mine geometry and strength properties of weak floor strata (claystone) are given in figure 9. The moisture content for weak floor strata is MC = 8 pct.

Step 1: Calculate UBC underneath a test plate using the regression equation (equation 1).

$$UBC = 1274.1 \exp(-0.112\ MC) = 520.09 \text{ psi } (3.586 \text{ MPa}).$$

Step 2: Determine cohesion of the upper and lower deformable layers.

$$c_1 = c_{0\,1}\,(1 - \sin\phi_1)/2\cos\phi_1 = 245.1 \text{ psi } (1.690 \text{ MPa}),$$

$$c_2 = c_{0\,2}\,(1 - \sin\phi_2)/2\cos\phi_2 = 637.1 \text{ psi } (4.393 \text{ MPa}).$$

Step 3: Calculate bearing capacity factors.

$$N_{c_1} = [\exp(\pi \tan\phi_1)\tan^2(\Pi/4 + \phi_1/2) - 1]/\tan\phi_1,$$

$$N_{c_1} = N_{c_2} = 14.86.$$

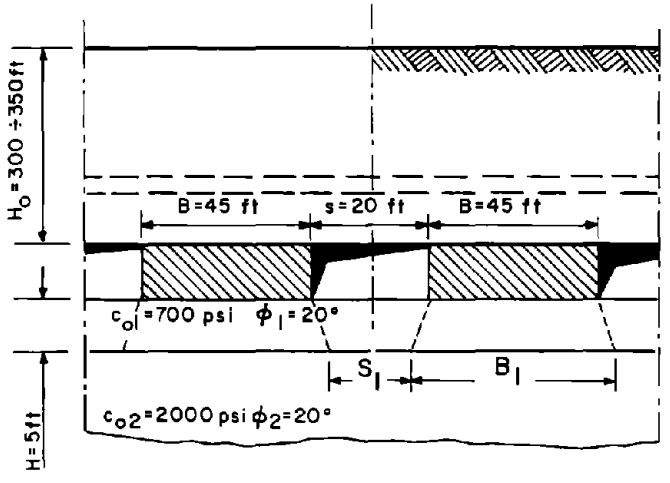

Figure 9.—Idealization of the physical problem.

Step 4: Calculate coefficient of stress distribution at a depth of 5 ft (1.52 m) underneath the center of pillar of width B = 45 ft (13.72 m).

$$\eta = \frac{2}{\Pi}\ \arctan\left[\frac{2H}{B}\left\{2 + 4\left(\frac{H}{B}\right)^2\right\}^{1/2}\right]^{-1}$$

$$+ 4\frac{H}{B}\left[\left\{2 + 4\left(\frac{H}{B}\right)^2\right\}^{1/2}\left\{1 + 4\left(\frac{H}{B}\right)^2\right\}\right]^{-1},$$

$$\eta = 0.922,$$

$$B_1 = B/\eta = 45/0.992 = 45.36 \text{ ft } (13.82 \text{ m}),$$

$$s_1 = s - B(1/\eta - 1) = 19.63 \text{ ft } (5.983 \text{ m}),$$

$$\alpha = 1/\eta^2 = 1.016.$$

Step 5: Calculate factor of majoration ξ (fig. 6).

$$\xi(2s_1/B_1, \phi_2) = \xi(2 \times 19.63/45.36, 20°) = \xi(0.865, 20°)$$

$$= 1.38.$$

Step 6: Estimate coefficients F_{c_1}, $\bar{F}_{c_1}$, $\bar{F}_{c_2}$ (fig. 5).

$$F_{c_1} = 3.136,\ \bar{F}_{c_1} = 0.585,\ \bar{F}_{c_2} = 0.585.$$

$$F_c^* = F_{c_1}/\bar{F}_{c_1} = 5.36.$$

Step 7: Determine ratio of bearing capacity for the two layers.

$$\bar{q}_1/\bar{q}_2 = c_1 N_{c_1} \bar{F}_{c_1}/c_2 N_{c_2} \bar{F}_{c_2} = 0.385.$$

Step 8: Calculate modified bearing capacity factor (N_t) from equation 16.

$$N_t = 1/(0.385/1.016 \times 1.38 + 1/5.36)$$

$$+ 0.385[1 - 1/(1/1.012 \times 1.38 + 1/5.36)] = 2.26.$$

Step 9: Calculate bearing capacity of floor strata underneath a coal pillar.

$$q = UBC_{(plate)}\ F_r(UBC)\ N_t = 520.09 \times 0.85 \times 2.26$$

$$= 999.09 \text{ psi } (6.889 \text{ MPa}).$$

Step 10: Calculate safety factor against foundation failure.

$$F_s = q/p = q/1.1\ H_o(1 + W/B)^2 = 1.450.$$

COMPARISON OF THREE PILLAR DESIGN APPROACHES USING FIELD OBSERVATION DATA ON FAILED AND STABLE PILLARS

In a recently completed study [Chugh, 1990 (*12*)] case history data were collected on failed and stable pillars for 114 cases in active mines in the Herrin (No. 6) coal seam. Three approaches discussed earlier (Vesic-Speck, Pytel-Chugh, Vesic-CHC) were used for calculating floor safety factors FSF for 114 cases. As specific values for C_o and MC were not available, the mean of the available values for a particular mine was used. A cumulative frequency plot for the total number of observed/reported failed or stable pillars against the calculated safety factor was drawn to determine an upper bound/critical value of the FSF below which failure would be likely to occur (figs. 10-11).

At any value of FSF for failed pillars below the critical value, there are some stable pillars whose performance remains unexplained. Similarly, some of the unstable pillars have an FSF value above the critical value. To investigate these discrepancies, a sensitivity analysis was done for each stable pillar using the variables in FSF calculation, such as moisture content and mining depth. The variation of these parameters was within the range of variability typically encountered at a particular mine. The objective of this analysis was to determine if, within the typical variability of selected parameters, the stable pillar could have failed. This analysis resulted in explaining performance of more than 90 pct of the failed pillars, i.e., if FSF was less than the critical value, either the failure was observed or it could be explained by the variability of parameters entering the calculation.

Based on 100 pct of the explained failed pillars, the critical FSF values are 2.0, 2.5, and 1.5 for the Vesic-Speck, Pytel-Chugh, and Vesic-CHC approaches (fig. 10). Similarly, the percentage of unexplained stable cases for these values of FSF are 40, 20, and 4 pct, respectively (fig. 11). Depending on the level of confidence desired, the critical values of FSF may be determined from figure 10. The percentage of unexplained cases, however, is the lowest for the Vesic-CHC method. The FSF value above is the minimum recommended values for pillars in room-and-pillar panels for long-term stability using different approaches. The above values of the critical FSF are based on analysis of limited data on failed pillars. More data should be collected and analyzed prior to recommending these values of safety factors for industry. Particularly, the most general Pytel-Chugh approach should be complemented by reliable data concerning changes in cohesion and angle of internal friction due to changes in rock moisture content. The effect of anisotropy should be also included in the UBC estimation.

Analysis similar to that mentioned above for failed pillars in abandoned mines should be undertaken to develop minimum FSF values based on a larger data base.

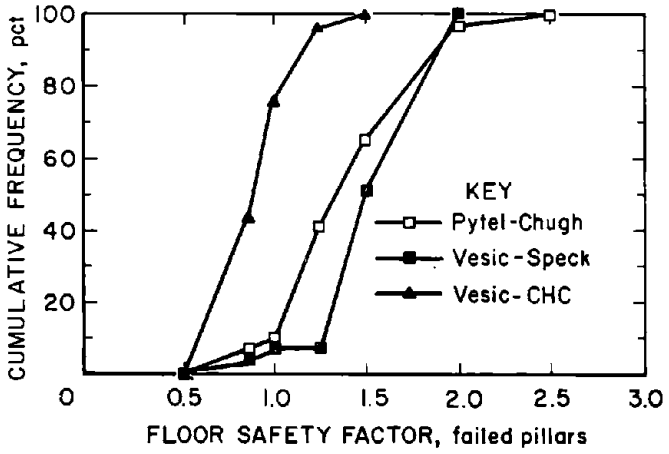

Figure 10.—Cumulative frequency plot of failed pillars for different floor safety factors (FSF) values.

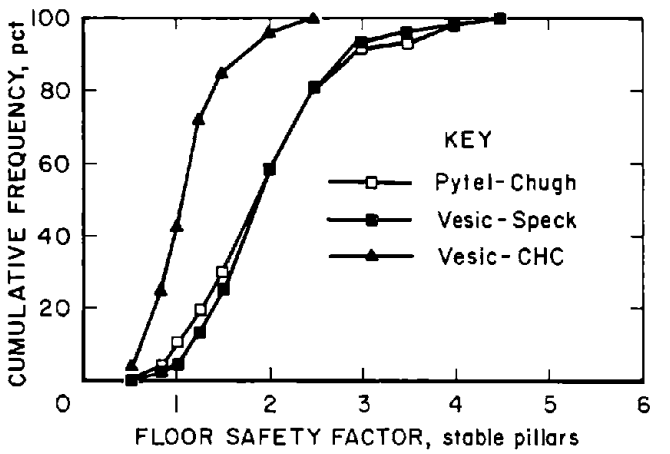

Figure 11.—Cumulative frequency plot of stable pillars for different floor safety factors (FSF) values.

ESTIMATION OF SETTLEMENTS UNDERNEATH FULL-SIZE PILLAR

GENERAL REMARKS

The stress distribution from field measurements corresponds reasonably well to that predicted by linear elastic analysis for homogeneous and layered systems [Perloff, 1975 (*26*)]. For saturated or nearly saturated cohesive soils subjected to moderate increments of stress, the elastic parameters can be assumed to be approximately constant throughout the soil mass, and stress-displacement relations can be assumed as linear for time-independent analyses. The elements to be considered for the design problem here then include the scale factor F_r for size effect and soil/rock behavior model.

SIZE EFFECT (SCALE FACTOR)

The relationship between the size of plate or pillar and settlement is not linear and it is different for different soils. This problem was studied by Bond [1961 (*1*)] and Terzaghi [1948 (*44*)] who proposed the following formula to compare the settlement ρ in sand of a foundation having a width B with the settlement ρ_1 of a square test plate with the area of 1 ft² (0.09 m²),

$$\frac{\rho}{\rho_1} = \left(\frac{2B}{B+1}\right)^2. \qquad (18)$$

The above formula may be used to calculate the load-settlement curve for any size foundation for the same type of sandy soil. Since weak floor strata is not a cohesionless material, an approximate approach for estimating pillar settlement or modulus of deformation underneath a pillar is given below.

$$\rho_{pillar} = \frac{\rho_{pl}}{F_r(DM_{50})}, \quad E_{pillar} = F_r(DM_{50})\, DM_{50}, \qquad (19)$$

where ρ_{pl} and DM_{50} are the test plate settlement and the deformation modulus and F_r (DM_{50}) is the size effect reduction factor obtained previously.

PILLAR SETTLEMENT ON LAYERED WEAK FLOOR STRATA

A general formula for foundation settlement may be expressed as follows.

$$\rho = \frac{pB}{E} I_\rho, \qquad (20)$$

where p is the foundation load and $I\rho$ is the settlement coefficient, which depends upon the Poisson's ratio ν, the relative thickness of deformable weak layer H/B, and shape of loaded area L/B. Figure 12 shows the relationship between $I\rho$ and H/B for a square foundation based on several methods available in literature [Janbu, 1956 (*19*); Giroud, 1972 (*15*); Perloff, 1975 (*26*); Steinbrenner, 1934 (*40*)]. A good correlation between Giroud's results based on an exact solution given by Burmister [1956 (*4*)] and Steinbrenner's approximation is observed. The Steinbrenner's approximation is based on the assumption that settlement ρ of a point on the surface of a deformable layer of thickness H is given by the compression of the material as a semi-infinite medium. Since this approximation yields settlement at the center of a foundation, a correction factor of 0.85 must be used to calculate average settlement of the foundation. Additional analyses were conducted by authors to compare solutions from finite element analyses and Steinbrenner's approximation for a plate-loading test as well as pillar on weak floor strata (fig. 13). Correlation between the two analyses techniques is very good.

Figure 14 shows surface settlements outside the foundation/pillar area based on Steinbrenner's approximation. For H/B < 0.2, the deflection of the foundation at center is directly proportional to stress applied at that point and almost independent of stresses applied at other points. This suggests the use of Winkler's model for

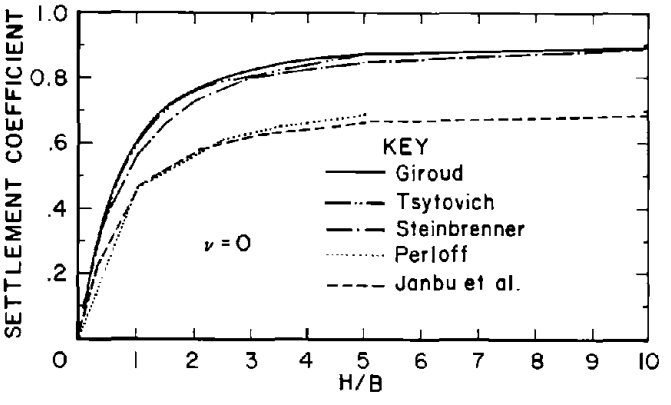

Figure 12.—Settlement coefficient I_ρ for a square footing.

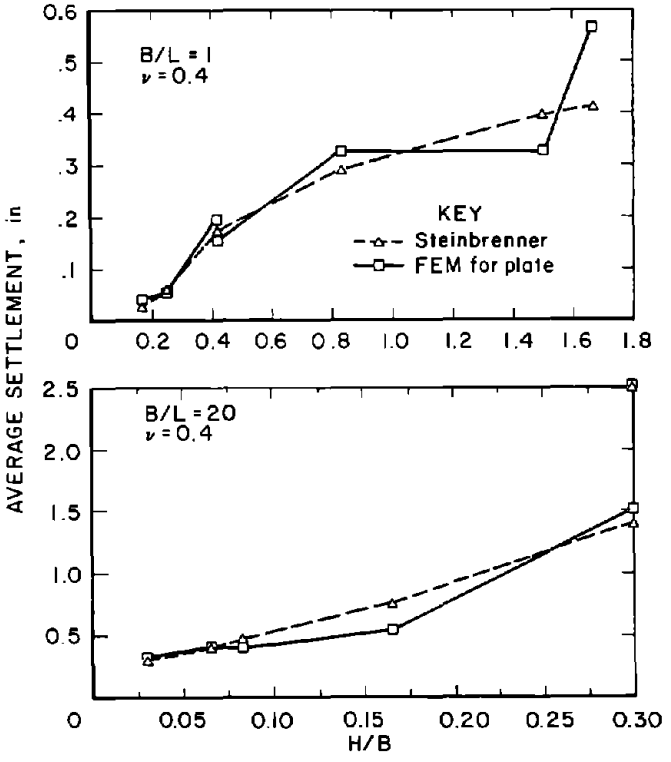

Figure 13.—Comparison of foundation settlement using finite element analysis and Steinbrenner approximation with correction factor of 0.85.

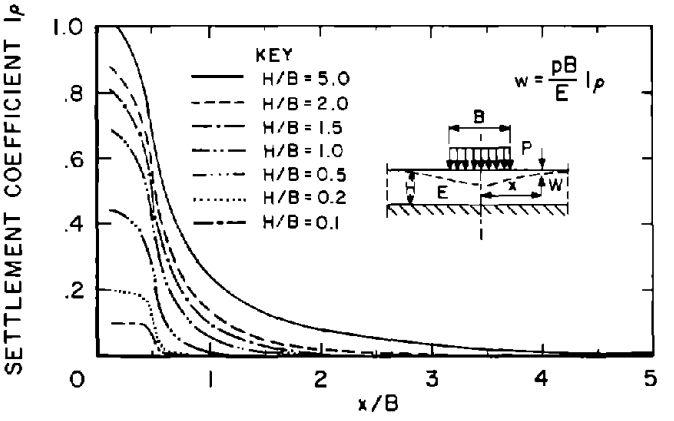

Figure 14.—Surface deflection of a deformable layer overlying a rigid layer (L/B=1, ν=0).

behavior of foundation material. The modulus of subgrade reaction K, for such material, is given by:

$$K = \frac{E(1-\nu)}{H(1+\nu)(1-2\nu)}, \qquad (21)$$

which is valid for compression conditions with no lateral strain. The settlement coefficient $I\rho$ may then be approximated as:

$$I_\rho \approx \frac{H}{B}\,\frac{(1+\nu)(1-2\nu)}{(1-\nu)}.$$

The Winkler model is not appropriate where the immediate weak floor stratum is underlain by other deformable strata. For such a case, the general Steinbrenner's solution should be used.

LOAD ACTING ON PILLARS AND ROOF-PILLAR-FLOOR INTERACTION ANALYSIS

Load acting on pillars may be calculated through an approximate two-dimensional or three-dimensional analytical technique based on the theory of beams or plates resting on elastic or nonelastic foundations [Pytel, 1988 (*29*); Pytel, 1991 (*33*)]. In the solution approach, the mine structure is modeled as an equivalent multi-indeterminate overburden elastic beam or plate supported by elastic-plastic pillars resting on a viscoelastic layer of immediate weak floor strata (see fig. 15). The problem solution, which consists of the vector or matrix of reactive uniformly distributed pressure p underneath pillars, is obtained using the Maxwell-Betti reciprocal theorem from a system of algebraic linear equations (SIU PANEL.2D two-dimensional model) or using the finite difference method suitable for a three-dimensional problem (SIU PANEL.3D model). The model output data include the average stress in all pillars, pillar settlements, and surface subsidence. The theoretical background of the model and its application are presented elsewhere [Pytel, 1988 (*29*); 1989 (*31*); 1991 (*33*)].

Time-dependent deflection of the overburden beam/plate is investigated based on rheological properties of floor strata and, separately, on time-dependent characteristics of the overburden plate [Pytel, 1990 (*30*)]. Since an actual dynamic approach requires consideration of the time-dependent underground mining geometry, the problem has to be solved using an incremental mining sequence. Therefore, all mine workings developed in the total period of time t_k are divided into (k) phases with an assigned extraction time Δt_j for each of the phases, and a suitable function of the load history H(t) = 1 (constant external load). The calculated elastic deformation state is transformed into the corresponding linear viscoelastic state using Alfrey's analogy. The transformation function

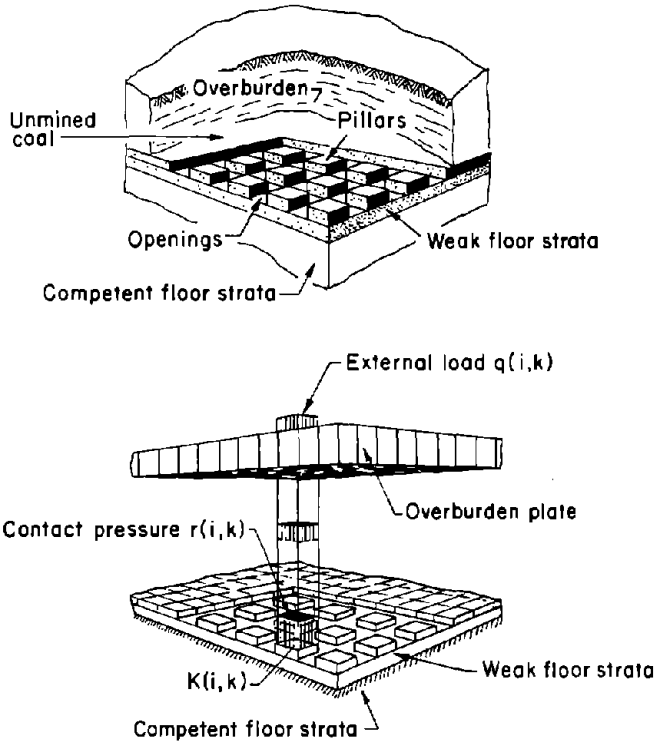

Figure 15.—Three-dimensional physical problem and its equivalent idealization.

equations for overburden and floor strata and their derivation were presented recently [Pytel, 1991 (*33*); 1990 (*30*)].

The transformation function f(t) (see equation 22) reflects strain-stress-time behavior of an assumed rheological model for immediate floor strata [Chugh, 1987 (*11*); Pytel, 1989 (31)]. For the standard Burger's model, the transformation (creep) function is as follows:

$$f(t) = 1 + \frac{E_2}{E_1}\left[1 - \exp\left(-\frac{E_1}{N_1}t\right)\right] + \frac{E_2}{N_2}t, \qquad (22)$$

where E_1, E_2, N_1, and N_2 are elastic and viscous parameters of the Kelvin-Voigt and Maxwell units, respectively. Assuming a linear hereditary model for weak floor strata behavior, the time-dependent deformation modulus of weak floor strata may be expressed as $E(t) = E_2/f(t)$. Modulus E_2 may be obtained from plate-loading tests or other available techniques. The remaining rheological model parameters have to be determined utilizing creep tests [Chen, 1990 (*7*)] or observations of surface subsidence and pillar settlement [Chugh, 1991 (*14*); Pytel, 1991 (*32*)].

The two- and three-dimensional models have been validated at several mines in the Illinois coal basin with very good results [Chugh, 1991 (124(*13*); Pytel, 1991 (*32*)]. The predicted results (subsidence and roof-floor convergence) from the model are generally within 10 pct of the field-observed data. One such comparison for the three-dimensional model is shown in figure 16 [Pytel, 1991 (*32*)].

DEVELOPMENT OF SETTLEMENT-BASED FAILURE CRITERIA FOR ROOF-PILLAR-FLOOR SYSTEM

Stability of the roof-pillar-floor system must be assessed once pillar settlements have been computed. Two failure criteria are proposed:

(1) Differential settlement within each opening that may lead to roof instability.

(2) Maximum average settlement of pillars in a panel.

Differential settlement criterion is based on the assumptions that (1) roof rock is homogeneous and linear elastic, (2) ends of the roof beam are rigidly clamped, and (3) flexure or shearing of the immediate roof beam is caused by gravitational loads $q = \gamma t$ and differential pillar settlements at the ends. The analysis approach is shown in figure 17, and the following expressions were developed for immediate roof displacements (u) and corresponding bending moments (M) and shearing forces (V):

$$u(x) = \frac{\gamma t x}{24E_rI}(W - x)^2 + \left(\frac{x}{W}\right)^2\left[3 - 2\left(\frac{x}{W}\right)\right]\Delta,$$

$$M(x) = \frac{\gamma t}{12}(W^2 + 6x^2 - 6Wx) - \frac{6E_rI}{W^2}\left[1 - 2\left(\frac{x}{W}\right)\right]\Delta,$$

$$V(x) = \gamma t\left(\frac{W}{2} - x\right) + \frac{12E_rI}{W^3}\Delta. \qquad (23)$$

where W is the width of opening, x is the distance from the edge of opening, t is the thickness of the immediate roof layer of unit weight γ, E_rI is the flexural stiffness, and Δ is the differential settlement between two adjacent pillars.

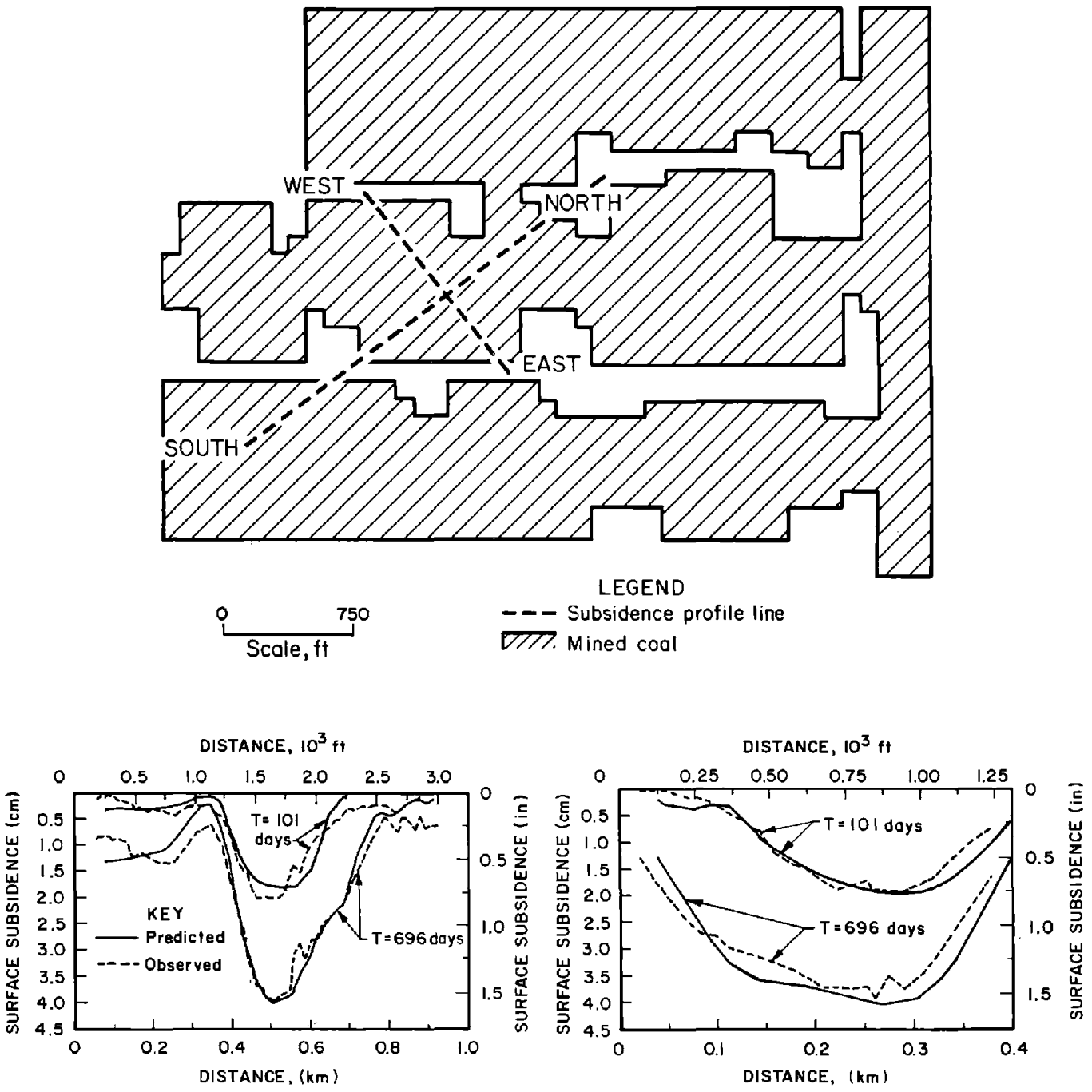

Figure 16.—Comparison of the predicted and observed subsidence profiles (Pytel and Chugh). *Top*, underground layout and panel subdivision. *Bottom left*, predicted and observed subsidence profiles (N-S direction). *Bottom right*, predicted and observed subsidence profiles (E-W direction).

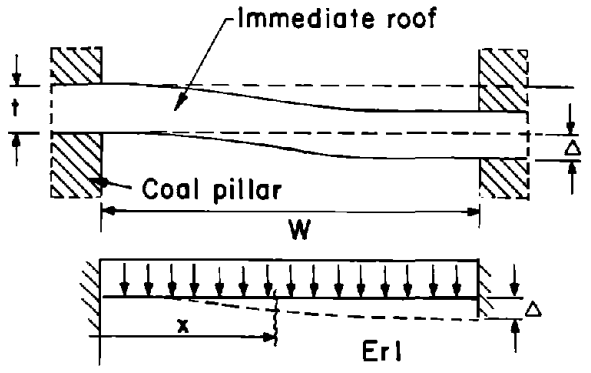

Figure 17.—Analysis for opening width design for weak floor strata conditions.

Using standard failure conditions:

$$\frac{R_o}{F_s} \geq \frac{M(x)\,t}{2I} \text{ (for bending),} \qquad (24)$$

and

$$V(x) \leq 0.75\,\frac{R_o\,t}{F_s} \text{ (diagonal tension),} \qquad (25)$$

where R_o is the flexural strength, I is the moment of inertia, t is the thickness, and γ is the unit weight of the immediate roof stratum, and F_s is the appropriate safety factor, the conditions that should be satisfied to maintain stable immediate roof were obtained in the form presented below. The term diagonal tension implies failure in the tension mode at an angle to the longitudinal axis of the beam due to rotation of the tensile principal stress. This occurs owing to the combined effect of tensile and shearing stresses in the beam and is most pronounced at the edges.

$$\left|\frac{\Delta}{W}\right|_b \leq \frac{1}{3}\left(\frac{W}{t}\right)\left[\frac{R_o}{EF_s} - \frac{\gamma t}{2E_r}\left(\frac{W}{t}\right)^2\right]$$

(failure in bending), (26)

$$\left|\frac{\Delta}{W}\right|_s \leq \left(\frac{W}{t}\right)\left[\frac{3R_o}{4E_rF_s}\left(\frac{W}{t}\right) - \frac{\gamma t}{2E_r}\left(\frac{W}{t}\right)^2\right]$$

(failure in diagonal tension). (27)

Figure 18 shows relative roof span $\left(\frac{W}{t}\right)$ versus allowable differential settlements based on equations 26 and 27. The maximum average settlement of pillars should be determined from the maximum value of heave, which is approximately linearly related with pillar settlement [Chugh, 1987 (*11*)]. Differential settlement of pillars with no associated lateral movement represents the worst case for stresses in the roof strata. The calculated safety factor therefore represents a conservative value.

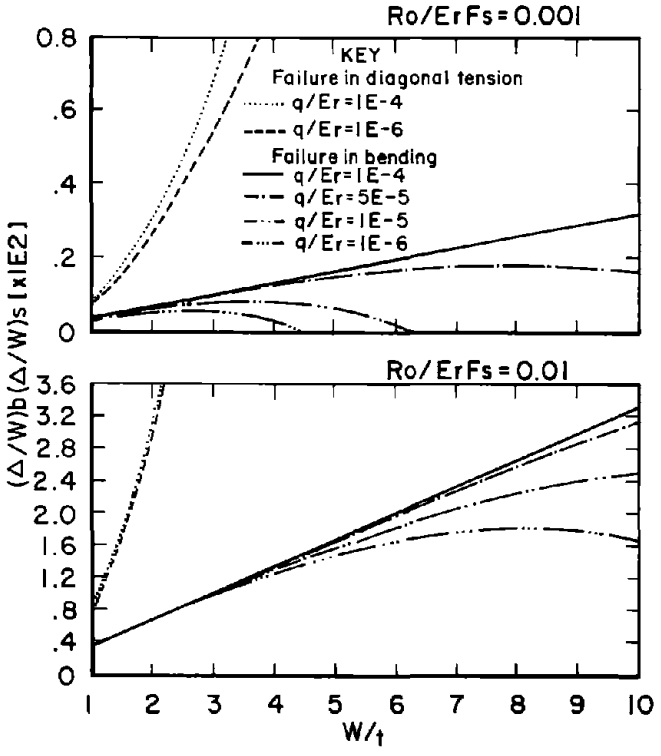

Figure 18.—Allowable differential settlements of adjacent pillars for roof span design.

DESIGN CRITERIA FOR COAL PILLARS FOR WEAK FLOOR CONDITIONS

Having calculated the UBC of weak floor strata q_i, load acting on coal pillars p_i, and pillar settlements ρ_i for each panel pillar, it is necessary to consider the following conditions to provide a stable roof-coal-floor system:

(1) The UBC of immediate floor strata must not be exceeded, such that:

$$p_i \le \frac{q_i}{F_s}, \qquad (28)$$

where p_i is the load acting on the i-th pillar, q_i is the UBC of the immediate floor strata under the i-th pillar, and F_s is the required safety factor.

(2) The strength of the coal pillar is larger than the load acting on the pillar, such that:

$$p_i \le \frac{\sigma_{pi}}{F_s}, \qquad (29)$$

where σ_{pi} is the strength of the (i)th pillar, and F_s is the safety factor against pillar failure. The acceptable F_s in equations 28 and 29 may not be the same.

(3) The differential settlements in an opening are below those indicated by equations 26 and 27.

(4) The maximum allowable pillar settlements are not exceeded, and these are governed by allowable floor heave value. This value depends on serviceability rather than safety requirements.

The safety factors defined above vary along panel cross sections and therefore depend on a given pillar location.

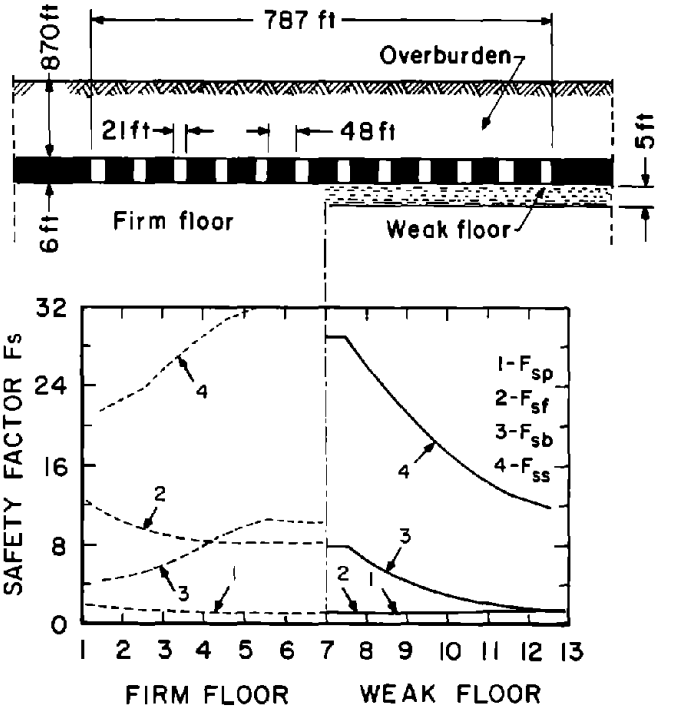

Figure 19.—Safety factors in a panel for different failure criteria, firm floor (left) and weak floor strata (right). F_{sp}=Pillar safety factor. F_{sf}=Floor safety factor. F_{sb}=Safety factor in bending. F_{ss}=Safety factor in diagonal tension.

The exemplary results based on the two-dimensional analysis approach are presented in figure 19 [Pytel, 1990 (*34*)].

CONCLUSIONS

This paper summarized a 5-year research effort related to rational approaches for design of partial extraction mining systems where weak floor strata conditions exist. Some of the major conclusions drawn from the study are (1) ultimate bearing capacity of weak floor strata underneath a small-size plate (6 to 18 in) may be estimated with confidence based on moisture content of weak floor strata, (2) the effect of plate size on UBC and deformability of weak floor strata may be estimated from equations similar to the Gaddy's formula for coal strength, (3) UBC and deformability of weak floor strata underneath full-size pillars may be estimated from the authors' modified analytical techniques that appear to fit the field observation data on failed and stable pillars, (4) mine openings may be designed based on allowable differential settlement of adjacent pillars, and (5) roof-pillar-floor interaction analysis may be conducted using simplified two- and three-dimensional analytical models developed and validated by the authors.

Studies are continuing to obtain field data on UBC and deformability underneath large size plates (24 in and above) to validate equation 1. A study has been initiated to obtain data on UBC and deformability of weak floor strata beneath full-size pillars by instrumenting longwall chain pillars. Another field study has been initiated to develop and to demonstrate alternate partial extraction mining geometries which will permit increased extraction

ratio with improved mine stability and controlled pillar settlements and surface subsidence. Based on field performance of pillars on weak floor strata, attempts are being made to develop adequate safety factors for failures based on bearing capacity and total as well as differential settlements. It is the authors' hope that the developed approach can be routinely applied in mine design after the next 1 to 2 years.

REFERENCES

1. Bond, D. The Influence of Foundation Size on Settlement. Geotechnique, v. 2, 1961, pp. 121-143.

2. Brinch Hansen, J. A Revised and Extended Formula for Bearing Capacity. Preprint of Lecture in Japan, 1968.

3. Brown, J. D., and G. G. Meyerhof. Experimental Study of Bearing Capacity in Layered Clays. Proc. 7th ICSMFE, Mexico City, v. 2, 1969, pp. 45-51.

4. Burmister, D. M. Stress and Displacement Characteristics of a Two-Layer Rigid Base Soil System: Influence Diagrams and Practical Applications. Proc. Highway Res. Board, v. 35, 1956, pp. 773-814.

5. Button, S. J. The Bearing Capacity of Footings on a Two-layer Cohesive Subsoil. Proc. 3rd ICSMFE, Zurich, v. 1, 1953, pp. 332-335.

6. Chandrashekhar, K. Effects of Weak Floor Strata Interaction on Underground Room-and-Pillar Mining. Ph.D. Thesis, Southern Illinois University at Carbondale, 1990.

7. Chen, G., and Y. P. Chugh. Application of Short-Term Time-Dependent Plate Loading Tests for Estimation of In-Situ Elastic and Viscous Parameters of Weak Floor Strata. Proceedings of the 9th International Conference on Ground Control in Mining, Morgantown, WV, ed. by S. S. Peng. 1990, pp. 238-249.

8. Chugh, Y. P., and A. Atri. Laboratory and Field Characterization of Immediate Floor Strata in Illinois Coal Mines. Final Report to IL Mine Subsidence Res. Program, Champaign, IL, 1988.

9. Chugh, Y. P., A. Atri, and J. Dougherty. Laboratory and Field Characterization of Immediate Floor Strata in Illinois Basin Coal Mines. Proceedings of the 30th U.S. Symposium on Rock Mechanics, WV Univ., Morgantown. 1989, pp. 47-54.

10. Chugh, Y. P., K. Chandrashekhar, and R. D. Caudle. A Field Geotechnical Study of the Effects of Weak Floor Strata on an Underground Coal Mine in Illinois. Proceedings of the 29th U.S. Symposium on Rock Mechanics, Univ. MN, 1988.

11. Chugh, Y. P., R. Nath, and S. Shankar. Time-Dependent Behavior of Immediate Weak Floor Strata From an Illinois Coal Mine. Proceedings of the 6th International Conference on Ground Control in Mining, Morgantown, WV. 1987, pp. 204-218.

12. Chugh, Y. P., M. Phillips, K. Chandrashekhar, A. Atri, and S. Haq. Identification of Mine Characteristics, Conditions, and Procedures for Design of Stable Partial Extraction Room-and-Pillar Mines in the Herrin (No. 6) Coal Seam in Illinois. Final Rep. to IL Mine Subsidence Res. Program, 1990.

13. Chugh, Y. P., and W. M. Pytel. Subsidence Prediction in a Room-and-Pillar Mining Area in Wabash Mine. Res. Rep. to AMAX Coal Co., 1991.

14. Chugh, Y. P., W. M. Pytel, Q.-W. Hao, and G. Chen. Subsidence Investigations for Design of Partial Extraction Mine Layouts for Black Beauty Coal Company. Res. Rep. for Black Beauty Coal Co., Dep. Min. Eng., South. IL Univ. at Carbondale, 1991.

15. Giroud, J. P. Settlement of Rectangular Foundation on Soil Layer. ASCE J. Soil Mech. and Found. Div., v. 98, 1972, pp. 149-154.

16. Graham, J., G. P. Raymound, and A. Suppiah. Bearing Capacity of Three Closely-Spaced Footings on Sand. Geotechnique, v. 34, No. 2, 1984, pp. 173-182.

17. Hanna, A. M. Bearing Capacity of Foundations on a Weak Sand Layer Overlying a Strong Deposit. Can. Geotech. J., v. 19, 1982, pp. 392-399.

18. Herdy, A. C., and F. C. Townsend. Preliminary Investigation of Bearing Capacity of Layered Soils by Centrifugal Modeling. Trans. Res. Rec., v. 872, 1982, pp. 20-24.

19. Janbu, N., L. Bjerrum, and B. Kjaernsli. Nor. Geotech. Inst. Publ., Oslo, v. 16, 1956.

20. Livneh, M. The Theoretical Bearing Capacity of Soils on a Rock Foundation. Proc. 6th ICSMFE, Montreal, v. 2, 1965, pp. 122-126.

21. Livneh, M., and J. Greenstein. The Bearing Capacity of Footings on Non-Homogeneous Clay. Proc. 8th ICSMFE, Moscow, v. 2, 1973, pp. 219-223.

22. Mandel, J. Interference Plastique de Semmelles Filantes. Proc. 6th ICSMFE, Montreal, v. 3, 1965, pp. 127-131.

23. Mandel, J., and J. Salencon. Force Portante d'un Sol Sut une Assise Rigide. Proc. 7th ICSMFE, Mexico City, v. 2, 1969, pp. 157-164.

24. Meyerhof, G. G. Ultimate Bearing Capacity of Footing on Sand Layer Overlying Clay. Can. Geotech. J., v. 11, 1974, pp. 223-229.

25. Myslivec, A., and Z. Kysela. The Bearing Capacity of Building Foundations. Elsevier, 1978.

26. Perloff, W. H. Pressure Distribution and Settlement. Foundation Engineering Handbook, ed. by H. Wintercorn and H.-Y. Fang. Van Nostrand Reinhold, 1975, pp. 148-149.

27. Pula, O., Y. P. Chugh, and W. M. Pytel. Estimation of Weak Floor Strata Properties and Related Safety Factors for Design of Coal Mine Layouts. Proceedings of the 31st U.S. Symposium on Rock Mechanics, Colorado School of Mines, ed. by W. A. Hustrulid and G. A. Johnson. A. A. Balkema, 1990, pp. 93-100.

28. Pula, O., and C. Rybak. Sur L'interaction de Semelles Filantes dans le Domaine Plastique. Proc. 10th ICSMFE, Stockholm, v. 2, 1981, pp. 235-237.

29. Pytel, W. M. Development of an Analytical Model for Solving Roof-Coal Pillar-Floor Interaction Problems. Internal Res. Rep., Dep. Min. Eng., South. IL Univ. at Carbondale, 1988.

30. ____. Development of a Simplified Roof-Pillar-Floor Interaction and Subsidence Analysis Model for Longwall Mining. Final Rep. to IL Min. and Miner. Resour. Res. Inst., 1990.

31. Pytel, W. M., and Y. P. Chugh. An Analysis of Roof-Pillar-Weak Floor Interaction in Partial Extraction Room-and-Pillar Mining. Proceedings of the 30th U.S. Symposium on Rock Mechanics, WV Univ., Morgantown, ed. by A. Wahab Khair. A. A. Balkema, 1989, pp. 621-628.

32. ____. Development and Validation of a Simplified Three-Dimensional Roof-Pillar-Floor Interaction Analysis Model. Proceedings of the 9th Annual Workshop, Lexington, Kentucky: Generic Mineral Technology Center, Mine Systems Design and Ground Control, 1991.

33. ____. Simplified Three-Dimensional Roof-Pillar-Floor Interaction Analysis Model Including Time Effect. Proceedings of the 32nd U.S. Symposium on Rock Mechanics, OK Univ., Norman, ed. by J. C. Roegiers, A. A. Balkema, 1991, pp. 781-790.

34. Pytel, W. M., Y. P. Chugh, and O. Pula. An Approach for Design of Coal Pillars in Partial Extraction Coal Mining Panels with Consideration of Roof-Pillar-Floor Interaction. Proceedings of the 31st U.S. Symposium on Rock Mechanics, Colorado School of Mines, ed. by W. A. Hustrulid and G. A. Johnson. A. A. Balkema, 1990, pp. 101-108.

35. Pytel, W. M., Y. P. Chugh, B. Zabel, and R. D. Caudle. A Simplified Two-Dimensional Analysis of the Roof-Pillar-Floor Interaction Problem in Coal Mines. Proceedings of the 7th International

Conference on Ground Control in Mining, WV Univ., Morgantown, ed. by S. S. Peng. 1988, pp. 271-281.

36. Rockaway, J. D., and R. W. Stephenson. Investigation of the Effects of Weak Floor Conditions on the Stability of Coal Pillars. Rep. No. BUMINES-OFR-12-81, 1979, 227 p.

37. Salencon, J. M. Barbier, and M. Benbat. Force Portante d'une Foundation sur Sol Non-homogenee. Proc. 8th ICSMFE, Moscow, v. 2, 1973, pp. 219-223.

38. Shield, R. T. The Plastic Indentation of a Layer by a Flat Punch. Q. Appl. Math., v. XIII, No. 1, 1955, pp. 27-46.

39. Speck, R. C. The Influence of Certain Geologic and Geotechnical Factors on Coal Mine Floor Stability - A Case Study. Proceedings of the 1st Conf. on Ground Control in Mining, WV Univ., Morgantown, 1981, pp. 44-49.

40. Steinbrenner, W. Tafeln zur Setzungberechnung. Die Strasse, v. 1, 1934, pp. 121-124.

41. Stuart, J. G. Interference Between Foundations With Special Reference to Surface Footings on Sand. Geotechnique, v. 12, 1962, pp. 15-20.

42. Suklje, L. Capacite Portante des Couches Cohesives peu Permeables et D'epaisseur Limitee. Proc. Yugoslav Soc. Soil Mech. and Found. Eng., v. 3, 1954, pp. 16-26.

43. Terzaghi, K. Theoretical Soil Mechanics. Wiley, ch. 8, 1943.

44. Terzaghi, K., and R. B. Peck. Soil Mechanics in Engineering Practice. Wiley, 1948.

45. Vesic, A. S. Research on Bearing Capacity of Soils (unpublished).

46. West, J. M. and J. G. Stuart. Oblique Loading Resulting From Interference Between Surface Footings on Sand. Proc. 6th ICSMFE, Montreal, v. 3, 1965, pp. 214-217.

47. Wilun, Z., and K. Starzewski. Soil Mechanics and Foundations Engineering. Wiley, 1972, p. 41.

PILLAR DESIGN IN BUMP-PRONE GROUND USING NUMERICAL MODELS WITH ENERGY CALCULATIONS

By Keith A. Heasley[1] and Joseph C. Zelanko[1]

INTRODUCTION

Coal bumps can be described as the sudden, violent expulsion of coal from a rib or active coal face into an adjacent entry or entries. Coal bumps are an extremely debilitating problem since they can result in severe personnel injuries, damaged equipment, reduced production, and lost reserves. In addition, the unpredictable nature of bumps has a profound negative effect on the morale of the work force. Commensurate with the seriousness of the problem, a significant effort has been expended over the years to better understand the coal bump phenomenon. The U.S. Bureau of Mines has long been active in this research area, as have been a number of coal companies and coal industry research groups. Historically, research has focused on improved mine designs and mining practices. In recent years, the Bureau has directed resources toward the development of numerical models as tools that provide insight into mine design in bump-prone ground.

As part of the modeling effort, an investigation of the geologic strain energy released in association with coal bumps was initiated. It was hypothesized that calculated energy values may provide better insight, or even a certain predictive capability, regarding the occurrence of coal bumps. For many years, it has been understood that energy changes occur in the rock mass during mining. Basically, the very act of creating an opening underground causes the gravitational potential and tectonic strain energy of the rock mass to be redistributed. Part of this redistributed energy goes to increasing the elastic strain energy of the nearby rock mass while another part of the redistributed energy is dissipated or released. This released energy can take a passive form such as heat, sound, etc., or it may appear as dynamic energy driving a damaging rock burst or coal bump.

It is not surprising, then, to find that in the past the energy release rate (ERR) has been found to correlate with the incidence or risk of damaging rock bursts. In the 1960's, the concept of ERR as an indicator of burst potential was pioneered in deep hard-rock mines in South Africa (*1-3*)[2]. More recently, energy release rate computation and application have improved (*4-5*), and use of the ERR concept at burst-prone hard-rock mines has become common. However, the application of energy concepts to bump-prone coal mines has been limited. Crouch and Fairhurst (*6*) applied a displacement-discontinuity model with an energy release calculation to simulated coal mining sequences and demonstrated a technique for selecting an optimum cut sequence for bump control based on the energy values. Similarly, Zipf and Heasley (*7*) applied an energy calculation to a set of idealized cut sequences for pillar retreat mining and demonstrated the superiority of the Olga Mine cut sequence for maintaining a uniform energy release and therefore minimizing bump potential. In a more practical situation, Maleki et al. (*8*) used energy calculations in conjunction with stress and displacement calculations to analyze and recommend alternative mining plans for an active mine experiencing bump problems.

This paper summarizes some recent work in which energy calculations available in MULSIM/NL were used to evaluate room-and-pillar retreat and longwall mine designs. Several pillar retreat cut sequences were evaluated in an effort to determine their relative suitability for use in bump-prone ground. Similarly, the dissipated energy from the longwall gate pillars and tailgate corner in several different multiple-seam mining scenarios was evaluated. Finally, MULSIM/NL was used in a back analysis of an actual bump event to evaluate whether dissipated energy values correlated with the actual observed bump behavior.

MULSIM/NL AND THE ENERGY CALCULATIONS

In this paper, energy calculations are implemented in the computer code, MULSIM/NL (*9*). This code uses the displacement-discontinuity variation of the boundary element method (BEM) to calculate three-dimensional stresses and displacements caused by mining tabular deposits such as coal seams. From these stresses and displacements, MULSIM/NL calculates energy quantities for

[1]Mining engineer, Pittsburgh Research Center, U.S. Bureau of Mines, Pittsburgh, PA.

[2]Italic numbers in parentheses refer to items in the list of references at the end of this paper.

the seam materials. The energy quantities discussed in this paper are called the "strain energy" values and consist of the total strain energy, the recoverable strain energy, and the dissipated strain energy. An explanation of these three quantities is best accomplished by reference to figure 1.

In figure 1, a typical strain-softening curve for an idealized coal is shown. As the coal is initially loaded along the elastic portion of the curve (line AB), the work needed to strain the coal is stored as elastic strain energy (area ABC). Since any unloading of the coal is assumed to occur along the same line, all of the input work is totally recoverable. However, as the coal is loaded past the point of peak stress (point B) to the residual stress portion of the curve (line DE), any unloading of the coal is assumed to occur along a line parallel to the initial loading (line EF) and not along the original loading curve (ABDE). Thus, the "recoverable" strain energy for a coal material at point E is equal to area EFG, while the "total" work energy applied to the material is equal to area ABDEG. The difference between the total energy area and the recoverable energy area is the area ABDEF, which is known as the "dissipated" energy since it must have been liberated to the environment.

The energy analyses in this paper will examine the changes in total dissipated strain energy between one mining step and another. By the Bureau's proposed coal model (fig. 1), any increase in dissipated strain energy between steps implies that energy was dissipated to the environment. It is postulated that the larger the increase in dissipated energy between steps the more likely that the energy will be dissipated dynamically as a coal bump.

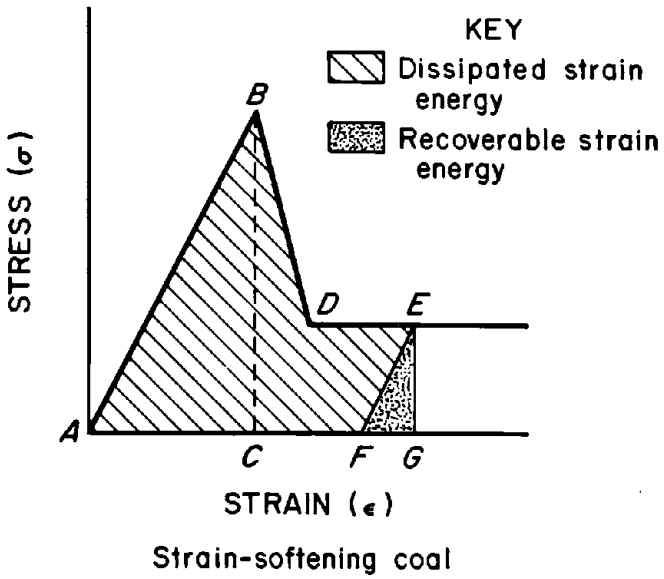

Figure 1.—Schematic of strain energy values.

Therefore, the model steps with the highest increases in dissipated energy would assumedly correlate with the greatest bump hazard. (The model of coal behavior and the calculation of dissipated energy used in this paper are not directly derivable from the first principles of mechanics. However, within the limitations of the boundary element method, the dissipated energy calculations should provide a reasonable indication, the realistic energy changes.)

PILLAR RETREAT CUT SEQUENCING ENERGY ANALYSIS

The first example of using energy calculations for mine design is an idealized scenario where four different pillar retreat cut sequences are analyzed as to their relative bump potential. Three of the cut sequences are standard room-and-pillar retreat practices: single split and fender, pocket and wing, and open ending. The fourth cut sequence was developed at the Olga Mine in southern West Virginia specifically to combat bumps. These four cut sequences are the same as those previously analyzed by Zipf and Heasley (*7*) and are shown in figure 2. In the previous work, elastic and elastic-plastic coal properties were used, and ERR values after Salamon (*4*) were calculated. The analysis in this paper builds upon the previous work by adding strain-softening coal properties and by calculating the dissipated energy values explained earlier. Also, the concept of a spatial and temporal density for the energy values is presented.

In these cut sequence models, the coal seam under evaluation is 66 in thick and is located at a depth of 1,000 ft. The fine grid elements, as shown in figure 2, are 9 ft square, and the mine plan is modeled with 18 ft wide entries and 54- by 72-ft pillars. The surrounding rock mass is modeled with an elastic modulus of 750,000 psi, a Poisson's ratio of 0.25, and a density of 158 lb/ft^3. The gob material has a linear elastic modulus of 7,500 psi, and the strain-softening coal properties that were utilized are shown in figure 3. These four strengths of coal are correlated in the model with the location of the element in respect to a free surface. The "external" coal material is located on the edge of the pillar and the material properties progressively increase in peak and residual strength toward the "core" material in the center of the pillar. This arrangement of coal elements is intended to incrementally account for strength increases owing to increased

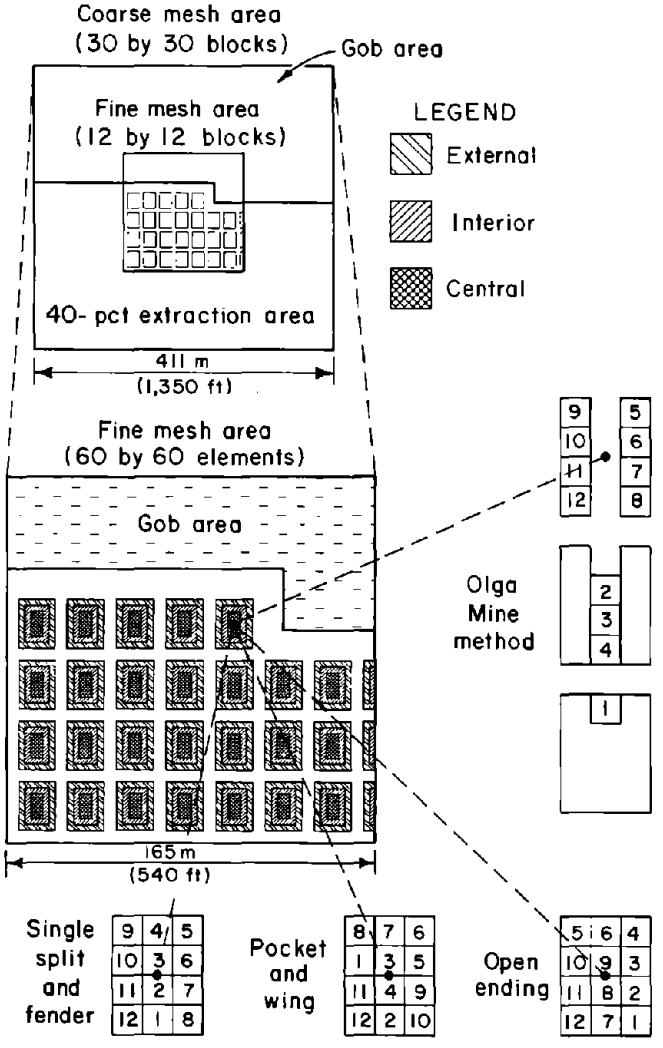

Figure 2.—Schematic of the four cut sequences.

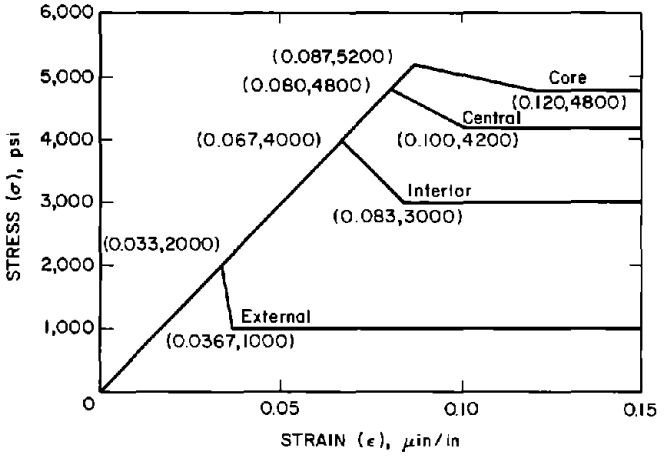

Figure 3.—The stress-strain curves for the coal elements.

confinement toward the center of the pillar. (These rock mass properties and coal stress-strain curves were originally derived in an extensive calibration of the Olga Mine model (*10*). However, they are used in these cut sequence models as average parameters.)

The first results from the cut sequence models show the dissipated energy increases for the entire fine mesh model (fig. 4). In general, these plots show a large increase in dissipated energy when the pillars are being split and minimal dissipated energy changes when the yield zones or remnant wings are mined. If, as proposed, the peak dissipated energy values are indicative of the greatest bump hazard, then the model clearly indicates that the greatest bump hazard occurs during pillar splitting. This model behavior nicely matches observed and intuitive pillar responses. If the relative magnitudes of the peak dissipated energy are used to determine the cut sequence with the least bump potential, then the open-ending sequence appears to be noticeably better than the other three cut sequences. This low bump potential of the open-ending cut sequence seems reasonable since the cuts are only taken from the yielded perimeter of the coal pillar. In fact, Crouch and Fairhurst (*6*) had previously noted the minimized peak energy release associated with only mining the yielded perimeter of a pillar. Also, the fairly successful "thin-pillar" mining method, which was developed for bump control, takes advantage of this principle (*11*).

It was originally thought that the Olga mining method would show a relatively low peak dissipated energy since this sequence was developed for minimizing bumps and was used fairly successfully. However, as shown in figure 4, the Olga sequence results in as much, or more, dissipated energy than either the pocket and wing or the single split and fender sequences. It has been hypothesized that part of the success of the Olga cut sequence was due to distributing the mining over three pillar rows thereby dissipating the gravitational potential energy over both a

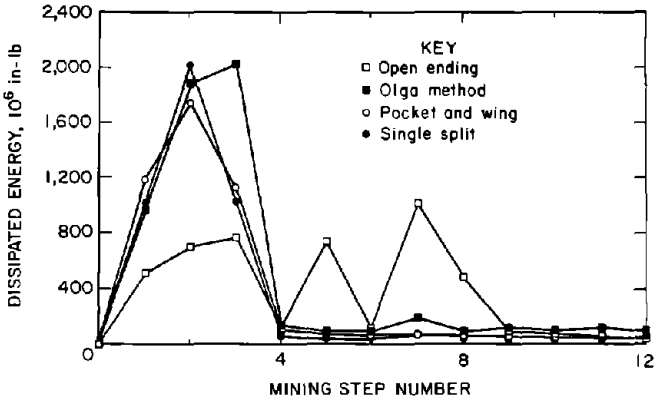

Figure 4.—Dissipated energy from the entire model.

wide area and a large time frame. To evaluate this hypothesis, the spatial density of the dissipated energy release from the Olga method was compared with the other methods by graphing the dissipated energy from only the pillar being split. This graph is shown in figure 5, and indeed the Olga method has a lower peak dissipated energy for the pillar being split. Also, if each of the cuts is considered as a measure of equal time, then the results in figure 5 indicate that the Olga method contains two cuts of relatively high-dissipated energy within a given time span whereas both the pocket and wing, and the single split and fender methods contain three cuts of high-dissipated energy within a similar time span.

While the dissipated energy analysis of these four cut sequences does not conclusively determine their relative bump hazard, the dissipated energy values have generally correlated well with observed field behavior. Also, the previous discussion has demonstrated the use of energy calculation for insight toward mine design and the possible significance of the spatial and temporal density of the dissipate energy was introduced.

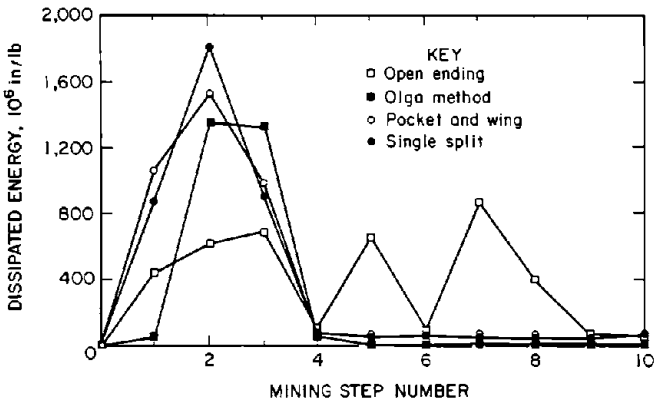

Figure 5.—Dissipated energy from the split pillar.

MULTIPLE-SEAM LONGWALL ENERGY ANALYSIS

The second example of using energy calculations for mine design in bump-prone ground is an actual situation in which multiple-seam interactions have appeared to influence bump occurrences on a longwall face. In this study, a room-and-pillar mine with pillar retreat sections overlies a longwall mine. Both mines are drift mines; however, due to the topographic relief, mining depths often exceed 2,000 ft. The lower longwall mine operates in a 9-ft-thick coalbed, which is approximately 140 ft beneath the 3-ft-thick coalbed of the upper room-and-pillar mine.

In the lower mine, a series of four adjacent longwall panels was extracted beneath various preexisting room-and-pillar configurations: barrier pillars between sections, development sections, and retreat sections (with associated gob zones). (In figure 6, the longwall panels were extracted left to right and bottom to top.) Underground observations in the lower mine revealed that the gate pillar ribs tended to be stable in areas beneath gob zones. However, beneath barrier pillars or in pillar-to-gob transitions, pillar ribs were heavily spalled and appeared to be highly stressed. During the extraction of the four longwall panels, numerous bumps occurred along the tailgate end of the face, and these face bumps appeared more frequently when mining beneath barrier pillars in the upper mine. After each major face bump, the tailgate abutment pillars were observed to have bumped either ahead of, or adjacent to, the longwall face. In fact, in one particular instance, gate pillars located beneath a barrier pillar were observed to have bumped in the tailgate several hundred feet ahead of the face (*12*).

In previous research, it has been postulated that the failure of tailgate abutment pillars contributes to longwall face bumps by allowing abutment stresses to override the gate pillar system onto the tailgate corner of the face. This research has demonstrated that appropriately sized abutment pillars can mitigate longwall face bumps by either preventing, or at least delaying, tailgate pillar failure (*13*). Based on this premise, multiple-seam longwall models were designed to evaluate the response of the gate pillars and the tailgate corner of the face in relation to the configuration of the upper mine. In order to provide this evaluation, three specific multiple-seam configurations consisting of longwall gate pillars located beneath: a barrier pillar (model 1), a room-and-pillar panel (model 2), and a gob zone (model 3) were modeled (fig. 6).

Using MULSIM/NL, the mine plans were discretized using 10-ft fine grid elements. For convenience, the model grid was aligned with the orientation of the longwall gate roads in the lower mine. This alignment allowed the longwall mine plan to be modeled with 20-ft-wide entries, and

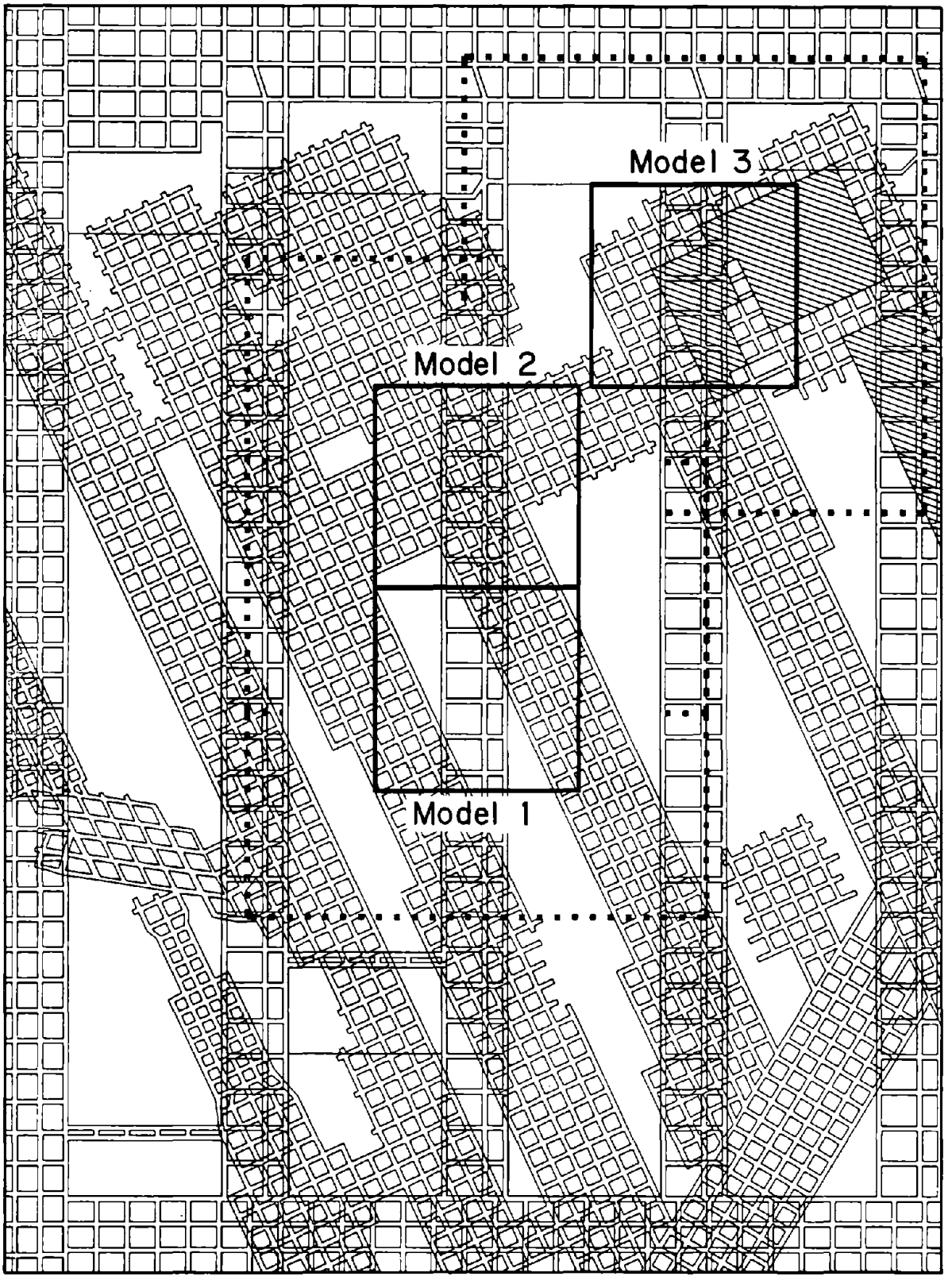

Figure 6.—Multiple-seam mine configuration.

140- by 120-ft and 60- by 120-ft gate pillars. Owing to the relative skewed orientation, however, the room-and-pillar workings in the upper seam were not aligned with the grid. Nevertheless, the 10-ft fine mesh elements were used to approximate the boundaries of the abutment and chain pillars as closely as possible. The rock mass surrounding the coal was modeled with an elastic modulus of 750,000 psi, a Poisson's ratio of 0.25, and a density of 158 lb/ft^3. Strain-softening coal properties were used in a manner similar to that described earlier; four coal stress-strain curves are correlated in the model with the location of the element in respect to the rib. These rock mass properties and coal stress-strain curves are similar to those developed in the calibration of the Olga Mine model. However, the exact coal properties used in these multiseam models have been calibrated such that the abutment pillars in the lower seam fail adjacent to the tailgate corner when they are located under barrier pillars in the upper seam, as was observed in the field (*12*).

In each of the three models, the longwall face was extracted in 14 separate 10 ft face advances (or steps). In each of these steps, the dissipated energy values were calculated for the entire fine mesh. However, since the majority of face bumps that occurred at this mine were concentrated near the tailgate, the dissipated energy associated with this area was of particular interest and is illustrated in figure 7. It can be seen in this graph that generally the highest dissipated energy values were observed when mining was conducted beneath a barrier zone (model 1), and successively lower energy values were present when mining beneath room-and-pillar sections (model 2) and gob zones (model 3).

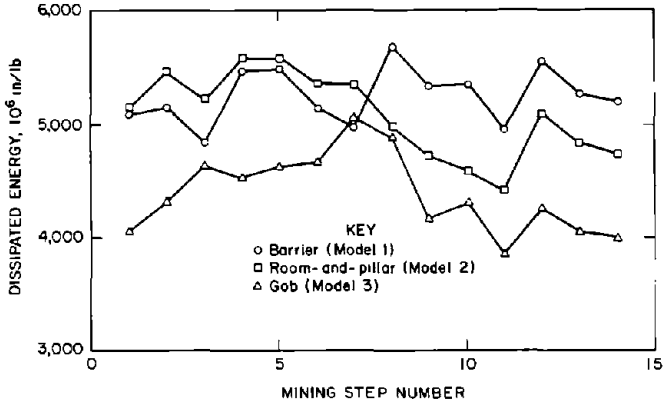

Figure 7.—Dissipated energy from tailgate corner of panel.

These dissipated energy results are encouraging in that the model trends generally match observed pillar responses in the field. That is, energy values are generally high in those multiple-seam settings associated with observed bumps. However, to further understand the energy results, it is instructive to observe the spatial distribution of the dissipated energy (fig. 8). The total magnitude of dissipated energy associated with areas beneath room-and-pillar sections and barrier pillars are similar for the first eight model steps (fig. 7). However, it can be seen in figure 8 that much of the dissipated energy in the room-and-pillar configuration results from the failure of the small pillar adjacent to the longwall panel. Once the small pillar reaches its residual stress state, the total magnitude of the dissipated energy in the room-and-pillar configuration (model 2, fig. 7) decreases significantly (steps 8-14). The larger abutment pillar in model 2 does not fail (reach residual stress) and, thus, continues to limit the transfer of load from the adjacent gob to the active panel. In contrast, under the barrier pillar (model 1), the early failure of the large abutment pillars outbye the face contributes to higher stress on the tailgate corner of the longwall panel and face. These higher stresses directly correlate to larger amounts of dissipated energy along the tailgate edge of the panel ahead of the face (fig. 8). This observed dissipated energy response agrees with the previous postulation that the failure of tailgate abutment pillars contributes to longwall face bumps by allowing abutment stresses to override the pillar system. In this multiple-seam situation, an energy analysis, such as the one described, may provide a tool for evaluating the bump potential of alternative gate pillar designs.

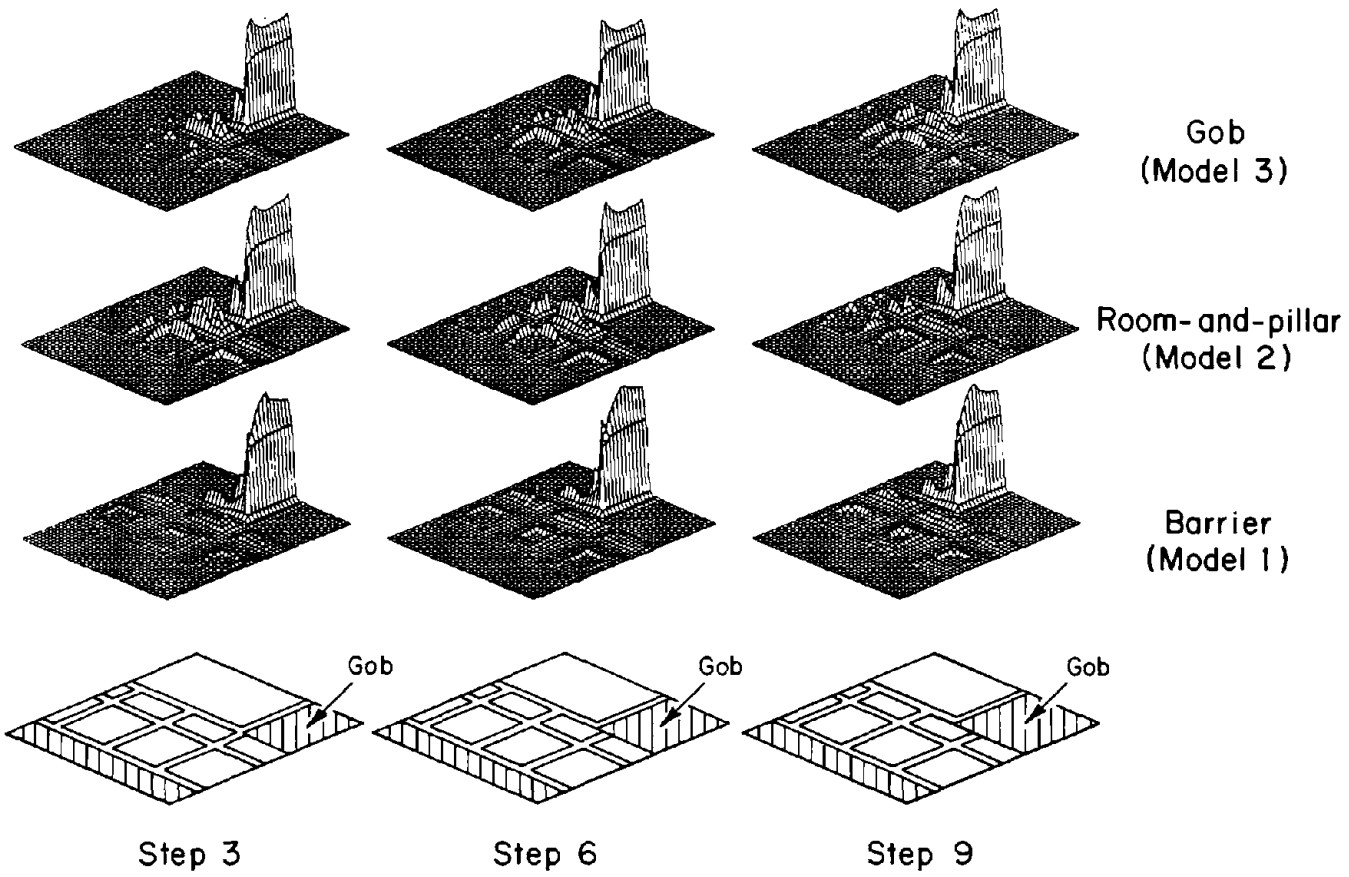

Figure 8.—Dissipated energy from steps 3, 6, and 9.

BACK CALCULATION OF THE ENERGY FROM AN ACTUAL BUMP EVENT

The third example of using energy calculations for mine design in bump-prone ground is the back calculation of the dissipated energy from an actual bump event. The specific site chosen for this back calculation was the 9-Right section at the Olga Mine located in McDowell County, WV. This section of the Olga Mine had been heavily instrumented with coal stress cells, coal extensometers, convergence stations, and microseismic transducers in the mid-1980's as part of an earlier Bureau coal bump research effort. The detailed monitoring and observation of the strata behavior in 9-Right provided valuable insight into the causes and possible control of coal bumps (*14-15*). Also, the abundance of convergence and stress data available from the instrumented 9-Right section provided excellent information for model calibration.

The Olga Mine operated in the Pocahontas No. 4 Coalbed, which is a friable coal with an average unconfined compressive strength of 2,400 psi (for 2-in cubes) (*14*). In the 9-Right study area, the coal averaged 66 in thick and the overburden ranged between 1,400 and 1,600 ft. The immediate and main roof at Olga is the very massive, strong, and stiff Eckman sandstone. Similarly, the floor of the No. 4 Coalbed in the 9-Right area is composed of 0 to 5 ft of siltstone and/or shale underlain by 50 to 75 ft of the massive Upper Pocahontas Sandstone, which does not heave or break readily.

At the time of the field study, mining at Olga was conducted exclusively by room-and-pillar methods using continuous mining machines, and the majority of the coal extraction was pillar retreat mining, which involved removing old barrier pillars that had been left to protect access roadways driven many years previous. The 9-Right section of the mine was initially chosen for the instrument site because it contained large (350- by 160-ft) barrier pillars (pillars A-G in figure 9) which were of the same size and shape as the pillars involved in previous bumps (*14*). The configuration of the study area at the beginning of the field investigation is illustrated in figure 9*A*. The full-extraction mining method at Olga involved first splitting the 350- by 160-ft barrier pillars into 55- by 70-ft chain

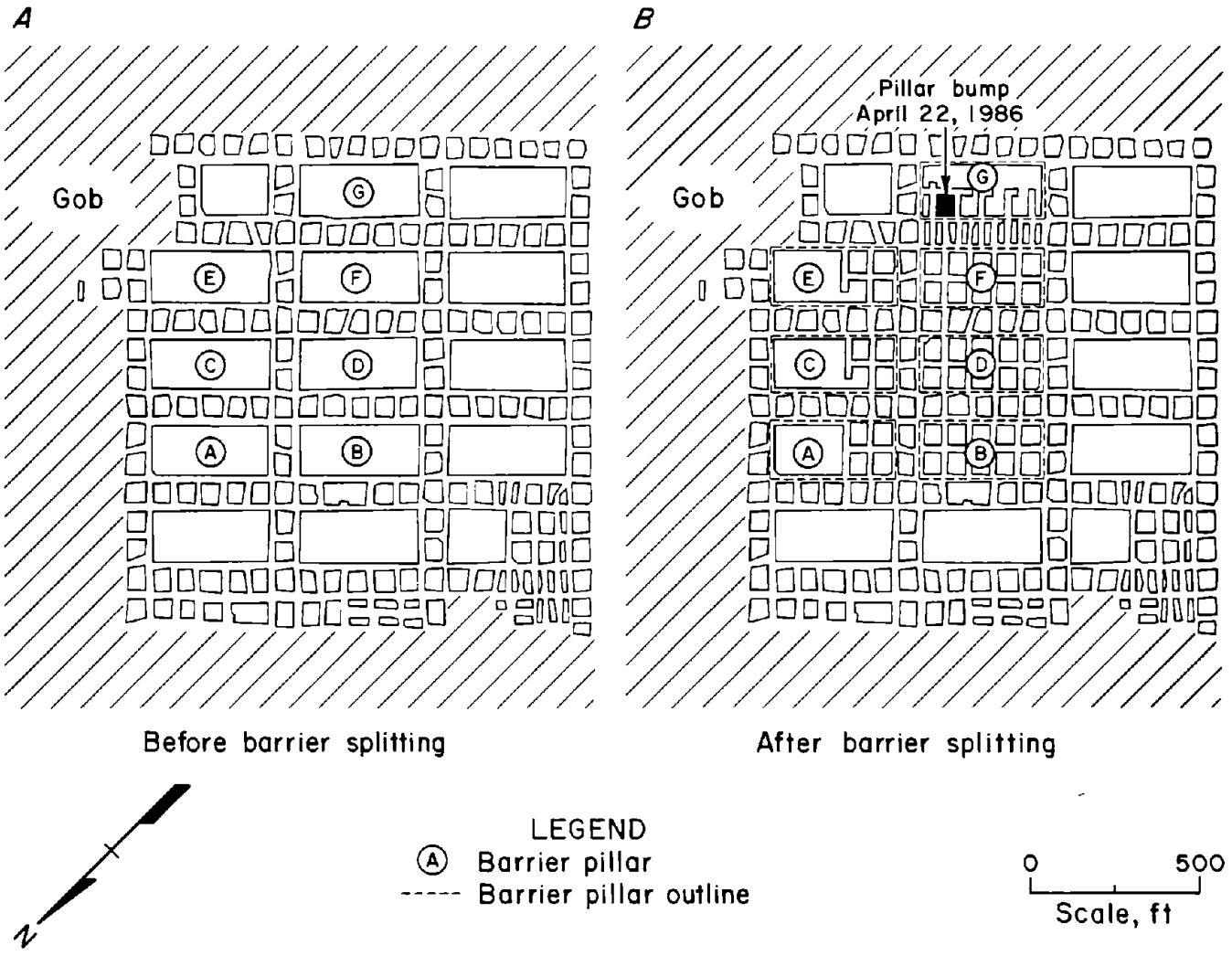

Figure 9.—The 9-Right section at the Olga Mine. *A*, Before barrier splitting; *B*, after barrier splitting.

pillars, then pulling the chain pillars in a retreating pillar line. During the time of the study, the large barrier pillars B, D, and F were each split into 10 chain pillars (fig. 9*B*). At the same time, barriers A, C, and E were each partially split into four chain pillars on the right, leaving a 200- by 160-ft barrier pillar on the left. The barrier pillar splitting in 9-Right was discontinued on April 22, 1986, when a lost-time injury occurred from a chain pillar bump during the splitting of barrier pillar G (fig. 9*B*). After the bump, a 9 by 9 array of 55- by 70-ft chain pillars had been outlined (fig. 9*B*). These chain pillars were subsequently pulled using the unique Olga Mine pillar recovery method explained earlier (*14*).

The first step toward back calculating the dissipated energy from the bump was to calibrate the model input parameters using actual field observations. In this calibration procedure, the input values for the elastic moduli of the coal, the elastic moduli of the surrounding media, and the failure strength of the coal were estimated by a systematic process in which the parameters were adjusted until the model results corresponded as closely as possible to actual observed convergence and pillar behavior. Details of this calibration were presented in an earlier paper (*10*) and will not be further discussed, except that the rock mass properties and coal stress-strain curves produced from the calibration and used in this back calculation are the same as given previously in the cut sequence model and in figure 2.

The second step in back calculating the dissipated energy from the bump was to formulate the 9-Right section of Olga into a model that specifically detailed the April 22, 1986, bump occurrence. The exact mining steps used in this MULSIM/NL model are shown in figure 10. Each modeled step consisted of 2 to 16 extracted elements, but since each group of elements was extracted in one location at approximately the same time, the energy calculations

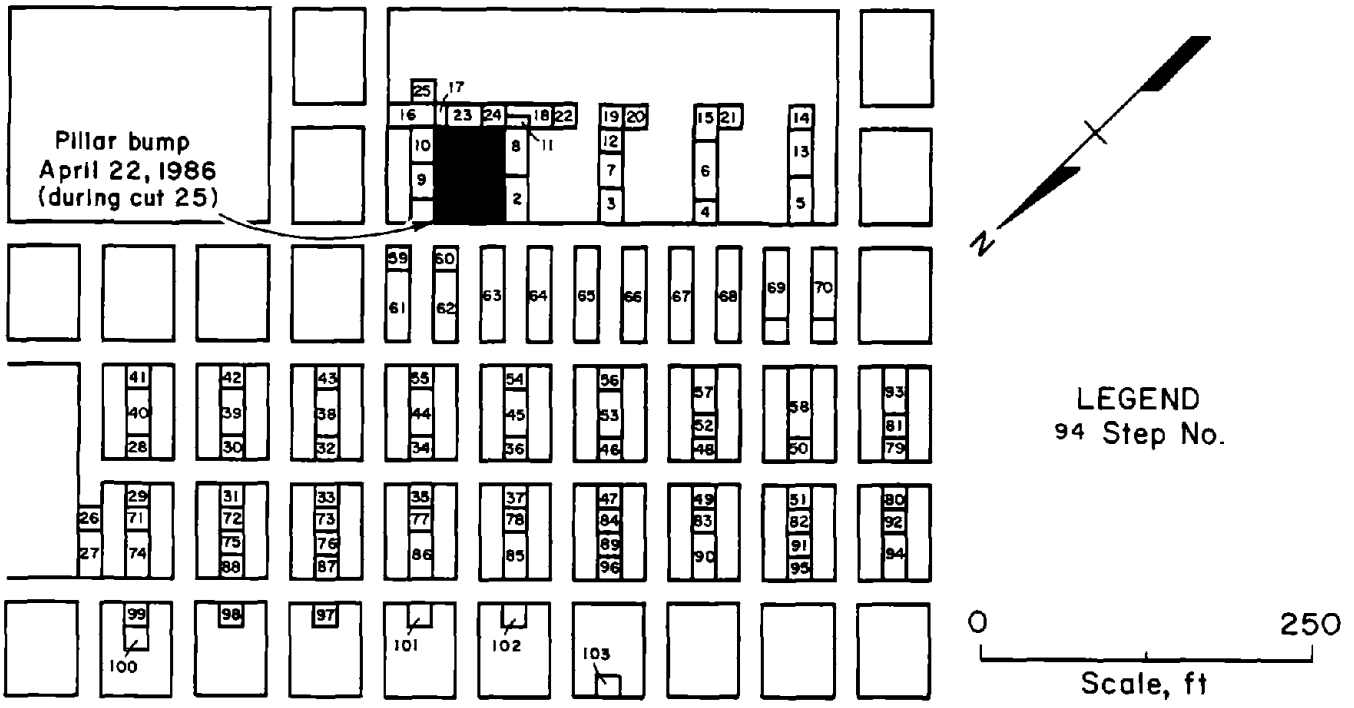

Figure 10.—Detailed cut sequence used in the Olga model.

from this model are assumed to be associated with one extraction event (step) at a specific location. To normalize the values of the energy calculations between different steps, all subsequent energy values are weight-averaged by dividing by the number of elements extracted in that particular step.

Figure 11 presents the energy results from the back calculation model and contains the changes in dissipated strain energy plotted against the mining step. When examining this figure, the absolute value of the dissipated energy is not important for analyzing bump potential since its absolute magnitude can vary greatly depending on model input parameters (*7*). Instead, it is the relative magnitude of successive dissipated energy values that can highlight an increase in energy activity and may be indicative of bump potential. In consideration of this point, two of the highest peaks in the dissipated strain energy curve in figure 11 correspond to steps 23 and 25. This result is encouraging since both steps 23 and 25 directly preceded and were in the area of the April 22d bump. Other steps in the model (30-37 and 46-49) also show considerable increases in dissipated strain energy. A look back at figure 10 shows that the extracted elements in these later steps with large increases in dissipated strain energy are what the Olga miners call "bump" cuts because this type of initial cut into a pillar has often been associated with bump activity.

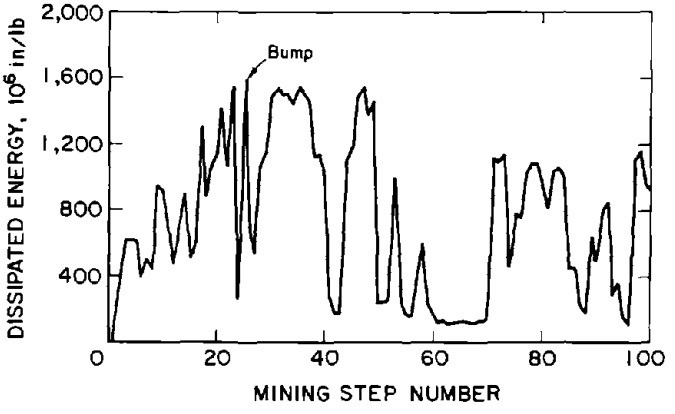

Figure 11.—Dissipated energy from the Olga model.

The question naturally arises as to why an actual bump occurred during step 25, but no noticeably large bumps occurred during the other mining steps, which also showed large increases in dissipated energy. One point to consider is the idea of the spatial and temporal density of the dissipated energy as mentioned earlier. The analyzed bump was associated with large dissipated energies from steps 23 and 25, both of which occurred in close proximity to and in the same time frame as the bump (fig. 12). On the other hand, the large dissipated energies associated with cuts 30-37 and 46-49 come from isolated cuts in separate pillars distributed over the section. As a second possible

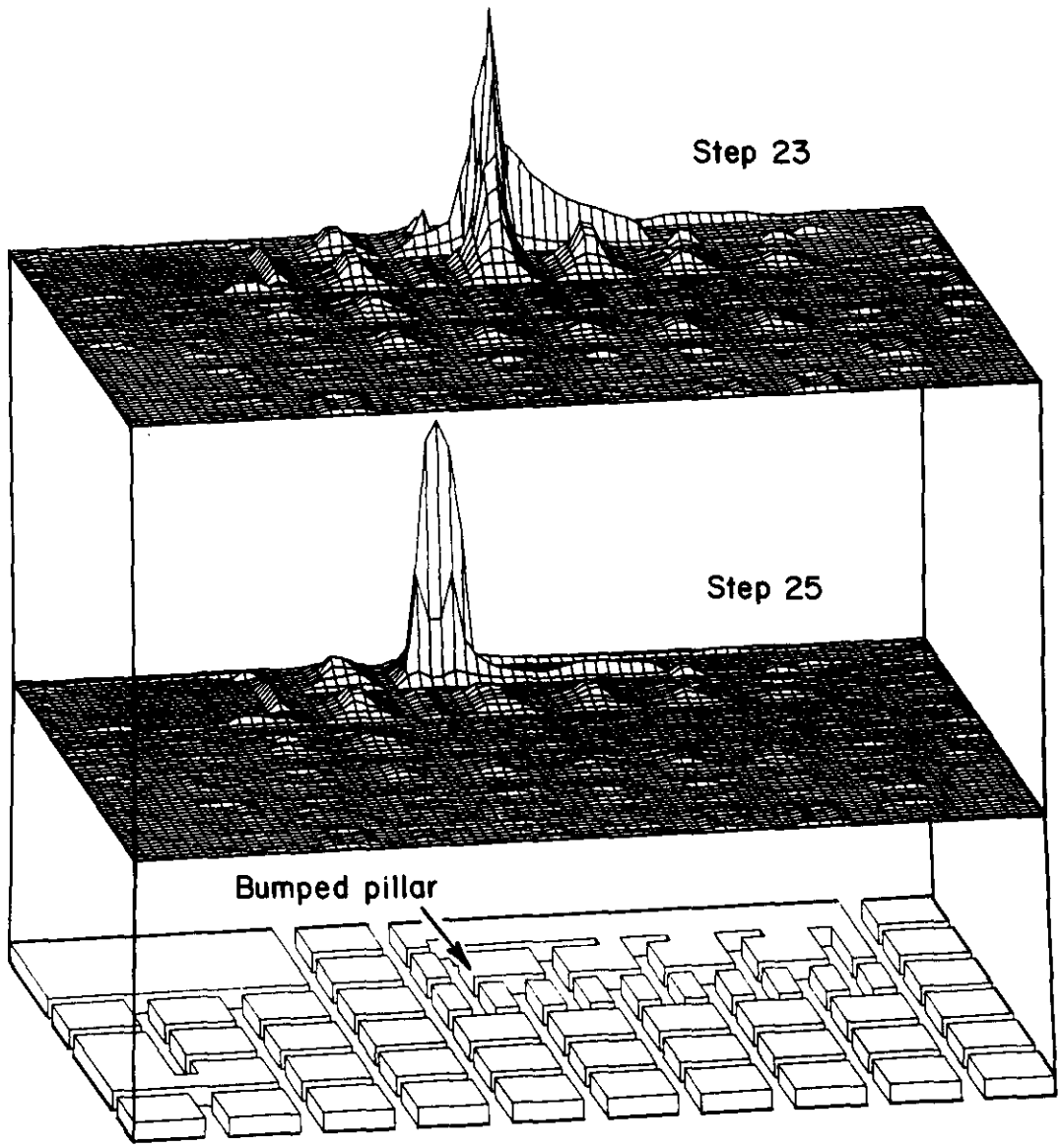

Figure 12.—Dissipated energy for steps 23 and 25.

explanation for the indefinite outcome of the dissipated energy analysis, it should always be considered that the model does not account for all of the possible inhomogeneities of the mining environment which may, in reality, determine the exact timing and location of a coal bump. For instance, some pillars may be slightly different (stronger, partings, slickensided, etc.) than others; the pillar may require some anomalous seismic source to trigger the actual dynamic failure; or the local mine stiffness may change from one location to another irrespective of the pillar configuration that is modeled. Any of these situations, and many others, could just as likely explain the exact timing and location of an actual bump and the reason why the dissipated energy calculated by the model does not unequivocally predict the bump occurrence.

However, the main point to be made from this entire back calculation of dissipated energy is that the model did show a large amount of dissipated energy in the same place and at approximately the same time as the actual lost-time bump accident and this energy behavior correlates well with the observed bump. Also, the model consistently indicates large increases in dissipated energy in general situations that historically have had a high incidence of bumps (i.e., the initial "bump" cut into the

pillars). Thus, the model appears to fairly accurately associate large increases in dissipated energy with potential bump situations and shows promise as a tool for investigating the coal bump potential of a mining plan.

CONCLUSIONS

The research presented in this paper has demonstrated the application of strain energy calculations as a mine design tool for bump forecasting in a room-and-pillar cut sequence analysis, a multiple-seam longwall analysis, and a back calculation of an actual bump event. In each of these analyses, the calculated amount of dissipated energy was found to correlate with the bump potential that was actually observed in the field. Also, the capability of the numerical models to quantify the relative bump potential of various mining plans and to extrapolate the relative bump potential to the design of new and different mining plans has been demonstrated.

Limitations to the practical utilization of the energy calculations also were mentioned in the paper. Essentially, the energy calculations were found to be extremely sensitive to the value of the geologic input parameters. The uncertainty of these geologic parameters and the impossibility of modeling all geologic anomalies that may be present in the field impose some strict limitations on the practical extension of energy calculations. However, the sensitivity of the energy calculations to geologic input parameters may very well parallel the true situation underground where small differences in geology or rock properties may ultimately dictate the precise location and timing of coal bumps.

The concept of a spatial and temporal density for the energy values was also presented. In each of the case studies, it was demonstrated that the location and chronology of large dissipated energy values was instructive to understanding the observed bump behavior. Thus, in addition to the total magnitude of the dissipated energy, it appears that the spatial and temporal densities of the energy may provide additional necessary insight for definitive energy analysis.

Even though the practical utilization of energy calculations may be limited, analysis of the energy values generated by the MULSIM/NL model can provide considerable insight into the possible locations, timing, and geometries associated with potential coal pillar bumps. In particular, with the judicious choice of input parameters and the proper analysis of the output energy values, it appears that the dissipated energy calculations may be used as a tool to investigate the coal bump potential of a mining plan or cut sequence. In fact, energy investigations of active bump-prone mines utilizing the techniques presented in this paper should increase operator awareness of potential bump situations and therefore help minimize bump-related accidents.

REFERENCES

1. Cook, N. G. W., E. Hoek, J. P. G. Pretorious, W. D. Ortlepp, and M. D. G. Salamon. Rock Mechanics Applied to the Study of Rock Bursts. J. S. Afr. Inst. Min. and Metall., v. 66, 1966, pp. 436-528.

2. Salamon, M. D. G. Elastic Analysis of Displacement and Stresses Induced by Mining Seam or Reef Deposits (Part I). J. S. Afr. Inst. Min. and Metall., v. 64, No. 4, 1963, p. 128-149.

3. Hodgson, K., and N. C. Joughin. The Relationship Between Energy Release Rate, Damage, and Seismicity in Deep Mines. Proc. 8th U.S. Symp. on Rock Mech., 1966, pp. 194-203.

4. Salamon, M. D. G. Energy Considerations in Rock Mechanics: Fundamental Results. J. S. Afr. Inst. Min. and Metall., v. 84, 1984, pp. 233-246.

5. Gay, N. C., W. D. Ortlepp, J. A. Ryder, O. Steffen, and H. Wagner. The Future of Rock Mechanics in South Africa. World Min. Equip., Jan. 1984, pp. 36-39.

6. Crouch, S. L., and C. Fairhurst. The Mechanics of Coal Mine Bumps and the Interaction Between Coal Pillars, Mine Roof, and Floor. BuMines OFR 53-73, 1973, 88 pp.

7. Zipf, R. K., and K. A. Heasley. Decreasing Coal Bump Risk Through Optimal Cut Sequencing with a Non-Linear Boundary Element Program. Proc. 31st U.S. Symp. on Rock Mech., 1990, pp. 947-954.

8. Maleki, H., J. Aggson, F. Miller, and J. F. T. Agapito. Mine Layout Design for Coal Bump Control. Proc. 6th Int. Conf. on Ground Control in Mining, 1987, pp. 32-46.

9. Zipf, R. K. MULSIM/NL Theoretical and Programmers Manual. BuMines IC, 1992, in press.

10. Heasley, K. A. An Examination of Energy Calculations Applied to Coal Bump Prediction. Proc. 32d U.S. Symp. on Rock Mech., 1991, pp. 481-490.

11. Campoli, A. A., C. A. Kertis, and C. A. Goode. Coal Mine Bumps—Five Case Studies in the Eastern United States. BuMines IC 9149, 1987, 34 pp.

12. Zelanko, J. C., G. A. Rowell, and T. M. Barczak. Analysis of Support and Strata Reactions at a Bump-Prone Eastern Kentucky Coal Mine, 1991 SME Annual Meeting and Exhibit, Denver, CO, Feb. 25-28, 1991, SME Preprint No. 91-91, 8 pp.

13. Campoli, A. A., T. M. Barton, F. C. Van Dyke, and M. Gauna. Mitigating Destructive Longwall Bumps Through Conventional Gate Entry Design. BuMines RI 9325, 1990, 38 pp.

14. Campoli, A. A., D. C. Oyler, and F. E. Chase. Performance of a Novel Bump Control Pillar Extracting Technique During Room-and-Pillar Retreat Coal Mining. BuMines RI 9240, 1990, 40 pp.

15. Condon, J. L., and R. D. Munson. Microseismic Monitoring of Mountain Bumps and Bounces: A Case Study. Proc. 6th Int. Conf. on Ground Control in Mining, 1987, pp. 1-9.

MSHA'S SIMPLE TECHNIQUE FOR PREDICTING STRESS DISTRIBUTION IN A MINE PANEL

By M. Terry Hoch,[1] George J. Karabin,[2] and James M. Kramer[3]

INTRODUCTION

People in the coal industry occasionally need to know how a room-and-pillar design will affect ground stability. Numerical modeling is effective in predicting stresses, but it is slow and requires a certain amount of technical prose to operate. A useful tool would be a computer program that quickly and easily determines the stability of a mine layout. The Mine Safety and Health Administration's (MSHA) Technical Support group is developing software to accomplish this goal. A significant portion of the development requires creating an algorithm to predict the effect that room-and-pillar geometry has on pillar stress.

This paper presents a technique that predicts the stress distribution, amount of yielding, and thus the stability in a series of pillars. The pillars can be different shapes and sizes. The first part of the paper introduces a curious equation for estimating stresses in a coal seam. The basis of the equation is from elastic theory concerning flat elliptical cracks. It is feasible to perceive an excavation in a coal seam as a crack in an infinite mass. The stress zone of influence at the crack tip is the same zone of influence that extends into a coal rib. The only parameters necessary for elastic analysis are entry width and seam depth. The equation compares well to the results of numerical modeling.

The second topic involves procedures for superpositioning the stress disturbance induced by each and every entry. A mine panel contains a thin grid of tunnels. Each entry or crosscut has an additive effect on the stress distribution in the pillar supports. To obtain the stress distribution in a mine panel, it is necessary to superposition the stress zone of influence for each excavation. The pillar equation and superposition technique permits instantaneous, two-dimensional, plane strain analysis of mine panels. A three-dimensional type of analysis may be possible.

The final section describes a procedure for simulating pillar yield. An assumption is made that coal behaves in an elasto-plastic manner. A technique is introduced to simulate pillar yield. The yield method is empirical in its present form. A more complicated "elastic" solution is available—it can be incorporated into the software at a later date. A dynamic zone of influence describes the area affected by the pillar yielding. As the pillar yields, this zone of influence increases. Several formulas are available that describe the stress distribution in a yielding coal seam. Most of these formulas are empirical in derivation. Any one of these equations can be used in the yield analysis—it is simply a matter of substituting the equation.

Computer software will incorporate all techniques described in this paper. The software already operates as a macro in Lotus 1-2-3 spreadsheet. Hewlett Packard markets a handheld computer that contains Lotus 1-2-3 as its operating system. It should be possible to operate the software in this palm-size computer. This would be convenient for performing analysis in the field.

Rock mechanics is not an exact science, especially in coal-bearing strata. Numerical techniques must make many assumptions to effectively model rock behavior. This paper describes techniques that predict stress distributions that correlate well with those predicted by two-dimensional numerical modeling. The MSHA technique is extremely fast and simple to use.

DEVELOPMENT OF THE PILLAR EQUATION

For years, MSHA Technical Support has been discussing a method for simulating pillar yield. In 1987, George Karabin and Larry Lauritzen wrote an in-house report describing computer algorithms that progressively yield pillars by comparing the stress on the pillar edge to the strength of the edge. The tributary area method predicts the stress, and Wilson's equation determines the strength of the edge. As the pillar yields, the insupportable load is transferred to adjacent pillars. This paper expands these techniques by incorporating an equation that predicts the stress distribution in the elastic core and

[1]Chief.

[2]Supervisory civil engineer.

[3]Mining engineer.

Roof Control Division, Technical Support, Pittsburgh Health and Safety Technology Center, Mine Safety and Health Administration, U.S. Department of Labor.

defines the dynamic zone of influence caused by the yielding coal. A superpositioning technique makes everything work to correlate well with numerical modeling predictions.

The MSHA Elastic Stress Equation (MSHA-ESE) was an accidental discovery.[4] A project was underway to better understand how a virgin stress field is altered by the presence of an entry. Two-dimensional numerical modeling using FLAC[5] software demonstrates how an excavation alters the stress distribution in the model. To speed up the analysis, FLAC output was loaded directly into Lotus 1-2-3 spreadsheet software in hopes of constructing a mathematical relationship for pillar stress distribution. Halfway through the FLAC investigations, a request came for a technical review of two reports written by R. Karl Zipf, Jr. (*1-2*).[6] After reviewing the reports and experimenting with a particular equation, a new equation emerged.

One of Zipf's reports referred to an analytic solution for stresses surrounding a crack. According to Zipf, Jaeger, and Cook (*3*) provide certain analytic solutions essential for checking boundary element method programs. The solutions are for an elliptic crack of length 2c subject to a stress P at infinity perpendicular to this crack plane (fig. 1). In more practical terms, this problem corresponds to an infinitely wide (into the page) slot of length 2c in an infinite medium. The vertical stress distribution along the edge of this opening is given by

$$\sigma_{yy} = P \coth(\epsilon) \qquad (1)$$

$$\epsilon = \cosh^{-1}\left[\frac{x}{c}\right],$$

where σ_{yy} = vertical stress into rib adjacent to crack,

P = stress at infinity perpendicular to the crack,

x = distance into rib,

and c = half the crack width.

This equation applies along the x axis for x/c > 1. Normal convergence across this opening is given by

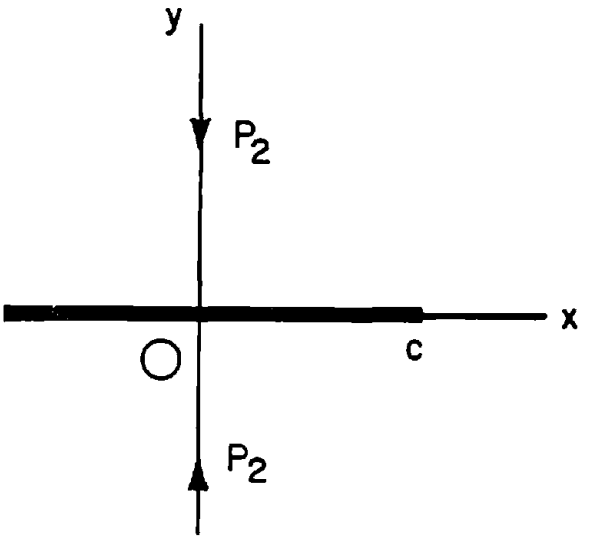

Figure 1.—Elliptical crack of length 2c.

$$V = \frac{4(1 - \sigma_{yy}^{\ 2})}{E} P\sqrt{(c^2 - x^2)}\ , \qquad (2)$$

where v = vertical convergence,

and E = Young's modulus of roof.

A software package named DERIVE[7] can analyze and simplify many complex mathematical equations. A very interesting thing happened while experimenting with equation 1 using DERIVE. After assigning values to the variables P and c (i.e., P = 1,000 and c = 50), a query was made for DERIVE to generate an equation of σ_{yy} in terms of x. DERIVE responded with the equation

$$\sigma_{yy} = \frac{1000x}{\sqrt{(x^2 - 2500)}}. \qquad (3)$$

It was immediately obvious the relationship was

$$\sigma_{yy} = \frac{Px}{\sqrt{(x^2 - c^2)}}. \qquad (4)$$

Equation 4 implies the ability to predict rib stresses with only knowledge of the seam depth and entry width. This equation is given the name (MSHA-ESE) MSHA Elastic Stress Equation. To test the validity of the equation, FLAC will analyze cracks of various widths and seam depths. A comparison will be made to the prediction of

[4]This paper includes several pillar equations of different names. In order to avoid confusion, it was decided to name the new equation the MSHA Elastic Stress Equation (MSHA-ESE).

[5]FLAC (Fast Lagrangian Analysis of Continua) is a commercial two-dimensional modeling software package marketed by Itasca Consulting Group Inc., Minneapolis, MN.

[6]Italic numbers in parentheses refer to items in the list of references at the end of this paper.

[7]Soft Warehouse Inc., Honolulu, HI.

the MSHA-ESE. Figure 2 is the result of the first comparison. In this model, the FLAC elements are 5 ft square (seam height = 5 ft).[8] Note the only discrepancy between the MSHA-ESE and the FLAC data is in the element immediately adjacent to the entry (2.5 ft into the rib). The question arises: Is this discrepancy due to the MSHA-ESE, or is it a limitation in FLAC due to edge effects? To study this problem, it is necessary to increase resolution by reducing element size of the FLAC model. Figure 3 (1-ft elements) demonstrates that with smaller elements, the only difference is at the edge element—stresses match well at 2.5 ft into the rib. This indicates that it is FLAC's limitations that account for the discrepancy.

To prove the validity of the MSHA-ESE, it is necessary to construct additional FLAC models varying the seam depth and entry widths.[9] The tabulation below displays the values of "P" and "c" used for each study. In each study, the MSHA equation compared well with the FLAC solution.

Study	Variable P, psi	Variable c, ft
2 . . .	1,000	50
3 . . .	1,000	100
4 . . .	1,000	25
5 . . .	500	25
6 . . .	250	25

The original formula of Jaeger and Cook (*3*) stipulates that the force is at infinity and the model is assumed homogeneous, which is not a real-life situation. In reality, the loading force is a gradient, and the rock is far from homogeneous. Two additional models investigate the effect on stress distribution caused by these differences.

[8]Since the element size is 5 ft, this implies that the crack thickness is 5 ft which is the average coal seam thickness; therefore, the name "entry" will be substituted for "crack."

[9]Seam depth is directly related to the force "P" used in the equation. The variable "c" is one-half the entry width.

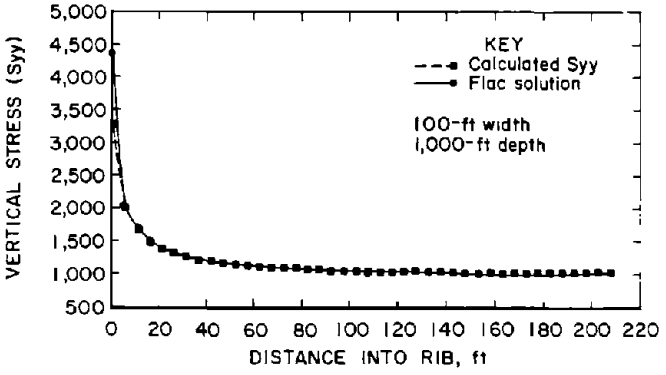

Figure 2.—Crack with 5-ft elements.

Figure 4 shows a model in which the coal's modulus is reduced by 50 pct—there is a slight difference between the FLAC solution and the pillar equation. It should be easy to compensate for this deviation. In figure 5, a gradient stress field is added to the model to simulate the effects of gravity. The results compare well with the MSHA-ESE. All in all, it appears the pillar equation will effectively model mine pillars.

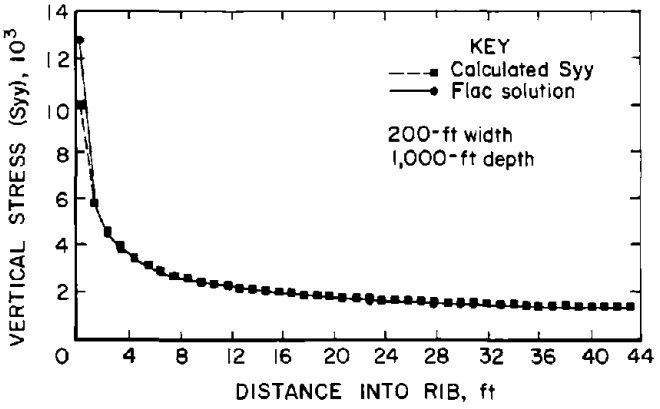

Figure 3.—Crack with 1-ft elements.

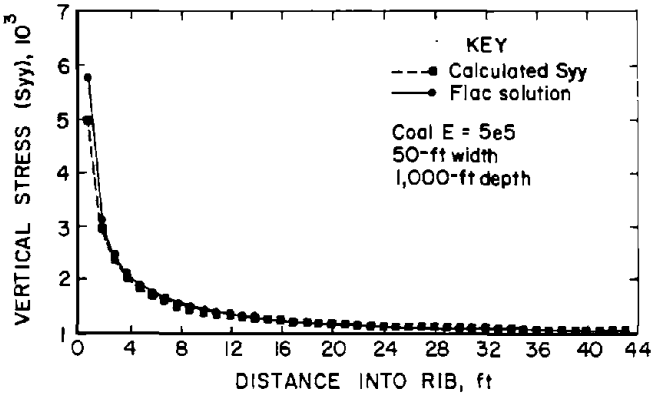

Figure 4.—Coal modulus 50 pct of surrounding strata.

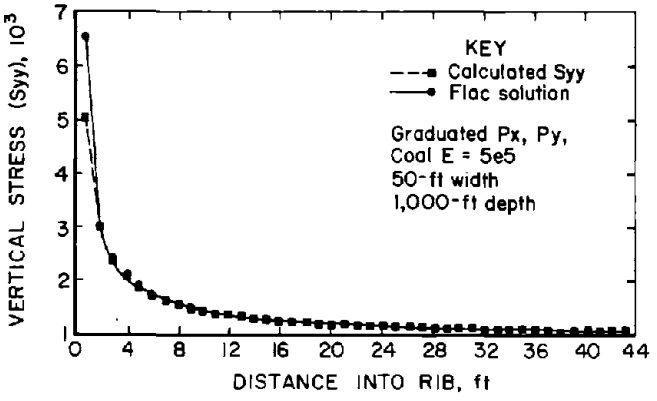

Figure 5.—Graduated stresses added to simulate gravity loading.

DETERMINATION OF PRINCIPAL STRESSES WITHIN PILLARS

Figure 6 shows σ_{yy} and σ_{xx} as predicted by FLAC. It can be seen that the σ_{xx} curve has the same shape as the σ_{yy}; however, it is a fraction less in amplitude. This fractional amount can be approximated by the expression:[10]

$$\sigma_{xx} = \gamma\sigma_{yy}, \quad (5)$$

where σ_{xx} = horizontal stress,

σ_{yy} = vertical stress,

and γ = Poisson's ratio.

SUPERPOSITION OF EQUATION TO SIMULATE PANELS

The MSHA-ESE successfully predicts the stress distribution for a single excavation. This section will discuss methods for determining the additive effect from several closely spaced excavations such as encountered in room-and-pillar mining.

The first subsection below describes modeling a single pillar subjected to the effects of two entries. The following subsection expands the technique to account for the combined effects from all entries that make up the mine panel. Using superposition, it is possible to combine the stress influence zone from all entries onto each and every pillar in the model. The last subsection discusses special treatment for small pillars.

STRESSES ON SINGLE PILLAR

There are three distinct σ_{yy} forces at work on a single pillar sandwiched between two entries: (1) the in situ stress due to gravitational loading, (2) the stress induced from the presence of the left entry, and (3) the stress due to the presence of the right entry (fig. 7).

Because the in situ (gravity) stress is considered separate from the entry-induced stress, the MSHA-ESE (equation 4) takes a slightly different form. The formula remains similar to the original; however, it is now necessary to subtract the in situ gravity stress P as shown below:

$$\sigma_{yy} = \frac{Px}{\sqrt{(x^2 - c^2)}} - P, \quad (6)$$

where σ_{yy} = additional stress attributed to mine opening,

and P = in situ gravitational stress (a product of depth and unit weight).

Figure 8 plots the superimposed stress distribution on a single pillar.[11]

[10]This has not been validated.

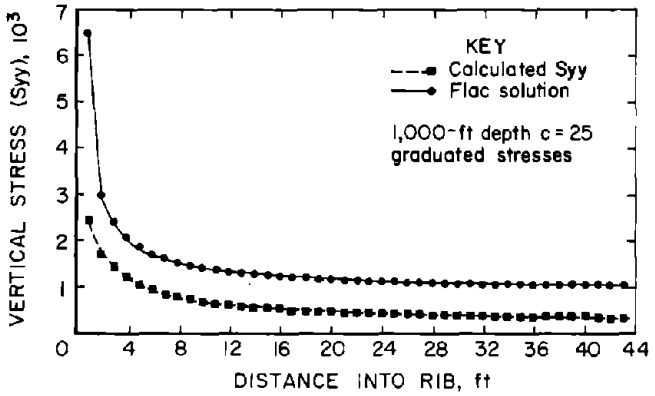

Figure 6.—Comparison of the shape of σ_{yy} and σ_{xx}.

STRESS SUPERPOSITION ON SERIES OF PILLARS

The stress on a series of pillars will be a combination of all the stresses induced by all the entries. Each entry will affect the stress on every pillar in the panel up to the point where the influence zone is far enough away from the entry as to produce a negligible result. The subsection "Zone of Influence" later in this paper will demonstrate this zone to equal the distance 4c. Each entry will affect stress distributions in both right and left directions across the entire panel. By superpositioning all the stress influence zones, it should be possible to accurately predict the stress distribution in the mine panel. Figure 9 demonstrates that superposition accurately predicts stress distribution over a mine panel.

STRESS SUPERPOSITION FOR SMALL PILLARS

Small pillars require additional superposition treatment. A small pillar is any that has a width less than the width of the adjacent entries (i.e., 2c in equation 4). Figure 10

[11]The superposition technique used on some of the earliest work (figs. 8 and 13) was not correct. The lastest superposition technique correlates well with the FLAC solution.

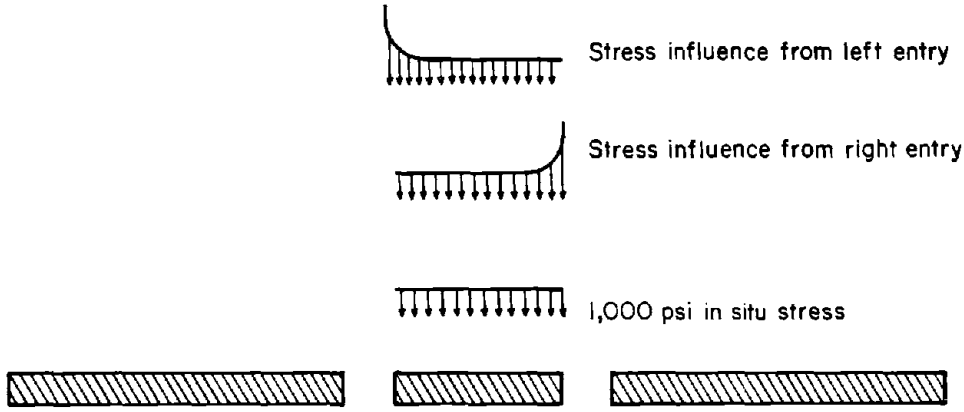

Figure 7.—Superposition of stresses on a pillar influenced by two adjacent entries.

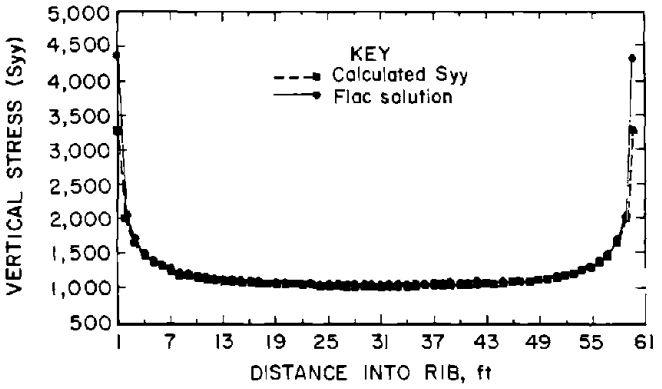

Figure 8.—Stress superpositioning to predict pillar loading. Early attempt; bad superposition technique.

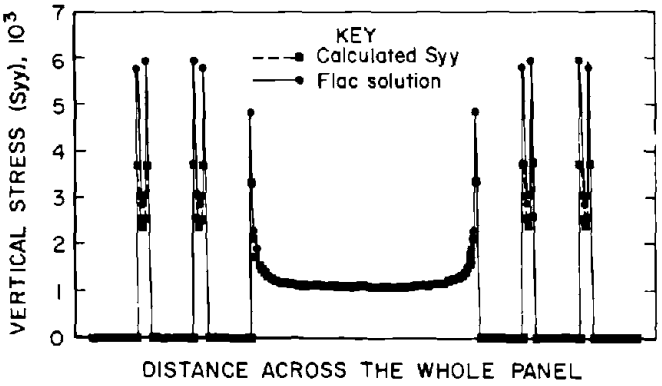

Figure 10.—Panel with small pillars (standard superposition method).

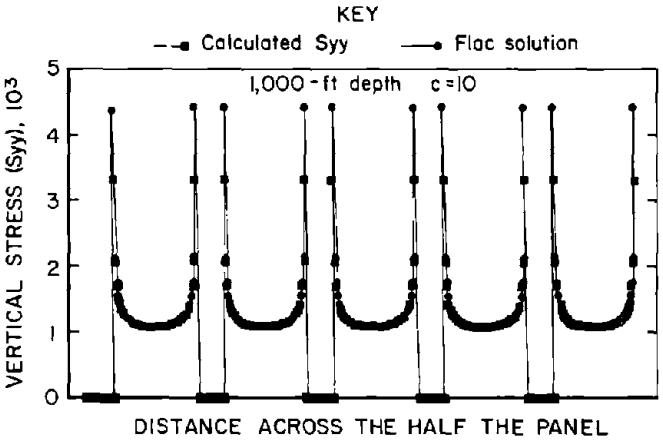

Figure 9.—Stress superpositioning for a series of pillars.

is a stress distribution comparison between FLAC and the standard superposition method. Notice the variance in stress predictions for the 5-ft-wide pillars. There is a small amount of stress that overrides these pillars. This is the cause of the variance. Therefore, it is necessary to average the rideover stress and then redistribute it back onto the pillar.

The rideover stress on one side of the pillar will determine the additional stress to add to that particular edge. The average rideover stress is assigned to variable P in equation 4 to determine the additional edge load. Figure 11 demonstrates how the superposition technique works on 5-ft pillars. Figure 12 illustrates the method on a panel of 20-ft-wide pillars; the center pillar is 5 ft wide.

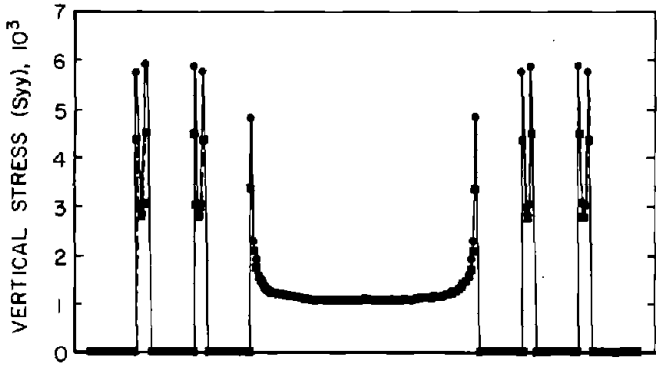

Figure 11.—Panel with small pillar design. Includes four 5-ft-wide pillars and a 100-ft-wide center pillar.

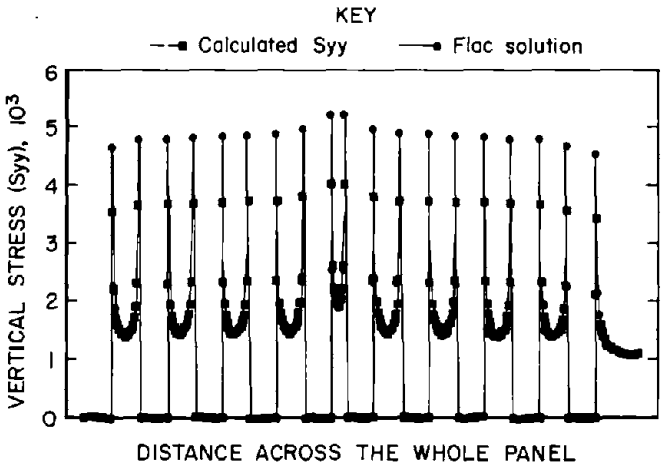

Figure 12.—Panel with 20-ft-wide pillars. Center pillar is 5 ft wide.

SIMULATING YIELDED PILLARS

An assumption is made that pillar behavior is more elasto-plastic then elastic—the pillar yields. It is possible to incorporate failure criteria into the MSHA software. Jaeger and Cook (*3*) provide Griffith failure criteria for flat elliptical cracks. These criteria may be perfectly suited for the pillar equation and superposition method. If so, they will be added at some future date. In the meantime, it should be possible to estimate pillar yield using pillar strength formulas.

The first section below will demonstrate that superposition can model the irregular pillar loading caused by an adjacent yielding pillar. Later sections demonstrate that pillar strength equations can be incorporated into the yielding process in an attempt to simulate the yielding behavior.

In the most critical situation, the pillar would completely yield and not offer any vertical support to the roof. While this situation is unlikely, it is easy to model and will demonstrate how the superposition techniques predict the pillar loading. Following this, an improved method is shown that permits the yielded pillar to retain a residual roof support.

The center pillar (i.e., pillar No. 5) in the model will completely yield and transfer its load to the remaining pillars.[12] Simulating complete pillar yield is simply a matter of removing the pillar, thus creating a very large opening—it is assumed that the yielded pillar does not support any load. This new opening will be the combined widths of yielded pillar No. 5 plus the two adjacent entries (i.e., 20 + 60 + 20 = 100 ft). The large opening will cause the superposition stress to be considerably higher on the ribs adjacent to the yielded pillar. Figure 13 is the stress profile for pillar No. 4 which is next to the completely yielded pillar No. 5.[13] The superimposed MSHA-ESE corresponds well to the FLAC solution. Figure 14 is a stress comparison of the right half of the panel—due to symmetry, the left half should be the same. The fifth pillar completely yields, offering no support to the roof. Superposition accounts for the close comparison between the pillar formula and FLAC.

[12]There are 10 pillars in the FLAC model. Because of symmetry, it is only necessary to plot half the model.

[13]Early superposition technique.

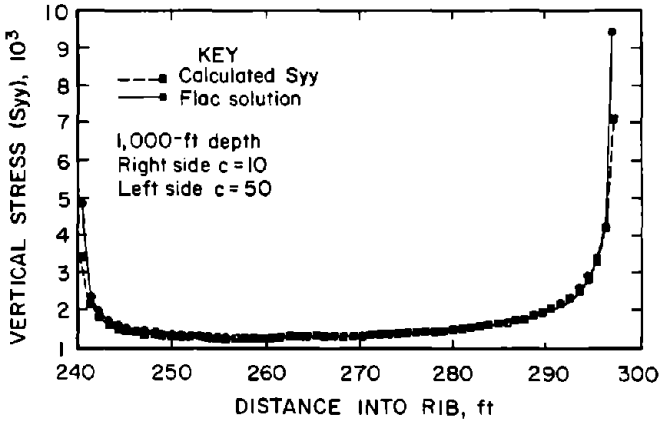

Figure 13.—Fourth pillar adjacent to yielded fifth pillar. Note increased load on right side. Early attempt; bad superposition technique.

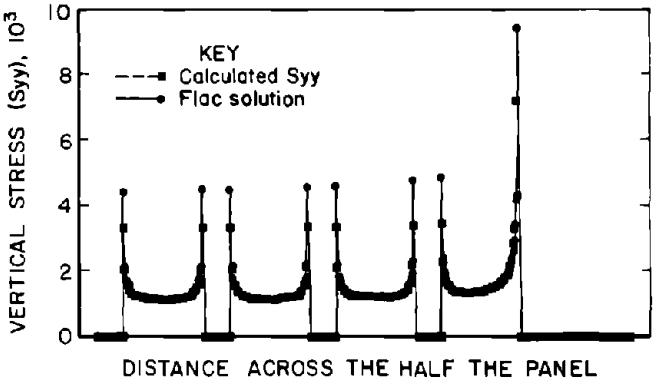

Figure 14.—Half section of panel. Fifth pillar yielded.

SIMULATING PROGRESSIVELY YIELDING PILLARS

The following paragraphs discuss an approach to simulate progressively yielding pillars. For analysis, it is necessary to divide the pillars into equal sections. A comparison is made between the strength of a pillar section and the stress on that section. If the stress exceeds the strength, the pillar yields. There are several equations that predict strength for every section of a pillar. Using these equations and knowing the related stress, it is possible to determine if the section will yield.

PILLAR STRENGTH EQUATIONS

Because of the high stress on the very edge of the pillar, an assumption is made that the pillar edge will fail and this failure will propagate in toward the center of the pillar. There is no confinement on the pillar edge, so the yielded coal supports no vertical load. However, the frictional resistance in the broken coal offers increasing confinement as the vertical load moves inward toward the core. This confinement provides vertical load supporting capacity. The propagation inward will continue until the frictional confinement of the broken coal is sufficient to support the vertical load of the roof. There are several pillar strength equations that predict the residual load-bearing capacity of broken coal.

The amount of load a section of pillar supports increases with confinement (i.e., distance into the rib). Two different techniques predict the load-bearing capacity of the yielded edge. Carr and Wilson (*4*) studied numerical modeling combined with Mohr/Coulomb failure criteria, whereas Mark, Listak, and Bieniawski (*5*) derived the capacity by integrating various popular empirical pillar strength formulas.

The following are some of the more popular empirical formulas for determining the residual load-bearing capacity of a yielded pillar edge. These equations approximate the residual load-bearing capacity as a function of distance from the rib into the pillar core.

The following equations are from Mark, Listak, and Bieniawski (*5*):

Holland-Gaddy/Hustrulid-Swanson: $\sigma_v = 2.65\, S_1 (x/h)^{1/2}$,

Obert-Duvall/Wang: $\sigma_v = S_1 (0.78 + 1.32\, x/h)$,

Bieniawski: $\sigma_v = S_1 (0.64 + 2.16\, x/h)$,

Wilson: $\sigma_v = k\, p' (2x/h + 1)^{k-1}$,

where σ_v = residual load capacity,

S_1 = unconfined compressive strength,

x = distance into rib,

h = height of pillar,

k = triaxial stress factor $= [1+\sin(\phi)]/[1-\sin(\phi)]$ ($\phi = 30° - 37°$),

and p′ = unconfined compressive strength of failed coal at pillar edge (14 psi).

As an initial attempt to model yielding, these empirical formulas will predict the failure stress as a function of depth into the pillar.

ZONE OF INFLUENCE

Saint Venant's rule suggests that an excavation only affects the stress distribution in the immediate area surrounding it. Figures 15 and 16 verify this fact. Figure 15 is from a publication on elasticity (source unknown) concerning radial and tangential stress and Saint Venant's effect. Figure 16 is a plot of the MSHA Elastic Stress Equation (equation 4). Both figures suggest that at a distance 4c from the excavation, the stress distribution is unaffected by the presence of the excavation. Also note in figure 16 the apparent effects of variables P and c in the MSHA equation.

YIELDING TECHNIQUE

The method of yielding incorporates the MSHA-ESE, superpositioning techniques, a pillar strength equation, and the dynamic zone of influence to predict the final stress distribution in a series of pillars. The pillar strength equation will determine the stress distribution in the broken pillar edges. The MSHA-ESE will indicate the stress distribution in the elastic core. The zone of influence will control the area in which conservation of energy is to be applied.

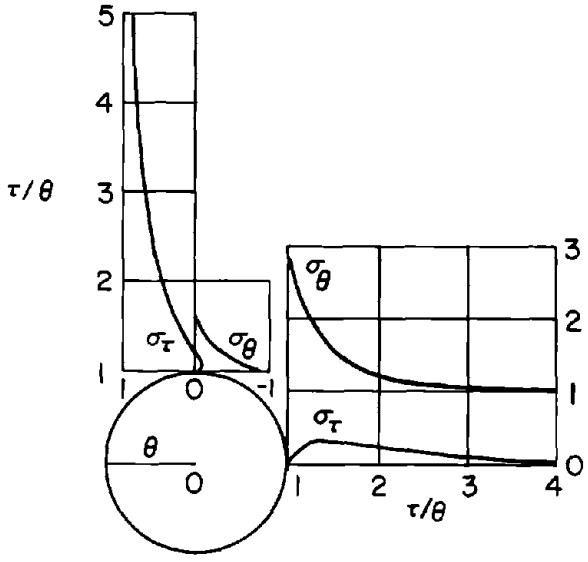

Figure 15.—Stress concentrations along axes of symmetry for circular openings subjected to a uniaxial stress field.

If the pillar completely yields, there is no elastic core, and the pillar strength equation predicts the stress distribution over the entire pillar. The variable c in equation 4 controls the size of the zone of influence (refer to the previous subsection). In a situation of total yield, the variable c extends from the center of the entry to the pillar center.

The failure analysis consists of comparing the strength of the pillar to the stress applied on the pillar. The pillar width is divided into sections. The failure analysis begins on the outermost section and works its way into the center. If the analysis predicts the section to be unstable, the section is allowed to yield. The amount of stress that the yielded portion can no longer support is transferred onto the pillar core. The failure analysis will then proceed on the next section. The process will continue inward until the failure analysis predicts stability. If it is not possible to achieve stability, the pillar will not accept any more load than that predicted by the pillar strength equation.

The MSHA-ESE predicts the stress in the elastic core. As the pillar edge yields, the core becomes smaller and receives increased loading. To reflect this effect, the variable c in equation 4 increases from the pillar edge to the new yield-elastic boundary. This results in an increase in stress on the elastic core as if the fracture section were mined away. However, the fractured pillar edge has a residual load-bearing capacity that must be taken into consideration. To insure conservation of energy, it is necessary to subtract this residual load from the load on the elastic core.

A dynamic zone of influence will dictate the area in which conservation of energy is to apply. This zone is equal to 4c (refer to the previous subsection), where c is equal to the distance from the center of the entry to the yield-elastic boundary. In the yielding process, the variable c increases; therefore, the zone of influence will also increase.

The three-dimensional plot of the empirical pillar strength formula will take on the shape of a pyramid. Similarly, the three-dimensional plot of the MSHA-ESE would take on the shape of an inverted pyramidal depression. To determine the stress acting at any particular section of the pillar would involve complex calculus and is impractical. It is much easier to analyze a thin vertical slice (unity in thickness) through the pillar center. The shape of this slice is similar to the shape of the two-dimensional plot in figure 8.

The yielding process involves dividing the pillar into many equal segments. The analysis begins on the outermost section and works its way into the core. The process can be divided into the following steps: (1) determine the value of c (i.e., the distance from the entry center to the pillar edge or yield-elastic boundary); (2) determine the

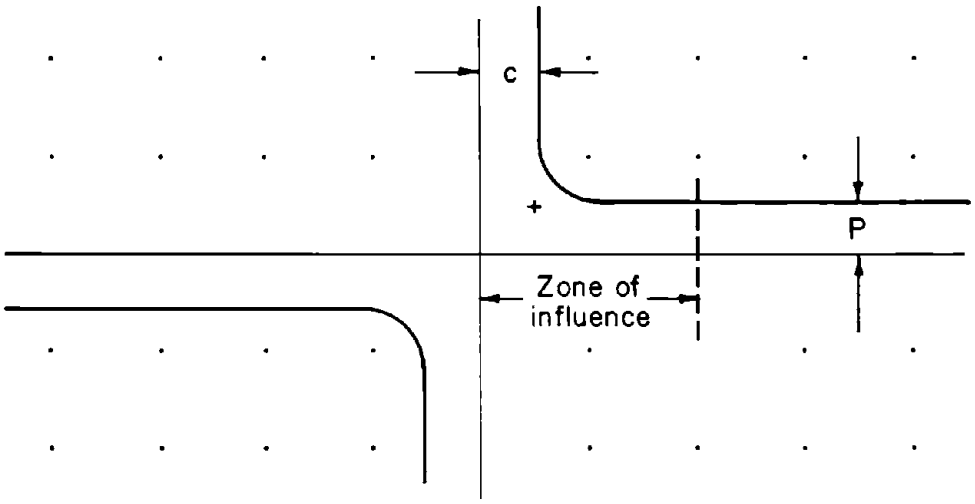

Figure 16.—Stress distribution predicted by MSHA pillar formula. At a distance 4c, the excavation has a minimal effect on stress distribution.

zone of influence caused by the presence of the entry; (3) determine the total in situ load in the zone of influence; (4) determine the value of the variable P by dividing the total in situ load by the zone of influence; (5) use the MSHA-ESE and superpositioning techniques to determine the load on the segment; (6) use a pillar strength equation to determine the strength of the segment; (7) if the load is greater then the strength of the segment, the pillar section is assumed yielded; (8) choose the next segment, and repeat the analysis on this segment beginning at step (1). This process will continue until either stability is achieved or the yield zone reaches the center of the pillar (i.e., the entire pillar yields).

The following is an example of the yielding process. The assumption is made that the pillar is wide enough so that stress superposition can be ignored. Carr and Wilson's equation (*4*) is chosen to provide the residual strength characteristics of the yield zone. To determine the load and strength over the entire section, it is necessary to take the integral of either equation for the limits defined by the edges of the section. Since comparison is made between two integrals, the limits of the integral can be in feet instead of inches.

Pillar Yield Method Incorporating Stress Influence Zone

MSHA Elastic Stress Equation:

$$\frac{Px}{\sqrt{x^2 - c^2}}. \qquad (7)$$

Initial conditions
c = 10
P = 1,000

Wilson Strength Formula:

$$KT\left[\frac{2x}{H} + 1\right]^{K-1}. \qquad (8)$$

Initial conditions
H = 5
K = 3
T = 14

Example

The section 0 to 5 ft into the pillar has yielded. Determine the stability on the next section 5 to 10 ft into the pillar.

c = c + 5
c = 15

$$\text{AREA OF INFLUENCE} = 4 \times c$$
$$= 60. \qquad (9)$$

$$\text{TOTAL ELASTIC LOAD} = P \times \text{AREA OF INFLUENCE}$$
$$= 60{,}000. \qquad (10)$$

Subtract Wilson's residual strength of yielded edge from Total Elastic Load.

Wilson's Strength Formula:

$$KT\left[\frac{2x}{H}+1\right]^{K-1}. \quad (11)$$

To determine the amount of Wilson residual strength for the section,

$$\int_0^5 KT\left[\frac{2x}{H}+1\right]^{K-1}dx. \quad (12)$$

Subtract Wilson residual strength from the Total Elastic Load:

TOTAL ELASTIC LOAD = TOTAL ELASTIC LOAD

$$-\int_0^5 KT\left[\frac{2x}{H}+1\right]^{K-1}dx. \quad (13)$$

TOTAL ELASTIC LOAD

$$= 60{,}000 - \int_0^5 KT\left[\frac{2x}{H}+1\right]^{K-1}dx$$

$$= 59{,}090. \quad (14)$$

Determine new value for P:

$$P = \frac{\text{TOTAL ELASTIC LOAD}}{\text{AREA OF INFLUENCE}}$$

$$= 984. \quad (15)$$

Determine stress on 5- to 10-ft section.
MSHA Elastic Stress Equation:

$$\frac{Px}{\sqrt{x^2-c^2}}. \quad (16)$$

MSHA Load on 5- to 10-ft section.
Remember that c = 15.

$$\text{SECTION STRESS} = \int_{15}^{20}\frac{Px}{\sqrt{x^2-c^2}}dx$$

$$= 13{,}028. \quad (17)$$

Determine Wilson Residual Strength of 5- to 10-ft section.

WILSON RESIDUAL STRENGTH

$$= \int_5^{10} KT\left[\frac{2x}{H}+1\right]^{K-1}dx.$$

$$= 3430. \quad (18)$$

Section Stress is greater than Wilson Strength. Therefore, Section Yields Analysis will continue on the next section (i.e., 10 to 15 ft).

This technique will continue until either stability is achieved or the yield zone extends to the pillar center.

NOTE: The value for the integral in equation 17 results in the formation of a complex conjugate due to the square root of 0, which can be attributed to solution of the lower limit. However, results are satisfactory if the value of the integral at the lower limit is assumed to equal 0.

As it turns out with this example, the yielding will continue up to section 22 ft into the pillar. The final analysis follows.

Determine new value for P obtained from analyzing section 20 to 22 ft into the pillar.

$$P = \frac{\text{TOTAL ELASTIC LOAD}}{\text{AREA OF INFLUENCE}}$$

$$= 726. \quad (19)$$

Determine MSHA load on section 22 to 24 ft.

$$\text{SECTION STRESS} = \int_{32}^{34}\frac{Px}{\sqrt{x^2-c^2}}dx$$

$$= 8{,}339. \quad (20)$$

Determine Wilson Residual Strength of section 22 to 24 ft.

WILSON RESIDUAL STRENGTH

$$= \int_{22}^{24} KT\left[\frac{2x}{H}+1\right]^{K-1}dx$$

$$= 8{,}744. \quad (21)$$

WILSON STRENGTH:

$$= \int_{22}^{24} KT \left[\frac{2x}{H} + 1\right]^{K-1} dx$$

$$= 8{,}743.84.$$

The Wilson Strength is greater than Section Stress; therefore, the section is stable. This implies that the yield zone is 22 ft into the pillar. Wilson has an equation that predicts the yield-elastic depth into pillar.

$$Q = \text{DENSITY} \times \text{OVERBURDEN THICKNESS}$$

$$Q = \frac{170}{144} \times 1000$$

$$= 1{,}181 \qquad (22)$$

Assuming H = 5, T = 14, K = 3,
The depth of the yield zone is

$$y = \frac{H}{2}\left[\left(\frac{Q}{T}\right)^{\frac{1}{K-1}} - 1\right]$$

$$= 20.5. \qquad (23)$$

This is close to the zone predicted from comparing equation 20 to equation 21.

Wilson also predicts the stress at the yield-elastic boundary as

σ = Kq on the yield side of the yield-elastic boundary

σ = KQ

σ = 3542.

Equation 11 indicates this value to be equal to 4033.68, which is close. Wilson predicts the stress on the elastic side of the yield-elastic boundary as:

σ' = KQ + Uniaxial compressive strength.

The MSHA equation (equation 7) predicts the stress 0.25 ft into the elastic core to equal 5840.18. This implies the uniaxial compressive strength is

$$= 5840 - 4033.68$$

$$= 1806.32.$$

This is slightly high but satisfactory. Actually the MSHA equation predicts the vertical stress at the extreme edge of the elastic boundary is infinity, which seems correct if you assume the edge is a sharp corner.

Jaeger and Cook (*3*, p. 277) describe failure criteria for the surface surrounding a flat elliptical crack. It should be possible to incorporate these yield criteria into the model. This would permit a more precise yield model.

FURTHER CONSIDERATIONS

PREDICTING ROOF STRESSES

Using equation 2, it is possible to determine the convergence of the entry roof. Using the beam or plate theory and the knowledge of roof convergence, it should be possible to predict the stresses in the immediate roof.

COMPUTER SOFTWARE

The first version of the computer software will operate in Lotus 1-2-3. The elastic version of the code is already functioning; most of the plots are taken from Lotus. Hewlett Packard markets a handheld calculator that uses Lotus 1-2-3 as its operating system. This code should be able to operate from within the calculator. Another version of the code will be written in C language. This code is nearly half complete.

CONCLUSION

The MSHA Elastic Stress Equation (MSHA-ESE) accurately predicts the stress distribution in the elastic core of a coal pillar. Using superposition techniques, it is possible to estimate the stress distribution throughout an entire mine panel. Superposition permits analysis of more irregular pillar geometries and yielding processes. Small pillars require additional superposition measures to account for rideover stress. Pillar edge strength can be estimated using any of the popular empirical formulas. If the load on the pillar edge exceeds the pillar edge strength, the pillar edge yields and redistributes the insupportable portion of the load onto the pillar core and adjacent pillars. The evaluation process will continue on the edge of the pillar core until a stable condition exists.

Computer software incorporates all these techniques to predict panel stability. The software is quick and easy to use. It provides the layperson with a tool to estimate mine design stability. It also could assist the experienced modeler as a tool to "hone in" on a design before final modeling, using more sophisticated software.

The yield portion is not the most elegant solution, but it does produce satisfactory results. Incorporation of the Griffith failure criteria for flat elliptical cracks should improve the validity of the failure analysis considerably. Rock mechanics is not an exact science, especially in coal-bearing strata. Numerical analysis is only a tool for estimating design considerations. The results from any numerical modeling software should not be taken at face value. Any unusual panel design should be tried on an experimental basis.

REFERENCES

1. Zipf, R. K., Jr. MULSIM/NL Theoretical and Programmer's Manual. BuMines IC, in press.

2. ____. MULSIM/NL Application and Practitioner's Manual. BuMines IC, in press.

3. Jaeger, J. C., and N. G. W. Cook. Fundamentals of Rock Mechanics. Chapman and Hall, 3d ed., 1979.

4. Carr., F., and A. H. Wilson. A New Approach to the Design of Multi-entry Developments for Retreat Longwall Mining. Paper in Proceedings 2nd Conference on Ground Control in Mining. WV Univ., Morgantown, WV, 1982, pp. 1-21.

5. Mark, C., J. Listak, and Z. T. Bieniawski. Field Measurements in Yielding Coal Pillars. Paper in BuMines Seminar on Ground Control for Longwall Mining, April 24, 1990.

IN SITU PILLAR STRENGTH AND FAILURE MECHANISMS FOR U.S. COAL SEAMS

By Hamid Maleki[1]

INTRODUCTION

As mining extends to greater depths, stresses exceed the strength of coal-measure rocks, resulting in failure of mine roofs, coal seams, and mine floors. In practice, coal mine operators have learned to control failure while maintaining stability and productivity.

For design purposes, there is a need to understand different failure mechanisms associated with coal-measure rocks and to calculate complete load-deformation behavior for site-specific conditions in U.S. coal mines. Existing methods for determining pillar strength are inadequate because these methods may only estimate peak pillar strength and are based on either laboratory testing [Bieniawski, 1968 (*3*); Hustrulid, 1976 (*8*)][2] or theoretical considerations [Wilson, 1972 (*17*); Baron, 1983 (*2*)]. Other studies for calculating pillar strength and postfailure load-deformation behavior were completed on South African coal by Salamon and Munro [1967 (*15*)] and Wagner [1974 (*16*)].

In this paper, both failure mechanisms and peak in situ strength measurements for several U.S. coal seams are characterized. The study is based on long-term observations, geotechnical monitoring, and back analyses of stresses that caused pillar failure in eight mines and seven coal seams in the United States. Results are important for developing improved coal pillar designs for site-specific conditions, including designs for yield pillars and control of coal bursts. For the first time, the influence of several structural parameters on coal pillar strength has been included.

COMPLETE LOAD-DEFORMATION CURVE

Wagner [1974 (*16*)] and Bieniawski and Van Heerden [1975 (*4*)] have discussed the significance of large-scale tests of coal for engineering and design purposes. Maleki [1981 (*10*); 1988 (*11*)] obtained complete load-deformation curves for the upper Hiawatha Seam using the split-platen technique [Hustrulid and Ramos, 1977 (*9*)] and proposed design criteria for yield pillars in western U.S. mines. Figure 1 presents typical results. Pariseau et al. [1977 (*14*)] reported laboratory test results, including postfailure characteristics, for the Blind Canyon coal seam.

Two types of postfailure are characteristic of U.S. coal: elastic-plastic and elastic-residual. The first mechanism is seen in coal seams with in-seam or near-seam weakness planes. In such seams, average pillar stresses tend to increase linearly until a peak strength is reached. Beyond this stress level, deformation continues at constant stress, followed by strain softening, as identified in figure 1 by the postfailure modulus.

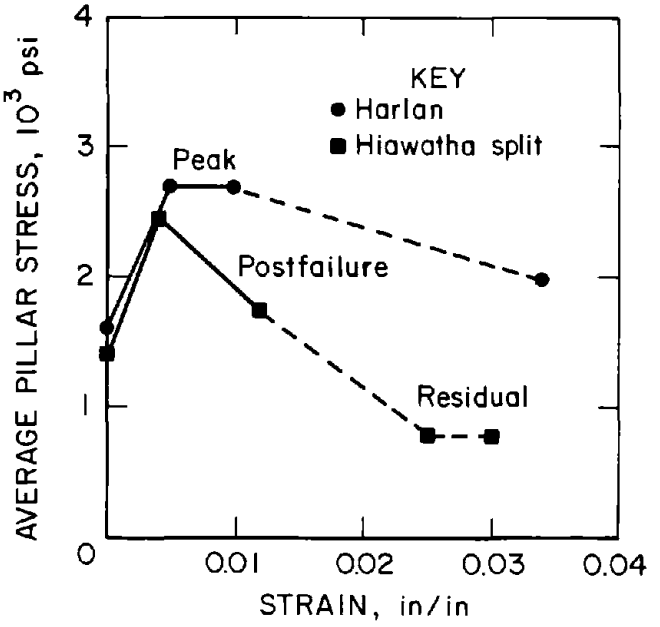

Figure 1.—Pillar stress-strain relationship. Dashed lines indicate estimated behavior.

[1]Mining engineer, Spokane Research Center, U.S. Bureau of Mines, Spokane, WA.

[2]Italic numbers in parentheses refer to items in the list of references at the end of this paper.

The second mechanism is commonly observed in highly cleated coal, where average pillar stress is reduced beyond peak strength to a residual strength (fig. 1).

Peak strength, postfailure modulus, and residual strength are important characteristics of coal pillars. To maintain stable pillars, pillar widths are selected so that average stresses will remain significantly below peak strength. For unstable or yield pillars, the postfailure modulus should be gradual to avoid excessive rates of roof movement. Similarly, bump-prone conditions may result if the postfailure modulus is too steep in comparison with the mine roof-floor modulus (stiffness).

METHODS OF ANALYSIS

Average peak vertical stresses on pillars were calculated on the basis of back-analyses of pillar failures using tributary loading methods, finite-element analyses [Maleki et al., 1988 (*13*), displacement-discontinuity analysis [Maleki, 1988 (*11*)], and a review of studies of pillar load monitoring conducted by the U.S. Bureau of Mines. These studies involved the use of borehole pressure cells, vibrating-wire strain gauges, and, in a few cases, overcoring stress measurements [DeMarco et al., 1988 (*6*); Maleki et al., 1988 (*13*); Haramy and McDonnell, 1988 (*7*); Bunnel and Ko, 1986 (*5*)]. Pillar failure was verified both through analyses of geotechnical data and numerical modeling for some cases [Maleki, 1988 (*11*)].

The premining stress field was estimated on the basis of depth of cover and published overcoring stress measurements in U.S. coalfields. Pillar stresses generated during retreat longwall mining were calculated using the data from both horizontally and vertically oriented borehole pressure cells and the procedure suggested by Babcock [1986 (*1*)].

IN SITU FAILURE MECHANISMS

As pillar stresses increase during retreat mining, a variety of failure mechanisms occur in weak horizons of coal-measure strata. Depending on the depositional and structural setting in a mine, it is possible to have a combination of two or more of these mechanisms. Figure 2 presents typical failures caused by excessive vertical stresses. (Mines with excessive horizontal stresses are excluded from this analysis because the focus is on stress-induced pillar stability problems.)

Figure 2*A* presents typical roof stability problems caused by excessive pillar loading. In this case, high stress concentrations caused lateral dilation of a claystone layer in the mine roof, which bent roof bolts (fig. 3) and contributed to the failure of the top coal. Extensive measurements and numerical modeling revealed pillar stresses exceeding 3,000 psi, which approached the strength of the coal pillar [Maleki, 1981 (*10*)].

Figure 2*B* illustrates schematically gradual pillar failure in a structurally controlled coal seam. This failure was associated with gradual rib slabbing and propagation of failure toward the pillar core. Lateral dilation in a pillar is a sensitive indicator of pillar unloading. Figure 4 shows rib conditions for a yield pillar of this type.

Figure 2*C* illustrates failure originating at seam contacts, such as bedding planes or rock splay contact planes. In these mines, pillar dilation was facilitated along favorable low-friction contact planes, which contributed to pillar failure in an elastic-plastic pattern.

Figure 2*D* presents development of failure in a mine floor and formation of excessive heave in a mine with strong coal seam, a strong roof, and a weak floor. Failure

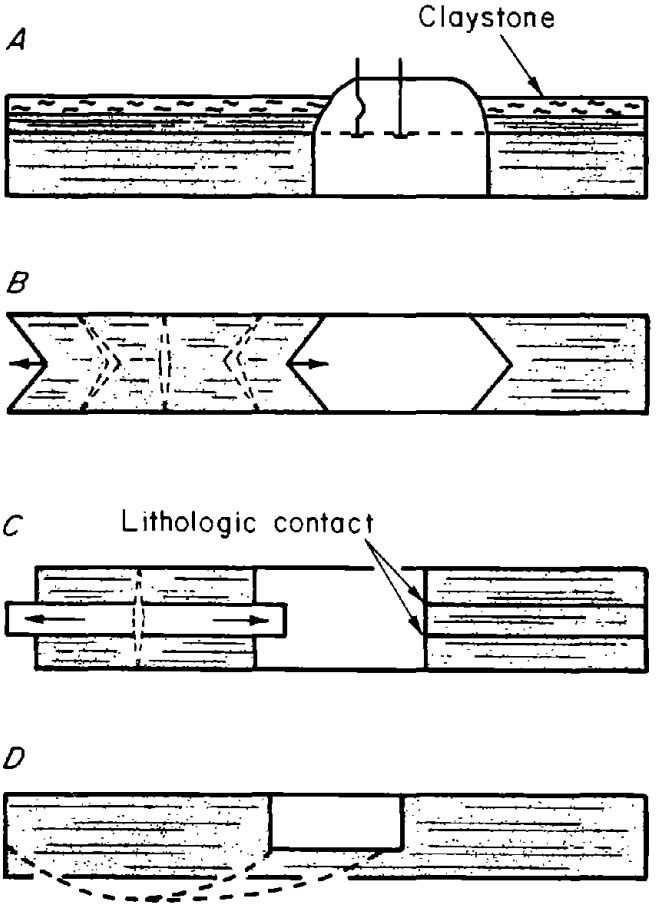

Figure 2.—Failures caused by excessive vertical stresses. *A*, in roof; *B*, in coal; *C*, at seam contact; *D*, in mine floor.

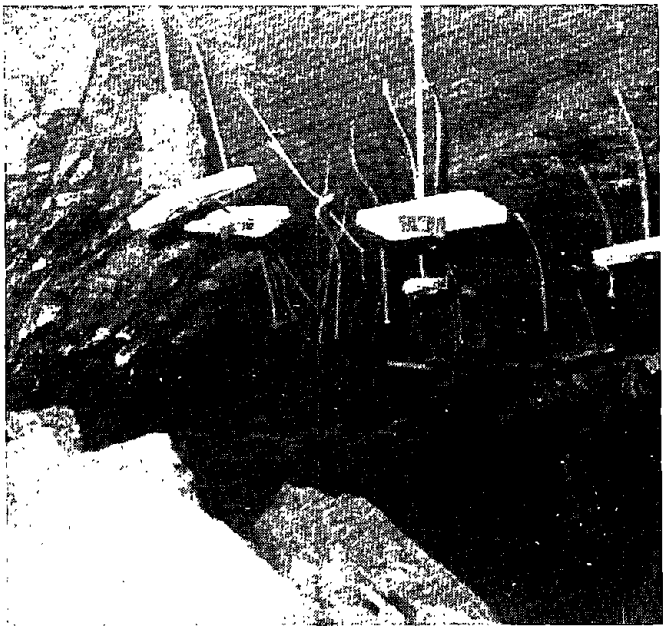

Figure 3.—Typical roof fall caused by excessive pillar loads.

Figure 4.—Gradual rib failure in a yield pillar.

in the mine floor created tensile zones within the pillar, contributing to pillar failure.

These simple descriptive mechanisms are important in recognizing pillar failure and for taking remedial action in the early stages of mine life. Based on these descriptive guidelines, pillar failure mechanisms can be identified and used for modeling in situ pillar behavior.

IN SITU PEAK PILLAR STRENGTH

Peak average strengths for pillars in seven coal seams mined in eight coal mines across the United States are characterized. In figure 5, dashed lines present an extrapolation of results based on observations and engineering judgment. These data are extremely useful for estimating the peak in situ strength of the pillars and as input to variations of pillar stability and pillar design.

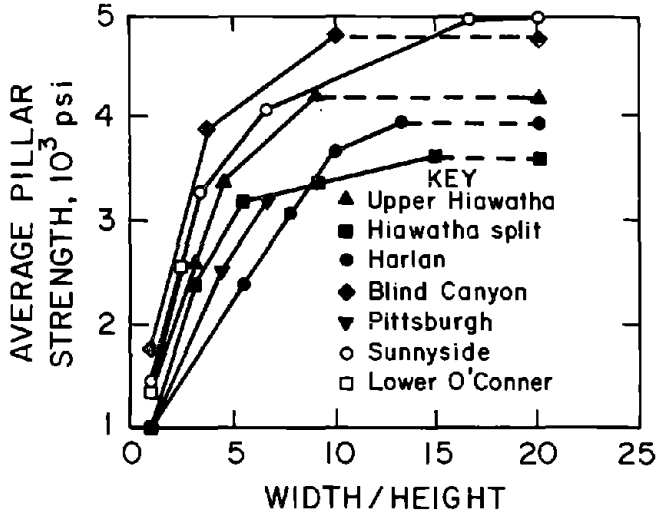

Figure 5.—Average in situ strengths for pillars in selected U.S. coalfields. Dashed line indicates extrapolations of results.

The data are grouped into two categories and fitted with a least squares fit as illustrated in figure 6. The high-strength curve is typical for mines with a large degree of

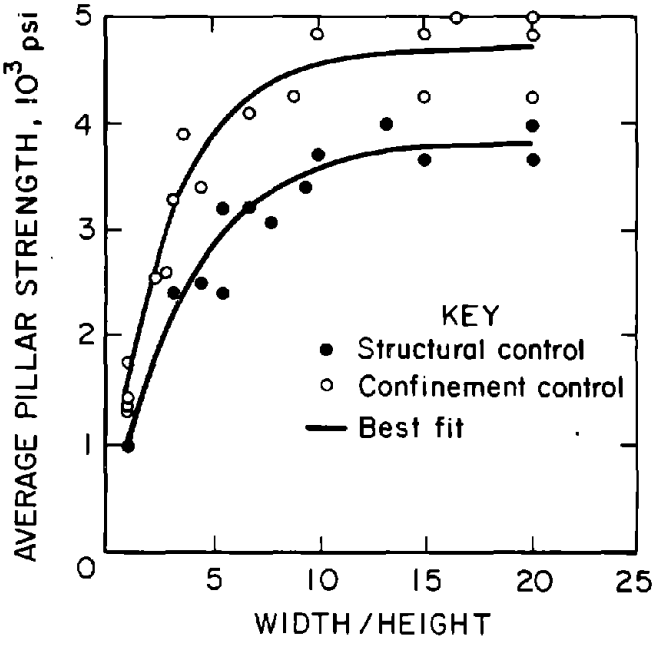

Figure 6.—Best-fit curves for in situ pillar strengths.

pillar confinement and the low-strength curve is typical for structurally controlled coal seams, including persistent cleats and in-seam contact planes.

The best-fit equations are as follows. Confinement control strength = 4700 × (1 - EXP (-0.339 w/h), and structural control strength = 3836 × (1 - EXP (-0.260 w/h), where w/h = pillar width-to-height ratio, strength = pillar average, psi, and EXP = exponential function.

Important conclusions are

1. Wide pillars, even with width-to-height ratios up to 15:1, have failed when loaded [Maleki, 1988 (*11*)]. This contradicts other pillar design formulas, such as Bieniawski [1968 (*3*)].

2. Depending on site-specific conditions, the design strengths of coal pillars may vary between 3,000 and 5,000 psi. Beyond these average stress levels, stability problems are likely to occur.

RESIDUAL STRENGTH

Figures 7 and 8 present peak and residual strengths for two western U.S. coal seams in three longwall mines. Postfailure moduli and residual strengths (fig. 1) are difficult to obtain, but are very important design parameters. Further research should focus on obtaining postfailure characteristics. Other factors influencing postfailure in pillars are cleat spacing, cleat orientation, and frictional properties of bedding planes.

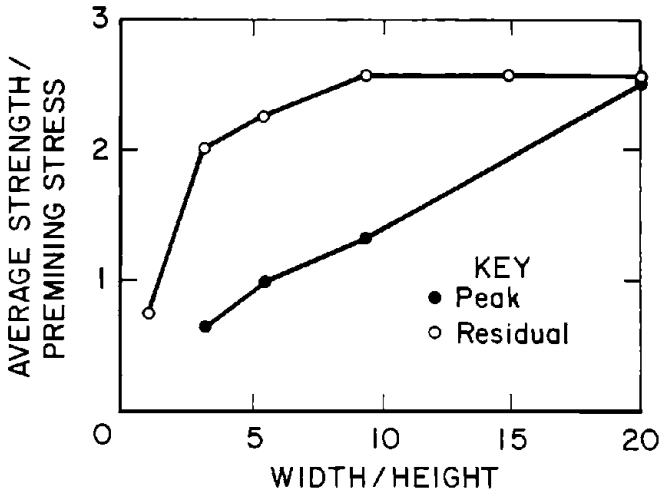

Figure 7.—Average pillar strength ratio for Hiawatha split-seam.

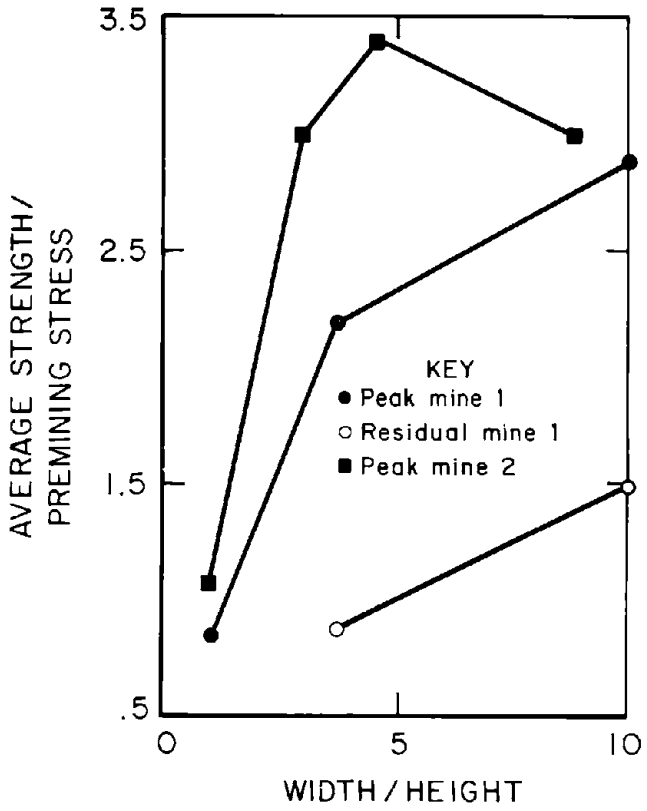

Figure 8.—Average pillar strength ratio for Hiawatha Seam.

CONCLUSION AND RECOMMENDATIONS

Strength curves for pillars were developed for seven U.S. coal seams based on observations, measurements, and analyses of failure. It was shown that coal pillars can sustain maximum stresses between 3,000 and 5,000 psi depending on geologic conditions. Beyond these stress levels, stability problems may occur as a result of failures in the roof, seam, and floor. Two postfailure behavior patterns were characterized: elastic-plastic and elastic-residual.

Further research is needed to obtain complete load-deformation curves for other U.S. coal seams. This is important to maintain pillar stability for resource recovery and the safety of miners as mining continues to greater depths. Coalbump control and prudent yield pillar design will significantly benefit from such efforts.

REFERENCES

1. Babcock, C. O. Equation for the Analysis of Borehole Pressure Cell Data. Proceedings, 27th U.S. Symposium on Rock Mechanics (Tuscaloosa, AL, June 1986), H. L. Hartman (ed.). SME, Littleton, CO, 1986, pp. 233-240.

2. Baron, K. An Analytical Approach to the Design of Pillars in Coal. Canada Center for Mineral and Energy Technology, 1983, 148 pp.

3. Bieniawski, Z. T. The Effect of Specimen Size on Compressive Strength of Coal. Int. J. of Rock Mech. Min. Sci., 1968, pp. 325-335.

4. Bieniawski, Z. T., and W. L. Van Heerden. The Significance of In Situ Tests on Large Rock Specimens. Int. J. Rock Mech. Min. Sci. and Geomech. Abst., v. 12, 1975, pp. 101-103.

5. Bunnel, M. D., and K. C. Ko. In Situ Stress Measurements and Geologic Structures in an Underground Coal Mine in the Northern Wasatch Plateau, Utah. Proceedings, 27th U.S. Symposium in Rock Mechanics (Tuscaloosa, AL, June 1986), H. L. Hartman (ed.). SME, Littleton, CO, 1986, pp. 333-337.

6. DeMarco, M. J., J. R. Koehler, and P. H. Lu. Characterization of Chain Pillar Stability in a Deep Western Coal Mine - Case Study. Min. Eng. (Littleton, CO), v. 40, No. 12, 1988, pp. 1115-1119.

7. Haramy, K. Y., and J. P. McDonnell. Causes and Control of Coal Mine Bumps. BuMines RI 9225, 1988, 35 pp.

8. Hustrulid, W. A Review of Coal Pillar Strength Formula. Rock Mechanics, v. 8, 1976, pp. 115-145.

9. Hustrulid, W., and G. Ramos. The Split-Plotter Technique for Determining the Load Deformation—Behavior of Model Coal Pillar. Paper presented at the SESA meeting, Dallas, TX, 1977, 56 pp.

10. Maleki, H. Coal Mine Ground Control. Ph.D. thesis, Colorado School of Mines, Golden, CO, 1981, 432 pp.

11. ____. Ground Response to Longwall Mining. Colorado School of Mines Quarterly, v. 83, No. 3, 1988, 14 pp.

12. Maleki, H. N., J. R. Aggson, F. Miller, and J. F. T. Agapito. Mine Layout Design for Coal Bump Control. 65th Int. Conf. on Ground Control in Mining (West Virginia University, Morgantown, WV, June 1987), 8 pp.

13. Maleki, H. N., M. Moon, and J. F. T. Agapito. In Situ Pillar Strength Determination for Two-Entry Longwall Gates. Paper in Proceedings of the 7th Int. Conf. on Ground Control in Mining (West Virginia University, Morgantown, WV, 1988), pp. 10-19.

14. Pariseau, W. G., W. A. Hustrulid, S. R. Swanson, and L. L. Van Sambeck. Coal Pillar Strength Study (The Design of Production Pillars in Coal Mines) (contract HO242059, University of Utah). BuMines OFR 166-77, July 1977, 417 pp.

15. Salamon, J. D. G., and A. H. Munro. A Study of the Strength of Coal Pillars. J. of So. Afri. Inst. of Min. and Tech., v. II B, 1967, pp. 55-67.

16. Wagner, H. Determination of the Complete Load-Deformation Characteristics of Coal Pillars. Proceedings, 3rd Congr. of the Int. Soc. for Rock Mechanics, Denver, CO, Sept. 1-7, 1974, 8 pp.

17. Wilson, A. H. An Hypothesis Concerning Pillar Stability. Min. Eng. (London), v. 131, 1972, pp. 409-417.

COAL PILLAR MECHANICS: THEORETICAL MODELS AND FIELD MEASUREMENTS COMPARED

By Christopher Mark[1] and Anthony T. Iannacchione[2]

INTRODUCTION

The scientific study of coal pillars dates back at least 100 years. The first pillar strength formulas were derived from laboratory testing of coal specimens of different sizes and shapes (*4, 33*).[3] Other measurement-based formulas incorporated results from large-scale compressive tests of coal specimens (*9, 3, 30*). The best known of the measurement-based pillar strength formulas are the Obert-Duvall/Wang formula (equation 1), the Holland-Gaddy/Hustrulid-Swanson formula (equation 2) and the Bieniawski formula (equation 3):

$$S_p = S_1 \times \left(0.78 + 0.22 \times \frac{w}{h} \right) \quad (1)$$

$$S_p = S_1 \times \left(\frac{w}{h} \right)^{0.5} \quad (2)$$

$$S_p = S_1 \times \left(0.64 + 0.36 \times \frac{w}{h} \right) \quad (3)$$

where S_p = pillar strength, psi,

S_1 = in situ coal strength, psi,

w = pillar width or least plan dimension, (psi),

and h = pillar height, ft.

In each of these formulas, a pillar's strength is determined by its geometry, in particular to its width-to-height ratio (w/h).

Another approach to pillar design relies on statistical analysis of previous experience with mine pillar performance. The first rigorous application of the method of *back analysis* was by Salamon and Munro (*24*) in South Africa. Their formula follows a power law:

$$S_p = S_1 \times \left(\frac{w^{.46}}{h^{.66}} \right) \quad (4)$$

Sheorey et al. (*27*) recently employed a similar approach, combined with extensive laboratory and in situ testing, in developing a pillar strength formula for Indian coal mines

$$S_p = S_1 + 0.28 \times H \times \left(\frac{w}{h} - 1 \right) \quad (5)$$

where H = depth of cover, ft.

Their formula is unique in that the depth of cover has an independent effect on the pillar strength.

These *empirical* methods have been validated through full-scale tests and many years of actual use. They contain considerable wisdom regarding coal pillar behavior. Their most significant drawback is that their predictions cannot be extrapolated with confidence beyond the data they were developed from, typically pillars with w/h ratios of less than 5.

More fundamentally, empirical formulas treat the entire coal pillar as a single structural element. Their goal is to estimate the average strength of the pillar, which is defined as the pillar's ultimate load-bearing capacity divided by its area. In reality, it has been known for some time that at ultimate load the stress within even a relatively small pillar is highly nonuniform. Tests conducted nearly 20 years ago by Wagner (*29*) demonstrated this quite dramatically (fig. 1). Moreover, pillar failure is typically *progressive*, rather than sudden. Large sections of a pillar often yield

[1]Mining engineer.
[2]Supervisory geologist.
Pittsburgh Research Center, U.S. Bureau of Mines, Pittsburgh, PA.
[3]Italic numbers in parentheses refer to items in the list of references at the end of this paper.

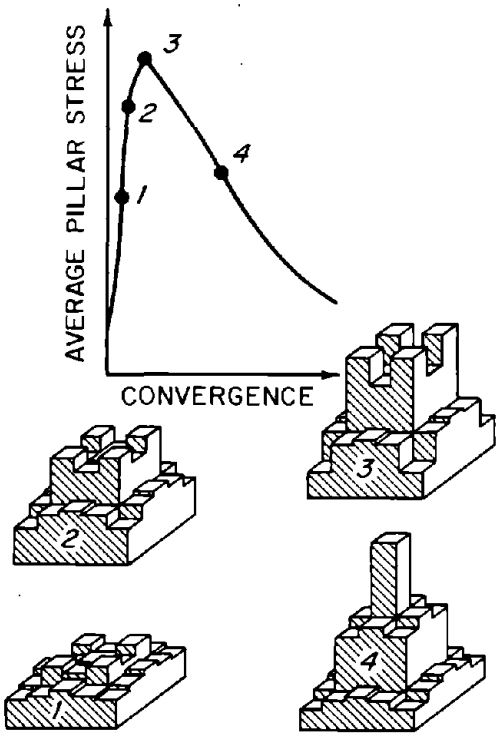

Figure 1.—Pillar stress profiles measured in small coal pillars (after Wagner, 1974).

long before the pillar as a whole attains its maximum load. Therefore, the concept of *pillar strength*, while useful for practical engineering design, is not very satisfactory from a scientific standpoint.

The *mechanics-based* approach to coal pillar design begins with the concept that a coal pillar can consist of an outer "yield zone" providing constraint to a "confined core." Perhaps the best-known of these mechanics-based methods was first proposed by A. H. Wilson in 1973 (*31*), and later revised (*32*). Wilson's model started with the assumption that coal follows a linear Mohr-Coulomb failure criterion. He then derived an expression for the vertical stress gradient within the yield zone:

$$\sigma_v = p' \times k \times \left(\frac{x + \frac{h}{2}}{\frac{h}{2}} \right)^{k-1} \qquad (6)$$

where σ_v = vertical stress in yield zone, psi,

k = triaxial stress factor = $(1+\sin\phi)/(1-\sin\phi)$,

ϕ = the internal friction angle,

x = distance from ribline, ft,

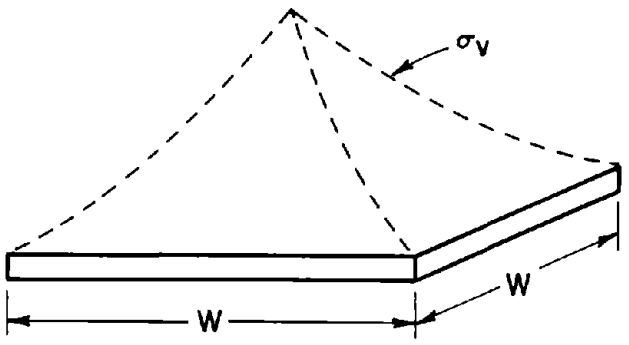

Figure 2.—Determination of pillar load bearing capacity as the integral of the pillar stress distribution.

and p′ = the unconfined compressive strength of the failed coal at the pillar edge, psi.

Wilson assumes that there is no further loss of strength or confinement once the coal has yielded, so the ultimate pillar resistance (R) may be determined by integrating equation 6 over the entire area of the pillar (fig. 2). The pillar strength is simply the ultimate pillar resistance divided by the pillar area. It can be seen that the stress distribution, and therefore the pillar strength, is highly dependent on the assumed values of p′ and k. Based on laboratory measurements, Wilson typically uses p′ = 14 psi and ϕ = 30° to 37°, implying an exponential stress rise in the yield zone. Salamon's squat pillar strength formula (*25*) follows a similar exponentially increasing trend:

$$S_p = S_1 \times \left(\frac{R_o^b}{V^a} \right) \times \left(\frac{b}{e} \times \left(\left(\frac{R}{R_o} \right)^e - 1 \right) + 1 \right) \qquad (7)$$

where R = width-to-height ratio,

R_o = critical w/h ratio = 5,

V = pillar volume,

e = rate of strength increase = 2.5,

b = 0.5933,

and a = 0.0667.

In part because an indefinite exponential stress rise within the yield zone appears unrealistic, Barron (*2*) presented an alternative formulation. His model limits the stress rise by two means:

1. A nonlinear Mohr envelope is assumed for the fracture strength of the intact coal, which allows the friction angle to gradually decrease, and
2. A "pseudoductile" failure mechanism is introduced at high stress, where the frictional strength exceeds the fracture strength.

The result is that pillar stress grows at a decreasing rate, until it reaches a final, limiting value in the "pseudoductile" zone.

"Closed form" analytical solutions for pillar strength, like Wilson's or Barron's, have, in recent years, increasingly been supplanted by numerical models. Like the analytical formulas, numerical models require failure criteria, a model of postfailure behavior, and material properties. The output from numerical models is typically a stress gradient that can be compared with equation 6. More sophisticated numerical models can consider roof and floor properties (*13*), nonlinear failure criteria (*23*), strain-softening behavior (*16, 18, 34*), and geologic contacts (*15*).

As the models become more complex, more material properties are required. In situ values for material properties are seldom available. Modelers have employed either linear Mohr-Coulomb or nonlinear Mohr failure criteria, generally derived from laboratory strength tests. These criteria usually generate exponential stress rises in the yield zone that are qualitatively similar to those predicted by Wilson.

It is evident that a wide variety of techniques for predicting coal pillar strength are available to today's rock mechanics specialist. The predictions of these different formulas can vary widely, however. Figure 3 compares five empirical formulas, three analytic formulas, and results from two numerical model studies. The formulas have been adjusted so that they yield the same strength prediction for a width-to-height ratio of 5.

Three general trends are evident in figure 3. The first, represented by the numerical models of Hsuing-Peng and Kripakov, Wilson's formula, and Salamon's squat formula, show an exponential increase in pillar strength as pillar width is increased. These theories all assume that confinement grows rapidly within squat pillars, allowing the core stress to build indefinitely. The other extreme, represented by the Salamon-Munro and Holland-Gaddy empirical formulas and Barron's analytic formula, indicate that the pillar strength tends towards some maximum, limiting value. An intermediate trend, an approximately

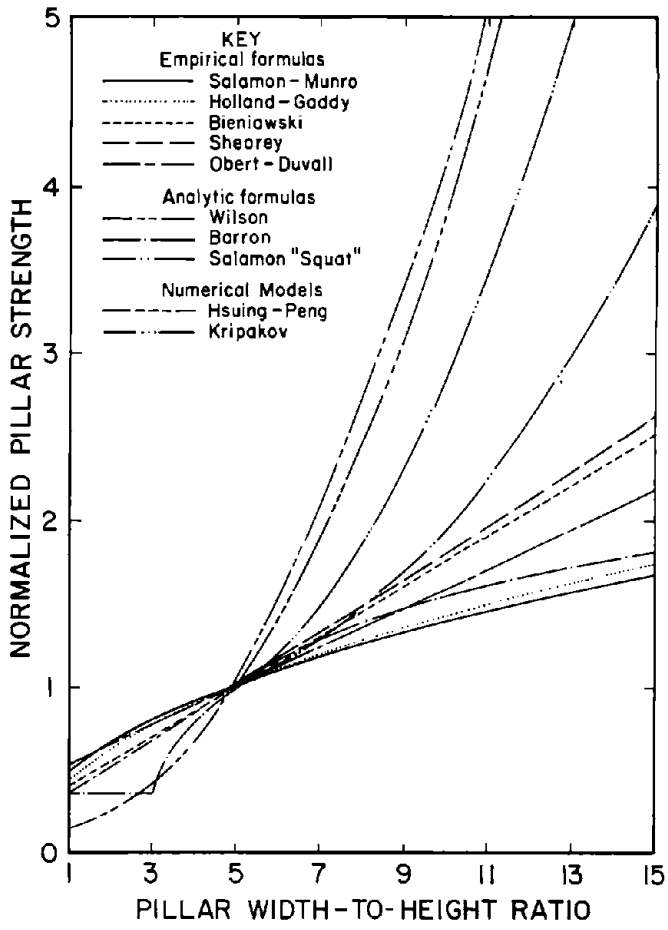

Figure 3.—Comparison of pillar strength predictions from various formulas.

linear increase in strength, is predicted by the empirical formulas of Bieniawski, Sheorey, and Obert-Duvall.

The practical implications of the variation in pillar strength prediction shown in figure 3 are enormous. As mines are worked at greater depth, and as mining methods like longwalls add to pillar loads, large pillars with w/h of 10, 20, and even more are becoming the norm. A better definition of the true trend in pillar strength is imperative if rock mechanics theory is to aid design practice.

The goal of this paper is to evaluate the current models of coal pillar strength. The basis of the evaluation will be a comprehensive data base of stress measurements from actual coal pillars.

STRESS DISTRIBUTION PROFILES FROM PILLAR STRENGTH FORMULAS

Since stress measurements are made at discrete points, they cannot be compared directly with pillar strength. Therefore, the first task is to develop stress distribution profiles from the various formulas. Stress gradients are readily obtained from analytic formulas, such as Wilson's. Numerical models also provide stress distribution profiles, though not normally in the form of an equation. Stress gradients are not so easily obtained from empirical formulas. It was stated earlier that the empirical formulas do not explicitly consider the effect of internal pillar mechanics. It is apparent, however, that they imply a nonuniform stress distribution because of the shape effect. Therefore, it should be possible to derive the stress gradients that are implied by the empirical formulas.

The derivation begins with two assumptions that are implicit in Wilson's and other analytical formulations:

1. The stress within the yield zone of a given pillar is a continuous function of the distance from the nearest rib (x) divided by pillar height (h), and independent of the pillar width (w).
2. The stress gradient within the yield zone of a given pillar does not change with time or load (i.e., the yielded coal is perfectly plastic).

The next step in the derivation is to calculate the ultimate resistance of a square pillar, R. Using the Bieniawski formula for illustration,

$$R = S_1 \times \left(0.64 + 0.36 \times \frac{w}{h}\right) \times w^2. \qquad (8)$$

Then, the increase in pillar resistance, dR, due to an increase in cross-section area (dA = 2w dw, fig. 4*A*) may be calculated by taking the derivative of equation 8 with respect to w,

$$dR = S_1 \times \left(1.28 + 1.08 \times \frac{w^2}{h}\right) \times dw. \qquad (9)$$

For the next step, the assumption that the vertical pillar stress is a continuous function of the rib distance, x, is applied. It may be seen (fig. 4*B*) that,

$$dR = \int_0^{\frac{w}{2}} \sigma_v dx dw. \qquad (10)$$

Equating 9 and 10 and simplifying,

$$S_1 \times \left(0.32 \times w + 0.27 \times \frac{w^2}{h}\right) = \int_0^{\frac{w}{2}} \sigma_v dx. \qquad (11)$$

The function σ_v that satisfies equation 11 and the two assumptions stated at the start is

$$\sigma_v = S_1 \times \left(0.64 + 2.16 \times \frac{x}{h}\right). \qquad (12)$$

Equation 12 is the stress gradient in the yield zone predicted by the Bieniawski formula. The equivalent equations for the other empirical formulas are:

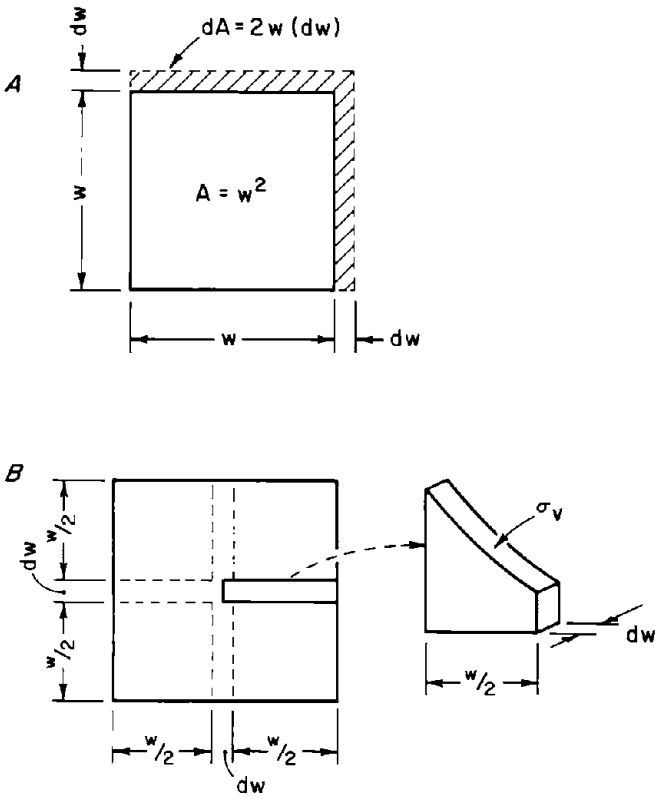

Figure 4.—Determination of pillar stress gradients from a pillar strength formula. *A*, Calculation of dR directly from the formula. *B*, Calculation of dR in terms of the vertical stress gradient.

OBERT-DUVALL:

$$\sigma_v = S_1 \times \left(0.78 + 1.32 \times \frac{x}{h} \right) \quad (13)$$

HOLLAND-GADDY:

$$\sigma_v = 2.65 \times S_1 \times \sqrt{\frac{x}{h}} \quad (14)$$

SHEOREY:

$$\sigma_v = \left(S_1 - 0.28 \times H \right) + \left(1.68 \times H \times \frac{x}{h} \right) \quad (15)$$

SALAMON-MUNRO:

$$\sigma_v = S_1 \times \left(\frac{2.47}{h^{0.2}} \right) \times \left(\frac{x}{h} \right)^{0.46}. \quad (16)$$

The most important conclusion is that in each case the form of stress gradient is the same as that of the parent formula (for example, a linear increase in pillar strength implies a linear stress rise within the yield zone).

FIELD STUDIES

During the past 20 years, a considerable effort has been directed towards studying pillar loading and pillar strength underground. Studies have been conducted by numerous research organizations, in every major U.S. coalfield, using several different types of instrumentation. Much of these data were reviewed for this report. In the end, studies conducted at six mines were selected. In each of these studies, the coal pillars were loaded by some form of retreat mining, either pillar extraction or longwall, and the cells were installed in a pattern that allowed stress profiles to be constructed. The characteristics of the instruments used in the studies are discussed, followed by brief descriptions of each of the study sites.

STRESS MEASUREMENT TECHNIQUES

Three different types of instruments were used in the studies to measure pillar stress. These are the vibrating wire stressmeter (VWS), the borehole pressure cell (BPC), and the borehole platened flatjack (BPF). Each cell has its own calibration procedure for relating cell response to rock stress or stress change.

The VWS is a "hard inclusion" device for measuring unidirectional stress *changes* in rock. Introduced in the early 1970's (*11*), the VWS consists essentially of a wire tensioned across a steel cylinder. As the rock stress changes, the cylinder deforms, causing the tension in the wire to change. A readout device plucks the wire electronically, and measures its natural period of vibration.

A review of 10 previously published VWS calibration studies (*20*) indicated that the calibration procedures originally proposed by Hawkes and Bailey (*11*) have largely been confirmed, both theoretically and experimentally. Several in situ, laboratory, and analytic studies have separately determined calibration coefficients for coal that fall within a range of ±25% (*6, 8, 11, 22, 28*). In practice, it appears that variations in setting procedure can be an important source of error. Hawkes and Bailey's calibration procedures, with an intermediate value of the calibration coefficient, was used to reduce all the VWS data used in this study.

BPC have been used to monitor pressure changes in coal pillars for more than 25 years (*21*). They consist of a hydraulic flatjack encapsulated in grout that is inserted into a cylindrical borehole. The BPF differs from the BPC primarily in that the grout is replaced by two aluminum platens.

Hydraulic cells are considered "soft inclusions," which complicates the development of calibration procedures. Although calibration of the BPC has been the subject of much discussion through the years (*1, 17*), much BPC data, including most of the data used in this study, are reported in terms of *cell pressure* rather than stress change. For BPF data, a calibration procedure called borehole platened flatjack calibration (BPFCAL) was developed by Heasley (*12*). BPFCAL combines analytical solutions for the displacements around a borehole and the borehole-platen interaction with the empirically determined stiffness behavior of the flatjack. All the BPF data reported here were reduced using BPFCAL.

Two additional issues may affect interpretation of pillar stress measurements. The first is the influence of the

biaxial stress field. In most of the studies described here, stressmeters were oriented in the vertical direction only. In general, however, three stressmeters would be necessary per installation to measure the complete biaxial stress field. Biaxial stress analysis is simplified in coal pillars because the directions of the major and minor principal stresses can usually be assumed to be vertical and horizontal. Horizontal stress changes would still be expected to influence the response of vertically oriented stress cells. Analysis supported by experimental evidence (*30*) indicates that where changes in the minor principal stress are less than 50% of changes in the major, they will affect VWS results by less than 20%. In the studies included in this paper, all the VWS data were adjusted using measured horizontal stress data, while the BPF and BPC data were not.

A second issue is the effect of coal failure on cell response. By definition, measurements of stresses in the yield zone are conducted where the coal is assumed to have failed. Yet very little research has addressed this issue, and all of the calibration procedures developed to date assume that the coal remains elastic. One finite-element model study has addressed the effect localized plastic behavior on VWS response, and it concluded that the measurements may be only marginally effected even when the rock yields entirely around the borehole (*22*). It may be added that measurements from within the yield zone, including those used in this study, usually appear reasonable and relatively consistent.

DESCRIPTION OF STUDY SITES

VP NO. 3 MINE

In the late 1980's, the U.S. Bureau of Mines instrumented 12 different pillars within three longwall gate entries of the VP No. 3 Mine near Vansant, VA, (*5, 14*). The Pocahontas No. 3 Coalbed averages 5.5 ft in thickness with an overburden ranging from 1,800 to 2,050 ft over the three instrumented sites. One stress profile given in table 1 (VP No. 3-1) is from an 80- by 80-ft 7-D gate entry pillar (fig. 5). Five other profiles (VP No. 3-[2 to 6]) are from a 120- by 180-ft gate entry pillars (figs. 6 and 7). All measurements were made with the BPF instrument.

FOIDEL CREEK MINE

The Bureau has monitored six different sites along three gate entries of the Foidel Creek Mine near Oak Creek, CO (*10*). The Wadge Coalbed averages 10 ft thick while the overburden averages 1,050 ft over the entire study area. Seven stress profiles (Foidel Creek-[1 & 8]) given in table 1 are from four 38- by 70-ft gate entry pillars (fig. 8). All measurements were made with the BPC instrument.

KEYSTONE NO. 1 MINE

The Colorado School of Mines under a Bureau contract (*30*) instrumented two 80- by 80-ft coal pillars with VWS at the Keystone No. 1 Mine in McDowell County, WV. These two pillars were reduced in size to determine the in situ deformation chacteristics and failure strength of coal. The Pocahontas No. 3 Coalbed was 5 ft thick and under 800 ft of overburden at the site. Four stress profiles (Keystone No. 1-[1 to 4]) were obtained when the pillar measured 62- by 62-ft, and four others (Keystone No. 1-[5 to 10]) were obtained when the pillar had been reduced to 42- by 42-ft pillar (fig. 9).

KITT MINE

The Pennsylvania State University instrumented four pillars at the Kitt Mine in Barbour County, WV (*20*). The Lower Kittanning Coalbed averaged 5 ft thick and was under approximately 700 ft of overburden at these two sites. Stress profiles (Kitt-[1 & 2]) were measured in two adjacent 42- by 72-ft gate entry pillars (fig. 10) and in a (Kitt-[3 & 4]) 22- by 110-ft gate entry pillar (fig. 11). The measurements were made with VWS.

PLATEAU MINE

The Bureau (*7*) and Agapito and Associates (*19*) both instrumented several 10-ft-thick pillars within the Wattis Coalbed at the Plateau Mine near Price, UT. The four stress profiles given in table 1 were from two 30- by 90-ft gate entry pillars under 1,400 ft (Plateau-[1 & 2]) and 1,500 ft (Plateau-[3 & 4]) of overburden (fig. 12). All measurements were made with BPC instruments.

LYNCH MINE

U.S. Steel Reseach (*26*) instrumented four pairs of longwall pillars, the longwall panels, and the barrier pillars with more than 80 VWS. The Harlan Coalbed at this site is 11 ft thick and under 1,560 ft of overburden. Two stress profiles listed in table 1 (Lynch No. 37-[1 & 2]) were obtained from a 72- by 92-ft T1 gate entry pillar (fig. 13).

Table 1.—Data used in analysis

ID	Over-burden	Cell type	h, ft	x, ft	σ_v, psi
Kitt-1	760	VWS	5	7	2079
				12	3011
				19	3342
				23	4254
Kitt-2	760	VWS	5	3	-65
				10	856
				18	2423
Kitt-3	640	VWS	5	2	-306
				4	580
				5	798
				9	1434
				11	1504
Kitt-4	640	VWS	5	3	213
				7	1118
				11	1504
Keystone No. 1-1	800	VWS	5.5	2.5	-427
				5	721
				10	3017
				15	3652
				20	4286
Keystone No. 1-2	800	VWS	5.5	2.5	-310
				5	548
				10	1878
				15	2880
Keystone No. 1-3	800	VWS	5.5	2.5	460
				5	2162
				10	2492
				15	3983
Keystone No. 1-4	800	VWS	5.5	2.5	1109
				5	1190
				10	1352
				15	4055
Keystone No. 1-5	800	VWS	5.5	2.5	-389
				5	1451
				10	4254
Keystone No. 1-6	800	VWS	5.5	2.5	-386
				5	1625
				10	3737
Keystone No. 1-7	800	VWS	5.5	2.5	204
				5	3071
				10	3505
Keystone No. 1-8	800	VWS	5.5	2.5	334
				5	2337
				10	4293
Keystone No. 1-9	800	VWS	5.5	2.5	1165
				5	1742
				10	3119
Keystone No. 1-10	800	VWS	5.5	2.5	-457
				5	1001
				10	1694
VP No. 3-1	1850	BPF	5.5	5	1494
				8	3920
				12	7449
				15	11348
VP No. 3-2	2050	BPF	5.5	4	160
				8	7975
				12	7815
				16	9597
VP No. 3-3	2050	BPF	5.5	5	3370
				10	5847
				15	6715
VP No. 3-4	2050	BPF	5.5	5	1495
				10	6917
VP No. 3-5	2000	BPF	5.5	5	730
				20	4160
				30	6080
VP No. 3-6	2000	BPF	5.5	5	386
				10	6664
Foidel Creek-1	1000	BPC	10	9	1250
				18	3450
Foidel Creek-2	1000	BPC	10	9	2550
				18	3450
Foidel Creek-3	1000	BPC	10	9	3646
				18	5449
Foidel Creek-4	1000	BPC	10	9	2313
				18	5449
Foidel Creek-5	1000	BPC	10	9	3802
				18	5958
Foidel Creek-6	1000	BPC	10	9	5000
				18	8200
Foidel Creek-7	1000	BPC	10	9	1350
				18	5700
Foidel Creek-8	1000	BPC	10	9	1500
				18	5700
Plateau-1	1500	BPC	10	5	0
				10	1950
				15	4440
Plateau-2	1500	BPC	10	5	200
				10	1260
				15	4440
Plateau-3	1500	BPC	10	5	960
				10	2640
				15	3320
Plateau-4	1500	BPC	10	5	1100
				10	1860
				15	3320
Lynch No. 37-1	1560	VWS	11	10	1920
				20	2450
Lynch No. 37-2	1560	VWS	11	10	170
				20	1960

h	Pillar height.
x	Distance from rib.
σ_v	Measured vertical stress.
VWS	Vibrating wire stressmeter.
BPF	Borehole platened flatjack.
BPC	Borehole pressure cell.

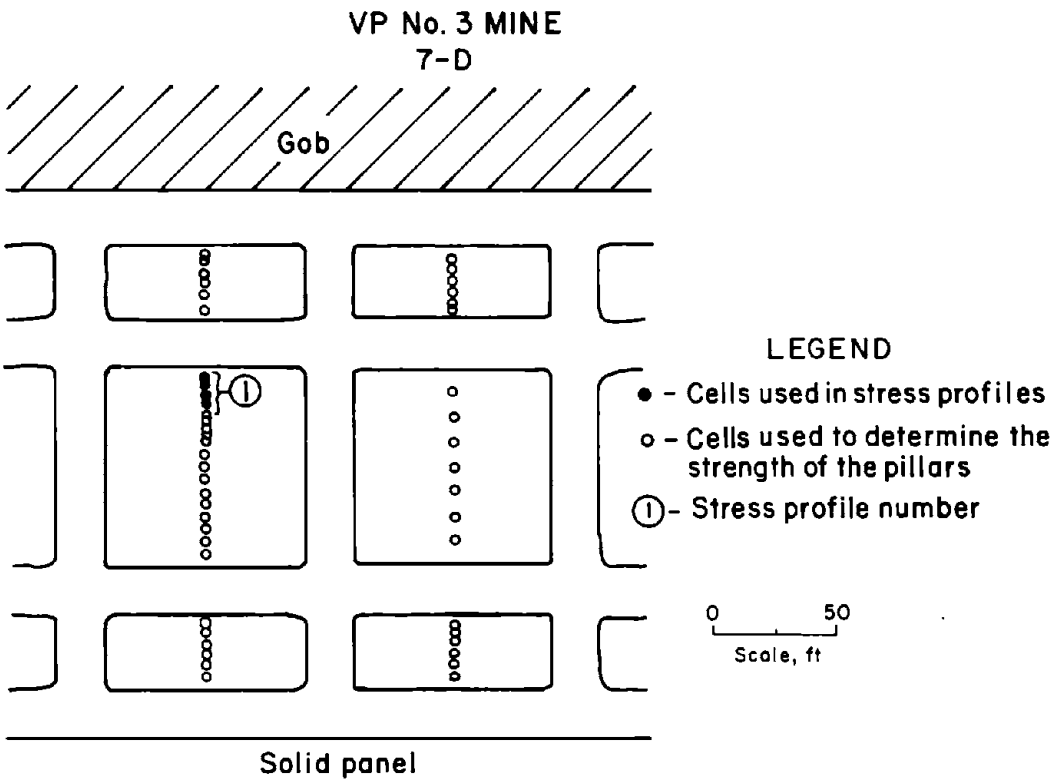

Figure 5.—First pillar study site at VP No. 3 Mine.

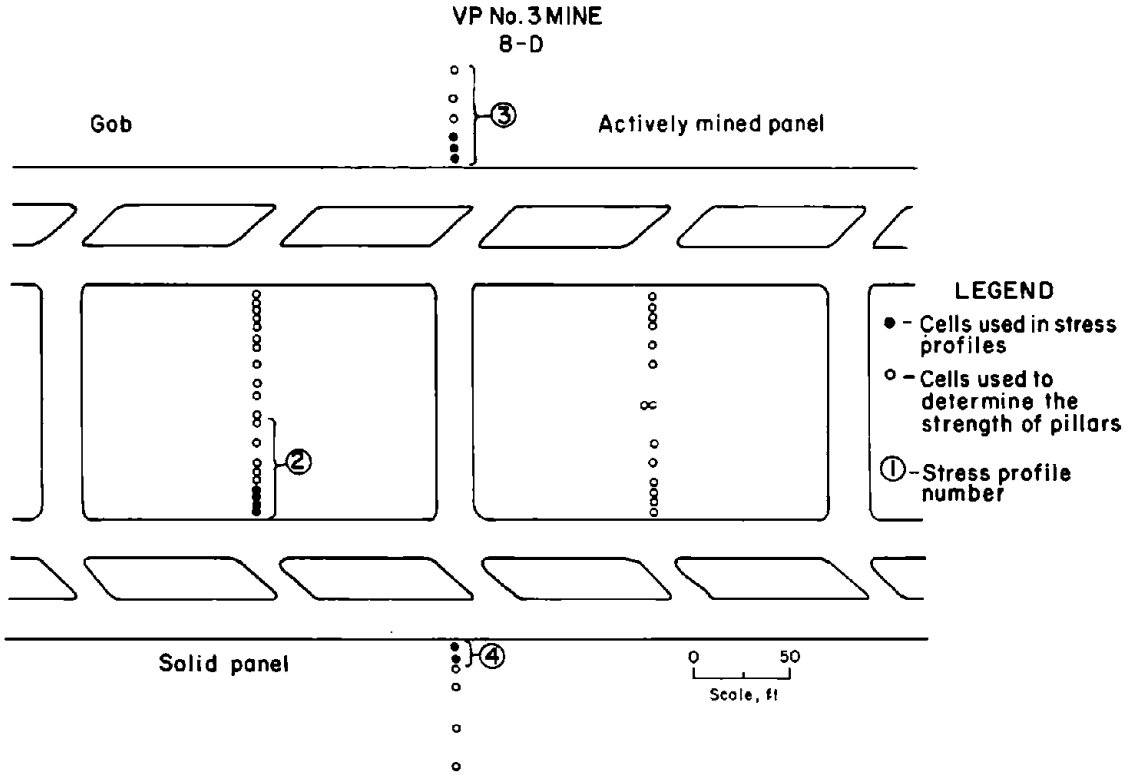

Figure 6.—Second pillar study site at VP No. 3 Mine.

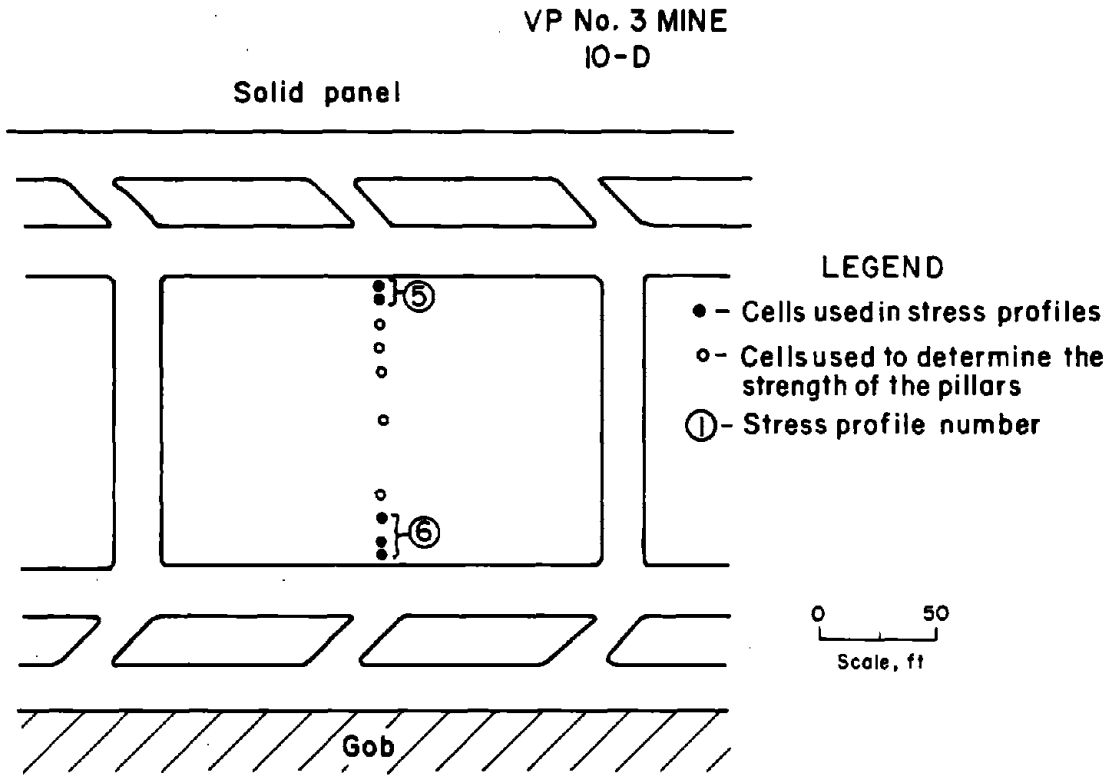

Figure 7.—Third pillar study site at VP No. 3 Mine.

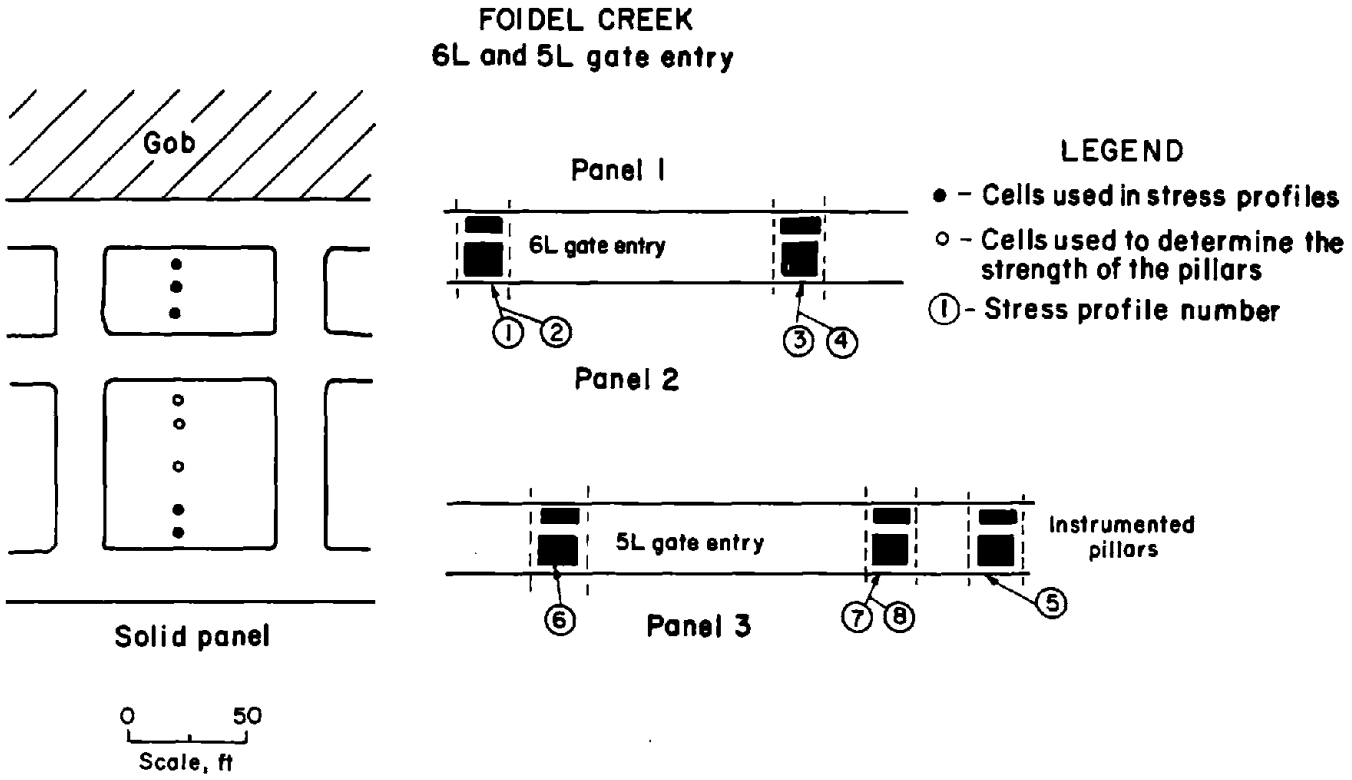

Figure 8.—Pillar study sites at Foidel Creek Mine.

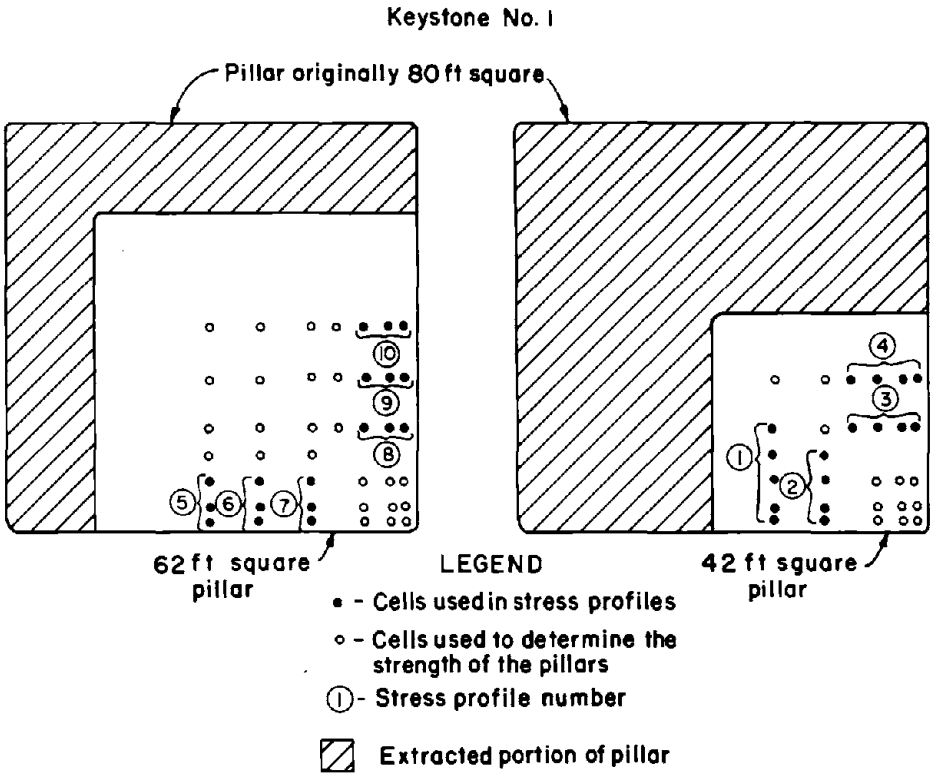

Figure 9.—Pillar study site at Keystone No. 1 Mine.

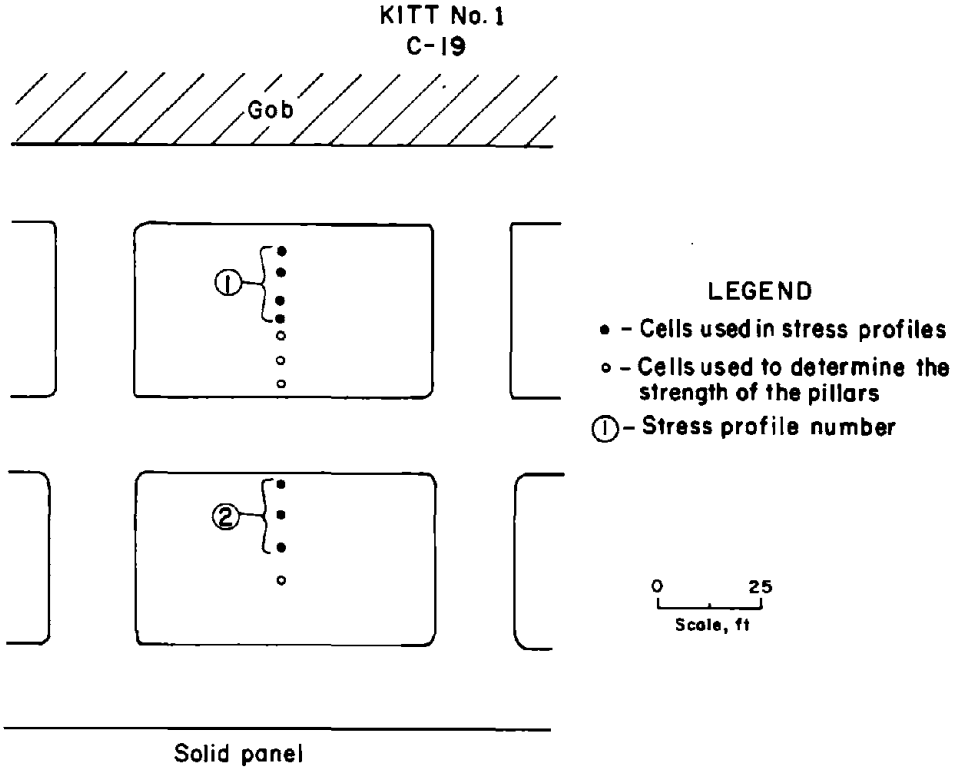

Figure 10.—First pillar study site at Kitt Mine.

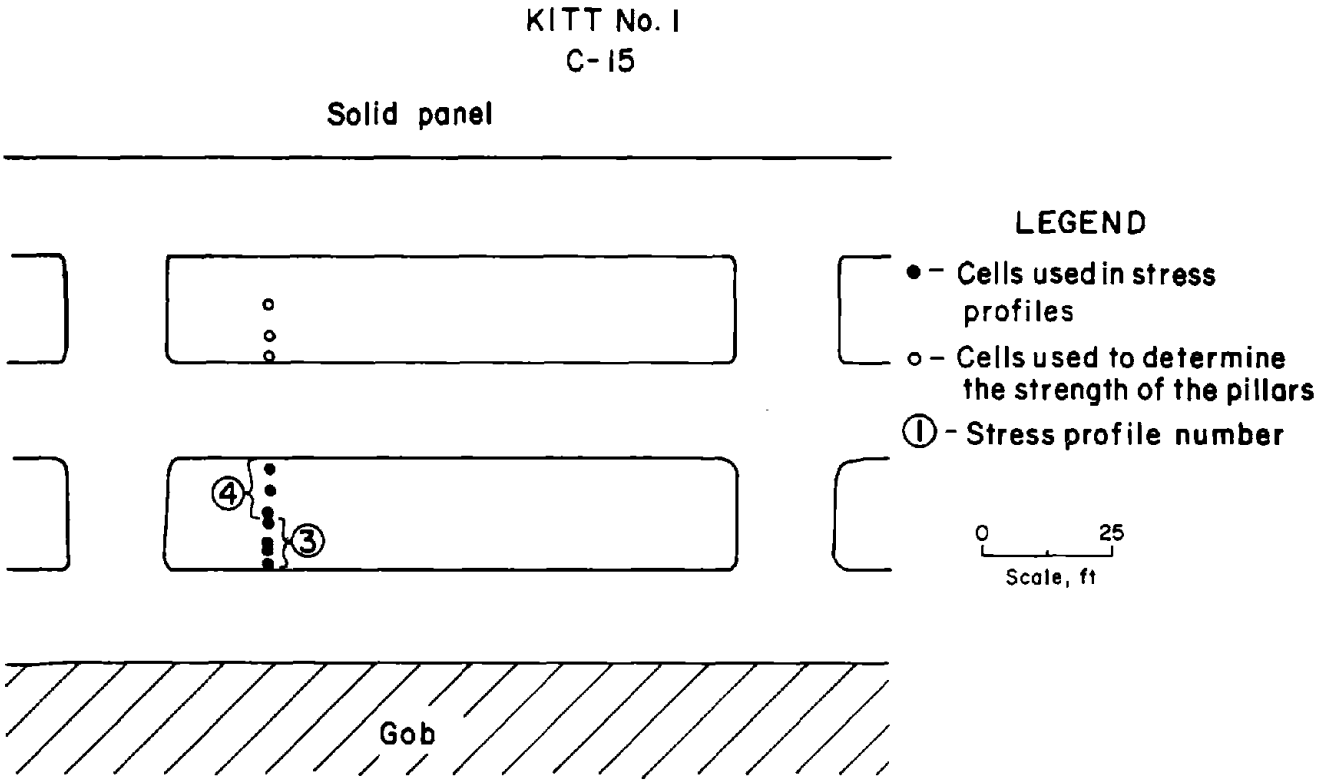

Figure 11.—Second pillar study site at Kitt Mine.

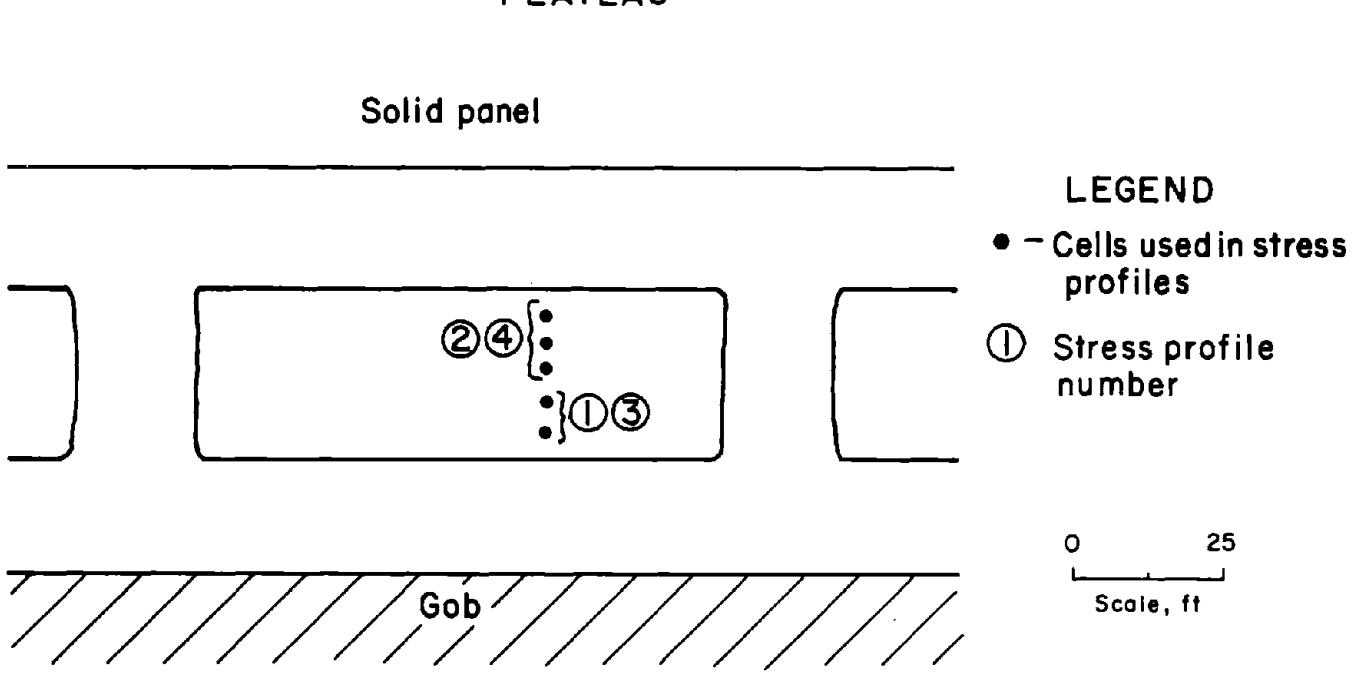

Figure 12.—Pillar study sites at the Plateau Mine.

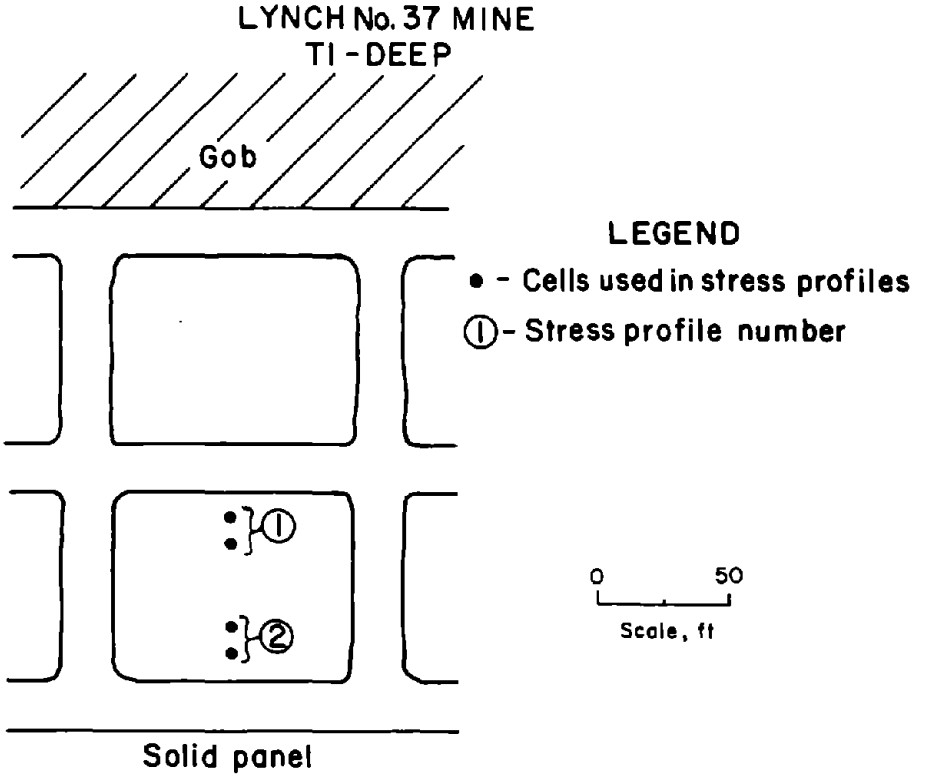

Figure 13.—Pillar study site at the Lynch Mine.

SELECTION OF STRESS PROFILES

As the goal of the study is to evaluate formulas predicting the stress rise within the yield zone, a key task was the selection of stress profiles from the field data. A typical stress profile is shown in figure 14. In the end, a total of 34 profiles from 15 pillars were selected. The profiles were identified using the following criteria:

1. The measurements indicated that the pillar reached its ultimate resistance, or at least that pillar failure extended a significant distance into the pillar.
2. Only cells that appeared to be giving valid readings were used in the profiles.

Details of the 34 stress gradients are shown in table 1, including the location of the cell and the actual measured stress change (or cell pressure). An average of 3.1 stressmeters were used in the construction of each profile. While most of the profiles extend less than two seam heights (2h) into the rib, the deepest profile (VP No. 3-4) is 5.5h, and nine other profiles are more than 2.5h deep.

The greatest problem encountered in choosing the profiles is that they were seldom static. In general, as a pillar's load increased, and the yield zone expanded, the stresses within the yield zone tended to decrease (see fig. 14). This "strain-softening" behavior within the yield zone may account for some of the scatter in the data.

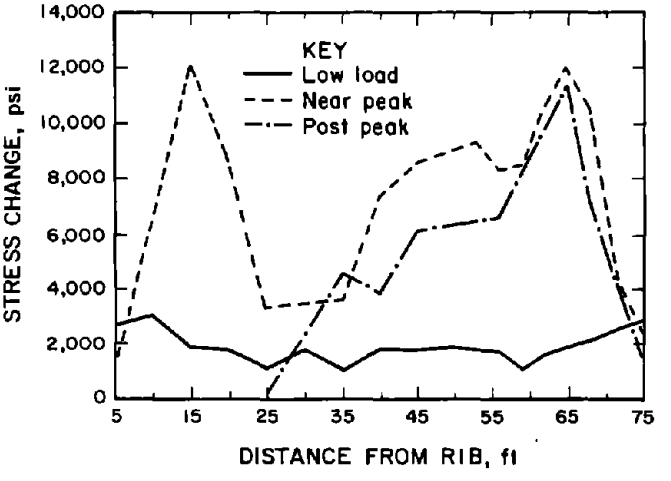

Figure 14.—Typical pillar stress profiles measured in the field.

ANALYSIS OF MEASURED STRESS GRADIENTS

Because of the limited number of stressmeters in each profile, linear regression was the only curve-fitting function applied to the data (table 2). The R-squared values obtained from the regression averaged 0.94 for three-cell profiles and 0.89 for four- and five-cell profiles. These results indicate that a linear model is reasonably appropriate for these data.

Table 2.—Calculated data

ID	$\Delta\sigma_v$, psi/ft	σ_v @ x=0, psi	$\Delta\sigma_v$, psi/h	σ_v @ x/h=1, psi	R^2
Kitt-1	122	1318	610	3424	.93
Kitt-2	167	-650	835	1681	.99
Kitt-3	188	-362	940	2084	.89
Kitt-4	161	-185	805	2126	.95
Keystone No. 1-1	269	-572	1479	2280	.91
Keystone No. 1-2	253	-809	1391	1955	.99
Keystone No. 1-3	246	273	1353	2997	.89
Keystone No. 1-4	222	124	1221	2716	.75
Keystone No. 1-5	611	-1791	3360	2943	.99
Keystone No. 1-6	532	-1442	2926	2856	.97
Keystone No. 1-7	390	-13	2145	3504	.69
Keystone No. 1-8	508	-644	2794	3522	.96
Keystone No. 1-9	263	477	1446	3296	.99
Keystone No. 1-10	266	-804	1463	2032	.85
VP No. 3-1	971	-3659	583	4667	.99
VP No. 3-2	704	-651	1969	3043	.74
VP No. 3-3	335	1966	5340	4770	.93
VP No. 3-4	1084	-3927	3872	6152	NAp
VP No. 3-5	215	-288	1842	6739	.99
VP No. 3-6	1256	-5892	5962	4966	NAp
Foidel Creek-1	244	-950	2440	3712	NAp
Foidel Creek-2	100	650	1000	3872	NAp
Foidel Creek-3	200	1840	2000	6062	NAp
Foidel Creek-4	348	-823	3480	4879	NAp
Foidel Creek-5	240	1646	2400	5861	NAp
Foidel Creek-6	356	1800	3560	7582	NAp
Foidel Creek-7	483	-3000	4830	4052	NAp
Foidel Creek-8	467	-2700	4670	4192	NAp
Plateau-1	444	-2310	4440	5496	.99
Plateau-2	424	-2273	4240	5333	.92
Plateau-3	236	-53	2360	5673	.94
Plateau-4	222	-127	2220	5459	.97
Lynch No. 37-1	53	1390	1182	3755	NAp
Lynch No. 37-2	179	-1620	6908	3876	NAp

σ_v Measured vertical stress.
x Distance from rib.
h Pillar height.
NAp Not applicable.

The magnitudes of the slopes, or stress gradients, were evaluated next. Two stress gradients were obtained for each profile, the first being the rate of stress rise per foot of distance from the rib ($\Delta\sigma_v$, psi/ft), and the second being the stress rise per seam height of distance from the rib ($\Delta\sigma_v$, psi/h). The stress gradients were also divided into three categories by cell type.

The results, summarized in table 3, indicate that the VWS measurements yielded the lowest stress gradients, and the BPF data the greatest, for both types of gradient ($\Delta\sigma_v$, psi/ft and $\Delta\sigma_v$, psi/h). Stress gradients from the BPC data were similar to those obtained from the VWS when evaluated as $\Delta\sigma_v$ (psi/ft), but approached those of the BPF when calculated as $\Delta\sigma_v$ (psi/h). Table 3 also indicates that there is considerable scatter within each group of measurements. The standard deviation of the slopes was approximately 50% of the mean for all three cell types.

Table 3.—Derived stress gradient parameters

Cell type	σ_v @ x=0, psi		$\Delta\sigma_v$, psi/ft		$\Delta\sigma_v$, psi/h		σ_{vt} @ x/h=1, psi	
	x	s	x	s	x	s	x	s
VWS	-331	893	277	151	1582	817	2820	752
BPF	-2075	2647	761	382	4184	2101	5043	1095
BPC	-525	1703	314	118	3136	1181	5181	1066

σ_v Measured vertical stress.
x Distance from rib.
h Pillar height.
x Mean.
s Standard deviation.
σ_{vt} Total vertical stress.

Multiple regression was employed to examine the effects of other parameters, including depth of cover, seam height, coal strength, and roof rock quality on the stress gradient. No meaningful correlations were observed when the data from each cell type were analyzed separately. With only two study mines for each cell type, however, the range of each variable was quite limited. When the data set was analyzed as a whole, a weak correlation (R-squared=0.22) was found between depth of cover and stress gradient. The most likely explanation for this is the strong correlation in the data base between depth and cell type. All but two of the VWS gradients were obtained at depths of less than 1,000 ft, while all the BPF data were from study sites located beneath at least 1,800 ft of cover. Indeed, the overwhelming influence of cell type may have masked effects due to the other parameters.

Further evidence of the strain softening discussed earlier can be found in the data. Of the 10 stress profiles obtained at the Keystone Mine, four extended to a depth of 15 ft or more. The average gradient for these profiles was 247 psi/ft, against 428 psi/ft for the profiles that only extend 10 ft into the pillar. Similar, though less pronounced,

trends can be observed in the VP No. 3 and Kitt Mine profiles.

The linear regression results were also used to evaluate the level of stress that is maintained near the rib. Table 2 gives the calculated intercept, or stress at x=0, for each profile. No actual measurements were made this close to the rib, so these intercepts must be considered hypothetical. Also, in the case of the VWS and BPF data, the development stresses present before the measurements began must be included in order to estimate the total stress. Using the pillar and entry dimensions shown in figures 5 through 13 and the depth of cover at each site, the development stresses were estimated using tributary area theory. Tributary area theory was considered appropriate because local extraction ratios were below 45% in all cases but two and because the subsequent stress measurements indicated that no significant pillar yielding had occurred at the time of development. The estimated total vertical stress at a distance of x=h from the rib was calculated as the development stress, plus the intercept, plus the stress increase due to the stress gradient. These data are also included in table 2 and summarized by cell type in table 3. They indicate that significant vertical stresses are maintained at a distance of one seam height from the rib: approximately 2,800 psi for VWS data, and 5,100 psi for BPC and BPF data.

PILLAR STRESS AND PILLAR STRENGTH FORMULAS FROM THE FIELD DATA

The field data may be used to construct pillar stress and pillar strength formulas that can be compared directly with the models. Using the data from table 3, and the estimated development loads (VWS and BPF data only), the estimated pillar stress gradients are

$$\text{VWS} = 1096 + 1582 \times \frac{x}{h}, \quad (17)$$

$$\text{BPF} = 592 + 4184 \times \frac{x}{h}, \quad (18)$$

$$\text{BPC} = -525 + 3136 \times \frac{x}{h}, \quad (19)$$

$$\text{Average} = 388 + 2967 \times \frac{x}{h}. \quad (20)$$

These stress gradients imply pillar strength as

$$\text{VWS} = 1360 \times \left(0.8 + 0.2 \times \frac{w}{h}\right), \quad (21)$$

$$\text{BPF} = 1289 \times \left(0.46 + 0.54 \times \frac{w}{h}\right), \quad (22)$$

$$\text{BPC} = 525 \times \left(\frac{w}{h} - 1\right), \quad (23)$$

$$\text{Average} = 882 \times \left(0.44 + 0.56 \times \frac{w}{h}\right). \quad (24)$$

Figure 15 shows the pillar stress gradients generated from equations 17 to 20, and figure 16 compares the calculated pillar strength formulas with three empirical models discussed earlier. For narrow pillars, the VWS and BPF measurements predict pillar strengths significantly greater than any of the current models. For more squat pillars, the BPC and BPF data predict strengths exceeding any of the empirical formulas. The rate of stress increase is still much less than that predicted by most analytical formulas, however.

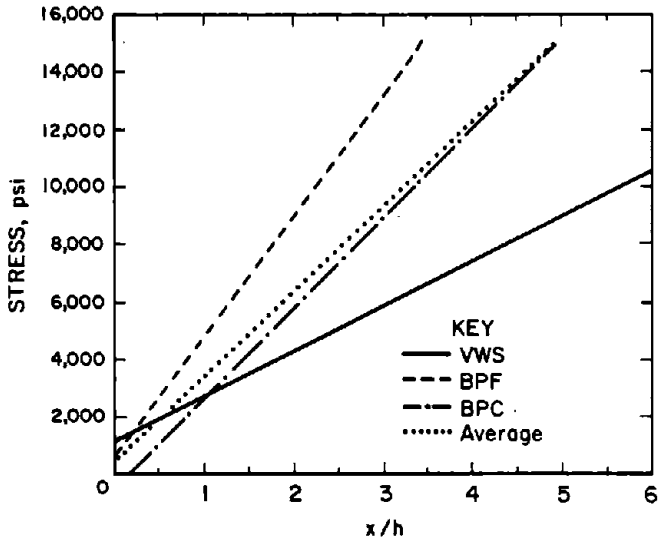

Figure 15.—Stress gradients generated from the field measurements.

The calculated pillar strength formulas were determined using measured stresses to x/h=4, and therefore apply to pillars of w/h=8. The only known study site at which a serious attempt has been made to collect data within failed coal pillars of w/h>8 was at VP No. 3. Although five such pillars have been instrumented (see figs. 5-7), the data have been ambiguous. Figure 14 shows typical results obtained from an 80-ft (w/h=13) pillar before it was destroyed by a series of small rib bumps. In this case, as in the others, no stress changes were measured in the core that exceeded the peak stresses measured at approximately x/h=4. One explanation is that the peak stress attain by a coal pillar is limited by some physical factor, such as interface slip or the "pseudoductile" failure described by Barron. Another possibility is that the BPF cells themselves failed at stresses exceeding 10,000 psi, which corresponds to gage pressures of more than 25,000 psi.

If the conservative interpretation that pillar stresses cannot exceed the level attained at x=4h is adopted, then the pillar strength may be adapted accordingly. Using the average stress gradient derived above (equation 24) for illustration, a formula for the strength of pillars in excess of w/h=8 is

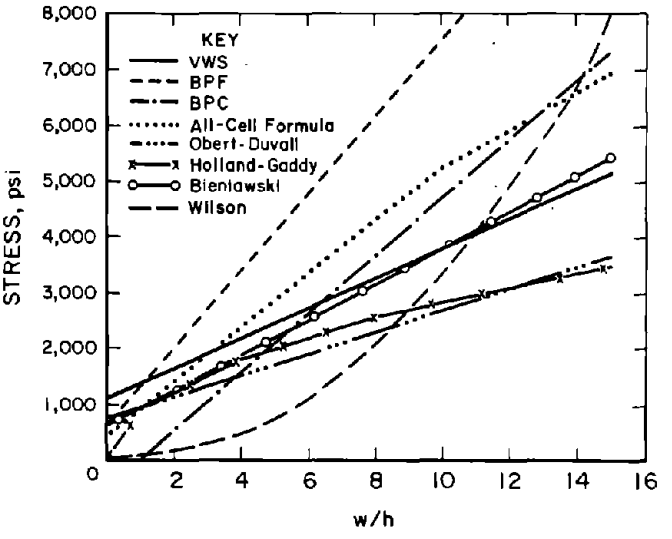

Figure 16.—Pillar strength formulas obtained from stress measurements compared with existing formulas.

$$Sp = \frac{\left(12{,}300 \times w^2 - 95{,}000 \times w \times h + 253{,}000 \times h^2 \right)}{w^2} \quad \left[\text{for } \frac{w}{h} > 8 \right]. \qquad (25)$$

This formula is also shown on figure 16 as the "all cell formula."

CONCLUSIONS

1. There is currently a wide range of opinion regarding the trend of the stress gradient within yielded coal pillars. One school of thought holds that the stress increases exponentially as the pillar core is approached, while another believes the stress approaches an asymptotic maximum. Various intermediate interpretations are also current.

2. Empirical pillar *strength* formulas may be converted to pillar *stress* formulas, using the concept that the pillar load-bearing capacity is the pillar stress gradient integrated over the load-bearing area.

3. Stress measurements are available from many pillars for x/h up to 4. The measurements display considerable variability, much of it apparently attributable to the different cell types and calibration procedures that have been used.

4. The field data generally support the interpretation that stress gradient within the yield zone is approximately linear, and that relatively high stresses may be maintained near the ribline.

5. "Pillar strength formulas" were derived from the field data. These generally predict higher strengths than current empirical formulas, but much lower rates of stress increase than most analytical or numerical models.

6. Little field data are available beyond a distance of x=4h from the ribline. What little data there are indicate that pillar stress may cease to increase. Another "pillar strength formula" was developed assuming the pillar stress remains constant beyond x=4h.

7. A number of areas for future research were identified:

- Better calibration procedures for stress cells, including the effects of biaxial stresses and coal yielding.
- Stress measurements within the cores of very squat pillars (w/h>8).
- The effects of strain softening and time on pillar strength.
- The effects of interfaces, seam height, depth, and material properties.

REFERENCES

1. Babcock, C. O. Equations for the Analysis of Borehole Pressure Cell Data. Proc. of the 27th U.S. Symp. on Rock Mech., Univ. of Alabama, Tuscaloosa, AL, 1986, pp. 233-240.

2. Barron, K. An Analytical Approach to the Design of Coal Pillars. CIM Bull., v. 77, No. 868, Aug. 1984, pp. 37-44.

3. Bieniawski, Z. T. Rock Mechanics Design in Mining and Tunneling. A. A. Balkema, 1984, 272 pp.

4. Bunting, D. Chamber Pillars in Deep Anthracite Mines. Trans. AIME, 1911, pp. 739-748.

5. Campoli, A. A., T. M. Barton, F. C. Van Dyke, and M. Gauna. Mitigating Destructive Longwall Bumps Through Conventional Gate Entry Design. BuMines RI 9325, 1990, 38 pp.

6. Conroy, P. A Demonstration of Longwall Mining - Appendix. BuMines OFR 86(2)-85, 1983, 371 pp.

7. DeMarco, M. J., J. R. Koehler, and P. H. Lu. Characterization of Chain Pillar Stability in a Deep Western Coal Mine - Case Study. Min. Eng., v. 40, No. 12, Dec. 1988, pp. 1115-1119.

8. Fossum, A. F., J. E. Russel, and F. D. Hansen. Analysis of the Vibrating Wire Stress Gage in Soft Rock. Exp. Mech., July 1977, pp. 261-264.

9. Greenwald, H. P., H. D. Howarth, and J. Hartman. Experiments on the Strength of Small Pillars in the Pittsburgh Bed. BuMines RI 3575, 1941, 7 pp.

10. Hanna, K., K. Haramy, and T. R. Ritzel. Automated Longwall Mining For Improved Health and Safety at the Foidel Creek Mine. AIME-Soc. Min. Eng. Preprint No. 91-165, 1991, 8 pp.

11. Hawkes, I., and W. V. Bailey. Low Cost Cylindrical Stress Gage. BuMines OFR 54-75, 1973, 145 pp.

12. Heasley, K. A. Understanding the Hydraulic Pressure Cell. Proc. of the 30th U.S. Symp. on Rock Mech., Morgantown, WV, 1989, pp. 485-492.

13. Hsuing, S. M., and S. S. Peng. Chain Pillar Design for U.S. Longwall Panels. Min. Sci. and Technol., v. 2, 1985, pp. 279-305.

14. Iannacchione, A. T. Behavior of a Coal Pillar Prone to Burst in the Southern Appalachian Basin of the U.S. Rockbursts and Seismicity in Mines, Fairhurst (ed.), 1990, Balkema, Rotterdam, pp. 295-300.

15. ____. The Effect of Roof and Floor Interface Slip on Coal Pillar Behavior. Proc. of the 31th U.S. Symp. on Rock Mech., Denver, CO, 1990, pp. 153-160.

16. Kripakov, N. P. Analysis of Pillar Stability on Steeply Pitching Seam Using the Finite Element Method. BuMines RI 8579, 1981, 33 pp.

17. Lu, P. H. Mining Induced Stress Measurement with Hydraulic Pressure Cells. Proc. of the 25th U.S. Symp. on Rock Mech., Northwestern Univ., Chicago, IL, 1984, pp. 204-211.

18. Maleki, H. Development of Modeling Procedures for Coal Mine Stability Evaluation. Proc. of the 31st U.S. Symp. on Rock Mech., CO Sch. Mines, Golden, CO, 1990, pp. 85-92.

19. Maleki, H. N., and M. Moon. In Situ Pillar Strength Determination for Two-Entry Longwall Gates. Proc. of the 7th Int. Conference on Ground Control in Mining, WV Univ., Morgantown, WV, 1988, pp. 10-19.

20. Mark, C. Analysis of Longwall Pillar Stability. Ph.D. Thesis, PA State Univ., University Park, PA, 1987, 414 pp.

21. Panek, L. A., and L. A. Stock. The Development of a Rock Stress Monitoring Station Based on the Flat Slot Method of Measuring Existing Rock Stress. BuMines RI 6537, 1964, 61 pp.

22. Pariseau, W. G., and I. M. Eitani. Post Elastic Vibrating Wire Stress Measurements in Coal. Proc. of the Int. Symp. on Field Measurements in Rock Mech., Zurich, Switzerland, 1977, pp. 255-273.

23. Park, D. W., and V. Gall. Supercomputer Assisted Three-Dimensional Finite Element Analysis of a Longwall Panel. Proc. of the 30th U.S. Symp. on Rock Mech., WV Univ., Morgantown, WV, 1989, pp. 133-140.

24. Salamon, M. D. G., and A. H. Munro. A Study of the Strength of Coal Pillars. J. S. Afr. Inst. Min. Metall., v. 68, Nov. 1967, pp. 55-67.

25. Salamon, M. D. G., and H. Wagner. Practical Experiences in the Design of Coal Pillars. Proc. of the 21st Int. Conf. of Safety in Mines Research Institutes, Sydney, Australia, 1985, pp. 3-10.

26. Schuerger, M. G. An Investigation of Longwall Pillar Stress History. Proc. of the 4th Conf. on Ground Control in Mining, WV Univ., Morgantown, WV, 1984, pp. 41-50.

27. Sheorey, P. R., M. N. Das, S. K. Bordia, and B. Singh. Pillar Strength Approaches Based on a New Failure Criterion for Coal Seams. Int. J. Min. Geol. Eng., No. 4, 1986, pp. 273-290.

28. Tanious, N. S. The Use of the Vibrating Wire Stressmeter in Coal. AIME-Soc. Min. Eng. Preprint No. 87-114, 1987, 8 pp.

29. Wagner, H. Determination of the Complete Load-Deformation Characteristics of Coal Pillars. Proc. of the 3rd Int. Congress on Rock Mech., Denver, CO, 1974, pp. 1076-1081.

30. Wang, F. D., W. A. Skelly, and J. Wolgamott. In Situ Coal Pillar Strength Study. BuMines OFR 107-79, 1976, 243 pp.

31. Wilson, A. H. An Hypothesis Concerning Pillar Stability. Min. Eng., London, v. 131, No. 141, June, 1973, pp. 409-417.

32. ____. The Stability of Underground Workings in the Soft Rocks of the Coal Measures. Int. J. of Min. Eng., v. 1, 1983, pp. 91-187.

33. Zern, E. N. Coal Miners' Pocketbook (12th ed.). McGraw-Hill, New York, 1928, pp. 641-645.

34. Zipf, R. K., and K. A. Heasley. Decreasing Coal Bump Risk Through Optimal Cut Sequencing with a Non-Linear Boundary Element Program. Proc. of the 31st U.S. Symp. on Rock Mech., Denver, CO, 1990, pp. 947-954.

STRENGTH AND STABILITY OF COAL PILLARS

By M. D. G. Salamon[1]

INTRODUCTION

Pillars are the most frequently used natural supports in coal mining. Coal pillars are employed in room-and-pillar workings as either permanent or temporary supports. Chain pillars are applied to protect the entries or gates of longwall faces. The role of pillars in each of these applications is diverse, and in each instance they are subject to different loading conditions.

Pillar failures can impair the efficiency of mining operations, the economic consequences of which, especially in capital-intensive longwalling, can be serious or even crippling. In addition, the history of mining is blemished by disasters emanating from pillar collapses.

Many attempts have been made in the past to put pillar design on a rational basis. The design methods, which have a reasonably long history of success, all seem to be based on some empirical pillar strength formula. A common feature of these empirical expressions is that they all predict a rise in pillar strength with an increase in the width-to-height ratio of the pillars.

Much of the earlier experience in the application of pillar strength formulas relates to pillars with relatively small width-to-height ratios. During the 1960's and 1970's, the interest in squat pillars awakened mainly owing to an increase in the application of retreating longwalls and the resulting wider use of chain pillars. The understanding of the failure process of such wide pillars is still inadequate.

There are two other aspects of the use of pillars which, because they represent serious threat to safety, warrant considerable further attention. These are the problems of coal bumps and the sudden or uncontrolled collapse of pillars. Although the occurrence of coal bumps is not restricted to pillars since they can happen at any highly loaded coal edge, a discussion of pillar mechanics cannot neglect the hazard represented by them.

Yield pillars are often discussed in technical papers because of their professed properties that can be used with advantage in certain applications, e.g., to control the conditions in longwall entries.

In this paper, an attempt is made to discuss the behavior of pillars with the object of aiding the more mechanistic definition of pillar strength and clarifying the ideas concerning stability as they influence the behavior of pillars and coal ribsides. To achieve this, first the present state of the art concerning pillar mechanics is reviewed from a somewhat restricted point of view, followed by the presentation of some reasonably novel ideas concerning pillar strength and stability.

STATE OF THE ART IN PILLAR MECHANICS

EMPIRICAL STRENGTH FORMULAS

A variety of pillar formulas have been proposed, mainly on the basis of laboratory tests and the back analysis of case histories. Most of the suggested expressions fall into one of two families of relationships. If the height and width of the pillars of square cross sections are M and W, respectively, then these families are defined by:

$$\sigma_{s1} = K_1 [r + (1 - r) (W/M)] \qquad (1)$$

$$\sigma_{s2} = K_2 (M/M_o)^{\alpha} (W/W_o)^{\beta}, \qquad (2)$$

where r, α, and β are dimensionless constants. Moreover, K_1 is the uniaxial compressive strength of a coal cube and K_2 is the strength of a reference specimen of volume $V_o = W_o^2 M_o$. Probably the most commonly used values of the parameters in equation 1 are

$$r = 0.64 \qquad K_1 = 900 \text{ psi} = 6.2 \text{ MPa}, \qquad (3)$$

where the value of r is due to Bieniawski (*1*)[2] and that of K_1 to Mark (*2*). The constants in equation 2, which have been obtained by back calculations from case histories and

[1]Distinguished professor, Mining Engineering Department, Colorado School of Mines, Golden, CO.

[2]Italic numbers in parentheses refer to items in the list of references at the end of this paper.

used by the coal mining industry in the Republic of South Africa since 1967, are (*3*):

$$K_2 = 7.2 \text{ MPa},$$

$$\alpha = -0.66,$$

$$\beta = 0.46,$$

$$W_o = M_o = 1 \text{ m}. \quad (4)$$

Figure 1 reveals that the expressions in equations 1 and 2, if the constants in (3) and (4) are used, do not result in greatly different pillar sizes.

The formulas in equations 1 and 2 can be rewritten in terms of the width-to-height ratio, R = W/M, and volume, $V = W^2M$. The new forms of these formulas are

$$\sigma_{s1} = K_1 [r + (1 - r) R] \quad (5)$$

$$\sigma_{s2} = K_2 (V/V_o)^a (R/R_o)^b \quad (6)$$

where

$$a = (\alpha + \beta)/3 \qquad b = (\beta - 2\alpha)/3. \quad (7)$$

The formula in equation 6 indicates the well-known property of coal that its strength is a function of the volume of the specimen. This relationship is usually given in the form

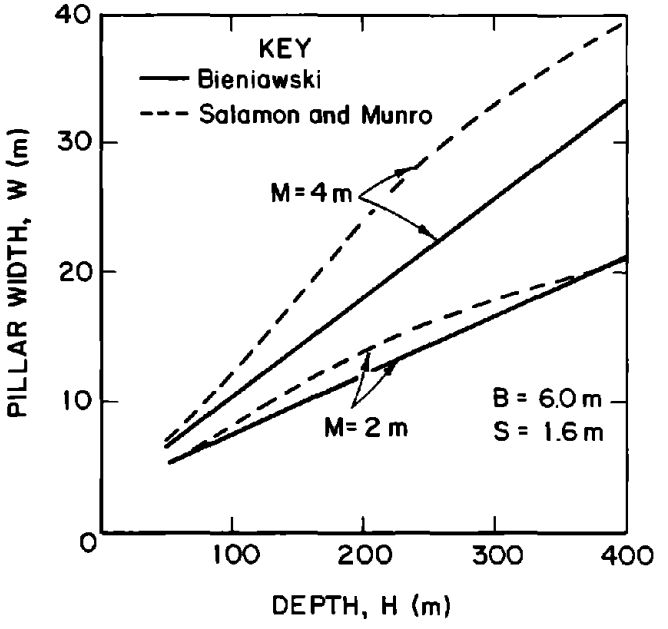

Figure 1.—Comparison of pillar widths obtained from the Bieniawski and South African pillar strength formulas (Salamon (*40*)).

$$K = K_{lab} (W/W_{lab})^{\delta}, \quad (8)$$

where δ is a negative constant, which reportedly ranges from -0.50 to -0.17. According to equation 6,

$$\delta = 3a = \alpha + \beta, \quad (9)$$

which yields $\delta = -0.2$ in the case of the values given in (4). The formula in equation 5 ignores the size dependency of coal strength because it assumes that K_1 corresponds to at least a minimum reference volume beyond which the effect of size can be neglected (i.e., 1.5 to 2.0-m edge length, (*1*)). The effect of specimen size on the uniaxial compressive strength will not be considered further in this paper.

A common feature of the expressions in equations 5 and 6 is that an increase in width-to-height ratio results in a rise in pillar strength. These formulas confirm a well-known feature of laboratory coal testing that generally also applies to coal pillars, as it has been amply substantiated by the observed behavior in the field. True to the nature of empirical relationships, these formulas do not reveal anything with regard to the reason for the stated influence of the width-height ratio. Thus, they cannot be the basis of an in-depth discussion of pillar mechanics.

CONFINED CORE CONCEPT OF PILLAR STRENGTH

The approach to provide a mechanistic explanation of the effect of the pillar's width-height ratio on its strength is usually referred to as the "confined core" concept. The main advocate of this idea has been A. H. Wilson (*4-5*), although his work in some respect had been preceded at least by one other publication (*6*). Many have contributed to the refinement and application of the concept, e.g., Abel and Hoskins (*7*), and Barron (*8-9*).

The basis of the idea is that the compressive strength of brittle materials, such as coal, is enhanced by confinement. For example, the Coulomb failure criterion defines this effect by requiring that to avoid failure, the major principal stress (compression is taken to be positive in this paper), σ_1, must obey the inequality

$$\sigma_1 \leq \kappa \sigma_3 + \sigma_c. \quad (10)$$

Here, σ_3 is the minor principal stress, σ_c is the uniaxial strength of the material, and κ is equivalent to the Rankine constant employed in soil mechanics, i.e.,

$$\kappa = \frac{1 + \sin \rho}{1 - \sin \rho}, \quad (11)$$

where ρ is the angle of internal friction. Since ρ usually is in the range of 25° to 50° for coal (*10*), the value of κ almost always exceeds 2.5. In practice, κ is likely to range from 3.0 to 5.5.

Underground, before yield is initiated, the stresses are highest at the pillar edges. Also, the coal located at the pillar sides is not confined. Owing these reasons, failure initiates here. After the failure has commenced, i.e., the maximum resistance of the unconfined coal has been overcome (see figure 2), the deformation of this material proceeds along the descending branch of the stress-strain curve. As the load-bearing capacity of the yielding coal diminishes, the pillar edge must shed load, and at least some of this load is transferred to coal further inside the pillar. If this coal is sufficiently confined, it will be able to accept the enhanced burden. If the confinement is still insufficient, the simultaneous yielding and load transfer proceed inward until the pillar is able to sustain the redistributed load, and a new state of equilibrium is reached. If it proves impossible to achieve a new equilibrium state, the whole pillar will fail.

It is clear from this that an increasingly squatter pillar can have higher strength only if the confinement of its core is intensified as a result of a growth in its width-to-height ratio. Fortunately, the process of pillar edge crushing can produce such a confining mechanism spontaneously. Clearly, the yielding coal at or near to the edges tends to migrate toward the open excavations. However, this movement induces frictional resistance at the interfaces between the seam and the neighboring beds, which restrains the migration. The magnitude of this restraint and the associated horizontal stress grow with increasing distance from the pillar sides. Thus, the opportunity appears to exist for greater core confinement in squatter pillars.

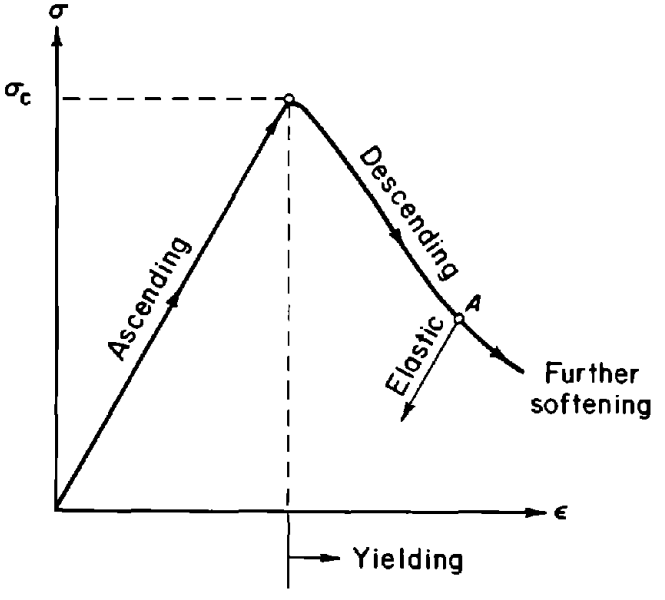

Figure 2.—Strain softening behavior of coal in unconfined compression, indicating at point *A* the possibility of elastic unloading or further yield.

Wilson (*4-5*) in developing his confined core approach to pillar design took advantage of this yielding mechanism and also ensured that the equilibrium of forces is satisfied, at least on a macro scale. His initial interest was in the siting or the protection of longwall gates, i.e., to determine the minimum distance from the edge of a panel at which an entry could be located safely. He reported (*5*) that in the case of a horizontal seam the vertical, σ_z, and horizontal, σ_x, stresses in the crushed zone are given by:

$$\sigma_z = p\,\kappa \exp(Fx/M), \qquad \sigma_x = p \exp(Fx/M), \quad (12)$$

where M is the extracted height, x is the distance from the edge, p is the horizontal edge restraint, and

$$F = \frac{\kappa - 1}{\sqrt{\kappa}} + \frac{(\kappa - 1)^2}{\kappa} \tan^{-1}(\sqrt{\kappa}). \quad (13)$$

Here, it is assumed that the crushed coal has no residual uniaxial strength.

In many instances, advocates of the confined core approach postulate that the uniaxial compressive strength of the crushed coal is nonzero. While this seems a dubious assumption, it is often unavoidable, since a stable yield zone can be obtained only if either the residual strength or the edge constraint is nonzero. Here, the latter approach is chosen. It may be mentioned that Wilson discussed two modes of yielding. He postulated either that yielding is restricted to the seam or, alternatively, he assumed that in addition to the seam, the roof and floor also yield. Here and in the sequel, it is postulated that the roof and floor remain elastic. This is done merely for the sake of brevity here and *not* to imply that the failure cannot occur in the roof and/or in the floor.

To deal with the conditions in the vicinity of longwall panels, Wilson (*5*) made some sweeping assumptions concerning (1) the pressure rise with distance into the caved waste, (2) the distribution of the transferred load over the ribside, and (3) the depth to which the yield zone penetrates into the ribside. These assumptions enabled him to deduce recommendations with regard to the minimum width of the pillars required to protect a longwall entry. While many of Wilson's assumptions can be questioned because of their tenuous physical basis, his work represents the first rational attempt to design longwall chain pillars. His work has gained fairly wide acceptance and is being applied by mining engineers in practical situations, (*11*).

Wilson has extended his approach to pillars of finite dimensions (*5*). Here, his work as applied to pillars of square cross section is reviewed (fig. 3).

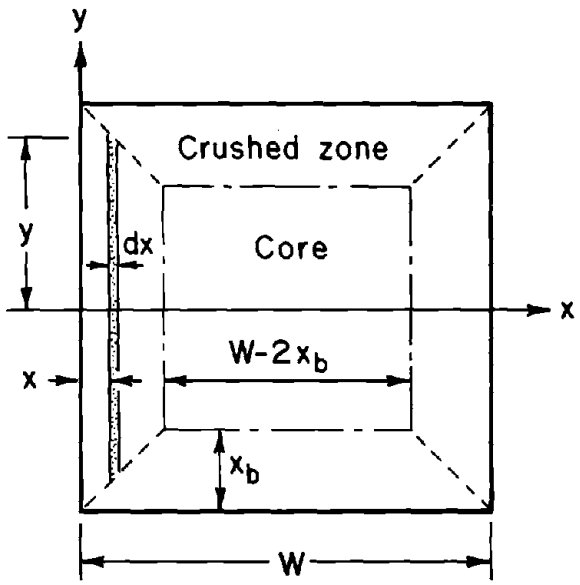

Figure 3.—Wilson's concept of a yielding pillar of square cross section with a crushed zone of width x_b and a confined core of width W - $2x_b$.

Assume that the pillar is symmetrically loaded. In such cases, the yield zone penetrates to the same depth x_b on all sides. Wilson appears to use two assumptions to determine the width of the yield zone. His more frequently used assumption is that yielding ends when the horizontal stress in the crushed coal reaches its premining value. He assumes that the horizontal and vertical virgin stresses are both equal to $q = \gamma H$, where γ is the weight of a unit volume of rock and H is the depth below surface. Thus, according to this assumption the width of the crushed region can be obtained from (12) and is given by:

$$x_b = (M/F) \ln (q/p). \quad (14)$$

At the interface between the crushed zone and the pillar core, there is a discontinuity in the vertical stress. On the crushed side

$$\sigma_z = p \kappa \exp (Fx_b/M), \quad (15)$$

and on the intact or core side the stress takes the form:

$$\sigma_z = p \kappa \exp(Fx_b/M) + \sigma_c. \quad (16)$$

Wilson then argues that the vertical stress in the core is virtually uniform and equals that given by equation 16.

If the pillar is so small that $W \leq 2 x_b$, then the pillar will not have a solid core. The critical width-to-height ratio, R_c, can be determined from equation 14:

$$R_c = (2/F) \ln (q/p). \quad (17)$$

Thus, if $R \leq R_c$ the total force, L_{tot}, acting on the pillar equals merely the sum of the loads born by the crushed coal, L_{y1}. Thus, on the basis of figure 3 the load carried by such a pillar is ($x_b = W/2$).

$\underline{R \leq R_c}$

$$L_{tot} = L_{y1} = 8 \int_0^{W/2} \sigma_z y \, dx = 4 \int_0^{W/2} \sigma_z (W - 2x) \, dx, \quad (18)$$

where σ_z is given in (12). After integration, the average pressure on the pillar is

$$\sigma_{av1} = L_{tot}/W^2 = \frac{2 \kappa p}{(FR/2)^2} \left(e^{FR/2} - FR/2 - 1\right). \quad (19)$$

This is also the ultimate strength of any pillar since it is assumed here that the whole structure is in a state of yield.

In general, the load supported by a pillar consists of the sum of the load on the crushed regions, L_{y2}, and the load sustained by the core.

$\underline{R \geq R_c}$

$$L_{tot} = L_{y2} + L_c,$$

$$L_{y2} = 8 \int_0^{x_b} \sigma_z \, y \, dx,$$

$$L_c = (\kappa q + \sigma_c) (W - 2x_b)^2, \quad (20)$$

and the average stress is given by:

$$\sigma_{av2} = \frac{4\kappa}{FR^2} \left\{ q \left[R - \frac{2}{F} \left[\ln \frac{q}{p} - 1 \right] \right] \right\}$$

$$- p \left[R + \frac{2}{F} \right] + \frac{\kappa q + \sigma_c}{R^2} \left[R - \frac{2}{F} \ln \frac{q}{p} \right]^2. \quad (21)$$

According to Wilson, σ_{av} represents the limit of mean stress on the pillar at which roadway stability is ensured. It will be observed that σ_{av} is defined by the width-height ratio (R), coal properties, (ρ, σ_c), lateral constraint (p), and the virgin ground stress (q). In figure 4, the variation of σ_{av} is shown as a function of the width-to-height ratio. Note that in accordance with expectation, an increase in R is associated with a growth in σ_{av}.

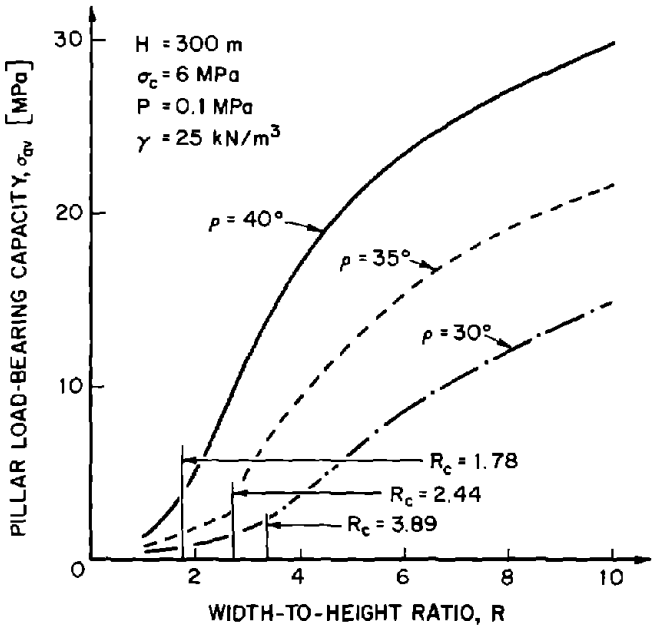

Figure 4.—Examples of load-bearing capacities (after Wilson).

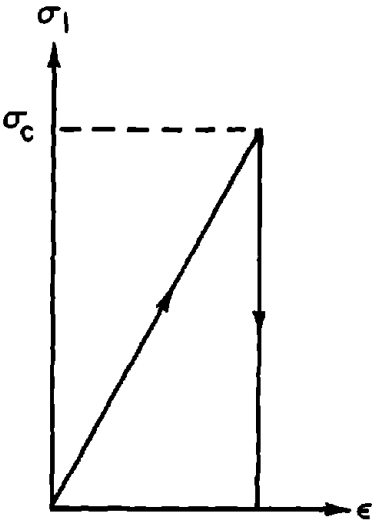

Figure 5.—Instantaneous drop in strength for unconfined coal.

The ultimate pillar strength represents the alternative assumption of Wilson with regard to width of the yield zone. This ultimate strength is given by equation 19 when it is used without restriction on the value of R.

CRITIQUE OF CONFINED CORE CONCEPT

Without wishing to diminish the credit due to its proponent, the original confined core concept of Wilson has a number of fundamental weaknesses. The most important of these warrant some discussion.

1. *The surrounding rock mass.* The rock mass within which the seam is sandwiched is an integral part of the mine system. In fact, this mass is the instrument of loading in the mine structure. On the basis of the analogy between this system and the laboratory system consisting of the loading machine (i.e., with its stiffness) and the specimen, the deformation of the rock mass is expected to play a major role in the loading and the stability of pillars. Unless the deformation behavior of this mass is taken into account, the pillar design problem cannot be solved satisfactorily. For example, the lack of this deformation mechanism forced Wilson to make weak assumptions with regard to the pressure distribution in the gob and in the still elastic rock mass.

2. *Unsatisfactory assumption concerning the penetration of yield.* There does not appear to be any rational explanation (except perhaps convenience) for the choice of σ_x = q at the interface between crushed and elastic coal (*12*). It will be necessary to replace this assumption with a more satisfactory interface condition.

3. *Discontinuous drop in cohesion at yield.* The comparison of the expressions in (10) and (12) reveals that Wilson accepted the underlying assumption that at the instant of yield the value of σ_c instantaneously reduces to zero (or at least to its residual value). Such reduction requires that the stress-strain curve follows the path depicted in figure 5. Nature cannot accommodate in a stable manner such abrupt changes.

4. *Residual uniaxial compressive strength.* A consequence of the problem under item 3 above is that the failed region of the pillar can remain stable only if the crushed coal has some uniaxial strength or if the pillar edge is laterally restrained. Both of these assumptions are unsatisfactory. It is difficult to accept that thoroughly crushed coal can sustain load without confinement. Also, lateral restraint obviously does not exist at the site of most coal pillars. This dilemma will have to be resolved if progress is to be made.

5. *Conditions at the interfaces between the seam and rock beds.* The buildup of core constraint depends on the ability of developing restraint, due to friction and even cohesion, at the seam's contact planes with the roof and floor. If this restraint fades, due to for example lubrication caused by moisture, the constraint of the core will decline, with possibly disastrous consequences. Wilson makes no provision to take the interface conditions into account.

6. *Coarse equilibrium of forces.* Wilson ensures, at least within the accuracy of his own assumptions, that the resultant of the transferred stresses is zero, as it should be.

This approach leaves open the satisfaction of the strict equations of equilibrium.

7. *Excessively high stresses in the pillar core.* According to (12), the horizontal stress in the crushed zone increases exponentially. This rapid growth creates the opportunity in wide pillars, if the problem in item 2 is removed, for the development of unduly high stresses both in the yield zone and in the elastic pillar core (*8*). The magnitude of these stresses may become sufficiently high to cause failure in the roof and/or in the floor.

Some of the problems have been overcome by Barron (*8-9*). First, he made an attempt to eliminate the untenable assumption concerning yield penetration as discussed in item 2 above. Secondly, he proposed that the failure of the intact rock is controlled by the nonlinear Hoek-Brown criterion (*13*) and the yield of the crushed rock by the linear Coulomb criterion. Since these curves intersect in the σ_1, σ_3 plane, Barron suggests that beyond the point of intersection a pseudoductile mechanism of failure develops. If this is so and if the interfaces are rough, then the horizontal confining stress no longer increases exponentially but *linearly*, according to a solution obtained by Prandtl in 1923 (*14-15*).

STABILITY OF SYSTEM SUPPORTED BY PILLARS

It has been known since about the mid-1960's that brittle rocks can, when tested in a stiff testing machine, exhibit strain-softening properties (*16-18*). This property implies that rock testing in the descending branch of the stress-strain curve is only conditionally stable (*19*). In a remarkable paper, Starfield and Fairhurst (*20*) point out that pillar failure, just the same as the failure of the rock specimen in the laboratory, can be rapid (explosive) or controlled.

The author (*19*) has shown that if the rock mass surrounding the seam is linearly elastic, it is possible to define a stiffness matrix for pillar workings and study the system's stability. Assume that a layout contains n pillars and that pillar forces P_i (i = 1,2, ... n) act at each pillar locations. Force P_i is distributed over the area occupied by the i-th pillar. Moreover, postulate that the forces act on a geometrically identical, but weightless rock mass.

If the compressive force P_j is applied to the roof and floor of the j-th location, the divergence at the position corresponding to the i-th pillar can be expressed as $- c_{ij}P_j$. The negative sign appears because convergence is taken positive. The total convergence induced by forces P_1, P_2, ... P_n can be obtained by superposition, hence:

$$s_i = -(c_{i1}P_1 + c_{i2}P_2 + \ldots + c_{in}P_n), \qquad (22)$$

where constants c_{ij} are real and are called the *influence coefficients*. The relationship, in matrix notation, between all values of convergence and those of force is given by

$$S = -CP. \qquad (23)$$

Here, S and P are $n \times 1$ vectors of s_i and P_i. The *influence* matrix $C = [c_{ij}]$ is an $n \times n$ symmetric, positive definite matrix. The inverse of C, i.e.,

$$K = C^{-1}, \qquad (24)$$

is called the *stiffness* matrix, the elements of which, k_{ij}, are termed the *stiffness coefficients*.

If the load-deformation relationship of the i-th pillar is defined by

$$P_i = f_i(s_i), \qquad (25)$$

then a state of equilibrium specified by force and convergence values P_i and s_i (i = 1,2, ... n) will be stable, *provided matrix K + Λ is positive definite* (*19*). Here, Λ is a diagonal matrix with elements (fig. 6):

$$\lambda_{ii} = df_i(s_i)/ds_i, \qquad \lambda_{ij} = 0 \qquad i \neq j. \qquad (26)$$

Some interesting additional information concerning the conditions of stability was obtained recently from A. M. Linkov, St. Petersburg (*21*). Since strain softening is an irreversible process, i.e., a point on the descending branch of the curve in figure 2, say point A, can move *only* either downward or revert to elastic behavior (but not upward), the requirement of positive definitiveness is too restrictive. Apparently, it has been shown in Russia (*22*) that the sufficient and necessary condition for a pillar system to remain stable is that matrix K + Λ is strictly *copositive*. A symmetric matrix is strictly copositive if its quadrative form is positive for all *nonnegative* (but not zero) vectors. Since all positive definite matrices are copositive, this conclusion indicates that the requirement of positive definiteness is a sufficient, but not necessary, condition of stability.

It is worth noting that a pillar layout, where the state of pillar loading is specified by the slope matrix Λ, will be stable if the algebraically smallest element of Λ is larger than $- \alpha_c$, where α_c is the smallest eigenvalue of K. This is again a sufficient, but not a necessary condition of stability.

Wagner (*23*) conducted a number of tests on model coal pillars, the widths of which were in the order of 2 m. A typical stress-convergence curve from his tests is shown in figure 7. It is interesting to observe in this illustration the variation in the distribution of load across the pillar's

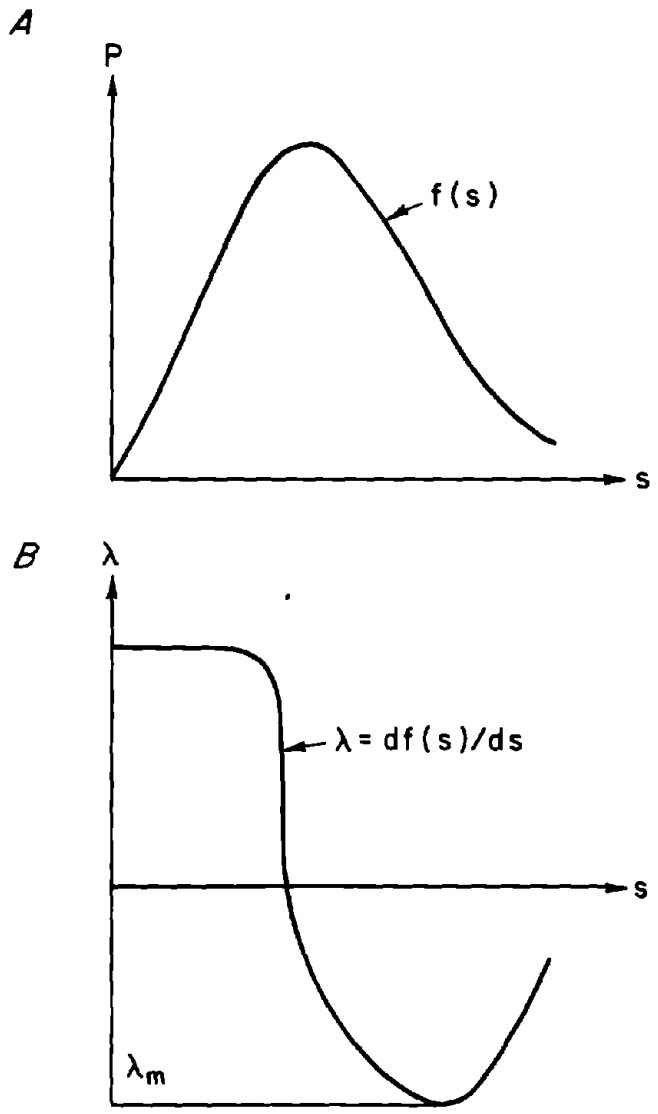

Figure 6.—Load deformation (*A*) and slope deformation (*B*) curves for coal pillars.

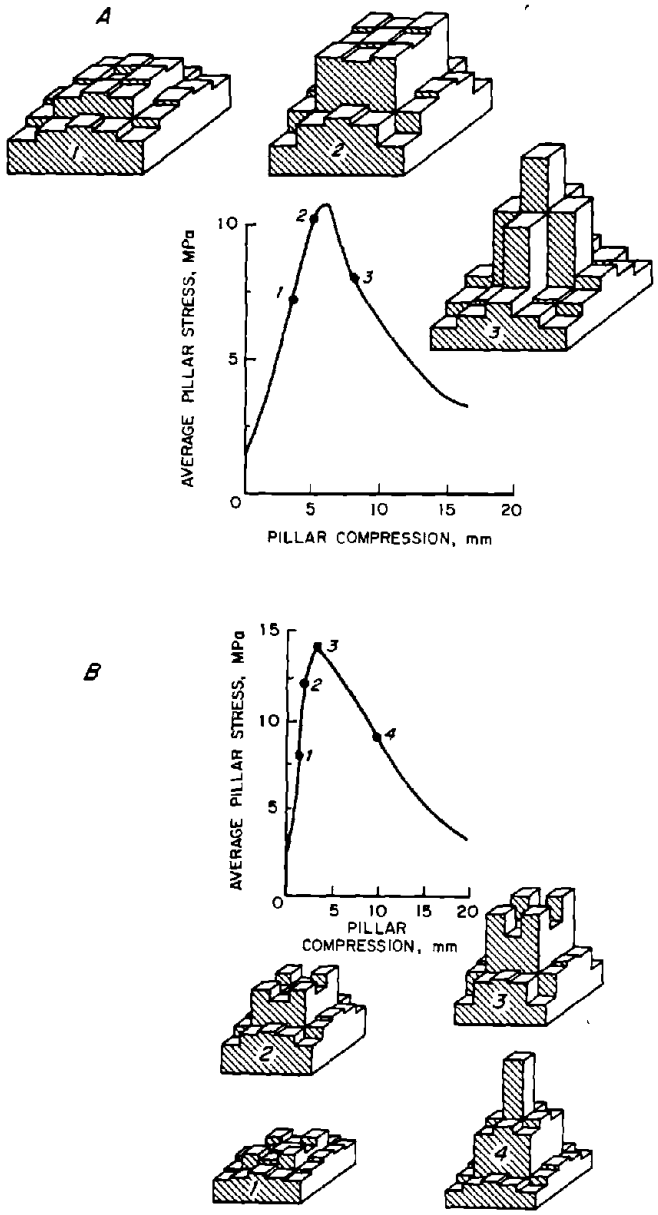

Figure 7.—Examples of complete load deformation curves and load distributions obtained by Wagner (*23*) on model coal pillars up to 2 m wide.

cross section as the loading proceeds. Yield at the pillar edges and the increase in load borne by the pillar core are clearly seen.

Wagner's tests prove conclusively that a pillar has significant load-bearing capacity even when its maximum resistance, which is traditionally regarded as the strength of the pillar, has been overcome. The slopes of the descending branches of the deformation curves observed by Wagner are plotted in figure 8 as a function of the width-height ratio.

To understand the difference between the "progressive" (gradual or controlled) and "sudden" (uncontrolled or catastrophic) pillar failures, suppose that there is a long isolated panel that is gradually being widened and more and more rows of regularly placed and equal pillars are being formed. During this process, the load on the pillars will increase. Let the pillar strength be σ_s and the pillar load calculated from the tributary area theory, or the modified coverload, be

$$q_m = q/(1 - e), \qquad (27)$$

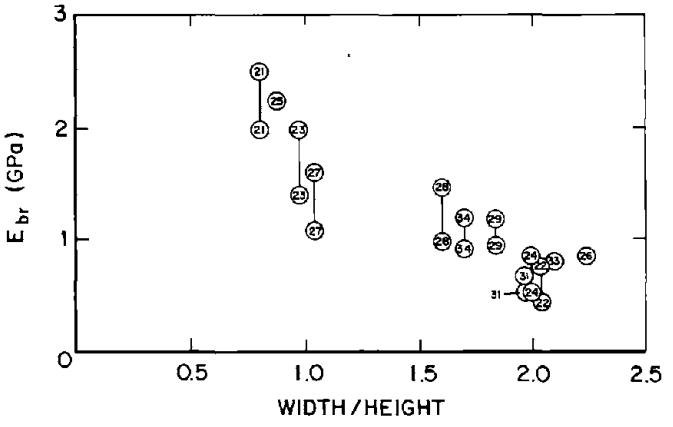

Figure 8.—Magnitudes of strain softening moduli, E_{br}, as a function of width-to-height ratio (after Wagner (23)).

where 100e is the percentage extraction. Two alternatives can arise:

- The pillar strength is greater than the modified coverload, i.e., $\sigma_s \geq q_m$, or
- The pillar strength is smaller than the modified coverload, i.e., $\sigma_s < q_m$.

Obviously, no collapse will occur when $\sigma_s \geq q_m$. This is so because q_m is the upperbound of the pillar load in this instance.

However, the case when $\sigma_s < p_m$ requires further investigation. Here, at a certain panel width the pillar strength in some rows, probably located at or near to the panel center, will be overcome. At this stage, some slopes of the pillar deformation curves turn negative, and consequently the smallest eigenvalue of matrix K + Λ may become zero or negative. If this happens, the stability of the pillar layout is in question, and an uncontrolled collapse of the pillars may occur.

If, however, at the time when the strength of some pillars is overcome matrix K + Λ is still positive definite (despite that $\lambda_{ii} < 0$ for some values of i), the layout will remain stable, but only conditionally stable. Gradual deterioration of pillars will commence at this stage. As the panel is widened further, the minimum eigenvalue of the stiffness matrix, α_c, decreases (fig. 9), so that sooner or later, if the pillars do not fail first progressively, matrix K + Λ will no longer be positive definite. At this stage, the workings could become unstable, and catastrophic collapse is likely to occur. A firm conclusion follows from this reasoning. If an extensive and uninterrupted area of room-and-pillar mining is planned, it is *essential* to design the

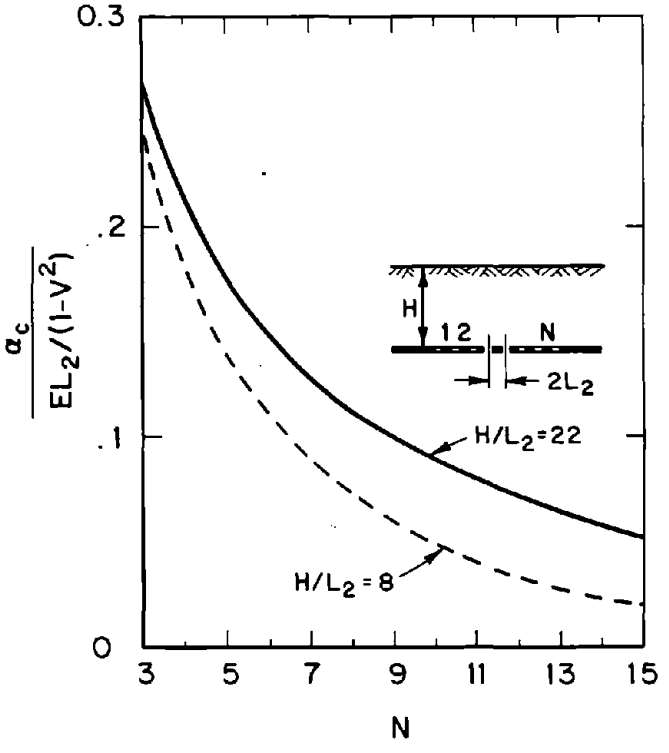

Figure 9.—Minimum eigenvalue of the stiffness matrix, α_c, of pillar workings as a function of panel width (after Salamon (41)).

pillars to have $\sigma_s > q_m$, with an acceptable margin of safety. It is in fact prudent to design pillar layouts in such a way that the "sea" of pillars is interrupted by more substantial stabilizing pillars.

The question of stability in mine workings has not been investigated in the English-speaking countries intensively since 1970's. An interest in the subject has been revived recently by a U.S. Bureau of Mines research team (*24-25*). Considerable work has been done, however, in the former Soviet Union and in Poland. Unfortunately, the results of this research have been available only in fragmented form (*26-27*).

The stability criterion requiring the positive definiteness of matrix K + Λ is a global condition. If this criterion is violated, then a catastrophic collapse of the workings is likely to follow. Pillar failure is possible while K + Λ remains positive definite, but the process will be non-violent. The question comes to mind that whether or not local violent events, such as coal bumps, can occur while the global stability conditions is *not* violated. This issue will be explored later.

ENHANCED CONFINED CORE METHOD

BASIC CONCEPTS

In the section "Critique of the Confined Core Concept," seven important shortcomings of the notion as proposed by Wilson were identified. Here, an attempt is made to address four of these deficiencies.

Wilson ignored the deformation of the rock mass surrounding the seam (item 1). Recent developments in the modeling of stratified rock masses (*30*) enable the removal of this failing of Wilson's approach.

Once the deformation of the rock mass can be modeled, it becomes possible to satisfy a set of boundary conditions that define the interface between the yield zone and the elastic pillar core and eliminates deficiency two of Wilson's method.

A new look at the behavior of crushed coal confined between the roof and floor planes provides a solution that accommodates frictional restraint at these interfaces with a coefficient of friction μ. Thus, the shear stress at the interfaces is either

$$\mu < \tan \rho \qquad \tau_{xz} = \mu \sigma_z \tag{28a}$$

or

$$\mu \geq \tan \rho \qquad \tau_{xz} = \tan \rho \, \sigma_z. \tag{28b}$$

Thus, the shear condition in (28b) corresponds to "rough" roof and floor surfaces where the slip actually takes place immediately off the interfaces and just inside the crushed coal. In effect, it is not plausible to have $\mu >$ tan ρ at these interfaces. The solution corresponding to the condition in (28a) offers the opportunity of investigating the effect of interface conditions. This facility, as stated in item 5, is lacking in Wilson's solution.

Finally, because the mathematical model of the layered medium facilitates the adherence to the equilibrium of forces in detail, one is not forced to accept the gross equilibrium condition used by Wilson (see item 6).

The solution presented here does not address the remaining weaknesses of Wilson's solution (items 3, 4, and 7).

RESISTANCE OF CRUSHED PORTION OF SEAM

Postulate that the crushed coal behaves like a loose granular medium (i.e., it has no residual unconfined strength). The yield criterion for such material is

$$(\sigma_1 - \sigma_3) - (\sigma_1 + \sigma_3) \sin \rho = 0. \tag{29}$$

Here, σ_1 and σ_3 are the major and minor principal stresses which can be expressed in terms of the rectangular stress components

$$\sigma_{1,3} = \frac{1}{2}\left[\left(\sigma_x + \sigma_z\right) \pm \sqrt{(\sigma_x - \sigma_z)^2 + 4\tau_{xz}^2}\right], \tag{30}$$

where σ_1 and σ_3 are defined using the upper and lower signs, respectively. The substitution of these expressions into equation 29 leads to

$$(\sigma_x - \sigma_z)^2 - (\sigma_x + \sigma_z)^2 \sin^2\rho + 4\tau_{x2}^2 = 0, \tag{31}$$

which is the yield criterion in terms of rectangular stress components. These stress components must also satisfy the equations of equilibrium:

$$\frac{\partial \sigma_x}{\partial x} + \frac{\partial \tau_{xz}}{\partial z} = 0 \qquad \frac{\partial \sigma_z}{\partial z} + \frac{\partial \tau_{xz}}{\partial x} = 0. \tag{32}$$

Equations 31 and 32 define the problem correctly, provided the third principal stress does in fact fall between σ_1 and σ_3.

If the definitions of stresses due to Airy are used, i.e., if (*28*)

$$\sigma_x = \frac{\partial^2 \Phi}{\partial z^2}, \qquad \sigma_z = \frac{\partial^2 \Phi}{\partial x^2}, \qquad \tau_{xz} = -\frac{\partial^2 \Phi}{\partial x \partial z}, \tag{33}$$

the equations of equilibrium in (32) are satisfied regardless of the form of function $\Phi(x,z)$. This function, appropriate to the solution of the present problem (fig. 10) can be written in the following form:

$$\Phi(x,z) = \exp\,[ax + f(z)] = X, \tag{34}$$

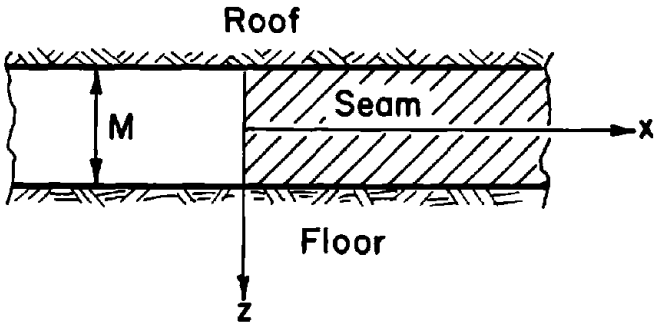

Figure 10.—Geometry near a coal pillar edge.

where a is a constant and f(z) is an unknown function of z to be determined from equation 31. The substitution of this function into (33) yields:

$$\sigma_x = [f''(z) + f'^2(z)]X,$$

$$\sigma_z = a^2X,$$

$$\tau_{xz} = -af'(z)X, \tag{35}$$

where $f'(z)$ and $f''(z)$ are the first and second derivatives of function f(z). The substitution of these expressions into equation 31 results in:

$$f''^2(z) + 2\left[f'^2(z) - a\,\frac{1+\sin^2\rho}{\cos^2\rho}\right]f''(z) + \left[f'^2(z) + a^2\right]^2 = 0, \tag{36}$$

which is a nonlinear second-order ordinary differential equation for f(z).

The solution of this equation is obtained in terms of a parameter ϵ and subject to the conditions (fig. 10) that at $z = \pm M/2$

$$|\tau_{xz}| = \mu\,\sigma_z, \tag{37}$$

where σ_z is the total or *resultant* vertical stress and that the *confining* stress on the exposed ribside (x = 0) is p, is given by

$$\sigma_x = \frac{p}{\mu}\,\frac{1+\sin^2\rho-2\sin\rho\,\cos\epsilon}{\cos^2\rho}\,Z, \qquad \sigma_z = \frac{p}{\mu}\,Z$$

$$\tau_{xz} = -p\,\frac{\sin\epsilon}{\sin\epsilon_m}\,Z. \tag{38}$$

In these expressions,

$$Z = \frac{1}{2}\,\eta\,\frac{1-\sin\rho\cos\epsilon_m}{1-\sin\rho\cos\epsilon}\,\exp\left[\eta\,\frac{x}{M} + \frac{1}{1-\sin\rho\cos\epsilon_m} - \frac{1}{1-\sin\rho\cos\epsilon}\right], \tag{39}$$

$$\eta = 2\tan\rho\left[\frac{\sin\epsilon_m}{1-\sin\rho\cos\epsilon_m} + 2\tan\rho\tan^{-1}\left(\frac{1+\sin\rho}{\cos\rho}\tan\frac{\epsilon_m}{2}\right)\right], \tag{40}$$

$$z = \frac{M\tan\rho}{\eta}\left[\frac{\sin\epsilon}{1-\sin\rho\cos\epsilon} + 2\tan\rho\tan^{-1}\left(\frac{1+\sin\rho}{\cos\rho}\tan\frac{\epsilon}{2}\right)\right]$$

$$|\epsilon| \le \epsilon_m \qquad \epsilon_m = \sin^{-1}(\mu/\tan\rho). \tag{42}$$

If $\mu \ge \tan\rho$, then $\epsilon_m = \pi/2$, which corresponds to the case of squeezing granular media between "rough" platens. This limiting solution, according to Nadai (*29*), was obtained and reported on by W. Hartmann in an unpublished doctoral dissertation in 1925. It can be shown that constant η introduced here reduces to parameter F of Wilson in equation 13 if $\mu = \tan\rho$ is substituted into equation 42 and then into equation 40. The more general solution presented here can be used to investigate the effect of the coefficient of friction μ on the development of core confinement.

It is easy to show that the use of $\epsilon = \pm\,\epsilon_m$ in equation 41 leads to $z = \pm\,M/2$, i.e., to the contact surfaces between the crushed seam and the surrounding beds. The total normal and shear stresses on these surfaces are given by

$$z = \pm\,M/2 \qquad \sigma_z = \frac{\eta p}{2\mu}\,e^{\eta x/M},$$

$$\tau_{xz} = \pm\,\frac{\eta p}{2}\,e^{\eta x/M}. \tag{43}$$

These formulas confirm that the solution does in fact satisfy the condition in (28a).

The resultant stress, $\bar{\sigma}_x$, on an x=constant plane ($|z| \le M/2$) is given by

$$\bar{\sigma}_x = p\,e^{\eta x/M}, \tag{44}$$

indicating that

$$\sigma_z = \frac{\eta}{2\mu}\,\bar{\sigma}_x. \tag{45}$$

The directions of the principal stresses are defined by:

$$\tan 2\rho = \frac{2\tau_{xz}}{\sigma_x - \sigma_z} = \frac{\cos\rho\,\sin\epsilon}{\cos\epsilon - \sin\rho}. \tag{46}$$

To illustrate the effect of the coefficient of friction, μ, between the crushed coal and the surrounding rocks, the parameter η is plotted in figure 11 as a function of the

ratio of the external and internal coefficients of friction, $\mu/\tan \rho$, for various values of angle ρ. Observe that if μ is significantly smaller than tan ρ, say $\mu < \tan \rho/2$, the value of η becomes much smaller than F.

To obtain an even better demonstration of the effect of μ, denote by x_0 and x_1 the depths at which the confining stress, $\bar{\sigma}_x$, will reach a certain value if $\mu = \tan \rho$ ($\eta = F$) and $\mu < \tan \rho$, respectively. Now from equation 44

$$\exp (\eta x_1/M) = \exp (F x_0/M),$$

therefore,

$$\frac{x_1}{x_0} = \frac{F}{\eta}. \qquad (47)$$

In figure 12, the variation in the ratio x_1/x_0 is shown as a function of $\mu/\tan \rho$. It is particularly important to note the slowness in the buildup of the confining stress if μ is a small fraction of tan ρ. Such low coefficients of friction may prevail in some circumstances, such as for example at slickensided interfaces. Perhaps, even more importantly, a reduction in the coefficient of friction, for example, due to the introduction of moisture, may destabilize an already developed yield zone.

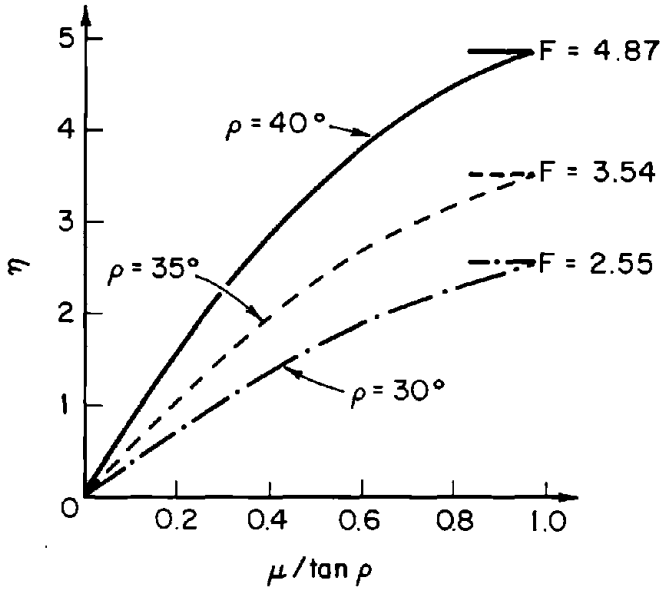

Figure 11.—Influence of the coal-rock interface coefficient of friction μ on the parameter η, which controls the growth of confinement with distance from the pillar edge.

DEFORMATION OF SURROUNDING STRATA

The rock mass surrounding coal seams is usually sedimentary and, hence, stratified. The behavior of such mass can be simulated by using an old (*38*) but recently reviewed and considerably generalized laminated model (*30*). This model is piece-wise homogeneous, consisting of a pile of thin, horizontal, and parallel-sided elastic plates (fig. 13). For simplicity, the interfaces between beds are free of shear stresses and cohesion. The continuity of stresses and normal displacements are assured across the

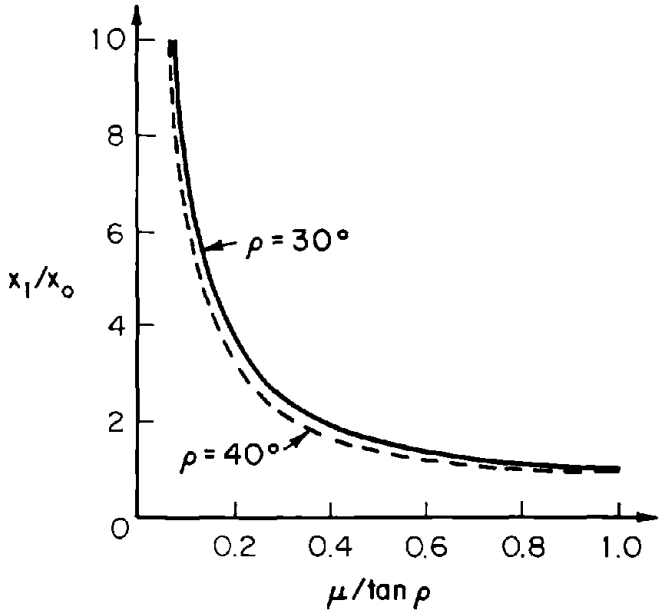

Figure 12.—Ratio of penetrations of crushed zone if $\mu < \tan \rho$, x_1, and if $\mu = \tan \rho$, x_0, as the function of $\mu/\tan \rho$.

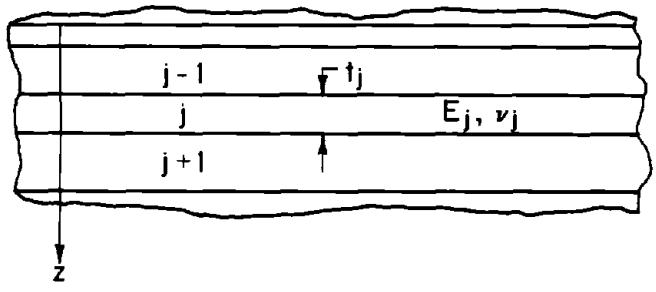

Figure 13.—Notations in the laminated model.

bedding planes, and the theory of thin plates is used as the kernel of the model (*31*). Here, only a much abbreviated discussion of the model is presented. Those who wish to obtain a more detailed view of this idealized layered medium are referred to an earlier publication by the author (*30*).

Let the Young's modulus, Poisson's ratio, and the thickness of the j-th bed in the pile be E_j, ν_j and t_j, respectively. The thin plate theory defines a relationship between the deflection of the middle plane of the j-th layer, w_j, and the transverse pressure acting on it, p_j, as

$$D_j \nabla^4 w_j = p_j, \tag{48}$$

where D_j is Love's "flexural rigidity" of the plate, i.e.,

$$D_j = E_j\, t_j^3/12\,(1 - \nu_j^2) \tag{49}$$

and ∇^4 denotes the biharmonic operator in the horizontal plane. The positive directions of p_j and w_j are both upward and coincide with the negative direction of the z axis. The transverse pressure is defined by

$$p_j = \sigma_j - \sigma_{j-1}. \tag{50}$$

Here, σ_j denotes the mean *induced* vertical stress acting between the middle planes of the (j + 1)-th and j-th beds. If these beds remain in contact after mining, this stress can be expressed as

$$\sigma_j = E_j^e \left(w_{j+1} - w_j\right)/d_j. \tag{51}$$

In this expression, d_j is the distance between the middle planes, and E_j^e is the effective modulus of the composite material residing in this space.

$$d_j = \left(t_{j+1} + t_j\right)/2$$

$$E_j^e = 2d_j\, E_{j+1}\, E_j / \left(t_{j+1}\, E_j + t_j\, E_{j+1}\right). \tag{52}$$

The substitution of the appropriate versions of σ_j from equation 51 into equation 50 and then into equation 48 leads to the equation that controls the continuity of the vertical-induced displacement and stress in the model.

$$\left(E_j^e/d_j\right)w_{j+1} - \left(D_j\nabla^4 + E_j^e/d_j + E_{j-1}^e/d_{j-1}\right) w_j + \left(E_{j-1}^e/d_{j-1}\right) w_{j-1} = 0. \tag{53}$$

Here, only the case of *homogeneous stratification* will be discussed, i.e., when the elastic constants and thicknesses of all beds are the same. In this instance

$$d_j = t,$$

$$E_j^e = E$$

$$D_j = D = Et^3/12(1 - \nu^2), \tag{54}$$

the substitution of which into equation 53 leads to

$$w_{j+1} - 2\left[\frac{t^4}{24(1 - \nu^2)}\nabla^4 + 1\right] w_j + w_{j-1} = 0. \tag{55}$$

Very useful further simplification occurs if all layers are thin and consequently the approximation

$$\left(w_{j+1} - 2w_j + w_{j-1}\right)/t^2 \simeq \frac{\partial^2 w}{\partial z^2}, \tag{56}$$

is acceptable. The substitution of this relationship into equation 55 results in the following partial differential equation:

$$\lambda^2 \nabla^4 w - \frac{\partial^2 w}{\partial z^2} = 0, \tag{57}$$

where the positive z axis points downward and

$$\lambda^2 = t^2/12(1 - \nu^2). \tag{58}$$

Under the same circumstances, the vertical induced stress in equation 51 can be rewritten as follows:

$$\sigma_z = E\, \partial w/\partial z,$$

$$\text{since } \partial w/\partial z \simeq (w_{j+1} - w_j)/t. \tag{59}$$

One further result is required to use this simplified model conveniently. This additional link is the relationship between the roof-to-floor convergence, s, and the induced stress, σ_z. The convergence is defined by the difference

$$s = w^+ - w^-, \tag{60}$$

where w^+ and w^- are the vertical displacements of the floor and roof, respectively. The convergence distribution is specified by

$$\nabla^2 s = \frac{2}{\lambda E}\left(\sigma_z - \sigma_m\right), \tag{61}$$

where ∇^2 is the Laplace operator in the x,y plane, σ_z is defined in equation 59, and σ_m is the vertical stress induced by the "mirror image" excavations. The concept of the mirror image seam is introduced to ensure that the ground surface halfway between the actual and mirror seams is stress-free (fig. 14). In the mirror image seam, the convergence induced in the actual seam is mirrored by divergence of identical distribution.

In the solution of equation 61, it is necessary to ensure that the convergence distribution is continuous and the resultant of the induced vertical stresses is zero. It has been shown that these requirements are satisfied if the convergence function and its first derivatives with respect to x and y are continuous (*30*).

The formulas in equations 57 to 61 define the vertical-induced displacement and stress in the *homogeneously stratified quasicontinuum*, i.e., in the idealized layered medium introduced here. Recent studies have indicated (*32-35*) that this model provides a reasonably accurate estimator of surface subsidence induced by coal mining, provided $\omega \approx 5 - 7$, where

$$\omega = (H/2\lambda)^{1/2}. \tag{62}$$

These are the results that will be used in the sequel to simulate the behavior of the rock mass surrounding the seam and which acts as the loading system of the pillars and ribsides.

LOADING OF PILLARS AND RIBSIDES WITH YIELDING EDGES

To deal with the problems tackled by Wilson, the convergence distribution in equation 61 needs to be determined for a variety of conditions. Solutions are required (1) in rooms or entries where the effect of artificial roof supports can be neglected, (2) in caved regions from where the coal has been extracted but pressure is transmitted between the roof and floor through the compacting caved rubble, (3) in the yielding edges of pillars or ribsides, and (4) in the nonyielding elastic core of pillars and nonyielding regions of the unmined seam. For the sake of simplicity, only two-dimensional solutions, corresponding to the use of long strip or rib pillars and long straight ribsides, are presented here.

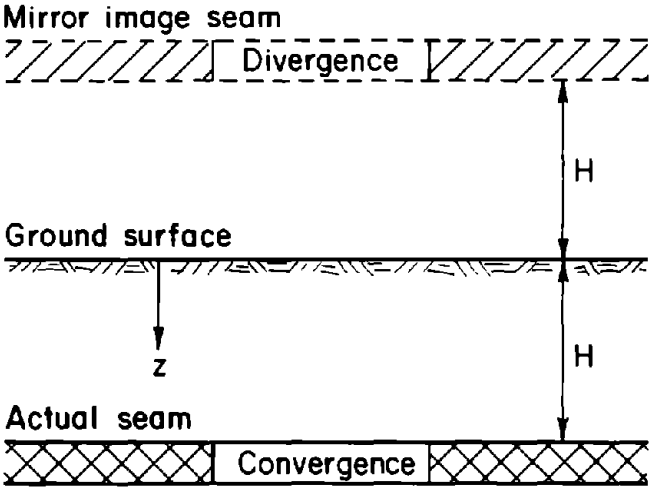

Figure 14.—Mirror image excavation concept.

In this instance, equation 61 reduces to an ordinary differential equation

$$\frac{d^2s}{dx^2} = \frac{2}{\lambda E}\left(\sigma_z - \sigma_m\right), \tag{63}$$

where, as before, σ_z is the induced vertical stress and σ_m is the stress induced by the mirror image excavation.

Next, the specific forms of equation 63 are presented to correspond to the four situations mentioned earlier. Actual solutions will be presented only for cases where the influence of σ_m can be neglected. This is certainly the case for room-and-pillar workings (fig. 15), provided the pillar center distance, W + B, is less than about one-half of the depth below surface, H. Moreover, for the sake of simplicity, the solution to be examined in detail corresponds to the instance where a wide area is supported by an uniform layout of pillars. In this case, and only in this case, the pillar load or mean pillar stress is determined purely by the geometry, i.e., by the tributary area theory:

$$q_m = \frac{W + B}{W}\, q = \frac{L_p + L}{L_p}\, q, \tag{64}$$

where $2L = B$ and $2L_p = W$ are the room and pillar widths, respectively.

1. The induced vertical stress in the case of unsupported *rooms* or *entries* is -q; therefore, in this case equation 63 becomes

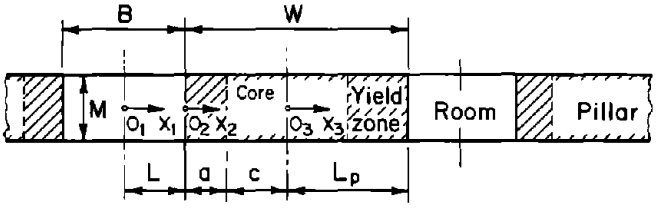

Figure 15.—Geometry and notations in a room-and-pillar layout.

$$\frac{d^2 s_r}{dx^2} = \frac{2}{\lambda E}\left(-q - \sigma_m\right), \qquad (65)$$

the solution of which for $\sigma_m = 0$ is

$$s_r = \frac{q}{\lambda E}\left(A_r + B_r x - x^2\right). \qquad (66)$$

Here and in all subsequent solutions of equation 63, two unknown constants are introduced that must be determined from the boundary conditions, i.e., from the continuity of the convergence function and its slope. In case of extensive room-and-pillar workings, it is advantageous to place the origin of the coordinate system to the center of the room, i.e., to point 0_1 in figure 15, in which case $B_r = 0$.

2. It has been suggested (*36*) that the compaction of *caved rock* can be approximated by a simple relationship between the bulking factor b and pressure $\hat{p}$:

$$b = \left(\hat{p} + b_o\, p_c\right)/\left(\hat{p} + p_c\right), \qquad (67)$$

where b_o is the initial or uncompacted bulking factor and p_c is a material constant ($p_c \approx 0.5 - 5.0$ MPa), fig. 16*A*. It has been shown by the author (*35*) that the formula in equation 67 leads to a simple relationship between gob compaction or convergence, s_g, and the pressure acting on the caved rubble:

$$\sigma_g = p_c\left(s_g - s_i\right)/\left(M - s_g\right) \qquad s_g \geq s_i \qquad (68)$$

Here, s_i is the initial convergence that occurs before the top of the caved pile comes into contact with the upper roof (fig. 16*B*).

Since σ_g represents the *total* pressure acting on broken rocks, the appropriate form of equation 63 in this case is

$$\frac{d^2 s_g}{dx^2} = \frac{2}{\lambda E}\left[-q + \frac{p_c\left(s_g - s_i\right)}{M - s_g} - \sigma_m\right]. \qquad (69)$$

A solution of this equation with $\sigma_m = 0$ has been published earlier by the author (*35*), but for the sake of brevity this problem will not be pursued here.

3. The resistance or the total vertical stress on the *crushed* parts of pillars or ribsides is given in (43):

$$\sigma_{zt} = \frac{\eta p}{2\mu}\, e^{\eta x/M}. \qquad (70)$$

The convergence in the yield zone, s_y, is therefore given by:

$$\frac{d^2 s_y}{d x^2} = \frac{2}{\lambda E}\left[-q + \frac{\eta p}{2\mu}\, e^{\eta x/M} - \sigma_m\right], \qquad (71)$$

where, as before, p is the restraining pressure on the exposed pillar side. The solution of this equation is ($\sigma_m = 0$):

$$s_y = \frac{q}{\lambda E}\left[-x^2 + \frac{M^2 p}{\eta\mu q}\, e^{\eta x/M} + A_y x + B_y\right], \qquad (72)$$

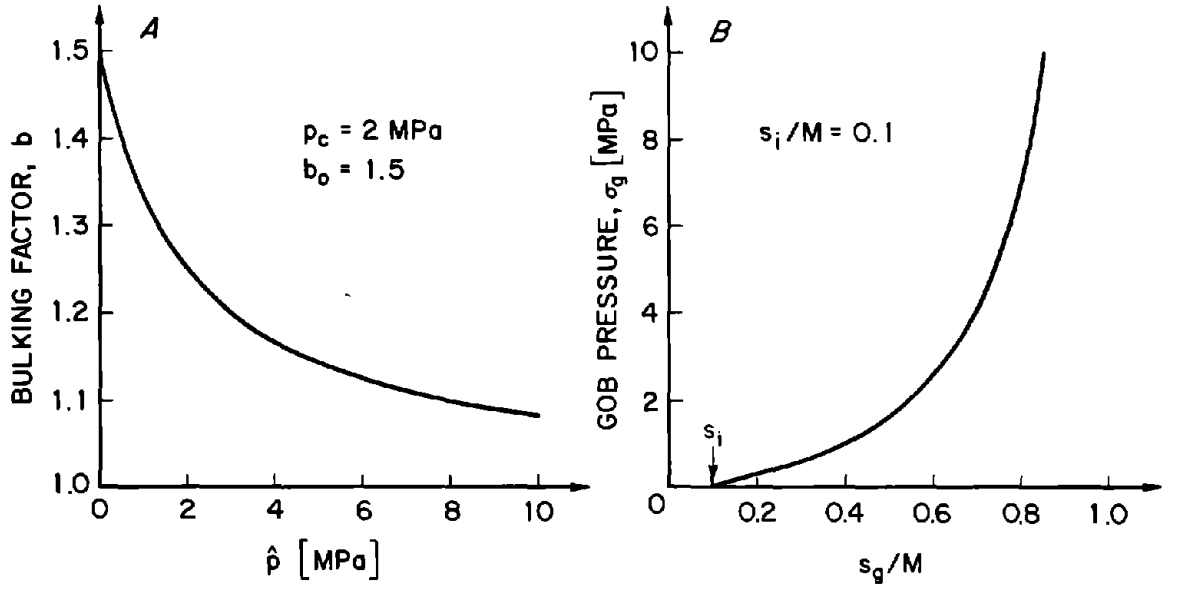

Figure 16.—Compaction of caved rubble. *A*, Bulking factor, b, as a function of pressure $\hat{p}$; *B*, gob pressure or resistance to compaction, σ_g, as a function of normalized compaction, s_g/M.

where A_y and B_y are constants to be determined from the boundary conditions.

4. It is assumed that in the *uncrushed* parts of the seam the coal is elastic and the induced stress is proportional to the roof-to-floor convergence, i.e.,

$$\sigma_z = \left[\left(1 - \nu_s\right) E_s / \left(1 - \nu_s - 2\nu_s^2\right)\right] s_e / M, \quad (73)$$

where E_s and ν_s are the Young's modulus and Poisson's ratio of the seam (*30*). Thus, equation 63 now takes the form:

$$M\frac{d^2 s_e}{dx^2} = \frac{1}{\theta^2}\frac{s_e}{M} - \frac{2M}{\lambda E}\sigma_m, \quad (74)$$

where

$$\theta = \left[\frac{\left(1 - \nu_s - 2\nu_s^2\right)\lambda E}{2\left(1 - \nu_s\right) M E_s}\right]^{1/2}. \quad (75)$$

The solution of this equation, with $\sigma_m = 0$, is

$$s_e = A_e \, ch\,(x/\theta M) + B_e \, sh\,(x/\theta M). \quad (76)$$

Since an extensive room-and-pillar layout results in symmetric stress distributions in the pillars, constant $B_e = 0$, provided the origin of the coordinate system is placed to point 0_3 in figure 15. The remaining constant A_e is to be determined from the continuity of the convergence slope at the interfaces between the crushed and uncrushed regions.

BEHAVIOR OF PILLARS IN EXTENSIVE ROOM-AND-PILLAR LAYOUTS

Now the task is to derive the distribution of the vertical total stress, σ_{zt}, across the pillars of extensive room-and-pillar workings, assuming that the value of a is known. This step is then followed by the determination of the depth of penetration of the yield zone into the pillars, i.e., the next step is to obtain the value of a. For these purposes, it will suffice to determine constants B_r, A_y, A_e, and B_e in equations 66, 72, and 76, respectively. If the origins of the coordinate systems with respect to s_r, s_y, and s_e are placed to 0_1, 0_2, and 0_3 in figure 15, it immediately follows that $B_r = B_e = 0$. Moreover, the requirement of continuity of the slope of the convergence curves at the pillar edges and at the transitions from crushed to elastic seam, results in

$$A_y = -\left[2L + \frac{Mp}{\mu q}\right],$$

$$A_e = \frac{2\theta M q}{\lambda E \, sh(c/\theta M)}\left[L + a - \frac{Mp}{2\mu q}\left(e^{\eta a/M} - 1\right)\right], \quad (77)$$

where 2c is the width of the elastic core of the pillars and a is the width of the crushed zone at each sides of the pillars (fig. 15).

In terms of these results, the total vertical stress acting across the pillar is defined in the crushed zone by $0 \le x_2 \le a$

$$\sigma_{zt} = (\eta p/2\mu) \exp(\eta \, x_2/M) \quad (78)$$

and in the elastic core by $-c \le x_3 \le c$ (see equation 79 below).

In order to use the expressions in equations 78 and 79, it is necessary to determine the value of a. Clearly, at the location of this transition the horizontal stress must be continuous and on the elastic side the Coulomb failure criterion for the intact coal must be satisfied. Thus, at $x_3 = \pm c$

$$\sigma_{zt} = \kappa \bar{\sigma}_x + \sigma_c, \quad (80)$$

where σ_{zt} and $\bar{\sigma}_x$ are given in equations 79 and 44, respectively. Hence, the equation that defines a is as follows:

$$\frac{q}{th\,(c/\theta M)}\left\{1 + \frac{1}{\theta}\left[\frac{L + a}{M} - \frac{p}{2\mu q}\left(e^{\eta a/M} - 1\right)\right]\right\}$$

$$= \kappa \, p \, e^{\eta a/M} + \sigma_c. \quad (81)$$

Before the results in this section can be used, it is necessary to determine at which stage the pillars will commence to yield. To determine this criterion, postulate

$$\sigma_{zt} = q\left\{1 + \frac{1}{\theta}\left[\frac{L + a}{M} - \frac{p}{2\mu q}\left(e^{\eta a/M} - 1\right)\right]\frac{ch\,(x_3/\theta M)}{sh\,(c/\theta M)}\right\}. \quad (79)$$

that a = 0 and $x_3 = c = L_p$ in equation 79. This substitution yields the maximum stress at the edge of a fully elastic pillar:

$$\sigma_{max} = q \left[1 + \frac{L}{\theta\ M\ th(L_p / \theta M)}\right]. \qquad (82)$$

Clearly, yielding will start if

$$\sigma_{max} \geq \kappa\ p + \sigma_c, \qquad (83)$$

where p is the pillar side restraint. Next, it is necessary to determine the *ultimate load-bearing capacity* of a fully yielded pillar. This can be obtained from equation 78 by integration:

$$S_{max} = \frac{1}{L_p} \int_0^{L_p} \sigma_{zt}\, dx_2 = \frac{Mp}{2\ \mu\ L_p} \left[\exp\ (\eta\ L_p/M) - 1\right]$$

$$= \frac{p}{\mu R} \left(e^{\eta R/2} - 1\right), \qquad (84)$$

where R is the width-to-height ratio of the pillar.

LOAD-BEARING CAPACITY OF PILLARS: EXAMPLES

In order to put into proper perspective the utility of the enhanced confined core method, it will be instructive first to design pillars using a well-tested empirical method, then to evaluate the behavior of these pillars as predicted by the results in the previous section. To do this, the South African formula in equation 2 with constants in (4) are employed. Since the pillars here are infinitely long, the effective pillar width, for the purposes of strength calculation, is obtained from the formula proposed by Wagner (*37*), which yields in this instance $W_{eff} = 2W$.

The South African design formula yields the pillar widths summarized in table 1 for M = 2 m and safety factor SF = 1.6.

Table 1.—Pillar widths obtained from the South African formula

H (m)	50	75	100	125	150	175
W (m)	2.07	2.91	3.71	4.60	5.48	6.39
H (m)	200	225	250	275	300	—
W (m)	7.34	8.32	9.36	10.52	11.42	—

M = 2 m, B = 7 m, SF = 1.6.

Next, the layout provided by the South African design is assessed using the results in the previous section. To perform these comparisons, reasonably typical values of the various parameters are introduced:

$$\sigma_c = 10\ \text{MPa},$$

$$\rho = 35^\circ,$$

$$\mu = \tan(25^\circ) = 0.466$$

$$\gamma = 25\ \text{kPa/m},$$

$$\omega = 7,$$

$$E = 20\ \text{GPa},$$

$$E_s = 2\ \text{GPa},$$

$$\nu_s = 0.2. \qquad (85)$$

The first test is to determine, using the criterion in equation 83, whether the edges of the pillars given in table 1 will yield. If they do not, the pillars remain elastic. If they do, the next task is to determine whether ultimate load-bearing capacity of the pillars, S_{max}, in equation 84 is greater than the load on the pillars determined by q_m in equation 64. If it is greater, then the pillars' edges will yield, but the pillars are able to sustain the load they are called upon to bear. The width of the elastic core can be obtained from equation 81 since 2c = W-2a. If the ultimate load-bearing capacity is less than the load, then of course the pillars will fail. This flow of logic is summarized in figure 17.

In the first series of comparisons, the side restraining pressure p is taken to be equal to that employed by Wilson (*5*), i.e., p = 100 kPa. The results of these computations are summarized in table 2. In the second row of this table, there is a comment specifying whether "no yield," "edges yield," or "failure" occurs.

A study of the data in table 2 reveals that the enhanced confined core method does not contradict the South African design method in this example. It is noteworthy that down to a depth of about 175 m, the pillars remain elastic and the safety factor calculated from the elastic load-bearing capacity is greater than unity, but decreasing with depth. It is important to observe also that at these depths the safety factor calculated using the ultimate yield strength, S_{max}, is *less* than unity. This indicates clearly that the confined core method is *unsuitable* to provide the strength of pillars with low width-to-height ratio. The geometry of such pillars prevents the development of significant confinement of the core, and the relatively thin crushed zone in itself has a low load-bearing capacity.

Table 2.—Confined core analysis of pillars in table 1 with p = 100 kPa

H, (m)	50	75	100	125	150	175	200	225	250	275	330
Comment	No yield	No yield	No yield	No yield	No yield	No yield	Edges yield	Edges yield	Edges yield	Edges yield	Edges yield
Core width, 2c	W	W	W	W	W	W	2.06	3.53	4.73	5.84	6.80
SF (elastic)	1.79	1.52	1.34	1.21	1.11	1.02	.95	.89	.84	.80	.75
SF (ultimate yield strength)	.13	.16	.22	.31	.46	.71	1.15	1.95	3.45	6.34	11.22

M = 2 m, B = 7 m, and the other data are in (85).

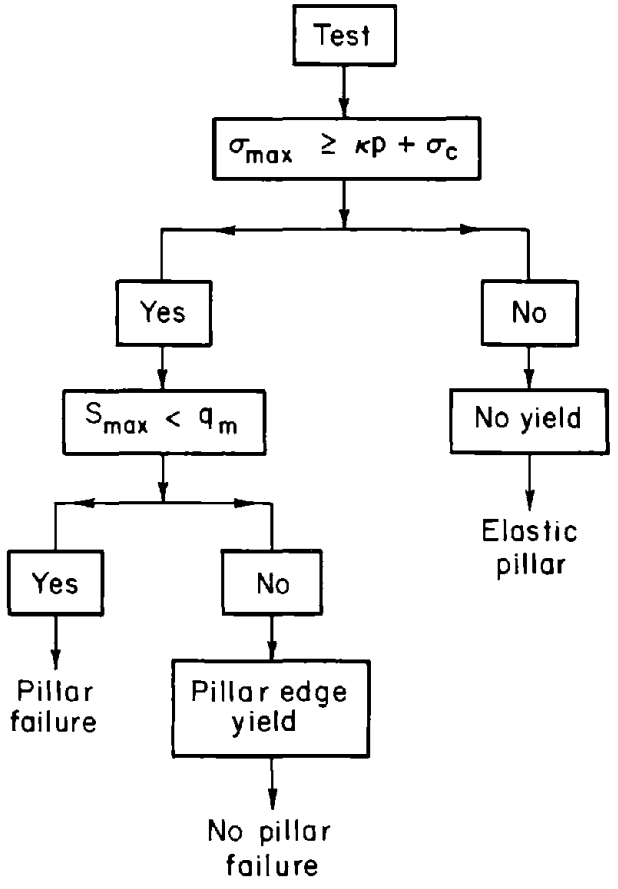

Figure 17.—Flow diagram for the determination as to whether or not pillar failure will occur when the modified Wilson method is applied.

At depths of 200 m and greater, the width-height ratio of the pillars in table 1 is greater than 3.7 and these pillars can develop increasingly effective confinement to assist their core. In figure 18, the distribution of total stress is illustrated for the depth of 250 m. A striking feature of this section of the table is the very rapid growth of the safety factor, SF, calculated from the ultimate yield strength. Such a rapid growth is probably unrealistic and will need to be mitigated by an approach such as suggested by Barron (*9*).

No evidence appears to exist to support Wilson's choice of p = 100 kPa for the value of the side restraint. It is difficult to justify such a high value when, in fact, most pillars do not have any side constraint at all. It will, therefore, be informative to examine the example analyzed in table 2 at a lower value of side pressure, say p = 20 kPa.

The data in table 3 reveal an interesting feature of the confined core approach to design. Between the depths of approximately 175 and 250 m (these values will be defined more accurately later), both safety factors are less than unity. This means that neither the elastic nor the ultimate (S_{max}) bearing capacities of the pillar are sufficient to support the pillar loads defined by q_m in equation 64. As the pillar width is increased with depth (see table 1), the squatter pillars can develop sufficient confinement to maintain an elastic pillar core. Therefore, at depths exceeding about 275 m the pillars do not fail.

To throw further light on this example, the actual pillar load, q_m, the elastic load-bearing capacity, and the ultimate yield strength of the pillars in table 1 are plotted in

Table 3.—Confined core analysis of pillars in table 1 with p = 20 kPa

H, (m)	50	75	100	125	150	175	200	225	250	275	330
Comment	No yield	No yield	No yield	No yield	No yield	Failure	Failure	Failure	Failure	Edges yield	Edges yield
Core width, 2c	W	W	W	W	W	0	0	0	0	1.92	3.38
SF (elastic)	1.74	1.47	1.30	1.17	1.07	.99	.93	.87	.82	.77	.73
SF (ultimate yield strength)	.03	.03	.04	.06	.09	.14	.23	.39	.69	1.27	2.24

M = 2 m, B = 7 m, and the other data are in (85).

figure 19 as a function of depth. This illustration shows that the load curve intersects the elastic load-bearing capacity line at the depth of 172 m and the ultimate strength curve at the depth of 256 m. Thus, between these depth values the confined core approach with p = 20 kPa predicts the failure of the pillars designed in accordance with the South African method.

The conflict between the deductions using p = 100 kPa and p = 20 kPa is serious. Since the South African method is well proven by 25 years of experience, it is tempting to conclude that Wilson's original p value is realistic. It is, however, too early to accept such a conclusion. Variations in the values of other parameters in (85) may also cause similarly conflicting conclusions. For example, little is known about the value of the μ, the value of the coefficient of friction at the interfaces.

STABILITY PROBLEMS WITH CONFINED CORE METHOD

Apart from the problems arising from the uncertainty of the numerical values of the various parameters, the

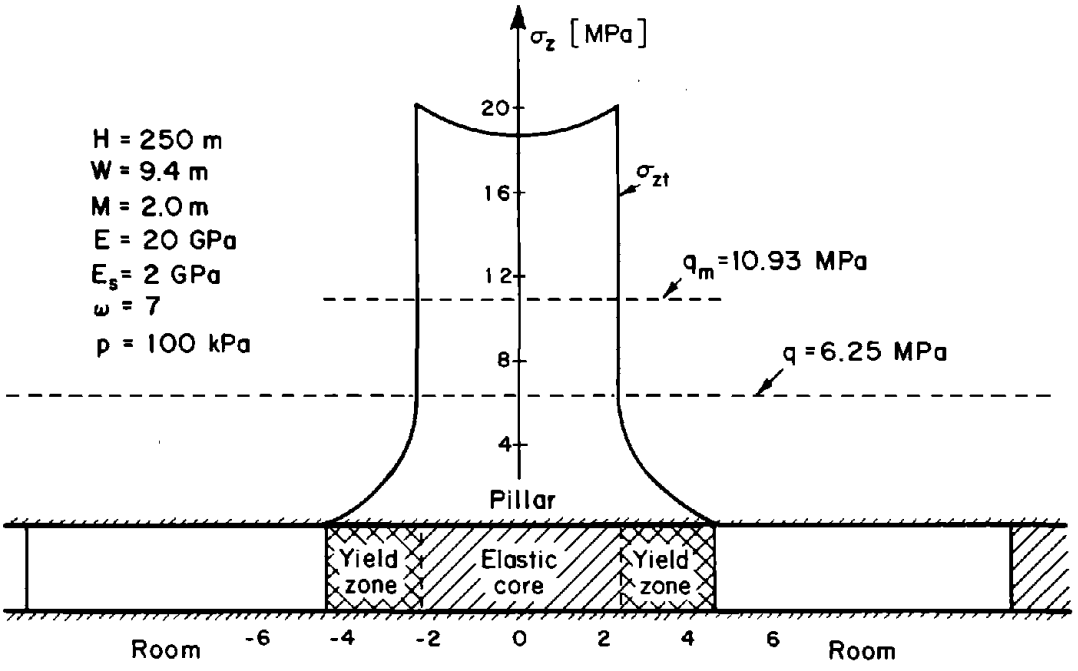

Figure 18.—Stress distributions in the yield zones and in the elastic core according to the modified Wilson approach.

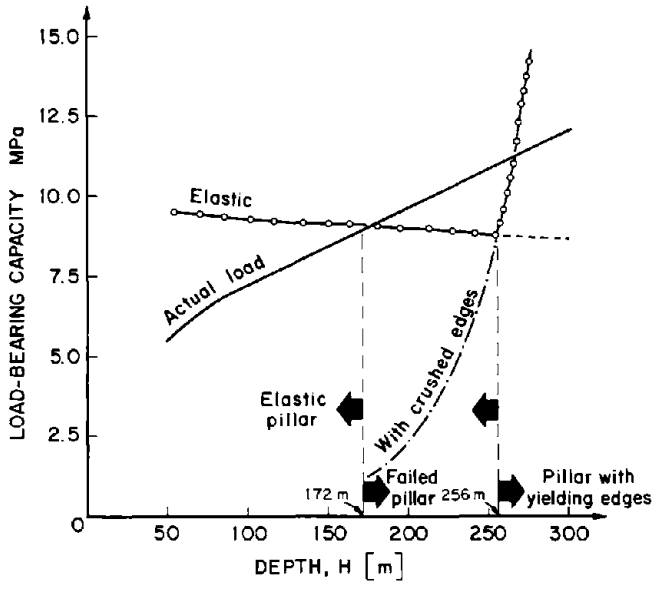

Figure 19.—Ultimate load-bearing capacity of the pillars in table 1, according to the modified Wilson method. Pillars remain elastic down to a depth of 172 m, fail between 172 m and 256 m, and yield but do not fail below 256 m (p = 20 kPa).

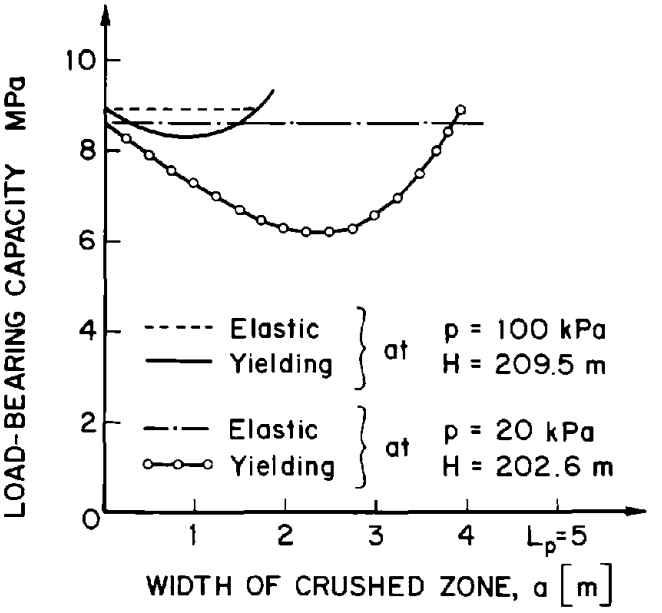

Figure 20.—The reduction in the load-bearing capacities of pillars immediately after pillar edge yield had commenced.

confined core method has a fundamental flaw. This weakness is a consequence of the assumption depicted in figure 5. The strength of real materials cannot reduce abruptly without causing instability and violent failure. It is best to illustrate this problem through an example.

Accepting the data in (85), postulate that B = 7 m, W = 10 m, and determine the depth at which the elastic stress at the edge of the pillar, σ_{max}, exactly satisfies the equality in equation 83, i.e., when $\sigma_{max} = \kappa\, p + \sigma_c$. Thus, at this depth the pillars remain entirely elastic. Next assume that either σ_c or p is reduced by an infinitesimal amount. Immediately, the pillar edge will start to yield and the process of yielding will penetrate into the pillar. However, during this process the load-bearing capacity of the pillar will start to diminish as shown in figure 20. In this figure, the load-bearing capacity of a pillar is plotted for the previously used two values of p (i.e., 20 and 100 kPa) as a function of yield penetration, a. Note the large depths of penetration that are required to rebuild the pillars' load-bearing capacities to the values that existed at the moment when yield had commenced. These values of penetration are 1.69 and 3.86 m, when the side restraints are 100 and 20 kPa, respectively.

Naturally, the crushing of such large volumes of coal cannot occur instantaneously, but require some period of time. Figure 20 indicates that, according to the model employed here, the load-bearing capacity of the pillars during this process of crushing is *less* than the load they are called upon to bear. Obviously, *no stable equilibrium can exist under these circumstances*. Such change can come about only if it is accompanied by a violent event. Another demonstration of the untenability of the proposition that the confined core model provides a realistic mechanism of pillar yield is shown in figure 21. Here two stress distributions are shown for the pillar featured in figure 20 (p = 20 kPa). In figure 21, curve A represents the stresses immediately before and curve B immediately after the pillar edges yield. Such a massive change in stress distribution, if it is to occur virtually instantaneously, would have to be accompanied by a large seismic event or a *coal bump*.

Thus, it appears that the confined core model, as outlined by Wilson and modified here, *inevitably* leads to a coal bump *every time* a pillar edge (or in fact any coal ribside) yields. Clearly, such events do not occur regularly. Coal bumps, fortunately, are rare occurrences in coal mines. Thus, the confined core approach cannot be accepted as a reasonable model of the behavior of coal pillars. While the concept has many merits, it does lead to a conclusion that is in conflict with reality in a fundamental sense.

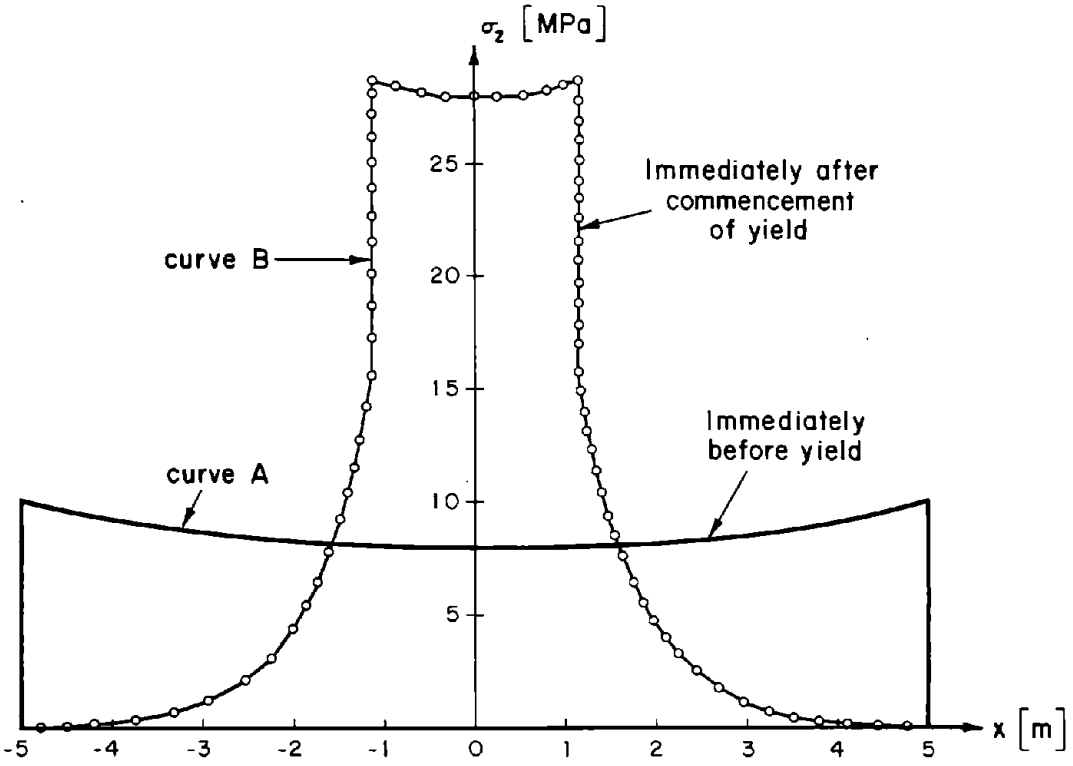

Figure 21.—Distribution of vertical stress, σ_z, across a pillar immediately before (curve A) and after (curve B) the commencement of yield.

The next step in this pursuit of an acceptable mechanism of coal pillar behavior is to retain the favorable features of the confined core concept and improve its most serious weakness. It would appear that it will be necessary to replace the abrupt drop in strength with a more realistic strain-softening constitutive law.

FUTURE RESEARCH TASKS

In the sequel, an attempt is made to outline an approach that may lead to a more satisfactory mechanism of coal pillar behavior. Unfortunately, due to time constraints, it has not been possible as yet to pursue these ideas to their logical conclusions, so here only the outline of some propositions is presented.

In developing this approach, significant inspiration was gained from the much earlier work of Deist (*17, 39*) and the more recent contributions of Mroz and Nawrocki (*27*).

STRAIN-SOFTENING CONSTITUTIVE LAW

The problem is discussed in two dimensions starting with the isotropic Hooke's law in plane strain:

$$\sigma_z - \sigma_x = 2G_s(\varepsilon_z - \varepsilon_x), \qquad \sigma_z + \sigma_x = \frac{2G_s}{1-2\nu_s}(\varepsilon_z + \varepsilon_x)$$
$$\tau_{xz} = 2G\gamma_{xz}. \tag{86}$$

It is assumed that these relationships are valid in the ascending branch of the stress-strain curve. Deist (*17*) suggested that the constitutive law may be taken to be rectilinear and, therefore, a simple linear generalization of the Hooke's law could be used in the descending branch of the curve. Retaining unchanged the relationship between the sums of normal stresses and strains, he proposed the following:

$$\sigma_z - \sigma_x = A_0 - A_1 (\varepsilon_z - \varepsilon_x) + A_2 (\varepsilon_x + \varepsilon_z) \quad (87a)$$

$$\sigma_z + \sigma_x = \frac{2G_s}{1-2\nu_s} (\varepsilon_z + \varepsilon_x). \quad (87b)$$

In addition, he accepted Coulomb's failure criterion which, if σ_x and σ_z are principal stresses, may be put into the following form:

$$\sigma_z - \sigma_x = (\sigma_z + \sigma_x) \sin\rho + \sigma_c (1 - \sin\rho). \quad (88)$$

Obviously, at the moment of failure both the elastic and the strain softening laws must be satisfied and the (principal) stresses must also obey equation 88. For simplicity, he proposed that

$$A_1 = 2\delta G_s, \quad (89)$$

where, clearly, δ is a positive parameter in strain softening. Its magnitude should be determined experimentally. The conditions that both sets of stress-strain relationships and also the Coulomb criterion are satisfied at the point of failure yield

$$A_0 = \frac{2(1 + \delta)\sigma_c}{\kappa + 1},$$
$$A_2 = \frac{2(1 + \delta)}{1-2\nu_s} \frac{\kappa - 1}{\kappa + 1} G_s, \quad (90)$$

where κ is given in equation 11. The substitution of these constants into equation 87a leads to

$$\sigma_z - \sigma_x = \frac{2(1 + \delta)\sigma_c}{\kappa + 1} - 2\delta G_s (\varepsilon_z - \varepsilon_x) + \frac{2(1 + \delta) G_s}{1 - 2\nu_s} \frac{\kappa - 1}{\kappa + 1} (\varepsilon_z + \varepsilon_x)$$

$$\sigma_z + \sigma_x = \frac{2G_s}{1 - 2\nu_s} (\varepsilon_z + \varepsilon_x), \quad (91)$$

which can be solved for σ_z

$$\sigma_z = \frac{1}{1 - \phi} \left[(1 + \delta)(1 - \sin\rho)\sigma_c + (1 + \phi)\sigma_x - 4\delta G_s \varepsilon_z\right], \quad (92)$$

where

$$\phi = (1 - 2\nu_s)\delta + (1 + \delta)\sin\rho. \quad (93)$$

The relationship in equation 92 describes the descending branch of the stress-strain curve as long as

$$0 \le \delta < \delta_c \qquad \varepsilon_0 \le \varepsilon_z \le \varepsilon_1. \quad (94)$$

Here the critical value of δ is given by

$$\delta_c = \frac{1 - \sin\rho}{1 - 2\nu_s + \sin\rho}. \quad (95)$$

It can be shown that $1 - \phi > 0$ as long as $\delta < \delta_c$. Therefore, on the basis of equation 92, $\partial\sigma_z/\partial\epsilon_z$ remains bounded. As illustrated in figure 22, ϵ_0 defines the point of failure and ϵ_1 signifies the strain at which the relation switches to the horizontal residual line. The bounding strains are given by:

$$\varepsilon_0 = \frac{1}{2G_s} \left[\frac{1 - 2\nu_s + \sin\rho}{1 - \sin\rho} \sigma_x + (1 - \nu_s)\sigma_c\right] \quad (96)$$

$$\varepsilon_1 = \frac{1}{4\delta G_s} \left\{(1 + \delta)(1 - \sin\rho)\sigma_c + \left[1 + \phi - (1 - \phi)\kappa_r\right]\sigma_x\right\}. \quad (97)$$

In equation 97, κ_r is the Rankine constant as defined in equation 11, but calculated from the residual internal angle of friction. In deriving equation 97, it was assumed that the crushed coal has no residual cohesion. This seems the appropriate assumption. On this basis, the maximum strain that can be reached in uniaxial compression is obtained from equation 97 by putting $\sigma_x = 0$. At this point, the yielding coal ceases to be a coherent substance.

DEFORMATION OF ROCK MASS-COAL SEAM SYSTEM

The goal here is to define a simple model of the interaction between the coal seam, which is being loaded in some places to the point of strain softening, and the strata in the roof and floor. Here, advantage is taken of the tabular geometry of the seam, the thickness of which, in most instances, is relatively small in relation to typical horizontal mining dimensions.

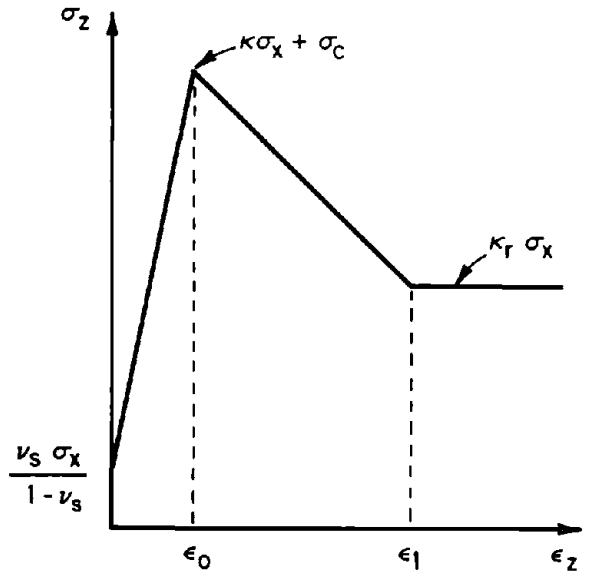

Figure 22.—The rectilinear stress-strain curve of coal, depicting the significance of ϵ_0 and ϵ_1.

In these circumstances, it is justified to expand, within the seam, the displacement functions with respect to z (fig. 10) and to retain only the first few terms. Thus, the approximate expressions of the induced displacements in the coal seam are

$$u^{(i)}(x,z) = u(x)\left[1 - 4b\left(\frac{z}{M}\right)^2\right]$$
$$w^{(i)}(x,z) = s(x)\,\frac{z}{M}, \tag{98}$$

where $u^{(i)}$ and $w^{(i)}$ are the components parallel with the x and z axes, respectively. These expressions do not yield the total displacement of points in the seam. It is argued that the neglected parts of the movement do not contribute significantly to the strains and, therefore, to stresses. Furthermore, function s(x) is the roof-to-floor convergence, u(x) is the unknown horizontal displacement in the middle plane of the seam, and b is a constant to be chosen later. It is noteworthy that for b = 0 the expressions in (98) coincide, at least formally, to those of Mroz and Nawrocki (*27*). There is, however, a substantive difference in interpretation. In their formulation, the function equivalent to s(x) denotes the deflection of the roof "beam," since they ignored the deformation of the floor.

The substitution into the definitions of strain components yields:

$$\varepsilon_x^{(i)} = \frac{\partial u^{(i)}}{\partial x} = \left[1 - 4b\left(\frac{z}{M}\right)^2\right]\frac{du}{dx},$$
$$\varepsilon_z^{(i)} = \frac{\partial w^{(i)}}{\partial z} = \frac{s(x)}{M}, \tag{99}$$
$$\gamma_{xz}^{(i)} = \frac{1}{2}\left(\frac{\partial u^{(i)}}{\partial z} + \frac{\partial w^{(i)}}{\partial z}\right) = \frac{1}{2}\left(\frac{ds}{dx} - 8b\,\frac{u}{M}\right)\frac{z}{M}.$$

The stresses and strains in the seam must satisfy the constitutive laws introduced in the previous section. Also, the same stresses must satisfy, at least in an approximate sense, the equations of equilibrium in (32). It will suffice to require that these equations are satisfied "in the mean" over each vertical section of the seam. To this end, introduce the "mean" horizontal stress

$$\bar{\sigma}_x = \frac{1}{M}\int_{-M/2}^{M/2} \sigma_x\, dz, \tag{100}$$

and integrate the equations in (32) with respect to z from -M/2 to M/2. This process leads to

$$M\,\frac{d\,\bar{\sigma}_x}{dx} + \tau_{xz}(x, M/2) - \tau_{xz}(x, -M/2) = 0$$
$$\sigma_z(x, M/2) - \sigma_z(x, -M/2) + \frac{d}{dx}\int_{-M/2}^{M/2} \tau_{xz}\, dz = 0. \tag{101}$$

Since σ_z and τ_{xz} are even and odd functions of z (the change in virgin stress between roof and floor is neglected here), the second of these equations is automatically satisfied and the first becomes:

$$M\,\frac{d\,\bar{\sigma}_x}{dx} + 2\,\tau_{xz}(x, M/2) = 0. \tag{102}$$

To complete the definition of the problem, the relationship provided by the laminated model between the convergence and the induced vertical stress is recalled next from equation 63

$$\frac{d^2 s}{dx^2} = \frac{2}{\lambda E}\left(\sigma_z^{(i)} - \sigma_m\right),$$

where, it will be recalled, σ_m is the effect of the mirror image excavation. Since the attention here is focused on room-and-pillar workings, it is permissible to take $\sigma_m = 0$. Hence, the simplified relationship to be used here is

$$\frac{d^2 s}{d x^2} = \frac{2 \sigma_z^{(i)}}{\lambda E}. \tag{103}$$

The constitutive relations in (86) or (91), the remaining equation of equilibrium in equation 102, and the relationship between convergence and induced vertical stress in equation 103 completely define the problem both in the elastic and strain-softening states.

Again, it is interesting to observe that the relationships in equations 102 and 103 are mathematically identical to those used by Mroz and Nawrocki (*27*). The physical content is, however, fundamentally different in the two approaches. The most important of these differences is that here the relationship in equation 103 follows from the homogeneously stratified quasicontinuum model, while Mroz and his colleague ignored the deformable rock mass in the floor and regarded the roof mass as a single beam, considering only its shear deformation.

Mroz and Nawrocki (*27*) indicated that two distinct situations can arise in the deformation of the seam. Either no relative movement takes place at the interfaces between the seam and the surrounding rocks, or slip occurs at these planes. They handle the former case in the elastic state (where this situation is more likely to arise) by taking u(x) = 0. A similar effect can be achieved by putting b = 1 in (98), but of course the solution in this case is more complex, although probably more realistic. The substitution of b = 1 ensures that at z = ± M/2 the horizontal displacement is 0.

Thus, it will be instructive to analyze three cases. In the elastic state, two situations can arise: (1) no slip between the surrounding strata and the seam occurs, (2) the seam tends to slip relative to the roof and floor. Case (3) corresponds to the situation when the *yielding* coal slips relative to the roof and floor.

1. *Elastic: No slip.* This situation can be simulated by putting b = 1 in (99). This solution seems to be of interest only when the seam is still elastic. Consequently, attention will be restricted only to this case.

In the virgin state the vertical and horizontal *principal* stresses are q and kq, respectively. Consequently, equation 102 is valid also for induced stresses.

$$M \frac{d \bar{\sigma}_x^{(i)}}{dx} + 2\tau_{xz}^{(i)} (x, M/2) = 0. \tag{104}$$

From the Hooke's law in plane strain, it is simple to obtain the induced stress components in terms of functions s(x) and u(x).

$$\sigma_x^{(i)} = \frac{2G_s}{1 - 2\nu_s} \left\{ (1 - \nu_s) \left[1 - 4 \left(\frac{z}{M} \right)^2 \right] \frac{du}{dx} + (\nu_s) \frac{s}{M} \right\}, \tag{105}$$

$$\sigma_z^{(i)} = \frac{2G_s}{1-2\nu_s} \left\{ \nu_s \left[1-4 \left(\frac{z}{M} \right)^2 \right] \frac{du}{dx} + (1 - \nu_s) \frac{s}{M} \right\}, \tag{106}$$

$$\tau_{xz}^{(i)} = G \left(\frac{ds}{dx} - 8 \frac{u}{M} \right) \frac{z}{M}. \tag{107}$$

From equation 105, the mean horizontal induced stress is

$$\bar{\sigma}_x^{(i)} = \frac{2G_s}{1 - 2\nu_s} \left[\frac{2}{3} (1 - \nu_s) \frac{du}{dx} + \nu_s \frac{s}{M} \right]. \tag{108}$$

The substitution of the appropriate stress components into equations 103 and 104 leads to the following pair of simultaneous ordinary differential equations:

$$\frac{2 M}{1 - 2\nu_s} \left[\frac{2}{3} (1 - \nu_s) \frac{d^2 u}{dx^2} + \frac{\nu_s}{M} \frac{ds}{dx} \right] + \frac{ds}{dx} - 8 \frac{u}{M} = 0 \tag{109}$$

$$\frac{d^2 s}{dx^2} - \frac{4(1 - \nu_s) G_s}{(1 - 2\nu_s) \lambda E} \frac{s}{M} = 0.$$

Omitting the details, the solution of these equations is given by the following expressions:

$$u(x) = - \frac{3 \alpha_o}{4 (1 - \nu_s) (\alpha_o^2 - \beta_o^2)} \left(B_1 \operatorname{sh} \alpha_o x/M + B_2 \operatorname{ch} \alpha_o x/M \right) \tag{110}$$

$$+ A_1 \operatorname{sh} \beta_o x/M + A_2 \operatorname{ch} \beta_o x/M,$$

$$s(x) = B_1 \text{ ch } \alpha_o x/M + B_2 \text{ sh } \alpha_o x/M, \quad (111)$$

where

$$\alpha_o^2 = \frac{2(1-\nu_s)\,ME_s}{(1+\nu_s)(1-2\nu_s)\,\lambda E}, \qquad \beta_o^2 = \frac{6(1-2\nu_s)}{1-\nu_s}. \quad (112)$$

The expressions of u(x) and s(x) permit the derivation of the stress components by substituting into equations 105 to 108.

2. *Elastic*: *Slip occurs*. If slip occurs, the induced shear stress at the contact surfaces is $\tau_{xz}^{(i)} = \mu\,(q + \sigma_z^{(i)})$. Therefore, the equation of equilibrium in equation 102 assumes the form:

$$M\frac{d\sigma_x^{(i)}}{dx} = 2\mu\left[q + \sigma_z^{(i)}(x, M/2)\right], \quad (113)$$

where, as before μ is the coefficient of friction at the interfaces.

In this instance, both elastic and nonelastic problems are of interest. First, the elastic case is analyzed.

In the elastic state, the relevant constitutive law can be obtained from (86),

$$\sigma_z = \frac{1}{1-\nu_s}\left(2G_s\,\varepsilon_z + \nu_s\,\sigma_x\right), \quad (114)$$

which, after the substitution of the strain components, yields the induced vertical stress:

$$\sigma_z^{(i)} = \frac{1}{1-\nu_s}\left[2G_s\frac{s}{M} + \nu_s\,\bar{\sigma}_x^{(i)}\right], \quad (115)$$

and the substitution of this into equations 103 and 104 results in:

$$\frac{d^2 s}{dx^2} - \frac{2}{(1-\nu_s)\,\lambda E}\left[2G_s\frac{s}{M} + \nu_s\,\bar{\sigma}_x^{(i)}\right] = 0, \quad (116)$$

$$M\frac{d\bar{\sigma}_x^{(i)}}{dx} - \frac{2\mu}{1-\nu_s}\left[\nu_s\bar{\sigma}_x^{(i)} + 2G_s\frac{s}{M}\right] = 2\mu q, \quad (117)$$

presenting a pair of ordinary differential equations for s(x) and $\bar{\sigma}_x^{(i)}(x)$. The solution of these equations takes the following form:

$$s(x) = M\left[C_2\exp(d_2x/M) + C_3\exp(d_3x/M) - (\nu_s/2)\,C_1\right] - \mu\nu_s qx/G_s, \quad (118)$$

$$\bar{\sigma}_x^{(i)} = -G_s\left\{\hat{\beta}\left[\frac{C_2}{d_3}\exp(d_2x/M) + \frac{C_3}{d_2}\exp(d_3x/M)\right] - C_1\right\} + 2\mu qx/M. \quad (119)$$

In these expressions, C_1, C_2, C_3 are arbitrary constants, d_2 and d_3 are given by

$$d_{2,3} = \left[\nu_s\hat{\beta}/2 \pm \sqrt{(\nu_s\hat{\beta}/2)^2 + 4\hat{\alpha}^2}\,\right]/2, \quad (120)$$

where the upper and lower signs correspond to d_2 and d_3, respectively. In addition, the following notations are employed:

$$\hat{\alpha}^2 = \frac{2ME_s}{(1-\nu_s^2)\,\lambda E} \qquad \hat{\beta} = \frac{4\mu}{1-\nu_s}. \quad (121)$$

3. *Yielding with slip*. Next, the solution corresponding to the *yielding* seam is sought, which must be obtained in terms of total strains and stresses. The total vertical strain is given by:

$$\varepsilon_z = \frac{q}{2G_s}(1-\nu_s-k\,\nu_s) + \frac{s}{M}. \quad (122)$$

Now, the total vertical stress in equation 92 assumes the following form:

$$\sigma_z = \frac{1}{1-\phi}\left[(1+\delta)(1-\sin\rho)\sigma_c + (1+\phi)\bar{\sigma}_x - \delta q(1-\nu_s - k\nu_s) - 4\delta G_s \frac{s}{M}\right]. \quad (123)$$

Two more equations are required to solve the problem. These are the equation of equilibrium in equation 102 and the relationship between convergence and induced stress in equation 103. Since $\tau_{xz} = -\mu\sigma_z$, equation 102 becomes:

$$M\frac{d\bar{\sigma}_x}{dx} = 2\mu\sigma_z, \quad (124)$$

and as $\sigma_z^{(i)} = \sigma_z - q$, the relationship in equation 103 assumes the form:

$$\frac{d^2s}{dx^2} = \frac{2(\sigma_z - q)}{\lambda E}. \quad (125)$$

The substitution of σ_z in equation 120 into these two relationships leads to the following pair of equations:

$$\frac{8\mu\delta G_s}{1-\phi}\frac{s}{M} + M\frac{d\bar{\sigma}_x}{dx} - \frac{2\mu(1+\phi)}{1-\phi}\bar{\sigma}_x = \mu\varsigma$$

$$\frac{d^2s}{dx^2} + \frac{8\delta G_s}{(1-\phi)\lambda E}\frac{s}{M} - \frac{2(1+\phi)}{(1-\phi)\lambda E}\bar{\sigma}_x = \frac{1}{\lambda E}(-2q + \varsigma), \quad (126)$$

where the notation

$$\varsigma = \frac{2}{1-\phi}\left[(1+\delta)(1-\sin\rho)\sigma_c - 2\delta q(1 - \nu_s k \nu_s)\right], \quad (127)$$

was employed. The solution of 126 is of the form (see equation 128 below).

where r_i (i = 1,2,3) are the roots of

$$r_i\left[r_i^2 - 2\mu\frac{1+\phi}{1-\phi}r_i + \frac{8\delta M G_s}{(1-\phi)\lambda E}\right] = 0. \quad (129)$$

At this point, it is advantageous to introduce a normalized value of δ:

$$\hat{\delta} = \delta/\delta_c \qquad 0 \le \hat{\delta} < 1, \quad (130)$$

where the critical value of δ is defined in equation 95. It is of interest to observe that on the basis of equation 92 this notation leads to:

$$\frac{\partial\sigma_z}{\partial\varepsilon_z} = -\frac{4G_s\hat{\delta}}{(1 - 2\nu_s + \sin\rho)(1-\hat{\delta})}, \quad (131)$$

which indicates that as $\hat{\delta}$ approaches unity, the coal loses its resistance instantaneously, and the stress-strain curve becomes similar to that depicted in figure 5. In terms of this new notation, the roofs of equation 129 can be expressed as follows (see equation 132 below).

$$s(x)/M = \sum_{i=1}^{3}\hat{A}_i\exp(r_i x/M) + \frac{1}{2\delta G_s}\left[\mu(1+\phi)qx/M - \frac{1-\phi}{4}(-2q+\varsigma)\right]$$

$$\bar{\sigma}_x(x) = \sum_{i=1}^{3}\hat{B}_i\exp(r_i x/M) + 2\mu qx/M, \quad (128)$$

$$r_1 = 0 \qquad r_{2,3} = \mu\frac{\kappa+\hat{\delta}}{1-\hat{\delta}}\left[1 \pm \sqrt{1 - \frac{4ME_s\hat{\delta}(1-\hat{\delta})}{\mu^2(1+\nu_s)(1-2\nu_s+\sin\rho)(\kappa+\hat{\delta})^2\lambda E}}\right]. \quad (132)$$

While in the elastic state the arguments of the exponential or hyperbolic function have always been real (see equations 110, 111, and 120), the situation might be different here in the yielding zone. Roots r_2 and r_3 are real only if the radicand in equation 132 is positive, and this will be so if

$$F(\hat{\delta},\ \rho,\ \nu_s,\ \nu) \le \mu^2 \frac{tE}{ME_s}. \qquad (133)$$

Here, the function on the left is defined by:

$$F(\hat{\delta},\rho,\nu_s,\nu) = \frac{8\sqrt{3(1-\nu^2)}\,\hat{\delta}\,(1-\hat{\delta})}{(1+\nu_s)(1-2\nu_s+\sin\rho)(\kappa+\hat{\delta})^2}. \qquad (134)$$

This function is positive through the permissible range of $\hat{\delta}$ and becomes 0 at both ends of this range (fig. 23). This means that it must have a maximum within this range. The maximum is attained at

$$\hat{\delta} = \hat{\delta}_o = \frac{\kappa}{2\kappa+1}, \qquad (135)$$

and the maximum value of the function is

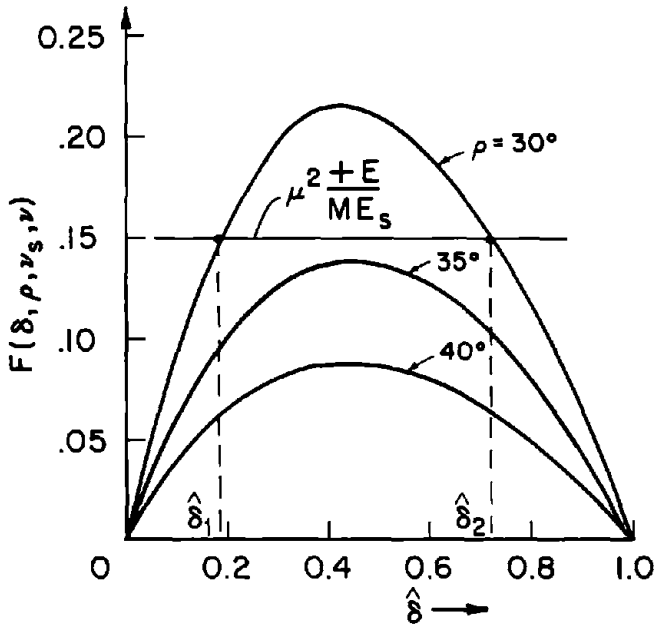

Figure 23.—$F(\hat{\delta},\ \rho,\ \nu_s,\ \nu)$ as a function $\hat{\delta}$. In the case illustrated, roots r_2 and r_3 are real for all values of $\hat{\delta}$ if ρ is about 34° or greater. If ρ = 30°, the roots are real if $\hat{\delta} \le \hat{\delta}_1$ and $\hat{\delta}_2 \le \hat{\delta} < 1$, but complex between these values.

$$F_{max} = \frac{2\sqrt{3(1-\nu^2)}}{(1+\nu_s)(1-2\nu_s+\sin\rho)\,\kappa(\kappa+1)}. \qquad (136)$$

Thus, r_2 and r_3 are real for *all* permissible values of $\hat{\delta}$ if

$$F_{max} \le \mu^2 \frac{tE}{ME_s}. \qquad (137)$$

If, however,

$$F_{max} > \mu^2 \frac{tE}{ME_s}, \qquad (138)$$

r_2 and r_3 are *real* only for certain ranges of values of $\hat{\delta}$, i.e., for

$$0 \le \hat{\delta} \le \hat{\delta}_1 \quad \text{and} \quad \hat{\delta}_2 \le \hat{\delta} < 1. \qquad (139)$$

The bounding values $\hat{\delta}_1$ and $\hat{\delta}_2$ are the roots of the quadratic equation that is obtained from

$$F(\hat{\delta},\ \rho,\ \nu_s,\ \nu) = \mu^2 \frac{tE}{ME_s}. \qquad (140)$$

If r_2 and r_3 are real, the solution in (128) contains ordinary exponential functions. If, however, the roots are complex, the solution will include some oscillatory terms which, in general, are unlikely to represent the behavior of the crushed coal.

It is instructive to examine the behavior of the roots in equation 132 at the two ends of the permissible range of $\hat{\delta}$. At $\hat{\delta}$ = 0, the roots become

$$r_2 = 2\mu\kappa, \qquad r_3 = 0, \qquad (141)$$

and at $\hat{\delta}$ = 1, i.e., when the descending branch of the stress-strain curve is vertical,

$$r_2 = \infty$$

$$r_3 = \frac{2ME_s}{\mu(1+\nu_s)(1-2\nu_s+\sin\rho)(\kappa+1)\lambda E}. \qquad (142)$$

These results suggest that well-behaved solution is feasible in the case of the classical plastic behavior ($\hat{\delta}$ = 0), but the infinitely large exponent r_2 indicates that no stable behavior can be expected when the strength drop is abrupt.

It has not been possible to obtain a full solution using the strain-softening model discussed in this section. The preliminary indication is, however, that stable solution is possible when the rate of strain softening, i.e., the value of $\hat{\delta}$, is small to moderate. Conversely, instability can be expected when the strength drop is sudden or even when the descend is steep.

Finally, it would appear that it might be possible to distinguish local stabilities, leading to coal bumps and global pillar instabilities that result in catastrophic pillar collapses. Local instabilities may occur at the edges of pillars or at ribsides where coal failure is initiated. As the inequality in equation 133 suggests, the main parameters that play a role in local instability are likely to be: the stiffness of the surrounding rock mass, λE; the "stiffness" of the yielding coal seam, $-4 M \hat{\delta} G_s/(1 - 2\nu_s + \sin\rho)(1 - \hat{\delta})$; the coefficient of friction at the interfaces, μ; and the internal angle of friction of the coal, ρ.

CONCLUSIONS

It has been shown that the confined core concept of Wilson contains the kernel of a mechanism that could lead to the explanation of the behavior of coal pillars when sandwiched between reasonably competent roof and floor strata. However, in its current state, this approach can hardly be regarded as more than an empirical method.

Many shortcomings of Wilson's basic idea can be removed by the introduction of a layered model of the stratified rocks in the roof and floor. Preliminary indications are that this model simulates the deformation and subsidence of sedimentary rock masses reasonably well. If further work confirms these initial conclusions, this model can be used with confidence as a realistic instrument of pillar loading when employed along the lines suggested in the main body of this paper. Another advance proposed here involves the direct study of the effects of the confining friction at the interfaces between the seam and the rock mass.

A closer study of the enhanced confined core approach reveals that the basic concept suffers from a fundamental flaw. Nature cannot cope in a stable manner with an abrupt change in the properties of substances. In deriving both the original and the enhanced confined core solution, it is implicitly assumed that the uniaxial compressive strength reduces abruptly to either zero or to a small residual value. As a result, at least theoretically, the confined core method should lead to a *violent* failure every time when the coal at the edge of a pillar or at a ribside starts to yield. Fortunately, reality does *not* support this conclusion.

In an endeavor to propose a more realistic model, in the final part of this paper an attempt is made to introduce an improved version of the complete stress-strain curve of coal, incorporating strain softening. While this part of the work is far from complete, the initial indications are that the favorable features of the earlier model have been retained, and the improved version of the model could provide the basis for investigating pillar strength and many of the factors affecting the occurrence of some of the coal bumps.

REFERENCES

1. Bieniawski, Z. T. Rock Mechanics Design in Mining and Tunneling. Balkema, Rotterdam, 1984, 272 pp.

2. Mark, C. Pillar Design Methods for Longwall Mining. BuMines IC 9247, 1990, 53 pp.

3. Salamon, M. D. G., and A. H. Munro. A Study of the Strength of Coal Pillars. J. S. Afr. Inst. Min. Metall., v. 68, 1967, pp. 55-67.

4. Wilson, A. H. A Hypothesis Concerning Pillar Stability. The Mining Engineer, v. 131, 1972, pp. 409-417.

5. ____. The Stability of Underground Working in the Soft Rocks of the Coal Measures. Ph.D. Thesis, Univ. of Nottingham, 1980.

6. Bryan, A., J. G. Bryan, and J. Fouche. Some Problems of Strata Control and Support in Pillar Workings. The Mining Engineer, v. 123, 1966, pp. 238-254.

7. Abel, J. F., and W. N. Hoskins. Confined Core Pillar Design for Colorado Oil Shale. Proc. 9th Oil Shale Symp., Quart. CO Sch. of Mines, v. 71(4), 1976, pp. 287-308.

8. Barron, K. An Analytical Approach to the Design of Coal Pillars. Part 1: The Analytical Model. Part 2: Application of the Model to Case Histories. Dept. Supply and Services, Ottawa, Ontario, Canada, Contract No. ISQ80-00151, 1983.

9. ____. A New Method for Coal Pillar Design. In "Ground Movement and Control Related to Coal Mining," ed. by N. I. Aziz. The Australasian Inst. of Min. Metall., Illawara Branch, Victoria, Australia, 1986, pp. 118-124.

10. Abel, J. F. Soft Rock Pillars. Int. J. Min. & Geol. Eng., v. 6, 1988, pp. 215-248.

11. Carr, F., and A. H. Wilson. A New Approach to the Design of Multi-Entry Developments for Retreat Longwall Mining. Proc. 2nd Conf. on Ground Control in Mining, Morgantown, WV, 1982, pp. 1-21.

12. Mark, C. The Wilson Approach to Estimating Coal Pillar Strength. BuMines, Pittsburgh Research Center, Internal Report 4690, July 1987, 28 pp.

13. Hoek, E., and E. T. Brown. Underground Excavations in Rock. Inst. Min. and Metall., London, 1980, 527 pp.

14. Nadai, A. Theory of Flow and Fracture of Solids, v. I. McGraw-Hill, New York, 1950, 572 pp.

15. Jaeger, J. C., and N. G. W. Cook. Fundamentals of Rock Mechanics. 3d ed., Chapman and Hall, London, 1979, 593 pp.

16. Cook, N. G. W. The Failure of Rock. Int. J. Rock Mech. Min. Sci., v. 2, 1965, pp. 389-403.

17. Deist, F. H. A Nonlinear Continuum Approach to the Problem of Fracture Zones and Rockbursts. J. S. Afr. Inst. Min. Metall., v. 65, 1965, pp. 502-522.

18. Cook, N. G. W., and J. P. M. Hojem. A Rigid 50-Ton Compression and Tension Testing Machine. S. Afr. Mech. Engr., 1966, pp. 89-92.

19. Salamon, M. D. G. Stability, Instability and Design of Pillar Workings. Int. J. Rock Mech. Min. Sci., v. 7, 1970, pp. 613-631.

20. Starfield, A. M., and C. Fairhurst. How High-Speed Computers Can Advance Design of Practical Mine Pillar Systems. Eng. & Min. J., v. 169, 1968, pp. 78-84.

21. Linkov, A. M. Personal communication, 1992.

22. ____. The Stability of Inelastic, Geometrically Nonlinear Discrete Systems. Proc. Acad. Sci. U.S.S.R., v. 294, 1987, pp. 44-47.

23. Wagner, H. Determination of the Complete Load-Deformation Characteristics of Coal Pillars. In "Advances in Rock Mechanics," Proc. 3rd Congress, Int. Soc. for Rock Mech., Denver, CO, v. II, Part B. Washington, Nat. Acad. of Sci., 1974, pp. 1076-1081.

24. Iannacchione, A. T., A. A. Campoli, and D. C. Oyler. Fundamental Studies of Coal Mine Bumps in the Eastern United States. Proc. 28th U.S. Rock Mech. Symp., Tucson, AZ, June 1987. A. A. Balkema, Rotterdam, pp. 1063-1072.

25. Zipf, R. K., Jr., and K. A. Heasley. Decreasing Coal Bump Risk Through Optimal Cut Sequencing With a Non-Linear Boundary Element Program. Proc. 31st U.S. Rock Mech. Symp., Golden, CO, June 1990. A. A. Balkema, Rotterdam, pp. 947-953.

26. Petukhov, I. M., and A. M. Linkov. The Theory of Post-Failure Deformations and the Problem of Stability in Rock Mechanics. Int. J. Rock Mech. Min. Sci., v. 16, 1979, pp. 57-76.

27. Mroz, Z., and P. Nawrocki. Deformation and Stability of an Elasto-Plastic Softening Pillar. Rock Mech. and Rock Eng., v. 22, 1989, pp. 69-108.

28. Timoshenko, S., and J. N. Goodier. The Theory of Elasticity. McGraw-Hill, New York, 1951, 506 pp.

29. Nadai, A. Theory of Flow and Fracture of Solids. McGraw-Hill, New York, 1963, 705 pp.

30. Salamon, M. D. G. Deformation of Stratified Rock Masses: A Laminated Model. J. S. Afr. Inst. Min. Metall., v. 91, 1991, pp. 9-26.

31. Love, A. E. H. A Treatise on the Mathematical Theory of Elasticity. 4th ed., Dover Publ., New York, 1944, 643 pp.

32. Salamon, M. D. G. Subsidence Prediction Using a Laminated Model. Proc. 30th U.S. Rock Mech. Symp., Morgantown, WV, June 1989. A. A. Balkema, Rotterdam, pp. 503-510.

33. ____. Some Applications of the Frictionless Laminated Model. Proc. 30th U.S. Rock Mech. Symp., Morgantown, WV, June 1989. A. A. Balkema, Rotterdam, pp. 891-898.

34. ____. Partial Extraction To Control Surface Subsidence Due to Coal Mining. Proc. 32nd U.S. Rock Mech. Symp., Norman, July 1991. A. A. Balkema, Rotterdam, pp. 861-870.

35. ____. Displacements and Stresses Induced by Longwall Mining in Coal. Proc. 7th Congress, Int. Soc. for Rock Mech., Aachen, Germany, v. 2. A. A. Balkema, Rotterdam, 1991, pp. 1199-1202.

36. ____. Mechanism of Caving in Longwall Coal Mining. Proc. 31st U.S. Rock Mech. Symp., Golden, CO, June 1990. A. A. Balkema, Rotterdam, pp. 161-168.

37. Wagner, H. Personal communication, 1980.

38. Salamon, M. D. G. An Introductory Mathematical Analysis of the Movements and Stresses Induced by Mining in Stratified Rocks. King's College, Univ. of Durham, Dept. of Mining, Res. Report, v. 9, Bulletin No. 3, 1961.

39. Deist, F. H. The Development of a Non-Linear Continuum Approach to the Problem of Fracture Zones and Rockbursts and Feasibility Study by Computer. Ph.D. Thesis, Univ. of the Witwatersrand, Johannesburg, Rep. of South Africa, 1966.

40. Salamon, M. D. G. Behavior and Design of Coal Pillars. The Australian Coal Journal, No. 32, 1991, pp. 11-22.

41. ____. Rock Mechanics of Underground Excavations. Proc. 3rd Congress, Int. Soc. for Rock Mech., Denver, CO, v. I, Part B. Washington, Nat. Acad. of Sci., 1974, pp. 951-1099.

PILLAR STRENGTH CONSIDERING IN SITU STRESSES

By P. R. Sheorey[1]

INTRODUCTION

The failure process in rock around any excavation depends on the total stresses which are a sum of the preexcavation or in situ stresses and excavation-induced stresses. These stresses are matched against a suitable failure criterion to define failure or stability. Coal pillars, which occur between roadways or gob excavations, must also be assessed for stability using this fundamental procedure in rock mechanics. This procedure in the case of pillars need not be followed rigorously, and in fact, an indirect method can be adopted for defining pillar strength because such factors as the influence of width-to-height ratio (w/h) and size on pillar strength are more or less well established.

The desirable features of a pillar strength equation are briefly given below.

1. It should fit as many case studies (both failed and stable) as possible.
2. It should preferably be applicable to all practical ranges of w/h.
3. The effects of w/h, end constraint, and size should be incorporated in the equation. The equation should be amenable to changes for unusual and conditions (e.g., soft bands in the roof/floor).
4. A suitable coal strength parameter should be included in the formula. The uniaxial compressive strength of small specimens (1-in cubes) is recommended, as the in situ large-scale strength is likely to be biased with cover depth (*1*).[2]
5. The influence of in situ stresses should be properly included.

A pillar strength equation was earlier developed based on these features (*1*). This paper examines the performance of this equation against case studies as well as against the Indian Coal Mines Regulations (1957) and suggests suitable refinement of the equation.

PERFORMANCE OF EARLIER FORMULA

The Central Mining Research Station (CMRS) formula reads as follows:

$$S = 0.27\sigma_c h^{-0.36} + \frac{H}{160}\left[\frac{w}{h} - 1\right], \qquad (1)$$

where S = pillar strength, MPa,

σ_c = strength of 1-in cubes of coal, MPa,

h = extraction height, m,

H = depth of rock cover, m,

and w = pillar width, m.

The first term on the right defines the effect of size on strength, and the second incorporates the influence of w/h, end constraint, and preexcavation stresses jointly. The formula is thus essentially a triaxial strength relation, with the first term defining the uniaxial strength of a unit cube of side h, and the second defining the increase in strength due to triaxial effects when $w/h > 1$ and decreases when $w/h < 1$.

Performance of equation 1 along with some of the better known equations was studied (*1*) against 23 failed and 20 stable pillar cases (tables 1-2) using the following two criteria specified by Salamon and Munro (*2*):

[1]Head, Bord and Pillar Design, Central Mining Research Station, Dhanbad, India.

[2]Italic numbers in parentheses refer to items in the list of references at the end of this paper.

Table 1.—Failed pillar cases

	Mine	Seam	H, m	h, m	w, m	B, m	w/h	σ_c, MPa
1.	Amritnagar	Nega Jamehari	30	4.5	3.6	5.7	0.8	45
2.	Amritnagar	Bega Jamehari	30	6.0	3.6	5.4	.6	45
3.	Begonia	Begonia	36	3.0	3.9	6.0	1.3	26
4.	Amlai	Burhar	30	5.4	4.5	4.5	.83	25
5.	Sendra Bansjora	X	23	8.1	4.65	5.55	.57	24
6.	W. Chirimiri	Main	90	3.75	5.4	6.0	1.44	45
7.	Birsingpur	Johilla top	129	3.6	7.5	6.0	2.08	38
8.	Pure Kajora	Lower Kajora	54	3.6	5.4	6.0	1.5	33
9.	Pure Kahora	Lower Kajora	56	3.6	4.95	6.45	1.38	33
10.	Shankarpur	Jambad bottom	42	4.8	4.5	4.5	.94	47
11.	Ramnagar	Begunia	70	1.8	2.85	3.15	1.58	26
12.	Ramnagar	Begunia	51	1.8	3.0	3.6	1.67	26
13.	Kankanee	XIII	160	6.6	19.8	4.2	3.0	27
14.	Kankanee	XIV	140	8.4	18.6	5.4	2.2	25
15.	Jitpur	XIV	450	3.6	18×34.5	6	6.5	19
16.	Jitpur	XIV	450	3.6	10.5×12	6	3.08	19
17.	Jitpur	XIV	450	3.6	12×12	6	4.13	19
18.	Jitpur	XIV	450	3.6	18×21	6	5.33	19
19.	Jitpur	XIV	450	3.6	18×25.5	6	5.83	19
20.	Jitpur	XIV	450	3.6	15×63	6	6.67	19
21.	Jitpur	XIV	450	3.6	18×30	6	6.25	19
22.	Jitpur	XIV	450	3.6	18×30	6	6.25	19
23.	Jitpur	XIV	450	3.6	15×32	6	5.67	19

NOTE.—In the case of rectangular pillars, the equivalent square pillar width was obtained from

$$\frac{2w_1w_2}{w_1 + w_2}$$

where w_1, w_2 are the two sides of a rectangular pillar.

Table 2.—Stable pillar cases

	Mine	Seam	H, m	h, m	w, m	B, m	w/h	σ_c, MPa
1.	Bellampalli	Ross	36	3.0	5.4	6.0	1.8	48
2.	Nimcha	Nega	48	6.0	9.9	6.0	1.7	50
3.	Morgan Pit	Salarjung	270	3.0	8.1	3.6	2.7	46
4.	Ramnagar	Ramnagar	75	2.7	9.9	6.6	3.7	28
5.	Lacchipur	Lower Kajora	38	5.1	7.2	3.9	1.4	33
6.	N. Salanpur	X	30	5.1	9.0	6.0	1.8	21
7.	Bankola	Jambad top	102	4.8	10.1	2.4	2.1	35
8.	Bankola	Jambad top	75	3.0	6.3	4.2	2.1	35
9.	Surakacchar	GI	106	3.5	16.0	4.0	4.6	29
10.	Lacchipur	Lower Kajora	38	5.1	18.3	4.2	3.6	33
11.	Sripur	Koithi	266	4.8	40.0	5.0	8.3	43
12.	E. Angarpathra	XII	30	2.1	6.0	6.0	2.9	19
13.	Kargali Incline	Kathara	36	3.6	9.3	5.7	2.6	40
14.	Jamadoba 6&7 Pits	XVI	80	2.1	5.8	5.5	2.9	29
15.	Topsi	Singharan	85	1.8	7.0	3.9	3.9	41
16.	Jitpur	XIV	450	3.6	21×39	6.0	7.6	19
17.	Jitpur	XIV	450	3.6	18×48	6.0	7.3	19
18.	Jitpur	XIV	450	3.6	19.5×30	6.0	6.5	19
19.	Jitpur	XIV	450	3.6	18×31.5	6.0	6.4	19
20.	Jitpur	XIV	450	3.6	18×42	6.0	7.0	19

1. In a plot of safety factors, the line of safety factor = 1 must pass through the middle of failed case data points.
2. All stable cases must have safety factors greater than 1.

For estimating the safety factor, pillar load P was estimated from

$$P = \gamma H \left[\frac{w + B}{w}\right]^2,$$

where γ = unit rock pressure = 0.025 MPa/m

and B = roadway width, m.

Figure 1 shows that the two conditions of Salamon and Munro are well satisfied.

Since the publication of this equation, the author and his mining colleagues had occasion to use it in a variety of situations. It was seen that the equation underestimated pillar strength to some extent under shallow covers. It was also observed that pillar sizes increased rather slowly at depths greater than 300 m. The first discrepancy was noticed from its application to the Indian Coal Mines Regulations, which specify pillar sizes at various depths (table 3). Generally, these regulations have given stable pillars except in very weak seams (σ_c < 20 MPa) or at greater depths (H > 400 m), when some side spalling has been evident. Figure 2 shows two example plots when the roadway widths are 3.0 and 4.8 m and the coal strength is σ_c = 15 MPa. The safety factor taken is 2.0 for long-term stability, which is the usual value taken in India.

Table 3.—Pillar sizes according to Regulation 99 of Indian Coal Mines Regulations, 1957

(h≤ 3m)

Depth of cover (H), m	Pillar size (center to center) for different roadway widths (B), m			
	B = 3.0	B = 3.6	B = 4.2	B = 4.8
Less than 60 . . .	12	15	18	19.5
60 to 90	13.5	16.5	19.5	21
90 to 150	16.5	19.5	22.5	24.5
150 to 240	22.5	25.5	30.5	34.5
240 to 360	28.5	34.5	39.5	45
More than 360 . .	39.5	42	45	48

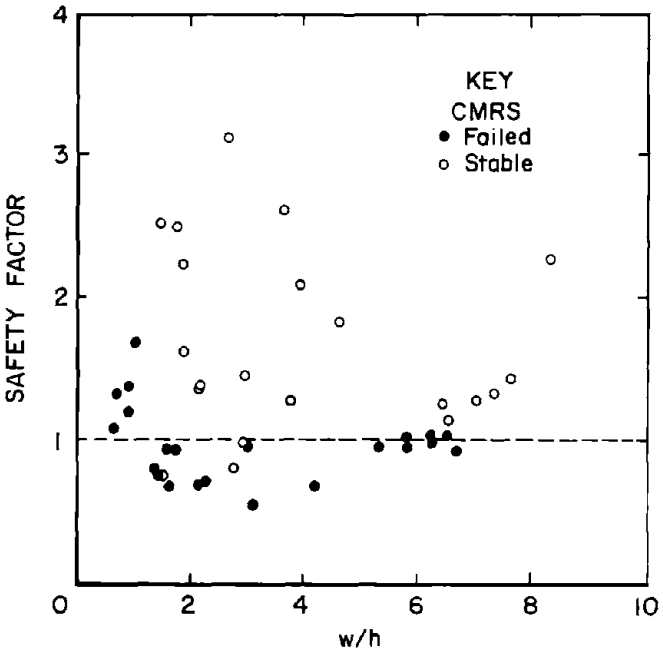

Figure 1.—Performance of equation 1 against case studies.

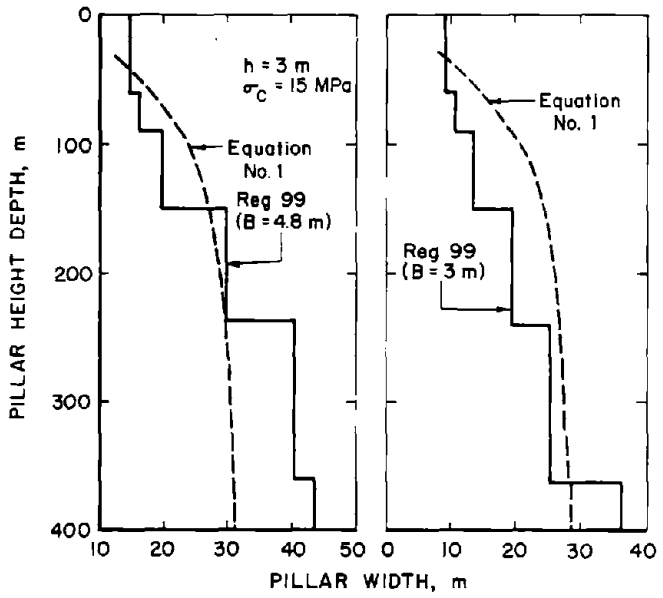

Figure 2.—Pillar sizes as per equation 1 and Regulation 99.

MODIFICATIONS OF CMRS FORMULA

The general form from which equation 1 has been derived is

$$S = \sigma_c h^{-\alpha} + am\,\gamma\,\frac{d\sigma_x}{d(w/h)}\left(\frac{w}{h} - 1\right),$$

where α = exponent defining size effect,

a = triaxial factor,

and m = horizontal-to-vertical in situ stress ratio.

The differential coefficient defines the rate of change of the total horizontal stress σ_x with w/h and end constraint. For simplicity, it is assumed to be directly proportional to depth so that

$$S = \sigma_c\, h^{-\alpha} + am\,\gamma\,cH\left(\frac{w}{h} - 1\right). \qquad (2)$$

Thus, H is the average vertical stress and the in situ stress ratio m is assumed to be constant at all depths. This assumption is incorrect as it has been shown that m reduces with depth according to the general form (*3*)

$$m = p + q/H, \qquad (3)$$

where p and q are empirical constants.

The constants p and q can vary considerably depending on local conditions. Unfortunately, in-seam stress measurement data are very scanty, and hence the values of these constants have been estimated from a theory being published elsewhere (*4*). This theory indicates that the average horizontal in situ stress depends on rock properties and is given by

$$\sigma_h = \gamma H\,\frac{\nu}{1-\nu} + \frac{\beta EG}{1-\nu}(H + 1000), \qquad (4)$$

where E = horizontal elastic modulus, MPa,

ν = Poisson's ratio,

β = coefficient of linear thermal expansion,

and G = thermal gradient, °C/m.

The depth H is in meters and the unit rock pressure γ is in megapascals per meter. This equation is derived for more or less horizontally disposed rocks.

Lindner and Halpern (*5*) have published a compilation of stress measurement data along with elastic modulus values. Equation 4 was checked for validity against these data using the following average values for crustal rocks:

γ = 0.027 MPa/m, ν = 0.2,

E = 50,000 MPa, G = 0.024 °C/m,

$\beta = 0.6 \times 10^{-5}$ /°C.

Figure 3, despite the inevitable scatter, indicates a reasonable correlation between the average measured horizontal stress and that predicted by equation 4.

This equation can thus be used for obtaining the average in-seam horizontal stress. The following average values may be assigned to coal seams (*6*):

γ = 0.025 MPa/m, ν = 0.3,

E = 3,000 MPa, G = 0.03 °C/m,

$\beta = 3 \times 10^{-5}$ /°C.

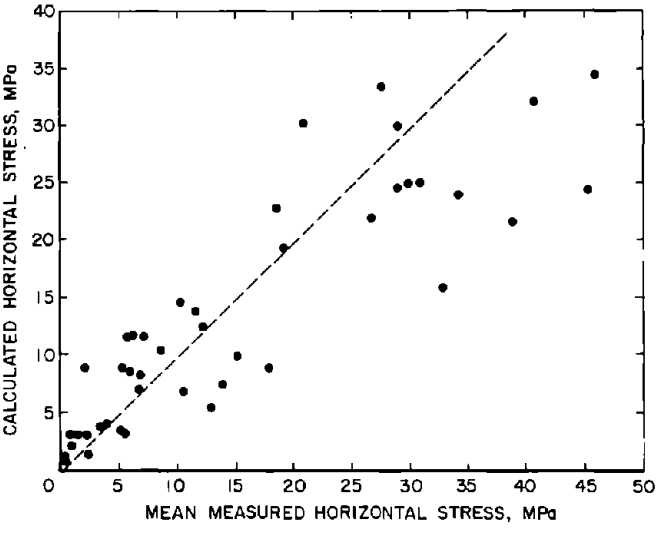

Figure 3.—Comparison between the mean horizontal stress predicted by equation 4 and measured values.

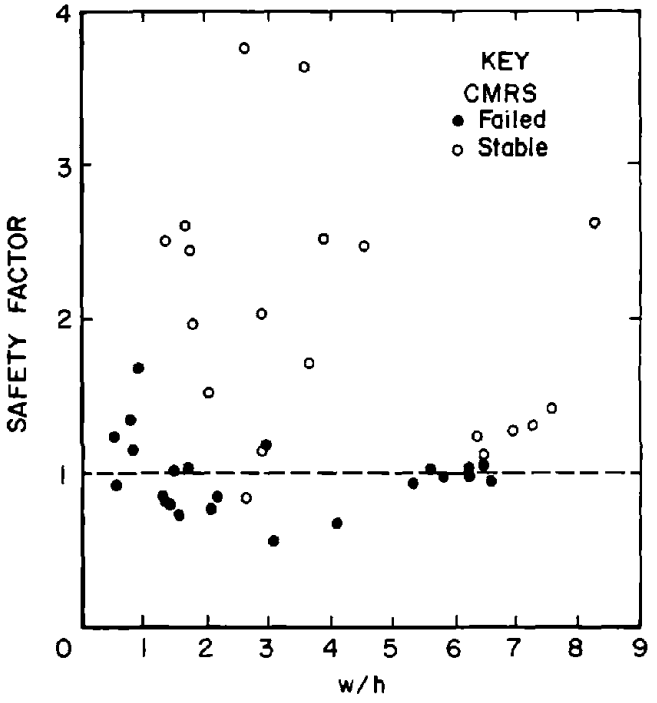

Figure 4.—Performance of equation 6 against case studies.

Dividing equation 4 by γH, the in situ stress ratio m was finally obtained as

$$m = 0.58 + \frac{154}{H},$$

or

$$m = 0.6 + \frac{150}{H} \quad \text{say.} \qquad (5)$$

Substituting equation 5 in equation 2, the general equation becomes

$$S = \sigma_c h^{-\alpha} + ac\gamma H \left(0.6 + \frac{150}{H}\right)\left(\frac{w}{h} - 1\right),$$

or

$$S = \sigma_c h^{-\alpha} + CH \left(0.6 + \frac{150}{H}\right)\left(\frac{w}{h} - 1\right).$$

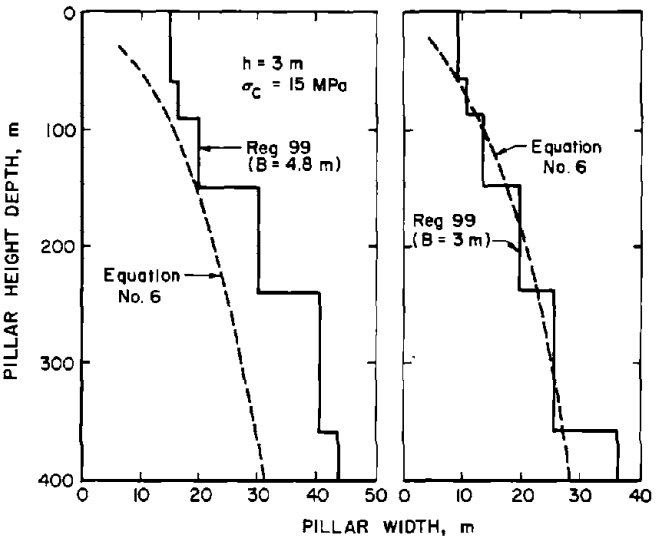

Figure 5.—Pillar sizes according to equation 6 and Regulation 99.

The value of $\alpha = 0.36$ as in equation 1 and the value of σ_c as the strength of 1-in cubes results in the equation in SI units:

$$S = 0.27\,\sigma_c h^{-0.36} + CH \left(0.6 + \frac{150}{H}\right)\left(\frac{w}{h} - 1\right) \text{MPa}.$$

The constant C was determined from the case studies of tables 1 and 2 such that the two criteria of Salamon and Munro were satisfied approximately, as shown in figure 4. The final pillar strength equation is obtained as

$$S = 0.27\,\sigma_c h^{-0.36} + \frac{H}{150}\left(0.6 + \frac{150}{H}\right)\left(\frac{w}{h} - 1\right) \text{MPa}. \qquad (6)$$

Figure 5 shows the performance of equation 6 against the pillar sizes of Regulation 99 for $\sigma_c = 15$ MPa. The improvement in the performance is apparent when compared with figure 2.

GENERALIZATION FOR IN SITU STRESSES

Equation 6 can be generalized to include any arbitrary in situ stresses. Equation 2 can be rewritten as

$$S = 0.27\,\sigma_c h^{-0.36} + m.\,ac\gamma\,\frac{\gamma H}{\gamma}\left(\frac{w}{h} - 1\right),$$

or $S = 0.27\,\sigma_c h^{-0.36}$

$$+ \frac{\sigma_v}{150\,\gamma}\left(p + \frac{q}{H}\right)\left(\frac{w}{h} - 1\right),$$

or $S = 0.27\,\sigma_c h^{-0.36}$

$$+ \frac{\sigma_v}{3.75}\left(p + \frac{q}{H}\right)\left(\frac{w}{h} - 1\right)\text{MPa}, \qquad (7)$$

in which γH is replaced by the vertical stress σ_v since the two are not necessarily equal.

Equation 7 may be used for coal pillar design in unusual in situ stresses.

CONCLUSION

Equation 6 is proposed for pillar design in average coal measures. It was derived with the help of case studies, and its performance is checked against Regulation 99 of the Indian Coal Mines Regulations for the seam strength of 15 MPa, which is one of the lowest values in India. These regulations generally provide stable pillar sizes, although they are not entirely true to logic since the pillar sizes increase slowly down to the depth of 150 m, whereafter they increase rapidly.

Equation 7 is proposed for unusual in situ stresses in coalfields. The vertical stresses σ_v and the constants p and q have to be determined by stress measurement in such cases.

Equation 5, which is proposed for the in-seam horizontal-to-vertical stress ratio, may be verified by stress measurement.

REFERENCES

1. Sheorey, P. R., M. N. Das, D. Barat, R. K. Prasad, and B. Singh. Coal Pillar Strength Estimation from Failed and Stable Cases. Int. J. Rock. Mech. and Min. Sci. (Geomech. Abstr.), v. 24, 1987, pp. 347-355.

2. Salamon, M. D. G., and A. H. Munro. A Study of the Strength of Coal Pillars. J.S.A. Inst. Min. and Metall., v. 68, 1967, pp. 55-67.

3. Hoek, E., and E. T. Brown. Underground Excavations in Rock, Inst. Min. and Metall., London, 1980, p. 527.

4. Sheorey, P. R. A Theory for In Situ Stresses in Isotropic and Transversely Isotropic Ground. Int. J. Rock Mech. and Min. Sci. (Geomech. Abstr.) (in press).

5. Lindner, E. N., and J. A. Halpern. In Situ Stresses in North America—A Compilation. Int. J. Rock Mech. and Min. Sci. (Geomech. Abstr.), v. 15, 1978, pp. 183-203.

6. Van Krevelen, D. W. Coal, Elsevier, Amsterdam, 1961, p. 514.

ANALYSIS OF STABLE AND UNSTABLE PILLAR FAILURE USING A LOCAL MINE STIFFNESS METHOD

By R. Karl Zipf, Jr.[1]

INTRODUCTION

Most coal mine pillar failures occur benignly by nonviolent yielding. Fracture systems in the overly stressed coal extend, and the failed coal, no longer able to sustain the applied stresses, transfers these stresses to other parts of the mine structure. Nonviolent yielding may be viewed as a *stable* failure process. In contrast, certain coal mine pillar failures occur catastrophically by violent bumps or progressive pillar failures. These violent failures may represent *unstable* failure processes. (A bump refers to the *instantaneous*, violent failure of overly stressed coal, and it is usually associated with significant seismic and microseismic activity. A progressive pillar failure refers to the *noninstantaneous* failure of a series of coal pillars. One pillar fails suddenly, which transfers stress to the adjacent pillar(s), causing it to fail, and so forth. In contrast to bumps, progressive pillar failures may occur without significant mining-induced seismic and microseismic activity.)

This paper describes ongoing research at the U.S. Bureau of Mines that seeks to develop and test analysis methods for describing the mechanics of pillar failure. This research could provide methodologies to distinguish why some pillars fail by nonviolent yielding when subject to high stresses whereas others fail by violent bumping. One mechanical explanation for distinguishing between stable (nonviolent) and unstable (violent) failures uses the local mine stiffness (LMS) concept introduced by Starfield and Wawersik (*1*)[2]. This concept stems from an understanding of the complete stress-strain behavior of a coal pillar and its relation to the mechanical properties of the surrounding rock mass. Stable failure occurs when $K_{LMS} - K_P < 0$, where K_{LMS} is local mine stiffness, and K_P is pillar stiffness. K_P is the downward slope of the strain-softening, stress-strain curve for the pillar at some point in the postfailure regime.

Discussions in this paper cover the origins of the LMS concept and show how it can explain the mechanics of certain kinds of unstable failures in mines. Bureau research efforts have incorporated K_{LMS} calculations into a three-dimensional (3-D) boundary-element-method (BEM) program. This experimental program, called LMSTIFF, calculates K_{LMS} and provides a means to distinguish between stable and unstable pillar failure. Bureau research described herein has provided practical understanding of the K_{LMS} calculations done by this new program. This paper systematically examines key factors controlling K_{LMS} in various room-and-pillar and longwall mining scenarios. Finally, the paper draws conclusions and makes recommendations on the practical use of K_{LMS} calculations to assess stable versus unstable pillar failure.

THE LOCAL MINE STIFFNESS CONCEPT

Prior to the 1960's, uniaxial compressive strength testing of laboratory-scale rock specimens in so-called "soft" testing machines produced stress-strain curves like the one shown in figure 1*A*. Typical tests ended suddenly and violently upon arrival at or shortly after reaching the "ultimate compressive strength," which is the maximum ordinate on the stress-strain curves in figure 1. Beyond a critical strain level, the specimen had no load-carrying capacity, usually because it had disintegrated completely.

In the 1960's, researchers (*2-4*) realized that the test specimen formed part of a larger test system that included the loading frame itself. Characteristics of that frame affected the outcome of the test. Later testing in so-called "stiff" testing machines produced *complete* stress-strain curves, such as shown conceptually in figure 1*B*. Typical tests did not end suddenly and violently, but continued beyond the ultimate compressive strength into the postfailure regime. Under properly controlled conditions, the rock test specimen could sustain considerable stresses at strain levels well into the postfailure regime.

Rigorous analysis of the specimen and loading frame test system by Salamon (*5*) provided a stability criterion

[1]Structural engineer, U.S. Bureau of Mines, Denver Research Center, Denver, CO.

[2]Italic numbers in parentheses refer to items in the list of references at the end of this paper.

able to distinguish between stable, nonviolent laboratory specimen failure and unstable, violent failure. Figure 1*C* illustrates this criterion with a hypothetical complete stress-strain curve. Initially, increases in strain lead to higher stress. With further increases in strain, the specimen enters the postfailure regime where increases in strain lead to lower stresses on the test specimen. A tangent to this stress-strain curve at some arbitrary point Q is the test specimen stiffness, K_P', at that point. Figure 1*C* also shows two other lines through point Q, one labeled soft and the other stiff, that represent the loading machine stiffness, K_{LMS}', for soft and stiff loading machines. The test system remains *stable* at any point Q as long as

$$K_{LMS}' < K_P', \quad (1)$$

and becomes unstable when

$$K_{LMS}' > K_P'. \quad (2)$$

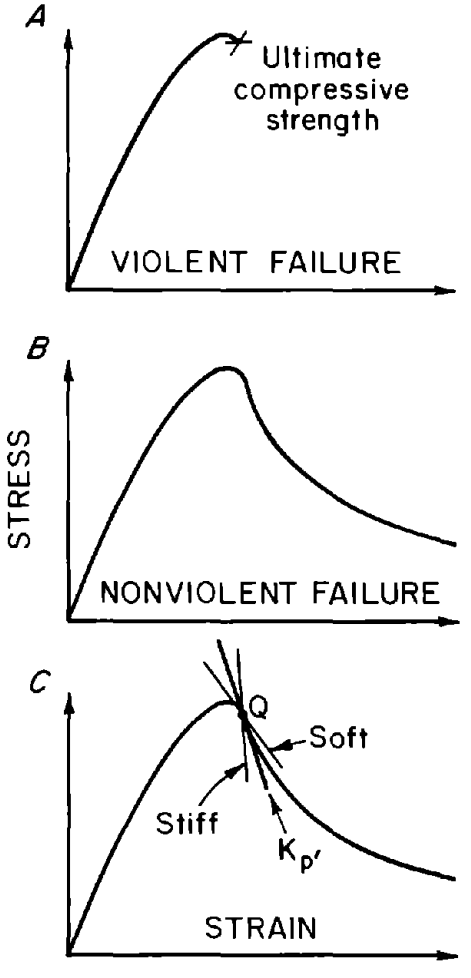

Figure 1.—Typical stress-strain curves for rock exhibiting stable and unstable failure. *A*, stress-strain curve with soft testing machine; *B*, stress-strain curve with stiff testing machine; *C*, criterion for stable and unstable failure of laboratory specimens.

Therefore, the stability criterion is

$$K_{LMS}' - K_P' < 0. \quad (3)$$

(Both K_{LMS}' and K_P' have *negative* values.)

For the situation with the stiff-loading frame, the stability criterion given by equation 3 is satisfied everywhere in the postfailure regime, so the system always remains stable. Failure proceeds in a nonviolent manner. However, with the soft-loading frame, the stability criterion is violated past the ultimate compressive strength. The system becomes unstable at that point, and failure proceeds in a violent manner.

Figure 2 shows the physical meaning of the loading machine stiffness, K_{LMS}'. The test specimen in the test frame is replaced with a simple hydraulic jack as shown in figure 2*A*, which is then pressurized to simulate a loaded test specimen. Relaxing the load on the jack causes the test frame to displace inward. The slope of the jack force versus test frame displacement relation, as shown in figure 2*B*, is the loading machine stiffness. Basically, it accounts for stretching of the loading frame posts, bending of the crosshead, and compressing of the main ram hydraulic fluid.

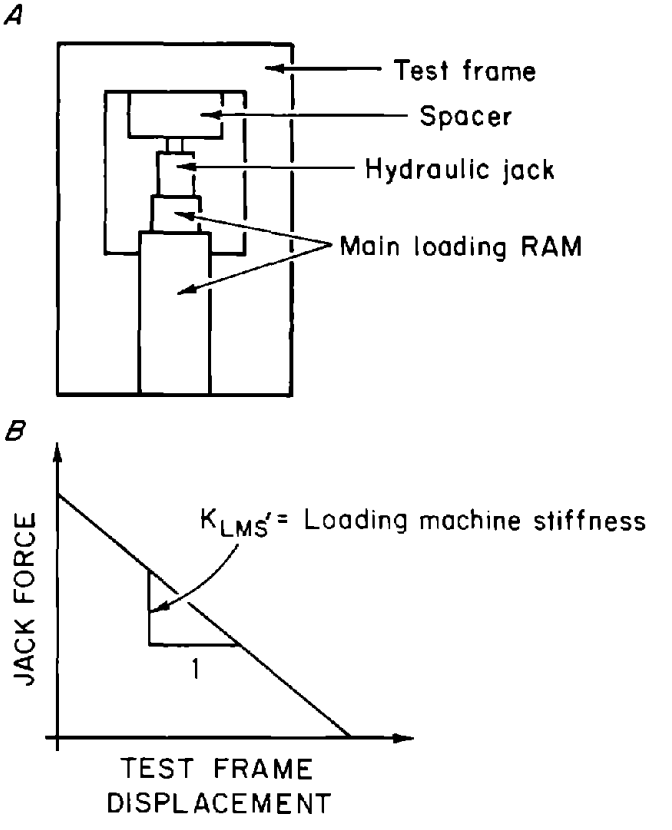

Figure 2.—Illustration of scheme to measure loading machine stiffness. *A*, jack replaces laboratory specimen in test frame; *B*, loading machine stiffness is slope of jack force versus test frame displacement diagram.

The laboratory test specimen loaded by a test frame, as shown in figure 3*A*, is analogous to a mine pillar loaded by the roof and floor, as shown in figure 3*B*. Understanding stable, nonviolent failure versus unstable, violent failure in the laboratory may provide possible explanations for full-scale pillar behavior in mines. Cook (*6*) suggested that rock bursts could occur owing to unstable failure in compression much like the violent failure in a soft-testing machine. Recently, Ryder (*7*) referred to rock bursts of this kind as "Class C" or crush and/or collapse events which occur in areas of high compressive stress concentration ahead of an active mining face.

Based on the analogy between a laboratory test specimen and a mine pillar, Salamon (*5*) and Starfield and Wawersik (*1*) developed an analogous stability criterion for mine pillars. A mine pillar will remain stable as long as

$$K_{LMS} - K_P < 0, \quad (4)$$

where K_{LMS} is the local mine stiffness and K_p is the pillar stiffness as defined earlier.

Similar to the means discussed earlier for measuring loading machine stiffness, figure 4 shows an analogous means to measure K_{LMS}. The mine pillar is replaced with a large hydraulic jack as shown in figure 4*A*, which is then pressurized to simulate a loaded mine pillar. Relaxing the load on the jack causes the mine roof and floor to displace inward. The slope of this force-displacement relation, shown in figure 4*B*, is K_{LMS}. To reiterate, *low* values for K_{LMS} (i.e., high *absolute* values) lead to stable, nonviolent pillar failures analogous to laboratory specimen failure in a stiff-loading frame. Similarly, *high* values of K_{LMS} (i.e., low *absolute* values) lead to unstable, violent pillar failures analogous to specimen failure in a soft test frame.

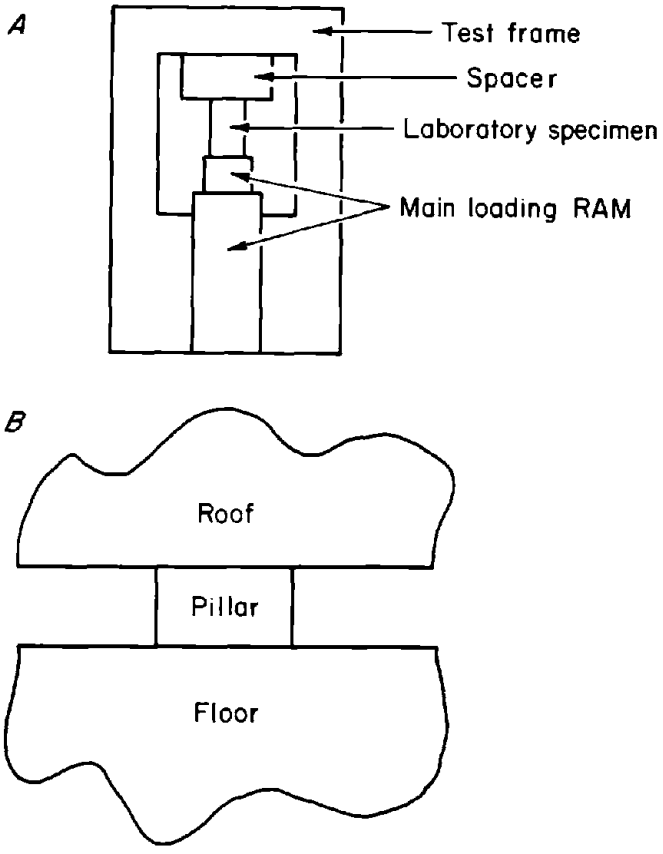

Figure 3.—Illustration of analogy between laboratory specimen loaded by test frame (*A*) and pillar loaded by mine roof and floor (*B*).

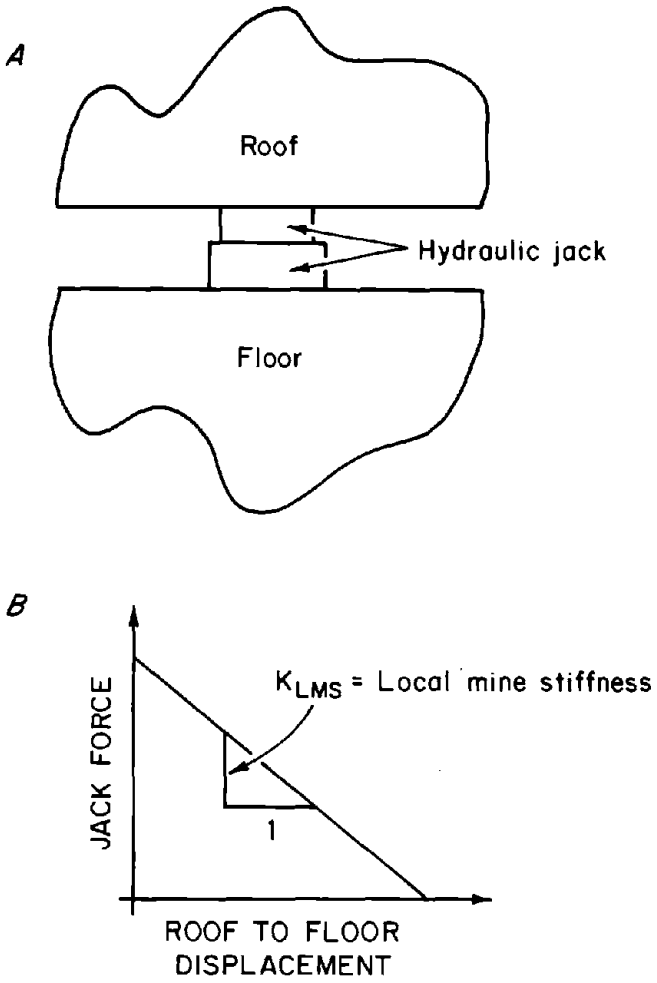

Figure 4.—Illustration of scheme to measure K_{LMS}. *A*, Jack replaces mine pillar; *B*, K_{LMS} is slope of jack force versus mine roof-to-floor displacement diagram.

IMPLEMENTING LOCAL MINE STIFFNESS CALCULATIONS

Two different approaches exist for computing K_{LMS} at a mine pillar, namely: an *eigenvalue approach* developed by Salamon (*5*) and a *perturbation approach* developed by Starfield and Wawersik (*1*). According to Salamon (5), the perturbation approach is equivalent to his more rigorous eigenvalue approach. Both approaches can be implemented into a variety of numerical methods including finite element and discrete element; however, implementation into a BEM program follows directly.

In a 3-D BEM program, a grid of square boundary elements approximates a tabular seam plane that is surrounded by a linear elastic rock mass. The stresses at each element are related to the displacements at every other element by a stiffness matrix that contains stress influence coefficients. Stated mathematically,

$$\sigma = K D, \tag{5}$$

where σ is the element stresses, D is the element displacements, and K is a stiffness matrix. This system of "n" equations contains 2n unknowns, namely n stresses, σ, and n displacements, D, where n is the number of elements.

Boundary conditions are prescribed at each element, and they provide the other n equations necessary for a solution. These boundary conditions take the form

$$\sigma_i = f_i (D_i), \tag{6}$$

where σ_i is the stress at element i, D_i is the displacement at element i, and f_i is a strain-softening, stress-strain function for element i. These prescribed strain-softening functions have derivatives, f'_i. At displacement D, this derivative has the value $f'_i(D)$. This slope $f'_i(D)$ is identical to the postfailure pillar stiffness K_p.

In the *eigenvalue approach*, evaluating stability requires a solution for the smallest eigenvalue of K, found as a root of the characteristic equation

$$|K + \lambda I| = 0, \tag{7}$$

where K is the stiffness matrix, I is the identity matrix, and λ are the eigenvalues. The eigenvalues, λ, are equivalent to the K_{LMS} at each element. Again, stability exists as long as equation 4 is satisfied. The eigenvalue approach has certain advantages aside from its analytical rigor. By finding (or estimating) the smallest eigenvalue of equation 7 and comparing it to the minimum slope of the stress-strain curves given by equation 6, the design engineer can decide whether a particular mine layout is conditionally or unconditionally stable. The safety advantages of an unconditionally stable mine layout are obvious.

Unfortunately, the eigenvalue approach may have certain disadvantages when implemented into a BEM program. Most such programs do not form K explicitly because of its huge size (commonly on the order of 10,000 by 10,000) and because it is *fully* populated. In addition, there appears to be no way of telling *where* the smallest eigenvalue (λ or K_{LMS}) lies in a particular BEM model. Knowing which element corresponds to a particular λ or K_{LMS} may be important if a design engineer wants to alter a mine layout to improve its stability.

The *perturbation approach* provides a computationally economic approach to calculating select eigenvalues of K, i.e., K_{LMS}, at select points in a model. This method begins by solving the boundary-element equations (*5*) and their boundary conditions (*6*) for equilibrium stresses and displacements throughout the model. Then, at a select point X, the equilibrium displacement, D_X, is increased by a small amount, ΔD, to obtain a "perturbed" displacement, D'_X; i.e.,

$$D'_X = D_X + \Delta D. \tag{8}$$

Next, the system is re-solved for the perturbed stresses and displacements. Finally, K_{LMS} at point X is calculated as

$$K_{LMS} = \frac{\sigma'_X - \sigma_X}{D'_X - D_X}, \tag{9}$$

where σ_X is the equilibrium stress at X, σ'_X is the perturbed equilibrium stress at X, D_X is the equilibrium displacement at X, and D'_X is the perturbed equilibrium displacement at X.

This mathematical approach to calculating K_{LMS} at a point is analogous to the mechanical approach shown in figure 4 for measuring K_{LMS}.

The experimental program LMSTIFF, uses the perturbation method of Starfield and Wawersik (*1*) in a practical 3-D BEM program. LMSTIFF calculates K_{LMS} at prescribed elements in the BEM model. Program MULSIM/NL (*8-9*), developed earlier at the Bureau, served as the basis for LMSTIFF.

For the in-seam material, program LMSTIFF has a strain-softening model. As shown in figure 5, the user specifies 10 points on a stress-strain curve to use this material model. With this material model, the user can also simulate elastic-plastic or linear elastic behavior for the in-seam material. LMSTIFF permits up to 26 different strain-softening materials. In addition, the program has multiple mining steps and multiple *loading* steps. Figure 6 gives a simplified flowchart of the structure of program LMSTIFF.

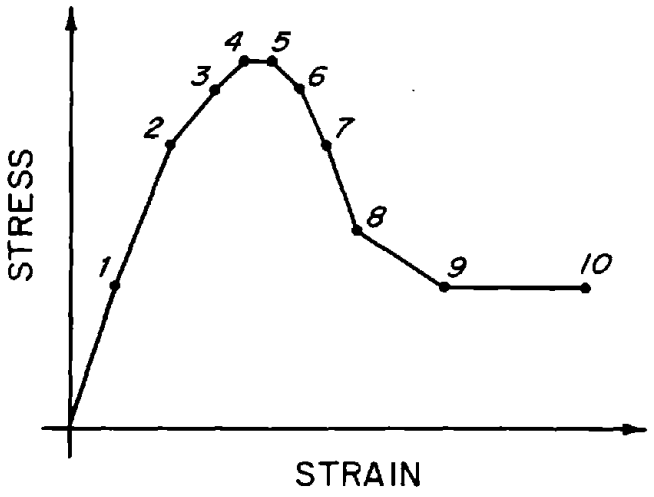

Figure 5.—Illustration of 10-point strain-softening material model in program LMSTIFF.

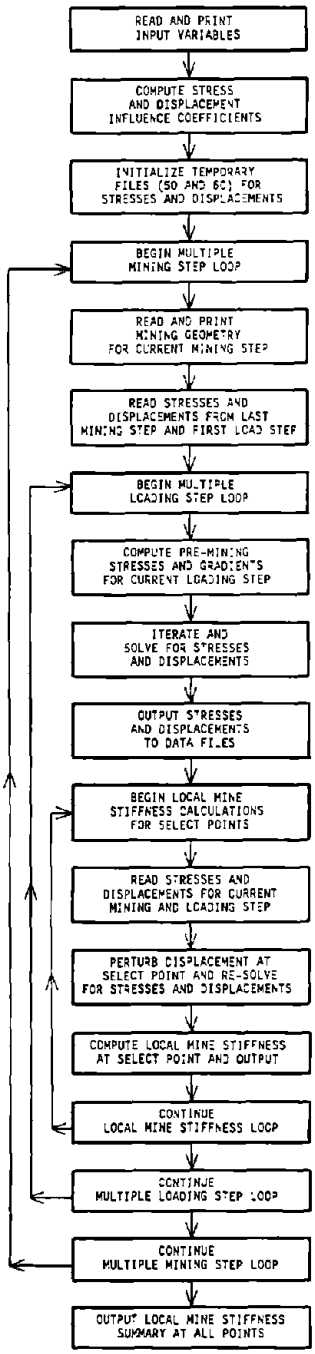

Figure 6.—Flowchart showing structure of program LMSTIFF.

ILLUSTRATION OF STABLE AND UNSTABLE PILLAR FAILURE

The following example demonstrates the capabilities of program LMSTIFF by showing an example of stable and unstable pillar failure. The BEM model in this example is a five-by-five array of 12-m by 18-m pillars with 6-m entries. Figure 7 shows this simple model, which uses 3-m elements in the fine mesh and 15-m blocks in the coarse mesh. The overall extraction ratio for this model is 50 pct. The surrounding rock mass has a modulus of 1,000 MPa, while the in-seam material follows one of the different strain-softening material models shown in figure 8. The stable example uses material model D, and the unstable case uses F. This example also uses the load-stepping capability of LMSTIFF. Applied vertical stresses on the model are 4, 6, 8, 8.9, 9.0, 9.1, 9.2, 9.5, 10.0, and 10.5 MPa. At each load step, LMSTIFF computes K_{LMS} at the central element shown in figure 7.

Figure 9*A* and *B*, presents these K_{LMS} computations for the stable and unstable cases, respectively. Points on the stress-strain curves indicate the calculated stress and strain at the central element of the model shown in figure 7. The sloping line through these points indicates the computed K_{LMS}, which for these cases has a value of about -700 MPa. The number above a K_{LMS} line gives the applied vertical stress on the model. For figure 9*A*, the computed K_{LMS} of about -700 MPa is less than the minimum pillar stiffness of -500 MPa, which occurs at strains between 0.010 and 0.015. This case satisfies the criterion given by equation 4 and, therefore, remains stable. For figure 9*B*, the K_{LMS} of -700 MPa is greater than the minimum pillar stiffness of -2,000 MPa, which again occurs between strains of 0.010 and 0.015. Since this case violates the criterion, an unstable pillar failure occurs.

The unstable pillar failure manifests itself as a sudden jump or increase in the computed pillar strain. Figure 10 illustrates this strain discontinuity. For the stable case, small increases in the applied vertical stress give small increases in the pillar strain at the select point in the model. However, for the unstable case, small increases in applied stress can give very large increases or a sudden jump in pillar strain such as that which occurs at an applied stress of about 9 MPa. The strain discontinuity also shows itself in figure 9*B*. Additional computations showed that increasing the applied stress from 8.93 to 8.94 MPa gives a sudden increase in pillar strain from 0.0099 to 0.0265. The transition from the stress-strain point (20, 0.0098) at an applied load of 8.9 MPa to point (10, 0.0265) at an applied load of 9.0 MPa follows the slope of the K_{LMS} quite closely.

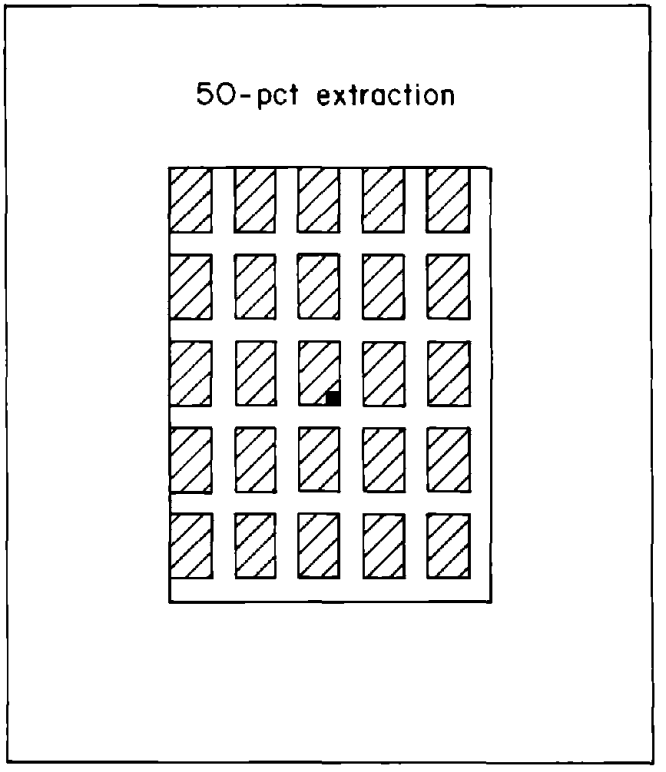

Figure 7.—Typical boundary element model used for stability analyses of room-and-pillar mines on development. Model uses 3-m elements in fine mesh and 15-m blocks in coarse mesh. K_{LMS} is evaluated at central shaded element.

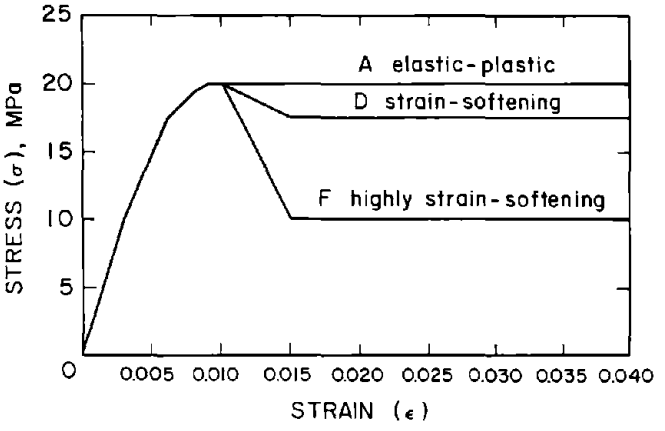

Figure 8.—Different strain-softening material models used to investigate K_{LMS} calculations.

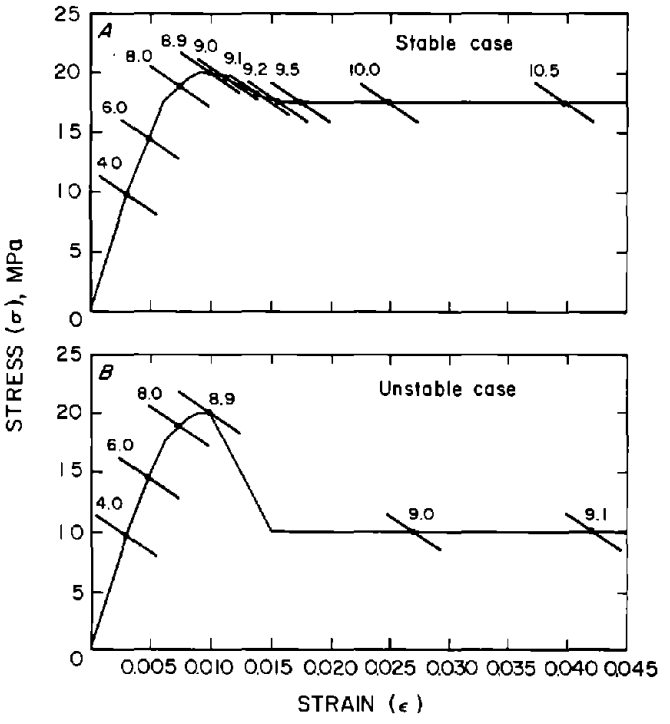

Figure 9.—Stress, strain, and K_{LMS} computations for stable case, *(A)* and unstable case, *(B)* using room-and-pillar geometry shown in figure 7.

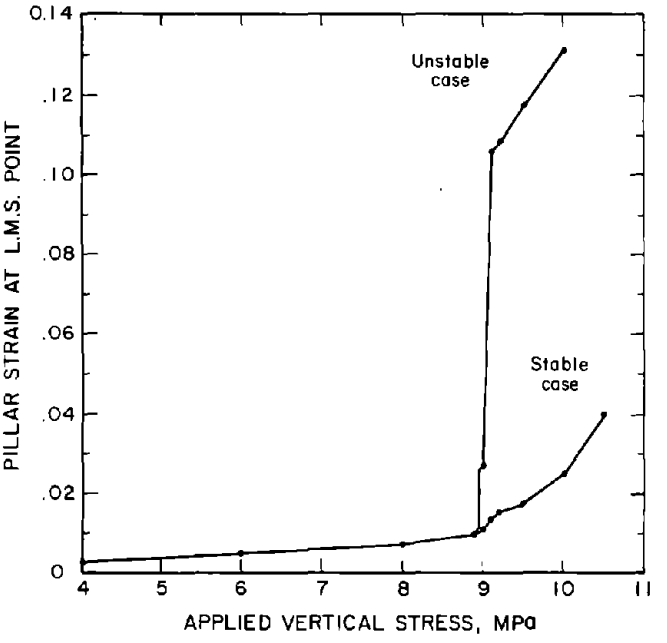

Figure 10.—Applied vertical stress versus pillar strain showing stable and unstable pillar failure of room-and-pillar geometry shown in figure 7.

PRACTICAL LOCAL MINE STIFFNESS CALCULATIONS WITH PROGRAM LMSTIFF

As discussed previously, initial trials with program LMSTIFF showed that K_{LMS} calculations can provide a distinction between stable and unstable pillar failure in mines through the stability criterion given by equation 4. This criterion considers K_{LMS} relative to the postfailure pillar stiffness, K_P. The user defines a priori one of the variables in the stability criterion, namely K_p, via the prescribed strain-softening, stress-strain curves for the boundary-element model. Program LMSTIFF computes the other variable, K_{LMS}, for the BEM model in question. Subsequent research with this program seeks to discern which parameters control calculations of K_{LMS} and their relative importance. The numerical experiments examined three different mining scenarios: room-and-pillar mining on development, room-and-pillar mining on retreat, and longwall mining. Major parameters considered in these studies include the rock mass modulus, stress-strain properties of the coal, mine geometry, and position within the BEM mesh. Additional factors considered were seam thickness and the relative size of the perturbation ΔD in equation 8. These minor factors had no influence on K_{LMS} calculations as theoretical considerations suggest.

ROOM-AND-PILLAR MINING ON DEVELOPMENT

Figure 7 shows a typical boundary-element model used in this phase of the room-and-pillar studies. The regular array of pillars effectively extends to infinity in all directions. These tests do not include the effect of any barrier pillars. The pillar geometries considered ranged from 6 by 6 m to 24 by 24 m, with various combinations in between. Extraction ratios ranged from 75 pct down to 33 pct. The 12- by 18-m pillar geometry at 50 pct extraction, shown in figure 7, is representative of the range of geometries considered. The numerical experiments with LMSTIFF increased the vertical stress on the mine model until the stress and strain at the select K_{LMS} calculation point extended far into the postfailure regime of the prescribed stress-strain curve. Comparisons use a calculated K_{LMS} at or near the peak stress for the select element.

For the wide variety of room-and-pillar geometries considered, computed K_{LMS} for the select element near the center of the BEM model showed *no* dependence on the mine geometry or the extraction ratio. Therefore,

additional K_{LMS} calculations for room-and-pillar mining scenarios consider an array of 12- by 18-m pillars only.

The initial studies completed with LMSTIFF demonstrated stable and unstable pillar failure. Increasing the vertical stress on a coal mine layout, such as that shown in figure 7, causes the pillar stress and strain to increase and follow the prescribed stress-strain curve as shown in figure 9. As the pillar strain increases, the computed K_{LMS} undergoes some slight changes. Figure 11 plots K_{LMS} as a function of increasing pillar strain induced by increasing the vertical stress on the BEM model. These studies used different rock modulus values, namely 1,000 and 10,000 MPa. Figure 8 shows the different stress-strain models for the coal considered in these studies: The curve labeled A exhibits elastic-plastic behavior, D shows moderate strain-softening, and F is highly strain-softening.

K_{LMS} computations exhibit a small dependence on strain level. In the initial elastic region, K_{LMS} starts with a high magnitude. As the pillar strain increases within the elastic regime, K_{LMS} magnitude decreases slightly (about 5 pct) until the peak stress is exceeded. Upon entering the post-failure regime, K_{LMS} magnitude continues to decrease and reaches a low value just after the strain at peak stress, which in this case occurs at 0.01 strains. K_{LMS} magnitude then increases back up to a plateau, which is about 10 pct to 15 pct less than the initial K_{LMS} magnitude in the elastic regime. Figure 11 indicates that the prescribed stress-strain curve for the coal does have some influence on calculated K_{LMS}. The "depth" of the K_{LMS} low shown in this figure depends on the degree of strain-softening prescribed for the in-seam material. More highly strain-softening materials seem to reach lower K_{LMS} magnitudes.

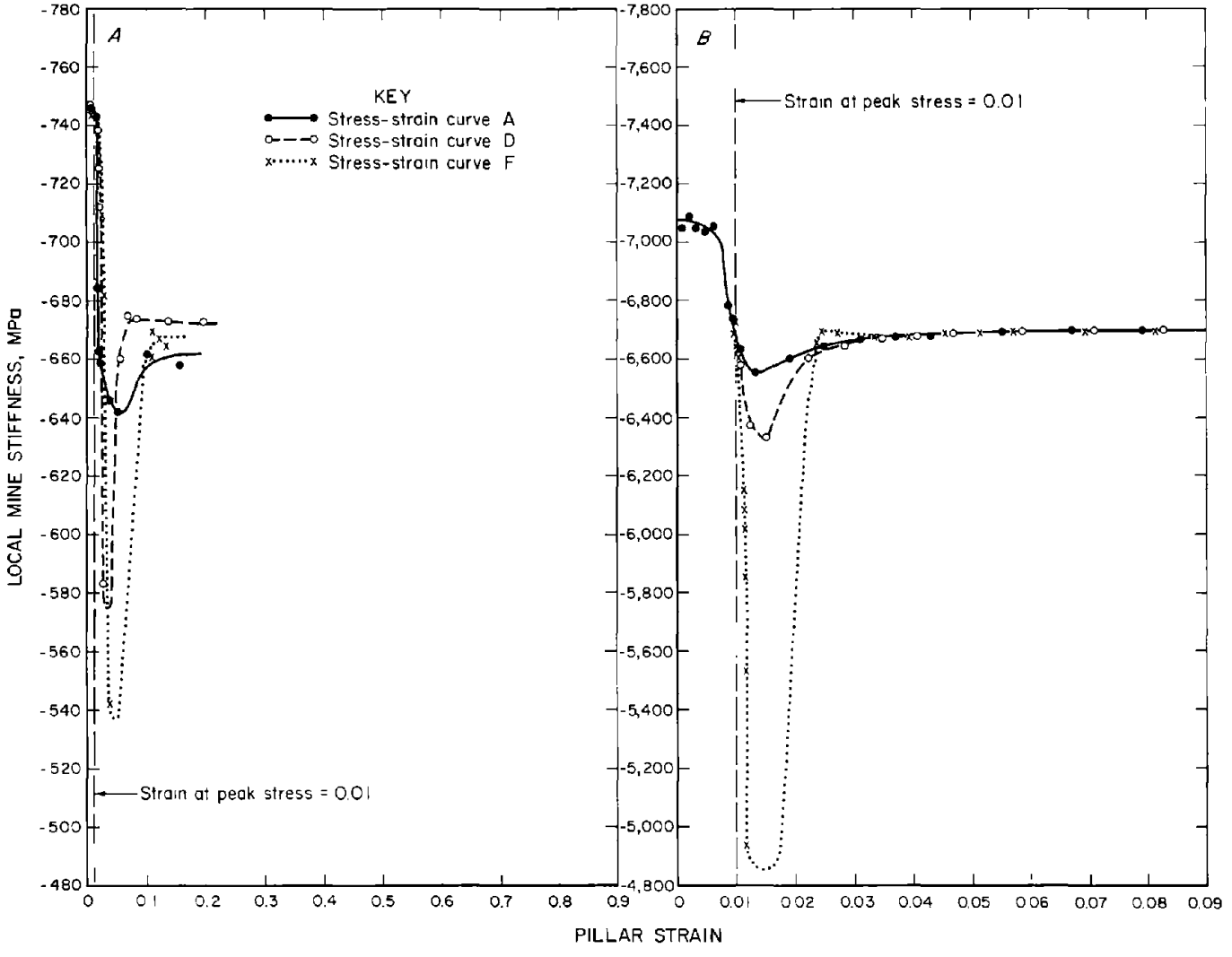

Figure 11.—K_{LMS} as function of pillar strain for room-and-pillar geometry shown in figure 7. *A*, rock mass modulus is 1,000 MPa; *B*, rock mass modulus is 10,000 MPa. A, D, and F refer to stress-strain models shown in figure 8.

However, beyond a sufficiently high strain level, different material models give almost identical K_{LMS} values. Except for the initial dip in K_{LMS} magnitude in the early post-failure regime, most practical applications can treat K_{LMS} as independent of the pillar strain level. However, the significance of this dip requires further investigation.

Prior calculations always computed K_{LMS} at the corner element of a pillar near the center of the BEM mesh. Further numerical experiments studied K_{LMS} as a function of position in the BEM mesh by calculating K_{LMS} at all elements in a central pillar and in the surrounding entry. Results show that K_{LMS} exhibits no significant dependence on position. In one typical set of calculations, K_{LMS} varied from about 6,700 to 6,800 MPa, i.e., less than 2 pct. Apparent variations in K_{LMS} with position are in reality caused by differences in the calculated strain levels in elements throughout the model.

Figure 12 plots K_{LMS} as a function of the surrounding rock mass modulus. As expected, the two correlate almost linearly. The ratio of K_{LMS} to rock modulus always remains about 0.7 for the room-and-pillar geometries considered. Factors controlling this ratio require further investigation. It appears that the element size has considerable influence and that the initial modulus of the coal has minor influence on this ratio.

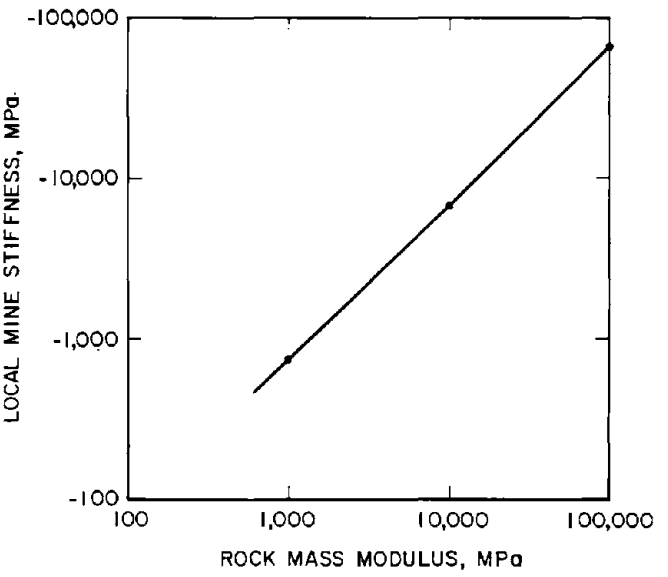

Figure 12.—K_{LMS} as function of rock mass modulus for room-and-pillar geometry shown in figure 7. This relation applies to a 3-m element size only.

ROOM-AND-PILLAR MINING ON RETREAT

Figure 13 shows the basic BEM model used to calculate K_{LMS} in retreat room-and-pillar mining scenarios. The upper part of this model is mined out completely, while the lower part is 50 pct extracted. Pillar dimensions are 12 by 18 m as in the previous models. This figure also indicates select elements where LMSTIFF calculates K_{LMS} at various applied vertical stress levels.

The retreat room-and-pillar mining studies considered strain level effects and position effects only. A few numerical experiments completed with various pillar geometries demonstrated that, as before, pillar geometry does not influence the calculated K_{LMS} at a select point. In addition, K_{LMS} scaled linearly with rock mass modulus, as was found earlier in the development room-and-pillar studies. When investigating strain level and position effects, the calculations use 10,000 MPa for the rock mass modulus and material model D, as shown in figure 8 for the in-seam coal. Different material models provided nearly identical numerical results that lead to similar conclusions.

Figure 14 plots K_{LMS} at select elements as a function of increasing pillar strain induced by increasing the vertical stress on the BEM model. Similar to figure 11 for the development room-and-pillar studies, K_{LMS} calculations exhibit a slight dependence on strain level. K_{LMS} starts with a high magnitude in the elastic regime and decreases

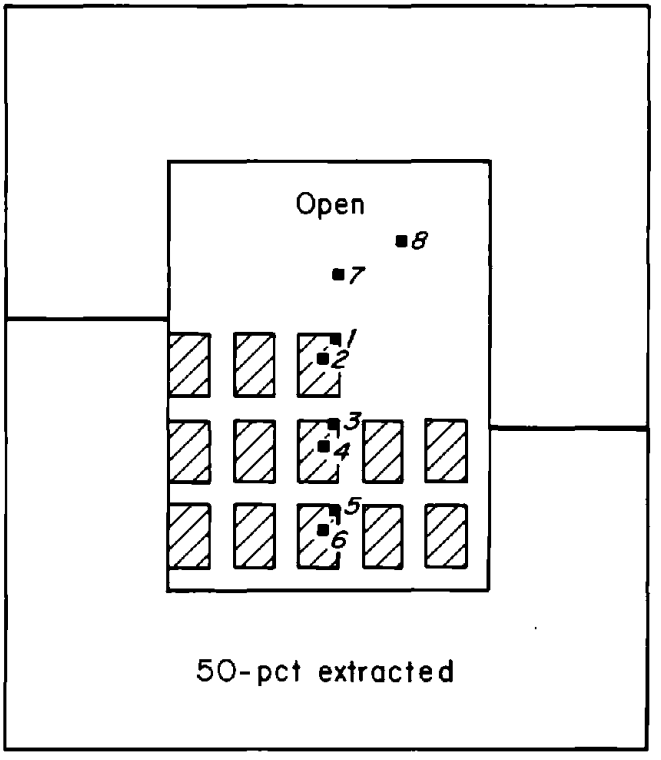

Figure 13.—Boundary-element model used for stability analyses of retreat room-and-pillar mines. Model uses 3-m elements in fine mesh and 15-m blocks in coarse mesh. K_{LMS} is evaluated at numbered elements.

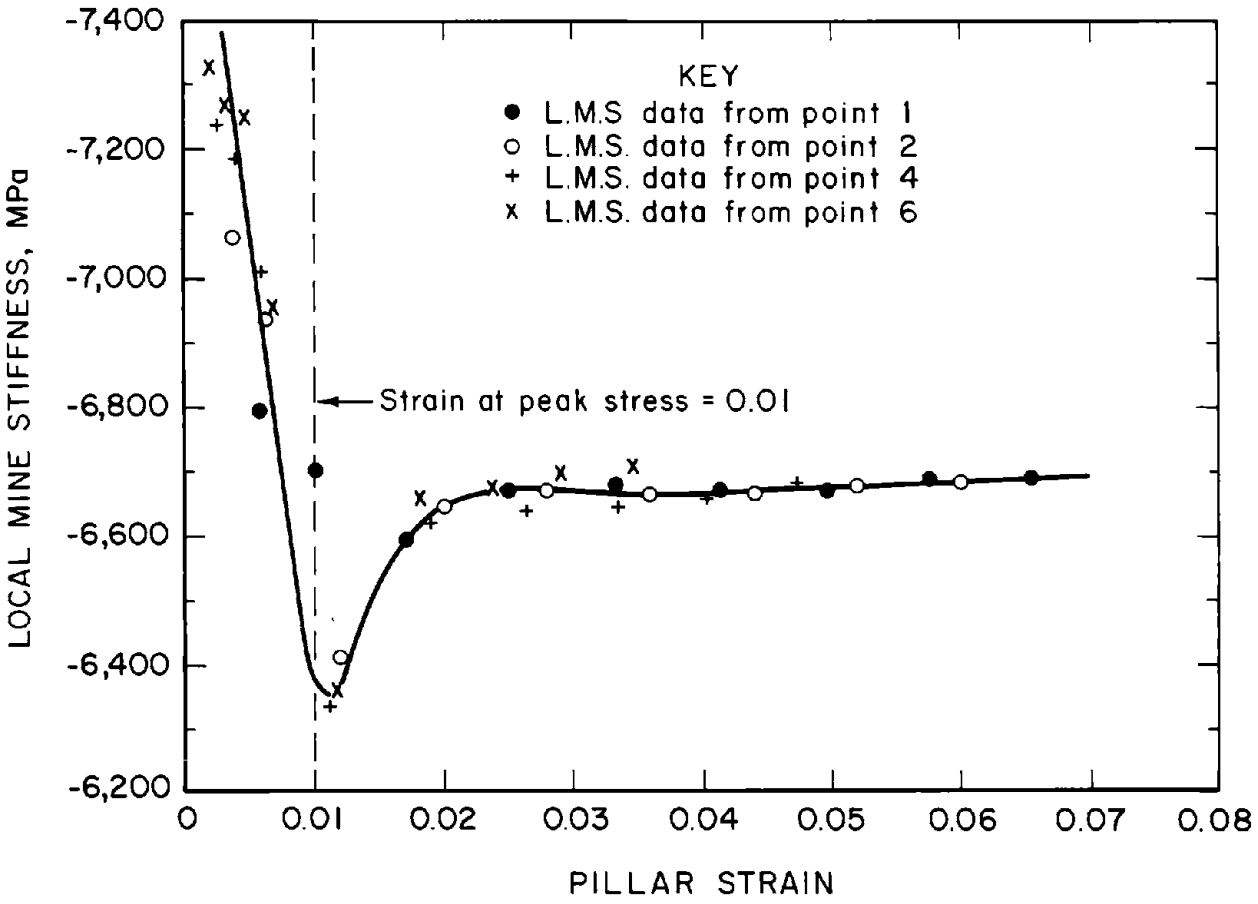

Figure 14.—K_{LMS} as function of pillar strain for retreat room-and-pillar geometry shown in figure 13. Rock mass modulus is 10,000 MPa, and coal follows material model D shown in figure 8. Numbers refer to elements indicated in figure 13.

slightly (less than 10 pct) until peak stress is exceeded at 0.01 strains. In the postfailure regime, K_{LMS} magnitude continues to decrease, then increases up to a plateau. K_{LMS} magnitude at this plateau is again about 10 pct to 15 pct below the initial value in the elastic regime. Evidently, all elements converge to the same K_{LMS} value at sufficiently high strain levels.

The BEM stress calculations clearly show development of high stresses in the pillars adjacent to the mined-out area and especially so in the pillar at the reentrant corner. However, the presence of this nonuniform stress field across the pillar array does not affect the K_{LMS} calculations significantly. Again, as shown in figure 14, different elements far into the postfailure strain regime have virtually identical K_{LMS} values, with less than 1 pct variation. In the elastic region prior to failure, K_{LMS} values show a slight increase for elements farther away from the mined-out area. However, this apparent position effect on K_{LMS} value is in actuality due to the variation in K_{LMS} with strain level.

LONGWALL MINING

Figure 15 shows the four longwall gate road models considered in this phase of the K_{LMS} evaluations, namely: abutment-abutment, yield-yield, yield-abutment, and abutment-yield systems. The model calculations occur in four mining steps. In step 1, mining has excavated the gate road pillars, which are then subject to "development loading." In step 2, longwall mining has extracted all of panel 1 on the right side of the model. The gate road pillars are subject to "side abutment loading" from the first panel. During mining step 3, half of panel 2 is mined out. The gate road pillars are subject to an additional "front abutment loading," and they reach their most critical state from a stability viewpoint. After mining step 4, all of panel 2 is mined out, and the gate road pillars are subject to side abutment loads from both panels. Abutment pillars are 24 by 24 m, and yield pillars are 9 by 24 m.

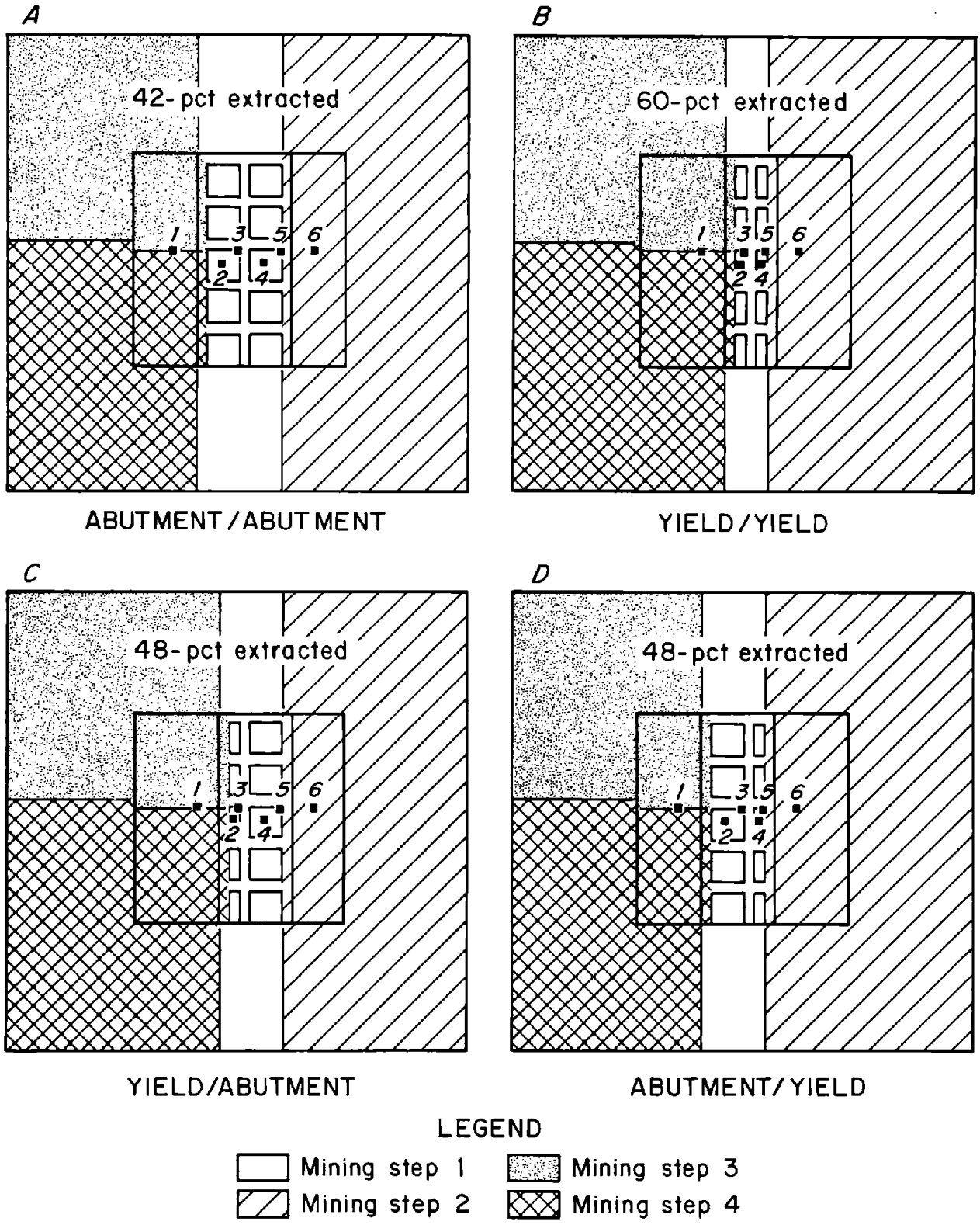

Figure 15.—Four BEM models used for K_{LMS} studies of longwall gate road systems. *A*, abutment-abutment; *B*, yield-yield; *C*, yield-abutment; *D*, abutment-yield.

The longwall mining studies differ from the previous room-and-pillar studies by the method of loading. The previous studies used the load step capability of program LMSTIFF to apply an explicit vertical stress increase on the overall BEM model. These studies use the multiple mining step capability of LMSTIFF to increase the stress on gate road pillars by the progressive mining activity. Rock mass modulus is either 1,000 or 10,000 MPa, and material model D (see figure 8) is used for the in-seam coal. These studies make a conservative assumption by allowing the mined-out areas to remain open and not replacing the mined-out coal material with a gob material. Therefore, the gate road pillars are subject to higher stresses than expected. Figure 15 also indicates the elements where K_{LMS} calculations are performed.

Figure 16 presents a composite of the calculated K_{LMS} versus pillar strain data for all the longwall gate road models. As in previous modeling exercises, K_{LMS} exhibits the same interesting behavior as a function of strain. Initially, when pillar strains are within the elastic region of the prescribed stress-strain curve, calculated K_{LMS} has a high magnitude. As pillar strain increases, K_{LMS} magnitude decreases on the order of 15 pct to 20 pct and reaches a low point just after the in-seam material has entered the postfailure regime. K_{LMS} magnitude then increases again and reaches a stable level about 10 pct to 15 pct below the initial value in the elastic regime.

These studies of various longwall mining scenarios identified clearly the various factors controlling K_{LMS} calculations for these cases. As before, rock mass modulus is the major factor controlling K_{LMS} magnitude. As indicated by data in figure 16, K_{LMS} and rock mass modulus correlate linearly, and the ratio of K_{LMS} to modulus is also about 0.7 as before. The actual gate road pillar geometry has *no influence* on K_{LMS} calculations. For the same rock mass modulus, different gate road geometries all seem to follow the same K_{LMS} versus pillar strain function as shown in figure 16. Furthermore, the position of an element within a BEM model does not affect K_{LMS} at that element. Apparent variations in K_{LMS} as a function of position are attributable to differences in the calculated strains across the model. In summary, except for the rock mass modulus, only the strain level has a small, but perceptible effect on K_{LMS} calculations. Figure 16 shows that relationship for two different rock mass moduli and one particular prescribed stress-strain relationship for the in-seam coal.

DISCUSSION

A major objective in this research is to develop and test methods applicable to the analysis of pillar failure. In early research on rock bursts, Cook (*6*) suggested that these violent failures are unstable failures brought about by differences between the postfailure pillar material stiffness and the surrounding rock mass stiffness. The LMS concept introduced by Starfield and Wawersik (*1*) and advanced by Salamon (*5*) may provide a means to distinguish between stable, nonviolent failures and unstable violent ones. Program LMSTIFF implements K_{LMS} calculations into a practical program. The examples shown in figures 9 and 10 indicate that K_{LMS} calculations and the stability criterion given by equation 4 can distinguish between a stable and an unstable pillar failure.

However, a major question in this research is whether the LMS stability criterion (equation 4) proposed by Salamon (*5*) applies to the violent failures known as coal mine bumps. Research for this paper suggests that while all coal mine bumps are unstable, violent failures, not all unstable, violent failures are coal mine bumps. For example, progressive pillar failures, such as the recent one documented and analyzed by Khair and Peng (*10*), constitute one form of unstable, violent failure quite distinct from a coal mine bump. The ideas presented in figure 17 may help clarify these distinctions.

In figure 17, the large box represents the set of all pillar failures, with unstable ones at the top and stable ones at the bottom. A dashed horizontal line separates violent and nonviolent failures. Placement of this line indicates that while all stable pillar failures are nonviolent, not all unstable failures are necessarily violent. The distinction between violent and nonviolent is strictly qualitative, hence the dashed line. The dashed vertical line separates short from long or instantaneous from noninstantaneous failure events, i.e., dynamic versus static failures. Again, the distinction is qualitative only. Next, this figure illustrates a hypothesis that separates pillar failures into two broad categories, namely, those that are driven by simple static stress increases and are not associated with significant mining-induced seismicity (i.e., the progressive pillar failures), and those that are driven by dynamic stress increases and are associated with mining-induced seismicity (i.e., coal mine bumps and rockbursts). As indicated in figure 17, all bumps and bursts are short-duration, unstable, violent failures. However, the progressive pillar failures can occur in either a stable or an unstable manner. The LMS stability criterion provides the distinction.

Several simple examples illustrate the utility of figure 17. In case A, the LMS criterion is satisfied. As stress increases on a pillar, it fails stably and nonviolently (i.e., yields), and the stress transfers to adjacent pillars. That stress transfer may drive adjacent pillars into the postfailure regime; however, as long as the LMS criterion

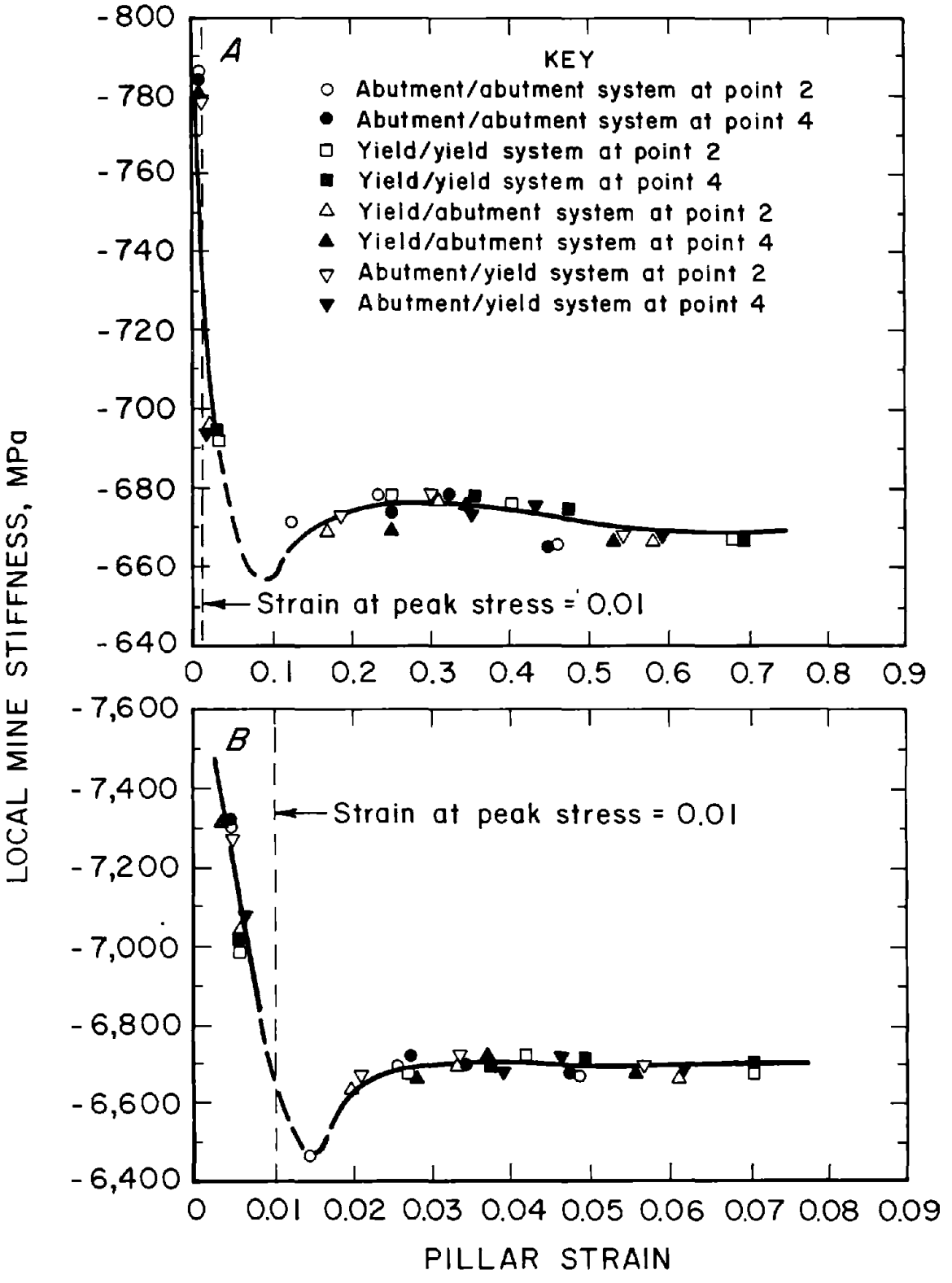

Figure 16.—K_{LMS} as function of pillar strain for longwall mining geometries shown in figure 15. *A*, rock mass modulus is 1,000 MPa; *B*, rock mass modulus is 10,000 MPa. In-seam coal follows stress-strain model D shown in figure 8.

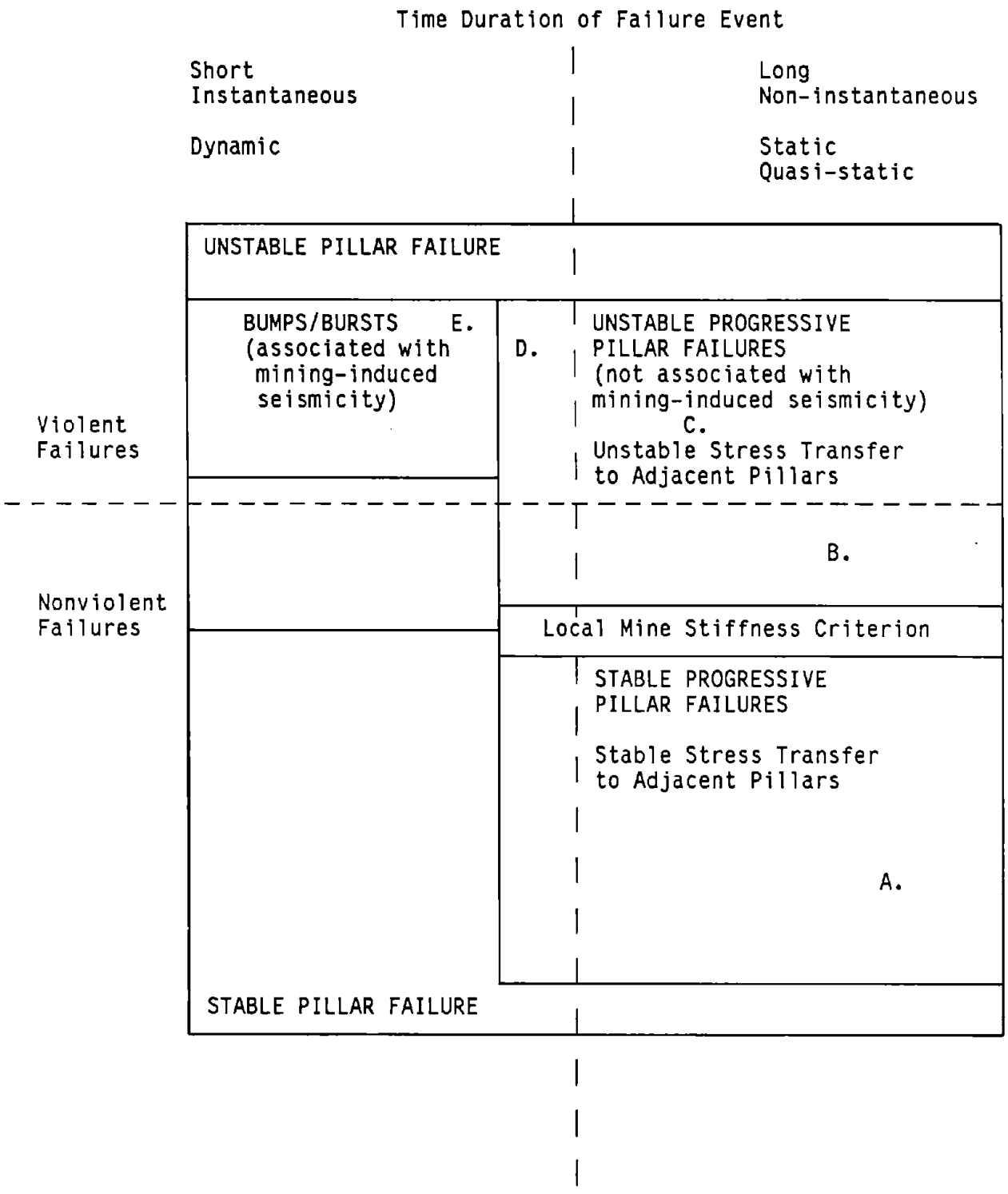

Figure 17.—Distinction between coal mine bumps and progressive pillar failures. Large box is set of all stable and unstable pillar failures. Horizontal dashed line separates violent and nonviolent failure. Vertical dashed line separates long- and short-failure durations. LMS stability criterion distinguishes between stable and unstable progressive pillar failures.

remains satisfied, the failure will not propagate catastrophically. In cases B, C, and D, the LMS criterion is violated, and failures proceed unstably. The stress transferred from the failed pillar causes neighboring pillars to enter the postfailure regime, and the failure begins to propagate catastrophically in a "chain reaction" or a "pillar run." In case B, the failure occurs slowly enough that it is nonviolent. In cases C and D, the propagation speed and the violence increase such that a potential hazard exists. In case C, the failure may propagate over a period of hours to days, such as that described by Khair and Peng (*10*), or it may occur over seconds as indicated by case D. Finally, case E shows an unstable, violent failure in the form of a bump or burst that occurs in a very short time.

This research suggests that the LMS concept applies to the analysis of unstable, violent failures in the form of progressive pillar failures. However, it does *not* apply to the analysis of unstable, violent failures in the form of coal mine bumps. The reason for this restriction stems from a very fundamental observation about the occurrence of coal mine bumps.

As shown in figure 12, an obvious linear correlation exists between rock mass modulus and K_{LMS}. Assuming that coals from both bump-prone and non-bump-prone mines have similar postfailure material properties (i.e., follow similar stress-strain curves), then according to the stability criterion given by equation 4, more negative values for K_{LMS} (i.e., high K_{LMS} magnitudes) will produce stable, nonviolent pillar failures. Many researchers (*11-12*) have observed that coal bumps occur in seams surrounded by stiff, massive, competent strata, such as thick sandstone layers, and not in seams surrounded by incompetent strata, such as shales. Assuming that competent sandstones have a higher rock mass modulus than incompetent shales, then according to the relationship shown in figure 12, mining in a high-modulus rock mass is *more* stable than mining in a low-modulus rock mass. Obviously, this implication does not agree with an important observation about the occurrence of coal mine bumps. Earlier research (*13*) raised an identical argument to show severe problems with the application of energy release rate calculations to the assessment of coal mine bump potential.

The LMS concept does apply to the analysis of unstable failures in the form of progressive pillar failures. In fact, its original intent was for the rational analysis of room-and-pillar layouts in order to prevent these catastrophes (*1, 5*). Most room-and-pillar mining operations subdivide the mine into panels separated by barrier pillars. In theory, pillars within the panel will yield and provide local roof support only, while the barrier pillars will carry the overburden stress. The barrier pillars isolate the panel and ensure that pillar collapse within the panel does not propagate beyond that panel. Salamon (*5*) provides a procedure for sizing panel pillars, panel dimensions, and barrier pillars based on the LMS concept. With the aid of program LMSTIFF, design engineers may have a realistic means to apply the LMS concept for rational room-and-pillar design.

Successful use of LMSTIFF in the sizing of panel and barrier pillars requires two main kinds of data. The first is quality rock mass modulus data. A variety of direct and indirect techniques exist to obtain rock mass modulus values with reasonable reliability and expense. However, only limited data exist for the postfailure behavior of full-scale coal pillars. Wang, Skelly, and Wolgamott (*14*), Iannacchione (*15*), Wagner (*16*), and Van Heerden (*17*) provide some complete stress-strain data for full-scale coal pillars in the postfailure regime. Such data are crucial for the application of the stability criterion given by equation 4. A clear need exists for more data on the postfailure behavior of coal in situ for a variety of different coals and different coal pillar sizes.

SUMMARY AND CONCLUSIONS

The LMS concept provides a mechanical basis to distinguish between stable, nonviolent failure and unstable, violent failure of coal mine pillars. This concept gives rise to the stability criterion presented in equation 4. According to this criterion, stable, nonviolent failure will occur as long as the local mine stiffness, K_{LMS}, is less than the pillar stiffness, K_P, at some point in the postfailure regime of the complete stress-strain curve for that pillar. Conversely, unstable, violent failure will occur when K_{LMS} equals or exceeds K_P at some point.

Bureau research has implemented the LMS concept into a practical 3-D BEM program called LMSTIFF. This experimental program computes K_{LMS} at any point in a boundary-element model and enables the user to assess stability based on the criterion of equation 4. As input, LMSTIFF requires the complete stress-strain relationship for the in situ coal, as well as the rock mass modulus and the mine geometry. LMSTIFF first calculates equilibrium stresses and displacements throughout the BEM model, then it computes K_{LMS} at select points using the so-called perturbation approach described by Starfield and Wawersik (*1*). Initial trials with the program indicate that it can distinguish between stable and unstable pillar failure as shown by the results in figures 9 and 10.

Preliminary research with program LMSTIFF considered three different mining scenarios, namely: room-and-pillar on development, room-and-pillar on retreat, and longwall mining. The experiments provided understanding of the effects of rock mass modulus, stress-strain properties of the coal, and mine geometry on K_{LMS} calculations at a point. Of all the mining scenarios and other parameters considered, rock mass modulus has the

greatest influence on K_{LMS} magnitude. Surprisingly, mine geometry, such as room-and-pillar layout and longwall gate road layout, had *no* apparent effect on K_{LMS}. Finally, the strain level has a small yet interesting effect on K_{LMS} at the select element. As shown in figures 11, 14, and 16 for room-and-pillar as well as longwall mining scenarios, the K_{LMS} magnitude appears to start with a high value in the elastic regime, decrease to a low after entering the postfailure regime, then increase to a plateau somewhat less than the initial K_{LMS} magnitude in the elastic regime. As shown in figure 11, the magnitude of the post-failure decrease in K_{LMS} depends on the degree of strain-softening exhibited by the in-seam material. The slight dependence of K_{LMS} on strain level accounts for the slight variations in computed K_{LMS} across a BEM model. Computed strains (displacements) change considerably throughout the model, which induce the small variations in K_{LMS}.

A major purpose in this research is to develop and test analysis methods for pillar failures. K_{LMS} cal-culations with program LMSTIFF provide one means to analyze certain kinds of stable, nonviolent versus unstable, violent pillar failures. Coal mine bumps and progressive pillar failures may both be unstable, violent events. However, the underlying mechanisms for each are possibly quite different. Numerical experiments conducted herein suggest that the LMS concept applies to the analysis of progressive pillar failures, as it was originally intended (*1, 5*), and not to the analysis of coal mine bumps. Future research with program LMSTIFF will focus on comparing its calculations with certain analytic solutions presented by Salamon (*5*) and also implementing the design procedure discussed therein for panel pillar, panel size, and barrier pillar layout in order to prevent catastrophic progressive pillar failures.

REFERENCES

1. Starfield, A. M., and W. R. Wawersik. Pillars as Structural Components in Room-and-Pillar Mine Design. Paper in Proceedings of 10th U.S. Symposium on Rock Mechanics, Rice Univ., AIME, New York, 1968, pp. 793-809.

2. Cook, N. G. W., and J. P. M. Hojem. A Rigid 50-Ton Compression and Tension Testing Machine. J. S. Afr. Inst. Mech. Eng., v. 1, 1966, pp. 89-92.

3. Wiebols, G. A., J. C. Jaeger, and N. G. W. Cook. Rock Property Tests in a Stiff Testing Machine. Paper in Proceedings of 10th U.S. Symposium on Rock Mechanics, Rice Univ., AIME, New York, 1968, pp. 297-329.

4. Wawersik, W. R., and C. Fairhurst. A Study of Brittle Rock Fracture in Laboratory Compression Experiments. Int. J. Rock Mech. and Min. Sci., v. 7, 1970, pp. 561-575.

5. Salamon, M. D. G. Stability, Instability, and Design of Pillar Workings. Int. J. Rock Mech. and Min. Sci., v. 7, 1970, pp. 613-631.

6. Cook, N. G. W. A Note on Rockbursts Considered as a Problem of Stability. J. S. Afr. Inst. Min. and Metall., v. 65, 1965, pp. 437-446.

7. Ryder, J. A. Excess Shear Stress in the Assessment of Geologically Hazardous Situations. J. S. Afr. Inst. Min. and Metall., v. 88, 1988, pp. 27-39.

8. Zipf, R. K., Jr. MULSIM/NL Theoretical and Programmer's Manual. BuMines IC, in press.

9. ____. MULSIM/NL Application and Practitioner's Manual. BuMines IC, in press.

10. Khair, A. W., and S. S. Peng. Causes and Mechanisms of Massive Pillar Failure in a Southern West Virginia Coal Mine. Min. Eng., (Littleton, CO), v. 37, 1985, pp. 323-328.

11. Campoli, A. A., C. A. Kertis, and C. A. Goode. Coal Mine Bumps: Five Case Studies in the Eastern United States. BuMines IC 9149, 1987, 34 pp.

12. Holland, C. T., and E. Thomas. Coal-Mine Bumps: Some Aspects of Occurrence, Cause, and Control. BuMines B. 535, 1954, 37 pp.

13. Zipf, R. K., and K. A. Heasley. Decreasing Coal Bump Risk Through Optimal Cut Sequencing With a Non-Linear Boundary Element Program. Paper in Proceedings of 31st U.S. Symposium on Rock Mechanics (CO Sch. Mines). A. A. Balkema, Rotterdam, 1990, pp. 947-954.

14. Wang, F. D., W. A. Skelly, and J. Wolgamott. In-Situ Coal Pillar Strength Study (contract H0242022, CO Sch. Mines). BuMines OFR 107-79, 1976, 243 pp.

15. Iannacchione, A. Behavior of a Coal Pillar Prone To Burst in the Southern Appalachian Basin of the United States. Paper in Proceedings of Rockbursts and Seismicity in Mines, ed. by C. Fairhurst. A. A. Balkema, Rotterdam, 1990, pp. 295-300.

16. Wagner, H. Determination of the Complete Load-Deformation Characteristics of Coal Pillars. Paper in Proceedings of 3rd International Congress on Rock Mechanics, Natl. Acad. Sci., v. 2B, 1974, pp. 1076-1081.

17. Van Heerden, W. L. In Situ Determination of Complete Stress-Strain Characteristics of Large Coal Specimens. J. S. Afr. Inst. Min. and Metall., v. 75, No. 8, 1975, pp. 207-217.

A REVISED MODEL FOR COAL PILLARS

By K. Barron[1] and Yuan Pen[2]

INTRODUCTION

A key consideration in the design and layout of underground coal mining operations is the design of pillars of a size that allows maximum coal recovery while maintaining overall stability. Wilson (*1*)[3] first proposed the concept that a pillar could be regarded as comprising a central, solid core surrounded by a peripheral zone of fractured coal and developed a model of pillar behavior based on these principles. However, application of Wilson's formulas in the highly disturbed coals of western Canada predicted fracture zones much less than those observed in the field. Consequently, work was commenced to modify Wilson's concepts to better fit Canadian conditions (*2-3*). It was found that the model resulting from this work could give a reasonable fit to observed field data on pillar stresses, strengths, and fracture zones provided that a judicious choice was made for the coal property parameters used in the model. However, to achieve this agreement between the field and model results, it was found necessary to choose coal parameters that appeared to bear little or no relationship to the generally accepted ranges of those values for coal.

It was believed that this problem was caused by a poor choice of the failure criterion used for the coal in the model. A second version of this model was therefore developed (*4-5*) in which the coal failure criterion was modified to the Hoek/Brown form (*6-7*) given by:

$$\sigma_1 = \sigma_3 + \{m\sigma_3\sigma_c + s\sigma_c^2\}^{1/2} \qquad (1)$$

where σ_1 and σ_3 are the major and minor principal stresses at failure, respectively; σ_c is the uniaxial compressive strength of the intact rock; and m and s are dimensionless parameters. The performance of this second version of the model was much improved, giving reasonable fits to field observations with much more realistic coal parameters. However, Salamon (*8*) pointed out an error in the manner in which the model dealt with the buildup of confining pressure in the pillar after the brittle/ductile transition point had been exceeded, such that equilibrium was not maintained in this region. This error has now been corrected to satisfy these equilibrium requirements, and a third version of the model has been prepared. While this major correction was made to the model, a number of minor changes were also made to allow the model to deal more satisfactorily with rectangular as well as rib pillars. In view of the number of changes that have taken place since the publication of the first version of this model and to avoid confusion, it is believed to be timely to present a detailed description of this third and, hopefully, final version of this coal pillar model.

SIMPLIFIED OUTLINE OF THE MODEL

This approach to pillar stability analysis stems from Wilson's concepts (*1*) whereby the coal pillar is considered to comprise a central, solid core of coal surrounded by a peripheral zone of fractured coal. A pillar is deemed to have failed (reached its maximum load-bearing capacity) when this peripheral zone reaches the center of the pillar.

The model has been developed by splitting the pillar into a large number of imaginary vertical slices, analyzing the elastic stresses acting on each slice, and comparing them with the failure criterion for the coal. If a slice fails, its residual stress capacity is calculated and the difference between this and the initial elastic stress is shed onto the remaining, as yet, unfailed slices. Successive analysis of each slice in turn allows the depth of the failed zone, the final stress distribution, the pillar strength and, for failed pillars, the residual stress capacity to be determined. Figure 1 gives a simplified flow diagram for the program. The key steps in this program will be outlined in more detail.

[1]Professor.

[2]Graduate student.

Department of Mining, Metallurgical and Petroleum Engineering, University of Alberta, Edmonton, Alberta, Canada.

[3]Italic numbers in parentheses refer to items in the list of references at the end of this paper.

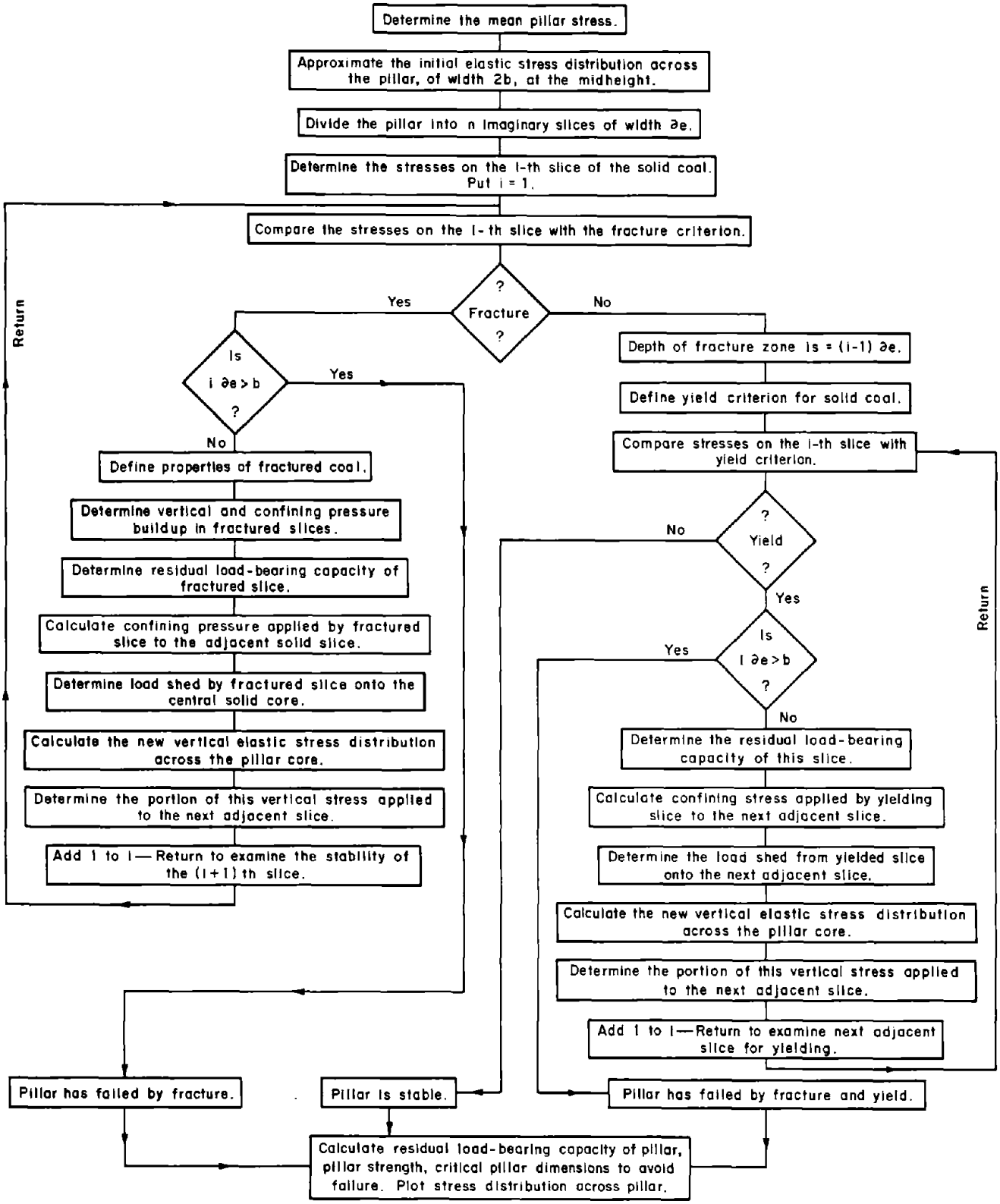

Figure 1.—Simplified flow diagram for the coal pillar model.

MEAN PILLAR STRESS

The starting point for the model is the calculation and/or input of the mean pillar stress, $\overline{\sigma_p}$. This can be determined by using the pillar dimensions, the field stresses, and the tributary area theory. Alternatively, a direct input of the mean pillar stress concentration factor is used; this might, perhaps, be the output from some other model such as MULSIM. (Earlier versions of the model also included the alternative of using Coates' pillar loading formula (*9*). However, this has now been dropped from the model since it was found in practice to be seldom used.)

APPROXIMATE INITIAL ELASTIC STRESS DISTRIBUTION ACROSS THE PILLAR

The model approximates the initial elastic stress distribution across the pillar at its midheight by making use of an approximate value for the boundary stress concentration factor at the midheight and assuming that the vertical stress concentration factor across the pillar diminishes as a hyperbolic function with depth into the pillar. These approximate equations are set up so as to ensure that the load represented by the area under this stress distribution curve is compatible with the mean load applied to the pillar determined in the "Mean Pillar Stress" section.

In the original version of the model, allowance was made for the adjacent opening shapes to be rectangular, ovaloide, or elliptical, and appropriate approximate expressions were developed for each case. For rectangular openings, fracture does not initiate at the midheight of the pillar but at the corners. The net result of such fracturing is that the shape tends toward that of an ovale and, once away from the pillar edge, the stress distributions are quite similar. Elliptical openings are not normally encountered in practice. It was therefore deemed sensible to simplify the model by eliminating this choice of shape, restricting it to the consideration of only adjacent ovaloide openings.

Approximate Maximum Stress Concentration Factor at the Midheight of a Row of Ovaloid Openings

Let Y_m be the maximum vertical stress concentration at the midheight of the sidewall of a row of ovaloid openings of height H and width W_B; let B be the width of the intervening pillars. Let L be the pillar length and W_L be the crosscut width. Let the field stress ratio be k = $\{S_H/S_v\}$, where S_H is the horizontal field stress and S_v is the vertical field stress. Let $\overline{Y} = \{\overline{\sigma_p}/S_v\}$ be the mean pillar stress concentration. Then it can be shown for rectangular pillars (*2*) that Y_m can be closely approximated by:

$$Y_m = (2.97 - 1.044\,k) + 1.327 \log_e \frac{W_B}{H} + 0.09 \left\{ \left[\frac{(W_L + L)(W_B + B)}{LB} \right]^2 - 1 \right\}, \quad (2)$$

or

$$Y_m = \overline{Y}, \quad (3)$$

whichever be the larger value.

Approximate Vertical Stress Distribution at the Midheight of the Pillars

For those cases when the maximum stress concentration at the midheight of the excavation boundary (calculated from equation 3) equals the average pillar stress concentration, then it follows that the stress distribution across the pillar must be constant and equal to $\overline{Y}$.

For those cases where the maximum boundary stress concentration is given by equation 2, it is assumed that the stress distribution curve is symmetrical about the center of the pillar and that it can be approximated by an equation of hyperbolic form, as illustrated in figure 2:

$$Y = \frac{k_1}{(X + k_2)} + k_3, \quad (4)$$

where Y is the vertical stress concentration factor $\{\overline{\sigma_p}/S_v\}$ at a distance e from the center of the room, where X = e/w and w is the semiroom width.

It is assumed that this stress concentration diminishes with distance from the opening, such that, if it were to extend 5 diameters (10w) away from the room, the stress

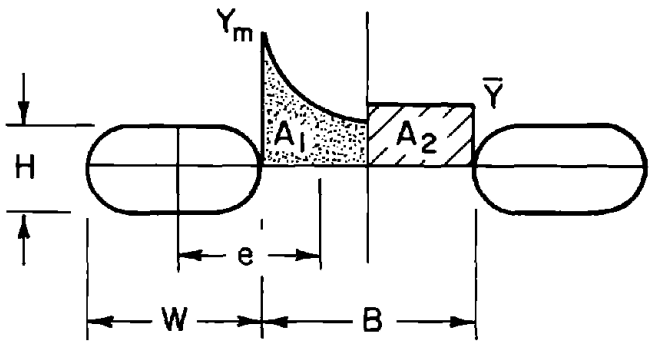

Figure 2.—Stress distribution across the pillar and nomenclature.

concentration would have reached the virgin stress concentration factor, i.e., when X = e/w = 10, then Y = 1.

Further, at the boundary of the opening X = 1 and Y = Y_m. Finally, for compatibility of loads, the load represented by the area under the stress distribution curve across half the pillar, A_1 in figure 2, must be equal to the load represented by the mean pillar stress acting across half the pillar (area A_2). Using these boundary conditions, it can be shown that the hyperbolic parameters k_1, k_2, and k_3 are given by:

$$k_1 = \frac{(Y_m - 1)(1 + k_2)(10m + k_2)}{9}, \quad (5)$$

$$k_3 = \frac{(10 - Y_m) - k_2(Y_m - 1)}{9}, \quad (6)$$

and k_2 is given by the solution of the equation:

$$\frac{(Y_m - 1)(1 + k_2)(10 + k_2)}{9} \log_e \left\{ \frac{1 + \frac{B}{W} + k_2}{1 + k_2} \right\} + \left\{ \frac{(10 - Y_m) - k_2(Y_m - 1)}{9} \right\} \left\{ \frac{B}{W} \right\} - \bar{Y} \left\{ \frac{B}{W} \right\} = 0, \quad (7)$$

and since Y_m is known, this equation can be solved for k_2. Having determined k_2, then equations 5 and 6 can be used to evaluate k_1 and k_3.

For example, Savin (*10*) has derived a theoretical solution for the stress distribution across the pillars between an infinite number of equally spaced circular holes under a uniaxial vertical field stress. Figure 3 compares Savin's results with the results using this approximation method. It is seen that the approximation gives an excellent representation of the theoretical solution in this case. It was shown (*2*) that this approximation worked well for other solutions given in the literature provided that 0.25 < (W/H) < 4. Outside this range, the approximation gradually breaks down; however, this is adequate for most practical cases. The program gives a warning if this range is exceeded, but still continues the calculation.

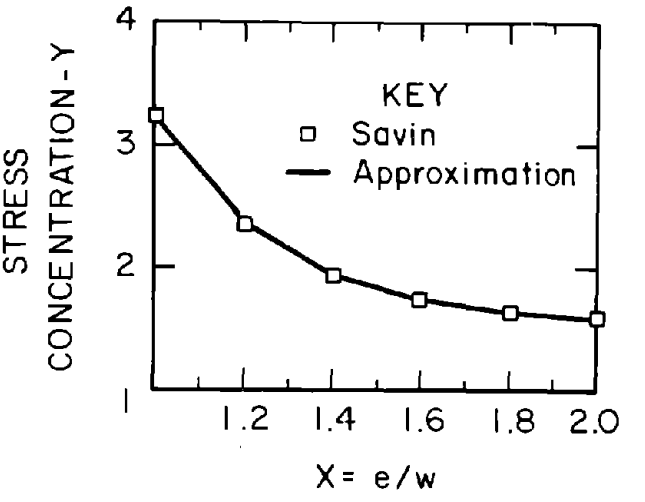

Figure 3.—Comparison of Savin's results with the approximation.

THE FAILURE CRITERION FOR COAL

The Failure Criterion Prior to the Brittle/Ductile Transition Point

Consider the typical differential stress-strain curves for triaxially tested specimens illustrated in figure 4*A*. At low-confining pressures (σ_{31}, σ_{32}), as the axial stress increases the shear and normal stresses both increase until the maximum shear stress exceeds the shear resistance of the rock and the specimen fractures. After fracture, the normal stress continues to act across the failed surface producing a frictional resistance. Thus, the peak stress level at fracture drops to the residual stress level where deformation continues by sliding on the fracture surface.

At high-confining pressures (> σ_{33}), the frictional resistance to sliding exceeds the shear resistance for fracture. Consequently, it is easier to form a new fracture surface than to produce displacement along existing fractures.

At an intermediate confining pressure, σ_{33}, the shear resistance to fracture just equals the frictional resistance to sliding on the fracture surface. Consequently, there is no drop from the peak to the residual strength and, after fracture, large deformations can take place with little or no increase in axial stress. Such deformation is called ductile when associated with plastic materials in which there is no loss of cohesion. However, as shown above, similar ductile deformation can be caused by brittle behavior followed by sliding on the fracture surface. This behavior has therefore been called pseudoductile behavior.

This failure mechanism has previously been applied to hard rocks at great depth (*11-13*). It is postulated that such failure can occur in coal in the range of confining pressures normally encountered in mining.

The point of transition between brittle failure and pseudoductile yield can be defined as the point of intersection between the peak stress failure criterion (equation 1) and the residual strength criterion. It is assumed that the peak strength curve is given by Hoek and Brown's expression:

$$\sigma_{1P} = \sigma_{3P} + \{m\sigma_{3P}\sigma_c + s\sigma_c^2\}^{1/2}, \quad (8)$$

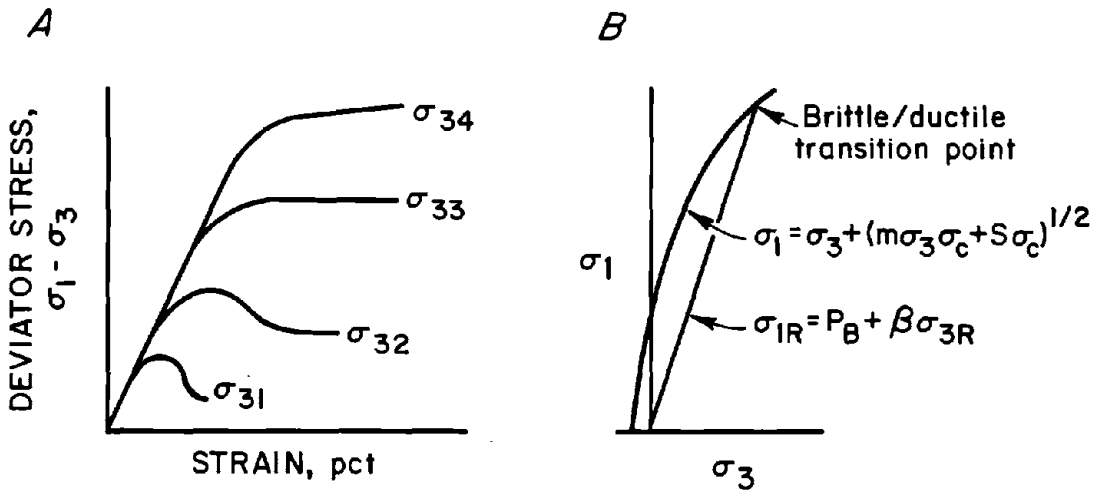

Figure 4.—Typical stress-strain curves at failure (*A*) and brittle/pseudoductile transition point given by intersection of peak and residual strength curves (*B*).

where σ_{1P} and σ_{3P} are the major and minor principal stresses at peak failure, σ_c is the intact uniaxial compressive strength of the coal, and m and s are constants for the coal (s = 1 for intact coal).

The residual stresses are assumed to obey the Coulomb-Navier theory and are related by:

$$\sigma_{1R} = P_B + k_R\sigma_{3R}, \quad (9)$$

where P_B is the uniaxial compressive strength of the broken rock, k_R is a constant for the coal and is related to the angle of friction, ϕ_B, of the broken coal by $k_R = (1 + \sin \phi_B)/(1 - \sin \phi_B)$.

Brittle/Ductile Transition Point

The transition from brittle to pseudoductile failure occurs at the intersection of these two curves (fig. 4*B*) and is given by putting $\sigma_{1P} = \sigma_{1R} = \sigma_{1T}$ and $\sigma_{3P} = \sigma_{3R} = \sigma_{3T}$ in the above equations, where the subscript T refers to the stresses at the transition point. Solving these equations for the stresses at the transition point gives:

$$\sigma_{3T} = \frac{-\beta + \{\beta^2 - 4(k_R - 1)^2(P_B^2 - s\sigma_c^2)\}^{1/2}}{2(k_R - 1)^2}, \quad (10)$$

and

$$\sigma_{1T} = P_B + k_R\sigma_{3T}, \quad (11)$$

where

$$\beta = \{2(k_R - 1)P_B - m\sigma_c\}. \quad (12)$$

The Failure Criterion Beyond the Brittle/Ductile Transition Point

Hoek and Brown placed a practical limitation on the use of their failure criterion (equation 1) because of the change from brittle to ductile behavior at high-confining pressures. They noted that, beyond the transition point, the σ_1 versus σ_3 curve bent over more rapidly than given by their equation and there was a gradual deviation of the experimental results from their equation when the brittle/ductile transition point was exceeded. Consequently, they used Mogi's criterion (*14*) for the transition from brittle to ductile behavior, given by $\sigma_1 = 3.4\ \sigma_3$ for many rocks. As a result, in deriving the m values for various intact rocks they specifically excluded any data where σ_1 was not $> 3.4\ \sigma_3$. Thus, equation 1 can be considered only to be valid for brittle failure prior to the brittle/ductile transition point. It remains, therefore, to determine or estimate the failure criterion applicable beyond this point.

If the failure relationships are viewed in τ/σ space (as illustrated in fig. 5*A*), the Mohr envelope for failure beyond the transition point gradually becomes parallel to the σ axis, i.e., the failure criterion will be asymptotic to a constant shear stress failure criterion and $\delta\sigma_1/\delta\sigma_3$ approaches unity (fig. 5*B*). It is therefore assumed that, beyond the transition point, the failure criterion can be approximated by a straight line that passes through the transition point and has a slope of unity. That is, it is assumed that the failure criterion beyond the transition point can be expressed by the linear relationship given by:

$$\sigma_1 = \sigma_3 + (\sigma_{1T} - \sigma_{3T}). \quad (13)$$

Further, this implies that beyond the transition point, $\phi_B = 0$ and $c_B = (1/2)(\sigma_{1T} - \sigma_{3T})$.

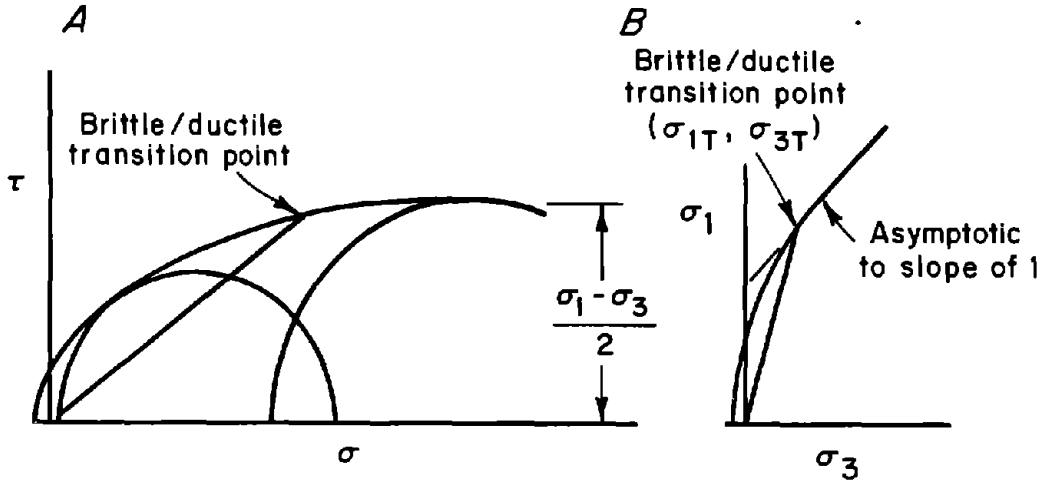

Figure 5.—Failure relationships viewed in τ/σ space (*A*) and in σ_1/σ_3 space (*B*).

CONFINING PRESSURE IN THE PERIPHERAL FAILED ZONE AROUND THE PILLAR

Consider an elemental vertical slice of width dx, at a depth x from the pillar edge, in the failed portion of the pillar periphery, as shown in figure 6.

Let the pillar have a height H = 2h and a width B = 2b; let τ be the shear stress across the ends of the slice, c_B be the cohesion, and ϕ_B be the angle of friction of the failed coal. Let P_1 be the vertical stress acting on this failed element, with P_3 and $(P_3 + dP_3)$ being the confining pressures acting on either side of the element. Then, ignoring the weight of the element, for equilibrium:

$$H\,dP_3 = 2(c_B + P_1 \tan\phi_B)\,dx. \qquad (14)$$

Prior To The Brittle/Pseudoductile Transition Point

Before the confining pressure has been built up to the level for brittle/pseudoductile transition, the vertical stress acting on the failed element, P_1, is the residual stress, σ_{1R}, given by equation 9 and $P_3 = \sigma_{3R}$. Hence:

$$P_1 = P_B + k_R P_3. \qquad (15)$$

Then, substituting from equation 15 into equation 14, and integrating between the limits x = 0, $P_1 = P_B$ and x = x, $P_1 = P_1$, the following expressions for the buildup of the vertical stress and the confining pressures in this fracture zone can be derived:

$$P_1 = P_B \frac{(1 + \sin\phi_B)}{2\sin\phi_B}\left[e^{k_R(\frac{x}{h})\tan\phi_B} - \frac{1}{k_R}\right], \qquad (16)$$

and

$$P_3 = \frac{P_1 - P_B}{k_R}. \qquad (17)$$

Further, if the transition point occurs at a depth d_T from the pillar edge, then d_T can be determined from equation 16 by putting $x = d_T$ and $P_1 = \sigma_{1T}$ and solving for d_T:

$$d_T = \frac{h}{k_R \tan\phi_B}\log_e\left\{\frac{2\sin\phi_B\,\sigma_{1T}}{(1 + \sin\phi_B)P_B} + \frac{1}{k_R}\right\}. \qquad (18)$$

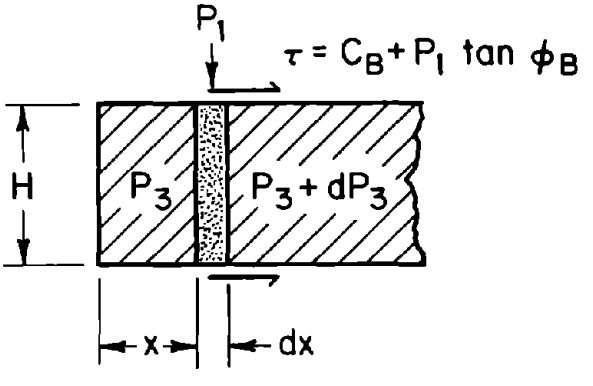

Figure 6.—Forces acting on a slice in the fractured pillar periphery.

After the Brittle/Pseudoductile Transition Point

In previous versions of this model it was assumed that, beyond the transition point, there would be no further

buildup of confining pressure and that the vertical stress on a slice reaches a maximum defined by that at the transition point. The assumption was shown to be in error (*8*) because slice equilibrium is not maintained. The following modification has therefore been introduced into the model to describe the confining pressure buildup once the transition point is exceeded.

For slice equilibrium beyond the transition point, equation 14 still applies. However, there is no drop from the peak to the residual stress when the slice yields; thus the stresses on the failed slice in this zone are given by putting $\sigma_1 = P_1^*$ and $\sigma_3 = P_3^*$ in equation 13, i.e.,

$$P_1^* = P_3^* + (\sigma_{1T} - \sigma_{3T}). \qquad (19)$$

Further, beyond the transition point $\phi_B = 0$ and $c_B = (1/2)(\sigma_{1T} - \sigma_{3T})$.

Substituting for P_1^* from equation 19 into equation 14 and integrating between the limits when $x = d_T$, $P_3^* = \sigma_{3T}$ and when $x = x$, $P_3^* = P_3^*$, gives:

$$2\int_{d_T}^{x} \frac{dx}{H} = \int_{\sigma_{3T}}^{P_3^*} \frac{dP_3^*}{\left\{\frac{(\sigma_{1T} - \sigma_{3T})}{2} + \tan\phi_B [P_3^* + (\sigma_{1T} - \sigma_{3T})]\right\}}. \qquad (20)$$

Hence, with $\phi_B = 0$, this integration gives:

$$P_3^* = \sigma_{3T} + \left[\frac{(x - d_T)}{H}(\sigma_{1T} - \sigma_{3T})\right], \qquad (21)$$

which gives the variation of P_3^* with the distance x beyond the transition point. The variation of P_1^* beyond the transition point is then given by equation 19.

LOAD SHEDDING MECHANISM

For Rib Pillars

For rib pillars, the pillar is split into n slices of equal width, δe, as illustrated in figure 7*A*. Before failure, the vertical stress, σ_{1i}, applied to the i-th slice is given by the initial elastic stress distribution plus the increments shed from previously failed slices. After failure, the residual stress capacity is given by P_1 or P_1^*. Hence, the load, ΔL_o, shed by a failed slice (of unit depth) onto the pillar core is:

$$\Delta L_o = (\sigma_{1i} - P_{1i}^{\#})\,\delta e, \qquad (22)$$

where $\delta e = B/n$ is the slice width and $P_{1i}^{\#} = P_{1i}$ or P_{1i}^*, depending whether the slice is in the fracture or the yield zone.

When $Y_m = Y$, then the initial stress distribution is uniform across the pillar and it can be assumed that, in the pillar core, it must remain uniform, i.e., this load must be shed equally between the remaining, as yet, unfailed slices. Hence, the incremental stress to be added to the elastic stress already applied to each of the remaining unfailed slices is given by:

$$\Delta\sigma_1 = \frac{(\sigma_{1i} - P_{1i}^{\#})}{(\frac{n}{2} - i)}, \qquad (23)$$

where n is the number of slices across a pillar of width B (= 2b).

When $Y_m > Y$, the initial stress distribution across the pillar is nonuniform and has been approximated by a hyperbolic function (see the "Approximate Vertical Stress Distribution at the Midheight of the Pillars" section). In this case, it is assumed that the excess load is shed onto the remaining slices by a general inverse distance function given by:

$$\Delta L = f(\frac{1}{g^{\alpha}}), \qquad (24)$$

where g is the distance from the failed slice to the receiving slice, and α is assumed to be a constant. A value of $\alpha = 0.5$ is used in this model, but it can be changed if so desired.

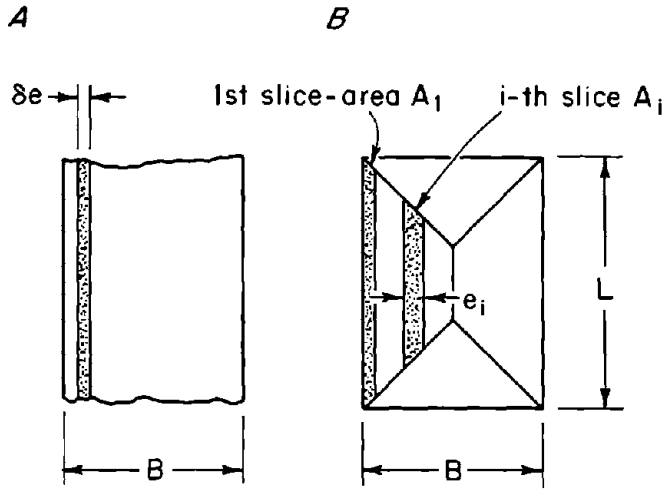

Figure 7.—Rib pillar with equal width slice (*A*) and rectangular pillar with equal area slice (*B*).

In this case, the incremental stress to be added to the j-th slice resulting from the failure of the i-th slice is given by:

$$\Delta\sigma_{1j} = \frac{\left\{\frac{1}{(j-i)^{\alpha}}(\sigma_{1i} - P_{1i}^{\#})\right\}}{\sum_{j=i+1}^{j=n/2}\left\{\frac{1}{(j-i)^{\alpha}}\right\}}. \qquad (25)$$

For Rectangular Pillars

For rectangular pillars of length L and width B, the failed zone will develop from all sides of the pillar. Hence in this case, the changing length of the slices must be taken into account, as illustrated in figure 7*B*. To simplify this case, instead of dividing the pillar into equal width slices as was the case for rib pillars, the pillar is divided into slices of different width, but of the same equal area. The width of each slice is determined by solving the following system of equations, which is obtained by equating the area of the first slice to the area of the remaining slices, as follows:

$$(L - e_1)e_1 = \{L - 2\sum_{j=1}^{j=1} e_j\}e_i - e_i^2, \qquad (26)$$

where i = 2, 3, 4,.....n. and e_1 and e_i are the widths of the first slice and i-th slice, respectively. The left term is the area of the first slice, and the right term is the area of the i-th slice.

Add to this the requirement that the sum of e_i has to be equal to half the pillar width, (b = B/2), i.e.,

$$e_1 + e_2 + \ldots\ldots + e_{n/2} = \frac{B}{2}, \qquad (27)$$

then the whole system of n equations can be solved by using a nonlinear approximation method. Having determined the requisite slice widths by this method, the same load shedding functions developed for rib pillars above can again be used for the cases where $Y_m = Y$ and $Y_m > \overline{Y}$.

PILLAR STRENGTH FORMULAS AND CRITICAL PILLAR DIMENSIONS

FOR RIB PILLARS

The use of the above key concepts in the model to successively analyze each slice in turn allows the depth of the fracture zone, the depth of the yield zone (if any), the stress distribution across fracture zone, the yield zone, and the pillar core to be determined. The pillar strength (average stress at the maximum load bearing capacity) can be determined by increasing the mean pillar stress until the failed zone just reaches the pillar center. Alternatively, a subprogram can be written to determine only the pillar strength without the necessity of determining the final stress distribution, the extent of the fracture, and yield zones, etc.

Several other important points can be demonstrated by the consideration of the equations that have been developed. These will now be discussed.

Let σ_p be the mean stress applied to the pillar of width B (= 2b) and height H (= 2h). S_v is the vertical field stress and Y (= σ_p / S_v) is the mean pillar stress concentration factor. Let σ_s be the pillar strength. Assuming symmetry, consider only the stress distribution across half the pillar at its midheight. Prior to fracture initiation, the vertical stress distribution is elastic and is similar to that shown in figure 8*A*.

The maximum vertical stress at the midheight of the pillar is that on the boundary. Hence for fracture to initiate, this stress must be equal to the uniaxial compressive strengh of the coal mass (σ_{cm}). This condition will occur when:

$$\sigma_{in} = \frac{\overline{Y}}{Y_m}\sigma_{cm}, \qquad (28)$$

where σ_{in} is the mean pillar stress for fracture initiation at the boundary and Y_m is the boundary stress concentration factor at the midheight of the pillar (and given by equations 2 or 3).

Once fracture initiates, the fracture zone will continue to grow until the confining pressure buildup is sufficient to prevent further failure. The stress distribution will then be as illustrated in figure 8*C* (left and right), in which there is a peripheral fracture zone, or a peripheral fracture plus yield zone, with a central elastic core. In this case, the area under the stress distribution curve will be equal to the area under the mean pillar stress line, and the pillar will be stable and will have a safety factor of >1. Finally, as the mean pillar stress increases, the failed zone will eventually propagate to the pillar center (as illustrated in figure 8*D* (left and right)) and the maximum load-bearing capacity of the pillar is reached. This is called the point of ultimate failure.

Behavior of Narrow Rib Pillars

The confining pressure in the failed coal builds up rapidly. However, for narrow pillars, once fracture has been initiated, the confining pressure buildup may not be sufficient to prevent the failed zone from reaching the center of the pillar. Hence, the failure propagates

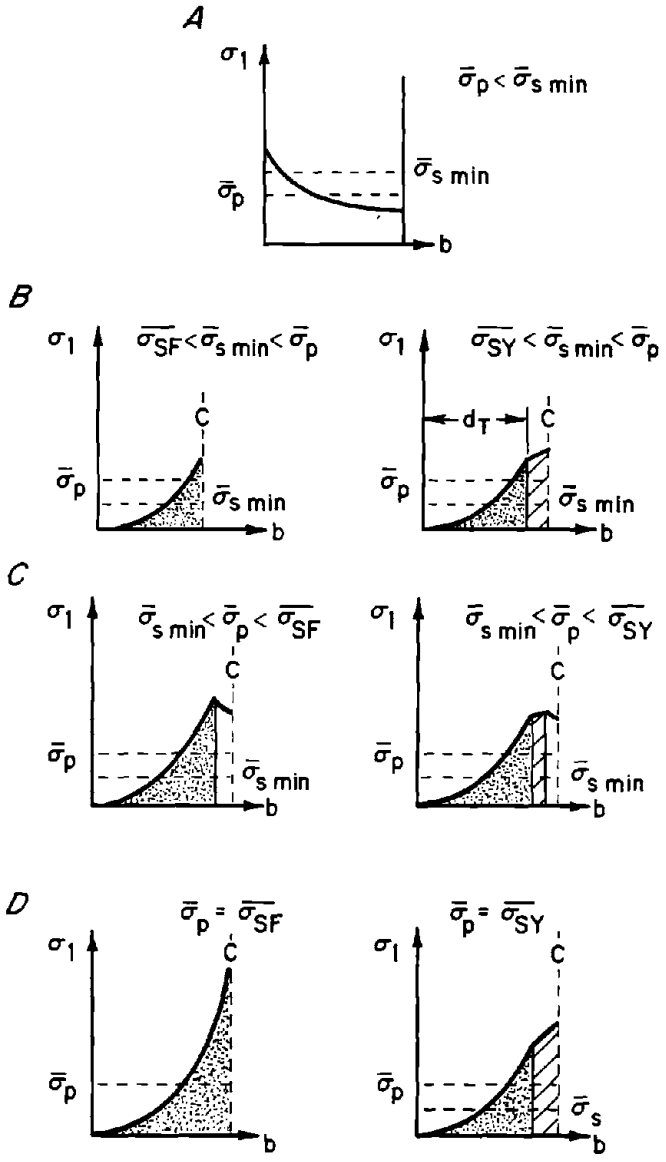

Figure 8.—Possible modes of pillar stability and failure. *A*, Stable pillar-elastic stress distribution; *B*, sudden fracture (left) and sudden yield (right); *C*, stable-partial fracture/elastic core (left) and stable-partial fracture/yield-elastic core (right); *D*, ultimate fracture (left) and ultimate yield (right).

immediately to the center of the pillar and the strength of the pillar must be equal to the mean pillar stress required to initiate fracture at the boundary, i.e., there must be some minimum pillar strength ($\bar{\sigma}_{s\,min}$) and this will be given by putting $\sigma_{in} = \bar{\sigma}_{s\,min}$ in equation 28:

$$\bar{\sigma}_{s\,min} = \frac{\bar{Y}}{Y_m}\sigma_{cm}. \qquad (29)$$

In this case, the area under the stress distribution curve (fig. 8*B* (left and right)) is less than that under the mean pillar stress line. This is an unstable situation; the pillar has a safety factor of less than 1 and will fail suddenly. (Note that "sudden" failure in this context does not imply that the pillar bursts. Whether this failure will be violent or gentle will depend on the stiffness of the failed pillar compared with the local mine stiffness.)

There will be some critical semipillar width, b_c, beyond which sudden failure cannot occur. For the case where the brittle/ductile transition point is not exceeded in the pillar, then the depth of the transition point, d_T (given by equation 21), must be greater than b_{cF} for sudden fracture. This critical pillar dimension can be determined by equating the minimum pillar strength with the area under the stress distribution curve:

$$\frac{\bar{Y}}{Y_m}\sigma_{cm}b_{cF} = \int_0^{b_{cF}} P_1\,dx,$$

where P_1 is given by equation 15, which defines the buildup of confining pressure in the fracture zone. Carrying out this integration gives the following equation:

$$\frac{\bar{Y}}{Y_m}\sigma_{cm}b_{cF} = P_B\theta\left[\frac{h}{\tan\phi_B}\{e^{k_R(b_{cF}/h)\tan\phi_B} - 1\} - b_{cF}\right], \qquad (30)$$

where

$$\theta = \frac{(1-\sin\phi_B)}{2\sin\phi_B}, \qquad (31)$$

which can be solved for b_{cF}.

For the case where the brittle/ductile transition point is exceeded in the pillar, then d_T is $< b_c$ and sudden yield may occur. Equating the minimum pillar strength with the area under the stress distribution curve gives the condition for the critical pillar dimension, b_{cY}, in this case:

$$\frac{\bar{Y}}{Y_m}\sigma_{cm}b_{cY} = \int_0^{d_T} P_1\,dx + \int_{d_T}^{b_{cY}} P_1^*\,dx, \qquad (32)$$

This yields the following expression, which can be solved for b_{cY}:

$$\frac{\bar{Y}}{Y_m}\sigma_{cm}b_{cY} = P_B\theta\left[\frac{h}{\tan\phi_B}\{e^{k_R(d_T/h)\tan\phi_B} - 1\} - d_T\right] + (b - d_T)\left[\sigma_{1T} + \frac{(\sigma_{1T} - \sigma_{3T})}{2H}(b_{cY} - d_T)\right]. \qquad (33)$$

In light of the above discussion, the term "narrow" pillar can now be defined as any pillar that, under the prevailing load, will fail suddenly, i.e., any pillar of semiwidth less than b_{cF} or b_{cY}.

Behavior of Wide Rib Pillars

When the pillar width is greater than the critical width, b_c, for sudden failure, the failed zone will propagate and stop, leaving the pillar with a central elastic core. As the load on the pillar increases, the failed zone will eventually reach the center of the pillar, at a width b_u, and it is then deemed to have failed (fig. 8*D* (left and right)). In this case, the area under the stress distribution curve just equals the area under the mean stress line. This stress level will be called the ultimate strength of the pillar. Let $\overline{\sigma_{SF}}$ and $\overline{\sigma_{SY}}$ be the mean pillar strengths at ultimate failure for the cases where there is only a fracture zone and where there is both a fracture and a yield zone, respectively.

Then, when $d_T > b_{uF}$ (i.e., there is only a fracture zone), $\sigma_{SF} b_{uF} = \int_0^{b_{uF}} P_1\, dx$ and integrating, as before, gives:

$$\sigma_{SF} = Y S_v b_{uF}$$

$$= \frac{P_B \theta}{b_{uF}} \left\{ \frac{h}{\tan \phi_B} \left[e^{k_R \left(\frac{b_{uF}}{h} \right) \tan \phi_B} - 1 \right] - b_{uF} \right\}. \quad (34)$$

When $d_T < b_{uY}$ (i.e., there is a fracture zone plus a yield zone),

$$\overline{\sigma}_{SY} b_{uY} = \int_0^{d_T} P_1\, dx + \int_{d_T}^{b_{uY}} P_1^*\, dx.$$

As before, integrating gives equation 35.

FOR RECTANGULAR PILLARS

For rectangular pillars, rather than rib pillars, the fracture zone develops from the ends of the pillars as well as from the sides, as illustrated in figure 9. This fact must be taken into account when calculating the pillar strength.

Behavior of Narrow Rectangular Pillars

As with the case for rib pillars, for narrow rectangular pillars, once fracture initiates, the confining pressure build-up is insufficient to prevent the failure from propagating to the pillar center. Failure propagates immediately to the pillar center and the pillar strength must be equal to the mean pillar stress required to initiate fracture and will again be given by equation 29. (Note: This assumes that Y_m, the maximum stress concentration at the midheight of the pillar boundary, is the same in the crosscuts as in the entries; i.e., that the crosscuts and entries have the same shape and dimensions.)

It also follows that the critical semipillar width to avoid sudden failure can be derived in a similar manner to that for narrow rib pillars, but taking into account the development of the failed zone from the pillar ends as well as from the sides.

For the case when $d_T > b$ (i.e., there is only a fracture zone), it can be shown that the semicritical width to avoid sudden fracture, b_{cFR}, is given by the solution of equation 36.

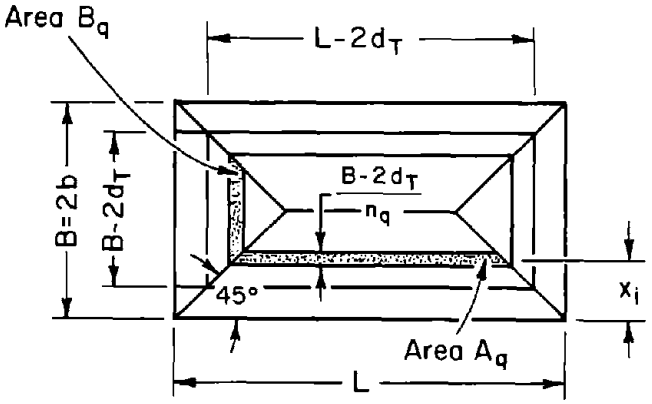

Figure 9.—Fracture/yield zone development in rectangular pillars.

$$\overline{\sigma}_{SY} = \overline{Y} S_v b_{uY} = P_B \theta \left[\frac{h}{\tan \phi_B} \left\{ e^{k_R (d_T/h) \tan \phi_B} - 1 \right\} - d_T \right] + (b_{uY} - d_T) \left[\sigma_{1T} + \frac{(\sigma_{1T} - \sigma_{3T})}{2H} (b_{uY} - d_T) \right]. \quad (35)$$

$$\frac{\overline{Y}}{Y_m} \sigma_{cm} b_{cFR} L = P_B \theta \left[\frac{h}{\tan \phi_B} \left\{ e^{k_R (b_{cFR}/h) \tan \phi_B} - 1 \right\} \left\{ L - 2b_{cFR} + \frac{4h}{k_R \tan \phi_B} \right\} - \left[L + \frac{4h}{\tan \phi_B} \right] b_{cFR} \right]. \quad (36)$$

For the case when $d_T < b$ (i.e., there is a fracture zone plus a yield zone), it can be shown that the semicritical width to avoid sudden yield, b_{cYR}, is given by the solution of equation 37.

Behavior of Wide Rectangular Pillars

When the pillar width is greater than the critical width, b_c, for sudden failure, the failed zone will propagate and stop, leaving the pillar with a central elastic core. As the load on the pillar increases, the failed zone will eventually reach the center of the pillar, at a width b_u, and it is then deemed to have failed. In this case, the area under the stress distribution curve just equals the area under the mean stress line. This stress level will be called the ultimate strength of the pillar.

Let $\bar{\sigma}_{SF}$ and $\bar{\sigma}_{SY}$ be the mean pillar strengths at ultimate failure for the cases where there is only a fracture zone and the case where there is both a fracture and a yield zone, respectively.

Then, when $d_T > b_{uFR}$ (i.e., there is only a fracture zone) and it can be shown that the pillar strength is given in equation 38.

When $d_T < b_{uYR}$ (i.e., there is a fracture zone plus a yield zone), then the strength is given in equation 39.

$$\frac{\bar{Y}}{Y_m}\sigma_{cm}b_{cYR}L = P_B\theta\left[\frac{h}{\tan\phi_B}\left\{e^{k_R(d_T/h)\tan\phi_B}-1\right\}\left\{L+2b_{cYR}-4d_T+\frac{4h}{k_R\tan\phi_B}\right\}-(L+2b_{cYR})d_T+2d_T^2-\frac{4d_Th}{\tan\phi_B}\right]$$

$$+(b_{uYR}-d_T)\left[\frac{4c_B}{3H}(b_{uYR}-d_T)^2+\frac{c_B}{H}(L-2b_{uYR})(b_{uYR}-d_T)+(L-2d_T)P_{1T}\right]. \quad (37)$$

$$\bar{\sigma}_{SF}b_{uFR}L = \bar{Y}S_vb_{uFR}L = P_B\theta\left[\frac{h}{\tan\phi_B}\left\{e^{k_R(b_{uFR}/h)\tan\phi_B}-1\right\}\left\{L-2b_{uFR}+\frac{4h}{k_R\tan\phi_B}\right\}-(L+\frac{4H}{\tan\phi_B})b_{uFR}\right]. \quad (38)$$

$$\bar{\sigma}_{SY}b_{uYR}L = \bar{Y}S_vb_{uYR}L = P_B\theta\left[\frac{h}{\tan\phi_B}\left\{e^{k_R(d_T/h)\tan\phi_B}-1\right\}\left\{L+2b_{uYR}-4d_T+\frac{4h}{k_R\tan\phi_B}\right\}-(L+2b_{uYR})d_T\right.$$

$$\left.+2d_T^2-\frac{4d_Th}{\tan\phi_B}\right]+(b_{uYR}-d_T)\left[\frac{4c_B}{3H}(b_{uYR}-d_T)^2+\frac{c_B}{H}(L-2b_{uYR})(b_{uYR}-d_T)+(L-2d_T)P_{1T}\right]. \quad (39)$$

INPUT ROCK PROPERTIES

FOR HARD ROCKS

Although this model has been developed primarily for coal pillars, it can also be applied to hard rock pillars. In this case, the intact m value for the rock can be obtained from direct triaxial testing of intact, laboratory-size specimens, and the broken coal parameters, P_B, c_B, and ϕ_B, can be determined from the residual strength curves from these tests. The rock mass m and s values for use in the equations can then be estimated, using Hoek and Brown's table (*6-7*), provided that a Council for Scientific and Industrial Research or a Norwegian Geotechnical Institute rock mass rating has been estimated for the rock mass.

FOR COAL

Hoek and Brown (*6-7*) did not study coal as one of their rock types; consequently, their rock mass rating approach to the estimation of the coal mass properties cannot be taken for coal. Bieniawski and Bauer (*15*) attempted to extend this work to coal, but showed that, contrary to Hoek and Brown's experience with other rocks, the m value for coal could not be regarded as a constant, but covered a wide range for intact laboratory size specimens. The reason for this has been attributed (*16*) to the fact that the coals tested were of various ranks and that laboratory-size test specimens of coal are not in fact

truly intact, i.e., there is a major influence of the test specimen size on the triaxial coal strength of coal.

This problem of estimating both the intact and coal mass properties from triaxial tests on nonintact, laboratory size specimens of coal was tackled by Barron and Tao (*17-20*). They showed that:

1. The intact m value (=M) for coal can be approximated from a knowledge of the E.C.E. rank number (R_e) for the coal and is given by:

$$M = e^{5.38 - 0.4\,R_e}, \tag{40}$$

or, alternatively, for a specific coal, it can be estimated from triaxial tests on nonintact, laboratory-size specimens of known height and width.

2. The intact uniaxial coal strength, σ_c, is given by:

$$\sigma_c = 5.266\,K, \tag{41}$$

and the coal mass uniaxial compressive strength, σ_{cm}, is given by:

$$\sigma_{cm} = 0.88\,K, \tag{42}$$

where K is the uniaxial compressive strength of a 1 meter cube of coal.

3. The Hoek and Brown parameters m and s for the coal mass (s_{mass} and m_{mass}) are given approximately by:

$$s_{mass} = 0.028, \tag{43}$$

and

$$m_{mass} = M\,s_{mass} = 0.028\,M. \tag{44}$$

It is the parameters σ_c, s_{mass}, and m_{mass} that are used to describe the peak strength failure criterion in the model.

In addition, Barron and Tao showed that the residual strength parameters for the coal are unaffected by the specimen size and can be estimated from the residual strength curves for triaxial tests on coal of any size specimen. A survey (*2*) of the ϕ_B values for coal (below the transition point) given in the literature gave a range of values from as low as 23° to as high as 45°, with a "typical" value of around 30°.

The estimation of the residual cohesion, c_B, and the residual uniaxial compressive strength, P_B, from the residual triaxial test results is not very accurate. P_B is small, and following the example of Wilson (*1*), a value of 0.1 MPa has been used in this paper (with a typical ϕ_B value of 25°, which corresponds to a c_B value of 0.029 MPa).

EXAMPLE: COMPARISON OF MODEL RESULTS WITH SALAMON'S PILLAR FORMULAS

SALAMON'S PILLAR FORMULAS

Salamon and Munro (*21*) developed a strength formula for square coal pillars in South Africa, given by:

$$\bar{\sigma} = K\,H^{\alpha}\,B^{\beta} = K\,V^{a}R^{b}, \tag{45}$$

where K is the strength of a 1 m cube of coal (in megapascals), H is the pillar height, B is the pillar width, V is the pillar volume, and R is the height/width ratio = B/H. $\alpha = -0.66$, $\beta = 0.46$, $a = -0.0667$, and $b = 0.5933$. This formula was deemed to be valid for pillars of width/height ratios up to about 4.

Later, Salamon and Wagner (*22*) extended this work to cover square, squat pillars where the ratio R exceeds 4. Their squat pillar formula is given by:

$$\bar{\sigma} = K\,V^{a}R_o^{b}\left\{\frac{b}{\epsilon}\left[\left(\frac{R}{R_o}\right)^{\epsilon} - 1\right] + 1\right\}, \tag{46}$$

where R_o is the ratio beyond which R can be considered "squat" ($R_o = 4$ is used in this paper), ϵ is a measure of the rate of increase of strength when $R > R_o$, and Salamon and Wagner suggested this value be 2.5 for deep South African collieries.

The variation of the ratio of the pillar strength to the K value for coal versus the width height ratio, R, calculated from these equations is shown in figure 10 for square pillars. In these calculations, the values of H = 3m and K = 5.7 MPa (see below) were used.

MODEL INPUT DATA

The pillar model developed here has been run with the objective of comparing these model results with the results from Salamon's formulas. For this purpose, the following input data were used.

The K value for South African coals has been estimated by Salamon and Munro (*21*) to be 7.17 MPa, by Madden (*23*) to be 5.24 MPa and by Bieniawski (*24*) to be 4.86 MPa. A representative value of 5.7 MPa was therefore chosen for use in the model calculations. Hence,

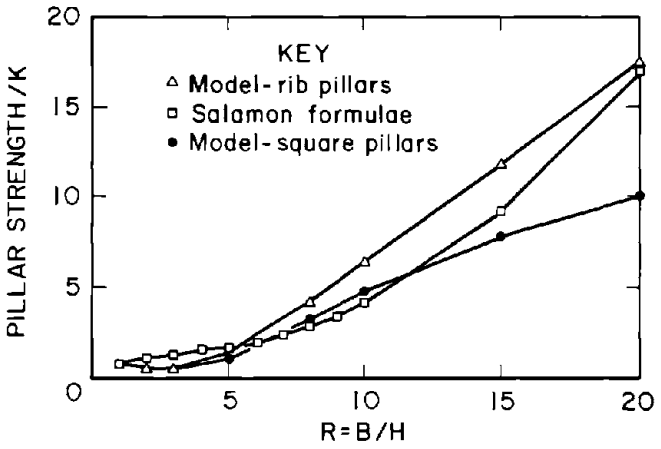

Figure 10.—Comparison of model results with Salamon's pillar formulas.

from equations 41 and 42, the intact and coal mass uniaxial compressive strengths are, respectively, σ_c = 5.266 K = 30 MPa and $\sigma_{c\,mass}$ = 0.88 K = 5 MPa.

The bulk of the data used by Salamon were derived from pillars in the Witbank coal seams. These have a volatile content of around 34% and a calorific value in the range of 32-35 MJ/kg (*25*) and may thus be classified as a high volatile, bituminous A rank or an ECE rank number of 6. Hence, using equations 40 and 44, the intact M value and the coal mass m value are given, respectively, by the equation below.

The broken coal properties used in the model were chosen as follows: A typical value of ϕ_B = 25° was chosen. The uniaxial strength of broken coal, P_B, was assumed to be 0.1 MPa and this corresponds to a cohesion of the broken coal, c_B, of 0.029 MPa.

A field stress ratio k = 1 was chosen for coal at depth. A room width of 6 m and a pillar height of 3 m were again chosen, and the model was run to determine the pillar strengths with variation of the width/height ratio, R, for both square and rib pillars. These results are also shown in fig. 10.

$$M = e^{5.38 - 0.4 \times 6} = 19.7,\ m_{mass} = 0.028\ M = 0.55, \text{ and } s_{mass} = 0.028 \text{ (see equation 43)}. \quad (47)$$

DISCUSSION AND CONCLUSIONS

It is seen from figure 10 that:

1. The model results for rib and square pillars effectively "bracket" the results from Salamon's formulas for square pillars. All the results show an increasing pillar strength as the width/height ratio increases.

Comparing the results for square pillars only, it is seen that:

2. At B/H ratios < 5, the model gives lower strengths than indicated by Salamon's formulas. This difference arises because the model includes the concept of a minimum pillar strength resulting from the minimum boundary stress level at which fracture can first initiate in the pillar. Salamon's approach does not consider the effect of the boundary stress concentration factor on fracture initiation in the pillar.

3. Over the range 5 < B/H < 12, the results of the two approaches are very similar and for all practical purposes are the same.

4. As B/H increases above about 12, Salamon's formulas give increasingly higher strengths than the model. The slower rate of strength increase indicated by the model is due to yielding of the pillar at high B/H ratios. Since Salamon's formulas are empirically based, it is difficult to be certain how far the squat pillar equation can or should be extrapolated to deal with very high B/H ratios.

It is concluded that this latest version of the model is a significant improvement on past versions, particularly since it indicates the increasing pillar strength with increasing B/H ratios. It compares well with Salamon's squat pillar formula for B/H ratios up to about 12. However, other pillar case histories need to be evaluated to further validate this model.

It is also important to note that this relatively favorable comparison has been achieved using coal parameters that are realistic and that can be estimated from laboratory testing or, in an extreme, from a knowledge of only the coal rank and the uniaxial compressive strength of a specimen of known dimensions.

REFERENCES

1. Wilson, A. H. Research Into the Determination of Coal Pillar Size. Part 1: An Hypothesis Concerning Pillar Stability, Min. Eng., v. 131, 1972, pp. 409-417.

2. Barron, K. An Analytical Approach to the Design of Coal Pillars. Part 1: The Analytical Model. Part 2: Application of the Model to Case Histories. Dep. Supply and Services, Ottawa, Rep. for contract

ISQ 80-00161, Jan. and Mar. 1983; available from Micro-Media Ltd., Front St., Toronto, Ontario, Canada.

3. Barron, K. An Analytical Approach to the Design of Coal Pillars, CIM Bull., Aug. 1984, pp. 37-44.

4. ____. A New Method for Coal Pillar Design, Paper in Proceedings of Symposium on Ground Control, Austr. IMM (Illawara Branch), Wollongong, New South Wales, Aug., 1988, pp. 118-124.

5. ____. A New Method for Coal Pillar Design, Aust. IMM Bull., v. 293, No. 8, 1988, pp. 87-91.

6. Hoek, E. and E. T. Brown. Empirical Strength Criterion for Rock Masses, J. Geotech. Div., A.S.C.E., Sept., 1980, pp. 1013-1035.

7. ____. Underground Excavations in Rock, Inst. Min. and Metall., London, 1980, pp. 140-177.

8. Salamon, M. D. G. Private communication, 1991.

9. Coates, D. F. Pillar Loading: Part 1: Literature Survey and New Hypothesis, CANMET, Dep. E.M.R., Ottawa, Canada, Res. Rep. R 168, Oct. 1965.

10. Savin, G. N. Stress Concentration Around Holes, Pergamon Press, London, 1983.

11. Orawin, E. Mechanism of Seismic Faulting, Rock Deformation, Geol. Soc. Am. Mem., v. 79, 1980, pp. 323-345.

12. Maurer, W. C. Shear Failure of Rock Under Compression, Soc. Petrol. Eng., v. 5, 1965, pp. 165-175.

13. Byerlee, J. D. Frictional Characteristics of Granite Under High Confining Pressure, J. Geophys. Res., v. 15, 1967, pp. 3634-3648.

14. Mogi, K. Pressure Dependance of Rock Strength and Transition from Brittle to Ductile Flow. Bull. Earthquake Res. Inst., Japan, v. 4, 1966, pp. 215-232.

15. Bieniawski, Z. T. and J. Bauer. Discussion of Empirical Strength Criterion for Rock Masses, J. Geotech. Eng. Div., ASCE, Apr. 1982, pp. 670-672.

16. Hoek, E. and E. T. Brown. Discussion of Empirical Strength Criterion for Rock Masses—Closure. J. Geotech. Eng. Div., ASCE, Apr. 1982, pp. 672-673.

17. Barron, K. and T. Yang. The Influence of Specimen Size and Shape on the Strength of Coal. Part 1: Size Effects on the Uniaxial Strength of Coal. Paper in these proceedings.

18. ____. The Influence of Specimen Size and Shape on the Strength of Coal. Part 2: An Approach to the Evaluation of the Intact and Mass Strengths of Coal from Triaxial Tests on Laboratory Size Test Specimens. Paper in these proceedings.

19. ____. The Influence of Specimen Size and Shape on the Strength of Coal. Part 3: Laboratory Test Results. Paper in these proceedings.

20. ____. The Influence of Specimen Size and Shape on the Strength of Coal. Part 4: Influence of Coal Rank. Paper in these proceedings.

21. Salamon, M. D. G. and A. H. Munro. A Study of the Strength of Coal Pillars, J. S. Afr. Inst. Min. and Metall., v. 68, 1967, pp. 55-67.

22. Salamon, M. D. G. and H. Wagner. Practical Experiences in the Design of Coal Pillars, Safety in Mines Research. Paper in Proceedings of the 21st International Conference (Sydney, Oct. 21-25, 1985, pp. 3-9).

23. Madden, B. J. A Re-Assessment of Coal Pillar Design. J. S. Afr. Inst. Min. and Metall., v. 91, 1991, pp. 27-37.

24. Bieniawski, Z. T. The Effect of Specimen Size on the Strength of Coal. Int. J. Rock Mech. and Min. Sci., v. 5, 1968, pp. 325-335.

25. Meintjes, A. A. The Grindability and Abrasive Properties of South African Coals. J. S. Afr. Inst. Min. and Metall., v. 66, 1965, pp. 631-634.

A METHOD REVISITED: COAL PILLAR STRENGTH FORMULA BASED ON FIELD INVESTIGATIONS

By Z. T. Bieniawski[1]

INTRODUCTION

The design of mine pillars involves the determination of proper sizes of pillars compatible with the expected load and the in situ strength of the coal strata. Thus, in deciding the most suitable dimensions for mine pillars, one needs to consider such factors as the pillar load (the stress on pillars), the pillar strength, and the factors of safety.

There are two approaches to coal pillar design. The *ultimate strength approach* contends that pillars will fail when the applied load reaches the compressive strength of the pillars. This approach presumes that the load-bearing capacity of a pillar reduces to zero the moment its ultimate strength is exceeded. *The progressive failure approach* emphasizes the nonuniform stress distribution in the pillar; failure initiates at the most crucial point and propagates gradually to ultimate failure. In the United States, the Federal Coal Mine Health and Safety Act of 1969 prescribes the safety concept of failure initiation as the criterion rather than ultimate failure. This results in an additional margin of safety. This paper summarizes a method developed by the author for determination of coal pillar strength that has been used successfully for more than 20 years. The recommended procedure is supported by a survey of approximately 200 coal mines, including 174 in the United States, in which typical mining conditions and pillar configurations were analyzed.

PILLAR LOAD

The simplest approach to determine the pillar load, or more correctly the average pillar stress, is by the tributary area method. This approach is generally only applicable to room-and-pillar mining and to sizing pillars for the development entries in longwall mining. If a number of well-known simplifying assumptions are made (e.g., uniform stress distributions, large extent of mining), the average pillar load for such cases can be calculated from

$$S_p = [1.1\ H\ (w + B)(L + B)]\ /\ (w \times L), \qquad (1)$$

where S_p = pillar load (average pillar stress) in psi,

H = depth below surface, ft,

B = width of opening (room or entry), ft,

w = pillar width, ft,

and L = pillar length, ft.

For longwall mining applications, where abutment loading is of prime importance, the Analysis of Longwall Pillar Stability (ALPS) method proposed by Mark and Bieniawski (1986) (*11*)[2] can be used to estimate the pillar stresses for headgate and tailgate loading conditions.

PILLAR STRENGTH

The strength of coal pillars, i.e., the ultimate load per unit area, is dependent upon three elements: (1) the size or volume effect (strength reduction from a small laboratory specimen of coal to a full-size coal pillar), (2) the effect of pillar geometry (shape effect), and (3) the properties of the coal material. Although for years many pillar strength formulas have been proposed, some dating back to 1911, two types of expressions are predominant:

$$\sigma_p = \sigma_{cube}\ [A + B\ (w/h)], \qquad (2)$$

and

$$\sigma_p = K\ w^a/h^b \qquad (3)$$

where σ_p = pillar strength,

σ_{cube} = in situ coal strength incorporating size effect,

A, B, a, b = constants expressing the shape effect,

[1]Professor of Mineral Engineering, The Pennsylvania State University, University Park, PA.

[2]Italic numbers in parentheses refer to items in the list of references at the end of this paper.

K = constant characteristic of a coal seam,

w = pillar width,

and h = pillar height (usually same as seam height).

SIZE EFFECT

The size effect is best characterized by the concept of the "critical size" (Bieniawski, 1968) *(1)*, which is very important in practical strata control engineering. It means that for cubical specimens of coal (no shape effect involved), the strength decreases with increasing specimen size until the strength becomes nearly constant from a certain "critical specimen size" onward. This phenomenon is depicted in figure 1, and its significance is that the strength values at the critical size, about 3 ft (1.0 m) for coal, are directly applicable to full-size pillars.

The size effect characterizes the difference in the strength between the small-size specimens tested in the laboratory and the large-size coal pillars mined in situ. Research in the United States has shown [Hustrulid, 1976 *(10)*] that the scaling of coal properties from laboratory-measured data to field values can be satisfactorily achieved by the following equations:

$$\sigma_{cube} = k / (36)^{1/2}; \quad (4)$$

applicable to cubical pillars if the height h is more than 36 in (0.9 m), or

$$\sigma_{cube} = k / h^{1/2} \quad (5)$$

applicable to cubical pillars if the height h is less than 36 in (0.9 m).

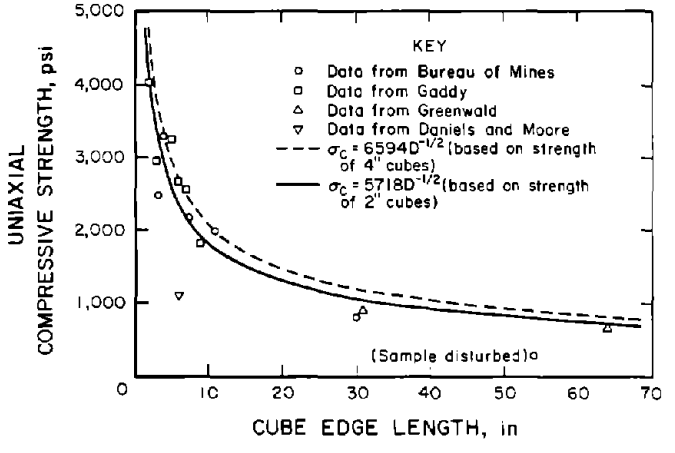

Figure 1.—Compressive strength as a function of cube size for Pittsburgh coal [Hustrulid, 1976 (*10*)].

In the previous equations, the constant k must be determined for each coal seam; k is obtained as shown by Gaddy (1956) *(7)*:

$$k = \sigma_c (D)^{1/2} \quad (6)$$

where σ_c = uniaxial compressive strength of coal specimens tested in laboratory, psi,

and D = diameter or cube side dimension, in.

While there is a difference in laboratory results depending on whether cylindrical or cubical specimens are used, for practical engineering purposes this difference is not significant within the range of D between 2 and 4 in (50 and 100 mm) [Hustrulid, 1976 (*10*)].

Although the strength of coal at the critical size is most conveniently determined by the Hustrulid equations, a number of other approaches can also be used. These are as follows: in situ large-scale tests, "petite sismique" geophysical tests, the Protodyakonov method, and the Hoek-Brown criterion for rock mass strength [Bieniawski, 1984 (*5*)].

SHAPE EFFECT

From all the available pillar strength formulas, the following five expressions are most commonly used in coal mining:

Obert-Duvall, 1967 (*13*):

$$\sigma_p = \sigma_{cube} (0.778 + 0.222\ w/h) \quad (7)$$

Holland-Gaddy, 1964 (*8*):

$$\sigma_p = k\ [w/h^{1/2}] \quad (8)$$

Holland, 1973 (*9*):

$$\sigma_p = \sigma_{cube}\ (w/h)^{1/2} \quad (9)$$

Salamon-Munro, 1967 (*14*):

$$\sigma_p = 1{,}320\ w^{0.46}/h^{0.66} \quad (10)$$

Bieniawski, 1968 (*2-4*):

$$\sigma_p = \sigma_{cube}\ (0.64 + 0.36\ w/h). \quad (11)$$

PILLAR STRENGTH FORMULA

The origin and the use of equation 11 are the prime topics of this paper. This pillar strength formula was proposed [Bieniawski, 1968 *(2)*] on the basis of extensive in situ tests performed on coal during 1966-73 in South Africa. The program of tests was initiated as a result of a coal mine disaster at Coalbrook Mine where 427 miners lost their lives in 1960 because of pillar collapse.

Conducted under the author's direction at Witbank Mine, the first series of tests (1966-68) involved 35 large-scale in situ tests on square coal specimens measuring from 24 in to 6 ft (0.6 to 2 m) in side length and of various heights. The influence of the width-to-height ratios of up to 3.1 was studied by testing specimens of different heights and with the same cross-sectional area. The second series of tests involved 12 specimens tested by Wagner in 1972 at Usutu Mine *(15)*. These tests included rectangular and square specimens up to 6 ft (2 m) in size and with width-to-height ratios of up to 2.2.

The third and last series of tests, also conducted under the author's direction, was performed in 1973 at New Largo Mine and involved 10 in situ coal specimens, 4.5 by 4.5 ft (1.4 by 1.4 m) in cross section and of various heights, with width-to-height ratios of up to 3.4. Full details of all the specimen preparation and testing techniques are given by Bieniawski and van Heerden (1975) *(3)*.

The Witbank coal formation was the weakest of the three tested, while the New Largo coal was the strongest. To make the in situ test results generally applicable (i.e., not only to the locality where the tests were carried out), a pillar strength formula is best expressed in a normalized form. For example, the original strength formula for the Witbank Coalfield [Bieniawski, 1968 *(2)*] was of the form

$$\sigma_p \text{ (psi)} = 400 + 220 \text{ w/h},$$

but this can be expressed dimensionlessly as

$$\sigma_p = 620 \ (0.64 + 0.36 \text{ w/h}),$$

where σ_{cube} = 620 psi (4.3 MPa) is the "critical size" strength for the Witbank coal.

Thus, the general (normalized) form of this pillar strength formula is

$$\sigma_p = \sigma_{cube} \ (0.64 + 0.36 \text{ w/h}),$$

which is equation 11 given earlier. In figure 2, all the in situ test results from the three coal mines are plotted, demonstrating the close fit of the experimental data with equation 11.

In essence, this pillar strength formula—confirmed by 57 large-scale in situ tests on coal performed in three mines—is applicable to any coal seam, provided the value of σ_{cube} is known from equation 4 or by other means. The formula can be used not only in room-and-pillar mining but also in longwall mining, provided the appropriate stability factors are established, as discussed in the next section. Note that although the original in situ test data in figure 2 were based on pillar width-to-height ratios of up to 3.4, when applied to full size coal pillars—as shown later in figure 7—the pillar strength formula given by equation 11 was found applicable even for pillar width-to-height ratios of up to 12.

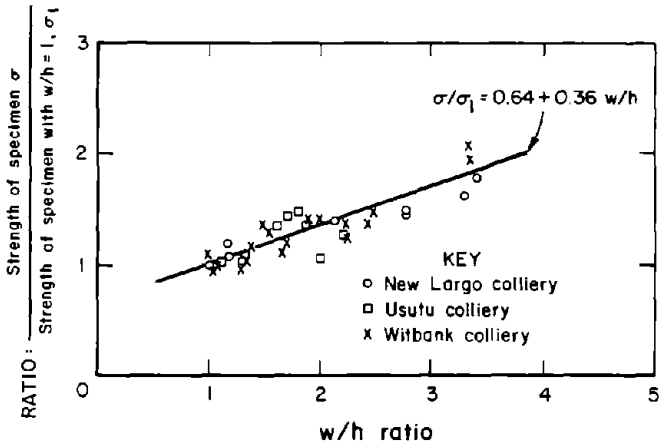

Figure 2.—Strength data from large-scale in situ tests on coal [Bieniawski and van Heerden, 1975 (*11*)].

CHOICE OF A STABILITY FACTOR

To use any pillar strength formula with confidence, the appropriate "safety factor" or "stability factor" must be used.[3] For the Bieniawski formula (equation 11), this was accomplished in a 1982 national survey of design practices and mining dimensions in the United States [Bieniawski, 1983 *(4)*]. This survey included a comprehensive study of such parameters as the depth below surface, seam thickness, roof span, pillar height, pillar width, pillar length, width-to-height ratios, percentage extraction, and method of design. A total of 174 cases were available for stability analyses of coal pillars (see table 1) plus 58 cases of roof falls for analyzing roof spans. The pillar cases included only three instances of pillar failure from the United States. However, 20 pillar failure cases in other countries were also collected by the author. Nevertheless, pillar failure cases were not essential for establishing the validity of a selected pillar strength formula for U.S. mining, contrary to an objective of a study by Salamon and Munro (1967) *(13)* in South Africa. There, no pillar strength formula was available at the time, while in the United States a number of formulas have been used since 1911. It was the aim of the 1982 national survey to select a formula that would be the most economical yet safe for coal pillar design in the United States.

Table 1.—Range of room-and-pillar parameters surveyed in U.S. coal mines[1]

Parameter	Range[2]	Typical value[2]
Depth below surface ..... ft ..	75-1,500	500
Seam or pillar height ..... ft ..	3-15	6
Entry width ..... ft ..	16-20	18
Pillar width ..... ft ..	15-75	48
Pillar length ..... ft ..	20-90	60
Width-to-height ratio ..... ft ..	2-16	8.0
Length-to-width ratio ..... ft ..	1-3	1.25
Extraction ..... pct ..	25-85	50

[1]Pennsylvania State University survey of 174 cases.
[2]To convert feet to meters, multiply by 0.30.

The results obtained are depicted in figure 3. The survey involved the coal seams commonly found in the United States. However, 38 pct of the data involved the Pittsburgh Seam. The average depth of room-and-pillar mines in the United States is 500 ft (150 m), with the range varying between 75 and 1,500 ft (25 and 480 m). The typical seam thickness, which is synonymous with pillar height, is 6 ft (2 m) varying between 3 and 15 ft (1.0 and 4.5 m). Roof spans (i.e., entry widths) in the United States are typically 16 to 20 ft (4-6 m) wide. The typical pillar width is 48 ft (15 m) varying from 15 to 75 ft (5 to 23 m) while the typical pillar length is 60 ft (20 m). The average percentage extraction is 50 pct varying between 25 to 85 pct. An important observation from figure 3 is that the typical pillar width-to-height ratio is 8.0 varying from 2 to 16. Based on this survey, the appropriate safety factors for the Bieniawski formula (equation 11) were established.

A factor of safety F is defined as the ratio of the strength of a pillar to the load acting on it. Thus,

$$F = \sigma_p / S_p. \qquad (12)$$

A factor of safety (stability factor) is necessary because in order to derive the pillar load as well as the strength formulas presented in the previous section, certain assumptions had to be made.

A structure is generally defined as stable when F is more than 1. In engineering practice, the factor of safety used is smaller when the conditions are well explored and understood. If the factor of safety is unity, the probability of failure is 50 pct. The factor of safety should be greater than unity to achieve a low probability of failure. What probability of failure is acceptable in coal mining?

Using a computer storage and retrieval system, the room-and-pillar dimensions from the Pennsylvania State survey were used together with the various pillar strength formulas. A histogram of safety factors for the strength formula in equation 11 is given in figure 4 for 171 case histories featuring stable pillars from the United States, 20 case histories involving failed pillars in other countries, and 3 cases of failed pillars in the United States.

It is concluded from figure 4 that factors of safety ranging from 1.5 to 2.0 are appropriate for room-and-pillar coal mining when using equation 11. For longwall mining, using the ALPS method developed at The Pennsylvania State University by Mark and Bieniawski (1986) *(11)*, the recommended factor of safety is 1.3. It must be emphasized, however, that these figures should be used as a guide only and the local mining experience should be taken into consideration.

More specifically, the guidelines for the stability factors using the Bieniawski formula are as follows:

[3]A better term would be "a factor of ignorance" because of the uncertainties inherent in any empirical approach.

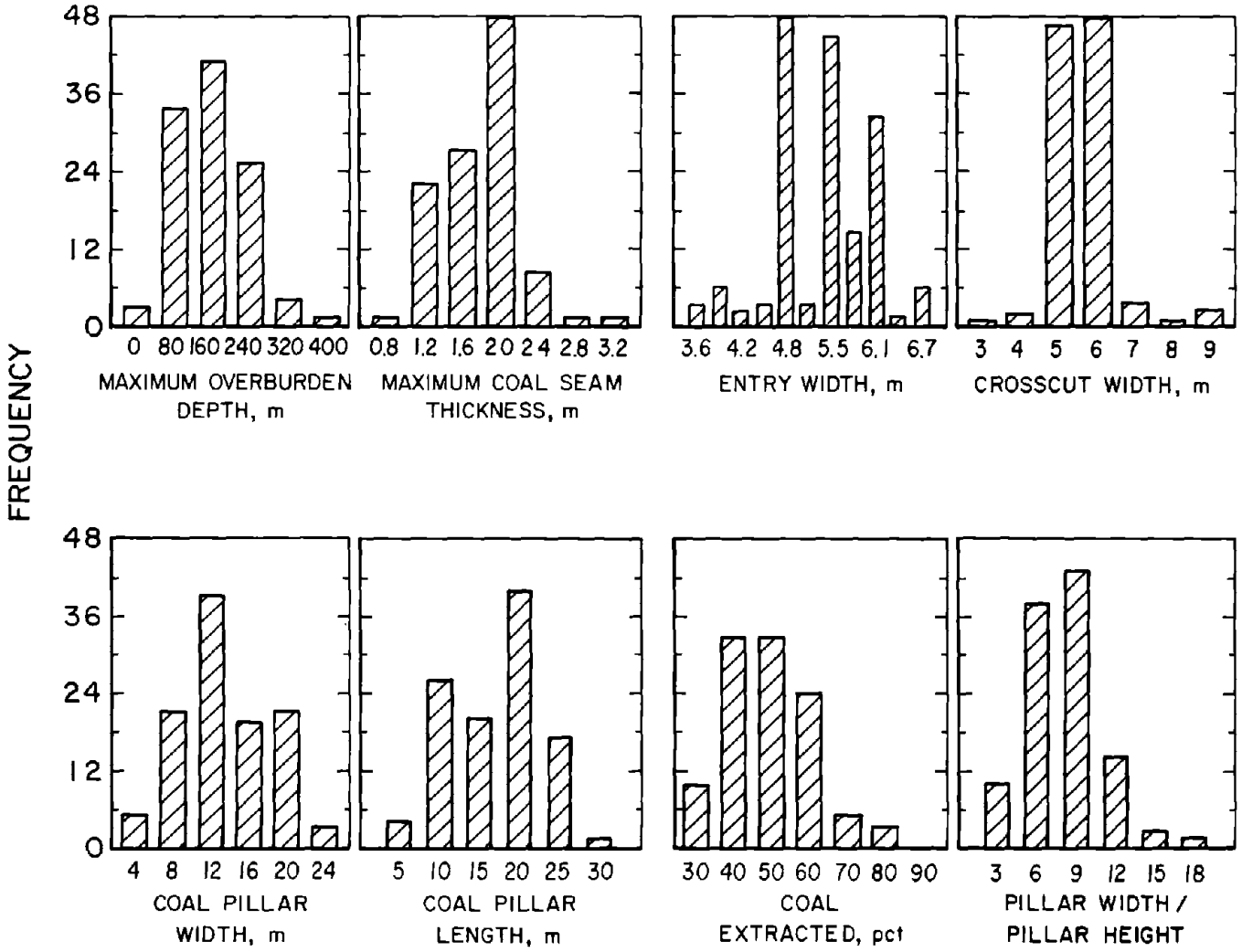

Figure 3.—Penn State survey of coal mining in the United States [Bieniawski, 1983 (*4*)].

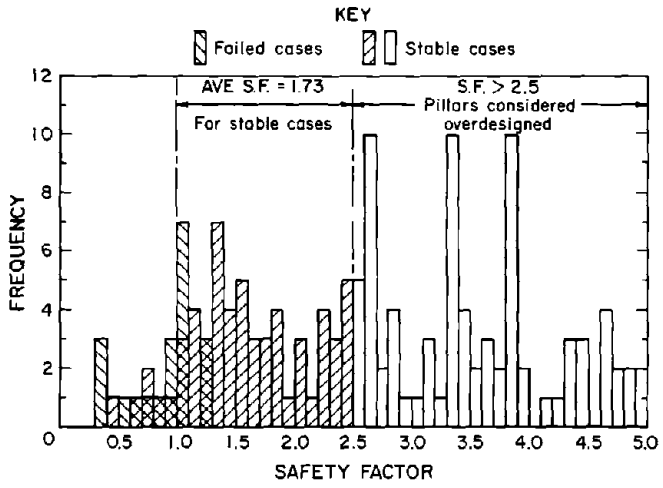

Figure 4.—Histogram of safety factors (S.F.) for the strength formula in equation 11 [Bieniawski, 1983 (*4*)].

Room-and-pillar mining:

Nonretreating panels	1.5
Retreat panels	2.0
Mains	2.0
Barrier pillars	2.5

Longwall mining:

Tailgate chain pillars	1.3
Pillars in bleeder entries	1.5 to 2.0
Mains	2.0
Barrier pillars	2.5.

To assess the stability of an existing mining operation, all the mining dimensions are known and the factor of safety can be determined for optimizing future designs.

COMPARISON OF PILLAR STRENGTH FORMULAS

The five pillar strength formulas listed earlier have been applied extensively in coal mining. Using the Pittsburgh Coal Seam as an example, these formulas may be compared. From the research by Gaddy (*7*), Hustrulid (*10*), and Bieniawski (*4*), the Pittsburgh coal has a typical value of k = 5,580, which can be used in equation 4. Thus, the in situ coal strength of the Pittsburgh Seam is estimated as

$$\sigma_{cube} = k / (36)^{0.5} = 930 \text{ psi (6.4 MPa)}. \quad (13)$$

The above value may now be used for equations 7, 9, and 11. For equation 10, the constant 1,320 represents the uniaxial compressive strength, in psi, of a 1-ft cube specimen of South African coal (equivalent to the strength of 7.2 MPa for 1-m cube of South African coal). For U.S. conditions, the appropriate constant may be determined by the Hustrulid equation (equation 5). Thus, for Pittsburgh coal, the appropriate constant for the Salamon-Munro formula is

$$K = k/(12)^{0.5} = 1{,}610 \text{ psi (11.1 MPa)}. \quad (14)$$

Consequently, the five pillar strength formulas may now be rewritten as follows for the Pittsburgh Seam:

Obert and Duvall formula:

$$\sigma_p = 930 [0.778 + 0.222 (w/h)] \quad (15)$$

Holland and Gaddy formula:

$$\sigma_p = 5{,}580 [w/h^{1/2}] \quad (16)$$

Holland formula:

$$\sigma_p = 930 (w/h)^{1/2} \quad (17)$$

Salamon and Munro formula:

$$\sigma_p = 1{,}610 \, w^{0.46}/h^{0.66} \quad (18)$$

Bieniawski formula:

$$\sigma_p = 930 [0.64 + 0.36 (w/h)]. \quad (19)$$

In figure 5, the above five formulas are plotted as the strength versus the width-to-height ratio. It is apparent that for higher width-to-height ratios equation 16 predicts the lowest strength while equation 19 predicts the highest strength. At the same time, the form of equations 17 and 18 is such that they will become very conservative at high

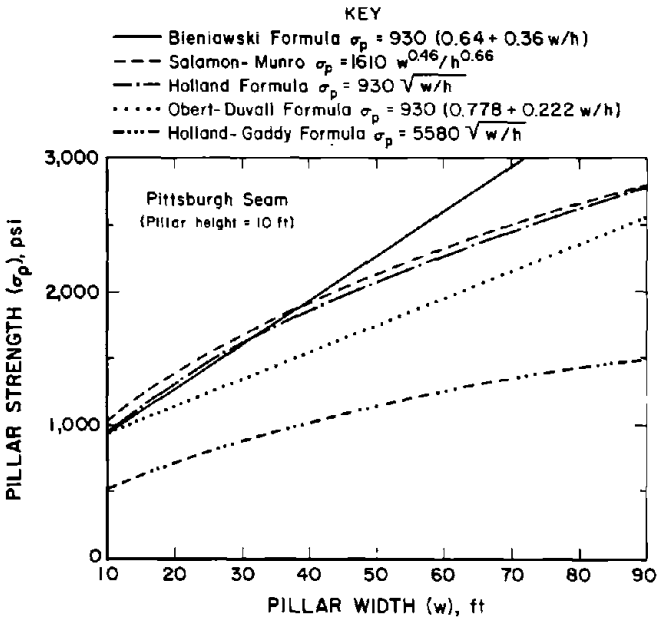

Figure 5.—Pittsburgh Seam: strength versus pillar width for h = 10 ft.

width-to-height ratios. The higher strength values predicted by equation 19 are consistent with the fact that for high width-to-height ratios there is a very rapid strength increase as shown by the experimental data plotted in figures 6 and 7. In fact, pillars were thought to be almost indestructible for width-to-height ratios greater than 10 [Cook and Hood, 1978 (*6*)]. This is further substantiated by figure 4 from which it is apparent that pillars are generally overdesigned in the United States. This is particularly so when the width-to-height ratios of coal pillars are eight or more. It is also evident from figure 7 that equation 11 is valid even for width-to-height ratios of up to 12, after which it will provide conservative values.

In fact, a detailed study of this aspect conducted at Pennsylvania State by Bauer in 1980 (*4*) has revealed that the theoretical strength of coal pillars is considerably higher than that predicted by equation 11. Bauer calculated the pillar strength based on rock mass properties such as: the cohesion and the angle of internal friction of coal; the cohesion and the angle of friction at the pillar-roof interface; and the pillar dimensions of width, length, and height.

The results of underground tests on coal pillars performed by Wagner (1974) (*15*) have shown that pillars of rectangular cross section are about 40 pct stronger than square pillars of the same width and height. He measured the stress distribution across pillars at various stages of deformation and found that the perimeter of a pillar is capable of carrying relatively little stress, but this

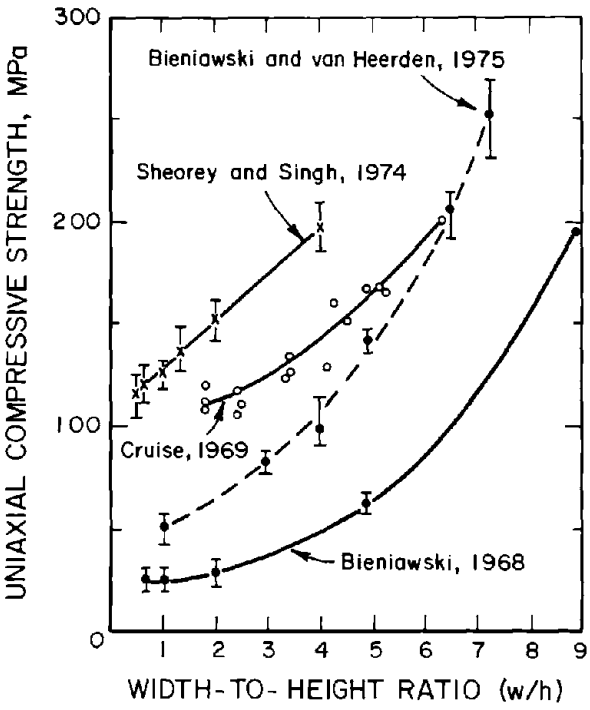

Figure 6.—The relationship between the strength and the width-to-height ratio of square sandstone specimens—published laboratory data (*3*).

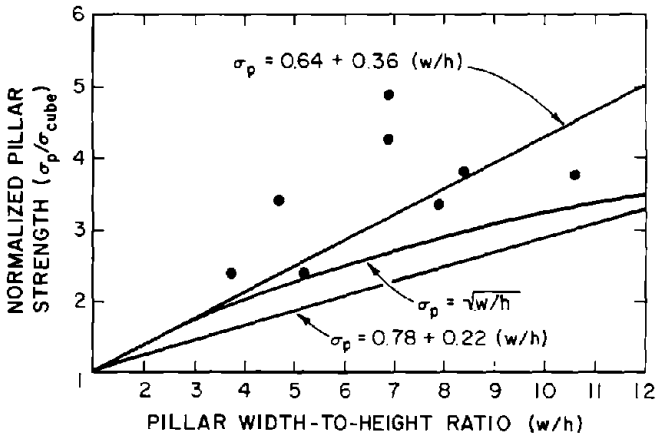

Figure 7.—In situ data: the effect of the width-to-height ratio on the strength of eight longwall coal pillars: observed data and predictions by three empirical formulas [Mark et al. 1988 (*12*)].

portion of the pillar provides lateral confinement, which enhances the strength at the center of the pillar. He also concluded that long rectangular pillars having a width greater than 10 times their height are unlikely to fail except for punching into the roof or the floor. However, recent studies (as yet unpublished) suggest that wide pillars—even with width-to-height ratios of 15 and over—may have failed, depending on the definition of "failure." It is not clear whether the pillar has failed throughout including the pillar core.

EXAMPLE

This simple example demonstrates the differences in pillar size estimates by the five pillar strength formulas. Consider an existing room-and-pillar coal mine in the Pittsburgh Seam, with an aim of improving its coal extraction:

Depth below surface (H)	500 ft (152 m)
Entry width (B)	18 ft (5.5 m)
Pillar width (w)	60 ft (18.3 m)
Pillar length (L)	80 ft (24.4 m)
Seam height (h)	7 ft (2.1 m)
Pittsburgh Seam in situ coal strength (σ_{cube})	930 psi (6.4 MPa)

The first step is to establish the current factor of safety F used by the mine and the percentage of the coal extracted.

$$F = \frac{930\,[0.64 + 0.36 \times (60/7)]}{1.1 \times 500 \times (78/60) \times (98/80)} = 3.95.$$

Clearly, this is not an efficient operation as evident by the uneconomical factor of safety and a low percentage of coal extraction e:

$$e = 1 - 60/78 \times 80/78 = 0.372 = 37.2 \text{ pct.}$$

To improve the coal extraction, the minimum pillar sizes may be determined using the five pillar strength formulas and retaining the pillar length-to-width ratio of 1.33 as practiced by the mine. The calculations must be performed for the appropriate factor of safety recommended by each formula, as shown in table 2.

Based on table 2, the author would recommend pillar dimensions of 29 by 39 ft (8.8 by 11.9 m) resulting in a

much improved coal extraction of 58 pct with a factor of safety of 1.52.

Table 2.—Estimates of maximum pillar sizes using the five pillar strength formulas and pillar length-to-width ratio of 1.33

Formula	Factor of safety	Pillar width, ft[1]	Pillar length, ft[1]	Coal extraction, pct
Obert-Duvall	2.0	44.1	58.6	45.6
Holland-Gaddy . . .	1.8	52.7	70.1	40.6
Holland	2.0	38.5	51.2	49.5
Salamon-Munro . .	1.6	28.9	38.4	57.9
Bieniawski	1.5	28.7	38.2	58.1

[1]To convert feet to meters, multiply by 0.30.

It is interesting to observe that if the mine would extend its operations to the lower seam, located at a depth of 1,000 ft (300 m) below the surface, the differences between the estimates for the pillar sizes by the five pillar strength formulas would be more pronounced, as shown in table 3.

Table 3.—Estimates of pillar sizes using the five pillar strength formulas at a depth of 1,000 ft (300 m)

Formula	Factor of safety	Pillar width, ft[1]	Pillar length, ft[1]	Coal extraction, pct
Obert-Duvall	2.0	81.6	108.0	29.7
Holland-Gaddy . . .	1.8	120.0	160.0	21.7
Holland	2.0	80.2	106.0	30.1
Salamon-Munro . .	1.6	57.0	75.9	38.5
Bieniawski	1.5	48.2	64.1	43.1

[1]To convert feet to meters, multiply by 0.30.

The above differences are due to the fact that some of the formulas are very conservative at greater depths for which they were not intended. The formulas by Holland-Gaddy and by Holland should not be used for depths of more than 500 ft (150 m). It is also clear that the economics of relatively low percentage of coal extraction from room-and-pillar mining at depths of more than 1,000 ft (300 m) may be questionable when compared to longwall coal mining.

CONCLUSION

A pillar strength formula for coal mining has been reviewed and shown to be both economical and safe. Although valid for use in other countries, the proposed design procedure is particularly relevant to the United States, where 174 coal mines have been surveyed using this formula. It has also been shown that, subject to an appropriate factor of safety, the formula has been used effectively in both room-and-pillar mining (*4*) and in longwall mining (*11*).

REFERENCES

1. Bieniawski, Z. T. The Effect of Specimen Size on the Strength of Coal. Int. J. Rock Mech. and Min. Sci., v. 5, 1968, pp. 325-335.

2. ____. In Situ Strength and Deformation Characteristics of Coal. Eng. Geol., v. 2, 1968, pp. 325-340.

3. Bieniawski, Z. T., and W. L. van Heerden. The Significance of In Situ Tests on Large Rock Specimens. Int. J. Rock Mech. and Min. Sci., v. 12, 1975, pp. 101-113.

4. Bieniawski, Z. T. New Design Approach for Room-and-Pillar Coal Mines in the USA. Paper in Proceedings of the 5th ISRM Congress on Rock Mechanics. Balkema, Rotterdam, 1983, pp. E27-E36.

5. ____. Rock Mechanics Design in Mining and Tunneling. Balkema, Rotterdam, 1984, pp. 55-92.

6. Cook, N. G. W., and M. Hood. The Stability of Underground Coal Mine Workings. Paper in Proceedings of the International Symposium on Stability in Coal Mining. Miller Freeman Publications, San Francisco, 1978, pp. 135-147.

7. Gaddy, F. L. A Study of the Ultimate Compressive Strength of Coal. Bulletin of the Virginia Polytechnic Institute Engineering Experiment Station, No. 112, August 1956, pp. 1-27.

8. Holland, C. T. The Strength of Coal in Mine Pillars. Paper in Proceedings of the 6th U.S. Symposium on Rock Mechanics. Univ. MO, Rolla, MO, 1964, pp. 450-466.

9. Holland, C. T. Pillar Design for Support of the Over Burden in Coal Mines. Paper in Proceedings of the 9th Canadian Symposium on Rock Mechanics. McGill Univ., Montreal, 1973, pp. 114-139.

10. Hustrulid, W. A. A Review of Coal Pillar Strength Formulas. Rock Mechanics, v. 8, 1976, pp. 115-145.

11. Mark, C., and Bieniawski, Z. T. An Empirical Method for the Design of Chain Pillars in Longwall Mining. Paper in Proceedings of the 27th U.S. Symposium on Rock Mechanics. AIME, New York, 1986, pp. 415-422.

12. Mark, C., J. Listak, and Z. T. Bieniawski. Yielding Coal Pillars - Field Measurements and Analysis of Design Methods. Paper in Proceedings of the 29th U.S. Symp. on Rock Mechanics. AIME, New York, 1988, pp. 261-270.

13. Obert, L., and W. I. Duvall. Rock Mechanics and the Design of Structures in Rock. Wiley, New York, 1967, pp. 542-545.

14. Salamon, M. D. G., and A. H. Munro. A Study of the Strength of Coal Pillars. J. S. Afr. Inst. Min. Metall., v. 68, 1967, pp. 55-67.

15. Wagner, H. Determination of the Complete Load Deformation Characteristics of Coal Pillars. Paper in Proceedings of the 3rd ISRM Congress on Rock Mechanics, Denver, 1974, v. IIB, pp. 1076-81.

TEN YEARS' EXPERIENCE OF THE WILSON/CARR PILLAR SIZING METHOD AT JIM WALTER RESOURCES, INC.

By Frederick Carr[1]

INTRODUCTION

In 1980, Jim Walter Resources, Inc. (JWR), was essentially a new company, mining in a new deep part of the Warrior Coal Basin, located in central Alabama. With a new longwall mining technique and a team of mining engineers having very varied backgrounds and experience in the United Kingdom and the Northern and Southern United States, it was a time of change when new ideas were the norm rather than the exception.

The primary strata control need at that time was to improve tailgate roadway conditions such that no delay occurred in the longwall operation. Tailgate supplemental support was shown to be inadequate even in the lightest stress conditions at No. 3 Mine.

A method of pillar design assessment, which has become known as the Wilson/Carr method, has evolved successfully at JWR over the last 10 years. During these years, the method has been described and detailed exhaustively at conferences and in published papers [Wilson (*9*), Carr (*1*), Martin (*5*), Hendon (*4*)].[2] However, a brief introductory description may be helpful.

The assessment is essentially a comparison of coal pillar load, which is determined by the tributary method and the coal pillar strength calculated by the Wilson approach. Where the load and strength are in balance, a stability factor of 1 is quoted; a stability factor above 1 indicates a pillar with greater support capacity. The introduction of yield pillar technology has allowed the practical design of large support pillars at depth in both mainline developments and in areas associated with longwall mining.

Main development design necessitates a stability factor of 1 as no additional loads are envisioned in the development's lifetime. The application of the method to longwall developments is more complicated since redistributed load from the adjacent longwall is imposed in addition to the coverload. It is assumed from theoretical considerations that the longwall load is limited to a certain calculable maximum and also imposed such that failure of a row of pillars adjacent to the longwall will transfer loads onto the remaining rows of pillars. The final transferred load to the adjacent future longwall panel or abutment pillar becomes the basis of a condition assessment for the tailgate entry.

A tailgate entry alongside a stable longwall pillar design may still have high stresses, which are associated with the primary longwall stress redistribution, imposed upon it. If this condition coincides with weak strata in the immediate roof or floor, observable roof side or floor movement can still occur.

Long-term abutment pillars associated with redistributed loads from a pillared or longwall area are assessed in a different way from those required in longwall panels. The long-term nature of the roadways next to the abutment pillar demands that no extra stress be imposed on the roadway. These stresses are dependent on the depth and stress decay factors.

As indicated previously, the successful use of yield pillars was the major reason why the Wilson/Carr method became applicable to JWR's deep mines. Until that time, longwall development chain pillars could not be driven large enough to satisfy the requirement of no transferred load in the main developments or from the chain pillar in either the first or second longwall phases.

Again, papers on the experience at JWR of yield pillars and their advantage have been presented previously [Martin (*5*); Serata (*8*); Carr (*2*); Martin (*6*); Gauna (*3*)].

[1]Vice President, Mining Engineering, Jim Walter Resources, Inc., Brookwood, AL.

[2]Italic numbers in parentheses refer to items in the list of references at the end of this paper.

EXPERIENCE AT NO. 3, NO. 4, NO. 5, AND NO. 7 MINES

The 10 years' experience at each of the JWR mines is expressed mainly in the form of diagrams, tables, and maps. In the 10 years, 33 miles of main developments have been driven, 80 miles of longwall development have been driven, 79 longwall panels have been extracted, and longwall face widths have increased from 450 to 850 ft, with 950 ft being projected.

Figure 1 shows the variation possible in the immediate roof and floor over the whole area mined by JWR. Variation can take the form of quality and thickness variations and can have an obvious effect on the condition of a roadway even under the same stress condition. This variation complicates any analysis of the effect of changes in pillar design and the transferring designs from mine to mine, and can account for some seemingly contradictory experiences.

EXPERIENCE AT NO. 3 MINE

Table 1 shows the different designs of main and longwall developments, indicates when they were driven, the starting and ending pillars associated with the longwall developments, and briefly comments on the condition of the longwall development's tailgate.

Figure 2 shows the location of the longwall panels and the development designs. The experience learned from this mine with pillar design is as follows:

1. The original design of the mainline developments was based upon C. Holland's principles of pressure arch formation and the use of insurance abutment pillars. There has been generally good experience with this design and a reluctance at this mine to change from a known

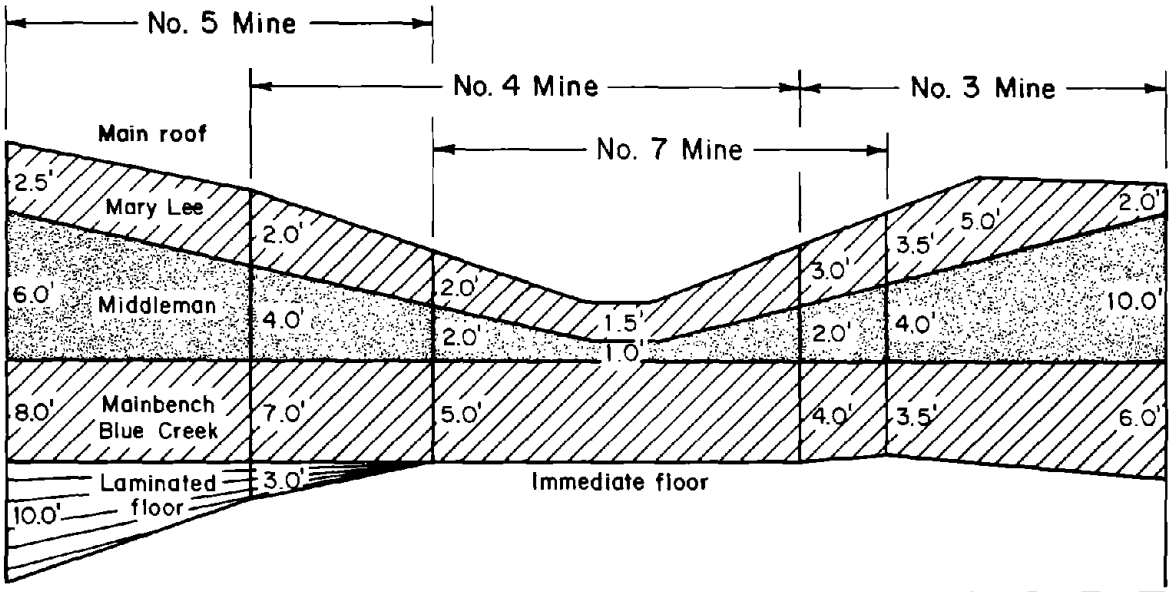

Main roof	25 to 30 ft shale, sandy shale, and siltstone	40 to 50 ft massive sandstone		35 to 45 ft sandy shale and siltstone
Mary Lee	15 in of coal, 12 to 18 in of partings	2 to 3 ft of rider seams overlying normal Mary Lee		Normal Mary Lee
Middleman	2 to 6 ft of sandy shale and shaley sandstone	Less than 1 ft of fire clay		Over 10 ft of sandy shale and shaley sandstone
Blue Creek	5 to 8 ft of coal, bone, and shale	Draw rock occasionally > 12 in	Thin but clean Blue Creek	Normal Blue Creek
Immediate floor	3 to 10 ft of laminated coal and rock	Sandstone	Fire clay	Hard fire clay / Fire clay

Figure 1.—Geological variation of the immediate roof and floor of the Blue Creek Seam at the Jim Walter Resources Nos. 3, 4, 5, and 7 Mines.

Table 1.—No. 3 Mine longwall and main developments, 1,500-ft depth

Design, ft	Panel	Date	Distance, ft	Starting pillar widths	Ending pillar widths	Comments
LONGWALL DEVELOPMENTS						
4 Entry chain:						
100 by 100	1st-SW	1978	2,770	250	470	1st t/g - weak roof - no major problems.
	3rd-S-H/G	1980	5,650	0	300	Poor conditions - last h/g.
3 Entry chain:						
100 by 100	2nd-SW	1978	3,750	500	200	Poor conditions - roof falls in t/g.
	3rd-SW	1979	4,020	360	320	Poor conditions.
	1st-S	1979	3,500	0	300	Poor conditions - roof falls in t/g - 1st t/g.
	2nd-S	1980	3,800	0	300	2nd t/g - poor condition.
	4th-SW	1980	3,950	400	360	Poor condition.
5 Entry chain:						
85 centers	1st-NE	1979	4,000	350	300	Very poor conditions - 3 roof falls on t/g - 1st t/g.
	2nd-NE	1980	4,100	350	450	Poor conditions.
2 Entry stable:						
200	5th-SW	1980	2,450	250	470	Improved conditions - weak roof - no major problems.
4 Entry chain:						
150 by 80 by 150	6th-SW	1980	4,000	250	600	Poor conditions.
100	1st-NW	1981	2,750	400	730	Poor conditions - 1st t/g.
120	2nd-NW	1982	4,240	230	620	Poor - h/g and t/g broken up.
3 Entry chain:						
120	7th-SW	1981	3,850	300	500	Poor conditions.
	3rd-NE	1981	4,450	330	250	Improved conditions - 1 roof fall in t/g.
	9th-SW-HG	1982	3,940	210	1,950	Poor condition - last h/g - t/g broken.
4 Entry chain:						
100-100-140	4th-NE	1982	5,300	320	460	Generally good roof - no major problems.
140-100-100	8th-SW	1983	2,850	210	1,950	Generally good roof - no major problems.
120-120-120	3rd-NW	1983	4,950	230	620	Weak roof - very poor conditions.
4 Entry:						
Y-S-C:						
40-200-120 ..	5th-NE	1984	3,000	360	280	Good conditions.
4 Entry chain:						
120-120-120	5th-NE	1984	2,400	260	430	Good conditions.
	4th-NW	1984	3,400	300	570	Fair conditions - no major problems.
4 Entry:						
C-S-Y:						
120-200-40 ..	4th-NW	1984	1,620	300	570	Fair conditions.
4 Entry:						
Y-S-Y:						
40-200-40 ...	6th-NE	1984	5,500	320	300	No problems.
	7th-NE	1985	6,400	320	360	No problems.
	5th-NW	1985	5,020	300	550	No problems.
	6th-NW	1986	5,040	300	550	No problems.
Y-Y-Y:						
45-45-45	8th-NE-HG	1986	6,300	320	360	No major problems.
Y-S-Y:						
45-135-45 ...	1st-SE	1987	2,250	400	300	1st t/g - no major problems.
45-200-45 ...	7th-NW	1987	5,120	320	460	Good conditions.
	2nd-SE	1988	3,700	750	150	Good conditions.
	8th-NW	1988	5,100	320	460	Good conditions.
	9th-NW	1989	4,340	320	450	Good conditions.
	3rd-SE	1989	4,400	220	150	Good conditions.
	9th-NW-HG	1990	3,600	320	450	Good conditions.

Table 1.—No. 3 Mine longwall and main developments, 1,500-ft depth—Continued

Design, ft	Panel	Date	Distance, ft	Starting pillar widths	Ending pillar widths	Comments
			MAIN DEVELOPMENTS			
5 Entry chain:						
100	—	1974-80	9,600	—	—	Fair conditions.
85	—	1974-77	6,600	—	—	Poor conditions.
6 Entry chain:						
100	—	1977-90	17,700	—	—	Fair conditions.
6 Entry:						
Y-S-Y-S-Y:						
45-135-45-135-45	—	1988-89	1,040	—	—	Poor conditions.
4 Entry chain:						
125	—	1989-91	3,450	—	—	Fair conditions - faulted area.

NOTE.—Dash indicates not applicable.

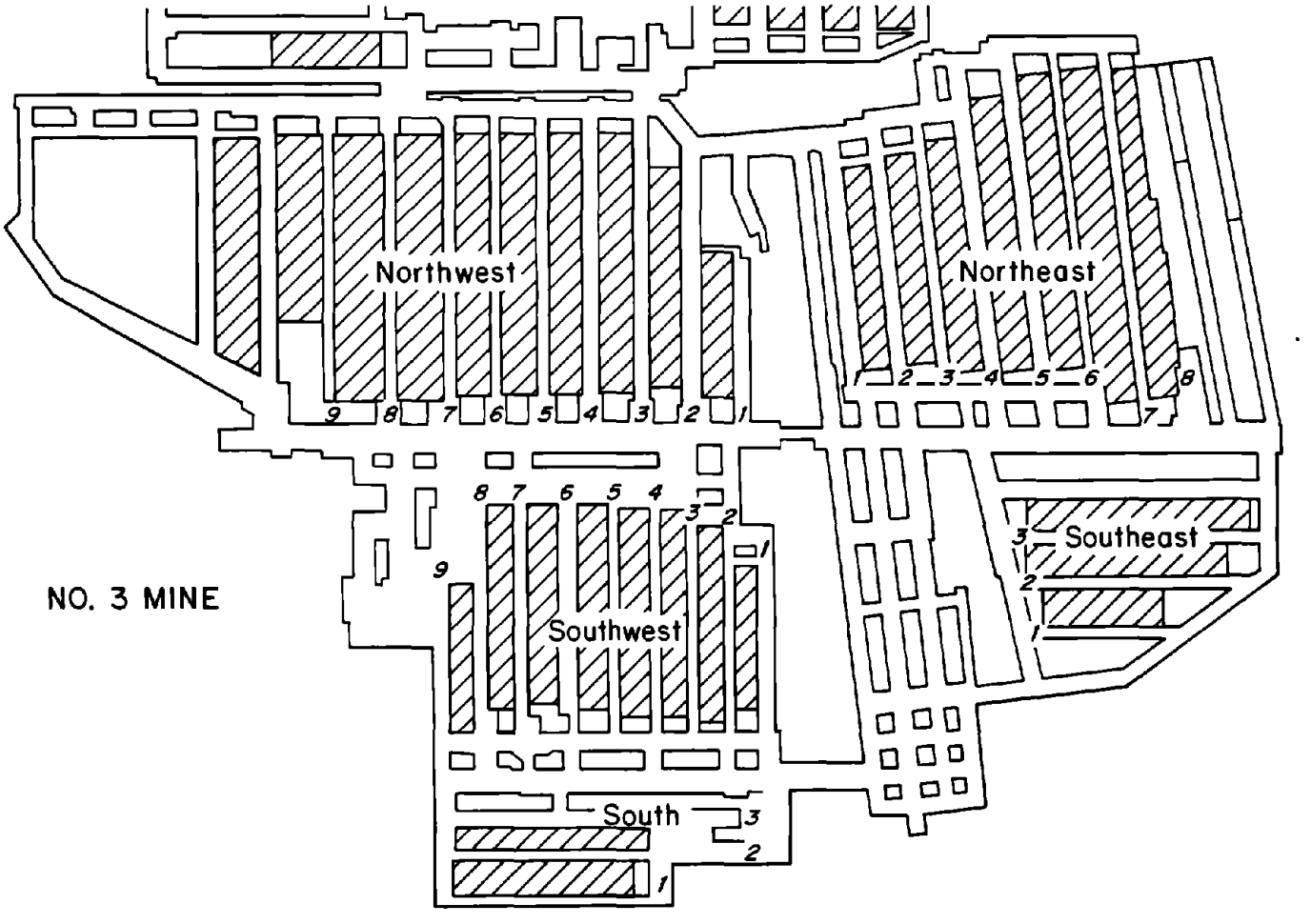

Figure 2.—Jim Walter Resources No. 3 Mine longwall and main developments.

success, especially in light of the yield pillar "failure" described later.

2. This mine was the initial site of the development of the Wilson/Carr approach for multientry roadways in association with longwall mining. The experiences of 1st-6th SW and 1st NE were included in the analysis leading to the defining of the method.

3. The two-entry longwall development driven on 200- by 200-ft centers and used as a tailgate for 5th SW established the desirability of large-stable pillars to isolate the longwall waste stresses from the adjacent future tailgate.

4. "Peep thru" stresses were encountered in the submains associated with the end position of the SW longwalls. One hundred by one hundred feet center-to-center pillars driven in the submains were unable to accept additional load and gradual deterioration spread into the mains themselves. A finishing pillar of at least 360 ft was established to counteract this effect. "Peep thru" was not completely cured, especially in weak ground conditions until it was decided that longwall developments should be based on the yield/stable/yield principle. This design change allowed for larger pillars at the transition area from longwall panel to submains.

5. Early in the introduction of yield pillar/stable pillar/technology to mains development, four-way junction failure occurred, which has restricted the use of this technology at this mine to longwall developments. The strata control explanation for this failure was primarily the undercasting of the junction after drivage and the subsequent weakening of the yield pillar.

6. Experiences with both longwall starting and finishing abutment pillars suggest that different stresses from the longwall process are developed on these pillars. JWR is now conducting trial-and-error experimentation at the ends of a series of panels with smaller starting pillars.

7. It has been found that three-way junctions are better in the longwall development yield/stable/yield pillar designs. Sensitivity of the main roof to the spanning needs of the design is suggested as an explanation.

EXPERIENCE AT NO. 4 MINE

Table 2 shows the different designs of main and longwall developments used at this mine. It indicates when they were driven, the starting and ending pillars associated with the defined panels, and briefly comments on the condition of the longwall tailgate of that development.

Figure 3 shows the location of the longwall panels and the development designs. The experience gained from this mine is as follows:

1. The longwall development design was changed from chain pillars to yield/stable/yield designs (tailgate development on 3rd NW, 3rd E, and 4th E panels) in midpanel of the 3rd NW panel. At the tailgate phase of the longwall extraction process, a coal bump condition occurred involving nine grouped chain pillars. It is suspected that the change in pillar support strength may have triggered the bump.

2. When 120- by 120-ft chain pillars were used in the longwall developments, "peep thru" stress developed in the submains and main bleeders (tailgate of 2nd E panel). The stress effect was mainly expressed as floor heave and was controlled by building a pillar lengthline of fiber concrete cribs in the main bleeders entries.

3. Half longwall panels 2-B-SW, 2-C-SW, and 2nd-SE show the use of yield/yield pillars in three-entry longwall development. No difficulties were experienced in the headgates of the panels. When the tailgates were supplementally supported by wooden cribs and roofed between with wire mesh, the only strata control difficulty was 2.5 to 3 ft of floor heave ahead of the longwall. This design was not continued because of ventilation difficulties associated with the longwall gob.

4. In the early designs of the mains and longwall development involving the yield pillar principle, 20- by 20-ft yield pillars were created where two yield pillar designs crossed each other. This created spanning problems even with the strong main roof condition found at No. 4 Mine. Present layouts are designed to eliminate 20- by 20-ft yield pillars.

5. Twin-seam conditions are often experienced both in main and longwall developments. Breakage of rib pins, sometimes very suddenly, was experienced in the headgate; bolted rib support was necessary in these conditions. Yield tube rib pins were designed to cure this problem by allowing the ribs to expand approximately 4 to 6 in under controlled support [Martin (7)]. The use of yield/stable/yield systems has also reduced the high-lateral stresses experienced at the headgate.

EXPERIENCE AT NO. 5 MINE

Table 3 shows the different main and longwall development designs used at No. 5 Mine. The table indicates when the developments were driven, the starting and ending pillars associated with the longwall panels, and briefly comments on the condition of the longwall tailgate associated with that development.

Table 2.—No. 4 Mine longwall and main developments, 1,800-ft depth

Design, ft	Panel	Date	Distance, ft	Starting pillar widths	Ending pillar widths	Comments
LONGWALL DEVELOPMENTS						
4 Entry chain:						
140	1st-E	1981	3,570	360	250	Major floor heave - roof o.k. - 1st t/g.
	2nd-E	1981-82	4,880	360	450	Major floor heave.
	3rd E	1982-83	3,800	310	400	Severe heave.
	4th-E	1982-83	3,300	320	400	Severe floor heave.
	2nd-NW	1982-83	4,920	320	360	Major floor heave.
125	1st-NW	1981-82	4,920	320	360	1st t/g - floor heave.
145-150-120	3rd-NW	1983	2,000	320	870	Chain pillar design changed to Y-S-C as shown below. Pillar burst at transition pillar - Y-S-C was stable.
4 Entry:						
Y-S-C:						
45-250-120	3rd-NW	1984	3,000	320	870	
4 Entry chain:						
120	1st-SW	1980-83	5,100	380	380	1st t/g - moved around fault - no major problems.
140	2-A-SW	1981	2,000	0	300	Some floor heave.
5 Entry chain:						
120	1st-SE	1986	2,380	0	220	1st t/g - no major problems.
Total yield:						
3 Entry:						
45-45-45	2-B-SW	1984	2,600	380	320	Good face conditions - squeeze behind longwall
	2-C-SW	1985	3,100	380	250	caused ventilation problems.
	2nd-SE-HG	1986	2,380	0	220	No major problems - single panel.
4 Entry:						
Y-S-Y:						
40-250-40	3rd-SW	1984	2,000	380	330	Good conditions.
40-180-40	3rd-SW	1985	2,800	380	330	Some roof breakup - no major problems.
40-230-40	5th-E	1985	4,400	360	460	Some heave - no major problems.
40-240-40	4th-NW	1984-85	5,100	320	360	No major problems.
40-220-40	4th-SW	1986	5,200	380	330	Hard footwall - no problems.
40-220-40	6th-E	1985-86	3,200	220	240	Some heave - no major problems.
40-220-40	7th-E-HG	1986	3,200	220	240	Some heave.
40-220-40	5th-NW	1985	5,100	320	360	Severe floor heave.
40-210-40	5th-SW	1987-88	5,200	380	360	Severe floor heave.
40-220-40	6th-NW	1986	5,100	320	360	Severe floor heave.
40-210-40	6th-SW	1988-89	5,200	380	360	Floor heave - increased crib density.
Y-S-Y:						
40-240-40	7th-SW-HG	1989	4,800	380	360	No major problems.
40-200-40	7th-NW	1987-88	5,100	320	360	No major problems.
40-220-40	8th-NW	1988-89	5,100	320	360	No major problems.
40-220-40	9th-NW-HG	1990	5,100	320	360	Mo major problems.
MAIN DEVELOPMENTS						
East:						
120 chain	—	—	—	—		Floor heave in all areas. High ribs in twin seam areas
6 Entry main	—	—	—	—		caused rib control problems.
4 Entry sub	1979-87	6,000	—	—		
4 Entry bleeder	—	—	—	—		
North West:						
120 Chain	—	—	—	—		Bleeders experienced major floor heave after panels
6 Entry main	—	—	—	—		were extracted. Mains and submains some spotty
4 Entry sub	1979-84	3,000	—	—		roof breakup in laminated zones.
4 Entry bleeder	—	—	—	—		
Y-S-Y-S-Y:						
40-150-40-150-40	—	—	—	—		Some problems with 20' × 20' pillars. Generally good
6 Entry main	—	—	—	—		conditions.
Y-S-Y:						
40-150-40	1984-89	5,000	—	—		
4 Entry sub and bleeders	—	—	—	—		

Table 2.—No. 4 Mine longwall and main developments, 1,800-ft depth—Continued

Design, ft	Panel	Date	Distance, ft	Starting pillar widths	Ending pillar widths	Comments
			MAIN DEVELOPMENTS			
South West:						
Y-S-Y:						
Submains	—	1983-89	6,000	—	—	Submains - no problems. Bleeders - floor heave prob-
40-150-40	—	—	—	—	—	lems.
Y-S-Y:						
Bleeders	—	—	—	—	—	

NOTE.—Dash indicates not applicable.

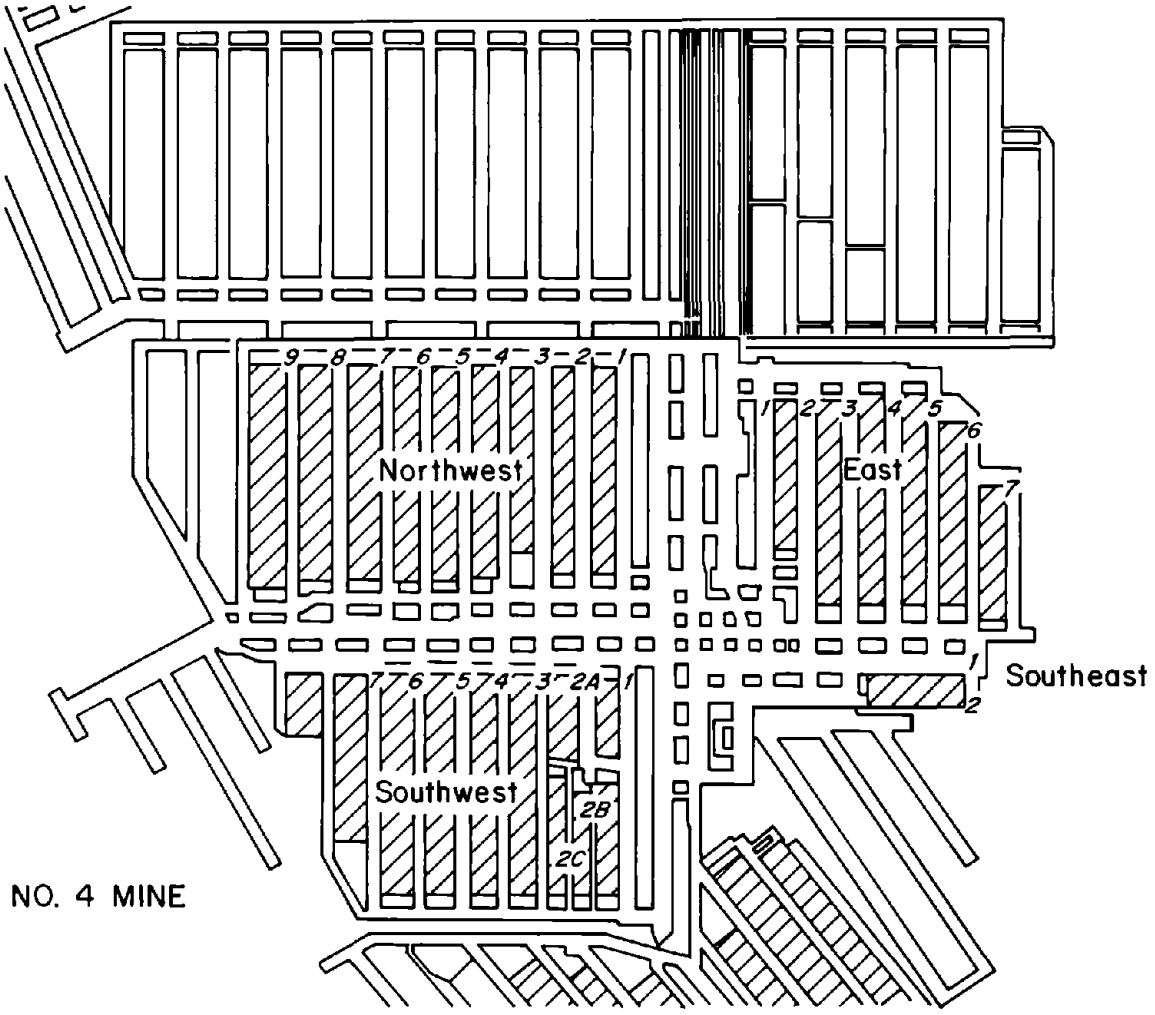

Figure 3.—Jim Walter Resources No. 4 Mine longwall and main developments.

Table 3.—No. 5 Mine longwall and main developments, 2,200-ft depth

Design, ft	Panel	Date	Distance, ft	Starting pillar widths	Ending pillar widths	Comments
LONGWALL DEVELOPMENTS						
Y-S-Y:						
40-150-40	1st-SW	1984-85	3,800	400	360	1st t/g - no major problems.
Y-S-Y-Y:						
40-240-40-40	2nd-SW	1985	3,800	350	360	No major problems.
	3rd-SW	1985-86	4,450	420	350	No major problems.
Y-Y-Y:						
45-45-45	1st-SE	1985	4,700	850	360	No problems - 1st t/g.
Y-S-Y:						
45-220-45	2nd-SE	1985-86	5,325	360	320	No problems.
40-140-40	3rd-SE	1985-86	3,300	0	610	No problems.
40-140-40	4th-SE-HG	1987	3,300	0	610	Last h/g - no problems.
40-140-40	1st-NE	1984-87	3,050	360	360	1st t/g - no problems.
40-230-40	2nd-NE	1987	4,750	320	360	No major problems.
40-230-40	3rd-NE	1987-88	4,800	350	360	No problems.
40-140-40	4th-NE-HG	1988	4,600	350	360	Last h/g - no problems.
40-140-40	1st-NW	1988	1,800	360	1,050	1st t/g - no problems.
Y-Y-Y:						
40-40-40	1st-NW	1988	800	360	1,050	1st t/g - no problems.
Y-Y-Y:						
40-40-40	2nd-NW	1989	800	400	360	No problems.
Y-S-Y:						
40-220-40	2nd-NW	1988	4,150	400	360	No major problems.
40-220-40	3rd-NW	1988-89	5,600	360	360	Severe floor heave - just outside expanded seam zone. H/G broken up at stopline.
40-230-40	4th-SW-HG	1988	5,000	420	360	Severe floor heave - areas of locally bad roof conditions.
40-220-40	4th-NW-HG	1989	5,700	360	360	Current h/g - some floor heave in h/g entry with locally broken roof areas near the stopline.
MAIN DEVELOPMENTS						
North Mains:						
6 Entry chain	—	1980-84	6,600	—	—	Some local areas of roof breakup - no major problems.
120 by 120	—	—	—	—	—	
West Mains:						
Y-Y-S-Y-Y:						
40 Yield - 170 stable	—	1986-91	6,200	—	—	General floor heave - areas of local roof breakup in areas with laminated main roof.
West Submains:						
Y-Y-S-Y-Y	—	1986-91	6,200	—	—	General floor heave - areas of local roof breakup in areas with laminated main roof.
South West Mains:						
4, 5, 6 Entry chain:	—	1980-82	2,600	—	—	Expanded seam area: severe floor heave. Many areas complete closure.
120	—	—	—	—	—	

NOTE.—Dash indicates not applicable.

Figure 4 shows the location of the longwall panels and the development designs. The strata control experience gained from this mine is as follows:

1. No. 5 Mine was the first to experience the expanded Blue Creek Seam condition where the seam thickens within a geological basin with inferior high ash and sulfur coal beneath the original Blue Creek Seam. In the expanded seam conditions, chain pillars were associated with very sudden and massive floor heave. Successful experimentation with yield pillars [Serata (*8*)] was the starting point of JWR yield pillar experience.

2. Because of the successful small-scale trials of yield/yield and yield/yield/yield pillar systems, these systems were applied in both normal and expanded seam conditions. Failure occurred initially in the four-entry yield development due to the main roof span being too great. Other spanning difficulties occurred when two yield pillar designs met and the three- or four-way junctions created were too wide. At present, yield/stable/yield systems are

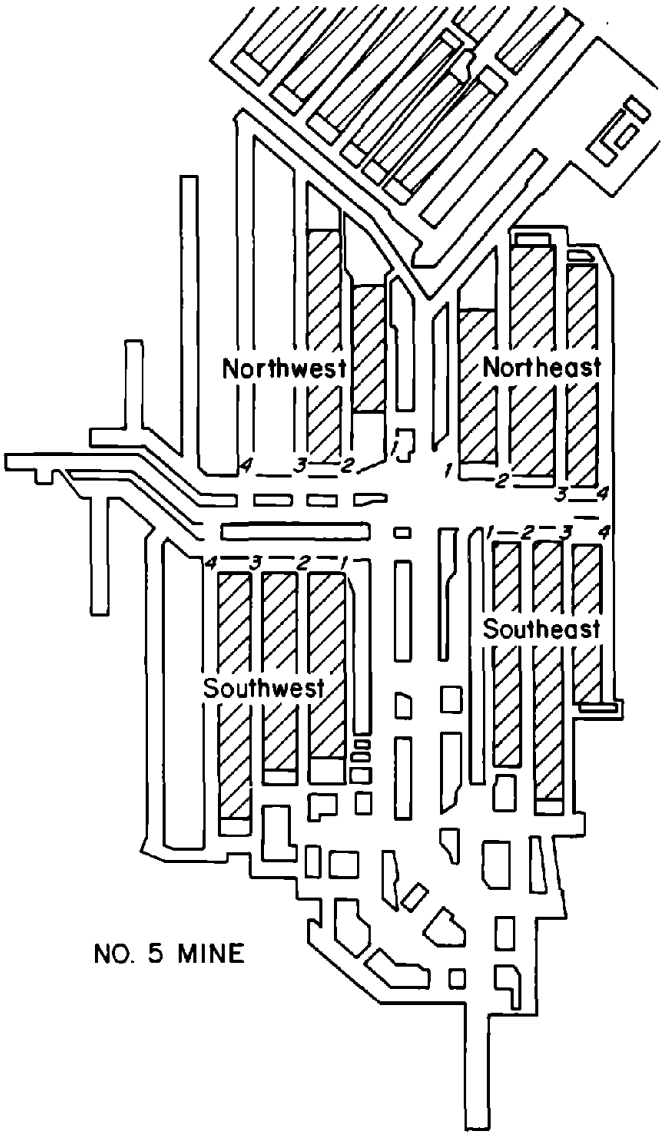

Figure 4.—Jim Walter Resources No. 5 Mine longwall and main developments.

generally used in nonexpanded seam conditions, in expanded seam conditions that are temporary (such as longwall developments), and where any floor heave is not a production problem. Yield/yield/stable systems are only used in main developments that are within the expanded seam and where it is considered that floor heave will be a long-term difficulty.

3. No. 5 Mine has had numerous problems with designs incorporating 20- by 20-ft yield pillars and have involved some massive main roof falls. Designs of mains, submains, and longwall turnouts are such that the spanning of the main roof is kept to a minimum while still obtaining the advantage of the floor heave reduction of the yield pillar systems.

4. No. 5 Mine was the first mine to attempt to drive a yield/yield development system through a small fault. The spanning quality of the main roof deteriorated to such a degree that the development had to be abandoned. In general, at all mines when faults are found in advance of the main development and have to be crossed, the design is changed to a large-chain pillar design to go through the fault. Yield pillar design systems are then reestablished beyond the fault, generally one to two crosscuts beyond the fault.

5. The inferior coal in the expanded seam contains a layer of high-sulfur pyritic coal approximately 2 to 2.5 ft below the floor of the upper bench Blue Creek Seam. Floor heave exposes this pyritic coal to the mine atmosphere, and spontaneous combustion has occurred. It is therefore of utmost importance that the number of roadways and the heave occurring in these roadways be kept to a minimum, especially in the longwall developments. This continues to be a difficult problem, but is helped by the yield pillar principle.

NO. 7 MINE

Table 4 shows the different main and longwall development designs that have been used at this mine. It indicates when they were driven, each panel's starting and ending pillar size, and briefly comments on the condition of the entry when used as the tailgate of a longwall panel.

Figure 5 shows the location of the longwall panels and the development designs. The strata control experience of the mine is as follows:

1. There has been in the NW series of panels a direct relationship between the size of the stable pillar in the yield/stable/yield longwall developments and the tailgate conditions and the supplemental support requirement. Experience has been obtained with 210, 220, and 230 ft stable pillars, mechanical bolts, full-column resin bolts, and point-anchored tab nut bolts.

2. This mine has had negative experiences with yield/yield/stable/yield longwall developments. Again, the difficulty is in the three-entry yield/yield portion of the development, where gradual failure of the main roof was evident. Sometimes when the spanning quality of the main roof is suspect or when the height of the yield pillar is above 8 ft, the size of the yield pillar can be increased to improve its support. This is generally successful in double-entry yield pillar systems, but in a three-entry system, any increase in yield pillar width without a decrease in entry width has the dubious effect of increasing the total span of the development, causing a greater chance of spanning failure.

3. The only experience to note from the main and bleeder designs is that the chain pillar designs were susceptible to "peep thru" stress created in a similar way to that described in Mines No. 3 and No. 4.

Table 4.—No. 7 Mine longwall and main developments, 2,200-ft depth

Design, ft	Panel	Date	Distance, ft	Starting pillar widths	Ending pillar widths	Comments
LONGWALL DEVELOPMENTS						
4 Entry chain:						
120 by 120	1st-SE	1981-83	6,400	360	320	1st t/g - no problems.
135 by 135	2nd-SE	1981-83	5,800	300	260	2nd t/g - pillars overloaded - poor conditions.
125 by 125	3rd-SE	1981-83	5,500	300	300	3rd t/g - pillars overloaded - very poor conditions.
120 by 130	1st-NW	1982-84	6,200	380	360	1st t/g - generally good conditions.
4 Entry Y-S-Y:						
40-210-40	2nd-NW	1985-86	6,200	380	620	2nd t/g - primary bolting overloaded (8' conv. 5/8") several falls in the t/g.
40-220-40	3rd-NW	1985-86	6,200	380	420	3rd t/g - some deterioration just outby active face. Primary support changed to 6' resin.
40-210-40	4th-NW	1986	6,200	380	360	4th t/g - primary 6' resin - poor conditions stress observed riding over 210' abutment pillar. Secondary bolting required in t/g.
40-220-40	4th-SE	1986	6,100	410	310	4th t/g - primary 1st 1/2 8' conv., 2nd 1/2 6' resin. No problems in 6' resin area. Bolts overload is 8' conv. requiring additional support.
40-230-40	5th-SE	1986	5,800	450	360	5th t/g - primary - 1st 1/3 conv. - last 2/3 6' resin. H/G and t/g rebolted with 8' tab nut bolts - no major problems.
40-220-40	5th-NW	1987	6,200	380	360	5th t/g - primary 6' resin rebolted with 8' T.N. bolts - no problems.
40-220-40	6th-SE	1987	4,800	380	360	6th t/g - primary T.N. rebolted with 8' T.N. No problems.
40-220-40	6th-NW	1988	6,200	380	450	Primary 6' resin, rebolted with 6' resin - no
40-220-40	7th-NW	1989	6,200	380	450	problems.
40-220-40	8th-NW-HG	1990	6,200	380	450	
5 Entry:						
120 by 120	1st-S	1983-84	4,000	400	360	1st t/g - Panel pulled 6 years after entry development - no major problems due to extensive rehabilitation work—1st East West panel at No. 7 Mine.
Y-Y-S-Y:						
45-45-210-45	7th-SE-HG	1987	4,600	380	360	H/G only - last panel in series. Generally poor conditions on development—5 entry system unstable in this area.
4 Entry:						
Y-S-Y:						
40-220-40	2nd-S	1988	5,600	570	220	2nd t/g - East/West panel. No major problems.
140	3rd-S-HG	1989	4,200	570	220	H/G only - last in series - fair condition - side abutment rode over 140' abutment pillar badly deteriorating outside entries.
MAIN DEVELOPMENTS						
North Mains:						
110 by 110 chain	—	—	—	—	—	General deterioration over time due to primary
Main-6 Entry	—	1982-85	6,600	—	—	support failing. No pillar design problems.
Submain-4 Entry	—	—	—	—	—	
North West Bleeders:						
5 Entry Chain	—	—	—	—	—	
110 by 120	—	1984-85	2,850	—	—	Same as North Mains.
5 Entry Y-S-Y-Y:						
40 Yield	—	—	—	—	—	
160 Stable	—	1985-86	3,200	—	—	System unstable. Design abandoned in this area.
4 Entry Y-S-Y:						
40 Yield	—	—	—	—	—	
200 Stable	—	1986-89	3,100	—	—	Good conditions.

Table 4.—No. 7 Mine longwall and main developments, 2,200-ft depth—Continued

Design, ft	Panel	Date	Distance, ft	Starting pillar widths	Ending pillar widths	Comments
			MAIN DEVELOPMENTS			
West Mains:						
Mains 6 Entry	—	—	—	—	—	
Sub 4 Entry	—	—	—	—	—	
Chain:						Stable conditions - primary support rusted in
105 by 120	—	1980-85	7,700	—	—	single seam areas.
Yield-Stable:						
45 Yield	—	—	—	—	—	
140 Stale	—	1987-91	2,500	—	—	No problems.
East Mains:						
6 Entry Main	—	—	—	—	—	No problems except in areas bolted with Resmech
4 Entry Submains	—	1984-86	5,000	—	—	bolts. Design generally stable.
Chain - 125	—	—	—	—	—	
Yield-Stable:						
40 Yield	—	—	—	—	—	
140 Stable	—	1987-91	1,500	—	—	No problems.
South Bleeders:						
5 Entry Chain:						General convergence due to peep through stress
110 by 120	—	1983-84	3,850	—	—	from longwalls - very poor conditions.
4 Entry Y-S-Y:			—			
40 Yield	—	—		—	—	
220 Stable	—	1985-86	3,200	—	—	No problems.
Old #1 Section:						
6 Entry Chain:						
120 by 120	—	1981	2,900	—	—	Design stable.
110 by 110	—	1981-82	3,300	—	—	Design stable.
85 by 125	—	1982-83	3,700	—	—	General convergence of entries, very poor conditions.
4 Entry Y-S-Y:						
40 Yield	—	—	—	—	—	
140 Stable	—	1983-84	4,000	—	—	No problems.

NOTE.—Dash indicates not applicable.

CONCLUSIONS

The following are conclusions derived from all of JWR's experience:

1. *The Wilson/Carr method has produced successful pillar designs at JWR for 10 years without any basic design difficulties and can be considered a safe initial design method for any green field mine.*

2. *The strength of the immediate roof and floor is a major factor regarding roadway condition even when adjacent pillars are stable.*

3. *The general application of the yield pillar principle is limited to a two-entry yield pillar system. A good spanning main roof is essential if three- or four-entry systems are required.*

4. *All designs incorporating yield pillars should eliminate any 20- by 20-ft yield pillars.*

5. *Yield pillar systems reduce floor stress and therefore floor heave in soft floor conditions.*

6. *The stability factor of any design pillar should be at least 1.*

JWR's initial experience in mains development was with C. Holland's design principles with stability factors of between 0.52 and 0.73 in the chain pillars. This approach was found to be adequate except in soft floor or deep conditions where floor heave was found to be a continual problem. The limitation of the pressure arch width on the number of roadways and the size of the insurance pillar sterilized a large amount of coal in the mains and submains development. The use of the yield stable principle has reduced the sterilized coal dramatically, produced more panel length to the associated longwalls, and allowed

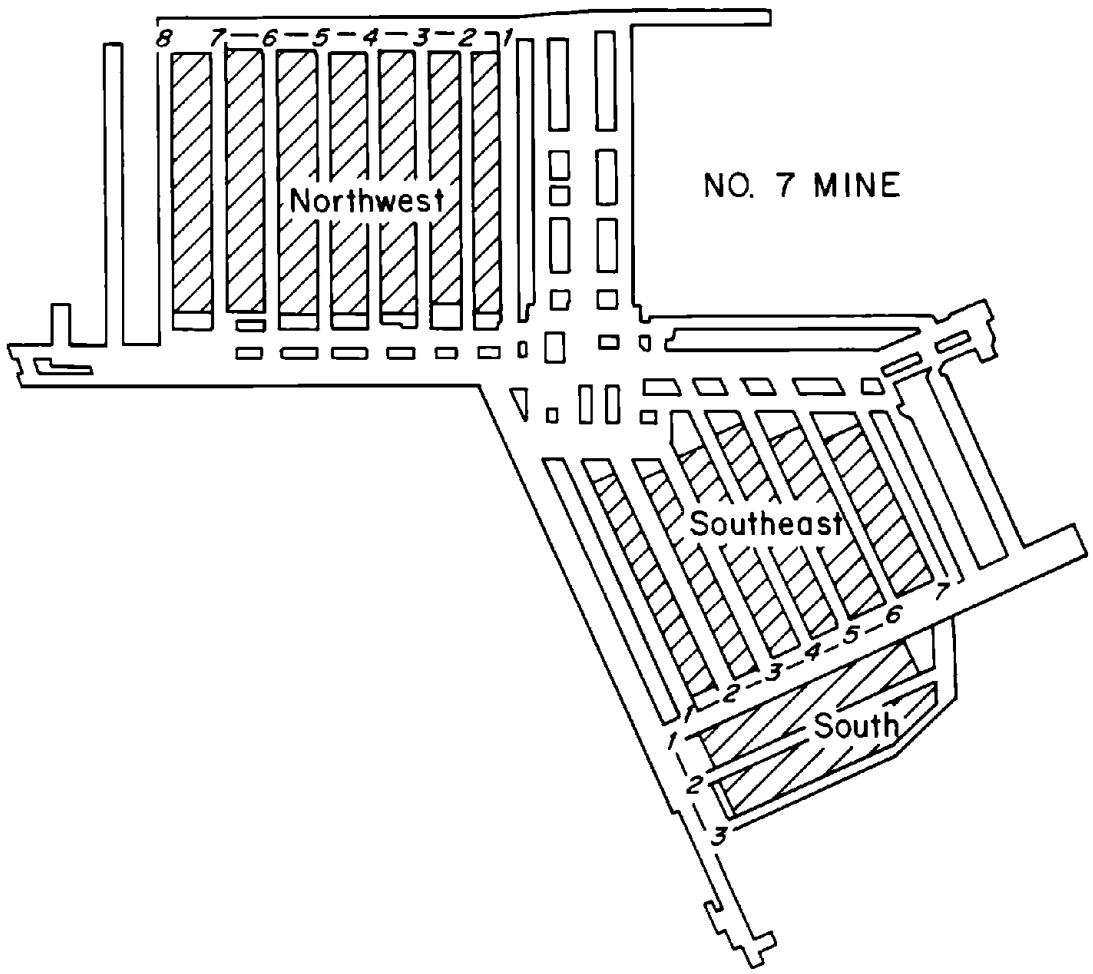

Figure 5.—Jim Walter Resources No. 7 Mine longwall and main developments.

for designs having a pillar stability of 1. In present designs of mains development, a yield/stable pillar is reproduced to the number of main entries required.

In longwall development, the stable pillar between two longwall wastes should be capable of supporting the load imposed by the longwall extraction. The size of the stable pillar required in the development design is then defined, and stability factors of the stable pillar in the development, first longwall phase, and second longwall phase can be calculated.

Table 5 shows the variation in safety factors with depth, pillar size, and through the different development and longwall phases. The stable pillar used at No. 3 Mine is 200 ft, No. 4 is 220 ft, No. 5 is 230 ft, and at No. 7 is 230 ft. As can be observed, the size of stable pillar at the deeper mines is not as big as that calculated by the Wilson/Carr method. It has been found that the upper limit is more determined by ventilation and development advance parameters than strata control reservations.

Table 5.—Stability factors for yield stable yield pillar developments (Roadway height - 7'0")

Stable pillar size (C to C), ft	Depth, ft	Stability factor		
		Development	After first longwall pass	After second longwall pass
200	1,400	3.57	1.86	1.26
180	1,400	3.02	1.52	1.01
175	1,400	2.88	1.43	.95
160	1,400	2.46	1.19	.79
135	1,400	1.79	.82	.53
240	1,800	3.57	1.82	1.22
220	1,800	3.19	1.58	1.05
210	1,800	2.98	1.46	.97
200	1,800	2.78	1.34	.88
140	1,800	1.49	.65	.42
250	2,200	3.06	1.49	.98
240	2,200	2.92	1.40	.92
220	2,200	2.61	1.22	.80
150	2,200	1.39	.59	.37

If the stable pillar is too small, load will be transferred from the common waste behind the second longwall to the front of the second faceline (as indicated in figure 6 by the dotted arrows), adding to the load already produced by the first longwall waste and the normal front abutment. Observations in the large crosscut roadways indicate that stress increases have occurred some 800 to 1,000 ft in front of the second longwall face.

At Mine No. 3, where the final stability factor of the longwall stable pillar is 1.26, very good tailgate conditions are a common feature. Any reduction of stable pillar size must be justified by ventilation or development advance against a possible deterioration in conditions. A trial reduction to 180 ft may occur in the near future. The size of the initial stable pillars at No. 5 Mine was 250 ft, and this has been successfully reduced to 230 ft.

7. *The condition of a designed tailgate is dependent upon the remnant redistributed stress, strength of the immediate roof and floor, and the effectiveness of the primary and supplemental support.*

A stable pillar with a design stability factor of 1 does not stop stress from the first longwall being redistributed onto the tailgate of the second face. Table 6 indicates the stress in tons per square foot and in percent of coverload at the second face tailgate at various depths and associated with various sizes of stable pillars.

Table 6.—Stress on 2nd face tailgates due to first face loading

Pillar size, ft (center & center)	Depth, ft	Stress at TG, (% above coverload)	Cover-load, t/ft^2	Stress @ tailgate, t/ft^2
180	1,400	33	110.88	147.97
200	1,400	27	110.88	140.97
360	1,400	5	110.88	116.53
220	1,800	37	142.56	195.70
360	1,800	12	142.56	159.97
240	2,200	45	174.24	253.21
360	2,200	21	174.24	210.72

The physical condition of the tailgate is dependent upon many factors:

1. Size of the stable pillar.
2. Size of the longwall load redistribution.
3. Type of immediate roof and floor and its ability to resist stress associated with factor (2).
4. The amount and effectiveness of artificial support, both primary and supplemental.

It is, therefore, difficult to give any definitive guidelines as to the amount of planned stress acceptable from the first

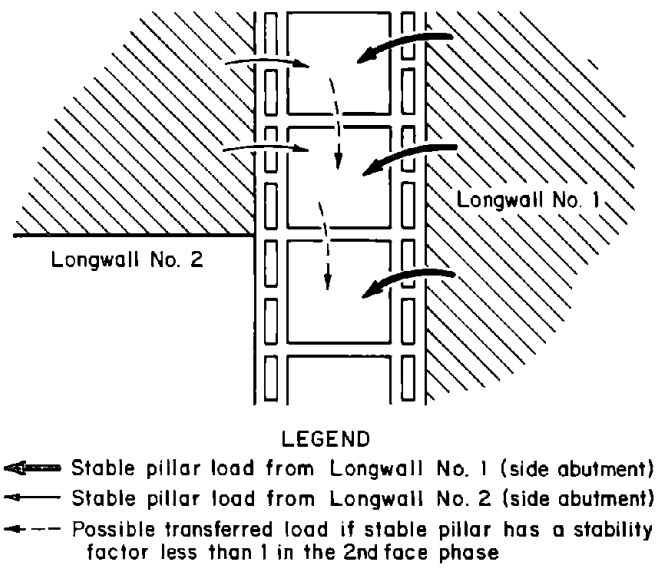

Figure 6.—Loading on stable pillars around a longwall panel sequence.

longwall face. Experience has shown that in some types of immediate roof and floor, up to 45 pct above coverload has been operationally acceptable.

A recent U.S. Bureau of Mines geological survey of development conditions has indicated that in situ horizontal stresses may create an initiating fracture in the immediate roof, especially where single-seam mining is used. This could create a weakness where further stress reactions could be concentrated. Direction of yield pillar development entry drivage and primary support pattern and density could influence the position and severity of this fracture. This may be very important to the support of the tailgate area of the second longwall since operational delays have been experienced where median thickness middleman is encountered.

At present, the U.S. Bureau of Mines is conducting investigations in a tailgate at No. 7 Mine to better understand the stress variations on development and first longwall and second longwall passage. JWR expects the results to indicate the best type of bolt to use in both primary and supplemental bolting systems and the design of those systems. This investigation has already indicated that "real-time" monitoring of bolt load and bed separation is possible from a surface-monitoring station.

Supplemental support is used in the tailgates of all the JWR longwalls. Where twin-seam development is practiced, a single row of wooden cribs is installed at 25-ft centers in the adjacent tailgate at the time of the first longwall passage. These have been required to control the periodic main roof caving effects in the immediate tailgate area.

Single-seam tailgates are reinforced by supplemental bolting and cribs. The contribution to entry condition stability is still being debated. An ongoing U.S. Bureau of Mines investigation of a current tailgate from its development phase will assist in distinguishing the effect of different forms of artificial support.

8. *The size of starting and ending barrier pillars is influenced by the longwall development pillar design.*

Initially, the starting and ending barrier pillars were based upon research and information given by A. Wilson. This indicated that both starting and ending barrier pillars should be 360 ft to eliminate any significant stress influence on the main entries from the longwall face.

The initial experience at No. 3 Mine was complicated by what is now called the "peep thru" stress effect, which occurs when the development pillars are too small, especially in weak immediate strata circumstances. Yield/stable/yield pillar developments eliminated the "peep thru" stress effect, but the 360-ft starting and ending design parameter is still used generally. There are theoretical and practical reasons to believe that this size can be reduced especially when the yield/stable/yield development system is utilized.

Trial-and-error reductions of starting pillars are now being tried at the end of a sequence of panels where the bleeder roads protected by the barrier pillars will be utilized for only a short time.

It has also been generally observed that the condition of mains and submains is worse than the condition of bleeder roads when protected by the same size barrier pillars. Further investigation of this is also necessary.

FUTURE DIRECTION

It is always interesting to look into the future to define one's goals if only to be able to measure one's future success or failure. The Strata Control Department at Jim Walter Resources has goals with respect to design of workings and they, for the most part, have been determined by past experience. The goals are:

1. To clarify the starting and finishing barrier pillar size by trial-and-error monitoring of smaller pillars and by computer simulation of pillar designs programmed by tailgate observations and measurements.

2. To confirm the reinforcing effects of primary and supplemental bolting as well as wooden and fiber crib support by real-time monitoring techniques. This could require a change of primary bolt patterns and density with a consequential reduction in supplemental support costs.

3. To confirm the destructive effect of in situ horizontal stress on roadway entries and the practical application of such confirmation.

4. To investigate the horizontal strata movement in the Blue Creek Coal Seam by in situ horizontal/vertical stresses and vertical redistributed stress, and to investigate the effect of reinforcing the longwall panel rib sides.

5. To investigate the limiting effect of the spanning strength of the main roof of the Blue Creek Seam in the yield pillar entries.

6. To investigate both theoretically and practically the two-entry yield pillar, longwall development.

REFERENCES

1. Carr, F., and A. H. Wilson. A New Approach to the Design of Multi-Entry Developments for Retreat Longwall Mining. First Int. Conf. on Stability in Underground Min., Morgantown, WV, 1982, pp. 2-21.

2. Carr, F., E. Martin, and B. Gardner. How To Eliminate Roof and Floor Failures With Yield Pillars. Coal Min., Dec. 1984, pp. 62-70.

3. Gauna, M., K. R. Price, and E. Martin. Yield Pillar Usage in Longwall Mining at Depth, No. 4 Mine, Brookwood, Alabama. 26th U. S. Symposium on Rock Mechanics, June 1985, pp. 695-702.

4. Hendon, G. W. and E. Martin. Longwall Gate Roads Theory, Design, and Results at Jim Walter Resources. Proceedings of Longwall USA Conference, Pittsburgh, PA, 1989, pp. 209-229.

5. Martin, E., and F. Carr. Control of Floor Heave in Mines. Second Int. Conf. on Stability in Underground Min., Morgantown, WV, 1983, pp. 13-33.

6. Martin, E., S. Stehney, J. Gambrell, M. Gauna, N. Bowne, and R. Southerland. Yield Pillar Applications—Impact on Strata Control and Coal Production. Fourth Conf. on Ground Control in Min., July 22-24, Morgantown, WV, 1985.

7. Martin, E., F. Carr, and G. Hendon. Strata Control Advances at Jim Walter Resources, Mining Division. 7th Int. Conf. on Ground Control in Min., Morgantown, WV, 1988, pp. 68-69.

8. Serata, S., F. Carr, and E. Martin. Stress Control Method Applied to Stabilization of Underground Coal Mine Openings. 25th U. S. Symposium on Rock Mechanics, Rapid City, SD, June 1984.

9. Wilson, A. H. The Effect of Yield Zones on the Control of Ground. Sixth Int. Strata Control Conf., Sept. 1977, pp. 52-93.

COAL PILLAR DESIGN FOR LONGWALLS UNDER THE OCEAN

By D. J. Forrester,[1] D. A. Payne,[2] and J. Kochhar[3]

INTRODUCTION

Coal pillar design in longwall mining must balance the need to ensure roadway stability with economic extraction of reserves. In particular, the design must accommodate the effects of stress redistribution providing stability not only during roadway formation but also by the extraction of longwall panels.

There are four types of pillars usually involved, as illustrated in figure 1, namely:

- Pillars between main access roadways;
- Pillars between access roadways and a longwall panel (start/stop pillars);
- Pillars between adjacent longwalls (rib pillars);
- Boundary pillars between adjacent mines.

This paper outlines the approach of the Cape Breton Development Corp. (CBDC), Nova Scotia, Canada, to meeting the challenges of designing pillars in modern longwall coal mining under the North Atlantic Ocean.

In addition to complying with regulatory requirements, other influences must be considered, such as:

- Protection from interaction effect of working other seams;
- Protection of the seabed by maintaining strata mass integrity.

After discussing the mainly empirical, current practices in pillar design, two longer-term strategies are discussed: (1) pillar reduction (smaller sizes), where appropriate, and (2) elimination of rib pillars completely, where possible. A key feature in developing these strategies is an innovative research and development program run jointly by CBDC and CANMET's Cape Breton Coal Research Laboratory (CBCRL). Several projects are summarized involving development of appropriate geotechnical monitoring and numerical modeling procedures.

BACKGROUND

The remaining economical reserves within the Sydney Coalfield mainly lie far from shore under the North Atlantic Ocean. Historically, as reserves under land were exhausted, workings extended out under the ocean. CBDC currently operates three underground coal mines using state-of-the-art longwall methods and producing approximately 3.5 million metric tons per annum salable coal. Colliery surface facilities are located on seam outcrops not far from the cliffs above the seashore. Main access roadways follow the seams, sloping down under the ocean at gradients up to 30%. Longwalling usually commences when solid cover exceeds 500 ft.

The Phalen Colliery is located in the Phalen Seam approximately 450 ft directly below Lingan Colliery in the Harbour Seam forming the second seam workings (fig. 2), whereas Prince is a first-seam working. Prince Colliery is located in the Hub Seam about 20 miles to the west. Current production features are listed in table 1.

Table 1.—Current production features

	Height, in	Panel width, ft	Panel length, ft	Metric tons/ Shift R.O.M.
Lingan Colliery:				
12E advancing wall . .	70	718	9,350	800
Prince Colliery:				
10W retreating wall . .	92	470	8,225	2,500
Phalen Colliery:				
4E retreating wall . . .	100	705	7,314	3,500

[1]Group leader.

[2]Strata mechanics engineer.

Cape Breton Coal Research Laboratory; Canada Centre for Mineral and Energy Technology (CANMET); Energy, Mines and Resources; Sydney, Nova Scotia, Canada.

[3]Chief planning engineer. Cape Breton Development Corp., Sydney, Nova Scotia, Canada.

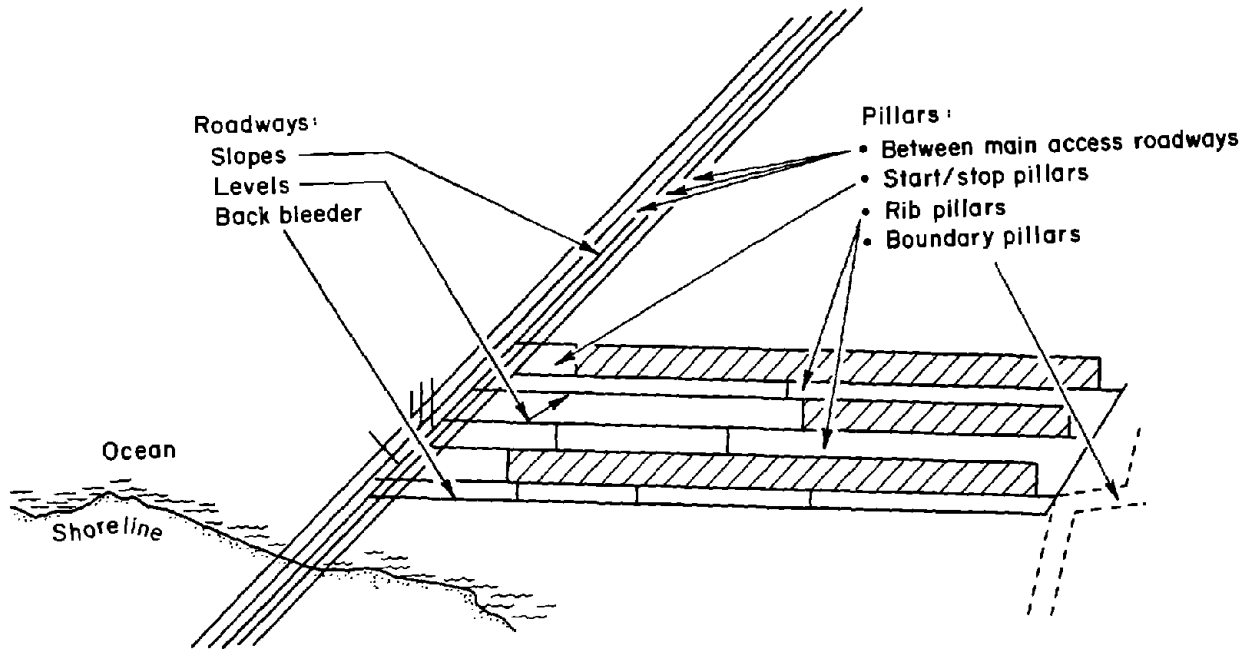

Figure 1.—Schematic mine plan: definition of types of pillars and roadways.

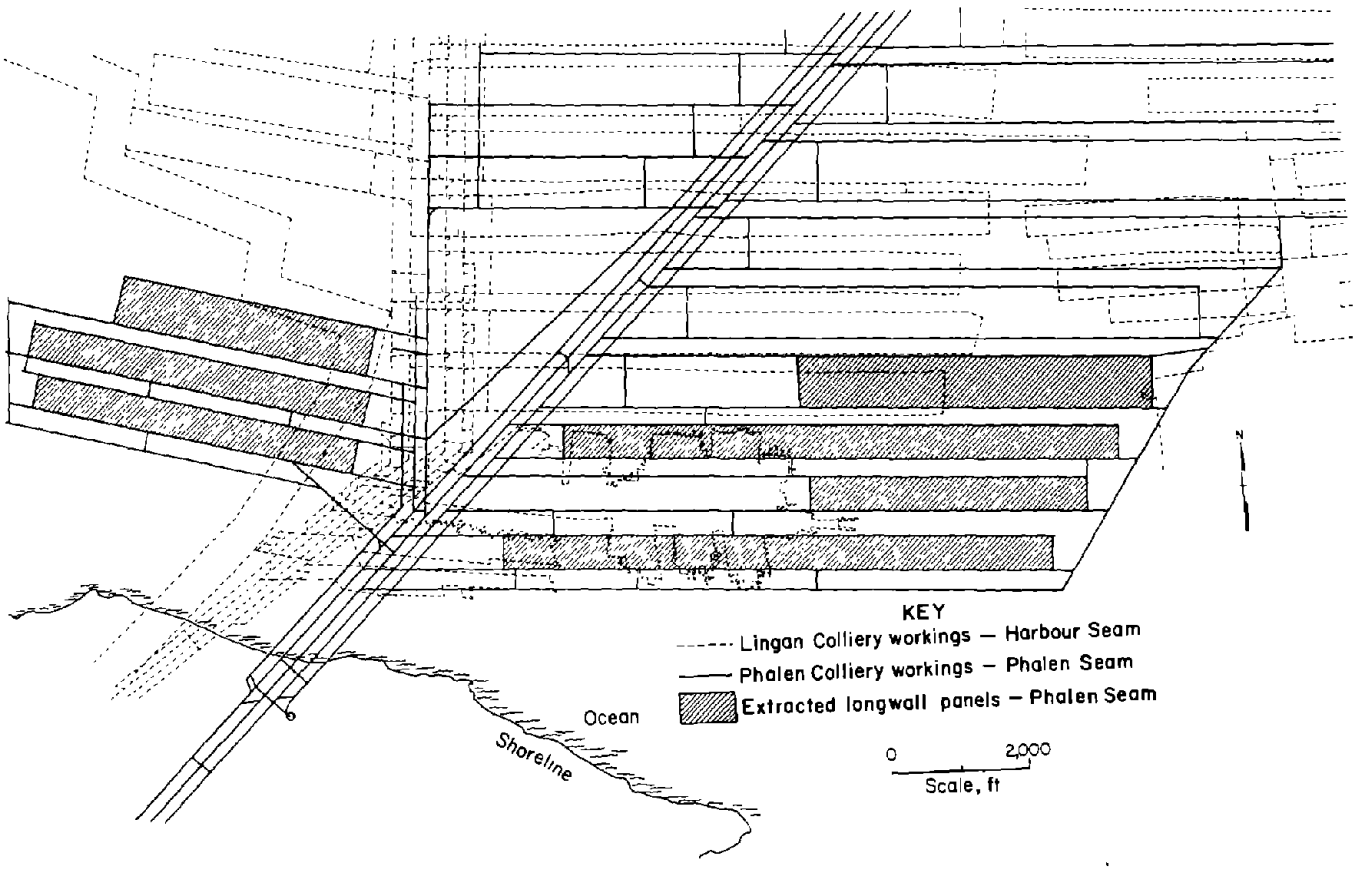

Figure 2.—Lingan and Phalen Collieries—superimposed mine plan.

For reference, the current production record is held by 4E wall at 5,618 mt in one 8-h shift.

CBDC has traditionally followed European mining practices adopting single-entry longwall methods usually supported by steel arch or rectangular supports. Seabed protection requirements have until now dictated a panel and pillar layout for modern heavy-duty mechanized longwalls. Relentless commercial pressures have led CBDC to adopt state-of-the-art technologies whenever possible, such as an electric shearer, 2/550-mt supports, etc. The best of ongoing technical developments have been examined, such as roof bolting, use of continuous miners, single-roadway shortwalls, yield pillars, etc. The first two of these have recently been introduced at Phalen Colliery. Such continual improvements are enabling CBDC to successfully compete in the international market.

PILLAR DESIGN

Historically, a variety of mining methods have been adopted in the Sydney Coalfield. These have included room-and-pillar, depillaring, advance and retreat longwalls (early mechanized), and pillarless shortwall panels. Significant experience with pillar design was developed over the last century, through extensive workings in up to four successive seams. During the 1960's and 1970's, however, as modern fully mechanized longwalls evolved utilizing shearer, panline, and powered support technologies, production rates increased enormously. This in turn led to associated ground movements of a larger and more rapid nature. Pillar design reflected this, and all mechanized longwalls since the mid-1970's in the Sydney Coalfield have been in panel/pillar layouts.

Reviews of design methods were also made by CBDC in the mid-1970's, and proven empirical methodologies developed elsewhere were evaluated against Sydney Coalfield experience. These resulted in two empirical design methods that are still used for coal pillar design in the coalfield:

- A pillar load formula;
- A maximum cumulative tensile strain on the seabed.

These are applied within the regulatory requirements, which stipulate minimum pillar sizes and cover depths for CBDC workings under the ocean. Section 55 of the Coal Mines (CBDC) Occupational Safety and Health Regulations (1990)(*1*)[4] requires that no coal mine shall be worked below the sea bottom or below a body of water or material that may flow, except under the following conditions:

1. A solid barrier of unworked mineral of 50 m (164 ft) or more shall be left between the workings of a submarine lease and another submarine lease.
2. Subject to paragraph (c), where coal seam or stratified deposit is worked, there shall be a cover of 55 m (180 ft) or more of solid measure.
3. Where a passageway is driven, there shall be a cover of 30 m (98 ft) or more of solid measure.

[4]Italic numbers in parentheses refer to items in the list of references at the end of this paper.

PILLAR DESIGN FORMULA

The pillar design formula developed is based on ratio of extraction by area and back calculation of a maximum pillar load required to maintain stability:

$$L = \frac{s \cdot D}{1 - r} = 7{,}500 \text{ psi}$$

where, L = pillar load, psi,

s = cover loading of 1 psi per ft of solid cover,

D = depth of cover, ft,

r = ratio of extraction by area = (w/w + p),

w = panel width, ft,

and p = pillar width, ft.

This has served well since 1977, providing for roadway stability from workings in the same seam. Occasionally, however, for example at Lingan, where pillar widths have at times been less than recommended (e.g., reduced from 0.11 × depth to 0.08 × depth), roadway deformation and floor heave have increased noticeably. The original Phalen Mine design was based on Wilson's revised analytical method also giving similar sizes (*2*). Typical pillar parameters adopted in CBDC's three submarine mines are shown in table 2.

Table 2.—Typical pillar parameters

	Lingan 11E/12E, ft	Prince 9W/10W, ft	Phalen 3E/4E, ft
Water depth	130	105	75
Depth of solid cover	2,050	600	1,360
Pillar Widths:			
Main access roadways	230	70	140
Stop/Start pillars	300	300	300
Rib pillars	250	200	230
Boundary pillars	>300	—	>300

SEABED PROTECTION

The United Kingdom approach to seabed protection based on a maximum tensile strain on the seabed was evaluated against key CBDC subsea workings in the mid-1970's. A figure of 8.5 mm/m was found to be more appropriate than the United Kingdom limit of 10 mm/m. This procedure ensures strata mass integrity and the necessity of preventing ingress of seawater into the workings.

The maximum tensile strain calculations are made by using a modified National Coal Board Subsidence Engineers Handbook (*3*) approach. The formula, for strain calculations, states:

$$E_{max} = \frac{kS}{D^{max}} = \frac{k\,a\,t}{D} \leq 8.5\ \text{mm/m (total cumulative)}$$

where E_{max} = maximum tensile strain,

k = a numerical constant, taken to be 0.75,

S_{max} = maximum subsidence caused by extraction of a critical or supercritical area in a given coal seam,

D = depth of cover between the workings and seabed,

a = subsidence factor, taken to be 0.65,

and t = thickness of total extraction.

It is critical to note that 8.5 mm/m is the maximum, whether from a single longwall, adjacent walls in the same seam, or in overlying seams. The individual subsidence and strain profiles must therefore be combined (fig. 3).

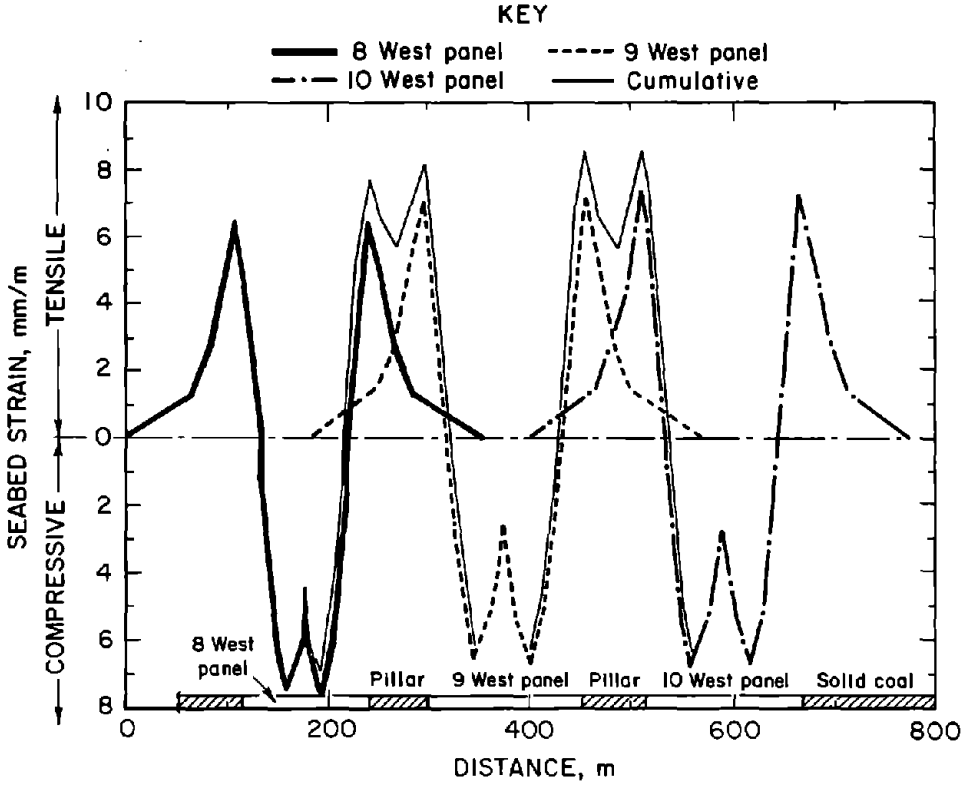

Figure 3.—Predicted seabed strains—panel and pillar layout.

PILLAR REDUCTION

While pillars are necessary, they do effectively sterilize coal reserves. The need to strive for optimum pillar size to maintain stability while minimizing sterilization continually drives coal operators to refine and improve pillar sizing methods. Two ways in which CBDC and CBCRL are doing this are outlined below.

MAIN SLOPE PROTECTION IN UPPER SEAM, FROM LOWER SEAM: STOP/START PILLARS

The Phalen west and center panels were designed with stop/start pillars large enough to prevent any disturbance in the overlying Lingan main slopes. However, the design criteria were largely based on appropriate European methodologies (predominantly surface subsidence-related, e.g., "angle of draw") owing to a lack of field data defining interseam interaction effects in the Sydney Coalfield.

To verify the design criteria, CBCRL monitored the Lingan slopes above first Phalen longwall, 1W, with no discernable interaction movements observed. Later, CBDC surveyed Lingan A above the third wall 2E stopline, with very little discernable movement observed. Thus, the original design intent was verified. However, this begged the question: How conservative is this design (i.e., how much coal is being unduly sterilized)?

To address this, CBCRL utilized horizontal borehole inclinometer and piezometer instrumentation techniques. A horizontal borehole was drilled in 1990 from Lingan 1 Slope over the underlying 2W stopline and its deformation monitored (*4*)(fig. 4).

While time-related movement is still occurring, the indication to date is that discernable strata movement ceases some 30 m away from the Lingan slopes (fig. 5). This represents apparent sterilization of coal worth several hundred thousand dollars. On this basis, the equivalent pillar on the next panel, Phalen 3W, was reduced by 20 m. A second instrumented horizontal borehole is being used now to verify that no movement will occur there in the Lingan slopes.

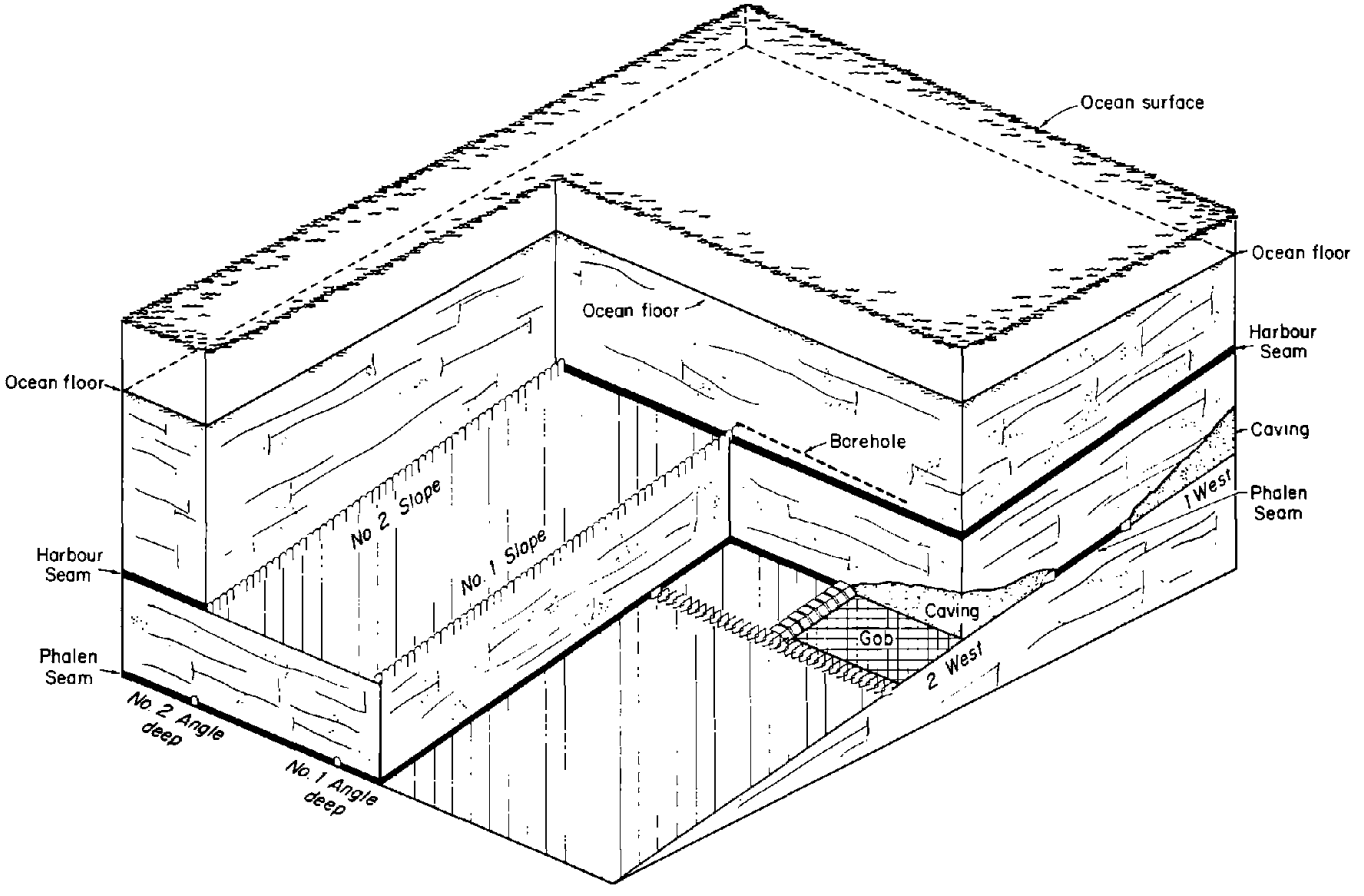

Figure 4.—Phalen 2W stopline: three-dimensional schematic of borehole.

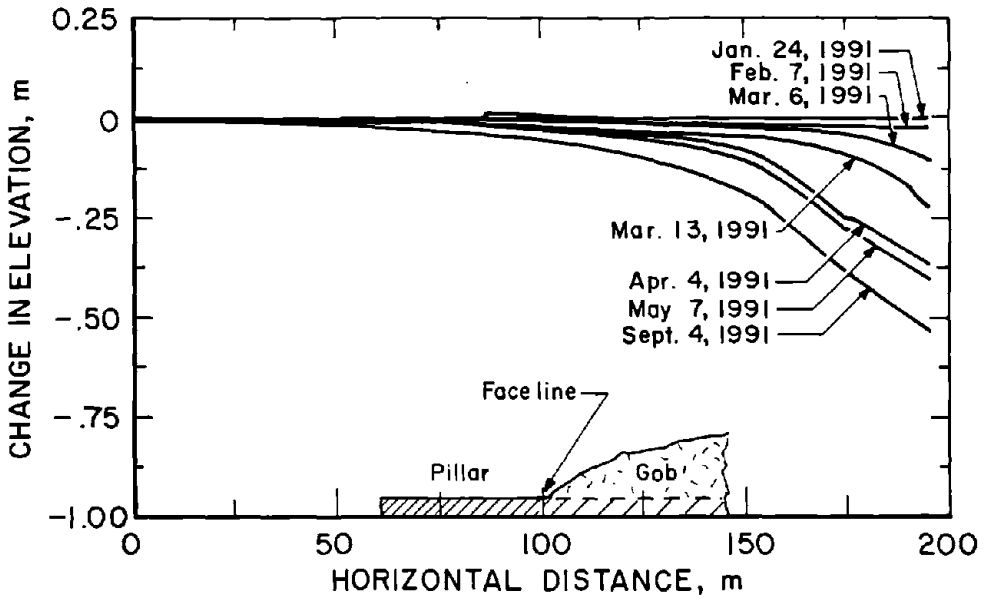

Figure 5.—Phalen 2W stopline: adjusted subsidence profiles.

SEABED PROTECTION: RIB PILLARS

While the pillar design approach outlined above accords sufficient support to the seabed, it is based on conservative interpretation of European-based empirical methodologies. Very few subsidence measurements are available over depillared workings under land in the coalfield. Thus, design verification is not possible without additional field data. The horizontal borehole program mentioned above will yield some data, but much more data are required.

CBCRL and CBDC started a long-term joint research project in 1983-84 to attempt to provide such data. This was to be accomplished by measuring seafloor subsidence directly, then producing a calibrated subsidence prediction model for more accurate seabed strain predictions.

This project is now nearing completion. Field work was done in 1987-89 (*5*), subsidence profile interpretation in 1990 (*6*) yielded six discernable seafloor subsidence profiles, and mining analysis is currently underway. The final stage will be to produce a calibrated prediction model, hopefully in late 1992. However, the data base is still severely limited, and efforts are continuing to expand it. Pillar sizes will subsequently be optimized for seabed protection.

PILLAR ELIMINATION

Prior to the introduction of modern longwall equipment, CBDC successfully deployed pillarless mining, whereby no rib pillars were left between panels (fig. 6). However, since the early 1960's, panel/pillar layouts have been adopted. These pillars not only sterilize reserves, but in retreat mining involve two costly single-entry drivages. There are great benefits potentially, in terms of resource recovery and economics of reduced development drivage, to be gained from trying to combine the old pillarless methods with current heavy-duty retreat methods. A recent review of European experience in applying pillarless mining to modern heavy-duty retreat workings revealed mixed results (*7*). Strata control aspects were found to be critical. If primary support and/or supplemental support is inadequate, then optimal support of the ground is lost. Subsequent floor heave can make mining the second panel very difficult due to crush of the common gate road (tailgate of second panel, fig. 7).

CBDC has therefore based its design approach for current effects on the successful designs in Europe. This incorporates heavy-duty primary roadway support, reinforcement of roadway support with additional roof bolts, center propping in the front abutment zone of the second wall, and packwalls behind the first wall to support the common gate during its second use.

A key factor in achieving success will be monitoring the first applications and feeding back findings to optimize both roadway and packwall designs. CBCRL will be closely involved in this work, designing and installing geotechnical monitoring for both roadway and packwall support performance throughout.

CBCRL has also been actively involved in researching the use of anhydrite packwalls to replace wood. Monitoring of initial trials, laboratory-scale testing, and a joint numerical modeling exercise with the U.S. Bureau of Mines (*8*) are currently underway. The modeling exercise is pursuing a threefold stepwise approach using the MULSIM boundary element, ADINA finite element, and USBMDE discrete element models. As mining trials unfold, field data are obtained to set up and later to refine modeling results. While such research and development is often long-term, CBDC is proceeding, with initial trials of pillarless retreat at Lingan with 13E wall scheduled to start in May 1992. Experience gained here will be fed back into the main trials with Phalen center panels scheduled for late 1992.

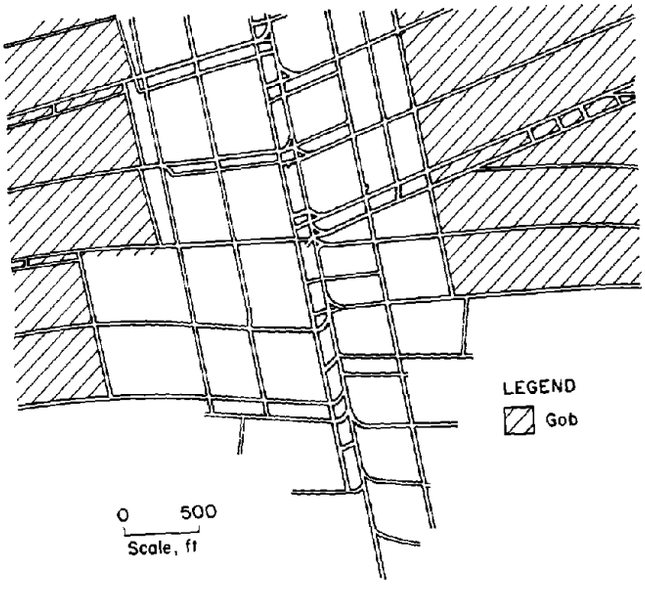

Figure 6.—Pillarless layout: No. 12 Colliery.

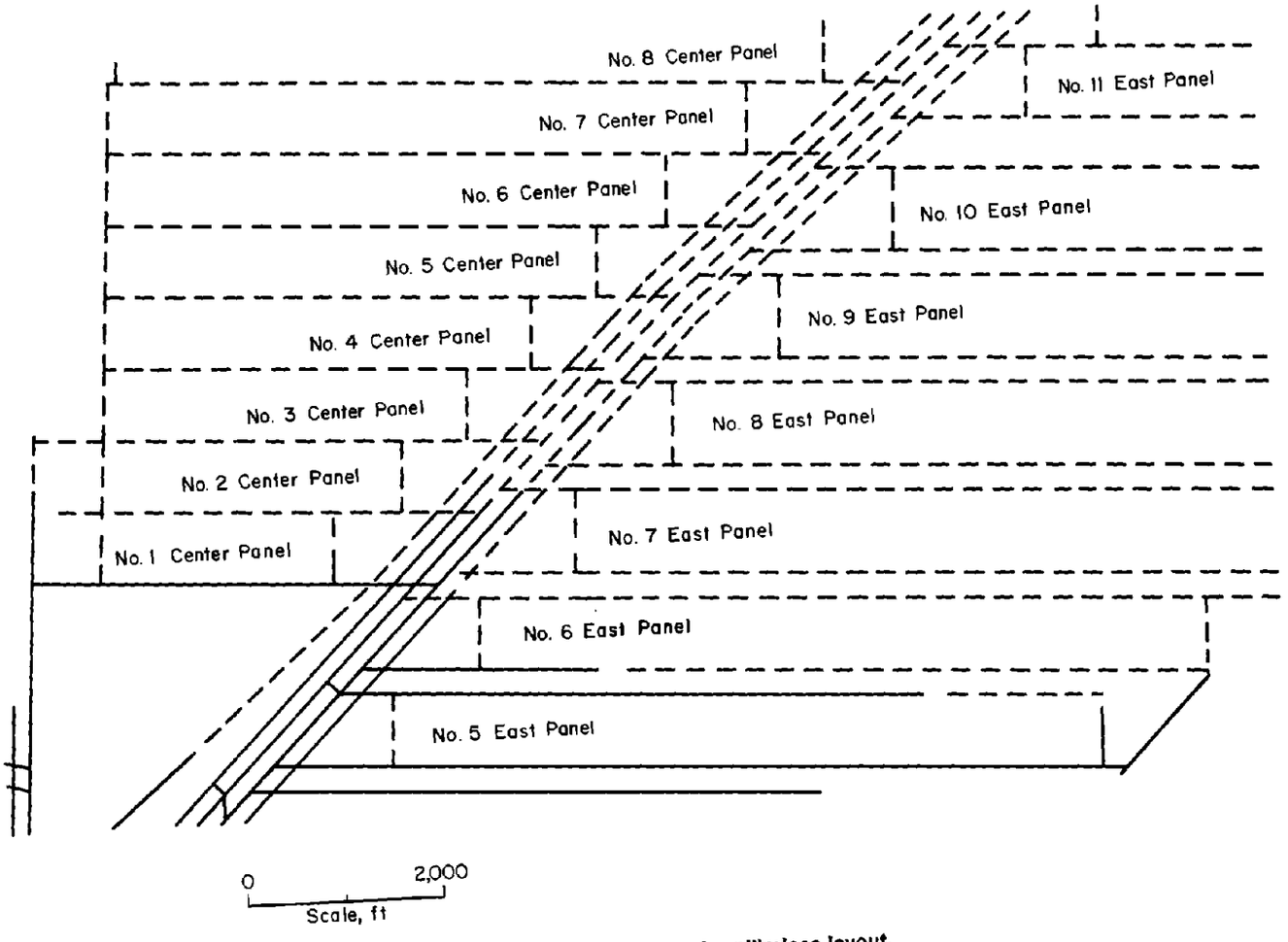

Figure 7.—Phalen center panels—pillarless layout.

CONCLUSIONS

Coal pillars in modern longwall mining under the ocean are essential but costly in terms of sterilized coal and additional development drivage. Traditional empirically based and pragmatic design approaches have largely provided sufficient and stable support. Relentless commercial pressures, however, are dictating that the successful operators are the most innovative ones. CBDC is not only using state-of-the-art technologies to improve longwall production and development performance, but is also devising long-term strategies to safely reduce and even eliminate some coal pillars whenever appropriate. Novel and innovative research and development projects have been carried out jointly by CBDC and CANMET to direct the development and implementation of these strategies. The critical trials needed to demonstrate the success of modern pillarless retreat mining will require intense and comprehensive monitoring. These needs will again be met by joint research and development activities. These modifications to traditional pillar design methods will significantly contribute to CBDC's continuing efforts to compete safely and successfully in the international coal industry.

REFERENCES

1. Coal Mines (CBDC) Occupational Safety and Health Regulations (1990).

2. Wilson, A. H. The Stability of Underground Workings in the Soft Rocks of the Coal Measures. International Journal of Mining Engineering, 1983, 1, 91-187.

3. National Coal Board Subsidence Engineers Handbook (1975).

4. Forrester, D. J., W. D. Gallant, and D. A. Payne. Determination of the Stopline Subsidence Profile of Phalen 2 West Panel From Within a Near Horizontal Borehole Over the Panel Stopline. Divisional Report CRL 91-39 (OP,J), 10th International Conference on Ground Control in Mining, June 10-12, 1991.

5. Aston, T. R. C., W. D. Gallant, A. Lapierre, and J. M. Stewart. Pre-Mining Seafloor Topography Determination Over the Phalen Mine Workings, Sydney Coalfield, Nova Scotia. Divisional Report CRL 89-1 (OP,J), Mining Science and Technology Journal.

6. Seabed Subsidence Profiles Over the Phalen Colliery Derived From Analysis of Seafloor Topography Data. McGregor Geoscience Ltd., CANMET/DSS Contract Report 33SQ.23440-0-9172, Mar. 1991.

7. Haslett, G. A. Longwall Retreat Mining - Its Practice With the Re-use of Single Gate Roads as Dual Life Gate Roads: Salvation or Suicide? Divisional Report CRL 91-47(CF), Sept. 1991.

8. Kripakov, N. Interim Report on Joint CBDC/USBM Numerical Modeling of Pillarless Mining. U.S. Bureau of Mines, Denver Research Center. In preparation, Feb. 1992.

A PILLAR DESIGN APPROACH

By Winton J. Gale[1]

INTRODUCTION

Coal mine pillar design formulas available to mine planners and geotechnical engineers in Australia are based on relationships determined from studies conducted abroad. These studies are notably those of Wilson (*1-2*)[2] undertaken in the United Kingdom, Salamon and Munro (*3*) undertaken on a statistical analysis of slender pillar mining operations in South Africa, and other design reviews provided [e.g., Hustrulid (*4*)]. The relationships determined from those workers have provided a sound basis for pillar design in their area of study and for the mining geometries used.

The application of such methods to Australian conditions has typically been problematical as other factors, either not relevant to or not addressed within those studies, may relate to the mining or geological conditions encountered. For this reason, experience and underground monitoring of pillar behavior have played a large role in pillar design considerations in Australia.

The potential range in geological conditions and the time required to obtain a comprehensive data base of pillar behavior relevant to mining at 400->600 m have required a design method that can account for geology and mine geometry by simulating the deformation mechanisms and stress redistributions within the coal and surrounding ground under various loading conditions.

During the past 6 to 8 years, Strata Control Technology Pty. Ltd. (SCT), New South Wales, Australia, has undertaken a review of pillar design methods and coal strength properties, together with field monitoring, of pillar behavior. This work and that of other workers have clearly shown that pillar strength and deformation characteristics are extremely sensitive to the in situ behavior of the rock surrounding the coal and mine roadway. The results of the study suggest that the mechanics of the deformation process, both within and about the pillar, must be addressed by any pillar design method applied to coal mining operations.

SCT has undertaken an assessment of such an approach, utilizing computational modeling, the deformational characteristics of roof rock, coal, floor rock together with their interfaces, interacting as a system under various loading conditions. This approach has been found to provide excellent correlation with existing monitored data. In situ monitoring of pillar loading and pillar strength, together with measurement of stress profiles above pillars, has been used to build a data base to assess the application of such methodology. This research is being currently undertaken by SCT within an Australian Mineral Industries Research Association Program.

METHODOLOGY

The approach undertaken has been fourfold:

1. Characterizing of elastic and postfailure strength properties of coals, host materials, and bedding planes.

2. Monitoring the stress redistributions and strength characteristics of small pillars (width-to-height ratio (W/H) <5) to assess the in situ coal strength in an effectively unconfined state and the appropriate "strength reduction characteristics" that relate to laboratory properties.

3. Defining a computer model geometry and loading to simulate the anticipated response of the coal and surrounding materials.

4. Obtaining field data of stress distributions above pillars having W/H >5 to assess results and provide validation. The validation and assessment have utilized:

   (a) monitoring of stress distributions above longwall chain pillars,
   (b) stress measurement over development pillars,

[1]Managing director, Strata Control Technology Pty. Ltd., Wollongong, New South Wales, Australia.

[2]Italic numbers in parentheses refer to items in the list of references at the end of this paper.

(c) monitoring coal and surrounding strata deformation, where possible,
(d) local experience of performance, and
(e) subsidence characteristics above extracted longwall panels.

RESULTS AND ISSUES OF INTEREST

In Situ Bulk Unconfined Strength of Coal

Monitoring of the peak strength of pillars having W/H ranging from approximately 3 to 5.4 has been undertaken in a number of mines. The method used has been to install stress cells above pillars prior to extraction operations and to monitor the stress distributions as the extraction process "loads" the pillars. Stress cells are placed either in advance development or from development roadways prior to longwall extraction.

An example provided in figure 1 details the stress history above the pillar.

The results of the sites for W/H <4 have allowed a good approximation of the "in situ cube strength" of the coals studied using available pillar strength formulas appropriate to that W/H range.

The strength relationship incorporating laboratory samples of various sizes is presented in figure 2, together with the defined in situ cube strength.

It has been found that the in situ results have provided good internal consistency and allow an adequate resolution of the effective bulk in situ unconfined compressive strength (UCS) of the coals studied.

Computer Modeling of Pillar Strength Characteristics

Computer modeling of the coal, rock, and associated boundaries has been undertaken to assess:

1. The interrelationships and effects of "host materials" to the coal. The modeling is used as a research tool to provide an understanding of the mechanisms involved and the implications of various geological situations in which pillars may be formed. The code used is FLAC (Cundall and Board) (*5*) and a two-dimensional section is studied. The implications for various rectangular-shaped pillars are assessed using available methods.

2. The effect of W/H on the strength of coal pillars via the development of confining stress in the "pillar core."

An initial application of modeling to the Bulli Seam for various W/H ratios is presented in figure 3. These results

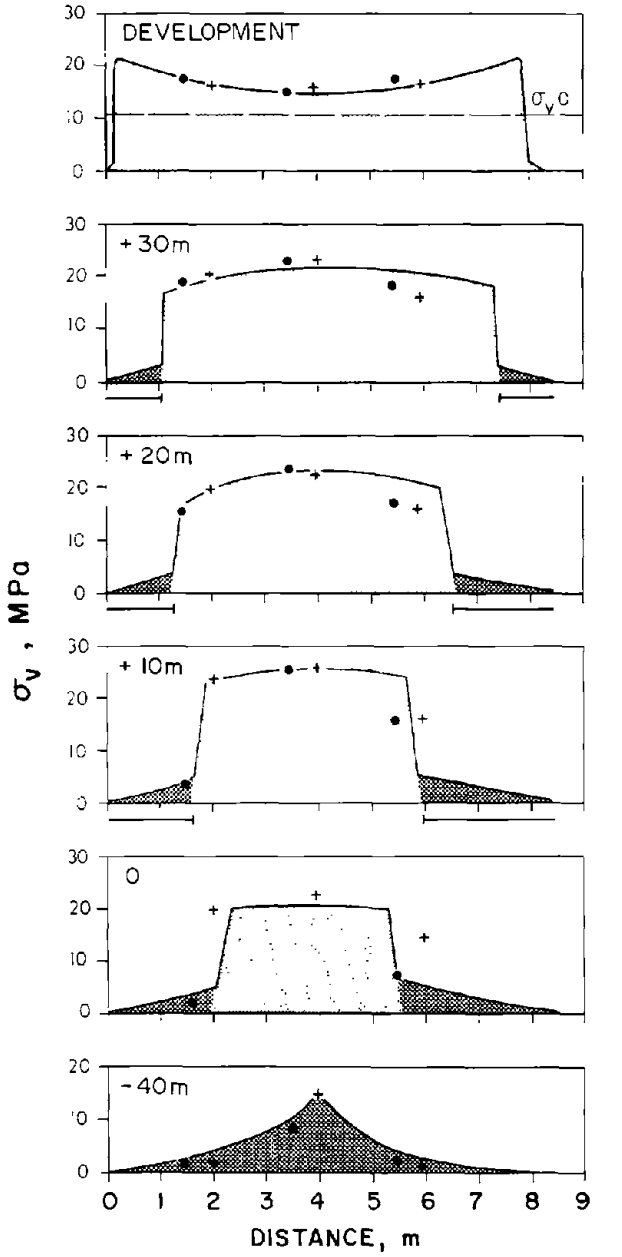

Figure 1.—Example of small pillar monitoring studies indicating pillar stress history.

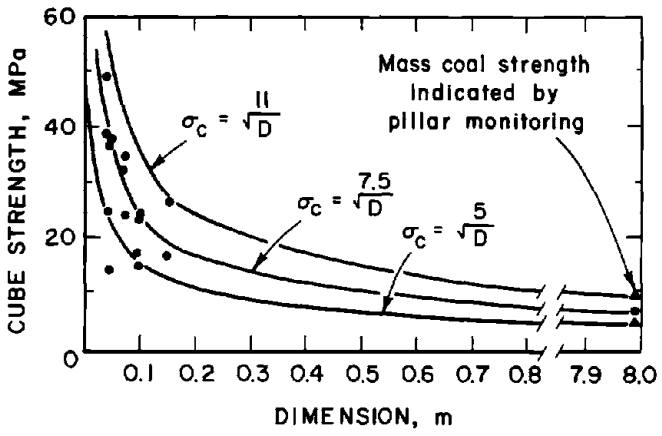

Figure 2.—Size effect determined from in situ monitoring.

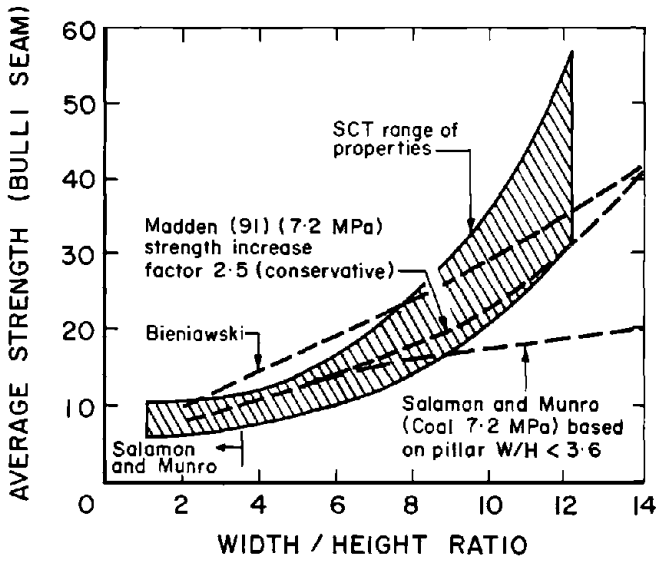

Figure 3.—Comparison of pillar strength relationships.

are compared with other formulas forwarded (e.g., Bieniawski, Salamon/Madden). A range of coal strength properties is used to provide the strength band. The boundary conditions for this example are relatively strong and relate to typically competent roof and floor strata. The results provided indicate a workable correlation in the areas where the formulas have been verified (e.g., W/H <5/6). The results defined in the modeling indicate that for W/H greater than approximately 5-6, confinement in the pillar is developed and the coal strength within the pillar is significantly increased. These results are in general agreement with those proposed by Carr and Wilson (*6*) and recently reported by Madden (*7*) to account for the development of confining pressure.

The advantage presented by modeling is that the factors that contribute to the strength increase into the pillar can be defined in terms of geotechnical properties of the rock/coal that relate to that particular site.

The results obtained have highlighted the effect of host material behavior on the coal pillar performance. The ability of the coal pillar to develop confinement, and hence additional strength above the in situ bulk strength, is dependent on the interface characteristics and the deformation occurring in the roof and floor of the seam. It has become apparent that the behavior of the host materials surrounding the coal has a much greater impact on pillar behavior than the variation in coal strength between seams. This is most relevant for W/H ratios above approximately 6.

Computer modeling is also being utilized to assess the potential deformation mechanisms that may relate to weak floors and their implications to pillar behavior. An example of deformation within a floor section is provided in figure 4. This figure represents a parametric example of the potential effect of floor strength under a pillar. The example indicates that in the case of the weaker floor, failure and displacement of the floor under the pillar may significantly modify the confinement distribution within the pillar and the ultimate strength characteristics achievable by the pillar. This example indicates that the occurrence of floor heave causes a major redistribution in stress within the pillar and leads to a strength adjustment. The implications of such deformation is dependent upon the material properties at the site. The use of this approach in a study of pillar strength characteristics within a coal seam bounded by weak roof and floor is presented in detail by Cassie and Mills (*8*).

Field Monitoring of Chain Pillar Loading

The aim of chain pillar monitoring is to assess the strength characteristics of pillars having a W/H >7 and to define the loading conditions of such pillars. Monitoring of longwall chain pillar stress redistributions has been undertaken for some time, and it is now being complemented with specific site studies for pillar strength analysis. Three-dimensional Commonwealth Scientific and Industrial Research Organization (CSIRO) stress cells are used to monitor stress redistributions. It has been found necessary to use a three-dimensional tool to assess the interactions of horizontal and vertical stresses, together with an appreciation of the confinement provided to the rock immediately above the pillar. Stress cells are placed at various heights above the coal, depending upon suitable strata and the data requirement. Typically, stress cells are placed less than 1.5 m above the coal when vertical stress distributions are being monitored.

An example is presented in figures 5 and 6 for a chain pillar extracted on both sides in goaf. These figures indicate the vertical stress distribution and horizontal stress redistribution occurring approximately 1.5 m above the coal during longwall extraction operations.

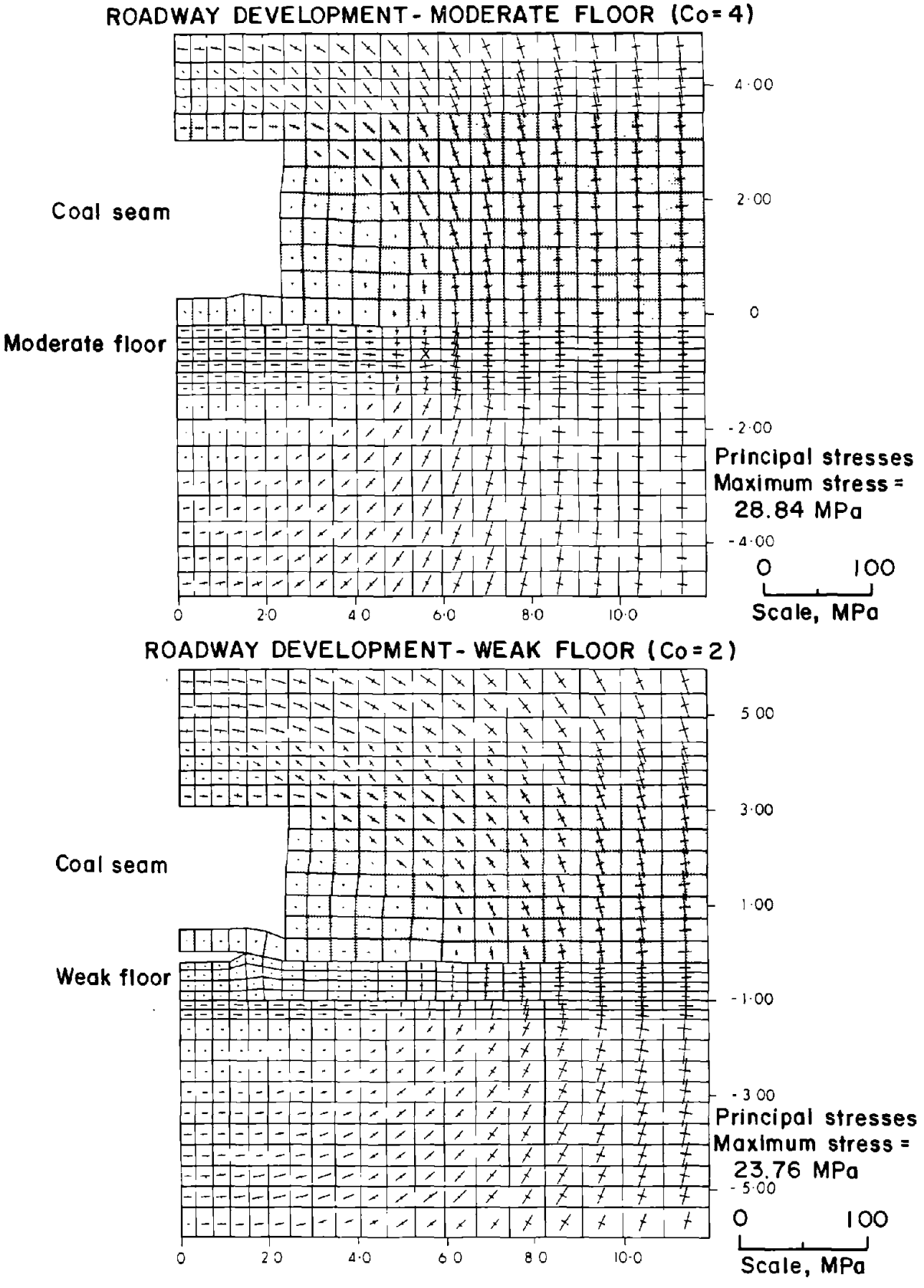

Figure 4.—Effect of floor strength on stress distribution in pillars.

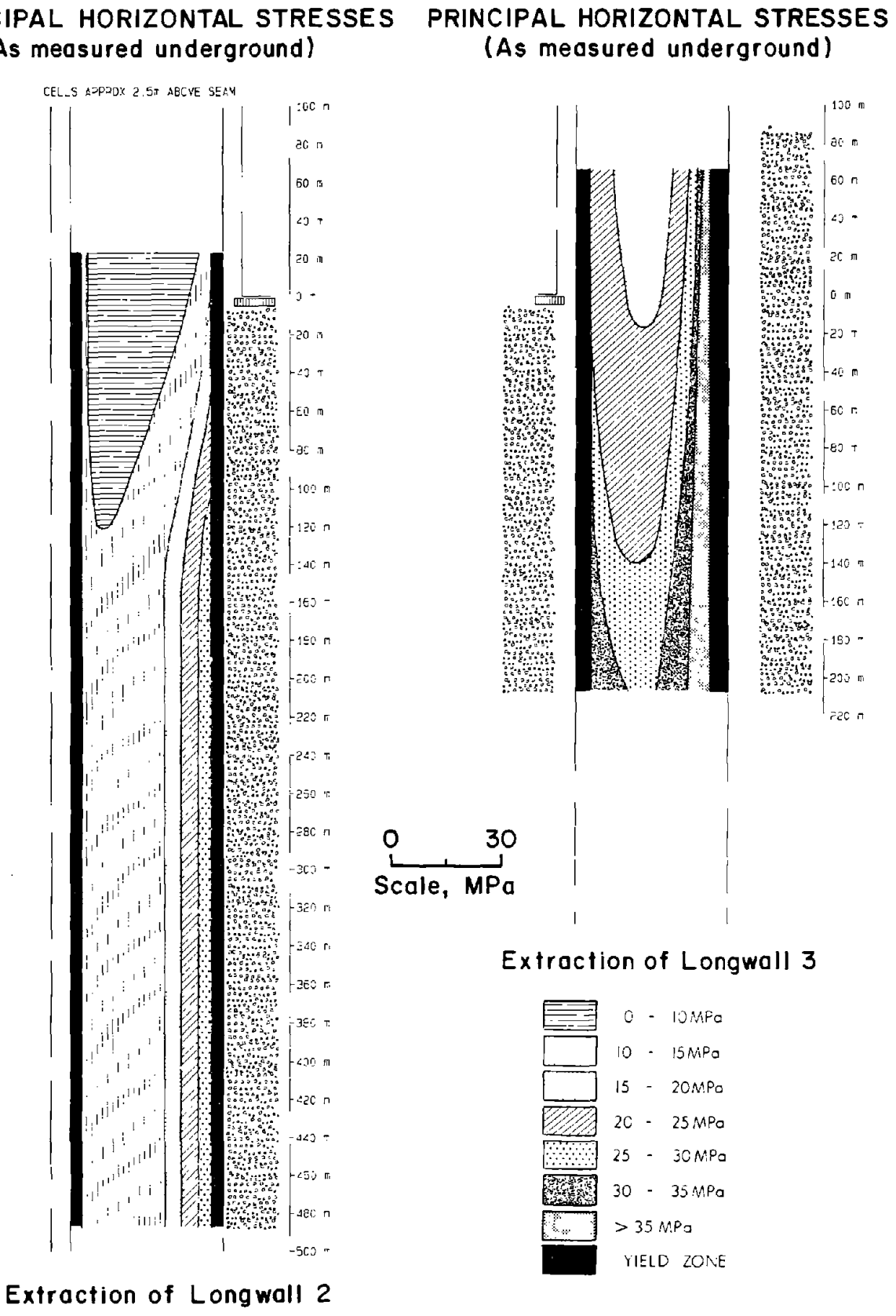

Figure 5.—Monitored vertical stress distribution immediately above a chain pillar during extraction.

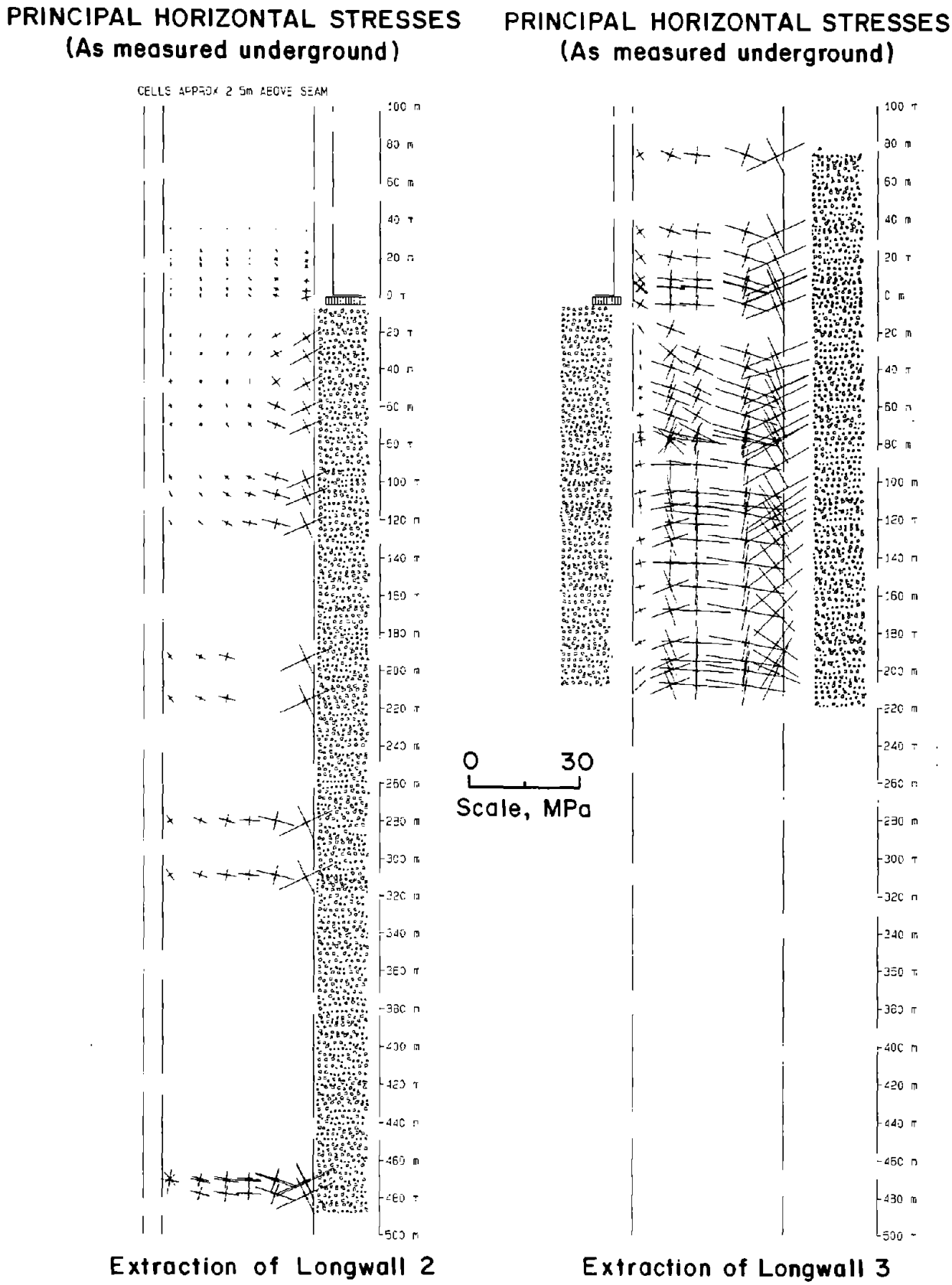

Figure 6.—Monitored horizontal stress distribution immediately above a chain pillar during extraction.

The results of such studies are also targeted to provide an estimation of the loading placed on pillars and that carried by goaf.

Coal Pillar Strength Characteristics

The results of current field monitoring studies, outlined above, are presented in figure 7. This represents the average strength determined for a two-dimensional cross section through rectangular pillars. Chain pillars in Australia are typically 80 to 100 m long, and a modification must be made to this information to correlate the results to square pillar strength estimates.

These results indicate that the strength of pillars display a gradual increase in strength up to a W/H of 6. Pillars having a W/H ratio greater than 6 display a rapid strength increase relative to W/H ratio. The increase in strength relative to W/H ratio is considered to reflect the confinement distribution developed within the pillar. It is considered that the boundary conditions and strength characteristics of the host strata will influence the pillar strength ultimately attained in any one geological environment (or minesite).

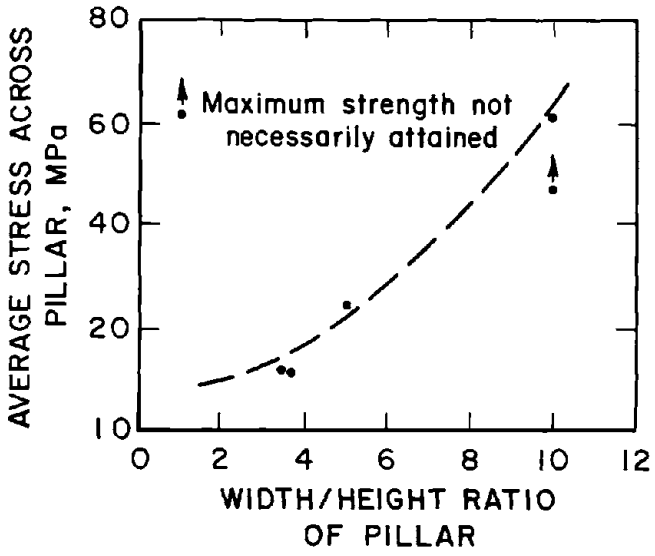

Figure 7.—Current pillar strength data obtained from monitoring studies.

CONCLUSIONS

This paper is presented to provide a general overview of research being conducted by SCT to assess pillar design guidelines and some of the results obtained.

Pillar design guidelines being researched are based on:

1. A definition of the loading conditions and mine geometry for which pillars are to be designed.
2. A definition of the in situ strength of the coal based on both underground monitoring of appropriately sized coal pillars and laboratory strength characteristics.
3. A design approach utilizing computational methods that accurately model the strength, confining conditions, and deformation occurring in the roof, floor, and coal seam.
4. Validation by monitoring stress distributions about pillars during mining operations.

The results to date indicate that:

1. The in situ strength of coal can be quantified from mine monitoring studies.
2. Accepted laboratory strength reduction relationships have been found to be consistent with the field strength of coal obtained.
3. Computer modeling is providing a good correlation with traditional methods, but has the advantage of being applied to a wider range of geological environments and stress regimes.
4. Monitoring of chain pillar loading is being undertaken to successfully monitor the three-dimensional stress redistributions occurring immediately above the coal seam. The data are forming a data base to verify computer simulation studies.
5. The initial results from field pillar monitoring indicate that strength characteristics rapidly increase in pillars having a W/H ratio greater than approximately 6. These field monitoring results display a good correlation with the computer modeling studies.

REFERENCES

1. Wilson, A. H. Research Into the Determination of Pillar Size. The Mining Engineer, 131, pt. 9, pp. 409, 417, pt. 2, 1972.

2. ____. The Stability of Underground Workings. Unpubl. Ph.D. Thesis, Univ. of Nottingham, 1980.

3. Salamon, M. D. G., and A. H. Munro. A Study of the Strength of Coal Pillars. J. S. Afr. Inst. Min. Detall., Sept. 1967, pp. 56, 67.

4. Hustrulid, W. A. A Review of Coal Pillar Formulas. Rock. Mech., 8, pp. 115-145, 1976.

5. Cundall, P., and M. Board. A Microcomputer Program for Modelling Large Strain and Plasticity Problems. In. Balkema Rotterdam, ISBN 906191809, 1988.

6. Carr, F., and A. H. Wilson. A New Approach to the Design of Multi-Entry Developments for Retreat Longwall Mining. Proc. 2nd Conf. on Ground Control in Mining. WV Univ., Morgantown, WV, 1982, pp. 1-21.

7. Madden, B. J. A Reassessment of Coal Pillar Design. J. S. Afr. Inst. Min. Metall., v. 91, No. 1, 1991, pp. 27-37.

8. Cassie, J. W., and K. W. Mills. Study of Pillar Behavior in the Parkgate Seam at Asfordby Colliery. Paper in these proceedings.

A REVIEW OF COAL PILLAR DESIGN IN AUSTRALIA

By J. Galvin[1]

INTRODUCTION

Coal was first discovered in Australia near Newcastle, New South Wales (NSW), in 1791 by a runaway convict named William Bryant. This was 3 years after the first settlement of the colony. William Bryant, his wife Mary, two children, and seven other convicts made good their escape to the East Indies, so news of the discovery did not become public until 1796.

The first coal mining ventures commenced in the colony in 1801 at Newcastle, although these were very fragmented. In 1804, however, a permanent penal settlement was established in the town to hold 34 of the "more desperate, dangerous and active" Irish convicts who had taken part in a rebellion against the English seated government. These convicts were put to work in the coal mines, which led to the first organized coal mining operations in the colony.

Coal mining in Australia has continued unabated since 1804 and today is the largest earner of foreign exchange for the country. Australia's total raw annual production is 197 mt, of which underground production comprises 60 mt. Almost all of this production occurs in NSW and Queensland, with longwall mining accounting for 45 pct of underground production. In NSW, most of the underground production comes from mines located in or adjacent to urban development or sensitive water catchment areas and from mines that work beneath tidal waters (lakes and ocean) and water storage dams.

Minimum pillar design standards are incorporated in NSW state government legislation. The first standards appeared in the NSW Coal Mines Regulation Act (CMRA) (1912) and these remained essentially unchanged until the review of the NSW CMRA in 1982. During the 1970's, specific guidelines were also developed for mining under tidal waters and stored waters in NSW. These were supplementary to statutory requirements and were not incorporated in legislation.

The pillar design standards incorporated in the NSW CMRA (1982) failed to recognize the significant advances of the last 50 years in understanding pillar behavior mechanisms and in applying these to design criteria. This is surprising, especially given the critical role that pillar design plays in safety and in strata control in sensitive mining environments.

There are no statutory requirements or guidelines relating to pillar design in Queensland. Pillar design is at the discretion of the mine manager.

It is encouraging that deficiencies in the local pillar design knowledge base have been recognized in recent years and that attention is now being focused on developing and implementing a coordinated approach to mine design based on up-to-date rock mechanics principles.

STATUTORY PILLAR DESIGN TO 1982

The predominant pillar design system applied in the Newcastle coalfield during the 1800's was to make roadways as wide as the roof conditions would allow, leaving substantial pillars of coal for support. This bord-and-pillar method of mining worked well in thick seams and at shallow depths. The system tended to become standardized and based on either 6- or -8-yd-wide bords and 4-yd-wide pillars cut through every 35 yd. In the Southern Coalfield of NSW, a variation of this system was utilized whereby bords were driven 10 yd wide and were separated by 55-yd-wide pillars, cut through every 100 yd. In both coalfields, these pillars were subsequently extracted.

By the 1890's, these systems of mining had given way to longwall mining in many other parts of the world. However, the methods persisted in Australia, with mining dimensions remaining fairly constant even though the depth of mining had increased significantly during the 1800's. By the close of the century, there were many problems with pillar stability in the Newcastle mines, especially when undertaking pillar extraction. This led to the following minimum pillar sizes being incorporated in the CMRA (1912):

> "Should the pillar and stall system be adopted, the percentage of coal to be left in the pillars after the bords, headings, drives and other workings shall have

[1]Mine manager, Angus Place Colliery, New South Wales, Australia.

been constructed, shall be as follows. Where the depth from the surface does not exceed 200 feet, 50 percent; from 200 to 500 feet, 50 percent to 60 percent; from 500 to 1000 feet, 60 percent to 70 percent; from 1000 to 2000 feet, 70 percent to 80 percent."

Only minor variations were made to these criteria up until 1982. The two most significant additions that occurred in the intervening years were

1. The stipulation of a maximum bord width of 5.5 m.
2. The stipulation of minimum pillar widths for the various given depth ranges.

No basis can be found for stipulating a maximum bord width of 5.5 m, although it is commonly suggested that this bord width was suited to handloading of rail skips from either side of the rails.

The requirements of the 1912 act were modified slightly in 1974 with the introduction of the metric system in Australia. The requirements of the act immediately prior to 1982 are summarized in table 1. As a point of reference, Salamon's 1966 pillar design formula [Salamon, 1966 (*2*)][2] and Salamon's 1990 squat pillar design formula [Madden, 1990 (*1*)] have been applied to pillar dimensions throughout this paper. This does not imply that the formulas are necessarily appropriate to NSW conditions.

Salamon's 1966 formula has been used to successfully design over 1.2 million pillars in South Africa. This success has led to the formula being applied outside the range of parameters on which it was derived. In particular, the formula was based predominantly on the behavior of coal pillars having a width-to-height ratio of 5 or less. It makes no provision for the exponential increase in pillar strength due to core confinement mechanisms once width-to-height ratio exceeds about 5. Salamon extended his 1966 formula in 1990 to address this issue.

The Salamon pillar design formulas have been applied to the parameters given in table 1 to come up with a range of design safety factors. These are summarized in table 2. Table 2 highlights the significant range in safety factors that arises from applying the CMRA (1912) requirements. This is due to grouping pillar dimensions within depth ranges and failing to account for the effect of mining height on pillar strength. Table 3 records the significance of the safety factors in terms of the probability of collapse.

[2]Italic numbers in parentheses refer to items in the list of references at the end of this paper.

Table 1.—Design requirements for bord-and-pillar workings, Section 53BA, CMRA (1912), No. 37

Depth, m	Extraction (in-panel), pct		Pillar width,	Bord width,	Mining height,[1]
	Min	Max	m	m	m
Less than 60 . .	NS	50	≥8	≤5.5	≤4
60 to 150	40	50	≥11	≤5.5	≤4
150 to 300	30	40	≥17	≤5.5	≤4
300 to 600	15	30	[2]≥24	≤5.5	≤4

NS Not stipulated.
[1]Where mining height exceeds 5 m, special mining approval required.
[2]No maximum depth restriction.

Table 2.—Range in pillar safety factors based on applying Salamon's design formulas (1966, 1990) to requirements of CMRA (1912)

Depth, m	Mining height, 2 m		Mining height, 3 m		Mining height, 4 m	
	1966	1990	1966	1990	1966	1990
Less than 60	+5	+5.2	+3.8	+3.8	+3.2	+3.2
60 to 150	6.9-2.0	8.9-2.1	5.3-1.5	5.4-1.5	4.4-1.3	4.4-1.3
150 to 300	4.0-1.4	8.6-1.8	3.1-1.1	4.0-1.1	2.5-0.9	2.7-0.9
300 to 600	3.5-1.0	31.0-2.1	2.7-0.8	11.5-1.0	2.2-0.6	5.9-0.7

Table 3.—Predicted probability of stability associated with Salamon's safety factor formulas

Safety factor	*Probability of stability, pct*	*Safety factor*	*Probability of stability, pct*
0.6	0.06	1.1	72.59
0.7	0.66	1.2	87.48
0.8	7.99	1.3	95.08
0.9	25.34	1.4	98.30
1.0	50.50	1.5	99.47

STATUTORY PILLAR DESIGN AFTER 1982

Under the regulations made pursuant to the CMRA (1982), the requirements for pillar dimensions were changed to:

"The dimension in plan of a pillar shall not be less than -

(a) A distance which is equal to one-tenth of the thickness of the cover (to the surface); or,
(b) ten meters,

whichever is the greater."

The maximum width of roadways was still prescribed as 5.5 m.

These design criteria fail to recognize:

1. The influence of mining height on pillar stability.
2. The influence of pillar width-to-height ratio on pillar stability.
3. Pillar stability in multiseam workings.

The stipulation of a minimum pillar width of 10 m represents a maximum extraction of 58.4 pct. This forces mine operators to use pillar extraction techniques to achieve higher percentage extraction. There are many instances of pillar extraction operations at depths of 30 m or less. These operations fail to achieve a higher percentage extraction than that of many well-designed bord-and-pillar first workings in some other overseas countries, although they can offer support costs and productivity advantages.

Table 4 compares the current CMRA (1982) design criteria for various mining heights with both the 1966 and 1990 Salamon design formulas. If a safety factor of 1.6 is accepted as reasonable under most practical circumstances, the table highlights that the CMRA (1982) requirements are conservative for a mining height of 2 m. Down to a depth of 300 m, the requirements are very similar to those corresponding to a safety factor of 1.6 at a mining height of 3 m under Salamon's 1966 formula. The CMRA (1982) requirement may result in an underdesigned pillar when applied to a mining height of 4 m at depths of less than 350 m.

Table 4 also highlights the increase in pillar strength based on Salamon's 1990 formula as pillar width-to-height ratio increases above 5. From the author's experience, coal pillars in normal geological environments are, indeed, capable of supporting any load imposed upon them once width-to-height ratio exceeds 10. However, care must be exercised with this approach, especially at depths exceeding about 350 m. Under these circumstances, while pillars may not fail, operators can be faced with the following problems due to the extremely high pillar loads

1. Bearing failure of floor or roof strata.
2. Excessive rib spall which increases effective roof and floor spans. The potential for roof and floor instability increases exponentially with increase in span.
3. High horizontal stresses induced at pillar, roof, and floor contact surfaces which may exacerbate roof and floor stability problems.

Table 4.— Range in pillar safety factors based on applying Salamon's design formulas (1966, 1990) to requirements of CMRA (1982)

Depth, m	Pillar width, m	Safety factor					
		Mining height, 2 m		Mining height, 3 m		Mining height, 4 m	
		1966	1990	1966	1990	1966	1990
50	10	4.4	[1]	3.3	[1]	2.8	[1]
100	10	2.2	2.2	1.7	[1]	1.4	[1]
150	15	2.3	2.5	1.7	[1]	1.4	[1]
200	20	2.2	3.0	1.7	1.8	1.4	[1]
300	30	2.1	9.8	1.6	2.2	1.3	1.5
400	40	1.9	7.0	1.5	2.9	1.2	1.7
500	50	1.8	9.1	1.4	3.7	1.1	2.0
600	60	1.7	12.5	1.3	4.7	1.1	2.5

[1]Pillar width-to-height ratio outside range of 1990 formula.

WARDELL'S GUIDELINES FOR MINING UNDER TIDAL WATERS

BACKGROUND TO GUIDELINES

By 1970, many of the coal mining operations in the Newcastle area had worked to the perimeter of the three major tidal lakes in the district (fig. 1). No guidelines existed at the time for designing mine layouts for working under the tidal waters. In view of the absence of such guidelines, Wardell and Partners (*3*) were appointed by the Mines Department of NSW in 1974 to make formal recommendations for the future undermining of the lakes.

Three geographical zones of influence (fig. 2) were identified, namely:

1. Land Zone [pillar design in accordance with CMRA (1912)].
2. High-Water Mark Subsidence Barrier Zone.
3. Tidal Waters Zone.

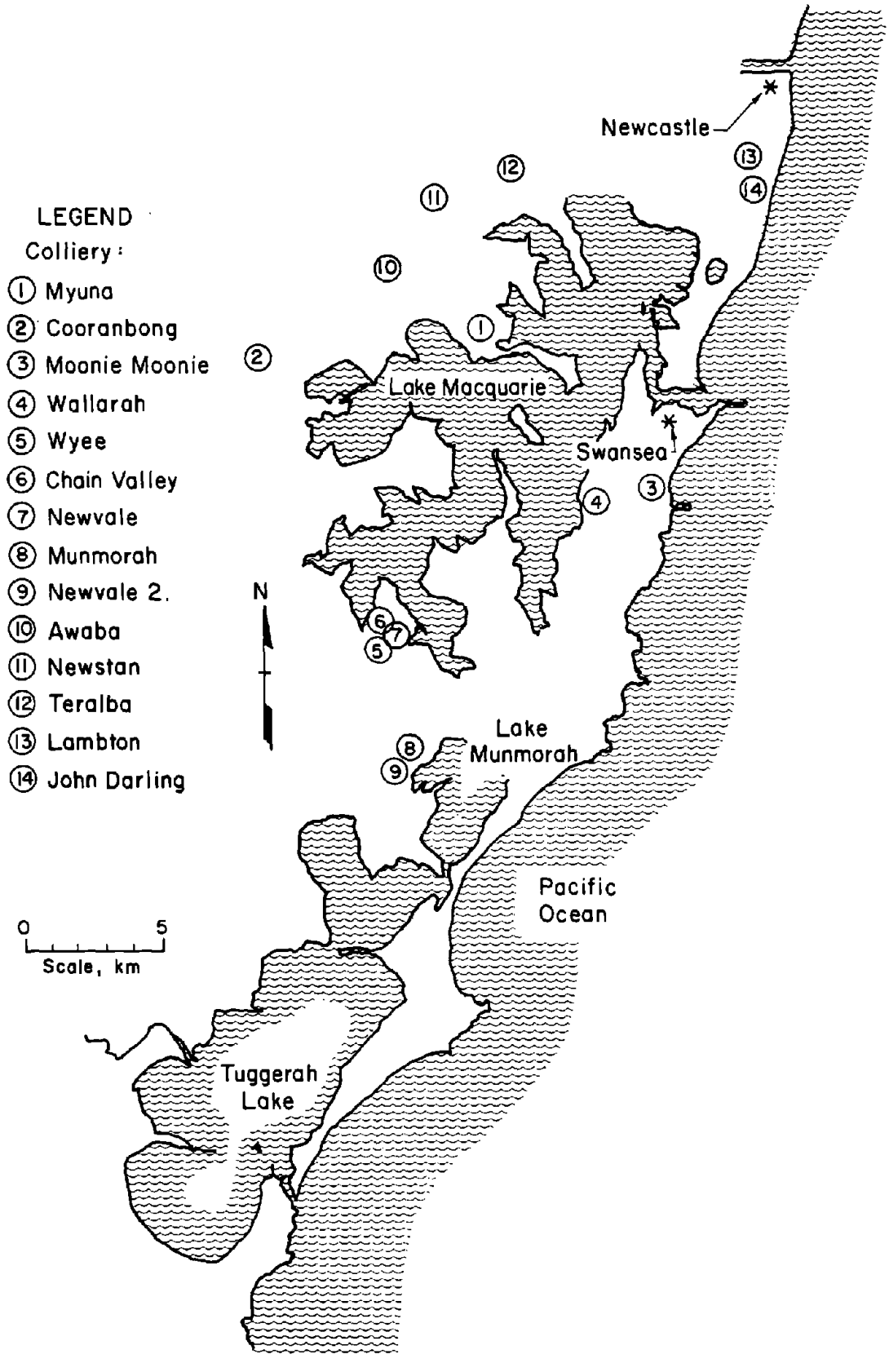

Figure 1.—Collieries adjacent to tidal lakes and ocean in the Newcastle District.

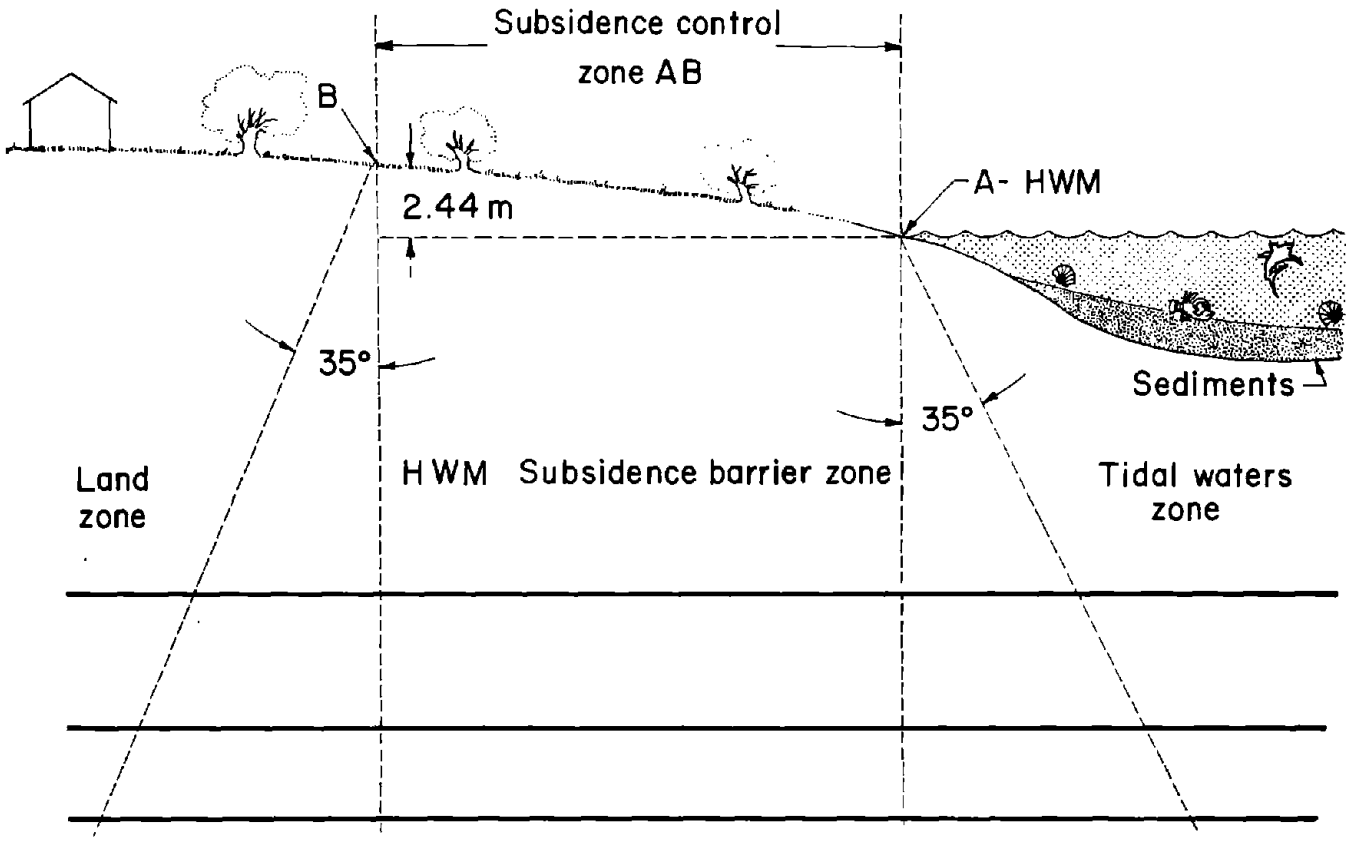

Figure 2.—Three geographical zones influencing the design of workings under tidal waters.

HIGH-WATER MARK SUBSIDENCE BARRIER ZONE

Surface subsidence in this zone must be restricted to prevent encroachment of tidal waters upon existing land surfaces. Long-term stability of mine workings is an essential prerequisite for achieving this aim. Investigations by Wardell revealed that an exceptional combination of natural circumstances could cause the water level of the coastal lakes to rise about 8 ft (2.44 m) above the standard high water mark (HWM). Thus, the zone AB, fig. 2, can be considered as the natural barrier to the encroachment of existing land surfaces by tidal waters. Wardell concluded that in order to prevent tidal waters encroaching beyond this barrier, subsidence within the zone AB was to be avoided or limited. Furthermore, the restrictions imposed upon underground mining to achieve this objective must ensure that the state is permanent.

Within the HWM Subsidence Barrier Zone, the nature, extent, and intensity of extraction would depend on the total amount of subsidence allowable. Wardell assumed that:

1. Subsidence up to a maximum of 150 mm would be tolerable within the Subsidence Control Zone AB around any of the tidal lakes.

2. Subsidence greater than 150 mm but less than 600 mm would be tolerable within the Subsidence Control Zone AB in certain areas where the lake shore was formed by a cliff or by very steeply rising ground.

3. Subsidence in excess of 600 mm would, generally speaking, not be tolerable within the Subsidence Control Zone AB.

Within the framework of these subsidence restrictions, Wardell proposed the guidelines (*3*) recorded in table 5. Basically, Wardell recommended that where subsidence within the subsidence control zone should not exceed 150 mm only bord-and-pillar mining should be employed. In areas where subsidence may exceed 150 mm but not 600 mm, restricted panel-and-pillar operations may also be conducted. ("Panel-and-pillar" is a colloquial term that refers to mining systems where the width of total extraction panels is restricted in order to restrict surface subsidence to defined limits. The restricted-width panels are separated by single rows of pillars, which are designed to be permanently stable.)

Table 5.—Guidelines recommended by Wardell (1975) for working coal in HWM Subsidence Barrier Zones

Upper / Lower	No mining	Bord-and-pillar	Panel-and-pillar	Longwall
No mining	Not applicable.	For $V_z \leq 150$ mm: 1. Widths of headings and cut-throughs should not exceed 5.5 m. 2. No pillar should have a smaller plan dimension than 8 times its height. For 150 mm $< V_z \leq 600$ mm: as per CMRA (1912).	For $V_z \leq 600$ mm: 1. The maximum width of any totally extracted panel section should not exceed 0.33D. 2. The minimum width of any abutment pillar between extraction panels should be 10 times its height or 0.16D, whichever is greater. 3. The two preceding recommendations could be applied to bord-and-pillar first workings as stipulated in this table, provided pillar extraction was limited to every third panel and the pillar extracted area did not exceed the maximum width of 0.33D.	$V_z > 600$ mm, in general, not tolerable.
Bord-and-pillar	For $V_z \leq 150$ mm: 1. Width of heading and cutthrough should not exceed 5.5 m. 2. No pillar should have a smaller plan dimension than 8 times its height. For 150 mm $< V_z \leq 600$ mm: as per CMRA (1912).	1. Widths of heading and cut-throughs should not exceed 5.5 m. 2. No pillar should have a smaller plan dimension than 8 times its height. 3. If the stratigraphic intervals between seams is not less than 10 times the extracted thickness of the lower seam, there is no necessity to superpose pillars.	See guidelines.	$V_z > 600$ mm, in general, not tolerable.

D Thickness below surface (of solid strata cover).
V_z Surface subsidence.

Table 5.—Guidelines recommended by Wardell (1975) for working coal in HWM Subsidence Barrier Zones—Continued

Lower \ Upper	No mining	Bord-and-pillar	Panel-and-pillar	Longwall
Panel-and-pillar	For $V_z \leq 600$ mm: 1. The maximum width of any totally extracted panel section should not exceed 0.33D. 2. The minimum width of any abutment pillar between extraction panels should be 10 times its height or 0.16D, whichever is greater. 3. The two preceding recommendations could be applied to bord-and-pillar first workings as stipulated in this table, provided pillar extraction was limited to every third panel and the pillar extracted areas did not exceed the maximum width of 0.33D.	No guidelines.	1. The maximum width of any totally extracted panel section should not exceed 0.33D. 2. The minimum width of any abutment pillar between extraction panels should be 10 times its height or 0.16D, whichever is the greater. 3. Superpositioning is imperative, irrespective of the thickness of strata between seams. 4. Panels in the lower seam must not be wider than those in the upper seams and the pillar dimensions in the upper seam must be determined by reference to parameters of the lower seam.	$V_z > 600$ mm, in general, not tolerable.
Longwall	$V_z > 600$ mm, in general, not tolerable.	$V_z > 600$ mm, in general, not tolerable.	$V_z > 600$ mm, in general, not tolerable.	$V_z > 600$ mm, in general, not tolerable.

D Thickness below surface (of solid strata cover).
V_z Surface subsidence.

Wardell's guidelines found widespread application up to the late 1980's and still form the basis for mining under tidal waters. Nevertheless, they contain a number of anomalies and deficiencies that have come to be recognized in recent years. These include:

1. *Surface subsidence.*—The fundamental criterion for the design of workings in the HWM Subsidence Barrier Zone is long-term stability. The subsidence values assigned to the mining methods in the zone (table 5) are incompatible with this criterion. Under most circumstances, a subsidence value of 150 mm cannot be equated to stable bord-and-pillar workings. It is widely accepted that, neglecting adverse floor or roof conditions, a pillar width-to-height ratio of 8 is sufficient to result in an indestructible pillar. As such, measured subsidence values are only of the order of millimeters.

Similarly, panel-and-pillar layouts cannot be considered stable in the long term where surface subsidence in the range 150 to 600 mm has occurred. Experience gained in the Lake Macquarie region since 1974 indicates that subsidence needs to be restricted to the order of 100 to 200 mm to ensure long-term stability.

2. *Superpositioning of workings.*—Wardell adopted the criterion that multiseam bord-and-pillar workings need to be superposed when the parting thickness between the seams is less than 10 times the mining height in the lowest seam. Rock mechanics principles do not support this criterion.

3. *Panel-and-pillar layout.*—The recommendation to superpose panel-and-pillar workings, irrespective of the thickness of strata between the seams, is reasonable but does have the potential to be relaxed when seams are separated by considerable thicknesses of competent strata. Of concern however, is that Wardell did not stipulate a minimum stratigraphic interval to be maintained between multiseam panel-and-pillar workings. Solid rock cover for a lower seam should be taken to be the distance between the roof of the lower seam and the floor of the upper seam. It may be argued that provided the upper seam was extracted first, collapse of the parting is of no significance since the panel width-to-depth ratio in the upper seam would still be sufficient to arrest caving. However, consideration must be given to the effect that such a collapse would have on the stability of the interpanel pillars, which carry the load of the bridging strata. Effectively, such a collapse results in a reduction in the pillar width-to-height ratio and thus a reduction in interpanel pillar strength.

TIDAL WATERS ZONE

In the Tidal Waters Zone, Wardell was primarily interested in ensuring stability of mine workings for at least the operational life of the mine. Wardell identified two areas of concern in regard to the inundation of mine workings by tidal waters. These were:

1. Natural features that could result in direct connection between mine workings and bodies of surface water.
2. Mining-induced changes in the permeability of the intervening strata between mine workings and bodies of surface water.

On the basis of overseas experience and limited local experience, Wardell recommended that a minimum thickness of 46 m of "solid" rock cover should overlie any workings. He also specified a maximum horizontal strain of 7.5 mm/m at rockhead. On the basis of limited subsidence measurements and observations in the Lake Macquarie/Newcastle area at the time (1974), Wardell interpreted this strain ratio as requiring the ratio of solid bedrock cover to extracted height be not less than 60:1. Wardell's guidelines for working in the tidal water zone are summarized in table 6.

A very large data bank of subsidence information now exists, and it is probably timely that Wardell's maximum horizontal strain criteria be reviewed. In particular, this should occur in instances where the guidelines are now being applied in different geological environments from those in which they were developed. The guidelines pertaining to double-seam panel-and-pillar mining in the tidal waters zone have the same shortcomings as those relating to the HWM Subsidence Barrier Zones.

Table 6.—Guidelines recommended by Wardell (1975) for working coal in the Tidal Waters Zones

Upper / Lower	No mining	Bord-and-pillar	Panel-and-pillar[1]	Longwall[1]
No mining	Not applicable.	1. D* ≥ 46 m. 2. To conform to CMRA (1912).	1. D* ≥ 46 m. 2. The maximum width of any totally extracted panel section should not exceed 0.4D. 3. The minimum width of any abutment pillar between extraction panels should be 8 times its height or 0.12D, whichever is greater.	1. D* ≥ 46 m. 2. A minimum of 60 m of solid strata cover for each 1 m of coal totally extracted.
Bord-and-pillar	1. D* ≥ 46 m. 2. To conform to CMRA (1912).	No guidelines.	No guidelines.	No guidelines.
Panel-and-pillar[1]	1. D* ≥ 46 m. 2. The maximum width of any totally extracted panel section should not exceed 0.4D. 3. The minimum width of any abutment pillar between extraction panels should be 8 times its height or 0.12D, whichever is greater.	No guidelines.	1. D* ≥ 46 m. 2. Panels and pillars should be superposed. 3. Panel dimensions should be determined by reference to the shallowest seam such that the maximum width of any totally extracted panel does not exceed 0.4D. 4. The minimum width of any abutment pillar between extraction panels should be 8 times its height in the thickest seam or 0.12 times the depth of the deepest seam, whichever is the greater dimension.	No guidelines.
Longwall[1]	1. D* ≥ 46 m. 2. A minimum of 60 m of solid strata cover for each 1 m of coal totally extracted.	No longwall mining permitted.	No longwall mining permitted.	1. D* ≥ 46 m. 2. Total or partial extraction in a seam underlying one already extracted must be planned so as to avoid the overlapping of tension zones and the creation of a maximum tensile strain at rockhead exceeding 7.5 mm/m.

D* Thickness of solid strata cover.

[1]No total extraction or pillar extraction to be permitted within a distance of 46 m of any known fault having a vertical displacement greater than 3 m nor any dike having a width greater than 6 m.

LONGWALL CHAIN PILLAR DESIGN

Mechanized longwall mining commenced in Australia in the late 1960's, but it was not until the early 1980's that its potential was proven. Australian legislation permits gate roads to comprise only two entries and, with special permission, single entry. Single entries service only one longwall block and are used in particular circumstances, for example, as the tailgate of the first longwall block in the new area of a mine or where a barrier has to be left between adjacent longwall panels to control spontaneous combustion.

The standard longwall layout is two entries. However, two circumstances result in some operators having to employ a three-entry development layout. These are

1. *High gas emissions*.—The third entry is required to increase ventilation during development drivage and to permit the next longwall block to be predrained of gas prior to mining. Longhole drilling and gas drainage take place in the third heading behind the current retreating longwall face.

2. *High lateral stress environments*.—In a conventional two-entry development, high lateral stress can result in the companion gate road becoming unserviceable prior to commencement of longwall operations in the adjacent block. A third roadway is driven in the stress-relieved zone of the gateway companion to serve as either the maingate or the tailgate of the next longwall (fig. 3*A*).

Chain pillar width in two heading developments has traditionally been based on numerical analysis and field measurements of the distribution of vertical stress around longwall blocks. Chain pillars are designed not to fail until both adjacent longwall blocks have been extracted. Typically, chain pillar widths range from 30 m at a depth of 150 m, 35 m at a depth of 300 m, to 40 m at a depth of 450 m. Pillar lengths range from 50 to 220 m and are based on operational considerations such as the ventilation system, gas make, and the coal clearance system.

In high horizontal stress environments, a third heading may be driven in the stress shadow of an adjacent heading either during primary development, or as a secondary operation (fig. 3). The best results are obtained during a secondary drivage operation by which time the adjacent heading has deteriorated to a sufficient degree to deflect lateral stresses deep into the roof and floor strata. However, driving a third heading as a secondary operation presents many operational problems and must be carefully planned to ensure longwall schedules are not affected.

When the third heading is driven as part of the primary operation, the reduced stress relief effect can result in the heading requiring floor brushing and/or additional backbye roof support before being brought into service. The potential also exists that the third heading is, in fact, the one to deform, thereby providing protection to the middle heading.

In a three-heading panel layout, the width of the abutment pillar still ranges from 30 to 40 m. The width of the protection pillar is typically 9.5 m.

It has only been recognized in recent years that many of the longwall gate road and gate end stability problems are associated with high lateral stresses. It is not uncommon for gate road support to comprise:

1. 17 to 20, 2.1 m by 25 mm diameter, fully encapsulated high tensile roof bolts per meter,
2. 3 "W" straps per meter,
3. mesh,
4. 4 rib bolts with straps per meter.

Not surprisingly, therefore, average development rates in these environments are less than 5 m per 7-h shift. These rates make the driving of a three-heading development a costly exercise and lead to development shortfalls. Considerable research is currently being undertaken to address these problems so that the full potential of longwall mining can be realized.

CASE STUDIES

BORD-AND-PILLAR MINING IN COMPLIANCE WITH COAL MINES REGULATIONS ACT (1982)

An uncontrolled collapse of multiseam bord-and-pillar workings recently occurred in NSW. Details of the mining operations in the bottom seam were

Seam depth	100 m.
Seam thickness	6 to 10 m in places.
Seam dip	0° to 7°.
Mining height	Up to 6 m.
Pillar size	Formed at 10 by 10 m; effectively 9.5 by 9.5 m.
Roadway width	Formed at 5.5 m; effectively 6 m.
Geology	The area was bordered by a large dike on one side and faulting on three sides. Fault displacement exceeded 2 m. Low-angle discontinuity planes were present in the pillars.

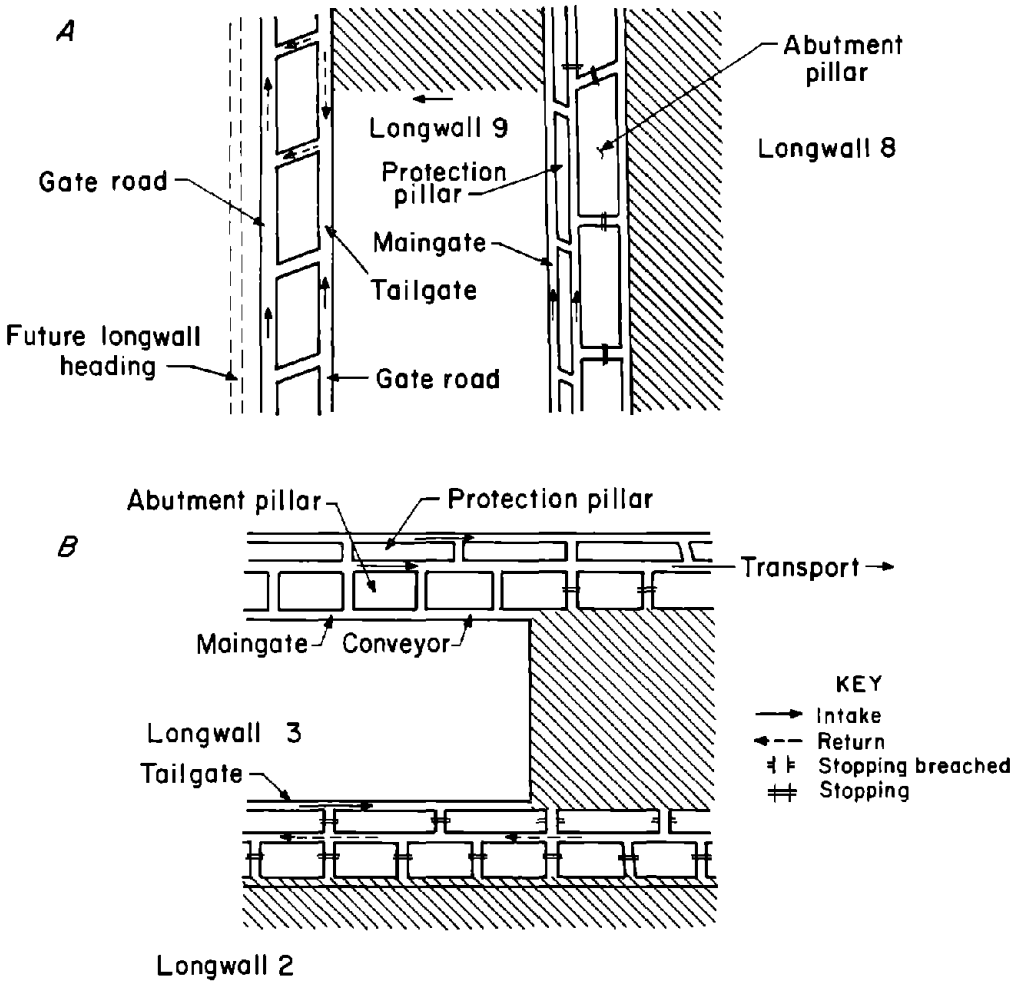

Figure 3.—Longwall development layouts designed to protect gate roads from the adverse effects of high lateral stress. *A*, Stress-relieved gate road driven as a secondary operation; *B*, stress-relieved gate road driven during primary development.

Sequence of events . . . After the area in the bottom seam was developed, mining transferred to another seam 40 m above. At the time of collapse, a four-heading main development panel at 35 m centers was directly over the lower seam workings. Workings were not superposed. Workings in the bottom seam collapsed suddenly, causing a major air blast. Workings in the upper seam were adversely affected and subsequently collapsed.

MULTISEAM WORKINGS UNDER TIDAL WATERS

Myuna Colliery commenced multiseam mining under tidal waters on the western side of Lake Macquarie in 1982 (fig. 4). Extensive residential areas are located around the lake foreshores. Three seams are mined simultaneously, namely the Wallarah, Great Northern, and Fassifern Seams. The deepest workings occur at a depth of 160 m in the Fassifern Seam, while all workings cease when the thickness of solid bedrock cover reduces to less than 40 m (lease conditions permit mining to within 40 m of solid bedrock cover, and not 46 m as contained in the Wardell guidelines).

The parting between the Fassifern and Great Northern Seams comprises 12 to 30 m of weak tuffaceous sediments. The Wallarah Seam lies 25 to 45 m above the Great

Northern Seam, the parting comprising conglomerate, sandstone, and claystone strata, rarely exceeding 3 m in thickness.

In general, the Fassifern Seam is mined to a height of 3 m, the Great Northern Seam to 2.5 m, and the Wallarah Seam to 2 m. Simultaneous extraction of each seam is essential in order to produce a blended product requiring no beneficiation.

The only potential for extensive total extraction is in the Fassifern Seam. However, such operations sterilize reserves in the overlying Great Northern and Wallarah Seams. Reserves in these upper two seams are critical to achieving a blended marketable product and therefore total extraction is not economically viable. Similar considerations also restrict the potential for panel-and-pillar operations to a negligible portion of the lease area Great Northern Seam.

Thus, bord-and-pillar mining is undertaken in all three seams. On the basis of the Wardell guidelines, workings in the Great Northern and Fassifern Seam within the HWM Subsidence Barrier Zone need to be superposed. While Wardell did not address this issue for Tidal Waters Zones, it has been presumed that similar considerations apply. Workings in the Wallarah Seam have also been superposed. Potential exists to relax this requirement in some areas of the lease, thereby allowing pillar size to be reduced in the Wallarah Seam. This aspect is currently being investigated.

Reference to figure 4 illustrates the scattered land mass/tidal waters distribution within the colliery lease area. Under these conditions, it is impractical to change design dimensions each time mine workings transgress from a HWM Barrier Zone to a Tidal Waters Zone, and back again. A conservative approach has been adopted and all mine design has been based on HWM Subsidence Barrier Zone guidelines.

These guidelines require a minimum pillar width-to-height ratio of 8, thereby necessitating a 24-m-wide pillar in the Fassifern Seam. A statutory bord width of 5.5 m results in a pillar center distance (PCD) of 29.5 m. As a matter of convenience and to take rib spall and mining deviations into account, a PCD of 30 m has been adopted.

To accommodate the effects that geological conditions in each seam can have on panel layout, and thus superpositioning of workings, a grid system has been adopted. The lease area is divided into a checkerboard of 30-m squares with both panel pillars and interpanel pillars being on a PCD of 30 m (fig. 5). The grid concept offers great flexibility especially in the following regards:

1. Main developments in any seam can be superposed with panel layouts in another seam.
2. At least two directions are available for turning panels off main developments.
3. Provided the grid itself is not altered, the mine layout can be changed without the need to reapply for approval for the mine layout from the relevant statutory departments.

The grid concept can be employed because all panel pillars have been dimensioned to HWM Subsidence Barrier Zone requirements and are therefore intended to be indestructible.

From personal experience, the Great Northern Seam is of a similar competence and toughness to that of South African seams, while the Wallarah and Fassifern Seams are marginally weaker. Under South African conditions, workings would be designed to a safety factor of 2.2 (based on Salamon's 1966 pillar design formula). The safety factor of Myuna workings ranges from 2.5 to 13.2. From table 3, it is obvious that even allowing for weaker coal strata, the workings are well designed by South African standards. A safety factor of 13.2 arises because the pillar width-to-height design approach makes no allowances for the limited cover load that a pillar has to support at shallow depth.

Deficiencies in the Wardell guidelines for superposing multiseam workings have had no adverse affect on the stability of the current workings. This is because, fortuitously, the lowest seam in the lease area is also the seam extracted to the greatest height, 3 m, resulting in a minimum pillar width of 24 m and superpositioning of workings when the parting thickness is less than 30 m.

Consider the consequences had the mine design been based on a 2-m mining height in all three seams. Under these circumstances, pillars would only have been 16 m wide instead of 24.5 m wide, while superpositioning would have been required only where the parting thickness was less than 20 m. As a result, average pillar stresses would have been almost 22 pct higher, while the Great Northern and Fassifern Seam workings would not have been superposed over a considerable area of the lease. In view of the weak nature of the parting between these two seams and the higher pillar stresses, bord stability may have been a major problem.

To date, the sequence in which the seams have been extracted has not been critical. Strata control in all three seams is excellent.

The leaving of interpanel pillars on a regular basis to prevent a pillar collapse within a panel from spreading throughout the mine workings is a fundamental design requirement in the layout of extensive bord-and-pillar workings. These interpanel pillars need to be designed to be indestructible. This design requirement may not appear to be satisfied by the grid concept since panel and interpanel pillars are the same width. However, it must be recognized that by usual standards, panel pillars have been overdesigned, panel pillars in the Great Northern and Wallarah Seams, for example, having width-to-height ratios of 9.8 and 12.2, respectively. Similar considerations apply to the interpanel pillars, in addition to the fact that they will be stronger because of their rectangular shape.

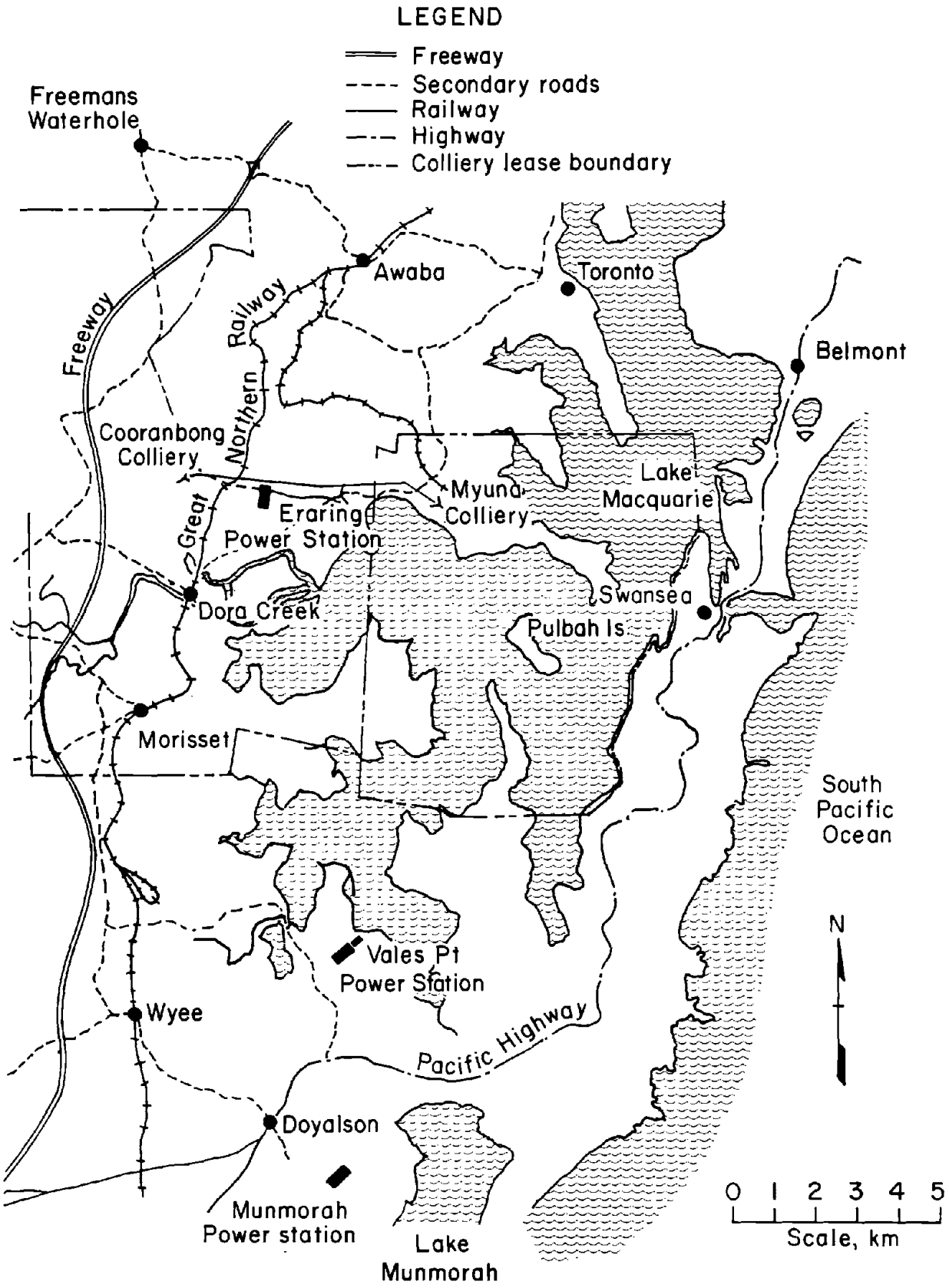

Figure 4.—Location and lease boundaries of Myuna Colliery.

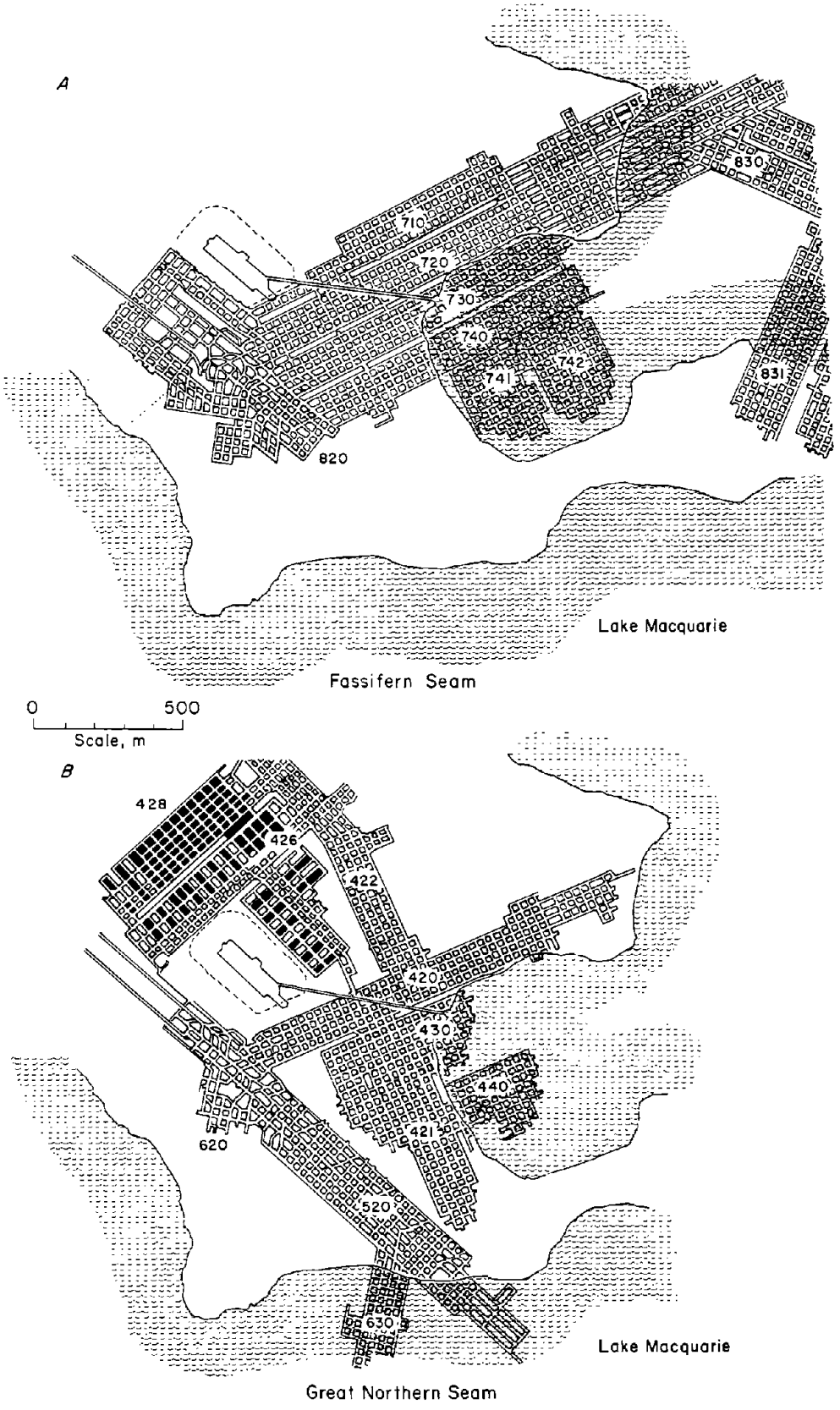

Figure 5.—Multiseam workings layout based on 30-m grid concept, Myuna Colliery. *A*, Fassifern Seam; *B*, Great Northern Seam.

PANEL-AND-PILLAR MINING

The panel-and-pillar layout shown in figure 6 is typical of that which developed out of the Wardell guidelines in the late 1970's and 1980's. There is a gradation from total pillar extraction under land to partial pillar extraction in the HWM Subsidence Barrier Zone.

The layout shown in figure 6 has a number of significant shortcomings, including:

1. Abutment pillars are square in shape and represent the minimum size required to conform to a maximum width-to-height ratio of 10. The number of cutthroughs increases the potential for pillar spalling, leading to a reduced width-height ratio. Pillar load and roof and floor bearing pressures are also higher than for rectangular or rib abutment pillars.
2. Some pillars are surrounded by goaf on three sides. This practice exposes these pillars to very high loads and increases the potential for pillar spalling, pillar failure and for bearing failures of the roof and floor strata.
3. The workings are not compartmentalized through the use of interpanel pillars. Thus, a collapse in one section of the workings could propagate through a larger area of the mine.

Vast areas of stable panel-and-pillar workings exist under the tidal lakes of the Newcastle district. However, design shortcomings have been evident in some cases. Surface subsidence tends to either stabilize at a value of less than 200 mm (and often less than 60 mm) very soon after the completion of mining operations, or else it tends to increase at a steady rate over many years to sometimes exceed 500 mm. In the latter cases, underground inspections reveal the pillars to be to size and in very good condition. However, floor heave is evident.

Limited studies to date indicate that the ongoing subsidence cases are associated with average pillar stress levels exceeding 15 MPa. Some designs are now being based on restricting average pillar stress to less than 13 MPa. The floor strata comprise an undrained low-permeability claystone, and further research is required to determine whether the problem is one or a combination of the following factors:

1. Drainage of floor strata with time.
2. Swelling of claystone when exposed to moisture.
3. Time-dependent creep of floor strata under stress.
4. Foundation bearing failure of floor strata immediately under the pillar.
5. Failure of floor strata in bords caused by induced horizontal stresses at the pillar/floor contact.

Only one total collapse of panel-and-pillar workings is known to have occurred. This developed in a controlled manner over many months, but owing to the absence of interpanel pillars, it spread through a considerable area of the mine workings.

The shortcomings associated with mine designs of the type depicted in figure 6 have been taken into account in recent panel-and-pillar designs by the author. The mine layout shown in figure 7, for example,

1. Avoids abutment pillars being surrounded by goaf on three sides.
2. Minimizes the number of cutthroughs in abutment pillars to those necessary for wheeling and ventilation purposes.
3. Compartmentalizes working sections through the use of interpanel pillars.
4. Achieves 65 pct extraction while restricting surface subsidence over the panel-and-pillar sections to a maximum of 35 mm.

LONGWALL MINING AT ANGUS PLACE COLLIERY

Angus Place Colliery commenced longwall mining in 1979 under the following conditions:

Depth range	75 to 150 m
Mining height	2.8 m
Face width including gate roads	142.5 m
Chain pillar width	29.5 m
Roadway width	5.5 m

Early operations broke many records and represented the first successful high-capacity longwalling operation in Australia. Gate road stability was excellent, and final surface subsidence above the chain pillars was only 25 to 30 mm.

In light of these successes, higher capacity equipment was installed in Longwall 8 in 1983. Relevant dimensions were

Depth range	160 to 220 m
Mining height	2.8 to 3.4 m
Face width	211 m
Chain pillar width	29.5 m
Roadway width	5.5 m

Problems were immediately encountered with major rib spall and floor heave. Roof and floor control were exacerbated by an increase in effective roadway width to 8 m.

Chain pillar width was increased to 34.5 m for Longwall 9 and maingate conditions improved significantly. However, some problems were still encountered in the tailgate. The introduction of rib bolting as part of the production cycle alleviated these problems and a chain pillar width of 35 m has remained the standard down to

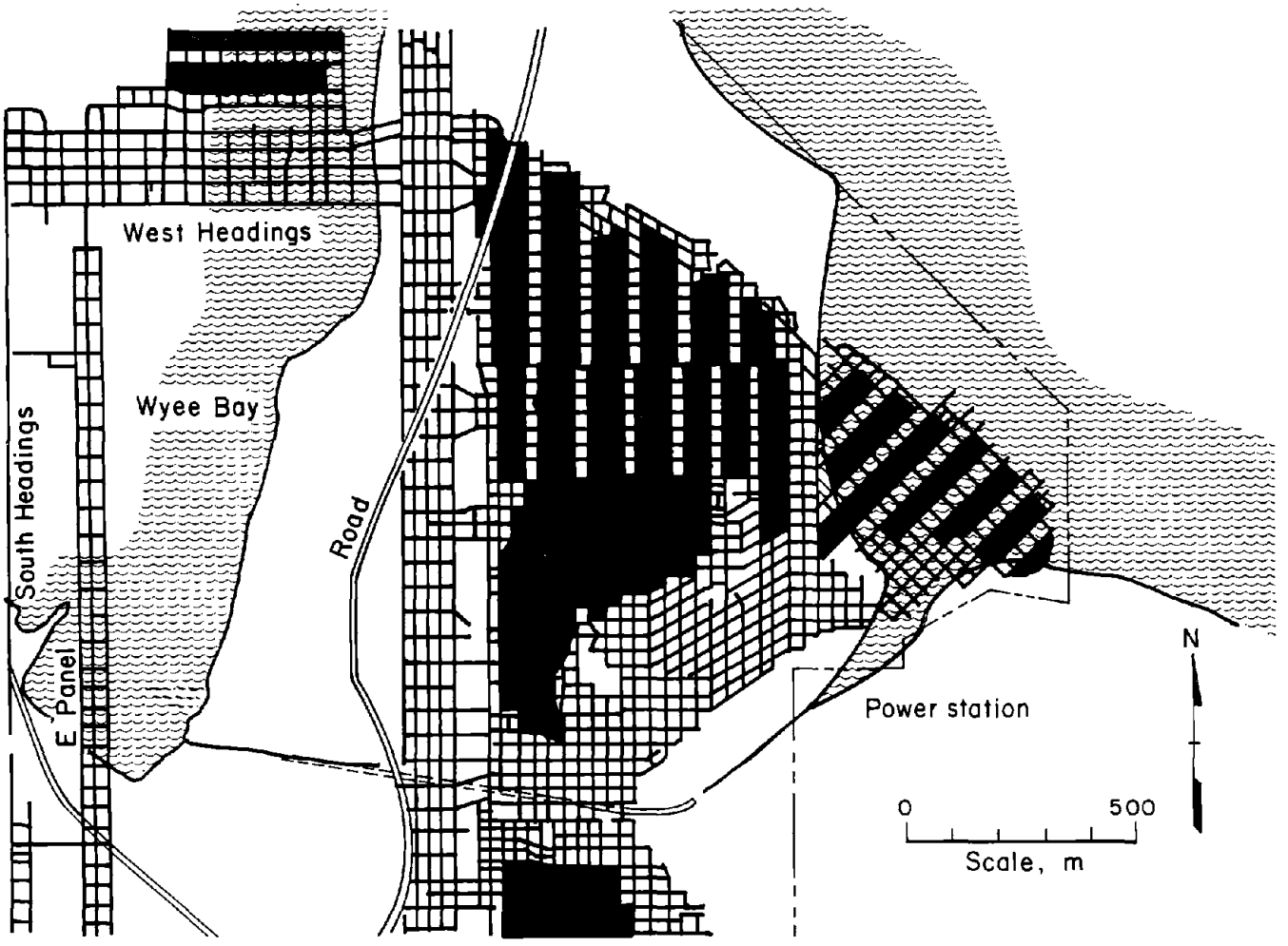

Figure 6.—An early panel-and-pillar layout.

current depths of 300 m. Surface subsidence above chain pillars at these depths is in the order of 500 mm. It has not been ascertained whether this subsidence reflects chain pillar failure, or interaction between angles of draw associated with the wider and deeper adjacent longwall goafs.

As mining operations have progressed deeper, severe lateral stress problems have been encountered. A principal horizontal stress of 2.5X vertical has been the norm since Longwall 10. The direction of this principal stress is sensitive to the mountainous topography and varies across the mining lease.

In order to minimize the adverse effects of high horizontal stress on gate road roof and floor stability and thus on development and longwall extraction rates, gate roads are orientated wherever practical to be within 30° of the direction of the principal horizontal stress. Cutthroughs are spaced at 100-m centers and are difficult to drive given the lateral stress direction. Currently ventilation and coal clearance systems prevent the use of longer pillars.

Although this layout results in improved development rates, it can cause significant problems when developing the 8-m-wide longwall face installation roadway. Following the loss of the installation roadway for Longwall 11, a study was undertaken into the viability of using the sacrificial roadway technique, to gain relief from high horizontal stress. A 9.5-m-wide pillar was left and a new installation roadway was driven outbye of the fallen roadway. This new roadway was driven in two passes. Roof and floor control were excellent and roof support requirements were less than in the fallen roadway.

The sacrificial roadway technique has been used in driving all five longwall face installation roadways since Longwall 11. A 4.7-m-wide, very heavily supported roadway is driven across the length of the block. This roadway

is then widened to 10 m on the retreat in a lifting off operation. The roof immediately falls to a height in excess of 5 m. A 9.5-m protection pillar is left and the 8-m installation roadway is driven full-face in excellent roof conditions requiring minimal roof support ("W" straps at 1-m centers with nine roof bolts).

In 1990, longwall operations commenced in a new section of the mine. Instrumentation and monitoring had indicated that the coal roof in this area was softening to a height of 3 to 5 m upon drivage at a roadway width of 4.7 m. Careful consideration was given as to whether this degree of roof softening alone would provide enough protection to the longwall face installation roadway without the need to cave the roadway. The decision was made to drive the sacrificial roadway at the maximum legal width of 5.5 m to encourage roof softening. The roadway was extensively instrumented. All indications were that this roadway need not be caved, thereby offering development, ventilation, and pumping advantages to the mine.

A 9.5-m protection pillar was left and the longwall face was driven 8 m wide, full-face from both directions. In the final stages of this operation, both the roof and floor strata became unstable. The installation roadway was salvaged through the use of cable bolting and floor brushing, but at an unacceptable cost. Analysis showed that the stress relief provided by the sacrificial roadway was inadequate and, in fact, the installation roadway, being wider, had failed and provided protection to the sacrificial roadway. Two years and two longwalls later, the sacrificial roadway remains open and in good condition.

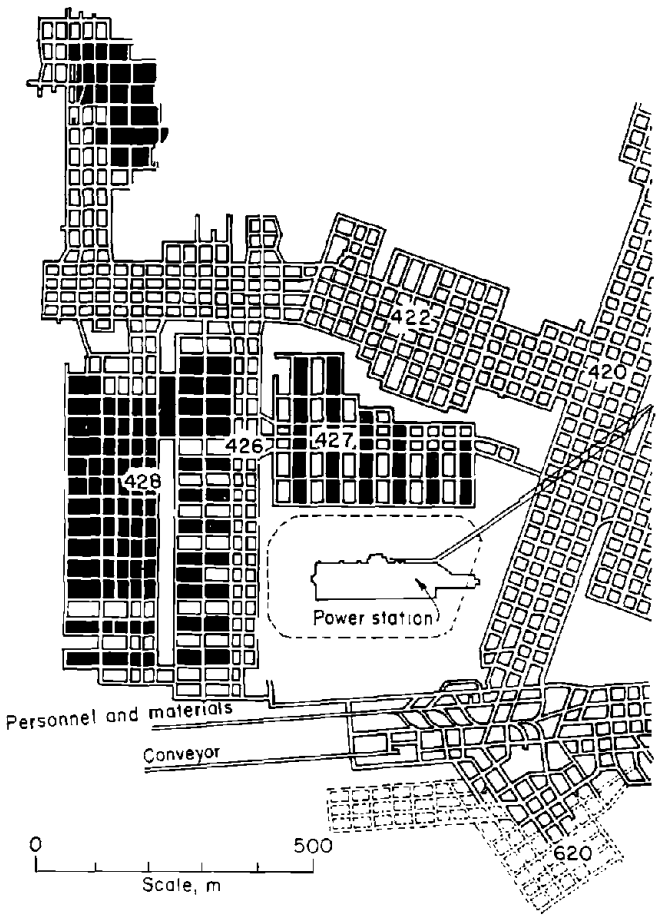

Figure 7.—A recent panel-and-pillar layout that addresses short-comings in earlier designs.

CONCLUSIONS

The prescription of roadway and pillar sizes in legislation in NSW has not encouraged the development of a pillar design knowledge base in that state. The predominance of successful rib pillar and longwall mining total extraction techniques in both NSW and Queensland in the last two decades has also resulted in little focus on the mechanics of pillar behavior and pillar design.

A series of recent unfortunate events associated primarily with the development and extraction of standing pillars has alerted the industry to a need to develop a local pillar design knowledge base. The requirements of NSW legislation appear to result in a conservatively designed pillar at mining heights of 3 m or less. However, they may be inadequate at greater mining heights. The requirements are inappropriate to multiseam mining.

The Wardell guidelines for designing single-seam workings under and adjacent to tidal waters have generally proved satisfactory. However, there is a need to review their basis in light of experience and greatly enhanced data and knowledge base. Emphasis needs to be placed on pillar foundation behavior.

An industrywide need exists to develop an understanding of interaction between multiseam workings.

Longwall chain pillar design has generally proven satisfactory. Pillar behavior itself is not an important issue, but roadway roof and floor control present major problems in high lateral stress environments. Pillar design has a role to play in strata control in these conditions. Research is in its infancy in this area, although the industry has gained significant benefit from stress relief techniques based on the use of protection pillars and sacrificial roadways.

Deficiencies in the local pillar design knowledge base have been recognized in recent years, and attention is now being focused on developing and implementing a coordinated approach to mine design based on rock mechanics principles.

REFERENCES

1. Madden, B. J. An Investigation Into the Factors Affecting the Strength of Pillars in South African Coal Mines. Ph.D. Thesis, Univ. Witwatersrand, Johannesburg, 1990.

2. Salamon, M. D. G. Method of Designing Bord-and-Pillar Workings. Chamber of Mines S. Afr. Research Rep. RR.72/66., 1966.

3. Wardell, K., and Partners. Mining Under Tidal Waters. Rep. pres. to Ministry for Mines and Power, NSW Gov., 1975.

COAL PILLAR DESIGN FOR DEEP CONDITIONS: AN OPERATIONAL APPROACH

By Michael Gauna[1]

INTRODUCTION

Under overburden conditions exceeding 1,500 ft, mining experience has shown that conventional pillar design guidelines are not generally applicable. A design method for deep mining is described in this paper where new pillar designs have been successfully implemented. The design technique involves determination of a pillar resistance/load (R/L) ratio which is used as a design guide. The implemented design change then utilizes monitoring to assess the impact of the modification. Monitoring primarily involves recording roadway deformation.

Two case histories are presented. One involves a longwall gate pillar design modification, which has been used for over 95,000 ft of longwall panel extraction. An improvement in ground control has been confirmed with the modified longwall gate pillar system. The other case study involves a new ventilation system pillar design involving a modified barrier pillar configuration. The new ventilation system pillar design has allowed a more efficient resource recovery with enhanced productivity. Roadway monitoring for over 2.5 years has confirmed that the design has maintained air course stability.

HISTORICAL PERSPECTIVE

Coal mine pillar strength formulas and pillar design criteria have been researched and published over the years. This information is well documented and typically relies on forming relationships between the laboratory strength of the coal and the in situ strength of the coal pillar. The design methodology usually involves determining the pillar strength and then dividing by a pillar tributary area overburden load. The resulting factor of safety, exceeding unity, is then considered a satisfactory design. In the situation where the floor strength is the critical parameter, pillar sizing criteria based on floor bearing strength should be applied (*1, pp. 174-205*).[2] However, in the situation where relatively firm floor conditions exist, where pillar strength is a critical parameter, and where overburden typically exceeds 1,500 ft, conventional pillar design guidelines are generally lacking in applicability.

Actual experience with deep coal mining, where overburden exceeds 1,500 ft, has shown that pillars having conventionally calculated factors of safety well under unity remain stable. This has been attributed to the pillar possessing a confined core that allows its strength to be in excess of what is usually determined from laboratory scaling. Also, the "Pressure Arch Concept" explains the apparent stability because the majority of the overburden stress is carried by the unmined flanks of coal surrounding the mining unit. The pillars mined in the development must cope with the loads imposed by only a portion of the overburden; usually assumed to be the region within the pressure arch. Unfortunately, the pressure arch geometry is not well understood or documented and has normally only been applied for rough estimations (*1, pp. 176-177*). In addition, mining methods employed in the United States rely heavily on multientry developments which tend to form complicated extraction geometries. The pillar design approach for deep conditions may be further complicated by abutment pressures from regions which have been fully or partially extracted. Although this complicated pillar loading relationship can be modeled, the implementation of pillar designs for deep conditions has often relied heavily on past experience with a reluctance to deviate appreciably from past practice.

DEEP COAL MINE PILLAR DESIGN

A design method for deep conditions is described in this section where new pillar designs have been successfully applied. The design method involves determining a pillar R/L ratio, which is then used as a design guide. Furthermore, the design change is then monitored to assess the impact of the modification. Monitoring primarily involves roadway deformation measurements and underground condition mapping.

The pillar R/L ratio calculation process follows the A. H. Wilson pillar strength approach, which was introduced in the United States in the 1970's. It was further developed for United States multientry development and published in 1981 (*2-3*).

[1]Manager mine engineering, Island Creek Coal Co., Oakwood, VA.

[2]Italic numbers in parentheses refer to items in the list of references at the end of this paper.

The design process for short-life roadways such as longwall gate developments involves calculating pillar ultimate strength as a function of a confined internal core which is capable of developing strengths in excess of laboratory derived strength (*4-5*). The pillar strength, or pillar resistance, is calculated using the formulas for ultimate pillar resistance with yield in roof, seam, and floor. The design process for long-life roadways, such as main developments, uses formulas for pillar resistance for limit of roadway stability with yield in roof, seam, and floor.

The tributary area load of the total overburden is assigned as the load imposed on the pillar(s). If abutment pressures from high-extraction mining also are to be applied, an abutment pressure loading technique as described by Carr and Wilson (*2-3*) is employed. The pillar design is then assigned a R/L ratio where pillar resistance is divided by imposed pillar load. Load reductions attributed to the "Pressure Arch Concept" are not applied because of the indeterminate nature of the arch load.

The R/L ratio is not considered a factor of safety. It is a design guide which, under greater overburden, can have a value less than unity. In some instances, the R/L ratios have been determined for proven stable designs and used as the guide for pillar design modifications. In order to verify the stability of the design change, underground monitoring is conducted.

It has been found that roof-to-floor convergence measurements and periodic repetitive mapping of roadway conditions are efficient and economical means of monitoring. Roadway roof-to-floor convergence stations are typically established with a pin in the floor and a bolt in the roof. Periodic measurements are taken with a dial-gauge instrument on a removable pole capable of measuring to 0.05 in of movement. Pillar rib rolls, roof falls, floor heave, elimination of coal pillar bumps, and improved airflows through longwall gob represent examples of conditions commonly documented with roadway mapping.

OPERATING CONSIDERATIONS

The necessity for multientry developments combined with the need for attractive mining productivity usually requires that pillar sizes be minimized. Consequently, stable pillar sizes for typical main development tend to have R/L ratios well under 1. Designing all pillars with R/L ratios greater than 1 is not economically practical for deep mining.

Pillar combinations of small, medium, and large pillars can be employed, as described in the case studies, to enhance mining efficiency as much as possible while simultaneously achieving the desired ground control. These combination pillar configurations must meet all ventilation, haulage, and travelway requirements. They also form complicated geometries where small pillars may purposely go into yield and force adjoining larger pillars and barriers to accept more loading. Since these loading relationships are difficult to precisely model, the application of R/L ratios, coupled with underground monitoring, has proved to be an efficient means of implementing pillar designs under these complicated scenarios.

CASE HISTORIES

A longwall gate pillar design study and a longwall ventilation system pillar design study will be presented to illustrate the R/L ratio design approach for deep mining conditions. The pillar designs were implemented in the four longwall coal mines of the Virginia Division of Island Creek Coal Co. situated in Buchanan County, VA (fig. 1).

The mines extract coal from the Pocahontas No. 3 seam, which is within the Pocahontas Formation (Lower Pennsylvanian). The Pocahontas No. 3 seam is typically 5.5 to 6 ft thick in the regions described in the case studies. The Pocahontas No. 3 seam overburden ranges from 1,200 to 2,200 ft. The immediate roof and floor consist of sandy shales and sandstones. All mined entries and crosscuts have been assigned a width of 20 ft for design purposes.

The pillar strengths for ultimate pillar resistance for yield in roof, seam, and floor are functions of the internal support resistance (plus cohesion), pillar height, and the coal pillar dimensions as described by Wilson (*2*).

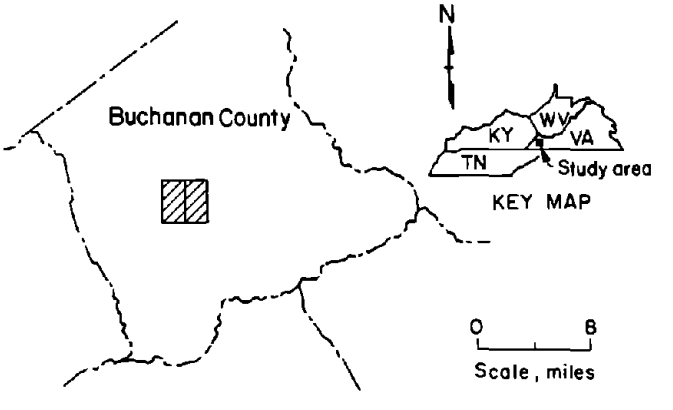

Figure 1.—Study area location map.

$$R_{r(y)} = (p+p') Q^2 \{3 M P + Q (P-M) - 0.5 Q^2\}/\{M^2 (P+W)\} \quad (1)$$

where $R_{r(y)}$ = pillar ultimate resistance for yielding conditions, st/ft development,

$p+p'$ = pillar internal support resistance and cohesion, st/ft^2,

Q = pillar width, ft,

P = pillar length, ft,

W = entry width, ft,

and M = pillar height, ft.

Support resistance and cohesion have been assigned a value of 1.04 st/ft^2. For a 6-ft pillar height, the calculated strength is similar to the equation presented by Carr and Wilson (*3*) for the Warrior Basin of Alabama.

The pillar strengths for limit of roadway stability for yield in roof, seam, and floor are functions of the internal support resistance (plus cohesion), pillar height, coal pillar dimensions, overburden load, triaxial stress factor, and in situ uniaxial compressive strength (*2*).

$$R_{r(y)} = [\{(12/M^2) (p+p') (A + B - C + D)\} + E]/(P+W) \quad (2)$$

where $R_{r(y)}$ = pillar strength for limit of roadway stability for yielding conditions, st/ft development,

$$A = M P Q X, \quad (3)$$

$$B = (P Q - M P - M Q) X^2, \quad (4)$$

$$C = 4/3 (P + Q - M) X^3, \quad (5)$$

$$D = 2 X^4, \quad (6)$$

and $$E = S (P - 2 X) (Q - 2 X). \quad (7)$$

For equations 3 to 7,

$$X = M/2 [\{(q H)/(p+p')\}^{1/(k-1)} - 1] \quad (8)$$

S = coal in situ uniaxial compressive strength, st/ft^2,

q = overburden density, st/ft^3,

H = overburden depth, ft,

and K = triaxial stress factor, unitless.

For load calculations, the overburden density is assigned a value of .0792 st/ft^3. The triaxial stress factor is assigned a value of 3, and the in situ uniaxial strength is assigned a value of 22 st/ft^2. The calculated pillar strengths are similar to the equation presented by Carr and Wilson (*3*) for the Warrior Basin of Alabama. It has been concluded that the Pocahontas No. 3 seam physical properties are similar to those of the Warrior Basin Blue Creek coal seam described by Carr and Wilson.

LONGWALL GATE PILLAR DESIGN

The previously existing longwall gate pillar design for the case study is shown in figure 2. The Pocahontas No. 3 seam is highly gassy. The resultant ventilation requirements necessitate a minimum of four entries for the longwall development. The original gate design had 100- by 100-ft center distance middle development pillars flanked by 50- by 100-ft center distance yielding pillars. The smaller pillars typically yield when subjected to abutment stresses and tend to become insusceptible to violent pillar bumps. The yield pillars also serve to narrow the total development width, which improves mining efficiency and enhances resource recovery.

However, with this design, abutment stresses from the adjacent previously extracted panel forced the use of a high tailgate crib density to maintain a travelway. Furthermore, roof-to-floor convergence immediately closed the tail side airways behind the face between the previous and active gob. The airway closure complicated the longwall face ventilation. In addition, the central abutment pillar proved to be bump-prone on the tailgate side, particularly when overburden exceeded 1,800 ft in the presence of strong roof and floor. The tailgate pillar bumps posed operational problems and contributed to face bumps during longwall mining.

MODIFIED LONGWALL DEVELOPMENT DESIGN

The objectives for the pillar design modification were to improve tailgate entry stability, control tailgate pillar bumps, and enhance ventilation between the active and previously extracted gob. To meet these objectives, greater middle abutment pillar strength was required.

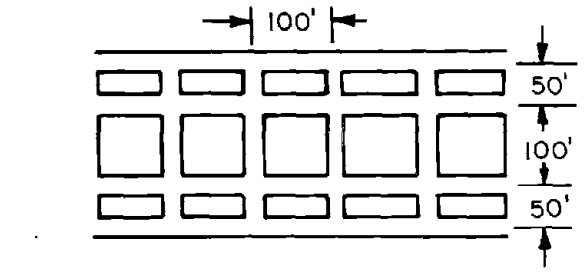

Previous longwall development pillar configuration

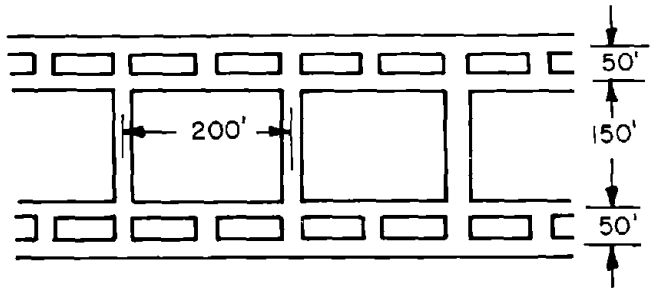

New longwall development pillar configuration

Figure 2.—Previous and new longwall development pillar designs.

Pillar strengths based on ultimate pillar resistance with yield in roof, coal, and floor were applied to determine R/L ratios. The original 100- by 100-ft center distance middle pillar had a calculated R/L ratio of 0.24 on first panel extraction and a R/L ratio of 0.15 on second panel extraction. A 1,900-ft mining depth and 5.5-ft pillar height were used for the Buchanan County mining conditions. The small resistance offered by the 50- by 100-ft center distance yield pillars was insignificant. The decision was made to increase the middle abutment pillar R/L ratio by a factor of approximately 4 by designing a middle pillar with a R/L ratio of approximately 1 for first panel extraction. The use of a R/L ratio of approximately 1 was based on the author's prior experience obtained in the Warrior Coal Basin of Alabama. The resulting nominal design consisted of a middle abutment pillar with 150- by 200-ft center dimensions flanked by yield pillars as shown in figure 2. The R/L ratios were 0.97 on first panel extraction and 0.63 on second panel extraction.

Sizing the pillar for a R/L ratio near unity for second panel extraction was not considered necessary because of the relatively short life of the Virginia Division longwall panels. The pillars are only required to resist closure between the active and previous gob for approximately 6 months. Gradual pillar system failure was considered acceptable within the gob. Also, in practice, the pillar

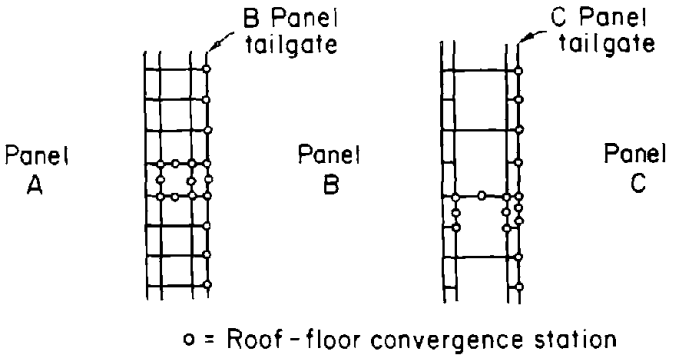

Figure 3.—Roof to floor convergence station locations for adjoining developments.

center width has been allowed to range from 140 to 160 ft and the pillar center length has been allowed to range from 200 to 270 ft depending on mining conditions and reserve constraints.

LONGWALL MINING RESULTS

In excess of 3 years of experience and approximately 95,000 ft of longwall, panel extraction have been achieved with the new pillar design. Monitoring and experience have shown an improvement in gate performance as noted by less tailgate roadway closure, enhanced ventilation, and a reduction in pillar bumps (*6*).

Tailgate Roadway Closure

Roof-to-floor convergence measurements were collected in a development having the 100-ft center width middle pillar and also in an adjacent development having the larger middle pillar. The monitoring areas are depicted in figure 3. Measurements were taken prior to and during longwall extraction. Overburden depth, geologic conditions, and roadway support were similar. Comparison of roadway closure between the two areas documented the results of the design change.

Figure 4 shows the convergence measured in the original design panel B tailgate and the modified design panel C tailgate. Closure is plotted versus the distance from the adjacent panel longwall face. The roof to floor convergence profiles are a composite of all the stations monitored. The movement at all stations is plotted versus distance from the longwall face at the time of measurement. The use of all stations generates a data point scatter along the profile; however, the convergence trend is apparent. The B panel tailgate exhibited rapidly accelerating closure after the passage of the A panel longwall face. Approximately 1,000 ft behind the A panel face, 0.5 ft of convergence occurred. The C panel tailgate did not exhibit the rapid convergence as the B panel face

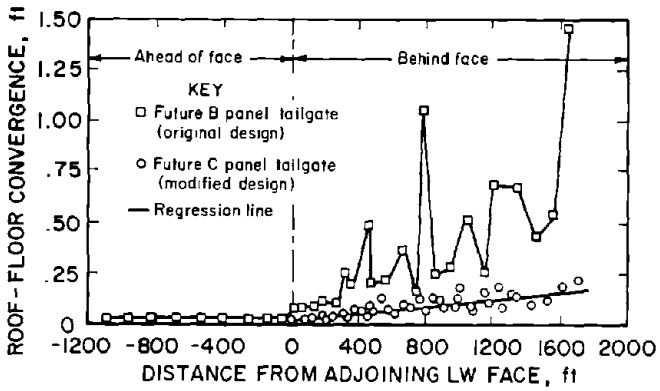

Figure 4.—Convergence in the original and modified pillar systems from the mining of the adjoining longwall panel (future B and C panel tailgates).

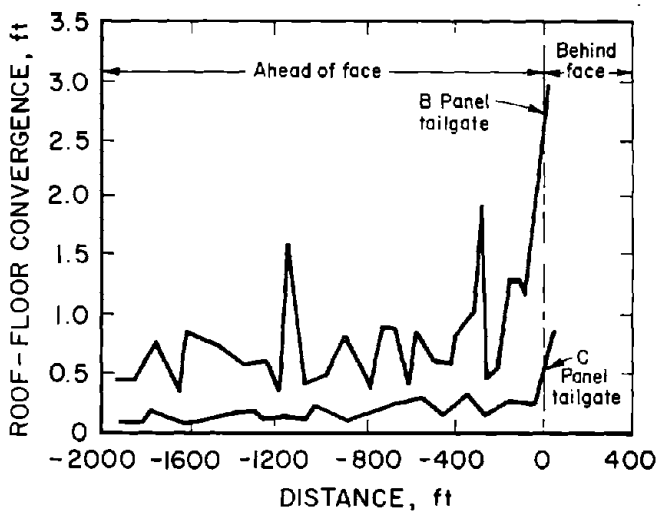

Figure 5.—Convergence in B and C panel active tailgate during longwall extraction.

passed. Approximately 1,000 ft behind the face, only 0.08 ft of movement occurred.

Figure 5 shows the closure in the B and C panel tailgates as the active longwall face approached the tailgate stations. The roof to floor convergence profiles are a composite of all the stations monitored as described for figure 4. The B panel, original-design tailgate rapidly converged as the face passed. Over 2.5 ft of movement occurred at the tailgate drive motor and was associated with broken roof conditions. The new pillar design only allowed approximately 0.5 ft of movement at the tailgate drive motor without roof breakage. The new pillar design has demonstrated a reduction of transferred abutment stresses as shown by the reduction of roof to floor tailgate convergence during both the extraction of the previous adjacent panel and the extraction of the active panel.

Ventilation Between Gobs

Mining experience has demonstrated an improved ability to ventilate between the active and previous gob for approximately 70% of the panels mined with the modified design. The previous designs have allowed similar enhanced ventilation for fewer than 10% of the panels mined. With the new gate design, ventilation restrictions occurred near the completion of the panels, whereas the old gate design allowed restrictions early in the life of the panels. Consequently, an improvement in longwall face ventilation has been noted.

Tailgate Pillar Bumps

The old and new longwall gate pillar designs were also evaluated and monitored in a bump-prone portion of the Virginia Division by the U.S. Bureau of Mines. The results of the Bureau studies are well documented (*5*).

The bump-prone area was approximately 2,000 ft deep and contained a massive quartzite sandstone within the overburden. The Bureau monitored two adjoining longwall gate developments. The first monitored development consisted of the old pillar design with a 100- by 100-ft center middle abutment pillar. The flanking yield pillars were on 50- by 100-ft centers. The second area monitored consisted of the new gate pillar design which incorporated a 140- by 200-ft center abutment pillar. The flanking yield pillars were 40- by 100-ft center distance. The two adjoining study areas had similar floor, roof, and overburden conditions. Monitoring by the Bureau involved measurements of pillar stress levels, pillar dilation, roadway roof to floor closure, and inspections of longwall operating conditions.

As the longwall panel was being mined in the first study area, the 100- by 100-ft center pillars exhibited rib spalling 1,000 ft ahead of mining and began bumping 500 ft ahead of the retreating longwall face. The pillar system failures allowed abutment stresses to concentrate at the tailgate corner of the panel face. This situation occasionally allowed tailgate corner face bumps as the shearer mined out the tail portion of the face.

During the extraction of the panel having the new tailgate pillar design (second study area), monitoring was conducted in a manner identical with the first study area. Measurements and observations revealed that tail- gate entry stability was undisturbed 200 ft ahead of the face. Mining the panel face did not generate severe face bumps at the tailgate corner. Furthermore, the large abutment pillars did not begin to bump until approximately 100 ft behind the face, and the bump intensity was greatly diminished in comparison to the events experienced with the old gate design. In summary, the severe tailgate pillar bumps were eliminated with the new design.

CONCLUSIONS

Improvements in gate performance have been accomplished by increasing the dimensions of the middle abutment pillar in a 4 entry longwall development. The larger abutment pillar formed a stronger pillar core, which provided more load resistance, and transferred the stress to the strong mine floor rather than allowing the pillar to fail violently. The new gate design slightly increased the total development width by typically 50 ft. The primary pillar stability improvement was accomplished by eliminating a middle pillar crosscut every 200 ft (fig. 2).

The modified design is efficient in that approximately a fourfold increase in calculated R/L ratio was accomplished with only a minimal increase in total development width. The 140- by 200-ft center distance pillar in the bump test area has a calculated R/L ratio approximately 360% greater than the 100- by 100-ft center distance pillar. The Bureau underground instrumentation determined that the new pillar design offered approximately a 270% increase in square feet of core per feet of gate development when compared with the old pillar system. The 360% calculation difference and the 270% instrumented pillar difference suggests that the R/L ratio is not a perfect design tool. However, the calculated R/L ratio and the Bureau instrumentation both signify that a major improvement has been accomplished. This indicates that the R/L ratio is a useful design guide for deep conditions.

LONGWALL VENTILATION SYSTEM PILLAR DESIGN

Pillar design experience and underground roadway monitoring experience were applied to optimize the design of a pillar configuration for a longwall ventilation system. The setting involved a series of adjoining longwall panels as shown in figure 6 positioned against the southern perimeter of the mine boundary. Along the southern periphery of the panels, a bleeder development was required. The bleeder development allowed the return air from the western side of the extracted longwall panels to course to the exhaust shaft shown in figure 6. Figure 6 depicts the

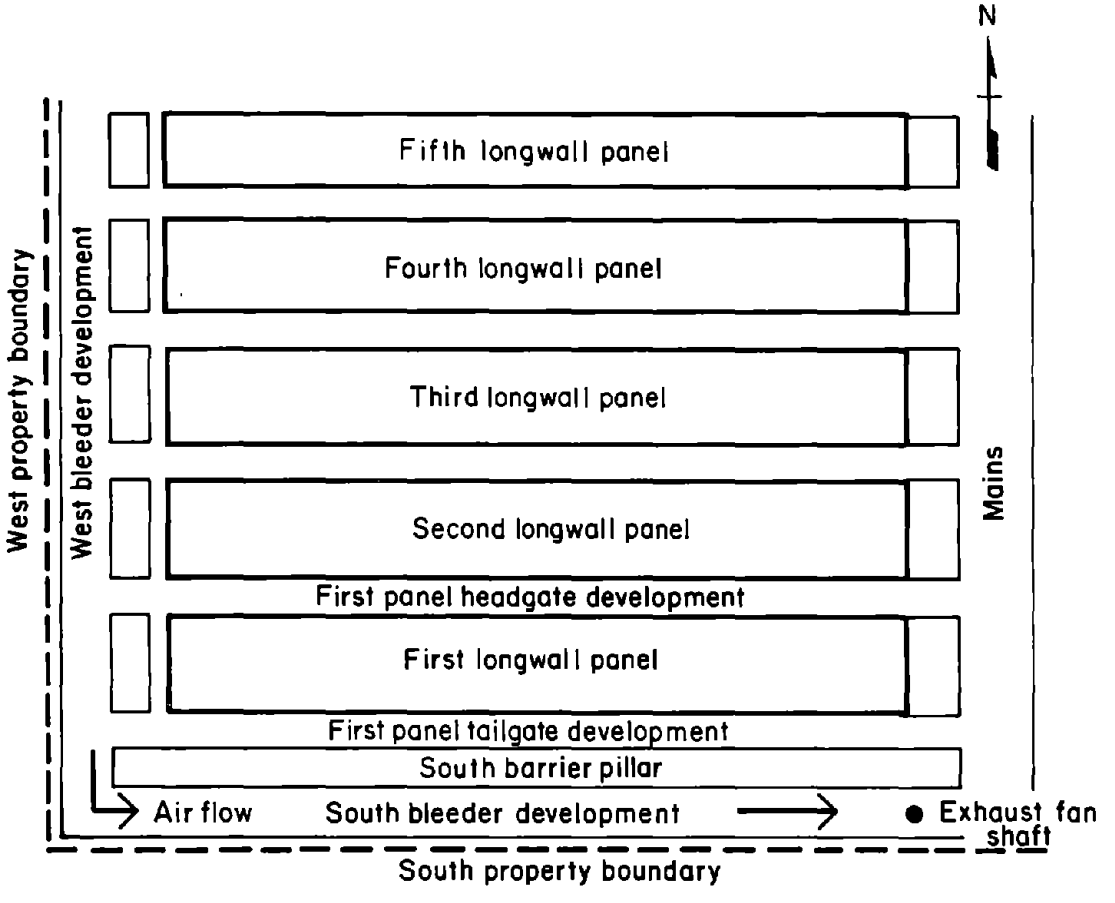

Figure 6.—Diagram of sequence of longwall panel extraction and position of exhausting fan shaft, south bleeder development, south barrier, and first panel tailgate development.

original conventional barrier and development configuration prior to the design modification discussed in the following section. The extremely gassy nature of the coal seam and the resulting high-ventilating airflows mandated that the bleeder development have a minimum of four entries for air courses. The south barrier pillar separated the bleeder and the first panel tailgate (fig. 6). The first panel tailgate and the order of panel extraction are shown schematically in figure 6.

MODIFIED LONGWALL VENTILATION SYSTEM

The pillar design work in this case study involved the south bleeder, south barrier, and the first panel tailgate development. Normally, the south bleeder and tailgate development are driven as two independent sections separated by a substantial barrier. The barrier pillar is traditionally sized at a 300- to 400-ft width to prevent roadway degradation in the bleeder from the abutment stresses from the extracted longwall panels. Furthermore, the bleeder and tailgate development must both be mined with a minimum of four entries in order to have sufficient air courses to ventilate the continuous mining units. The traditional development widths ranged from 250 to 300 ft.

The south bleeder was only required to have a life of approximately 4 years (3 years minimum to 5 years maximum). Consequently, a life of mine barrier design was not necessary. Furthermore, the decision was made to enhance mining efficiency by mining the bleeder and first panel tailgate with only one continuous miner crew. The resulting pillar configuration for the bleeder, barrier, and tailgate is the six-entry system shown in figure 7.

The modified bleeder system and combined tailgate pillar system design is a six-entry development with a short-term barrier pillar incorporated into the design between the fourth and fifth entries. A five- or six-entry development with traditional near equal size pillars was not feasible because of the magnitude of the longwall abutment stresses. The region is situated under 1,500 to 1,900 ft of overburden. If a barrier was not incorporated into the design, the resulting pillar and floor failure would probably destroy the ventilation stopping between the longwall gob and bleeder entries, making methane ventilation control impossible. Also, the resulting stress transfer into

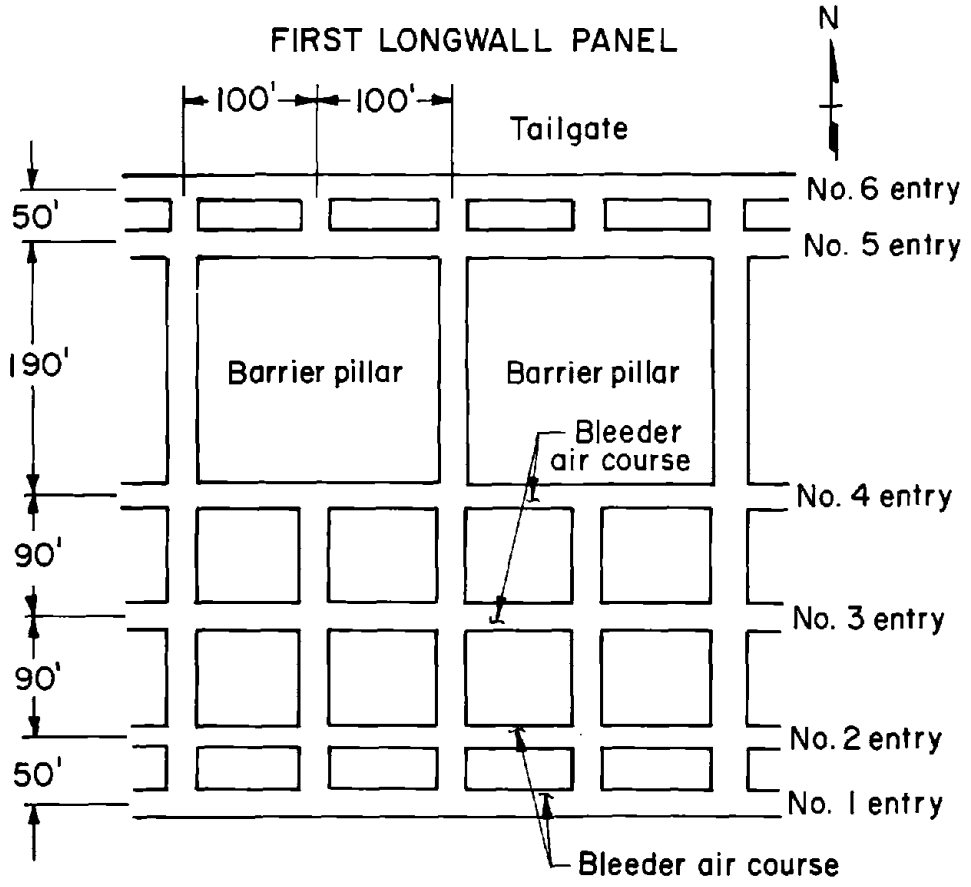

Figure 7.—Modified pillar configuration for the south bleeder, barrier pillar, and first panel tailgate.

the bleeder entries would generate roof falls and roof-to-floor closure, substantially restricting the bleeder air courses. A bleeder ventilation system failure would jeopardize the productive extraction of the bank of longwall panels.

BLEEDER SYSTEM PILLARS DESIGN

The pillars shown in figure 7 are discussed based on their relative placement.

Small Perimeter Pillars

Small perimeter pillars were established along the south and north flanks of the development at 50- by 100-ft center distance as shown in figure 7. Pillars of these dimensions have essentially zero pillar strength when calculated using resistance for Limit of Roadway Stability with yield in roof, seam, and floor. Consequently, the R/L ratio is 0, and the pillar is considered to be a yield pillar for deep mining conditions. The southern perimeter yield pillars serve as ventilation partitions where overburden control is maintained by the flanking unmined barriers and middevelopment pillars. These yield pillars increase mining efficiency by minimizing gate development width and by reducing the bleeder system total width of excavation, which allows more longwall panel width to be extracted within the property boundary. The northern perimeter yield pillars allow the mining of the large abutment pillars. The gassy Pocahontas No. 3 coal seam operating constraints require that these yield pillars serve as ventilation partitions which allow the excavation of the large abutment pillar. Under less gassy mining conditions, the northern perimeter yield pillars would not be necessary and the bleeder system design could encompass only five entries.

Roof to floor convergence monitoring on continuous miner developments as well as the Virginia Division mining experience has shown that, for main entry development, the roadways surrounding the 50-ft center distance yield pillars remain as stable as the roadways surrounding the larger abutment pillar systems. However, the data indicate that the yield pillars must be placed adjacent to barriers in order to maintain the most stable roadways.

Middle Development Pillars

Conventional pillars with a center size of 90 by 100 ft are placed near middevelopment in the bleeder system shown in figure 7. These pillars have a R/L ratio of 0.53 with pillar strength based on Limit of Roadway Stability with yield in roof, seam, and coal. R/L ratios from 0.5 to 0.6 have been shown to be satisfactory for the Virginia Division mains development. No longwall extraction abutment stresses are added to the loading condition in determining the R/L ratio for main pillars because these pillars are normally protected from such stresses by barrier pillars.

Yield pillars at midsection were considered. However, previous monitoring data suggest that yield pillars placed at midsection allow a higher rate of roof to floor roadway convergence. Visual inspection cannot distinguish the degree of such movement. Roadway roof to floor convergence stations with dial-gauge instruments capable of measuring to 0.05 in of movement are required. Yield pillar roadways surrounding yield pillars placed at midsection have shown approximately twice the closure rate when compared with roadways surrounding yield pillars positioned alongside barriers. Consequently, the yield pillars are placed only on the outside of the development for the bleeder system design to achieve the most stable configuration.

Barrier Pillar

The barrier pillar was positioned to slow the longwall abutment stress transfer onto the bleeder air courses. The monitoring data from the previous longwall development case study were used to assess the barrier size requirement. That study involved a 150- by 200-ft center distance pillar subjected to longwall abutment stresses. After extraction of the first panel, longwall abutment stresses crossed the 150-ft-pillar. However, the degree of roadway deformation and damage was considered to be acceptable for roadways which must only serve as 4-year air courses. An R/L ratio of 0.48 was calculated for the 150- by 200-ft pillar by applying the pillar strength based on limit of roadway stability and load transfer off the extracted longwall panel as described by Carr and Wilson (*3*). To ensure that the bleeder roadways would only require minimal supplementary support, the bleeder barrier pillar R/L ratio was increased by 25% to 0.60. The resulting barrier is the 190- by 200-ft center distance pillar shown in figure 7.

In the previous case study, it was determined that the 150- by 200-ft center distance pillar allowed a calculated transferred load across the system in excess of 30,000 st/ft. This calculated magnitude of load transfer, for the Virginia Division mining conditions, generates only limited roadway damage. In contrast, a calculated 30,000 st/ft load transfer in the mining conditions described by Carr and Wilson (*3*) generates a severely damaged roadway. Consequently, the application of R/L ratios for pillar design modifications must be based on the proper overburden, immediate roof, and floor horizon geologic conditions to achieve a proper design modification.

OPERATING CONSIDERATIONS

The total development width of the bleeder system was 470 ft. In contrast, the conventional bleeder, barrier, and tailgate design previously used would have a total width of approximately 820 ft. The net effect is that 350 ft of longwall panel width is gained with the modified bleeder system, which corresponds to a gain of 370,000 st of additional, highly efficient longwall production.

Developing with the modified six-entry bleeder system reduced continuous miner excavation by 28% compared with a traditional design. Continuous miner efficiency is typically hampered by the gassy Virginia Division mining conditions. Consequently, minimizing continuous miner excavation achieves an operating benefit. Furthermore, mining with the new design only required one operating unit rather than the two independent units required if the bleeder and tailgate were separated by a traditional barrier.

The implementation of the new ventilation design required that heavy-duty ventilation stoppings be constructed in the barrier pillar crosscuts to withstand the roof to floor closure which would occur within the barrier pillars. The heavy-duty ventilation stopping consisted of steel fiber reinforced concrete crib blocks. The stopping wall was 0.67 ft wide with three solid, 2- by 2-ft, concrete cribs incorporated into the wall design for stopping reinforcement. Minimal supplemental support, primarily consisting of five wood cribs per intersection, was installed to reduce the potential for roof falls within the bleeder air courses.

BLEEDER AIR COURSE RESULTS

Mining of the new ventilation system began in mid-1988. Longwall extraction of the first panel began in April 1989, with the first panel extraction completed in 6 months. The changing air course conditions within the bleeder were monitored through periodic roadway mapping.

The new design has been subjected to over 2.5 years of exposure to abutment stresses from the adjacent extracted longwall panel. The extraction of the first four longwall panels has been completed. The remaining panel to be mined consists of a remnant barrier, which is to be mined on retreat as the final mining in the southern reserves. Only two roof falls and minimal roof degradation have materialized in the bleeder air courses after the inception of longwall mining. After 30 months, only two barrier pillar stoppings required repair.

Roof to floor closure (floor heave) changes have been most evident. Mapping the floor heave conditions offers an understanding of the transferred pillar load situation. Only the four bleeder entries and associated crosscuts were mapped with the roadways categorized based on the conditions listed in table 1. Roof-to-floor convergence stations were not established because it was believed that the overall conditions in the bleeder system could be assessed through broad areal extent roadway mapping.

Table 1.—Bleeder air course roof to floor closure condition

Category	Approximate condition
A	Normal
B	0.5 to 1 ft closure
C	1 to 1.5 ft closure
D	1.5 to 3 ft closure
E	3 ft to 75% closure
F	Greater than 75% closure
R	Roof fall

The barrier pillars reacted first to the loads imposed by the extracted longwall panel. Eight months after the beginning of longwall mining (2 months after first panel completion), the barrier pillar crosscuts typically exhibited type B closure. Approximately 12 months after the beginning of longwall mining, the abutment pillar crosscuts typically exhibited type C closure and stress transfer became evident in portions of the bleeder system.

Bleeder air course deformation was documented. Figure 8 depicts the roof to floor convergence conditions within the bleeder at the 12-month elapsed period after the beginning of longwall mining. Over the subsequent months, conditions generally remained unchanged, except a 600-ft region exhibited slow gradual floor heave. This region is shown in figure 9, which depicts the roof to floor closure conditions within the bleeder at the 30-month elapsed period after the beginning of longwall mining.

In summary, the air courses have remained sufficiently stable for bleeder system ventilation. The roof fall situation and closure rates indicate that the bleeder system pillar design will maintain satisfactory air courses for at least an additional 2 years, which is well beyond the required operating life.

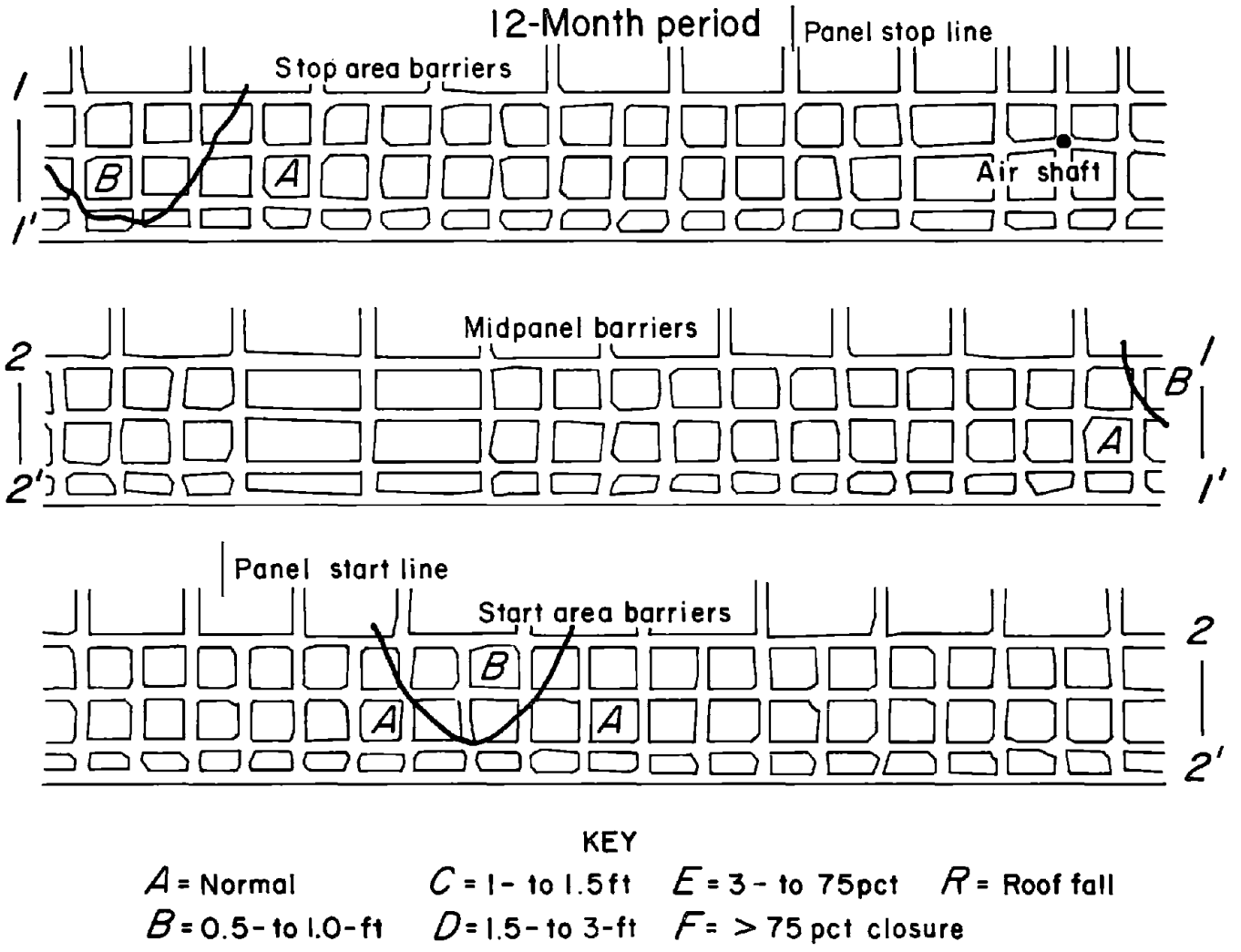

Figure 8.—Bleeder air course roadway closure conditions 12 months after the beginning of longwall mining.

DESIGN APPROACH LIMITATIONS

Monitoring may be applied to optimize an existing pillar design without the need for the R/L ratio design approach. The R/L ratio design approach is most suited for substantial design changes where a strong operational need must first exist for the new pillar design. The R/L ratio design approach relies heavily on studying the implemented design. However, the design philosophy must not be considered to be a random trial-and-error process. The process is driven by a calculation methodology with the calculation process being heavily reinforced through underground monitoring of the new or previous designs. Consequently, experience and time play extremely important roles in design implementation and optimization. In addition, the design process requires an individual or organization devoted to documenting the design consequences.

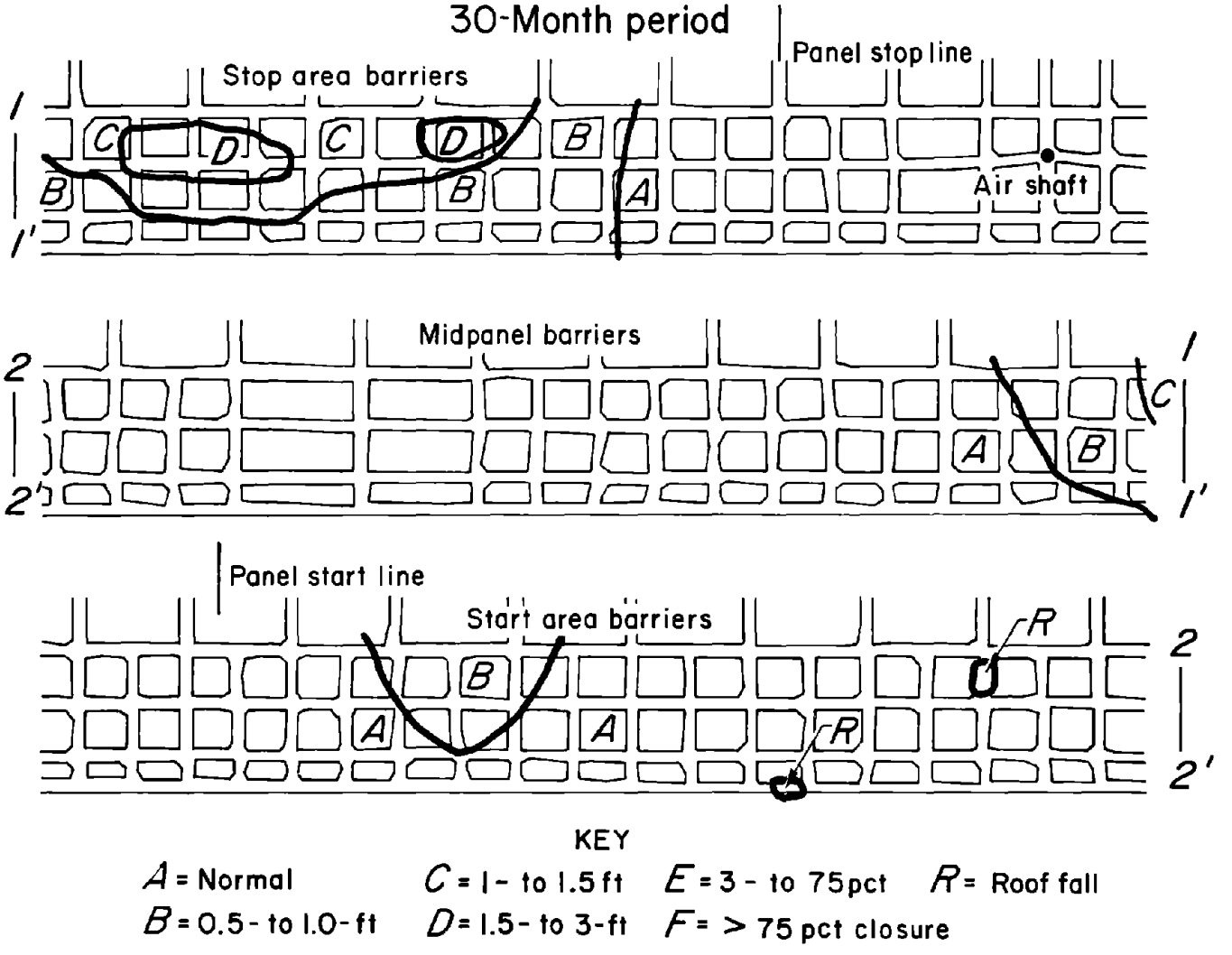

Figure 9.—Bleeder air course roadway closure conditions 30 months after the beginning of longwall mining.

REFERENCES

1. Peng, S. S. Coal Mine Ground Control. Wiley, 1979, 450 pp.

2. Wilson, A. H. Technical presentation, personal communications, and lecture, Jim Walter Resources, Inc., Brookwood, AL, 1981.

3. Carr, F., and A. H. Wilson. A New Approach to the Design of Multi-Entry Developments for Retreat Longwall Mining. Paper in Proceedings of the Second Conference On Ground Control In Mining, WV Univ. July 1982, pp. 1-21.

4. Campoli, A. A. and K. A. Heasley. Coal Mine Bump Research: Providing Tools For Rational Longwall Design. Paper in Proceedings of the 23d International Conference of Safety in Mines Research Institutes, Washington, DC, Sept. 11-15, 1989, comp. by E. T. Wallace and T. H. Koslosky. BuMines OFR 27-89, p. 667; NTIS PB 89-225262/AS.

5. Campoli, A. A., T. M. Barton, F. C. Van Dyke, and M. Gauna. Mitigating Destructive Longwall Bumps Through Conventional Gate Entry Design. BuMines RI 9325, 1990, p. 34.

6. Gauna, M., H. Epperly, and K. R. Price. Longwall Gate Pillar Design For Deep Gassy Environment. Paper in Proceedings, Twenty-First Annual Institute On Coal Mining Health, Safety, and Research, Dept. of Min. Miner. Eng., VA Polytechnic Inst. and State Univ., Blacksburg, VA, 1990, pp. 83-90.

COMPREHENSIVE INTEGRATED APPROACH FOR LONGWALL DEVELOPMENT DESIGN

By G. J. Hasenfus[1] and D. W. H. Su[2]

INTRODUCTION

Coal pillar design practices, including those for longwall development, often rely on a pillar safety factor concept to provide a means of assessing the overall development design stability. Designs based on traditional coal pillar safety factors have been found to be suitable in many standard room-and-pillar applications, particularly where roof and floor instability and large abutment loads are not present. However, this conventional design approach often fails to account adequately for the more complex design necessities of longwall development. These design factors include not only pillar stability, but also the stability of the roof, floor, and ribs, which are necessary for safety, ventilation, and longwall productivity. Most design methodologies also fail to address potential effects on the environment. In addition, important geomechanical effects on pillar loading, such as those due to roof and floor constraint, floor heave, and overburden caving and deformation, are not considered in many conventional designs.

The primary objectives for any longwall development design should be safety and entry stability. Any design approach must therefore account foremost for the stability of the roof, floor, and ribs along all vital passageways for both the headgate and tailgate mining phases. In addition, in areas where there is a potential for bumping, bump control considerations are vital. The use of yield pillars, with or without abutment pillars, to control complex multiple-seam interactions, deep overburden abutment stress, or high horizontal stresses may also be warranted and should be an integral part of the design approach.

From a ventilation standpoint, the longwall development design should provide an open air course to ventilate the longwall face and to provide bleeder air for the gob. Thus, prevention of large roof falls and floor heave is very important, even for the gob stage of longwall development entries. From a production standpoint, high productivity requires that the immediate headgate and tailgate entries and the headgate T-junction remain free from roof falls and floor heave that could limit ventilation and obstruct the free passage of miners, supplies, and longwall face equipment. The longwall pillar design should also consider the effects on the environment, such as the protection of surface structures and possible near-surface hydrological effects.

Other factors not related to stability also may play an important role in determining the pillar sizing and configuration for longwall development. For example, ventilation and methane experience may require a given number of entries. The areal extent of the minable reserve may dictate the panel-to-development width ratio. Development mining concerns may also have to be considered. These can include optimizing miner section advance rates, development pillar geometry, and miner equipment accessibility (i.e., place change versus satellite miners, or battery or diesel versus cable-operated equipment). The availability and cost of main and supplemental roof support are also important. Finally, one must always respect valid opinions based on experience and past design performance, namely: "don't fix what ain't broke."

In traditional longwall development designs based on pillar stability, the average coal pillar stress state is typically defined by depth, overburden rock density, coal recovery, and abutment loading factors. The pillar strength is often defined by a normalized coal strength value, pillar size and shape factors, and a triaxial confinement factor. However, even for pillar stability alone, it is recognized that contemporary designs must account for roof and floor frictional confinement, the potential for pillar unloading or settlement due to floor heave, caving and overburden deformation, and in situ horizontal stresses. All of these factors can contribute to a nonuniform, triaxial state of stress in mine pillars. In fact, the ratio of uniaxial compressive strength (or estimated pillar strength based on any existing formula) to average vertical pillar stress is often not accurate and may be meaningless as an index of safety, especially for pillars subject to high variable longwall abutment pressures or for yield pillars. Therefore, computation of the distribution of the local factor of safety in the pillars and for the surrounding entryways provides a more

[1]Research engineer.
[2]Senior research engineer.
CONSOL Inc., Library, PA.

accurate assessment of the longwall development stability because the effect of roof and floor geology can be included.

Not all of these design considerations and parameters can be accounted for by any current model. However, it is important that any attempt at a comprehensive pillar design model include all pertinent geotechnical parameters and that the results address the major geomechanical concerns, including not only pillar stability, but also roof and floor stability, overburden deformation, and surface subsidence. This paper advocates a comprehensive integrated longwall development design methodology based largely on the use of finite-element modeling and supported by a program to determine the geomechanical properties of the coal seam, floor, roof, and overburden. Subsequent observations of overburden deformation and surface subsidence, and underground pillar stress and roadway convergence are used to validate and refine the model.

COAL PILLAR DESIGN MODELS

In general, five coal pillar design model classifications can be defined according to decreasing reliance on empirical data and experience: empirical models, semiempirical models, semianalytical models, analytical models, and numerical models. Although each model concept may provide acceptable results, they become less applicable to previously unmined regions to the extent that they rely on experience and empirical data.

Pre-1960 designs tend to rely almost exclusively on empirical models based only on past experience and observations. Many companies still employ this approach for lack of other resources. In addition, barrier pillar formulas tend to be empirically based (*12*).[3]

Semiempirical approaches to pillar design became very popular in the early 1960's and are still considered applicable for room-and-pillar designs under shallow-to-medium cover. The Obert and Duvall (*11*), Holland-Gaddy (*8*), Salamon and Munro (*16*), and Bieniawski (*4*) formulas for coal pillar design are examples of this approach. Typically, these design formulas rely upon coal strength characteristics and empirically derived strength relationships for pillar size and shape. Rarely considered, however, are roof or floor conditions, coal strength mechanics, pillar stress distribution, or the in situ horizontal stress state, all of which affect pillar and entry stability.

Most of the models categorized as semianalytical were developed to specifically account for high-extraction or longwall mining. Examples in this category include those advocated by Mark (*10*), Choi and McCain (*5*), and Wilson (*21*). Semianalytical models typically account for abutment loading and abutment load distribution, and are thus more acceptable for longwall mining design than semiempirical models. In addition, models based on the Wilson approach also account for the individual pillar stress distribution, progressive pillar failure, and roof and floor constraints. One disadvantage of the semianalytical models is that they are usually applicable only in areas where sufficient experience with the model and mining conditions have been attained. This is due to the model constraints and input assumptions, which often simplify the many geomechanical relationships that affect longwall development stability. As such, safety factor adjustments are often necessary. One example of this shortcoming is the inability of most semianalytical models to adequately calculate pillar safety factors for longwall development under deep cover (>1,000 ft) since they tend to underestimate the effect of confinement on coal strength in large pillars. Another disadvantage of these models is that they usually base entry stability on the stability of the pillar and do not directly consider roof and floor stability as integral parts of the model.

The fourth model classification is purely analytical and relies almost entirely upon geomechanical theories and principles typically placed in a closed form solution. An example of this approach is that proposed by Salamon (*15*). While almost nonreliant upon empirical relationships, this approach may suffer from its inability to account for many possible geological, geometric, and time-related complexities in a closed form solution. Therefore, designs based on analytical models may be oversimplified.

The last category, the numerical model approach, can provide a more rigorous estimation of the longwall development design response and the corresponding safety factors then are possible by models in the first four categories. This is because numerical models can incorporate the many geomechanical, geometrical, and time-dependent complexities of longwall mining, including those of the roof, floor, and overburden. In addition, numerical models do not rely upon site-specific, empirically derived assumptions or correlations and thus are well suited for coal pillar design in new mining areas. The disadvantages to this approach include difficulties in material behavior simulation; reliance upon detailed, accurate input data; and the need for powerful computing capabilities.

While the numerical modeling approach is advocated in this paper, it is acknowledged that this is not the only means suitable for pillar design. In fact, with sufficient

[3]Italic numbers in parentheses refer to items in the list of references at the end of this paper.

experience, any of the design classifications can be utilized to provide satisfactory results. For situations in which sufficient input data are not available, the semiempirical and semianalytical approaches, coupled with experience and a field monitoring effort, may provide acceptable results.

COMPREHENSIVE INTEGRATED LONGWALL DEVELOPMENT DESIGN APPROACH

The following sections pertain to the longwall development design methodology advocated by the authors. This integrated methodology relies heavily upon a finite-element model. The model, in turn, relies upon a premodel program to measure or estimate the geomechanical characteristics of the coal, roof, floor, and overburden. Upon mining, a field-monitoring program is employed to verify the design and to recalibrate the model, if necessary, based upon mine level, overburden, and surface measurements. Underground measurements also can be used to augment the premining geomechanical test estimates.

GEOMECHANICAL CHARACTERIZATION

Geomechanical or rock strength characterization of the coal, roof, floor, and overburden is well documented and understood. This stage of design typically includes some form of laboratory testing of rock samples obtained from coreholes in advance of mining. In addition, for a preexisting mine, it may include in situ measurements of coal or near-seam rock characteristics and the measurement of in situ horizontal stress. All premodel testing is geared toward model input requirements or information that supports the input data.

Input requirements for the finite-element model employed in this approach include the following coal and rock strength parameters for each stratum:

- elastic constants or nonlinear stress-strain characteristics,
- cohesion,
- internal friction angle.

In addition, other rock mass stress and deformation characteristics are required, including:

- magnitude and orientation of in situ horizontal stress,
- deformation characteristics of the gob,
- location of overburden slip-shear horizons and their frictional characteristics.

An estimation of coal and rock strength characteristics usually is achieved from a combination of International Society for Rock Mechanics (ISRM) or American Society for Testing and Materials (ASTM) approved laboratory tests on rock core. These tests include uniaxial compression, triaxial compression, indirect tensile, direct shear, and/or strength index tests. Alternatively, the rock strength and deformation characteristics can be estimated from sonic and density logs based on proven acoustical-mechanical correlations. In situ measurement through the use of a Goodman Jack and Borehole Shear Tester may sometimes provide a better estimate of in situ coal strength characteristics, considering the well-known problems typically associated with estimating coal strength from drill core.

Where feasible, in situ horizontal stress estimates can be made by overcoring techniques utilizing instruments such as the U.S. Bureau of Mines deformation gauge, the Commonwealth Scientific and Industrial Research Organization (CSIRO) hollow inclusion cell, or by hydrofracture techniques utilizing tools such as the Mindata Minifrac system. In lieu of such measurements, in situ stress should be estimated based on previously accepted measurements that are characteristic of the mine or region.

The keys to the geomechanical test program are that it adequately addresses the model input requirements and that a sufficient number of tests are conducted to account for the variability that may occur throughout the mine area of concern. In addition, whereas most models require only near-seam data, a rigorous finite-element approach requires complete overburden characterization.

FINITE-ELEMENT MODEL OVERVIEW AND VERIFICATION

Unlike many traditional longwall development design approaches that rely heavily on past experience and on many assumptions about pillar and entry response to longwall abutment pressure, the longwall development design concept based on a finite-element approach is a more rigorous, theoretically exact method. The approach presented in this paper has evolved as part of a long-term study designed to evaluate the influence of caving and subsequent overburden response on surface subsidence, stability of chain pillars, and the hydrological effect of longwall mining. Extensive field monitoring has been conducted to validate model applicability.

The finite-element technique was selected because of its ability to account for both near-seam and overburden responses to longwall mining. For instance, caving characteristics of the immediate and main roof strata are known to play a very important role in surface subsidence as well as in overall pillar pressure redistribution, which in

turn determines the maximum abutment pressure and the width of the influence zone. The finite-element approach can be used to simulate caving and fractured areas above a mined-out longwall panel. In addition, slip-shear horizons in the overburden at weak-to-strong rock interfaces, which effectively reduce the flexural rigidity of the overburden rock mass, can be modeled accurately. At the mine horizon, pillar constraint effects such as those from roof and floor frictional confinement can be simulated. The effect of floor heave or roof failure on redistribution of stress in the pillar also can be modeled, as can progressive pillar yielding. The finite-element approach can be used to provide a truly three-dimensional analysis and can account for complex geometries. Finally, in addition to static response, finite-element modeling may be used to analyze possible dynamic effects of pillar loading and unloading.

The finite-element method (FEM) is a powerful numerical modeling procedure, and its applications to solving engineering problems have been discussed in detail by Zienkiewicz (*22*). However, many previous applications of the finite-element method to problems related to underground coal mining achieved only limited success. This can be attributed to computer hardware constraints and program inabilities to incorporate effective interface elements, appropriate nonlinear material models with strain softening, and dynamic capabilities. Fortunately, such limitations have been removed over the past decade, and these advanced capabilities are available in a few selected general purpose programs.

One of the finite-element programs typically employed in this research is MSC/NASTRAN, which possesses the capability of modeling shearing and separation along existing planes of weakness and nonlinear material behavior. To describe the modeling procedure and demonstrate its applicability to coal pillar design, information and results obtained from a subsidence and pillar pressure study conducted at a northern Appalachian coal mine [Su and Hasenfus (*17*)] will be used as an example.

Figure 1 shows a symmetric, two-dimensional, three-panel model, which includes 28 layers of interface elements for simulating shearing and separation. By thoroughly examining corehole geologic logs, planes of weakness were defined by identifying layers of relatively soft and thin material when compared with layers immediately above and below. The planes of weakness were assumed to have a friction coefficient of 0.3 and possess little cohesion. When positive pressure exists, the interface elements used to simulate these planes can carry any transverse shear load which is less than the coefficient of friction times the normal load.

Nonlinear analysis adopting elasto-plastic material behavior with strain softening was used to simulate the plastic deformation in coal and rocks surrounding the longwall excavation. The Drucker-Prager criterion was chosen as the yield criterion. The laboratory-determined mechanical properties of the rocks are summarized in table 1. Depending on the size of the element representing different layers, the rock moduli and strengths shown in table 1 were reduced by a scale factor of approximately 1/6 for input into the model to account for discontinuities and effects of pore pressure. The reduction factor was estimated according to $(V/V_o)^{0.167}$, where V_o is the volume of the rock used in the laboratory testing and V ($\leq$125 ft^3) is the volume of the element used in the finite-element model (*9, 20*).

The behavior of the rubblized zone or gob, which was assumed to be formed under an initial bulking factor of 1.50 (*12*), was simulated by a series of interface elements. After reviewing published data (*14, 18*) regarding the properties of broken rocks, the gob elements were assumed to possess very low initial stiffness ($E \approx 1{,}050$ psi) and to acquire much higher stiffness ($E \approx 42{,}000$ psi) after a gob compaction of approximately 22%. The gob material, with a relatively high width-to-height ratio, thus behaves as though it is constrained and follows a nonlinear load deformation curve.

Results from the finite-element modeling are presented in terms of predicted fracture zones above the longwall, predicted overburden deformation and associated shearing along planes of weakness, predicted pillar pressure distribution in the headgates, and predicted surface subsidence. These predictions are compared with field observations to verify the versatility and accuracy of the model.

Figure 2 illustrates the predicted fracture zones above a longwall panel that is 640 ft wide under 710 ft of cover. The extraction thickness is assumed to be 6 ft. The highest elevation of fracturing is seen near the edges of the panel at a horizon 164 ft above the mining level. For the purpose of comparison, the extent of the fracture zone estimated from observing fractures in postmining cores of the overburden strata was approximately 165 ft above the mining level (*17*).

Overburden deformation above the longwall panels and the associated shearing along planes of weakness are indicted in figure 3. The small voids along the interface elements near the edge of the panel do not indicate bedding plane separation, but rather a combination of shearing and compressive deformation along the planes of weakness. To correlate model results with time domain reflectometry (TDR) field measurements shown in figure 4 (*17*), however, shear deformations or shear stress along the traveling (longitudinal) profile are needed. Since coaxial cables used for TDR measurements are usually embedded in a grout column, which constitutes a circular inclusion in a multiple-phase material in the horizontal plane, shear stress rather than shear deformation provides a better means for correlating model predictions with field

Table 1.—Mechanical properties of overburden rocks as determined from laboratory testing

Rock type[1]	Young's modulus × 10^6 psi	Poisson's ratio	Unconfined compressive strength, psi	Cohesion, psi	Friction angle, °
(1) Sandstone	3.15	0.22	8,831	1,966	42
(2) SW sandstone	2.10	.22	8,837	2,600	33
(3) RS limestone	2.52	.22	9,472	2,310	38
(4) FP limestone	4.20	.18	12,610	2,940	40
(5) Shale with sandstone	1.68	.25	5,200	1,625	26
(6) BW limestone	3.15	.22	5,480	1,336	38
(7) Limey shale	2.10	.25	8,060	1,966	35
(8) Interbedded shale sandstone	1.68	.25	6,530	1,700	35
(9) Surface material	.168	.35	660	210	25
(10) Coal	.42	.35	3,450	900	35
(11) Claystone	1.26	.30	2,620	756	30

[1]Numbers in parentheses refer to rock type shown in figure 1.

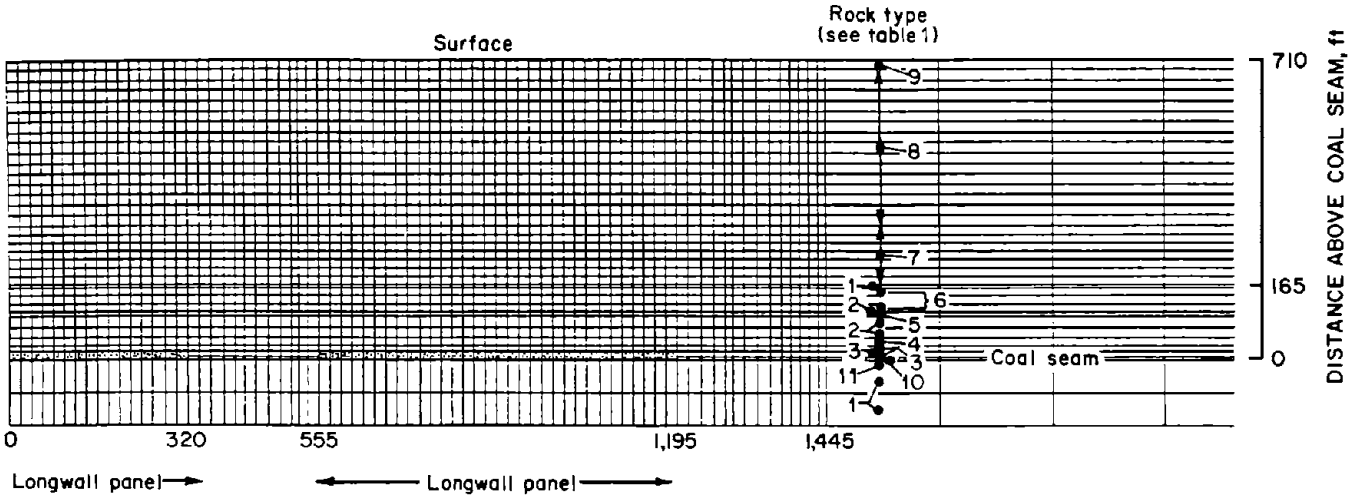

Figure 1.—A three-panel finite-element model.

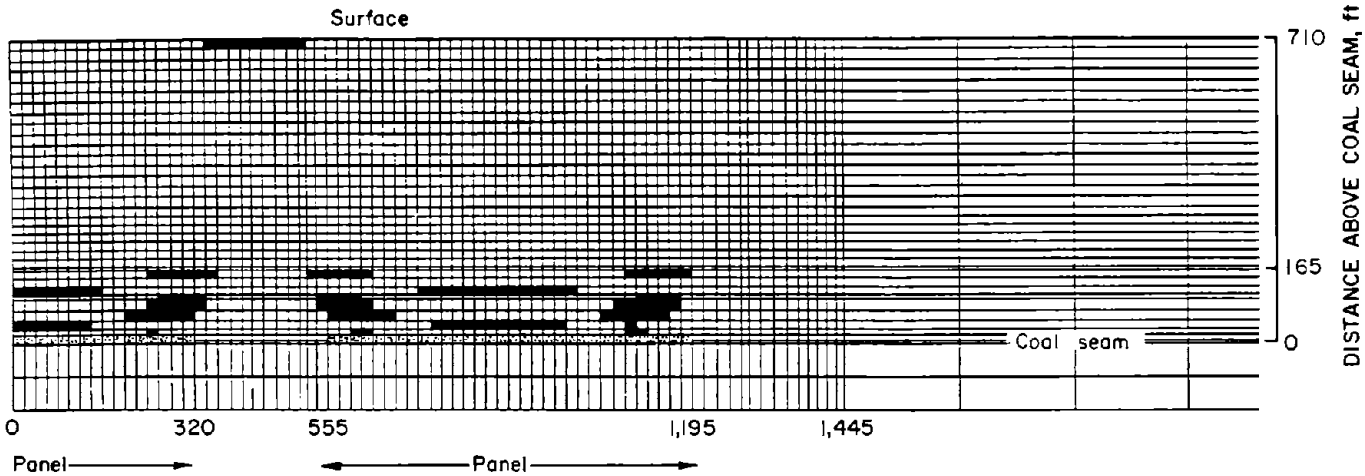

Figure 2.—Induced fracture zones above longwall panels. Darkened area represents fractured zones.

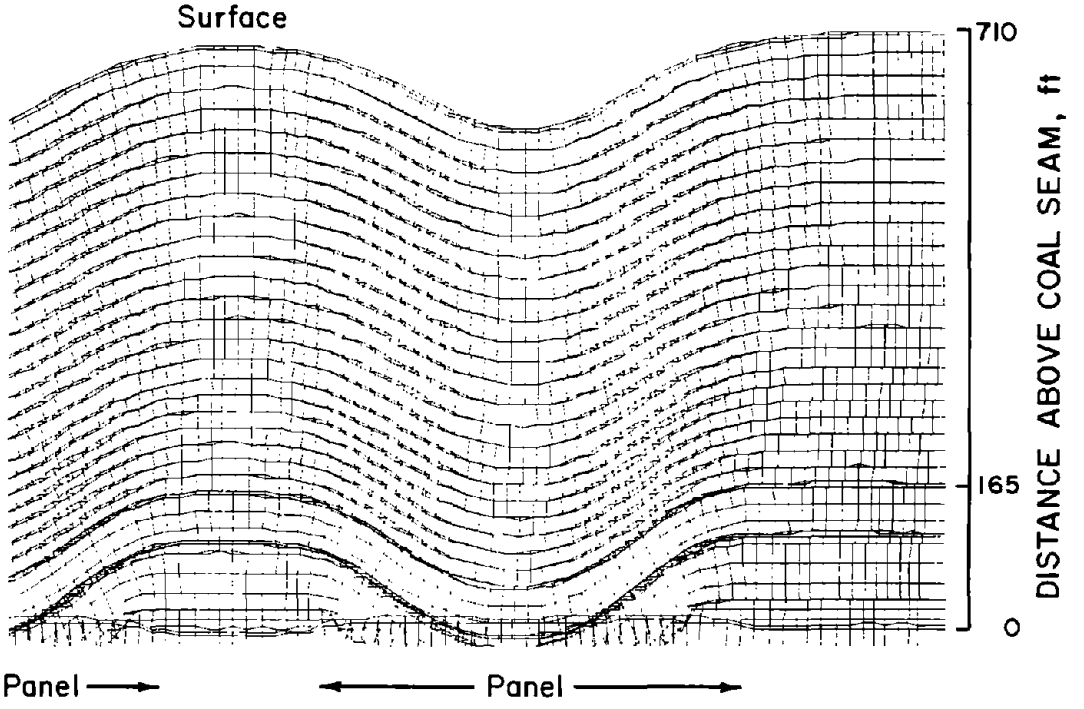

Figure 3.—Overburden deformation over longwall panels (vertical displacment magnified 40 times).

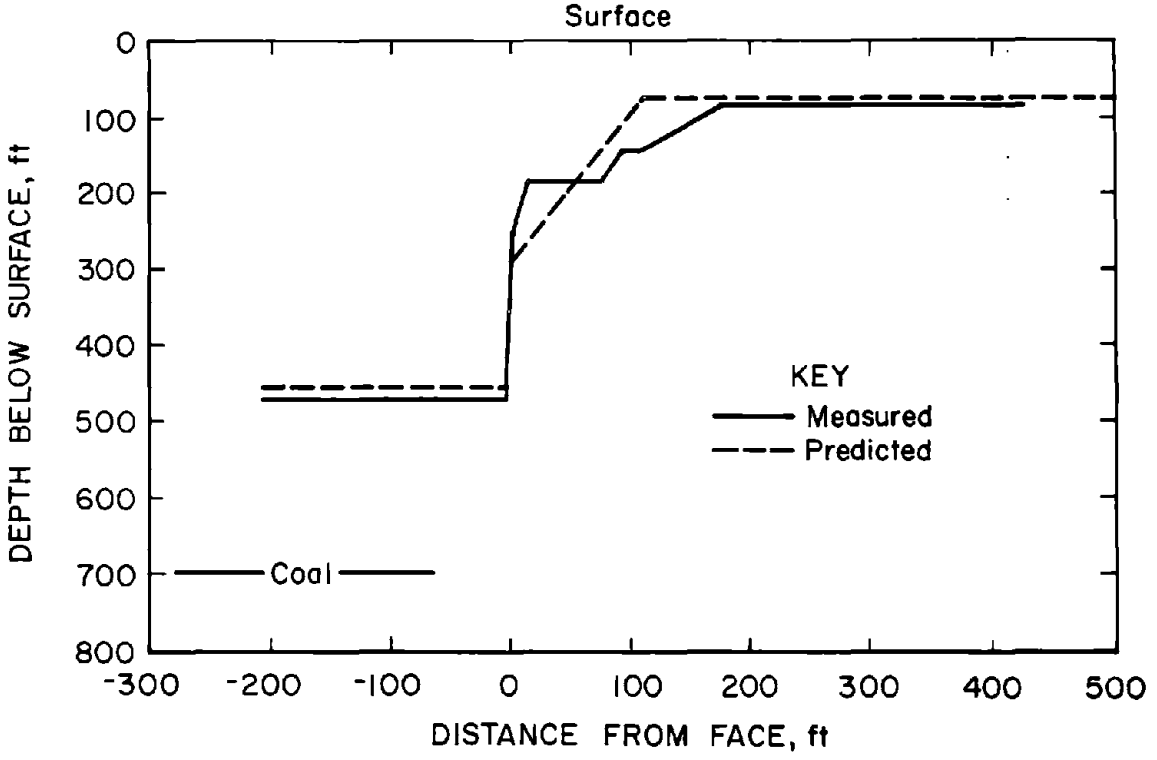

Figure 4.—TDR response above a longwall panel versus face position.

TDR measurements. Table 2 lists the predicted shear stress acting along the longitudinal profile on a grout column with a diameter of 3.25 in. Assuming that a shear stress of 400 psi is required to completely sever the grout column and that the embedded coaxial cables have a diameter of 0.25 in, the predicted TDR response is as shown in figure 4. The predicted TDR response is in close agreement with that observed in the field.

The predicted surface subsidence as a result of longwall extraction is shown in figure 5. The surface subsidence observed in the field (*17*) is included for comparison. The predicted subsidence is in close agreement with that observed in the field.

The predicted distribution of pillar pressure increase across the headgates is shown in figure 6. Note that a second model slightly different from that shown in figure 1 was used to calculate the pillar stress distribution. Mesh refinement was incorporated into the regions surrounding the chain pillars, and near surface layers were removed to optimize the computation cost. However, the important interface shearing and deformation characteristics of the gob were preserved in this model. The pillar pressure increase as recorded by vibrating wire stressmeters (*18*) is included for comparison in figure 6. The predicted distribution of pillar pressure increase is in good agreement with that recorded underground.

In summary, the finite-element model incorporating shearing along planes of weakness and material nonlinearity yields accurate predictions of induced fracture zones, overburden deformation, the resulting surface subsidence above longwall panels, and pillar pressure distribution across the headgates.

FIELD MONITORING

Monitoring to verify the longwall development design is an essential step in the design process. Monitoring typically involves some form of stress (load) and deformation measurement. In the case of coal pillar design, most monitoring programs are conducted only at the mine horizon. As shown in the previous example, with the ability to account for surface and overburden effects and to estimate the resulting deformational and stress state, an integrated finite-element approach also utilizes measurement of overburden deformation as well as surface subsidence. In addition to verification of the design, these observations are used to verify and develop a more accurate model of the complete longwall effect than could be done with underground measurements alone.

Field monitoring measurements also are utilized to formulate a better understanding of the pillar, floor, roof, and overburden response that occurs as a result of longwall extraction. Some examples of observations resulting from field monitoring that have been used to advance understanding of pillar and overburden response to longwall mining are:

- The presence of shear deformation along discrete weak horizons in the overburden as observed by TDR monitoring and supported by increases in hydraulic conductivity measurements from packer testing (fig. 7) (*6*).
- The loss of confinement and subsequent stress reduction in pillars caused by premature yielding of the floor (fig. 8).

Table 2.—Shear stresses acting on a grout column 3.25 in. in diameter

Depth below surface, ft	Shear stress, psi				
	200 ft prior to face passage	Directly above face	100 ft after face passage	150 ft after face passage	500 ft after face passage
30	16.3	53.2	120.5	138.0	75.3
50	57.3	159.5	345.0	347.6	71.0
75	49.6	252.9	500.9	523.6	74.6
100	31.5	289.8	633.3	677.2	74.6
125	12.7	311.5	756.6	816.0	75.9
150	5.94	326.7	877.7	949.7	76.7
175	25.8	342.2	986.1	1,079.0	77.9
200	47.5	354.6	1,105.0	1,204.7	79.5
225	71.7	366.5	1,234.6	1,329.6	80.3
250	100.4	379.9	1,267.4	1,456.3	80.8
275	133.7	391.0	1,294.7	1,582.5	81.5
300	171.4	404.1	1,325.9	1,715.4	82.3
325	213.2	412.4	1,346.8	1,854.2	82.3
350	257.8	416.8	1,367.7	1,955.1	80.8
375	303.7	413.9	1,364.4	2,029.7	77.4
400	349.2	429.2	1,308.6	2,002.6	77.3
420	382.7	423.2	1,277.2	1,948.9	66.1
440	397.9	424.3	1,264.8	1,961.6	66.3
460	400.0	405.4	1,255.0	1,992.8	64.0

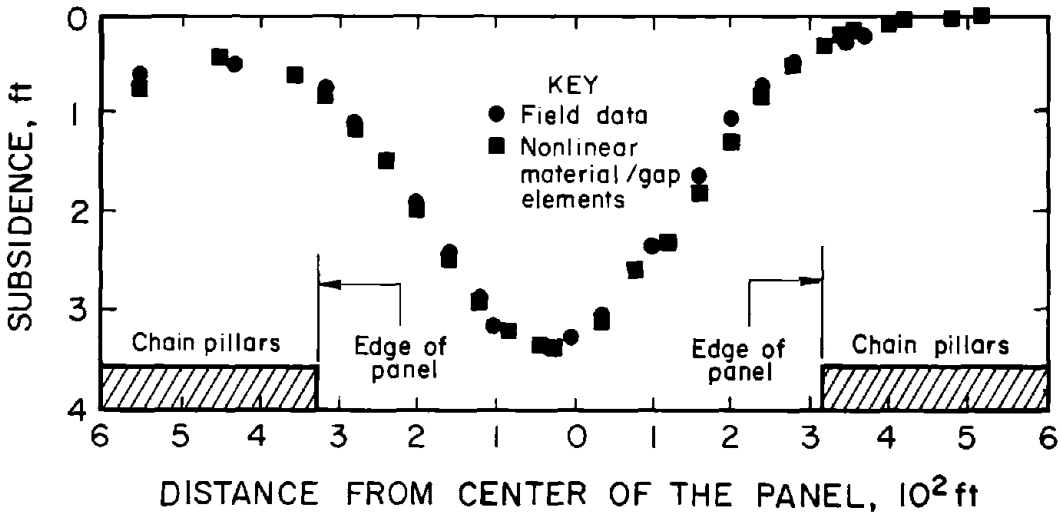

Figure 5.—Measured and predicted subsidence profiles over a 640-ft-wide longwall panel.

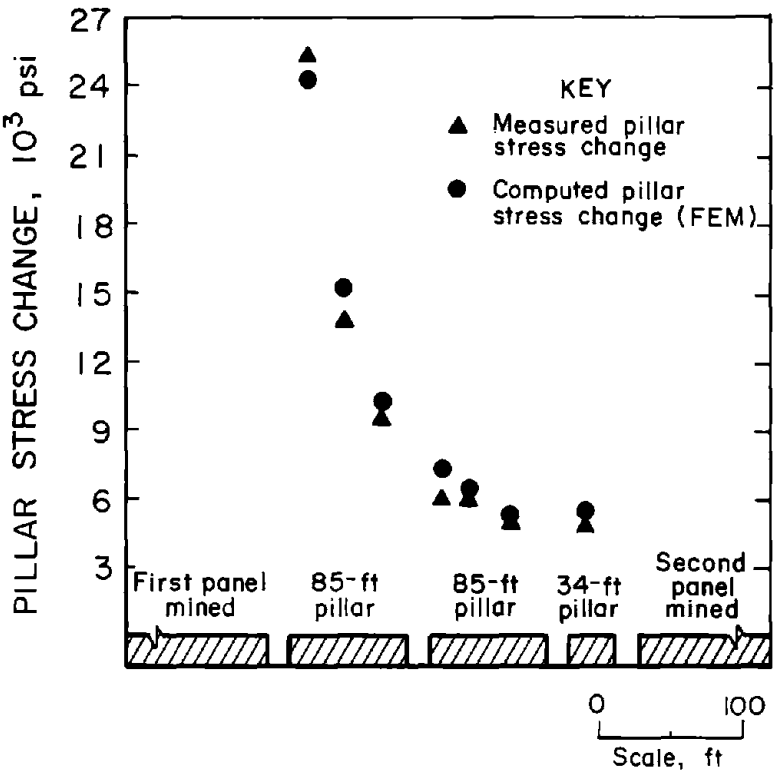

Figure 6.—Comparisons between measured and computed stress changes.

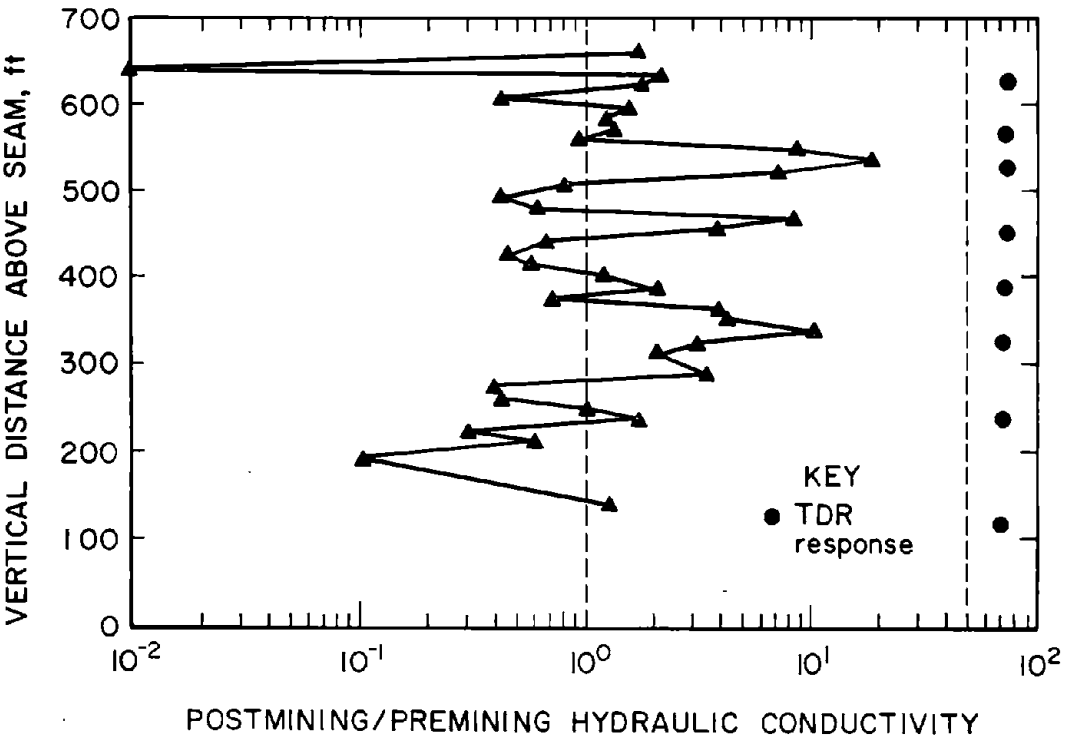

Figure 7.—Postmining-to-premining hydraulic conductivity compared with TDR response horizons.

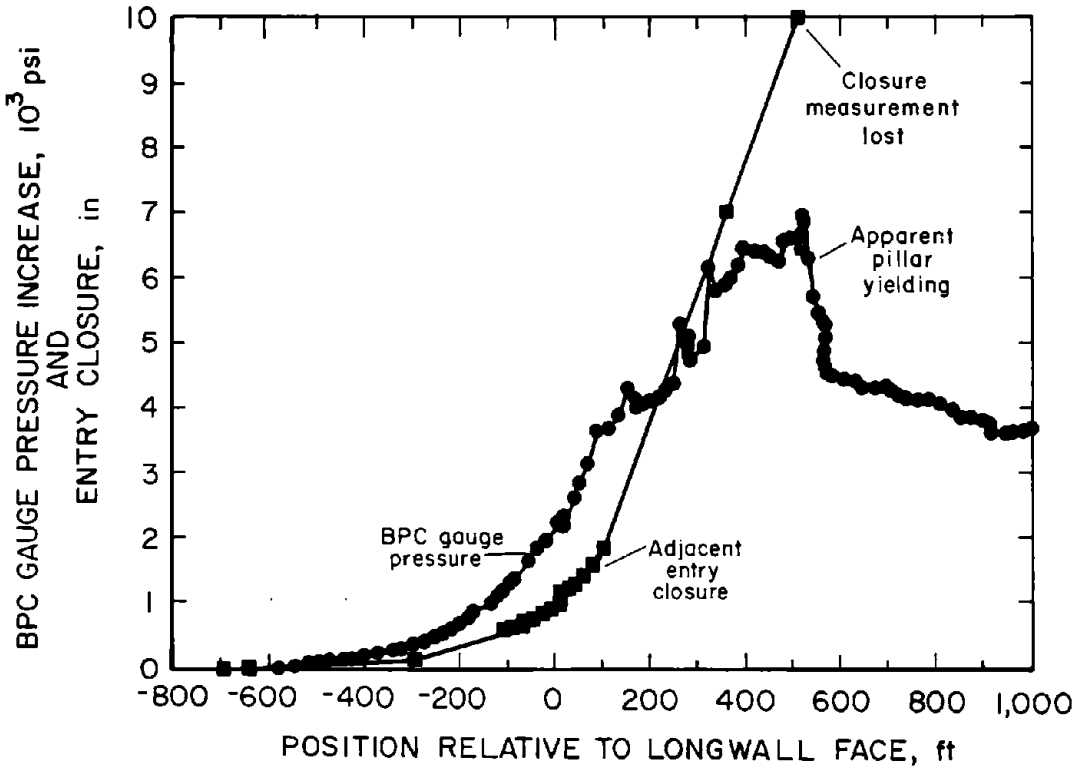

Figure 8.—Premature pillar yielding due to floor heave in deep cover and soft floor; BPC gauge installed 30 ft deep.

- The limited height of the so-called fracture zone determined by postmine coring (*6*).
- The large pressure levels sustained by deep cover pillars as a result of pillar core confinement (fig. 9).
- The apparent yielding around a borehole in a pillar subject to high pressures prior to complete pillar yield (fig. 10).

To institute an effective longwall development design monitoring program, it is necessary to identify the critical parameters and conditions of interest. For example, it is of little use to monitor pressures at only one or two locations in a pillar. The variable pressure distribution within an abutment pillar dictates that a sufficient number of locations be monitored to obtain a pillar stress distribution profile. This requirement can be met by the use of pillar symmetry for instrumentation layout (fig. 11) or the use of multiple pressure gauges per hole. Another example may be the placement of convergence monitoring instruments. If entry convergence measurement is sought to validate pillar stress distribution or stress attenuation (fig. 12), locating the convergence instrument directly adjacent to the pillar is superior to a location near the center of the entry where floor heave and roof sag may increase convergence, thereby skewing the results.

Another important consideration with pillar monitoring is the calibration and understanding of instrument response to in situ conditions. For example, Babcock (*2*), Bauer (*3*), Heasley (*7*), and Su and Hasenfus (*18*) all have addressed the complex issues of calibration of hydraulic pressure cells for measurement of coal pillar stress. The latter authors found that the standard vibrating wire stressmeter, often used to measure coal pillar pressure response, is not applicable for use in soft coals or where the rock mass around a borehole may become plastic or yield. This is because failure in an open borehole will precede the yield of the pillar. Since the vibrating wire stressmeter is not a total inclusion instrument, the borehole collapses into the void around the instrument and the stressmeter unloads prematurely (fig. 13).

Finally, the use of automated monitoring to collect and process field instrumentation is desirable. Aside from the obvious advantage of providing an efficient data acquisition process void of manual data collection errors, automated data acquisition can provide data quality assurance owing to the large quantity of data collected. For example, entry convergence data can often be misleading due to instrument disturbances that may occur in the entryways around a longwall operation. Manual data collection typically does not occur often enough to substantiate these disturbances. However, with frequent, regular, automated sampling, such disturbances can be readily identified and corrected. In addition, automation of data acquisition allows for the possibility of real-time monitoring from remote locations in situations that are of vital interest.

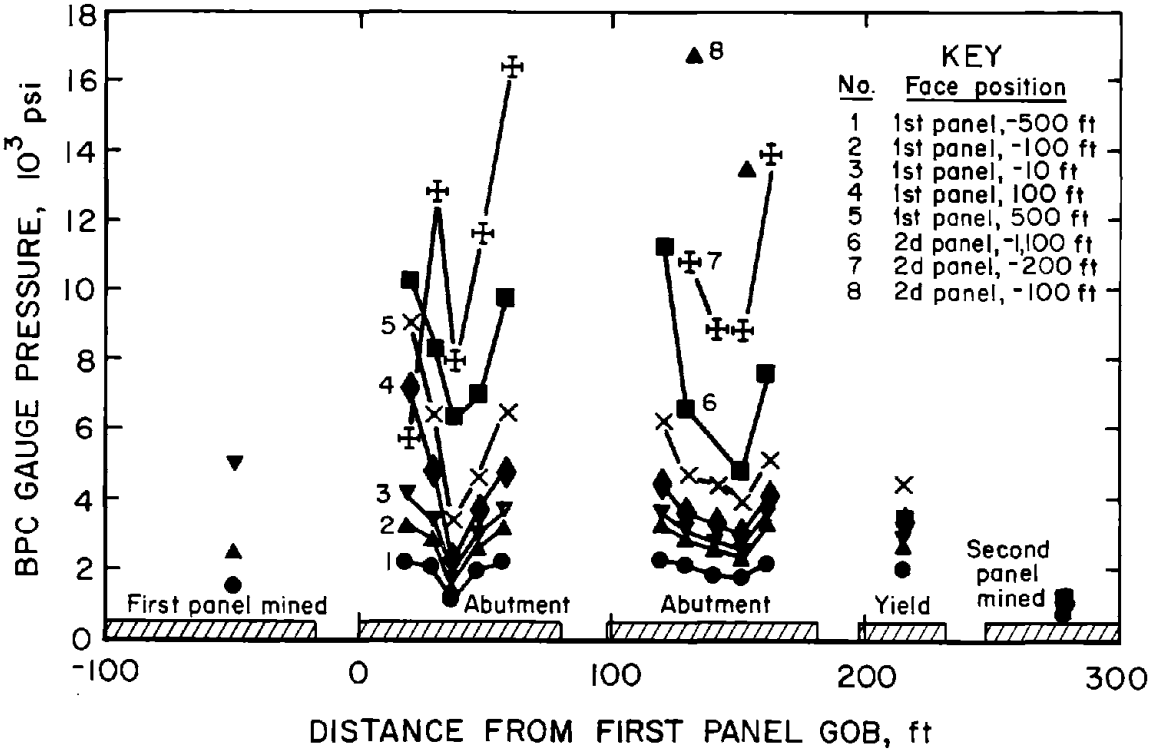

Figure 9.—Apparent pillar pressure profiles indicating the high stresses attained under deep cover with strong roof and floor.

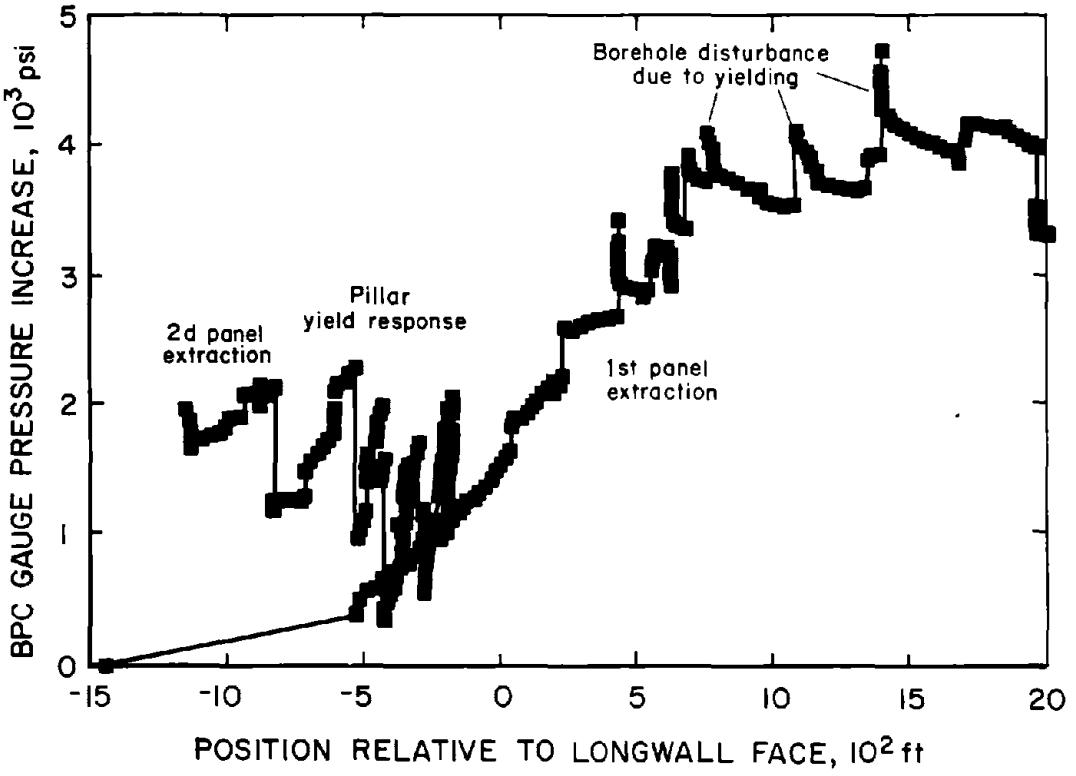

Figure 10.—Typical response of BPC to small pillar yielding; soft coal, deep cover.

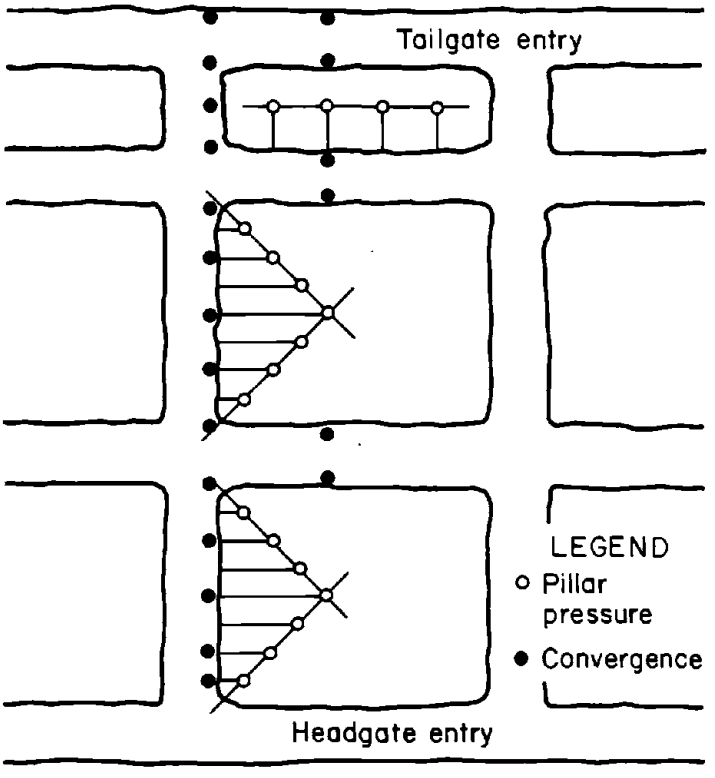

Figure 11.—Example of pillar monitoring instrumentation using symmetry of design.

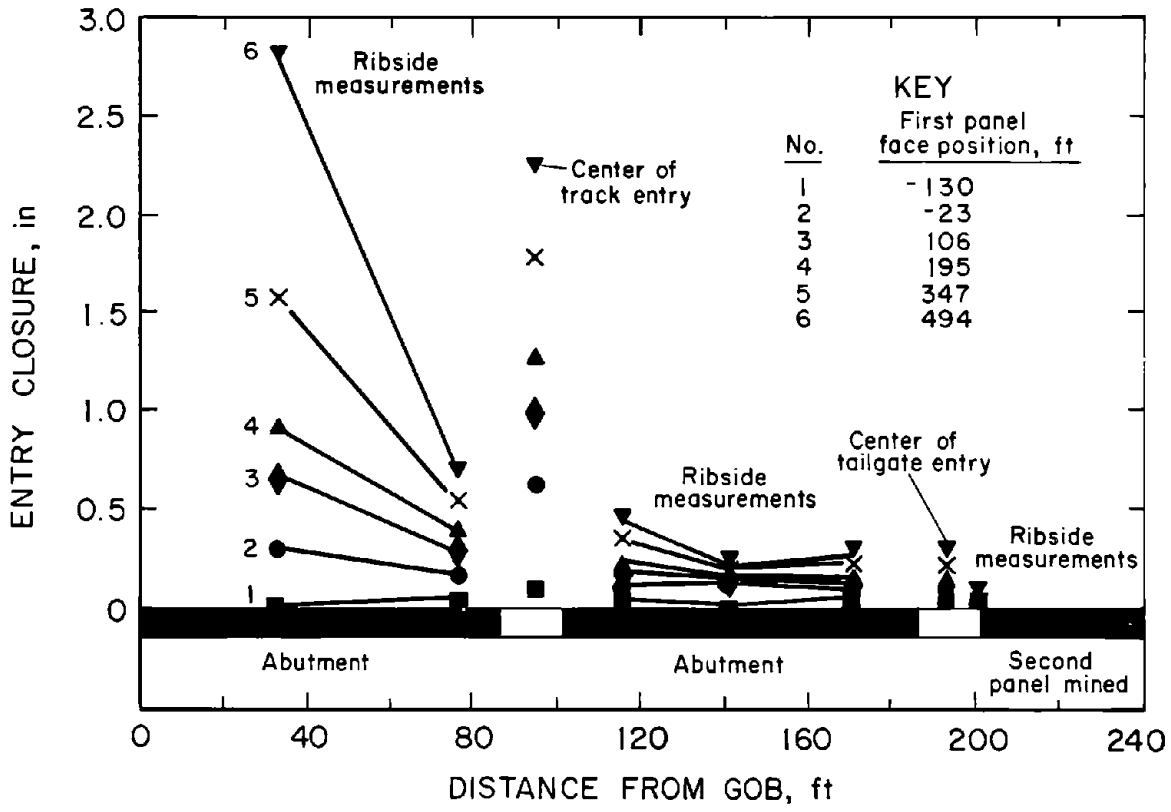

Figure 12.—Stress attenuation as depicted by entry closure measurements.

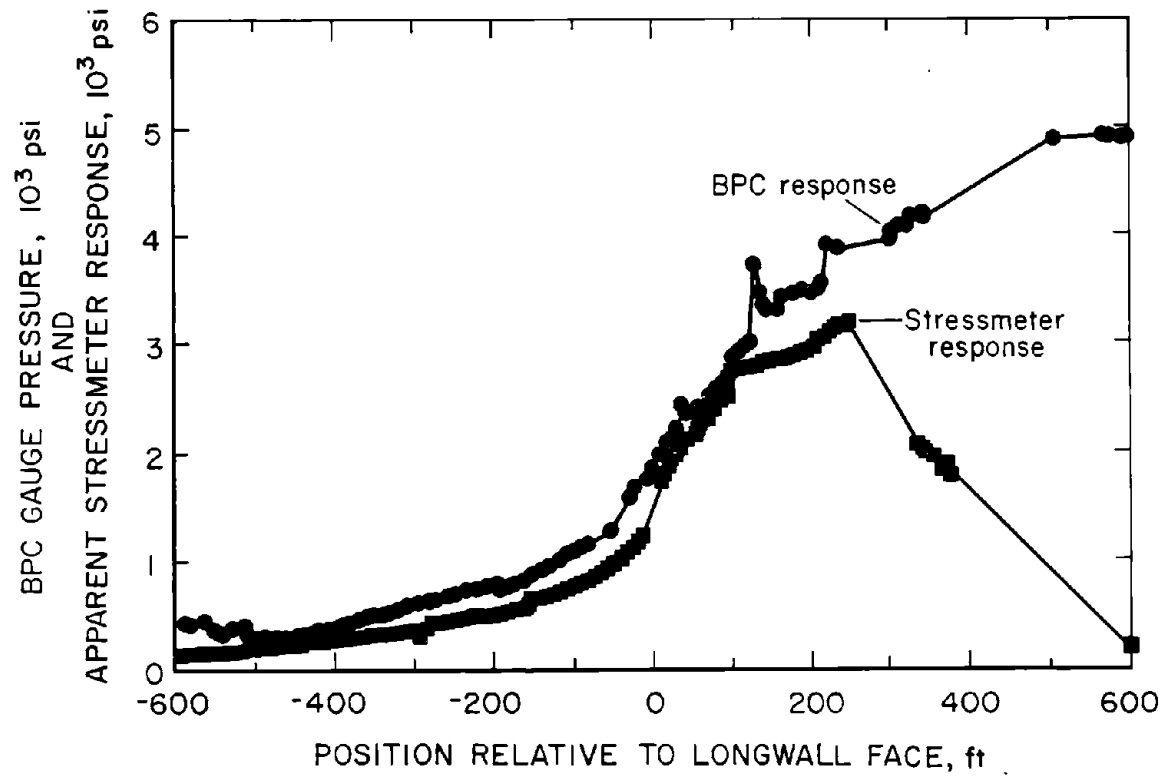

Figure 13.—Stressmeter versus BPC response illustrating premature decrease in stressmeter response due to borehole yield; deep cover, soft coal, 30-ft-depth installation.

The following observations are typically made during field monitoring programs—

- In-mine: Pillar stress measurement,
  Entry convergence measurement,
  Visual mapping of roof, rib, and floor stability.
- Overburden: Time domain reflectometry,
  Hydrological response measurements,
  Postmining core drilling.
- Surface: Vertical subsidence.

The above observations generally provide sufficient information for both verification of the longwall development design and overall finite-element model calibration.

SUMMARY

A comprehensive integrated approach to longwall development design is advocated in this paper. The approach encompasses three major tasks: geomechanical characterization, finite-element modeling, and field monitoring. Results generated from geomechanical characterization provide the necessary input to the finite-element model. Data obtained from the field monitoring program are used to calibrate the model and verify the design accuracy. Unlike other conventional coal pillar design methods, this integrated approach considers all important geomechanical effects associated with longwall mining such as entry stability, floor heave, overburden impact, and surface subsidence. Since this approach does not rely upon empirical observations, it is more suitable for applications in new mining and geological environments where little, if any, underground experience has been attained.

REFERENCES

1. Babcock, C. O. Equations for the Analysis of Borehole Pressure Cell Data. Paper in Proceedings of 27th U.S. Symposium on Rock Mechanics, Univ. of AL, Tuscaloosa, AL, 1986, pp. 233-240.

2. Babcock, C. O., P. Lu, F. Horvino, and R. Harmel. Field Test and Evaluation of USBM Borehole Pressure Cells for the WIPP Project. Final Report to DOE on Contract DE-AI04-82AC20398, 1982, 35 pp.

3. Bauer, E. R., G. J. Chekan, and J. C. Hill. A Borehole Instrument for Measuring Mining-Induced Pressure Changes in Underground Coal Mines. Proceedings of 26th U.S. Symposium on Rock Mechanics, SD School of Mines, Rapid City, SD, 1985, v. 2, pp. 1075-1084.

4. Bieniawski, Z. T. Improved Design of Coal Pillars for U.S. Mining Conditions. 1st Annual Conference on Ground Control in Coal, 1981, pp. 13-22.

5. Choi, D. S., and D. L. McCain. Design of Longwall Systems. Trans. Soc. Min. Eng. AIME, v. 268, 1980, pp. 1761-1764.

6. Hasenfus, G. J., K. L. Johnson, and D. W. H. Su. A Hydrogeomechanical Study of Overburden Aquifer Response to Longwall Mining. Paper in Proceedings, 7th International Conference on Ground Control in Mining. WV Univ., Morgantown, WV, 1988, pp. 149-162.

7. Heasley, K. A. Understanding the Hydraulic Pressure Cell. Proceedings of the 30th U.S. Symposium on Rock Mechanics, WV Univ., Morgantown, WV, 1989, pp. 485-492.

8. Holland, C. T. The Strength of Coal in Mine Pillars. Proc. of the Sixth Symposium on Rock Mechanics, Univ. of MO, Rolla, MO, Apr. 1964, pp. 450-456.

9. Hult, J., and B. Hall. Slope Stability in Rock in Connection With Mining, Swedish Mining Assoc., 1965, Ser. B, No. 72.

10. Mark, C. Pillar Design Methods for Longwall Mining. BuMines IC 9247, 1990, 53 pp.

11. Obert, L., and W. I. Duvall. Rock Mechanics and the Design of Structures in Rock. Wiley, 1967, pp. 531-545.

12. Peng, S. S., and H. S. Chiang. Longwall Mining. Wiley, 1984, 708 pp.

13. Peng, S. S. Coal Mine Ground Control, Wiley, 2d ed., 1986, pp. 255-256.

14. Rice, G. S. Tests of Strength of Roof Supports Used in Anthracite Mines of Pennsylvania. BuMines, B 303, 1929, 44 pp.

15. Salamon, M. D. G. Displacements and Stresses Induced by Longwall Mining in Coal. Proceedings of the 7th Congress of International Society of Rock Mechanics, Aachen, Germany, Sept. 1991.

16. Salamon, M. D. G., and A. H. Munro. A Study of the Strength of Coal Pillars: J. S. Afr. Inst. Min. Metall., v. 68, 1967, pp. 55-67.

17. Su, D. W. H., and G. J. Hasenfus. Field Measurements of Overburden and Chain Pillar Response to Longwall Mining. Paper in Proceedings, 6th Conf. on Ground Control in Mining, WV Univ., Morgantown, WV, 1987, pp. 296-311.

18. Su, D. W. H., and G. J. Hasenfus. Intrinsic Response of Borehole Pressure Cells—Laboratory Calibration and Nonlinear FEM Simulation. Paper in Proceedings, Ninth Conference on Ground Control in Mining, 1990, pp. 260-271.

19. Trueman, R. A Finite Element Analysis for the Establishment of Stress Development in a Coal Mine Caved Waste. Min. Sci. and Technol., 1990, pp. 247-252.

20. Weibull, W. A Statistical Theory of the Strength of the Materials, IVA Handl., No. 151, Stockholm, Sweden, 1939.

20. Wilson, A. H. Stress and Stability in Coal Ribsides and Pillars. Proc. 1st Annual Conference on Ground Control in Mining, Morgantown, WV, 1981, pp. 1-12.

22. Zienkiewicz, O. C. The Finite Element Method. McGraw-Hill, 1977, 787 pp.

ANALYSIS OF LONGWALL PILLAR STABILITY (ALPS): AN UPDATE

By Christopher Mark[1]

INTRODUCTION

Longwall pillars perform the essential function of protecting the gate entries, which provide the only access to the face. Blockages in the gates disrupt ventilation patterns and close off emergency travelways, posing serious safety hazards. In addition, the impact of any downtime is magnified on a longwall because such a high proportion of the total mine productive capacity is concentrated at the longwall face.

Ten years ago, there was very little theory available to assist mine planners in sizing longwall pillars. As many mines introduced longwalls, they first tried pillar dimensions that had been successful in their previous room-and-pillar developments. All too often the results were unfortunate (*1*, *5*, *7*, *10*).[2] Then pillar sizes would be increased over the course of several panels until satisfactory conditions were achieved. Other longwalls experienced difficulties only on some panels and were often at a loss to explain them. Still others settled early on a successful design, then continued to use it without regard to whether the pillars might be wastefully oversized.

Developing a pillar design method for longwalls required some new thinking. The goal of entry protection differs from the traditional function of pillar design, which is to prevent squeezes caused by widespread pillar failure. The long and narrow geometry of typical gate entry layouts makes a classic squeeze highly unlikely. Second, the abutment loads applied to longwall pillars are significantly greater and more complex than those assumed by traditional pillar design methods. Effective longwall pillar design requires some knowledge of abutment loads during all phases of longwall mining, from development all the way into the tailgate.

The Analysis of Longwall Pillar Stability (ALPS) method was developed in 1986 to answer these needs. First, design estimates of abutment loads were obtained through an extensive series of underground stress measurements. Then, back analyses of longwall case histories was used to develop an empirical relationship between pillar design and entry performance. Since it was first presented, the method has been tested by back analysis of a growing number actual mining case histories. This ongoing field verification process has been the key to the success of the method and its acceptance by the mining industry.

The goal of this paper is to discuss practical applications of ALPS, in light of the experience that has been gained to date. Several of the method's shortcomings are also described, as are current efforts to improve it and expand its scope.

ANALYSIS OF LONGWALL PILLAR STABILITY METHOD (ALPS)

The fundamental premise of the ALPS method is that there is a strong correlation between pillar performance and gate entry stability. Specifically, it has been found that if the pillars maintain a proper load-bearing capacity relative to the applied load, then good mining conditions can be maintained. The method, therefore, has three components:

1. A formula for estimating the load applied to the pillars;
2. A formula for estimating the load-bearing capacity of the pillar system; and
3. Calculation of a stability factor (SF) based on a comparison of the load to the load-bearing capacity.

The ALPS method is applicable to *conventional* longwall pillar designs, in which the pillars are expected to carry the abutment loads to which they are subjected. Approximately 95 pct of all longwall installations in the

[1]Mining engineer, Pittsburgh Research Center, U.S. Bureau of Mines, Pittsburgh, PA.

[2]Italic numbers in parentheses refer to items in the list of references at the end of this paper.

United States employ some form of conventional pillar design. ALPS is not suitable for yielding designs where the pillar system is purposely made too small to carry the abutment loads.

ESTIMATION OF LONGWALL PILLAR LOADS

ALPS divides the loads applied to longwall pillars into two parts. These are *development loads*, which are present before longwall mining, and *abutment loads*, which arrive during longwall panel extraction. Development loads are due to the weight of the overburden directly above the pillars and the gate entries. The tributary area theory is used by ALPS to estimate the longwall development load per foot of gate entry (L_d) as:

$$L_d = (H)(W_t)(\tau), \quad (1)$$

where H = depth of cover ft,

W_t = width of the pillar system ft,

and τ = unit weight of the overburden pcf.

Abutment loads are the key to longwall pillar design. ALPS began with a simple conceptualization of the side abutment (L_s) proposed by King and Whittaker (*13*) and Wilson (*18*) (fig. 1). The pillar loading is the wedge of overburden defined by the abutment angle ß. Two equations are used to quantify the side abutment, one for critical and supercritical panels (equation 2) where the panel width P exceeds twice (H tan ß), and the other for subcritical panels (equation 3):

$$L_s = H^2(\tan ß)(\tau/2), \quad (2)$$

and

$$L_{ss} = [(HP/2) - \{P^2/(8 \tan ß)\}]\,\tau, \quad (3)$$

where P = panel width ft.

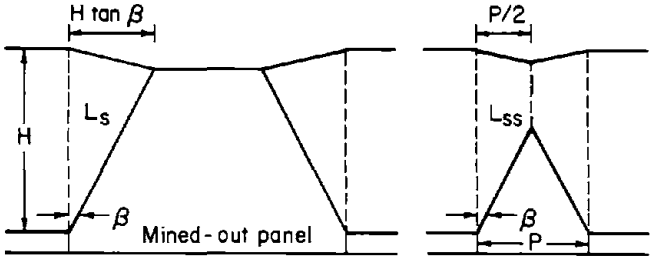

Figure 1.—Conceptualization of side abutment load used in ALPS. β = Abutment angle; H = depth of cover; L_s = side abutment for critical panels; L_{ss} = side abutment for supercritical panels; P = panel width.

The two-dimensional model of the side abutment shown in figure 2 is only applicable once the longwall face is long past by, as in bleeder entries. From a mining standpoint, the most critical abutment loads are the front abutments (L_f) experienced by the pillars at the face ends or T-junctions. The magnitude of the front abutment (L_f) is more difficult to determine analytically, because the load transfer at the T-junctions is a complicated three-dimensional problem. ALPS assumes that the front abutment is some fraction of the side abutment, and can be represented as

$$L_f = F(L_s), \quad (4)$$

where F is a front abutment factor with a value of less than 1. It was thought that two front abutment factors were needed, one for a headgate (or first panel) front abutment (F_h) and the other for the tailgate front abutment (F_t).

An extensive program of field measurements was conducted to determine values of ß and F appropriate for mining conditions in the United States. At each of 16 longwall panels in 5 mines and 4 States, instruments were installed in the pillars to monitor the stress increases that occurred as the panels were extracted. Details of the field studies have been given elsewhere (*13*).

It was concluded that values of ß = 21°, F_h = 0.5, and F_t = 0.7 would yield appropriately conservative estimates of the side abutment load for longwall pillar design. The

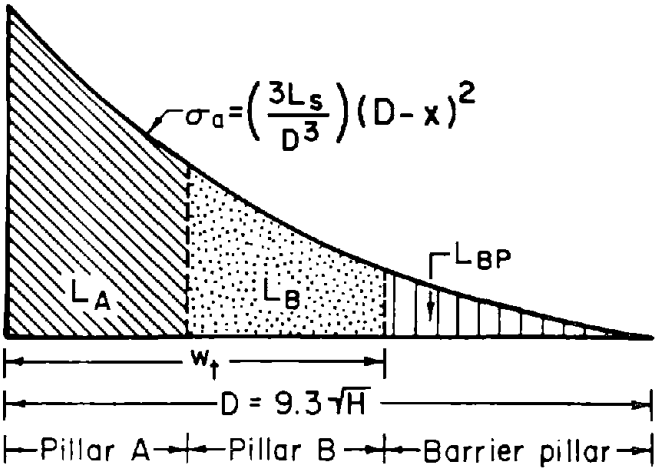

Figure 2.—Distribution of side abutment load. H = depth of cover; W_t = width of the pillar system; L_S = side abutment; L_A = pillar A abutment; L_B = pillar B abutment; L_{BP} = barrier pillar abutment; D = extent of side abutment influence zone; x = distance from edge of longwall panel; σ_a = abutment stress distribution function.

data were also used to develop a formula for estimating the distribution of the side abutment load (fig. 2):

$$R = 1 - \left[\frac{D - W_t}{D}\right]^3, \quad (5)$$

where $D = 9.3\sqrt{H}$, and where W_t is less than D. Where W_t is greater than D, or where there is no adjacent unmined panel or barrier pillar, then R = 1.

Using equations 1 through 5, three loading conditions may be defined. The loading experienced by pillars at the T-junctions in the headgate, or in the tailgate during first panel mining, is called headgate loading. Headgate loading (L_H) consists of the development loads plus the first front abutment:

$$L_H = [L_d + (L_s)(F_h)(R)]. \quad (6)$$

Pillars that are expected to protect bleeder entries will be subjected to the development load and the first full side abutment, or bleeder loading (L_B):

$$L_B = [L_d + (L_s)(R)]. \quad (7)$$

Barrier pillar loads may also be determined from equation 7, except that R = 1. The most severe longwall loading is tailgate loading (L_T), experienced during the mining of the second and subsequent panels. Tailgate loading consists of the development load, the first side abutment, and the second front abutment:

$$L_T = [L_d + (1 + L_s)(F_t)]. \quad (8)$$

ESTIMATION OF PILLAR LOAD-BEARING CAPACITY

The second component of ALPS is the estimation of the load-bearing capacity of the longwall pillar system. For multientry gates, it is first necessary to determine the strength of the individual pillars. ALPS uses the Bieniawski formula:

$$S_p = S_1\,(0.64 + 0.36\ w/h), \quad (9)$$

where S_p = pillar strength, psi,

S_1 = in situ coal strength, psi,

w = pillar width, ft,

and h = pillar height, ft.

As will be discussed, S_1 = 900 psi is normally used in ALPS.

The load-bearing capacity of a longwall pillar system per foot of gate entry (B) is then calculated as the sum of the individual pillar resistances:

$$B = [\Sigma(S_p)(A_p)]/(C), \quad (10)$$

where C = spacing between crosscuts, ft.

Once the maximum design load (L) has been determined using one of equations 6, 7, or 8, the stability factor (SF) is calculated as:

$$SF = B/L. \quad (11)$$

The SF is defined as the *total* load-bearing capacity of the longwall pillar system divided by the *total* applied load. Experience has indicated that although abutment loadings are not distributed evenly among the pillars (see fig. 2) and that individual pillars may become overloaded and yield, satisfactory tailgate conditions can be maintained as long the pillar system maintains an adequate overall SF.

The question then becomes, what is an adequate stability factor? The question is more urgent because *pillar* stability per se is not really the issue. Rather, the ALPS stability factor is to be used as an *index* to predict *gate entry stability*. The quantitative correlation between ALPS SF and gate entry performance has been established by back analysis of longwall case histories.

VERIFICATION OF THE ALPS METHOD

A total of 90 case histories are now included in the ALPS data base, some from the literature, but most from personal observations and discussions with mine personnel. As shown in figure 3, the case histories are distributed all over the U.S. coalfields.

The details of each case history are shown in tables 1 and 2. The case histories have been separated into unsuccessful and successful designs. The unsuccessful designs (table 1) were those in which intolerable entry conditions occurred, including roof deterioration and falls, severe pillar sloughing and floor heave, and in one case even pillar bumps. In all cases, the problems were apparently caused by excessive vertical stresses. Often the mine subsequently changed the gate entry design, either by increasing the pillar size or by installing more supplemental support.

The successful designs, shown in table 2, are ones in which no stress-related problems were reported. Most of these designs have been in use for many years. About one-half of the successful designs are from mines that also reported unsuccessful designs described in table 1. In these cases, the improved ground conditions can only be attributed to a change in pillar design or to a decrease in the depth of cover.

Table 1.—ALPS results for unsuccessful case histories

Seam and location	Depth of cover, ft	Pillar widths, ft	Pillar height, ft	Panel width, ft	ALPS SF
U. Hiawatha, UT	1,400	30,80	9.0	550	0.35
Pocahontas No. 3, VA	2,000	30,80,30	5.5	600	.36
Imboden, KY	1,800	100,28	6.5	700	.41
Wattis, UT	1,100	50,50	8.0	420	.41
Castlegate, UT	1,600	85	7.0	600	.41
Harlan, KY	1,700	92,52	8.5	500	.42
Blue Creek, AL	2,200	20,120,20	6.5	650	.44
Wadge, CO	1,000	71,41	9.5	640	.45
Powellton, WV	800	41,41	6.0	580	.53
Pocahontas No. 3, WV	1,400	42,42,42	4.5	360	.54
Castlegate, UT	1,900	120	7.0	600	.57
Harlan, KY	2,000	92,52	11.0	500	[1].57
Campbell Cr., WV ..	900	41,41,41	6.0	650	.58
Campbell Cr.,WV ...	1,050	41,41,41	7.0	700	[1].60
Eagle, WV	1,250	71,51	5.5	520	.62
Campbell Cr., WV ..	990	71,51	7.0	700	.62
Taggart, VA	1,300	72,82	7.0	685	.63
Elkhorn No. 2, KY ...	1,025	55,55	5.0	500	.66
Campbell Cr., WV ..	965	73,53	6.5	600	.72
Blue Creek, AL	1,500	80,80	6.0	500	.73
Blue Creek, AL	1,500	64,64,64,64	6.0	450	.73
Campbell Cr., WV ..	965	51,51,51	6.0	600	.75
Powellton, WV	725	50,30	4.2	365	.75
Campbell Cr., WV ..	1,000	81,41	7.0	700	.75
Jawbone, VA	1,150	66,66	4.8	650	.80
Pocahontas No. 3, WV	1,400	42,42,72	4.5	360	.80
Pittsburgh, PA	640	43,43	6.5	600	.81
Blue Creek, AL	1,300	40,110,40	6.0	700	.85
U. Freeport, WV	550	43,43	8.0	750	.89
Pittsburgh, PA	850	68,43	6.0	500	.90
Warfield, KY	800	50,30,30,50	5.0	600	.92
Pittsburgh, WV	1,300	84,84,84	7.0	800	.93
Blue Creek, AL	2,000	115,115,115	7.0	600	.94
Blue Creek, AL	2,000	20,188,20	6.5	850	.96
Pittsburgh, WV	1,140	64,84	6.5	480	.99
Hanna, WY	600	81	12.0	600	1.01
Blue Creek, AL	2,000	115,115,115	6.5	600	1.01
D Seam, CO	800	72,72	8.5	620	1.02
Pittsburgh, PA	875	73,73	7.0	630	1.02
Pittsburgh, WV	875	37,37,37	7.0	480	[1]1.05
Pittsburgh, OH	680	52,62	7.0	500	1.08
Splashdam, VA	725	45,45	3.3	700	1.09
Lower Kittanning, PA	800	62,62	5.0	800	1.24
Pittsburgh, WV	700	69,69	7.0	420	1.26
U. Freeport, MD	600	64,64	8.5	750	1.28
L. Banner, VA	700	70,45	4.0	600	1.58

SF Stablity factor.
[1]Headgate failure.

The most important conclusion from the case histories is that 77 pct of the failed cases had stability factors of less than 1.0, while 71 pct of the successful cases had stability factors of 1.0 or more (fig. 4). In other words, the data support the conclusion that there is a strong empirical correlation between ALPS stability factor and tailgate performance. Based on this observation, stability factors of 1.0 to 1.3 are currently recommended as the design criteria for use with ALPS.

Table 2.—ALPS results for successful case histories

Seam and location	Depth of cover, ft	Pillar widths, ft	Pillar height, ft	Panel width, ft	ALPS SF
E Seam, CO	740	36,51	9.8	750	0.50
U. Hiawatha, UT	1,000	30,80	9.0	550	.54
Pocahontas No. 3, VA	2,000	21,121,21	5.0	600	.67
B Seam,CO	1,200	80,80,80	9.0	600	.76
Campbell Cr.,WV	1,000	81,41	6.0	600	.78
Elkhorn No. 6, KY	900	55,55	5.0	500	.78
Elkhorn No. 6, KY	700	35,55	5.0	500	.85
Campbell Cr., WV	700	41,41,41	6.0	650	.86
Pittsburgh, WV	1,175	64,64,64	6.5	700	.87
Eagle, WV	1,050	73,73	6.0	700	.90
Jawbone, VA	1,000	76,46	4.8	650	.91
Imboden, KY	1,000	100,28	6.5	700	.92
Jawbone, VA	1,150	66,66,66	4.8	650	1.03
Eagle, WV	800	71,51	6.0	520	1.04
Lower Kittaning, WV	720	32,32	5.0	980	[1]1.09
Herrin No. 6, IL	650	44,64	7.5	750	1.14
Blue Creek, AL	2,000	20,200,20	7.0	630	1.16
Blue Creel, AL	2,200	20,210,20	6.5	650	1.16
Blue Creek, AL	2,000	20,230,20	6.5	850	1.16
Pittsburgh, PA	875	90,90	7.0	630	1.18
Dorchester, VA	850	71,41	4.0	625	1.21
Pittsburgh, PA	900	34,74,84	6.0	750	1.23
Pittsburgh, WV	770	34,84	6.0	450	1.28
Pocahontas No. 3, WV	1,400	42,42,107	4.5	360	1.29
Herrin No. 6, IL	650	44,42	7.5	750	[1]1.30
Herrin No. 6, IL	625	57,65	7.5	625	1.33
Herrin No. 6, IL	625	85,58	7.5	625	1.33
Lower Kittaning, PA	750	62,62	5.0	585	1.38
Herrin No. 6, IL	700	84,84	9.8	620	1.38
Pittsburgh, WV	1,000	84,84,84	7.0	800	1.38
Pittsburgh, PA	825	90,90,90	7.0	630	1.40
Lower Kittanning, WV	720	62,62	5.0	980	1.43
Pittsburgh, WV	900	85,85,85	7.0	520	1.47
Pittsburgh, WV	900	93,93	6.4	420	1.48
Pittsburgh, OH	680	34,94	7.0	500	1.57
Blue Creek, AL	1,500	130,60,130	6.0	500	1.58
U. Freeport, WV	550	83,33	8.0	750	1.59
Pittsburgh, PA	600	20,83	6.5	600	1.61
Blue Creek, AL	1,500	20,180,20	6.0	850	1.67
U. Kittanning, PA	400	42,42	4.0	750	1.72
Pittsburgh, WV	1,000	84,84,84	6.0	730	1.77
Splashdam, VA	750	75,45	3.3	700	1.85

SF Stability factor.
[1]Design used in headgate only.

A second observation is that ALPS seems to work well over a wide range of coal seams, locations, and depths of cover. Tables 1 and 2 ables also contain examples of two-, three-, four-, and even five-entry systems; designs that employed equal-sized pillars; and designs that used pillars of different sizes.

Finally, there is a range of stability factors (approximately 0.5 to 1.3) in which both successful and unsuccessful designs occur. This indicates that other variables, in addition to the ALPS stability factor, may determine tailgate performance. A later section of this paper discusses some of the possibilities.

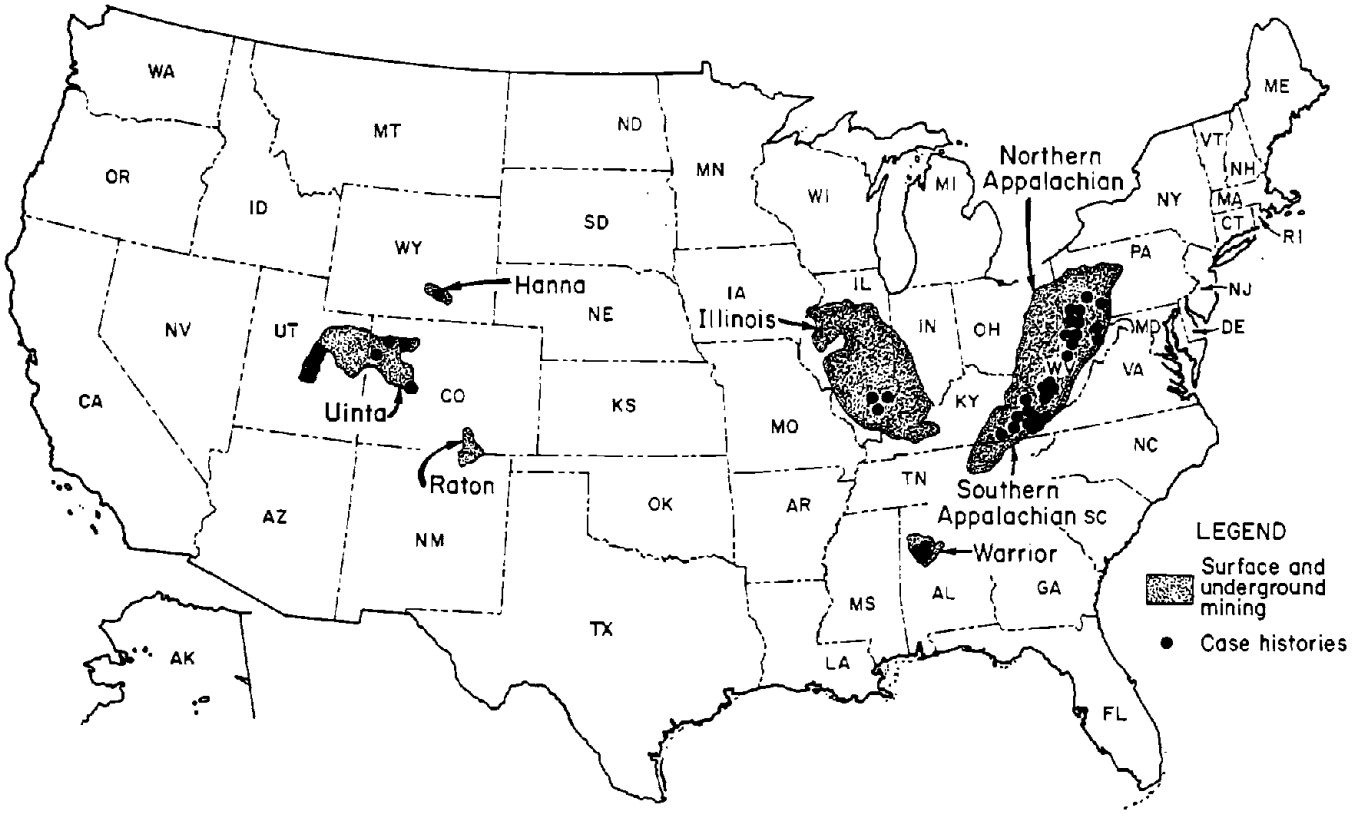

Figure 3.—Locations of ALPS case histories.

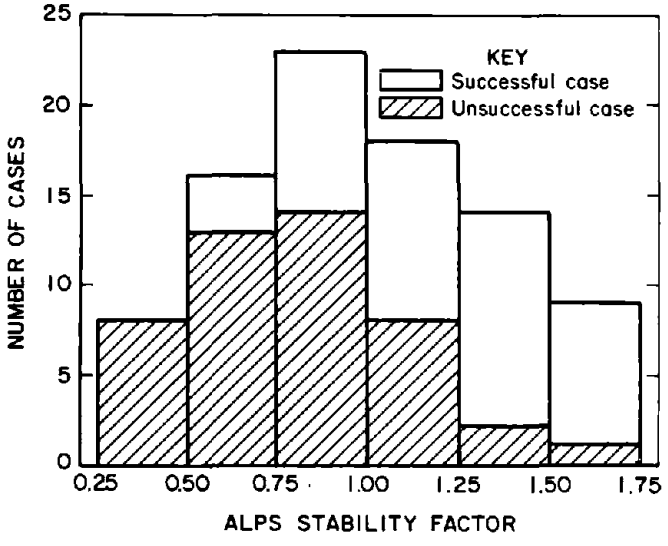

Figure 4.—ALPS stability factors calculated for 60 longwall case histories.

A computer program has been prepared to aid mine planners in using ALPS. The program is written in BASIC for an IBM personal computer or compatible. In the analysis mode, the user provides all the necessary input data, including pillar widths, and the program calculates stability factors. In the sizing mode, the program calculates the necessary pillar widths after being given the required stability factors. Single copies of the ALPS program may be obtained by sending one double-sided, double-density diskette to:

Christopher Mark
U.S. Bureau of Mines
Pittsburgh Research Center
Cochrans Mill Road
P.O. Box 18070
Pittsburgh, PA 15236-0070

USE OF ALPS IN DESIGN PRACTICE

ALPS assists the design process by reducing a multitude of variables (e.g., depth of cover, pillar widths, seam height, entry width) into a single meaningful design parameter—the stability factor. The stability factor can be used in at least four different applications.

PRELIMINARY DESIGN

Few things can cause more distress to a new longwall operator than to have an otherwise highly successful longwall slowed by serious ground control problems on its first or (more often) second panel. ALPS can give realistic, conservative estimates of pillar sizes for use in feasibility studies or initial longwall panel design. Two recent, successful examples of preliminary design with ALPS were reported at Kerr-McGee's Galatia Mine in Illinois (*8*) and at Wolf Creek Collieries in Kentucky (*6*).

ADAPTATION

No two longwall panels are alike, and as conditions change, ALPS can help mine planners *anticipate* rather than *react* to potential problems. Once a specific stability factor has been shown to be adequate for a given mine, then different designs employing the same stability factor can be used elsewhere on the property with some confidence. In other words, pillar design formulas can be calibrated with site-specific experience.

The depth of cover is the single most important parameter affecting gate entry performance, and in many parts of the coalfields it may change radically from one panel to the next. For example, a Kentucky longwall extracted its first three panels under 1,000 ft of cover with excellent conditions. The pillar design employed a 28- and a 100-ft pillar, yielding an ALPS stability factor of 1.0. When the same design was used at 1,800 ft, the stability factor was reduced to 0.5, and ground conditions were so poor that supplemental support had to be tripled just to maintain a travelway. ALPS formulas indicated that the width of the large pillar should have been increased to 150 ft to maintain the original stability factor under the greater depth of cover (*3*). At a nearby Virginia longwall, pillar widths were increased from 90 to 120 ft as the cover increased from 850 to 1,300 ft, and no significant degradation of ground conditions occurred.

Human-made conditions may change as well as natural ones. A common change is a switch from a four- to a three-entry system, or vice versa. Other mines have kept the same number of entries, but have gone from equal to unequal entry centers. ALPS can show how these changes can be made without beginning all over again at the bottom of the learning curve.

OPTIMIZATION

Longwall pillars that are too large constitute a needlessly wasted resource. An evaluation of survey data collected from 70 longwalls in the early 1980's indicated that the ALPS stability factor for tailgate loading was greater than 1.5 approximately 50 pct of the time (*13*). In some cases, it was as high as 4.0. The same data also indicated that little improvement in gate entry performance is achieved once the stability factor exceeds 1.5. Design methods can be used to safely reduce oversized pillars, thereby improving development drivage rates and adding to the life of the mine.

FAILURE ANALYSIS

Several factors may be responsible for the failure of a gate entry, and it is not always obvious what to do about it. ALPS can quickly indicate whether increasing pillar size could be the solution. In the case of the Kentucky longwall described earlier, the increased depth of cover was clearly identified as the problem, and increasing the pillar size could be expected to help. Many similar cases are included in tables 1 and 2, from the rolling hills of southwestern Pennsylvania to the dipping coalbeds of Wyoming.

Increasing the size of the pillars will not always solve the problem, however. A relatively large stability factor can be a clear signal that some other solution is required. For example, hazardous roof conditions developed along the length of one tailgate in Alabama despite an ALPS stability factor of 1.4. In this case, the problem was apparently low-quality roof support. Once select hardwood cribs were substituted for second-quality mixed hardwood, the improvement was sudden and dramatic. In another instance, steel beams had to be used in the tailgate of a Pennsylvania longwall because of roof conditions. The panel was a first panel, however, and its stability factor of 1.7 was much higher than had been safely employed on previous panels. Severe horizontal stress, due to the presence of an overlying stream valley, was identified as the source of the problem.

GEOLOGIC FACTORS AND ALPS

A perfect longwall gate entry design methodology would accurately predict tailgate performance in *all* cases. As figure 4 shows, the ALPS stability factor explains much of the variation in gate entry performance, but by no means all of it. This is perhaps not so surprising, because ALPS focuses on *geometric* parameters (e.g., depth of cover and pillar dimensions). Including some site-specific *geologic* variables might improve the predictive ability of ALPS. Some possibilities include the caving characteristics of the overburden, the in situ coal strength, and the quality of the roof rock.

OVERBURDEN CAVING CHARACTERISTICS

Overburden geology can vary dramatically from longwall to longwall. For example, figure 5 shows stratigraphic columns from two neighboring Virginia longwalls. Massive sandstones comprise most of the overburden at the first mine, while weaker shales predominate at the second. Subsidence research suggests that such differences in geology can have a large effect on surface movements (*11*), and abutment loads are surely an underground expression of the same phenomena. In general, where the overburden is strong, less complete caving, more bridging across the gob, and a larger effective abutment angle might be expected, while weaker conditions might result in more complete caving, more gob loading, and a smaller abutment angle. In the ALPS computer program, the abutment angle is preset at 21°, though this may be changed at the user's option. Can better results be achieved by adjusting the abutment angle on a site-specific basis?

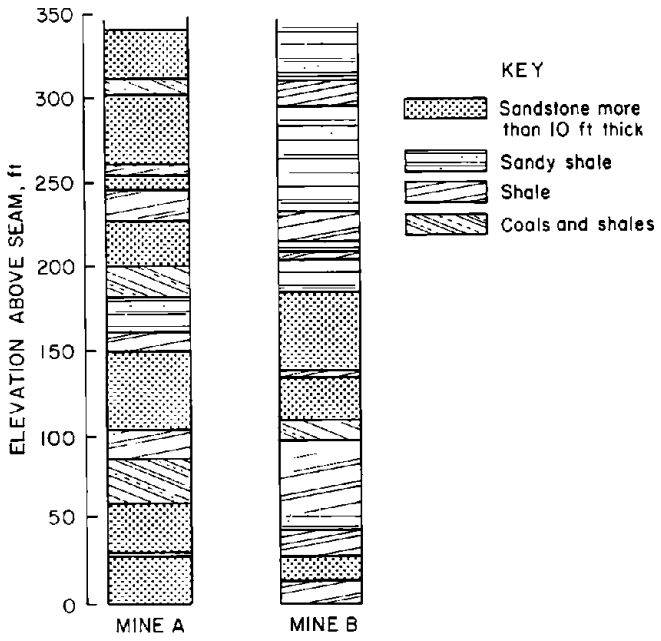

Figure 5.—Stratigraphic columns from neighboring Virginia longwalls. *A*, 60 pct of overburden is massive sandstone; *B*, 25 pct of overburden is massive sandstone.

The field studies used in the development of ALPS found a range in abutment angles of approximately 10° to 25° (*13*). The studies were not very helpful in identifying the causes of the variation, however. Both the largest and the smallest abutment angles were measured at the same mine. Current Bureau studies may eventually help to better define the effects of overburden geology on abutment load. Measurements of abutment stresses are being conducted in several deep-cover longwalls with very different overburden characteristics. In another study, the stiffness of different gob materials is being measured in laboratory tests. These results will be used in numerical models of abutment load distributions around longwalls.

In practice, however, the effect of the abutment angle may not always be as significant as it might first appear. To begin with, development loads typically make up almost half of the tailgate loading, and they would not be affected by overburden geology. In addition, for subcritical panels where the depth of cover is more than twice the panel width, variations in ß have relatively little effect on predicted loads. For example, with a 600-ft-wide panel at 2,000 ft of cover, increasing the abutment angle from 21° all the way to 90° increases the abutment load by less than 20 pct and the total load by only about 10 pct.

Some other factors may affect abutment loads in ways that might be difficult to simulate by adjusting the abutment angle. These include the capacity of abandoned pillars from previous panels to support abutment loads and the effect of longwall panel width on the ability of strong strata to bridge the gob. Evaluating these factors with field measurements would also be extremely difficult, however.

COAL STRENGTH

Probably the single question most often asked by ALPS users is: What value should be used for the in situ coal strength? Like the abutment angle, the in situ coal strength is soft-wired in the ALPS computer program, with a value of 900 psi. The author's experience is that little is to be gained by adjusting the coal strength. There are a number of possible explanations.

The traditional method for determining the in situ coal strength has been to apply a size-effect scaling factor to the strength of small coal specimens tested in the lab (*4*). Two serious drawbacks largely invalidate this laboratory test approach. First, it is very difficult to determine a meaningful *specimen-size* coal strength. Laboratory tests on coal are notoriously unreliable because of sampling bias, integrity loss during specimen preparation, and platen effects during testing. An example of the problems with laboratory testing was recently provided by a Kentucky operator who was trying to carry out a longwall feasibility study. Three different consultants were called in to carry out compressive strength tests on coal specimens from the same coal seam. The average values reported back were 2,700, 5,000, and 8,500 psi—a range approximately as great as that reported for all U.S. coal seams put together (*17*).

Better sampling and testing procedures can improve consistency, but leave the second problem of the size effect. There is now considerable evidence that the size-effect scaling factor varies considerably from seam to seam. As figure 6 shows, 2-in specimens from the Pittsburgh coalbed are approximately twice as strong as similar specimens from the Pocahontas No. 3 coalbed. The disparity in strength is rapidly reduced as the specimen size is increased because of the different size effects in the two seams.

Yet another problem is that the uniaxial compressive strength may not be very important when considering the strength of the large width-to-height ratio pillars typical of longwalls. It is widely accepted that the strength of such squat pillars is largely *triaxial* strength derived from the confinement that is generated within them. Laboratory studies (*9*) have indicated that the uniaxial compressive strength does not correlate very well with the internal friction angle, the most important triaxial strength parameter. Other issues associated with estimating the strength of squat pillars are addressed in another paper in these proceedings (*14*).

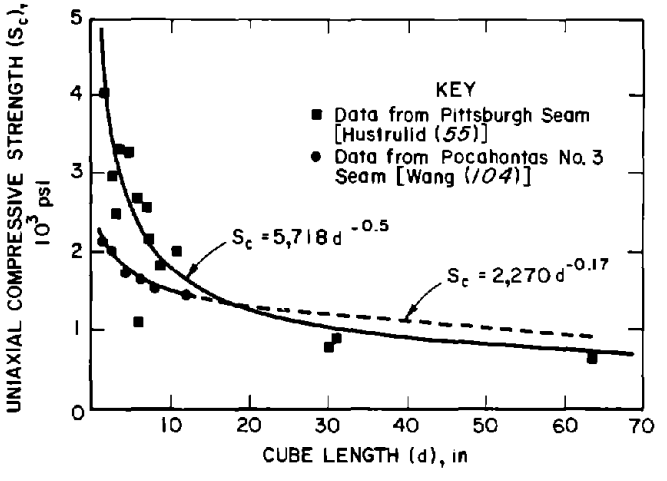

Figure 6.—Effect of specimen size observed on compressive strength of two coal seams.

Fortunately, it may be that while the laboratory strength varies considerably from seam to seam, the in situ strength is more consistent, as suggested by figure 6. Barton and Bandis (*2*) observed a similar scale effect on the strength of rock joints. In their classic statistical study of pillar performance, Salamon and Munro (*16*) also found that a single coal strength parameter could be used for design throughout the South African coalfields, despite the wide range in compressive strengths reported there (*4*). There is similarly little indication that the predictive capability of ALPS could be improved by considering variations in coal strength.

One aspect of pillar strength that does appear to have immediate practical implications for longwall pillar design is the effect of time. It is well known that the strength of rock decreases the longer the load is applied. In longwalls, the maximum design loading at the tailgate is applied for a relatively short time. As stated earlier, the design criterion for this application is an ALPS stability factor in the 1.0-1.3 range. It should be expected that long-term applications, such as bleeders or mains, should have other criteria. At one gassy Pittsburgh Seam longwall, four separate bleeder systems had been blocked by roof falls. Analysis indicated that the problems occurred when the stability factor dipped below 1.5. It appears that such long-term applications may require the stability factors originally suggested by Bieniawski (1.5-2.0). The effect of time also becomes more important when designing for super longwall panels because of the longer period of time that the gates will be in use.

GATE ENTRY STABILITY

Abutment loads and pillar mechanics relate directly to longwall *pillar* stability. Two other factors must be considered in a successful gate entry design: *roof rock quality* and *artificial support/entry width*.

The following example illustrates the relationship between these three elements. Geotechnical surveys were conducted underground at three longwalls operated by a major coal company. The data are summarized in table 3.

From the information in table 3, the ALPS stability factors were calculated, and ratings were applied to the roof quality and tailgate roof support (table 4).

Table 3.—Data from geotechnical surveys of three longwalls

Parameter	Mine A	Mine B	Mine C
Depth of cover . . . ft . .	650	1,000	900.
Pillar design	3 entries on 55- and 70-ft centers.	3 entries on 90- and 60-ft centers.	2 entries on 100-ft centers.
Roof rock	Strong, massive siltstone and sandstone.	4 ft of laminated shale overlaid by siltstone.	Weak, slickensided mudstones and laminated shales.
Primary tailgate roof support.	6-ft resin bolts on 5-ft centers.	5-ft point-anchor resin bolts on 5-ft centers.	6-ft point-anchor resin bolts and trusses.
Secondary tailgate roof support.	3 rows of wood cribs . . .	2 rows of wood cribs.	1 row of yielding steel posts.

Table 4.—Ratings for roof quality and tailgate roof support

Parameter	Mine A	Mine B	Mine C
ALPS stability factor . .	0.6	0.5	1.0.
Roof quality	Much better than average.	Better than average.	Much less than average.
Tailgate support	Better than average.	Average.	Average.

Based on pillar design alone, mine A and mine B both seemed like candidates for tailgate failure. When roof quality and support were considered, however, mine C was actually at greater risk than mine A. Serious tailgate roof control problems later did occur at both mines B and C, while mine A remained untroubled.

Preliminary indications are that these factors—roof quality and artificial support—explain the bulk of the variability in figure 4. Recent research has focused on incorporating them into the ALPS design methodology. Geotechnical surveys have now been conducted at nearly 50 longwalls to collect data that is now being evaluated with multivariate statistical techniques. The key has been the development of a prototype Bureau of Mines coal mine roof classification system (RCS) to quantify roof rock quality. The RCS builds on earlier rock mass classification systems by incorporating 20 years of Bureau studies of coal mine geology and ground control. The output from the RCS is a roof rating (RR) that is roughly comparable with Bieniawski's (*4*) rock mass rating (RMR). The RCS is currently being field-tested in several U.S. coal basins, and a final version should be available by the end of 1992.

Some results from preliminary statistical analyses using the RCS with ALPS are shown in figure 7. These indicate that as roof rock quality increases, the required stability factor decreases. The width of the entry also appears to have an important influence on tailgate stability. The analyses to date have not identified the role of artificial support because extra supports are often installed in a last-ditch effort in difficult conditions, leading to a false correlation between heavy support and failed designs.

Further statistical analyses will refine these relationships. The ultimate goal is to develop guidelines for selecting the appropriate ALPS stability factor, and the artificial support, based on site-specific geologic evaluations.

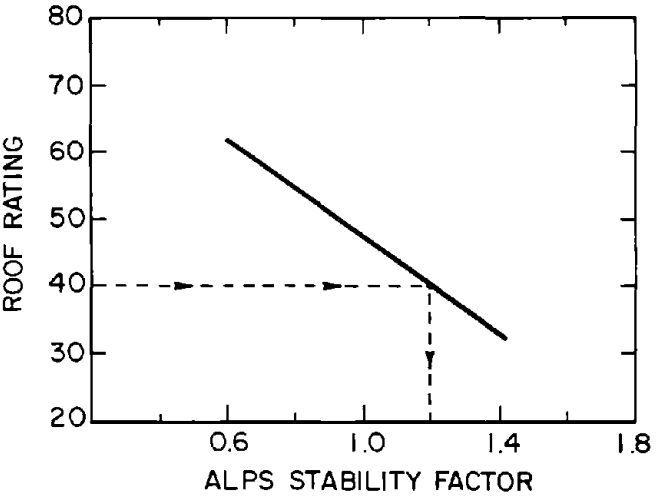

Figure 7.—Preliminary results of statistical analyses relating ALPS stability factor and Roof Rating obtained from Bureau's Roof Classification System.

ALPS AND DESIGN OF RETREAT PILLAR SECTIONS

While the longwall method has been the center of research attention since the 1970's, pillar extraction with continuous miners remains an important section of the U.S. coal industry. Approximately 25 pct of all underground mines still include pillar retreat in their roof control plans. Pillar extraction was also responsible for at least 10 pct of all roof fall fatalities during a recent 9-year period (*15*). Retreat pillaring also generates abutment loads that are essentially similar to those created by longwall mining. A current Bureau research project is investigating whether the ALPS approach can be modified to aid in the design of pillar retreat sections.

A literature review yielded 26 case histories of pillar retreat mining. Nineteen cases were determined to be unsuccessful because of pillar squeezes, severe pillar sloughage, pillar bumps, or other problems. In nearly all unsuccessful cases, the troubled section was abandoned. All cases were analyzed using a modified version of ALPS, called Analysis of Pillar Retreat Stability (APRS). The results are shown in figure 8. It appears that a retreat pillar design may require a greater stability factor than does longwall mining, perhaps 1.5. The greater stability factor may be explained by the longer time that a pillar line is subjected to the maximum abutment loading.

Further research, including a program of underground site visits, is ongoing. These visits will address the role of geology in design performance, again using the RCS. Another task is to adjust the APRS program to better accommodate the complicated three-dimensional panel geometries that are typical of pillar sections.

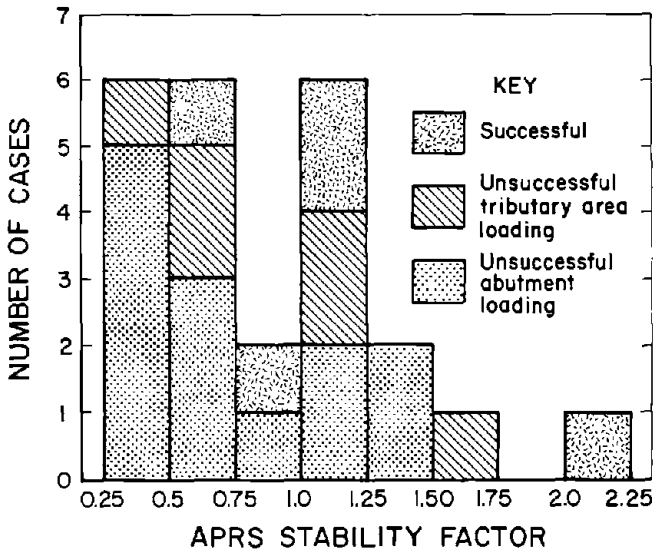

Figure 8.—Preliminary results from analysis of pillar retreat case histories using modified version of ALPS.

CONCLUSIONS

The ALPS method has found wide acceptance within the mining industry. More than 200 copies of the ALPS computer program have been distributed, with users found at almost every U.S. coal company employing the longwall technique. ALPS has been used to help size pillars for new longwalls in Illinois, West Virginia, Colorado, Alabama, and Kentucky. Mining consultants and regulatory agencies have also made extensive use of ALPS, and many leading mining schools have included the ALPS method in undergraduate, graduate, and extension courses.

Current research continues to build upon the ALPS approach. The next big step will be the incorporation of roof rock quality and artificial support into complete longwall gate entry and pillar retreat mining design packages.

REFERENCES

1. Artler, R. L. Pillar Design—Continuous Miner Butt Section and Longwall Development Section. Paper in Proceedings of the 4th Conference on Ground Control in Mining. WV Univ., Morgantown, WV, 1985, pp. 160-165.

2. Barton, N., and S. Bandis. Effects of Block Size on the Shear Behavior of Jointed Rock. Paper in Issues in Rock Mechanics, Proceedings of the Twenty-Third Symposium. Univ. CA, Berkeley, CA, 1982, pp. 739-760.

3. Barton, T. M., and C. Mark. Field Evaluation of Three Longwall Pillar Systems in a Kentucky Coal Mine. BuMines RI 9283, 1989, 13 pp.

4. Bieniawski, Z. T. Rock Mechanics Design in Mining and Tunneling. Balkema, 1984, 272 pp.

5. Brass, J. F. The Evolution of a Longwall System to Suit the Deep Mines in Alabama. Paper in Longwall-Shortwall Mining, State of the Art. Soc. Min. Eng. AIME, 1981, pp. 179-182.

6. Cole, J. D., M. Zik, P. M. Lin, P. Tsang, and S. S. Peng. Design of Three-Entry System for Super Longwall Panels. Paper in Proceedings of the 9th International Conference on Ground Control in Mining. WV Univ., Morgantown, WV, 1990, pp. 107-116.

7. Dangerfield, B. Longwall Experience in the Pittsburgh Seam. Suppl. to the Proceedings of the 1st Conference on Ground Control in Mining. WV Univ., Morgantown, WV, 1981, 6 pp.

8. Doney, E. D. Birth of a Longwall—Initial Planning to Post-Subsidence Mitigation—A Case Study. Paper in Proceedings of the 9th International Conference on Ground Control in Mining. WV Univ., Morgantown, WV, 1990, pp. 298-302.

9. European Community. A Study of Yield Zones Around Mine Roadways. Report EUR 5825e, Appendix 1. Luxemburg, 1977; available upon request from C. Mark, BuMines, Pittsburgh, PA.

10. Gauna, M., B. R. Pothini, and H. E. Hamilton. Practical Rock Mechanics for Safety and Productivity Improvement. Paper in Proceedings of the 7th International Conference on Ground Control in Mining. WV Univ., Morgantown, WV, 1988, pp. 126-136.

11. Karmis, M., T. Triplett, C. Haycocks, and G. Goodman. Mining Subsidence and Its Prediction in the Appalachian Coalfield. Paper in Proceedings of the 24th U.S. Symposium on Rock Mechanics, Assoc. Eng. Geol., 1983, pp. 665-675.

12. King, H. J., and B. N. Whittaker. A Review of Current Knowledge on Roadway Behavior. Paper in the Proceedings of the Symposium on Roadway Strata Control. Inst. of Min. Metall., 1971, pp. 73-87.

13. Mark, C. Pillar Design Methods for Longwall Mining. BuMines IC 9247, 1990, 53 pp.

14. Mark, C., and A. T. Iannacchione. Coal Pillar Mechanics: Theoretical Models and Field Measurements Compared. Paper in Proceedings, Workshop On Coal Pillar Design and Mechanics, BuMines IC 9315, 1992, in press.

15. Montague, P. G. Pillar Recovery—The Lost Art? Paper pres. at AMC Coal Conv., Chicago, IL, 1988, 24 pp; Available upon request from C. Mark, BuMines, Pittsburgh, PA.

16. Salamon, M. G. D., and A. H. Munro. A Study of the Strength of Coal Pillars. J. S. Afr. Inst. Min. Metall., v. 68, 1967, pp. 187-192.

17. Singh, M. M. Strength of Rock. Ch. in Physical Properties of Afr. Rocks and Minerals. McGraw-Hill, 1981, pp. 83-119.

18. Wilson, A. H. An Hypothesis Concerning Pillar Stability. Min. Eng. (London), v. 131, No. 141, June 1972, pp. 409-417.

NUMERICAL MODELING AS A TOOL FOR MINE DESIGN

By Duk-Won Park[1]

INTRODUCTION

Designing proper dimensions of pillars, panels, and entries is very important for underground mining. Until recently, mine operators have determined those dimensions according to previous experiences, rules of thumb, or simple analytical methods. According to traditional pillar design techniques, the compressive strength of coal is first tested for different sizes in the laboratories, then pillar sizes are estimated considering the tributary loading concepts and width/height ratios of the proposed pillars. These concepts, developed by Gaddy [1956 (*2*)][2], Holland [1973 (*6*)], and Bieniawski and Van Heerden [1975 (*1*)], are widely being used, but they do not fully take into consideration of horizontal confinement of the pillars and interactions between pillar and roof, and pillar and floor. Wilson's approach [Wilson and Ashwin, 1971 (*18*)], however, considers confinement and progressive yielding of the pillars. So far, there are no clear design criteria available for panel and entry design.

This paper discusses the experiences on applications of numerical modeling for underground mines and attempts to use the finite-element method as a tool for mine design in the Warrior Coalfield. The Warrior Coalfield, which covers an area of 9,420 square miles, is located in Alabama at the south end of the Appalachian Mountains. This coalfield contains more than 25 coal seams [Tolson, 1990 (*17*)], from which more than 26 million tons of high-quality coal is produced annually. In 1990, about 16.5 million tons of coal was produced from underground coal mines and 11.7 million tons from surface mines [Kelce, 1991 (*7*)]. The recent trend shows that underground production is increasing, while surface coal mine production is decreasing. Two coal mining techniques are used in the 15 underground coal mines of Alabama: room-and-pillar and longwall mining. There are nine active longwall sections in this area. Their production rate is far superior to room-and-pillar sections, and longwall mining is continuing to gain popularity.

For the last 10 years, The University of Alabama research team has been involved with various projects to provide information on the ground response caused by longwall mining, as well as some room-and-pillar mining cases in the Warrior Coalfield. The research included field observation, data analysis, computer simulation, and model analysis. Throughout the study, emphasis was given to the application of numerical modeling for simulating ground behavior. This paper discusses a portion of the effort involved with a two-dimensional and three-dimensional finite-element modeling, combined with the progressive failure simulation technique.

This project was supported by the Office of Mineral Institutes, U.S. Bureau of Mines, through the grant, G1125151.

GEOLOGY

The Warrior Coalfield is bounded on the east by the Opossum Valley Fault and the Blue Creek anticline. The rock units dip steeply away from the structures and are displayed as broad shallow folds that extend into the basin. These folds contain a series of north-northwest trending normal faults with varying dips. The major structures are typically several miles long and seldom possess throws that are greater than 100 ft [Kidd, 1982 (*8*)]. The Pottsville Formation is the uppermost geological unit in the basin and consists of an alternating sequence of conglomerates, sandstones, siltstones, shales, and coalbeds of early Pennsylvanian age. A typical stratigraphic sequence is shown in figure 1.

As a base study, in situ stress measurements were also carried out at one of the local underground coal mines using the U.S. Bureau of Mines overcoring method [Park, Sanford, Simpson, and Hartman, 1983 (*15*)].

[1]Professor of Mineral Engineering, The University of Alabama, Tuscaloosa, AL.

[2]Italic numbers in parentheses refer to items in the list of references at the end of this paper.

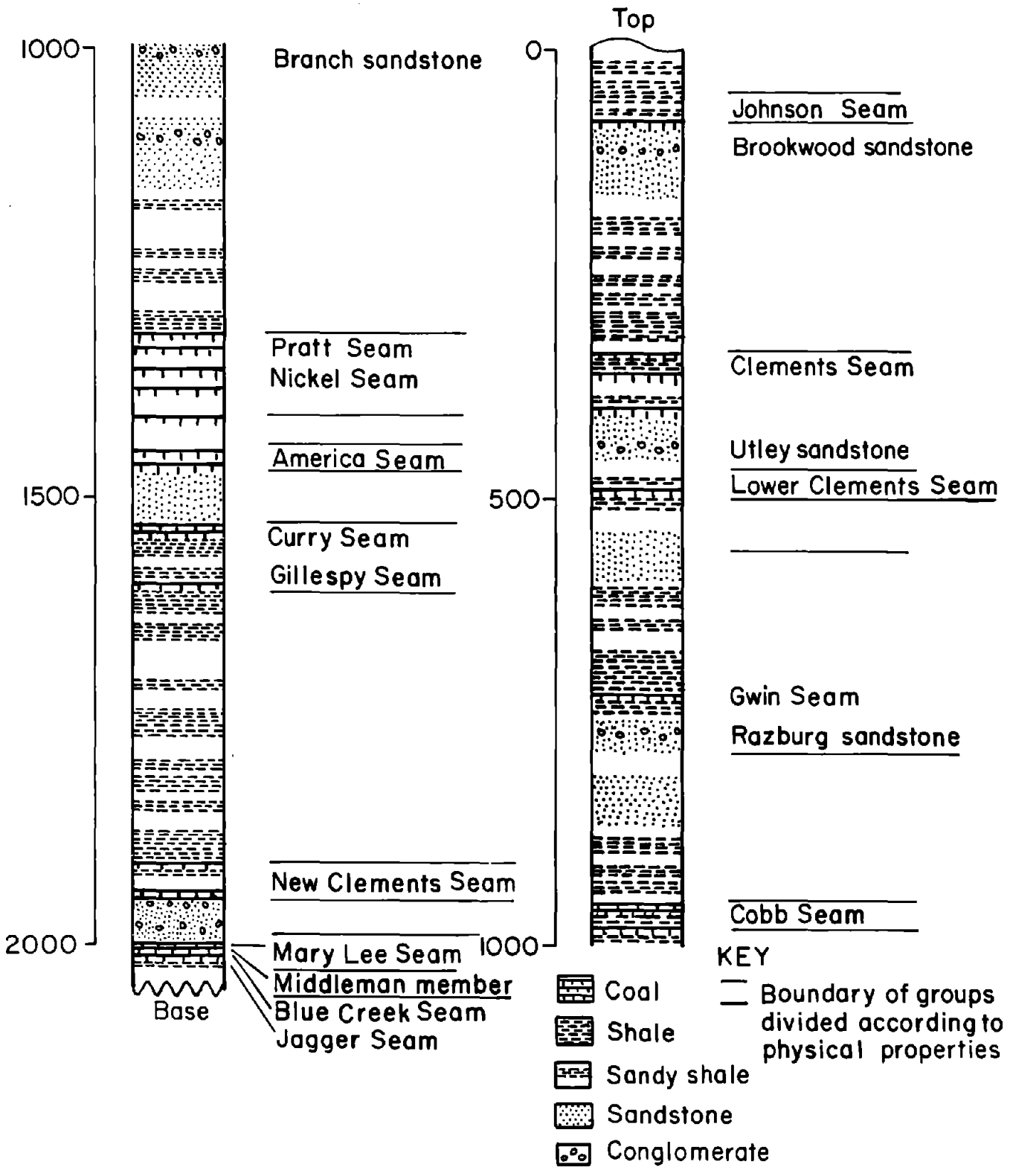

Figure 1.—Typical stratigraphic sequence in Warrior Coalfield.

FINITE-ELEMENT ANALYSIS OF PILLAR STRESSES

The purpose of using the finite-element technique in the study was to simulate stress distribution, deflection, and progressive failure around entries and in pillars and panels due to longwall mining. Throughout the study, the MSC/NASTRAN program was used in the finite-element analysis. This program is capable of solving problems varying from linear and nonlinear statics to dynamics and heat transfer. Rock mass input data that satisfy the actual conditions in a mine are difficult to obtain because of the many structural and geological variations that exist in rock masses. Models were made in two-dimensional as well as three-dimensional configurations. In order to simulate the progressive failure characteristics of coal and rock in the vicinity of openings and gob areas, both Mohr-Coulomb's failure criterion and Hoek and Brown's failure criterion were used. These criteria were applied, combined with a special iterative technique.

TWO-DIMENSIONAL STRESS ANALYSIS

Commonly, rock and coal in the coal mine do not fail violently, except for rock bursts or coal bumps. Before a roof fall or pillar failure occurs, a period of gradual yielding proceeds, accompanied with stress redistributions. Therefore, the initial simulation does not give the full history of stress development in the surrounding strata and coal seam. To simulate progressive failure phenomenon, an iterative procedure was used. The procedure was developed on the numerical analysis previously used by Kripakov [1981 (*10*)] and Kripakov and Melvin [1983 (*11*)], adopted from the theoretical concept developed by Kidybinski and Babcock [1973 (*9*)] and Pariseau and Eitani [1981 (*16*)].

The iterative technique is based on the accepted criterion, which states that failure can occur in one of the three failure modes: shear, compression, or tension. This is a method of simulating gradual change of stress utilizing safety factors, assuming there is some strength maintained during the process of failure unless it occurred in a sudden mode. However, this effect is minimal for the tensile failure mode. Therefore, if an excess tensile stress, higher than the tensile strength, is applied in an element, the element is considered to be completely failed. For two-dimensional cases, the safety factor (SF) for both shear and compression are calculated using the following relationships, which are based on Mohr-Coulomb's criterion:

$$\text{SF (shear)} = \frac{S_o + \sigma_n \tan\phi}{\tau_n} \qquad (1)$$

$$\text{SF (compression)} = \frac{C_o + \sigma_{min}\tan\beta}{\sigma_{max}} \qquad (2)$$

where S_o = shear strength,

C_o = uniaxial compressive strength,

ϕ = angle of internal friction,

$\tan\beta = \dfrac{1+\sin\phi}{1-\sin\phi}$,

σ_{max}, σ_{min} = maximum and minimum principal stresses,

σ_n = normalized compressive stress,

and τ_n = normalized shear stress.

If the calculated factor of safety value is greater than 1, the same modulus of elasticity (E) is used. Otherwise, the least safety factor (SF_{min}) is selected, and a new modulus of elasticity (E_{new}) is calculated according to:

$$E_{new} = SF_{min} \times E_{original} \qquad (3)$$

E_{new} is used for the next iteration. Similarly, new compressive and shear strength values are also decided for the element, assuming that strength values are also reduced as a rock mass goes through the yielding stage. This process is repeated until all elements become stable and the mine structure reaches an equilibrium condition.

THREE-DIMENSIONAL STRESS ANALYSIS

In order to account for rock mass behavior in the three-dimensional mode, the Hoek and Brown failure criterion was used in the determination process of the maximum allowable stress levels in the elements [Park and Gall, 1989 (*13*)]. Principal stress relationships were developed by Hoek and Brown [1980 (*4*)] in the general equations:

$$\sigma_{1n} = \sigma_{3n} + \sigma_c(m\sigma_{3n} + s)^{1/2} \qquad (4)$$

for principal stress relationship; and

$$\tau_n = A(\sigma_n + \sigma_{tn})^B \qquad (5)$$

for shear stress reltionship, where,

m, s, A, and B = material constants that depend on the rock types and rock mass quality,

σ_{1n} and σ_{3n} = normalized principal stresses, $\frac{\sigma_1}{\sigma_c}$ and $\frac{\sigma_3}{\sigma_c}$,

σ_c = uniaxial compressive strength of the intact rock in the rock mass,

τ_n and σ_n = normalized shear and compressive stresses expressed as $\frac{\tau}{\sigma_c}$ and $\frac{\sigma}{\sigma_c}$,

and σ_{tn} = normalized tensile strength, expressed

$$\frac{1}{2m} - (m^2 + 4s)^{1/2}.$$

The table for the Hoek and Brown criterion contains sets of these equations grouped according to lithology and quality of the rock mass. Each set of equations is assigned with numerical values for m, s, A, B, and σ_{tn} [Hoek and Brown, 1988 (*5*)].

The progressive failure of a rock mass is simulated by first choosing equations for each strata group according to the rock mass properties. In the case where two sets of equations are chosen, one is selected for the rock mass in its undisturbed state and the other for those of disturbed strata [Hoek and Brown, 1980 (*4*)]. The parts in the yield pillars or those around the pillar edges, as well as along the edge of the abutment pillars in the coal seam, are considered to be disturbed when the elements in those areas are classified as failed or yielded elements. This is based on the analysis of the initial run of the finite-element method.

The three-dimensional finite-element solution provides three principal stresses, σ_1, σ_2, and σ_3; shear stresses, τ_{xy}, τ_{xz}, and τ_{yz} acting on the stress planes, x-y, x-z, and y-z, respectively; and the normal stresses to these planes, σ_z, σ_y, and σ_x. Using the minor principal stress from the solution, the maximum allowable major principal stress can be calculated. Modification of equation 4 yields:

$$\sigma_{1,\,\text{allowable}} = \sigma_{3N} + \sigma_c\,(m\,\sigma_{3n} + s)^{1/2} \qquad (6)$$

where $\sigma_{1,\,\text{allowable}}$ is the maximum allowable principal stress.

The maximum allowable shear strength can be obtained using similar modifications. For instance, the maximum allowable shear stress, $\tau_{xy,\,\text{allowable}}$, acting on the x-y plane can be calculated using the following equation modified from equation 5:

$$\tau_{xy,\,\text{allowable}} = A\sigma_c\left(\frac{\sigma_z}{\sigma_c} + \sigma_{TN}\right)^B. \qquad (7)$$

The remaining shear stresses τ_{xz} and τ_{yz} are treated the same way. The ratios of the values from equations 6 and 7 and the calculated major principal stress, $\sigma_{1,\,\text{FEM}}$, and shear stress, $\tau_{xy,\,\text{FEM}}$, $\tau_{yz,\,\text{FEM}}$, or $\tau_{zx,\,\text{FEM}}$, from the finite-element solution are computed as the safety factors:

$$SF_1 = \frac{\sigma_{1,\,\text{allowable}}}{\sigma_{1,\,\text{FEM}}} \qquad (8)$$

for principal stress; and

$$SF_2\,(SF_3, SF_4) = \frac{\tau_{xy\,(yz,\,zx),\,\text{allowable}}}{\tau_{xy\,(yz,\,zx),\,\text{FEM}}} \qquad (9)$$

for shear stresses.

If the minimum of the four factors of safety is less than 1, then the modulus of elasticity for the element being analyzed is reduced by the minimum safety factor (SF_{min}) according to equation 3.

Every element in the model is analyzed in this manner, except those representing the longwall shields, gob, and mine openings. After adjusting all the material properties, the model is then rerun. The process is repeated until all of the calculated factors of safety exceed 1. Because a large number of elements and calculations are involved in the simulation of progressive failure, a computer program was written in Fortran to handle the computations of the new input data. The program also produces an input file compatible with the NASTRAN code for each subsequent iteration. The flow chart for the iteration technique is illustrated in figure 2.

PILLAR STABILITY ANALYSIS IN A LONGWALL MINE

The stability of longwall entries is greatly affected by the size of supporting pillars. The conventional system of pillars, consisting of equal-sized pillars, has frequently created problems. Examples are floor heave and roof and pillar failures caused by high stresses in the head entry area of a local longwall section. The recent development of a yield pillar system has shown improvements over the conventional system. Yield pillars are narrow pillars

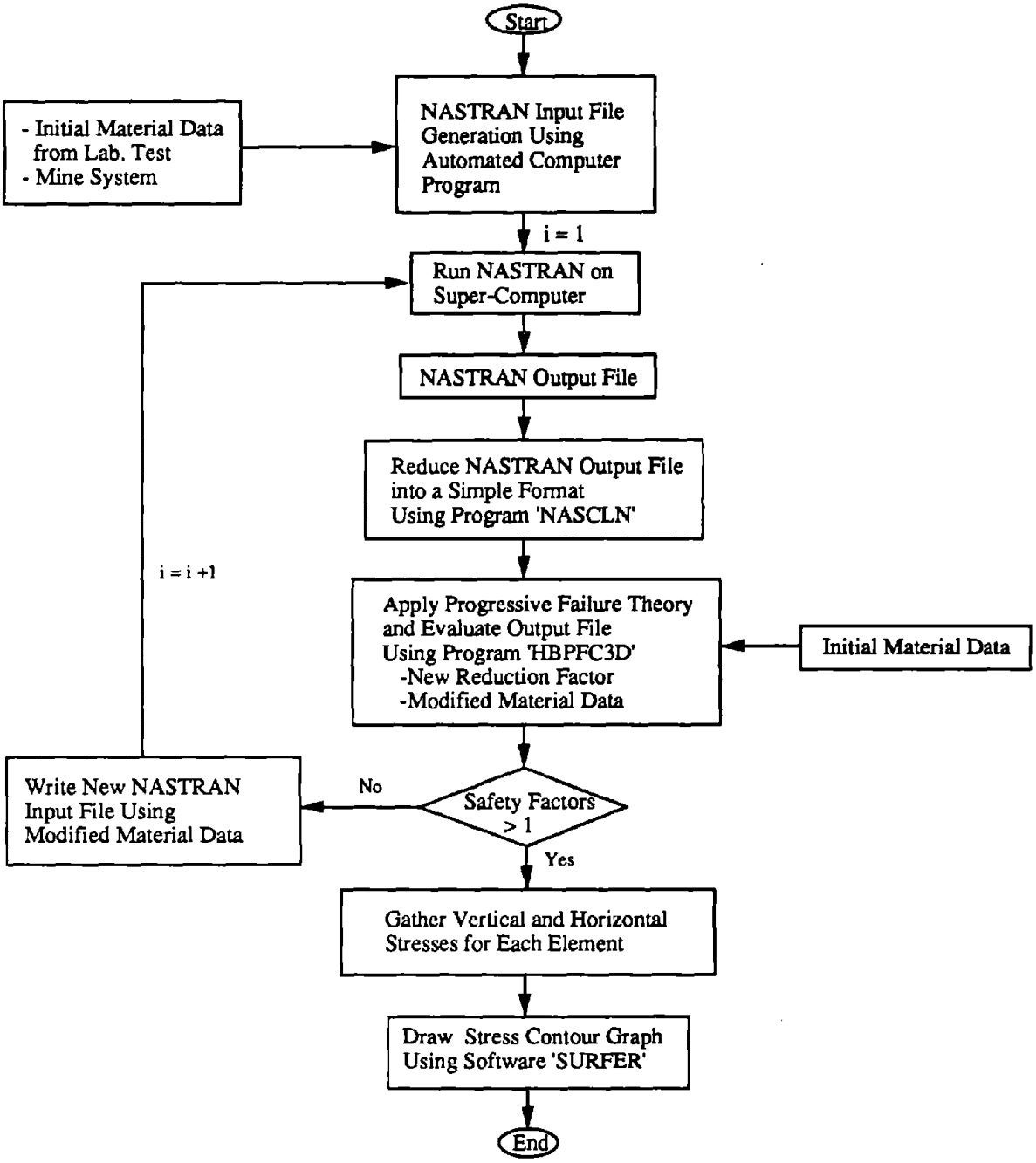

Figure 2.—Flowchart of numerical mine model simulation.

situated closest to the panel to yield, thus minimizing stress concentration problems and allowing the high stresses to transfer to a relatively larger pillar (abutment pillar) situated further away from the longwall panel. Therefore, stresses are relieved in the critical sections to be protected, such as head entry area.

Two-dimensional numerical modeling was performed to simulate a local longwall panel where the yield pillars were experimented [Park and Ash, 1985 (*12*)]. As shown in figure 3, the mine used two different entry systems to compare the characteristics of the chain pillars. As the first stage of the study before modeling, stress measurements were conducted using vibrating wire stress meters [Park, Sanford, Simpson, and Hartman, 1983 (*15*)]. The stress meters were placed at various depths, as indicated in figure 3.

A substantial number of tests were performed on coal and rock samples taken from the Warrior Coalfield in the previous studies [Park, Sanford, Simpson, and Hartman, 1983 (*15*)]. Based on the results, rock mass input data were carefully determined. The two-dimensional regular-pillar model consisted of 877 plate-elements with 1,038 nodes, while the yield-pillar model was formed combining 984 elements and 1,158 nodes, as shown in figure 4 [Park and Ash, 1985 (*12*)]. Roller-type boundary conditions for both models were placed along two edges of the models, and gravitational and excessive horizontal loadings were imposed on the other two surfaces in order to account for in situ stresses. The models were analyzed using the progressive failure simulation scheme (described earlier) combined with the Mohr-Coulomb's failure criterion. An IBM[3] 3086 mainframe computer was used for the processing.

[3]Reference to specific products does not imply endorsement by the U.S. Bureau of Mines.

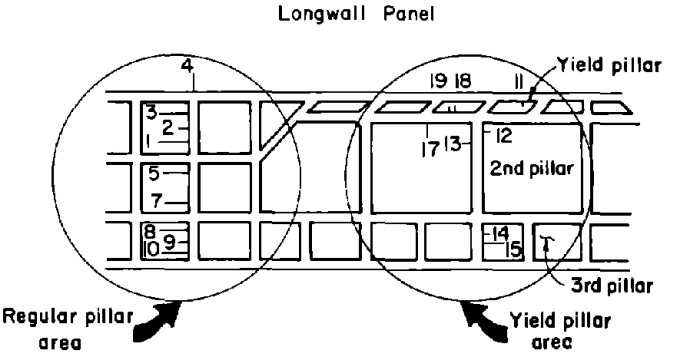

Figure 3.—Regular pillar and yield pillar areas and gauge locations.

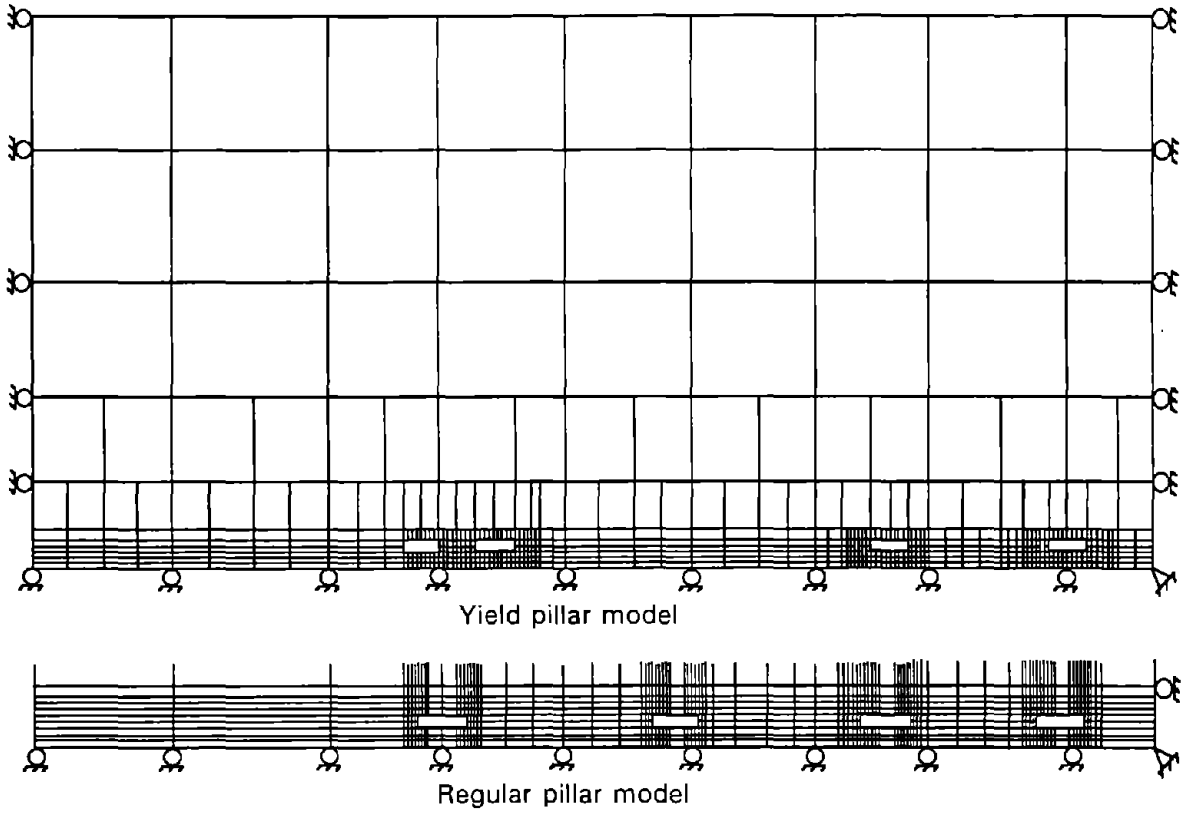

Figure 4.—Two-dimensional mine models.

Stress distribution for the initial run of the regular-pillar model, as shown in figure 5, showed high peak stresses at the edges, but the third iteration (stage), the final run, described a distinct yield zone and competent inner core area. The yield-pillar model showed similar stress redistributions in the abutment pillar and the intermediate pillar, but the yield pillar showed a gradual yielding, as it was designed (fig. 6). The vertical stresses in the yield pillar were lower compared with the regular pillar system. The stress values showed a close agreement with the field data.

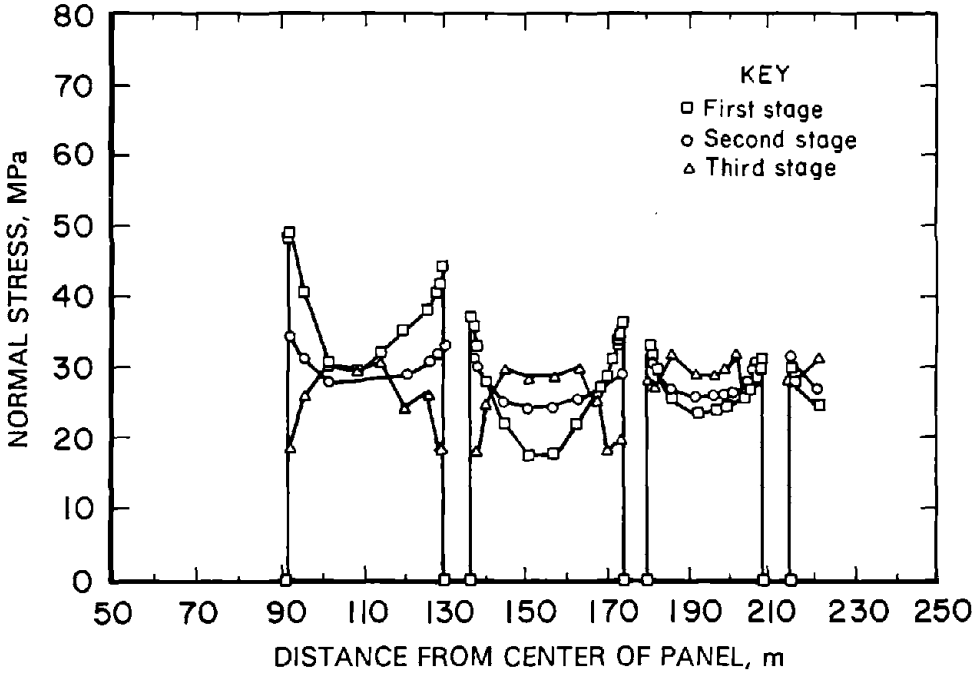

Figure 5.—Stress distribution of regular pillar area.

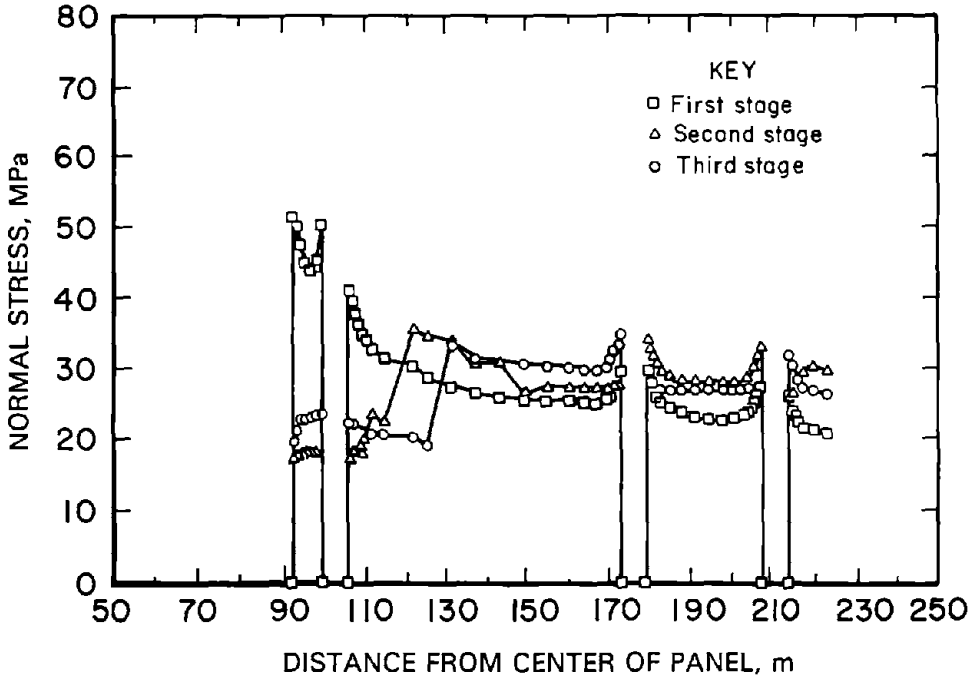

Figure 6.—Stress distribution of yield pillar area.

In this mine, floor heave caused by insufficient floor bearing capacity was one of the more serious problems. Floor movement was compared between the two models as shown in figures 7-8. Movement around the second entry (A-B) was drastically reduced in the yield pillar model. Since failures in the immediate floor are often caused by pillar punching into floor and subsequent deterioration by floor heaving, the results of this analysis show the advantage of the yield pillar system.

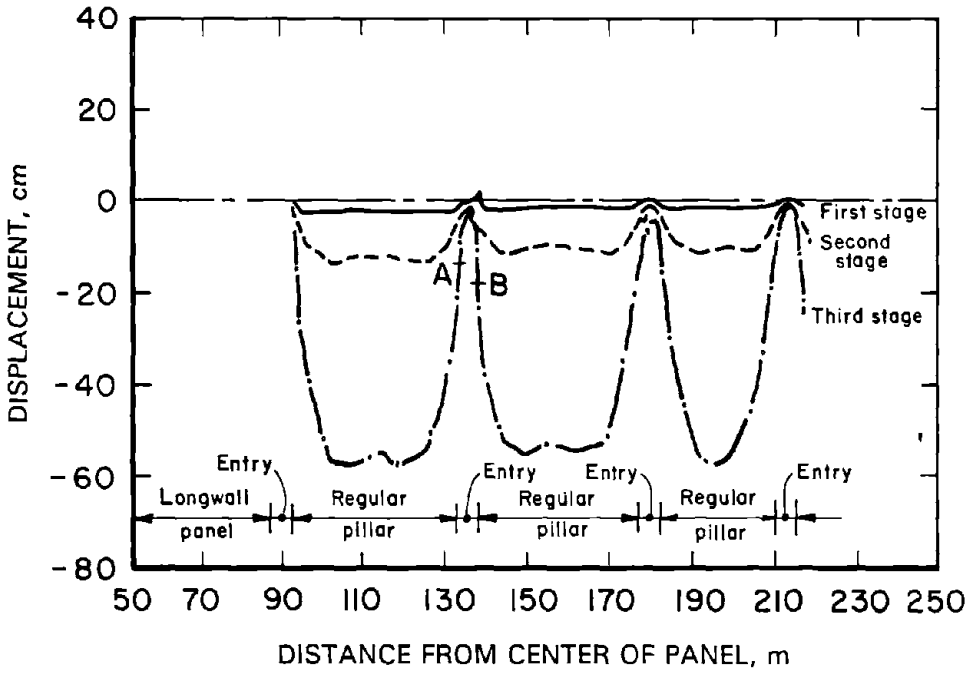

Figure 7.—Floor movement at regular pillar area.

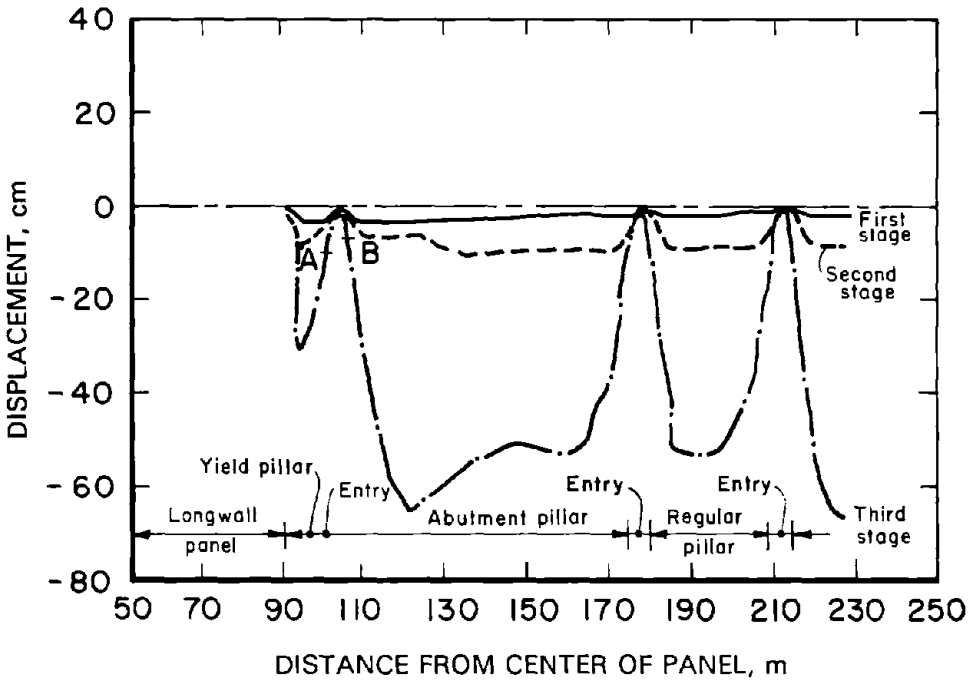

Figure 8.—Floor movement at yield pillar area.

THREE-DIMENSIONAL LARGE-SCALE SIMULATION

Two-dimensional models can only provide information limited to one profile and cannot account for longwall face movement or gob conditions. Therefore, a three-dimensional model was made for the same site [Park and Gall, 1989 (*13*); Gall and Park, 1990 (*3*)]. The model covers a horizontal area of 1,160 by 1,050 ft that consists of three rows of regular pillars and two half longwall panels situated on both sides of the chain-pillar entry system (fig. 9). The total height of the model is 2,130 ft, accounting for an overburden above the coal seam of about 2,000 ft and incorporating two layers below the coal seam. The model is discretized vertically into 14 layers of strata groups. Each layer consists of 531 eight-noded hexahedral elements, resulting in a total of 7,434 elements.

The progressive failure technique was utilized combining the Hoek and Brown failure criterion. Because of the size of the model and its complexity, a CRAY X-MP/24 supercomputer was used for the simulation. Even then, about 1 h of computer time had to be consumed for each run. To facilitate the process involved in the application of the progressive failure technique, a computer program was made.

The results of the analyses included stresses and displacements in the panels, pillars, and entries for different longwall face locations. Some examples of the results are shown in figures 10 through 12, which show stress distributions in the study area. The results compared favorably with the field measured stress data [Park and Gall, 1989 (*13*); Park, Sanford, Simpson, and Hartman, 1983 (*15*)]. The combination of a large-scale finite element model and progressive failure simulation provides a tool that can generate a large amount of information related to the behavior of rock and coal as a response to the longwall mining operation.

PILLAR AND PANEL DESIGN USING NUMERICAL MODEL

The numerical method was utilized as a preliminary design tool for a longwall mine to be located in the Warrior Coalfield [Park and Lee, 1992 (*14*)]. At this mine, the same coal seam is to be mined and the geological conditions are similar to other mines where numerical simulations were performed earlier. In this study, a total of five finite-element models were developed with various combinations of sizes of abutment pillars, yield pillars, and panels. The height of the model was 1,420 ft, accounting for an overburden above the coal seam of approximately 1,325 ft and incorporating two rock layers below the coal seam. Each model was discretized vertically into 12 layers of strata groups dictated by the stratigraphic sequence. As shown in figure 13, the models consisted of one row of abutment pillars, two rows of yield pillars, and two half longwall panels.

The detailed dimensions of the models are listed in table 1. The effect of change of yield pillar width was examined using models 1, 2, and 3, and the effect of variations of panel width was examined using models 1, 4, and 5. Influences of different abutment pillar sizes were studied through all models.

The results of the first three models (1-3) were used for comparing the effects of different yield pillar sizes. Outputs of models 1 and 2 were almost the same, with the exception of a slight increase in the overall sections due to the reduction of yield pillar width from 20 to 18 ft. As shown in figure 14, yield pillars yielded along the head entry, and the panel and other pillars were intact. Model 3, however, showed excessive stresses caused by floor failures (fig. 15). Therefore, 18-ft-wide yield pillars were recommended.

The panel width was increased from 600 to 800 ft, and the abutment pillar size was decreased from 200 by 220 ft to 150 by 220 ft in model 4 compared with model 1. As shown in figure 16, the edges of the abutment pillars and a small portion of the panel corner yielded. Model 5, with a panel width of 1,000 ft, resulted in an additional failure along the face and the yield pillar area on the other side of the abutment pillar (fig. 17). From these results, it was recommended that the maximum panel size would be between 800 and 1,000 ft, and the abutment pillar size of 150 by 220 ft is recommended.

Table 1.—Dimensions of mine models

	Panel width		Abutment pillar		Yield pillar		Total area covered	
Model	ft	m	ft	m	ft	m	ft	m
1 . . .	600	182.9	200 by 220	61 by 67.1	20 by 100	6.1 by 30.5	920 by 940	280.4 by 286.5
2 . . .	600	182.9	200 by 220	61 by 67.1	18 by 100	5.5 by 30.5	916 by 940	279.2 by 286.5
3 . . .	600	182.9	200 by 220	61 by 67.1	15 by 100	4.6 by 30.5	910 by 940	277.4 by 286.5
4 . . .	800	243.8	150 by 220	45.7 by 67.1	18 by 100	4.6 by 27.5	966 by 940	294.4 by 286.5
5 . . .	1,000	304.8	150 by 220	45.7 by 67.1	18 by 100	4.6 by 27.5	1,066 by 860	324.4 by 286.5

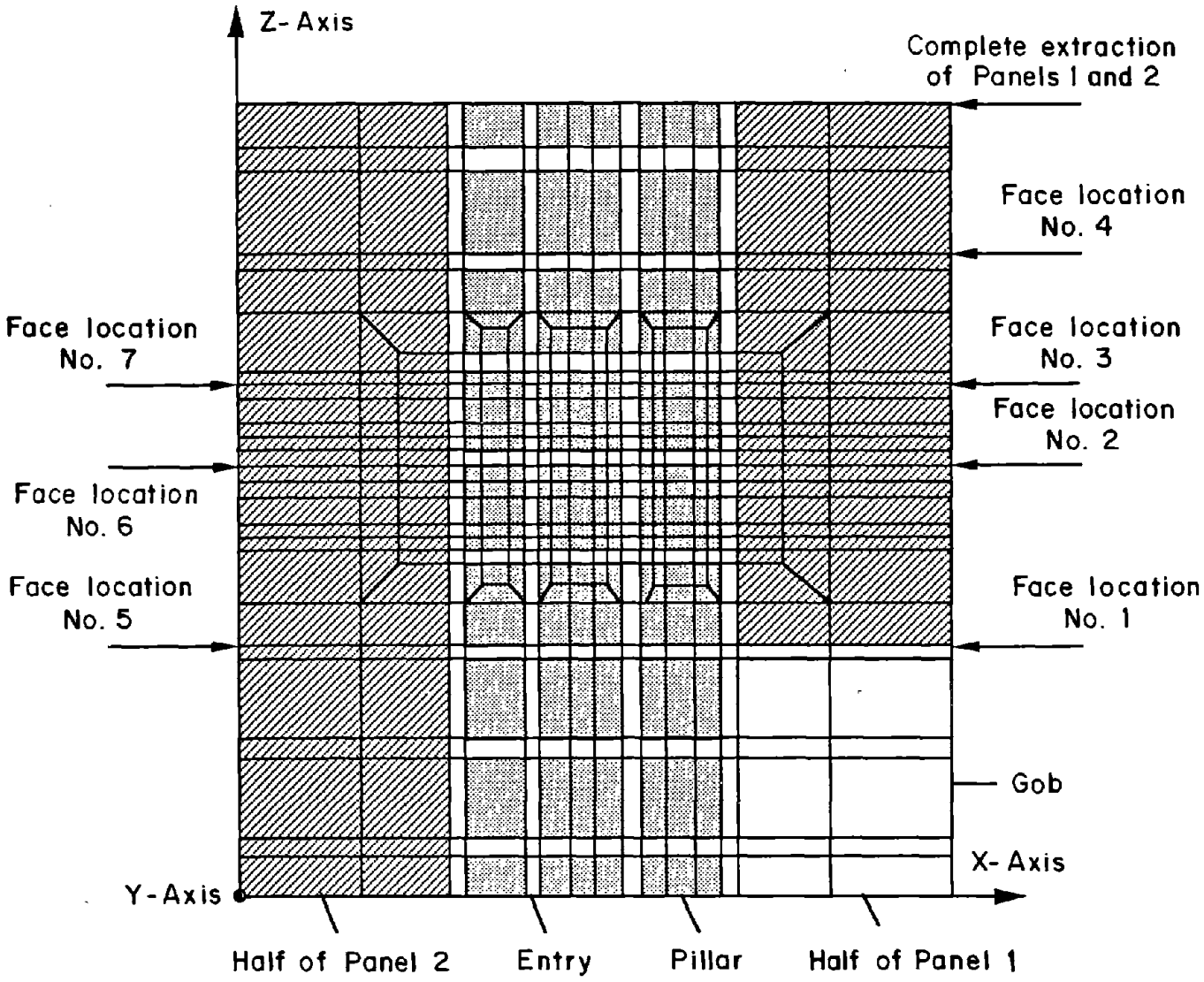

Figure 9.—Plan view of three-dimensional mine model.

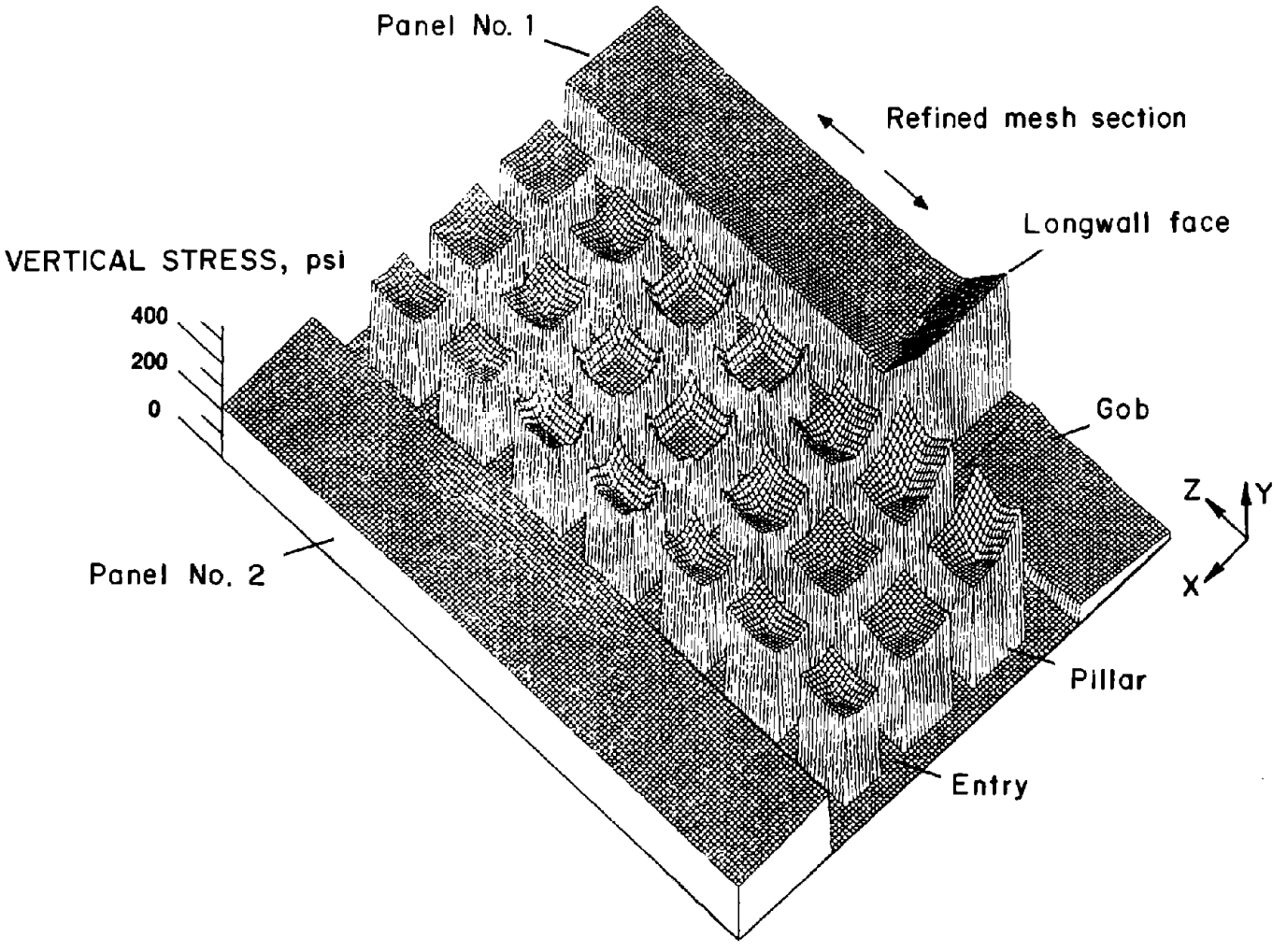

Figure 10.—Stress distribution for face location 1.

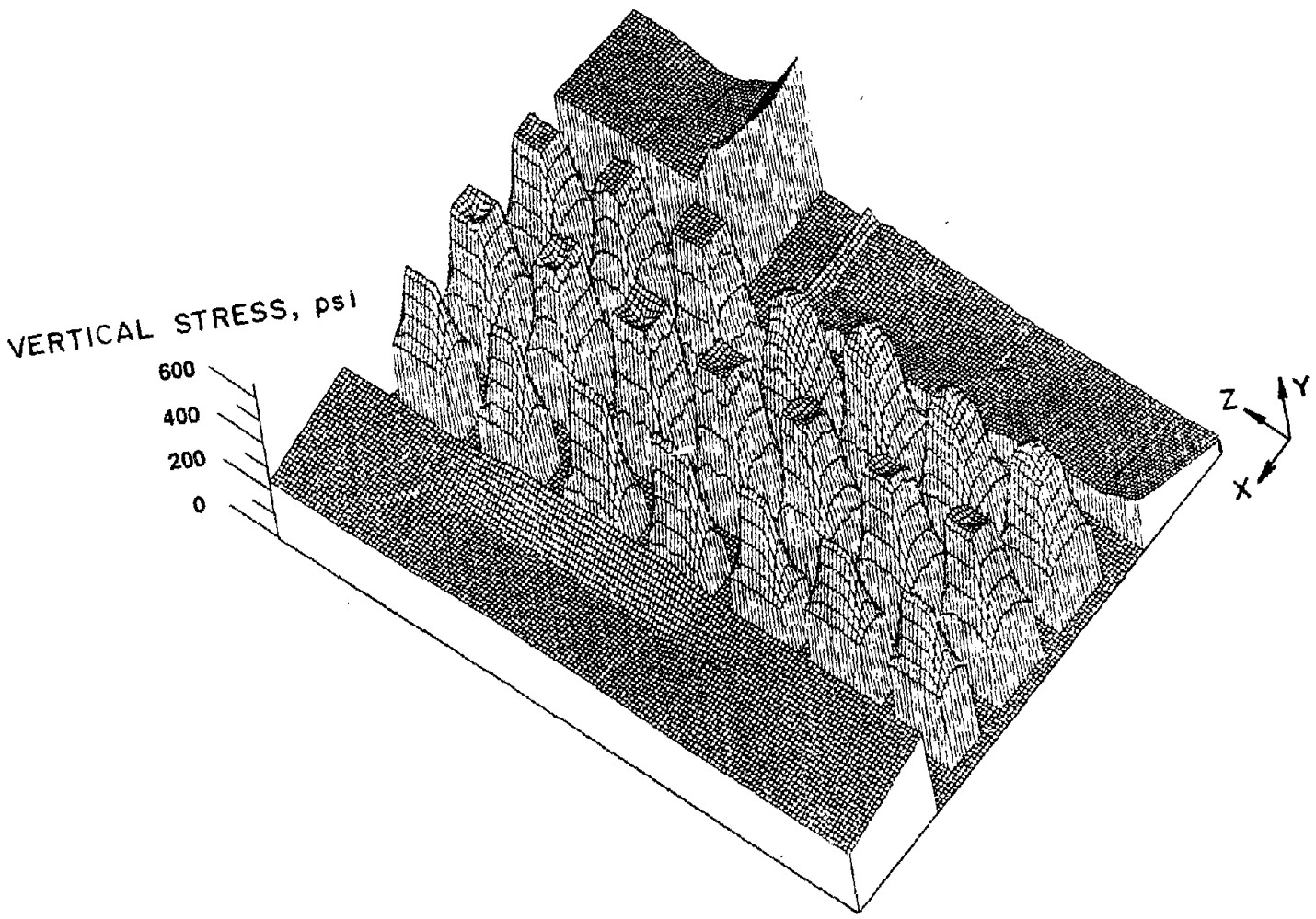

Figure 11.—Stress distribution for face location 3.

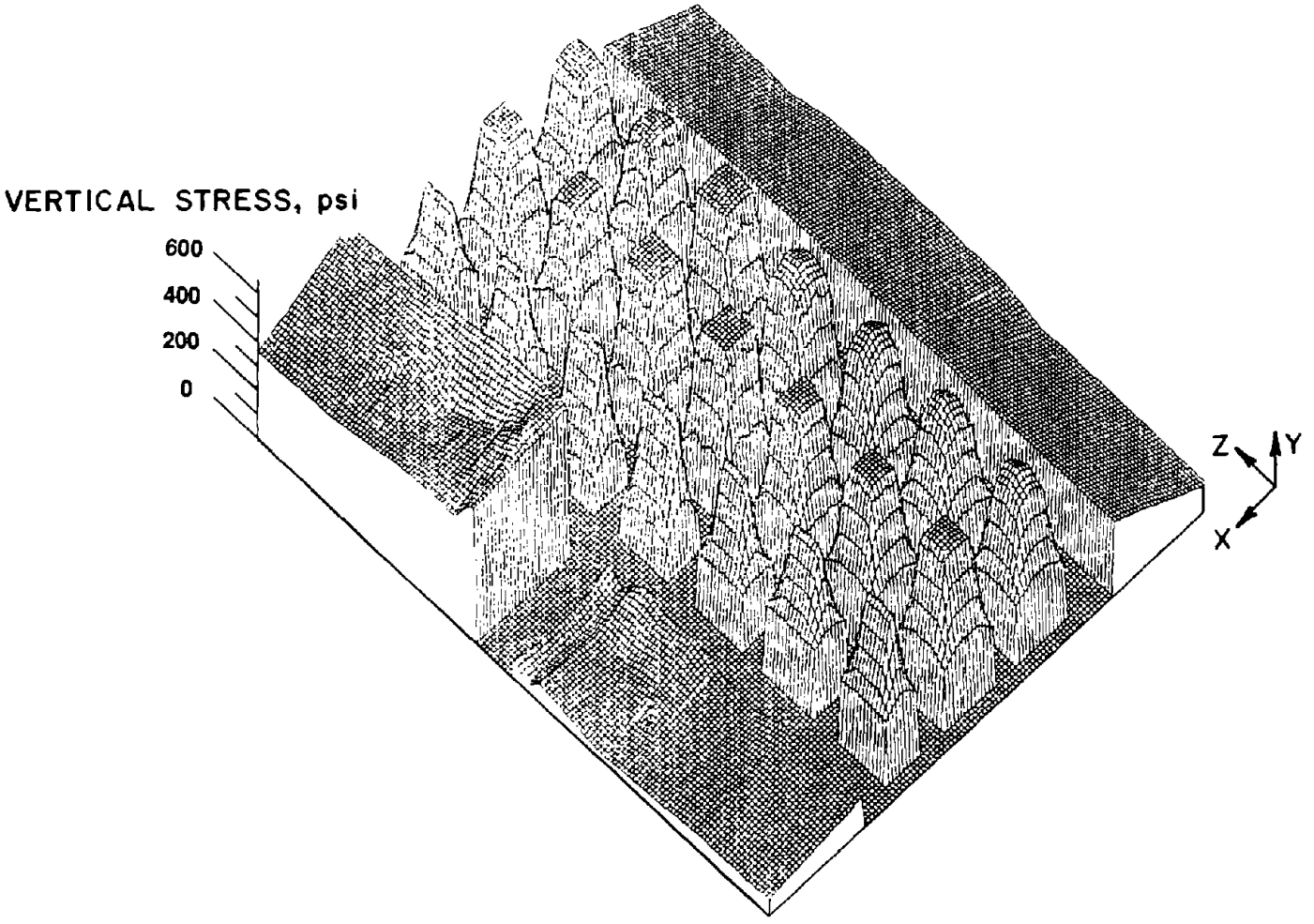

Figure 12.—Stress distribution for face location 6.

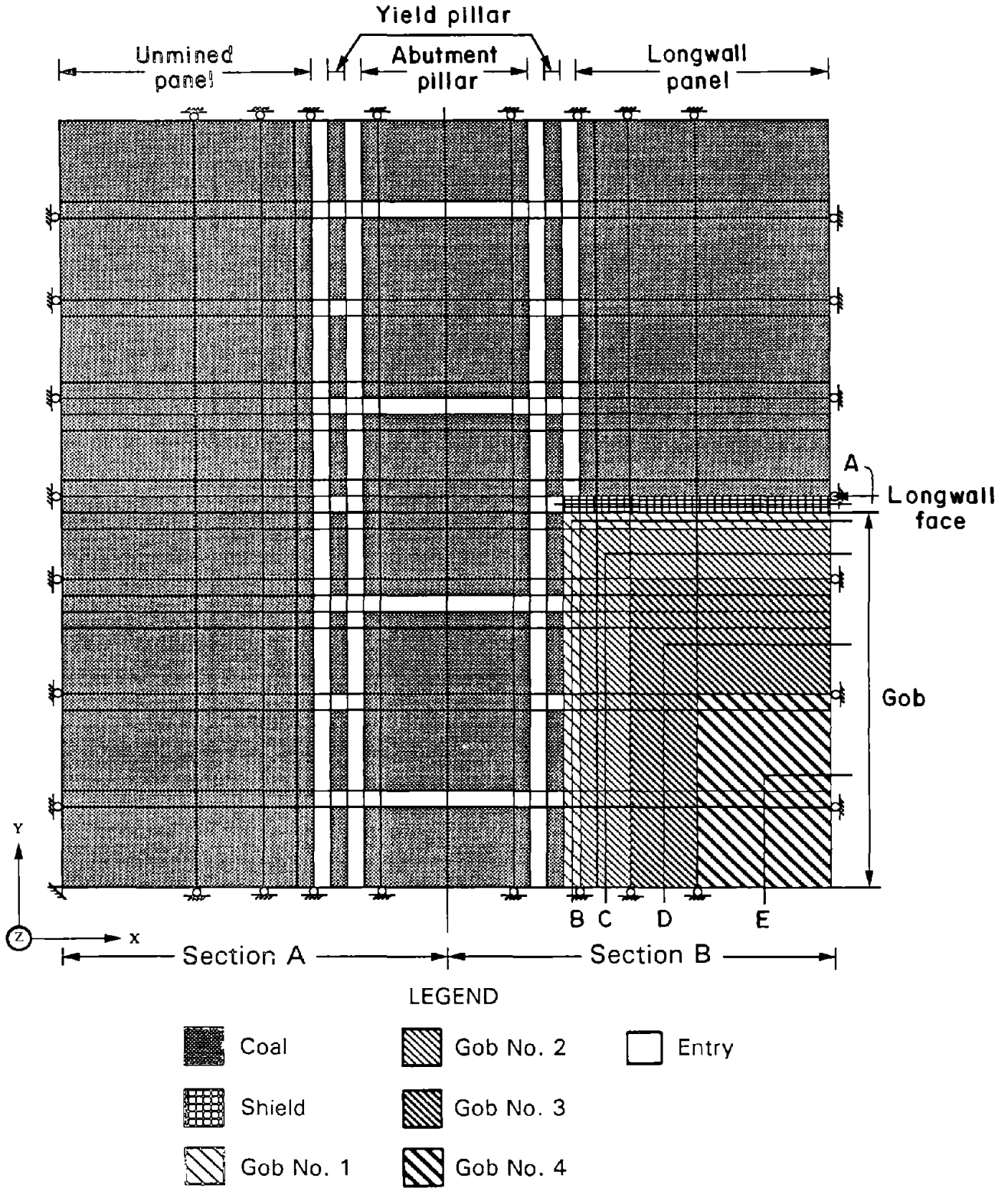

Figure 13.—Plan view of three-dimensional mine design model.

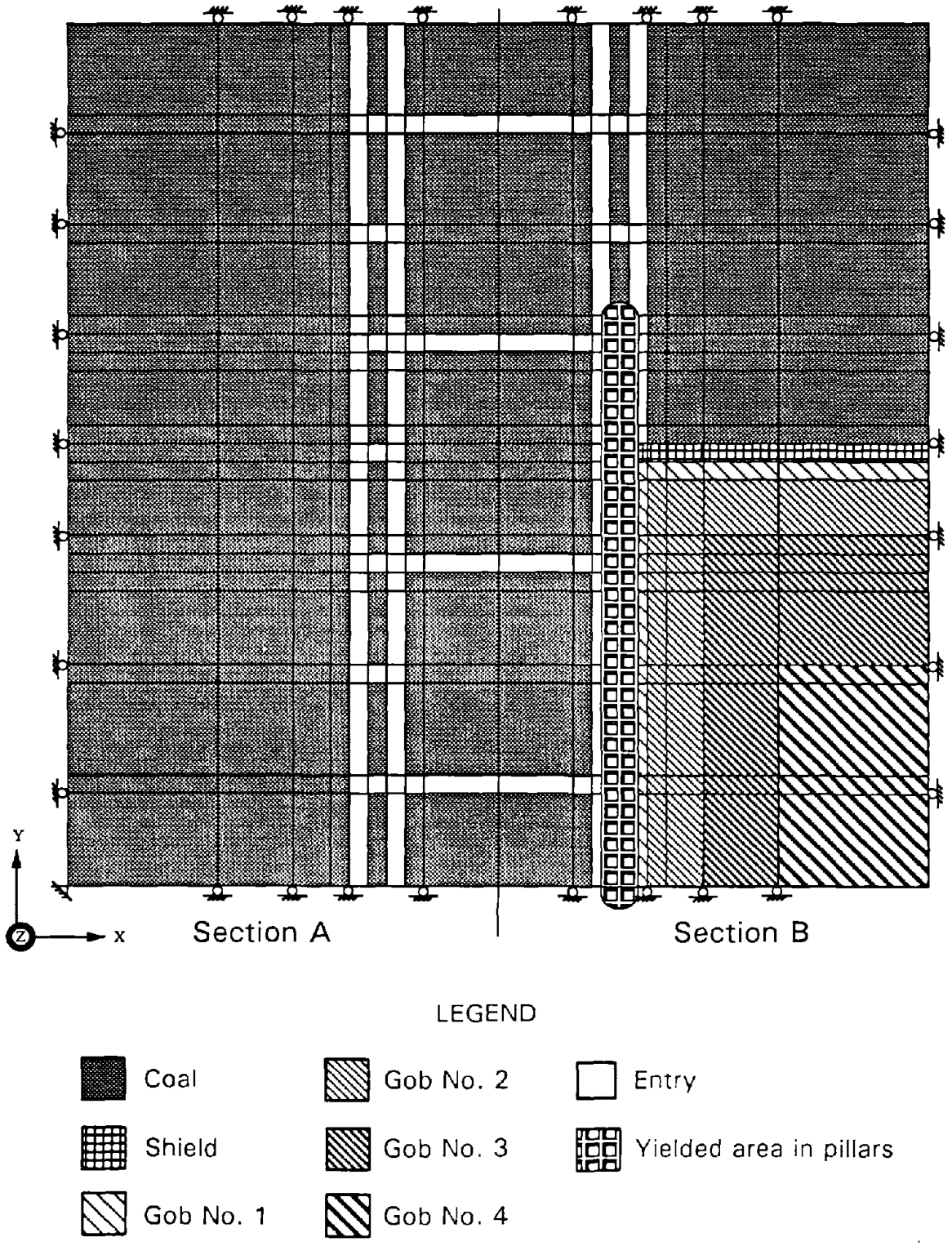

Figure 14.—Location of yielded areas in mine models 1 and 2.

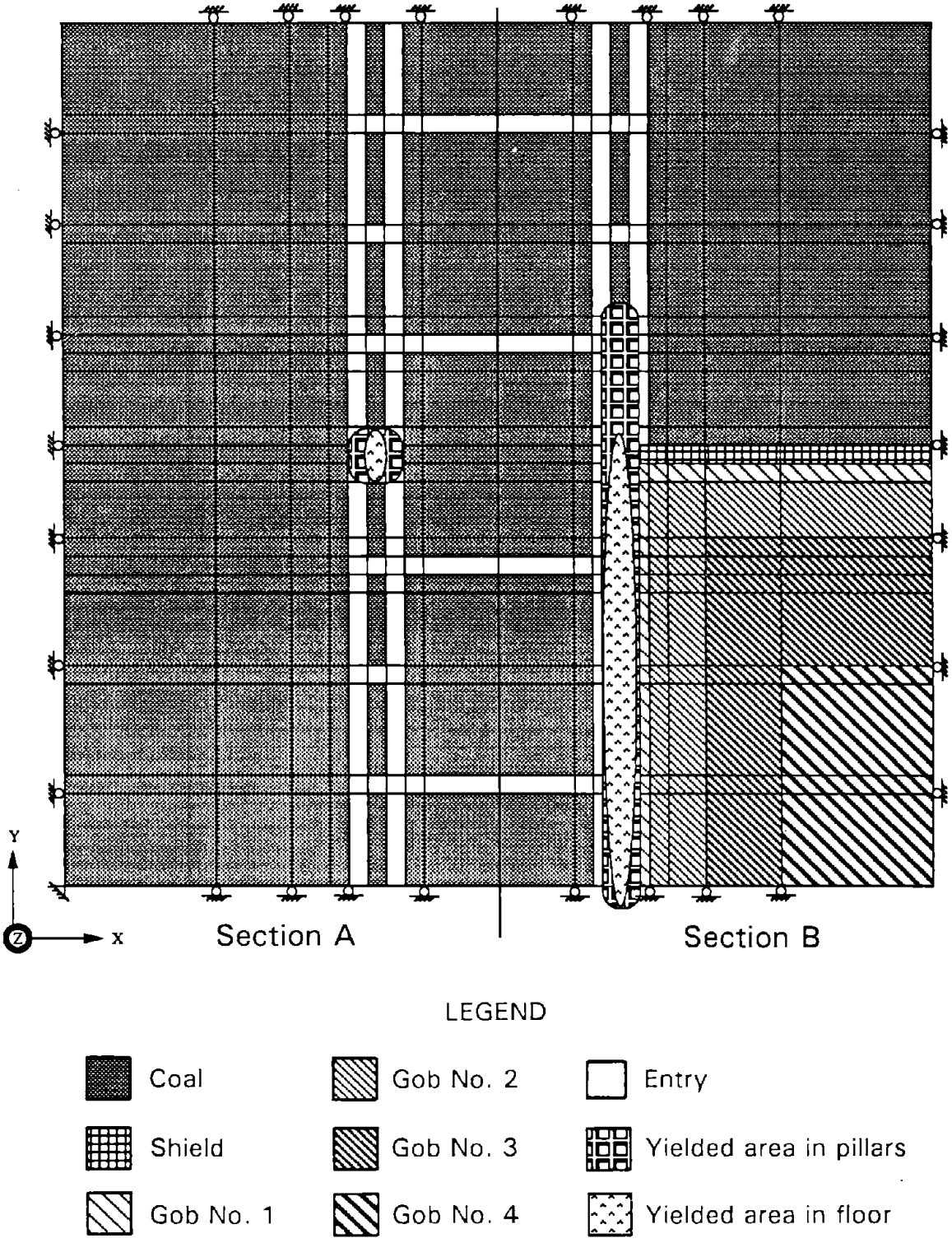

Figure 15.—Location of yielded area in mine model 3.

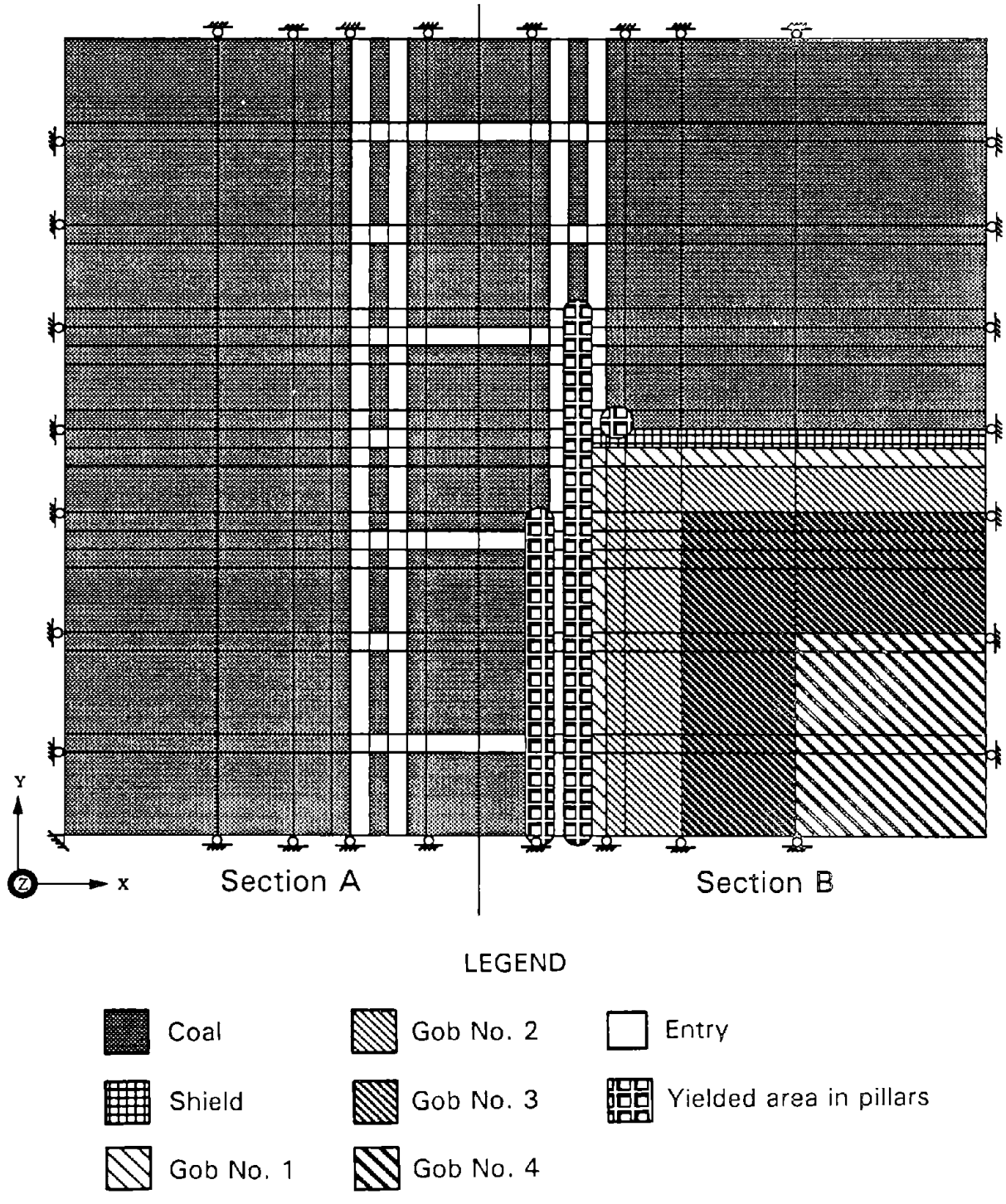

Figure 16.—Location of yielded area in mine model 4.

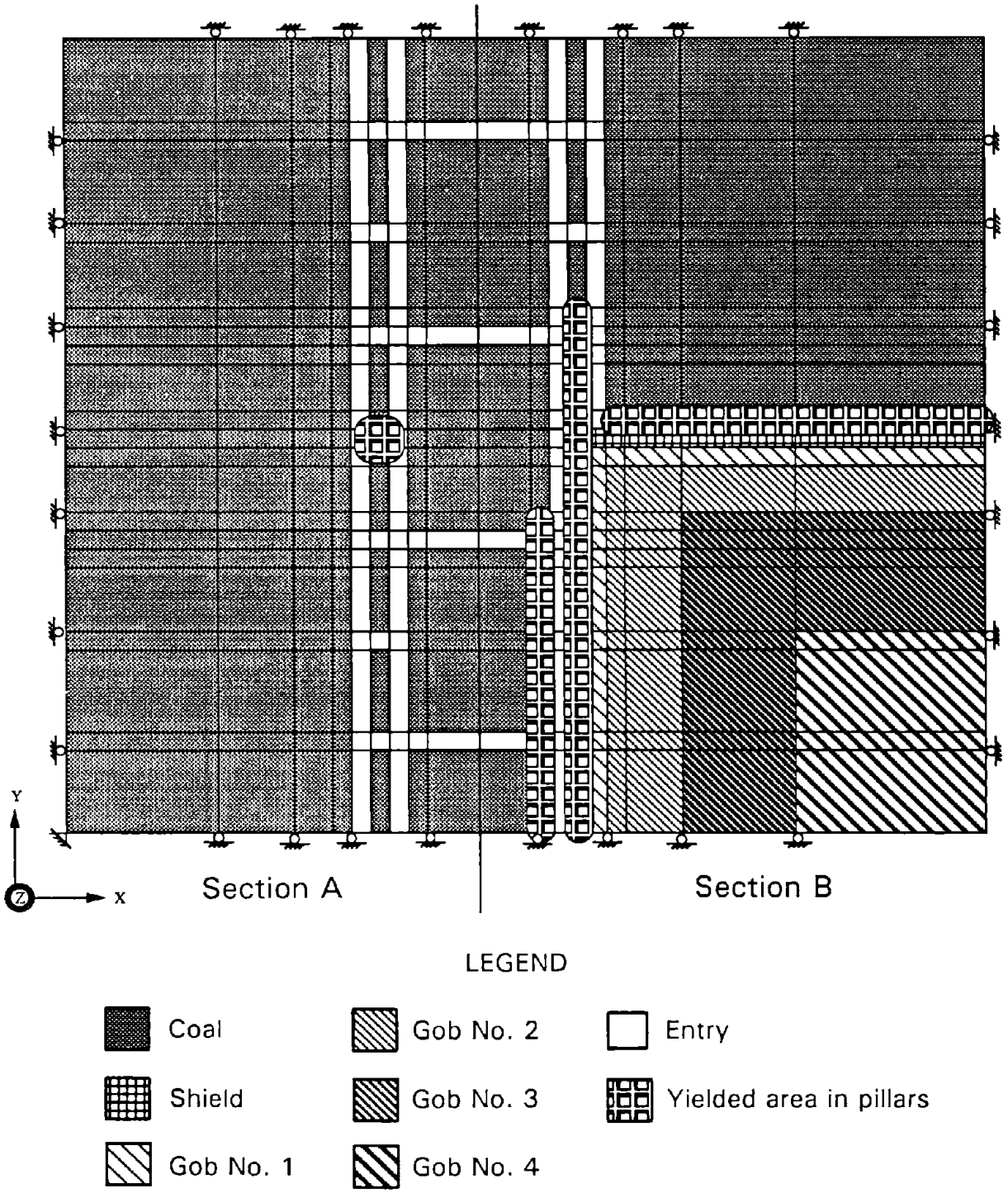

Figure 17.—Location of yielded area in mine model 5.

CONCLUSIONS AND RECOMMENDATIONS

Numerical modeling techniques are not commonly used as a means of mine design because of the complexity in mine structures, geology, and rock mass properties. However, the iteration method has shown encouraging results owing to its capability of simulating progressive failure and yielding. The same technique in combination with the Hoek and Brown failure criterion is especially promising because it accounts for rock mass properties. The results of the study were realistic because the method took into consideration the progressive failure phenomenon using the iterative technique and rock mass properties, and the availability of a supercomputer made it possible to simulate large areas that include multiple pillars, entries, and panels.

Additionally, the numerical technique seems to be a valid tool for mine design if it is properly used. In order to improve the technique, the following should be considered:

1. Although the Hoek and Brown failure criterion recognizes rock mass characteristics, it was originally designed for hard rock mines. Therefore, some modifications may be required for rock mass associated with coal mines, especially coal seams.
2. Since rock mass properties are the most critical, more detailed rock mass classification methods should be developed for coal measure rock masses.
3. Results from numerical simulation should be compared with field measurements for back calculations and improved input data.
4. Since the number of elements for a model is limited even though a supercomputer is used, element sizes sometimes have to be too large for simulation of the area where a large variation of stresses is imposed. A supercomputer with a larger capacity would be helpful.
5. More experiences are needed in comparative study between numerical simulations and other analytical methods.

REFERENCES

1. Bieniawski, Z. T., and W. L. Van Heerden. The Significance of In-Situ Tests on Large Rock Specimens. Int. J. of Rock Mech and Min. Sci., Geomech. Abs. No. 12, 1975.
2. Gaddy, F. L. A Study of the Ultimate Strength of Coal as Related to the Absolute Size of the Cubical Specimens Tested. VA Polytech. Inst. Bull., 1956.
3. Gall, V., and D.-W. Park. Large Scale Three-Dimensional Numerical Simulation of Longwall Mining. Paper 90-24 in 119th SME Annual Meeting, Salt Lake City, UT, Feb. 1990.
4. Hoek, E., and E. T. Brown. Underground Excavations in Rock. The Institution of Mining and Metallurgy, London, 1980.
5. Hoek, E., and E. T. Brown. The Hoek-Brown Failure Criterion-A 1988 Update. Proc. 15th Canadian Rock Mechanics Symp., Toronto, Ontario, Canada, 1988.
6. Holland, C. T. Mine Pillar Design. SME Mining Engineering Handbook, ed. by A. B. Cummins and I. A. Givens, AIME, New York, 1973.
7. Kelce, W. Personal communication, 1991.
8. Kidd, J. T. Structural Geology of the Black Warrior Basin in Alabama. Depositional Setting of the Pottsville Formation in the Black Warrior Basin, ed. by L. J. Rheams and W. J. Benson. Guidebook for the 19th Annual Field Trip of the Alabama Geological Survey, 1982.
9. Kidybinski, A., and C. O. Babcock. Stress Distribution and Rock Fracture Zones in the Roof of Longwall Face in a Coal Mine. Rock Mechanics J., v. 5, No. 1, 1973.
10. Kripakov, N. P. Finite-Element Analysis of Yield Pillar. Comput. and Struct., v. 13, 1981.
11. Kripakov, N. P., and M. T. Melvin. A Computer Procedure To Simulate Progressive Rock Failure Around Coal Mine Entries. Paper in Proceedings, the First Conference on the Use of Computers in the Coal Industry, WV Univ., Morgantown, WV, 1983.
12. Park, D.-W., and N. F. Ash. Stability Analysis of Entries in a Deep Coal Mine Using Finite-Element Method. Mining Science and Technology. Elsevier, v. 3, 1985.
13. Park, D.-W. and V. Gall. Supercomputer Assisted Three-Dimensional Finite-Element Analysis of a Longwall Panel. Paper in Proceedings of the 30th U.S. Symposium on Rock Mechanics, Morgantown, WV, June 1989.
14. Park, D.-W. and S. M. Lee. Application of Three-Dimensional Numerical Modeling for Longwall Mine Design. 121st SME Annual Meeting, Phoenix, AZ, Feb. 1992.
15. Park, D.-W., R. L. Sanford, T. A. Simpson, and H. L. Hartman. Pillar Stability and Subsidence Study at a Deep Longwall Coal Mine. Proceedings, Annual Workshop, Generic Mineral Technology Center, Mine Systems Design and Ground Control, Blacksburg, VA, Nov. 28-29, 1983.
16. Pariseau, W. G., and I. M. Eitani. Comparisons Between Finite-Element Calculations and Field Measurements of Room Closure and Pillar Stress During Retreat Mining. Int. J. Rock Mech., Min. Sci. and Geomech. Abstr., v. 18, 1981.
17. Tolson, J. S. Alabama Coal Data for 1989. Inf. Ser. 58K, Geol. Surv. AL, 1990.
18. Wilson, A. H., and D. P. Ashwin. Research Into the Determination of Pillar Size—Part 1. An Hypothesis Concerning Pillar Stability. Mining Engineer 141, 1971.

EVALUATION OF VARIOUS PILLAR DESIGN METHODS: A CASE STUDY

By S. S. Peng[1] and D. Dutta[2]

INTRODUCTION

Pillar design, or more accurately, the determination of pillar dimension, is frequently used in coal mining operations. Especially in recent years, more emphasis has been placed on the prevention of surface subsidence, and stable pillar design has become a critical factor.

Pillar design follows two distinct approaches in recent years: the conventional (or pillar strength formula) method and the finite element structural analysis method. Obviously, the conventional method is more widely used than the finite element method, because it is much simpler and easier to use for general practicing engineers than the finite element method, which requires more in-depth knowledge about elasticity theory and computers.

The conventional pillar design method involves the determination of a proper pillar dimension by matching pillar strength with pillar loading. Thus it only considers the behavior of pillar alone and assumes the roof and floor are rigid materials that will not deform with pillar. Underground observations and case histories have demonstrated that in many cases entry roof falls, floor heaves, or both while pillar remains intact. When this happens, the entries or sections containing those entries must be rehabilitated or abandoned. The prevailing concept among practicing mining engineers is that roof falls or floor heaves or both are associated with poor pillar design. In other words, a good pillar design not only requires a stable pillar condition but also prevents the roof from falling and the floor from heaving. This concept is valid because a stable pillar may penetrate into the roof and floor and cause roof falls or floor heaves. Therefore, a sound pillar design must consider the interaction between roof, coal, and floor. In order to achieve this, finite element method is one of the best choices.

In this paper, a case study is described to illustrate the necessity to consider the interaction between roof, coal, and floor when selecting a successful pillar size.

CASE DESCRIPTION

Smoot Mine is located in Bolair, Webster County, WV. It extracts the Firecreek Seam, 4 to 6 ft thick and 800 to 1,000 ft deep, by room-and-pillar method. In order to determine a proper pillar size for the mine, a test section 600 ft wide by 1,000 ft long was developed in which three sizes of chain pillar, i.e., 70 by 80 ft, 50 by 50 ft, and 60 by 60 ft, center-to-center, were used. Entry width was held at 18 ft in all cases (fig. 1). The three pillar sizes were selected for convenient operation of the continuous miner's cutting sequence during pillar extraction, i.e., to allow fast cutting and maximum recovery. In this section, the seam was flat and relatively uniform, approximately 6 ft thick and 875 to 912 ft deep. The immediate roof was gray shale and/or sandy shale 13 to 18 ft thick while the floor was soft shale or fire clay up to 5 ft thick. Figure 2 shows the stratigraphic column in the test section, and table 1 shows the mechanical properties of the immediate roof, coal, and floor rocks.

Table 1.—Mechanical properties of immediate roof, coal, and immediate floor in Smoot Mine

Material	Uniaxial compressive strength, psi	Brazilian tensile strength, psi	Young's modulus, 10^6 psi	Poisson's ratio
Sandy shale . .	11,498	809	1.85	0.23
Coal	2,068	NA	.29	.33
Fire clay	5,722	268	1.19	.27

NA Not available.

The areas with chain pillars of 70 by 80 ft and 60 by 60 ft center-to-center remain intact and stable even now—4 years after development (fig. 3). However, the area developed by chain pillars of 50- by 50-ft center-to-center deteriorated rapidly soon after development. It began with sudden buckling of the immediate floor in the entry center and hove up 2 to 3 ft. Then, pillar ribs on both sides of the entry started to spall off 5 to 10 ft thick (fig. 4). Therefore, it was decided that 50- by 50-ft center-to-center chain pillars could not be used. Instead, the 60- by 60-ft center-to-center pillars were selected for use in this mine.

[1]Chairman and C. T. Holland professor.
[2]Graduate student.
Department of Mining Engineering, West Virginia University, Morgantown, WV.

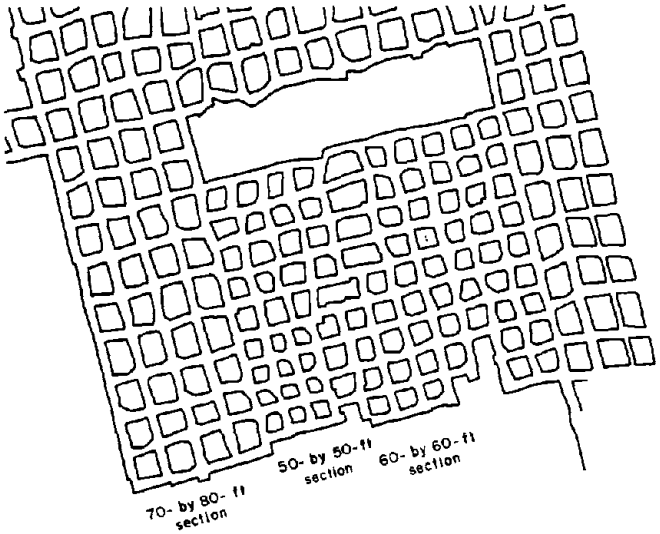

Figure 1.—Section map showing three areas with three different chain pillar sizes.

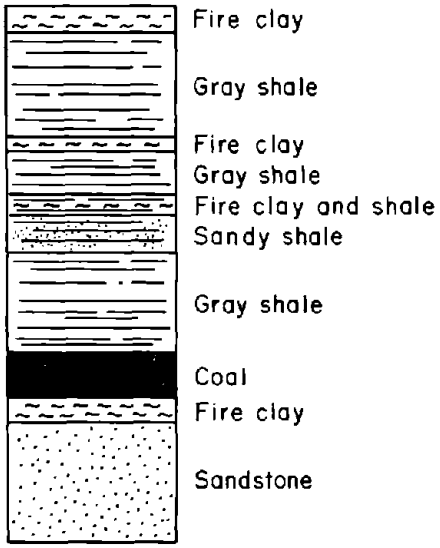

Figure 2.—Near-seam stratigraphic column of test section.

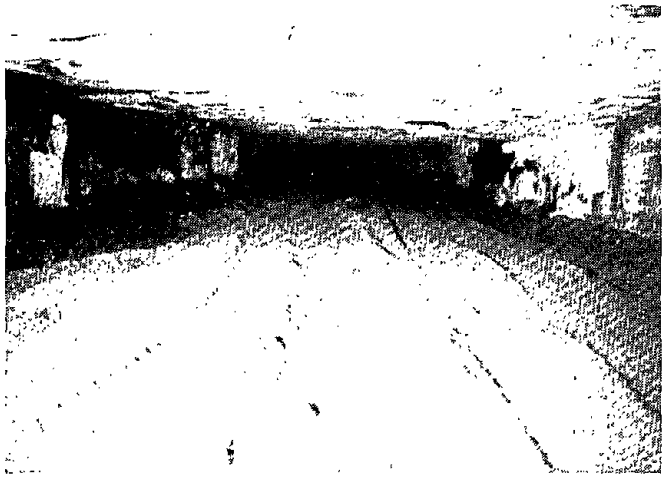

Figure 3.—Stable entry condition long after development in 60- by 60-ft center-to-center chain pillar block area.

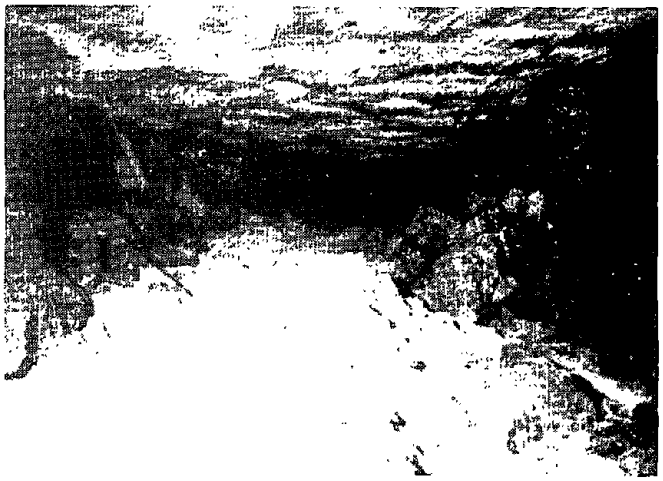

Figure 4.—Severe floor heave at entry center and pillar spalling on both sides in 50- by 50-ft center-to-center chain pillar block area.

CONVENTIONAL METHOD OF PILLAR DESIGN

METHODOLOGY

In conventional pillar design method, the ultimate goal is always to determine the safety factor of the coal pillar selected, and a safety factor of 1.5 to 2.1 has been recommended. The determination of pillar safety factor involves three steps:

1. Calculation of average pillar stress;
2. Calculation of ultimate pillar strength; and
3. Calculation of pillar safety factor defined, as the ratio of ultimate pillar strength to average pillar stress.

Calculation of Average Pillar Stress

Average pillar stress is calculated by using the tributary area loading concept [Obert and Duvall, 1967 (*9*)].[3] In

[3]Italic numbers in parentheses refer to items in the list of references at the end of this paper.

case of room-and-pillar workings, average pillar stress, σ_a (in pounds per square inch), in the center of development headings is

$$\sigma_a = \frac{(W_p + W_o)(L_p + W_o)}{W_p L_p} \sigma_v, \quad (1)$$

where W_p = pillar width, in,

L_p = pillar length, in,

W_o = entry width, in,

σ_v = vertical stress, psi,

= (1.1)(h),

and h = depth of cover, ft.

For a square pillar, L_p is equal to W_p.

Calculation of Ultimate Pillar Strength

The ultimate pillar strength is calculated in two steps. In the first step, uniaxial compressive strength data, obtained from laboratory testing of cubical coal specimens, are scaled down to represent in situ coal strength. (This is the so-called size effect.) So far, there is no consensus as to how this scaling should be done. Different authors have suggested different methodologies [Hustrulid, 1976 (*7*); Peng, 1986 (*10*)].

According to Wilson [1981 (*13*)], a strength reduction of 5 for coal should be done. So, by Wilson's method

$$S_1 = \sigma_c/5, \quad (2)$$

where S_1 = scaled down compressive strength of coal, psi

and σ_c = compressive strength of laboratory specimen, psi.

Gaddy [1961 (*4*)] had suggested a relationship of the form

$$\sigma_c = k_1 d^{-0.5}, \quad (3)$$

where k_1 = a constant

and d = side length of cubical coal specimen, in.

Hustrulid [1976 (*7*)] had suggested a relationship between S_1 and k_1, which is

$$S_1 = k_1/6. \quad (4)$$

Hustrulid's equation given above holds true if the pillar height is more than 3 ft.

In the second step, ultimate pillar strength, S_2 (in pounds per square inch), is calculated by using formulas developed by various researchers. The most commonly used formulas are as follows:

$$S_2 = S_1(0.778 + 0.222\, W_p/H) \text{ [Obert and Duval, 1967 (9)]}, \quad (5)$$

$$S_2 = S_1(0.64 + 0.36\, W_p/H) \text{ [Bieniawski, 1983 (3)]}, \quad (6)$$

$$S_2 = S_1(W_p/H)^{0.5} \text{ [Holland, 1964 (6)]}, \quad (7)$$

$$S_2 = k_1 (W_p)^{0.5}/H \text{ [Holland and Gaddy, 1957 (5)]}, \quad (8)$$

where H = pillar height, in.

Calculation of Safety Factor

Pillar safety factor, F, is calculated as

$$F = S_2/\sigma_a. \quad (9)$$

APPLICATION TO SMOOT MINE

In applying the conventional pillar design method to evaluate the three different sizes and shapes of coal pillars tested in Smoot Mine, the following parameters are used:

Pillar 1 . . . . Rectangular, 62 ft (L_p) by 52 ft (W_p)
Pillar 2 . . . . Square, 42 ft (L_p) by 42 ft (W_p)
Pillar 3 . . . . Square, 32 ft (L_p) by 32 ft (W_p).

Mining height is 6 ft, entry width is 18 ft, and overburden is 894 ft thick.

The average vertical pillar stress, calculated by using the tributary area concept, on the three sizes of pillar are as follows:

Pillar 1 . . . . σ_a = 1,708 psi
Pillar 2 . . . . σ_a = 2,007 psi
Pillar 3 . . . . σ_a = 2,401 psi.

Sampling and Testing of Roof, Coal, and Floor Property

Sampling of rock/coal specimens for the determination of rock/coal properties is a very crucial step, mainly because of rapid variation of coal property within different parts of a pillar. The method of sampling used must be such that it comes from the undisturbed parts of the pillar and that it covers samples from the whole seam height in any sites of sampling.

A custom-made chain saw was used to cut coal specimens in underground coal pillars. A channel, 2 to 3 ft wide, was cut 4 to 6 ft deep into the pillar beyond the zone of loose edges. Then coal blocks of various sizes were cut loose from the solid pillar core and evenly distributed from the top to the bottom of the seam. In the laboratory, 2.5-in-long cubical coal specimens were made with a minimum of four specimens from each foot of coal seam. Thus, a total of 24 cubical coal specimens were prepared and tested in this case.

Three-inch-diameter drill holes were drilled 2 to 4 ft deep and NX cores obtained from the roof and floor, respectively. Again, at least four specimens are prepared and tested for the immediate roof and floor, respectively.

Specimen preparation and property testing followed ASTM standard [ASTM, 1991 (*1-2*)]. Table 1 shows the mechanical properties of coal, roof, and floor determined in the laboratory.

Mean uniaxial compressive strength of coal was determined to be 2,068 psi (see table 1).

Determination of Pillar Safety Factor

Applying Wilson's method of scaling,

$$S_1 = 2068/5 = 413.6 \text{ psi.}$$

Applying Gaddy's and Hustrulid's methods in sequence, then

$$k_1 = (2068)(2.5)^{0.5} = 3{,}270,$$

and

$$S_1 = 3270/6 = 545 \text{ psi.}$$

The ultimate pillar strengths for the three sizes of pillars are, then, calculated by using the four formulas discussed above (tables 2 and 3).

Table 2.—Ultimate pillar strength determined by using Wilson's scaling method, pounds per square inch

Pillar number, (ft)	Obert and Duvall	Bieniawski	Holland	Holland-Gaddy
1 (70 by 80) . .	1,118	1,555	1,218	1,134
2 (60 by 60) . .	965	1,307	1,094	1,019
3 (50 by 50) . .	812	1,059	955	892

Table 3.—Ultimate pillar strength determined by using Gaddy-Hustrulid's scaling method, pounds per square inch

Pillar number, (ft)	Obert and Duvall	Bieniawski	Holland	Holland-Gaddy
1 (70 by 80) . .	1,473	2,049	1,605	1,134
2 (60 by 60) . .	1,271	1,722	1,442	1,019
3 (50 by 50) . .	1,069	1,395	1,259	892

The Holland-Gaddy method of determining ultimate pillar strength does not depend on the scaling technique. Because, in the Holland-Gaddy pillar strength formula, the constant k_1 is directly determined from the uniaxial compressive strength of coal obtained from laboratory testing.

Pillar safety factors for the three sizes of pillars are shown in tables 4 and 5.

Table 4.—Pillar safety factor determined by using Wilson's scaling method

Pillar number, (ft)	Obert and Duvall	Bieniawski	Holland	Holland-Gaddy
1 (70 by 80) . .	0.65	0.91	0.71	0.66
2 (60 by 60) . .	.48	.65	.54	.51
3 (50 by 50) . .	.34	.44	.39	.37

Table 5.—Pillar safety factor determined by using Gaddy-Hustrulid's scaling method

Pillar number, (ft)	Obert and Duvall	Bieniawski	Holland	Holland-Gaddy
1 (70 by 80) . .	0.86	1.20	0.94	0.66
2 (60 by 60) . .	.63	.85	.72	.51
3 (50 by 50) . .	.45	.58	.52	.37

SUMMARY

It is quite obvious that the results in this case study indicate that safety factor of a pillar depends very much not only on the pillar strength formula but also on the strength scaling method.

The pillar design formulas predict unstable pillar behavior for the three sizes of pillar tested assuming that a safety factor of 1.5-2.0 must be used.

FINITE ELEMENT STRUCTURAL ANALYSIS OF PILLAR DESIGN

TWO-DIMENSIONAL FINITE ELEMENT MODEL

The field results clearly indicate that in pillar design it is not sufficient to merely consider the coal strength versus overburden weight. The properties of roof and floor rocks must also be considered.

To simulate the interaction of roof, pillar and floor, two-dimensional finite-element modeling was carried out. Figure 5*A* shows the cross section XX of the test section used for modeling. Figure 5*B* (with exaggerated vertical scale) represents entries and pillars along the XX cross section. In figure 5*B*, entries and pillars are grouped into four sections. In sections A and D, there are four pillars in each section, and the width of each pillar is 52 ft. Section B has three pillars, each with a width of 32 ft. In section C, there are eight pillars, each 42 ft wide. All the entries are 18 ft wide. On each side of sections A and D, solid coal of 200 ft was considered. Fifty feet of roof and 20 feet of floor were also included in the model.

Two-dimensional isoparametric quadrilateral elements were used throughout the model. Plane strain formulation of unit thickness was considered. Nodal points were constrained in Y (vertical) direction at the bottom and in X (horizontal) direction at each side of the model. Uniform load of 928 psi (overburden load) was applied at the top of the model, and the elements were subjected to gravity loading, also. A total of 2,548 elements were formulated in the model. MSC/NASTRAN [1986 (*8*)] program, a large-scale finite-element program to solve a wide variety of engineering problems, was used to carry out the finite-element analysis. Figure 6 shows a section of the finite-element mesh.

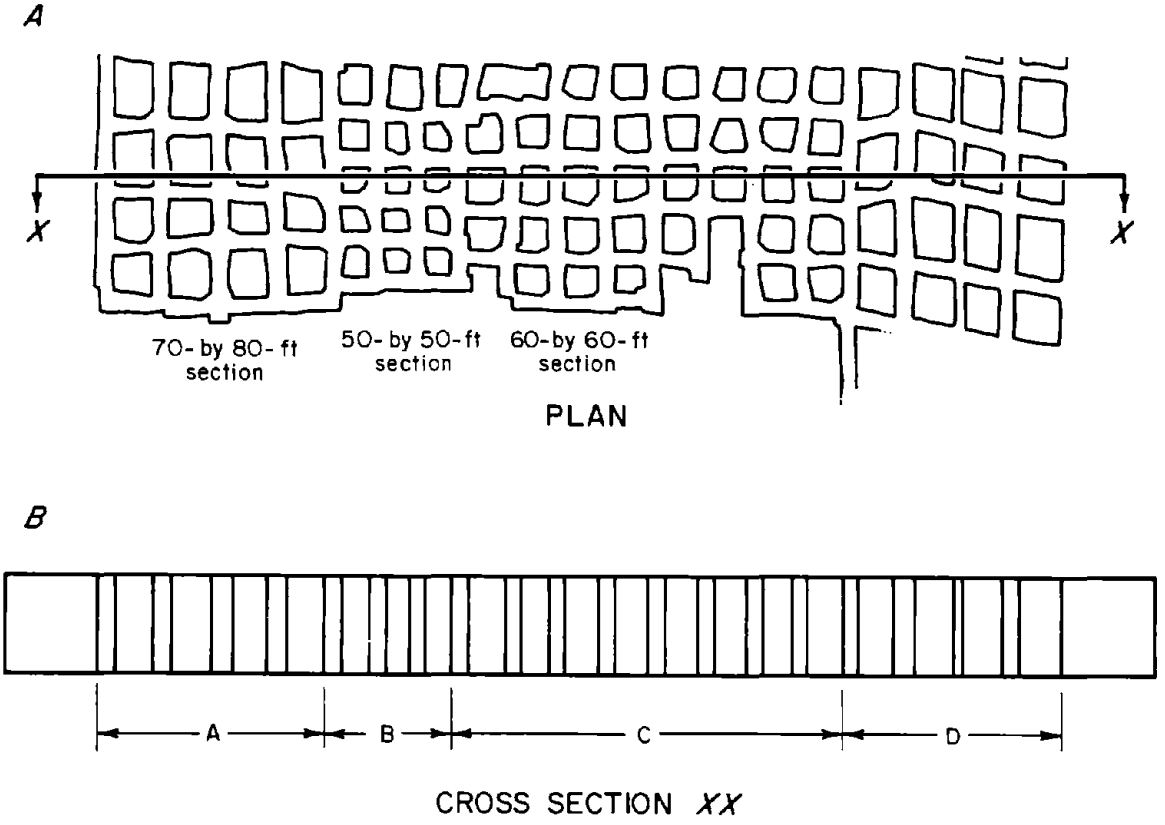

Figure 5.—*A*, Cross section XX of test section used for modeling. *B*, Entries and pillars along XX cross section.

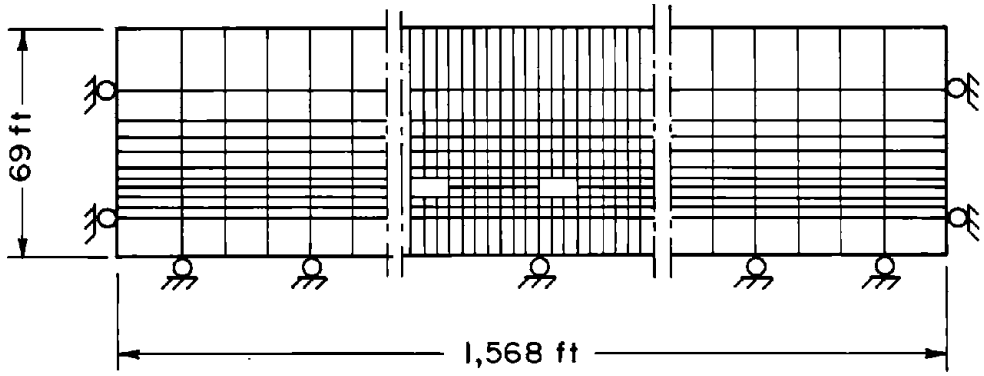

Figure 6.—Section of finite-element mesh.

To evaluate the stability of pillar and floor, the Coulomb failure criterion was applied to the stress output of the MSC/NASTRAN analysis. Factor of safety of each element is defined as

$$F = \frac{\sigma_c + q\sigma_3}{\sigma_1}, \qquad (10)$$

where q = triaxial stress factor,

$$= \frac{1 + \sin\phi}{1 - \sin\phi},$$

ϕ = angle of internal friction, deg,

σ_1 = maximum principal stress in the element, psi,

and σ_3 = minimum principal stress in the element, psi.

SUMMARY

The safety factor of individual pillar was calculated by averaging the safety factor of each element in the pillar. Compressive strength of coal was scaled down to one-fourth from the laboratory-determined value as reported in table 1. Angle of internal friction for coal was taken to be 31°. Figure 7 is the bar chart of individual pillar safety factors in sections A, B, C, and D.

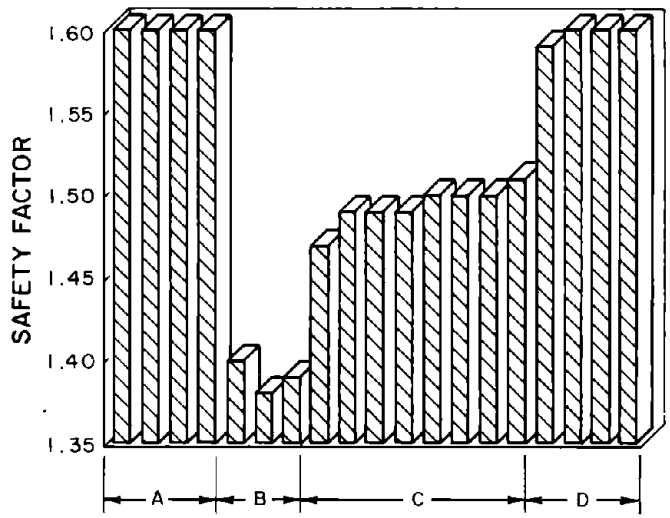

Figure 7.—Pillar safety factors in four sections.

Figure 7 shows that the pillars in sections A and D (with pillar widths 52 ft) have maximum safety factors of 1.6. In section C, where each pillar has a width of 42 ft, maximum pillar safety factor is 1.51. All the pillars in section C have safety factors equal to or greater than 1.47. Pillar safety factors in section B, where the pillars are 32 ft wide, vary between 1.37 and 1.41. Minimum safety factor for the 32-ft-wide pillar is the one surrounded by 32-ft-wide pillars. Figures 8*A*, 8*B*, and 8*C* show typical distribution of safety factors in 52-ft, 42-ft, and 32-ft-wide pillars, respectively. In all the pillars, pillar safety factors are larger in the cores of the pillars than the two edges.

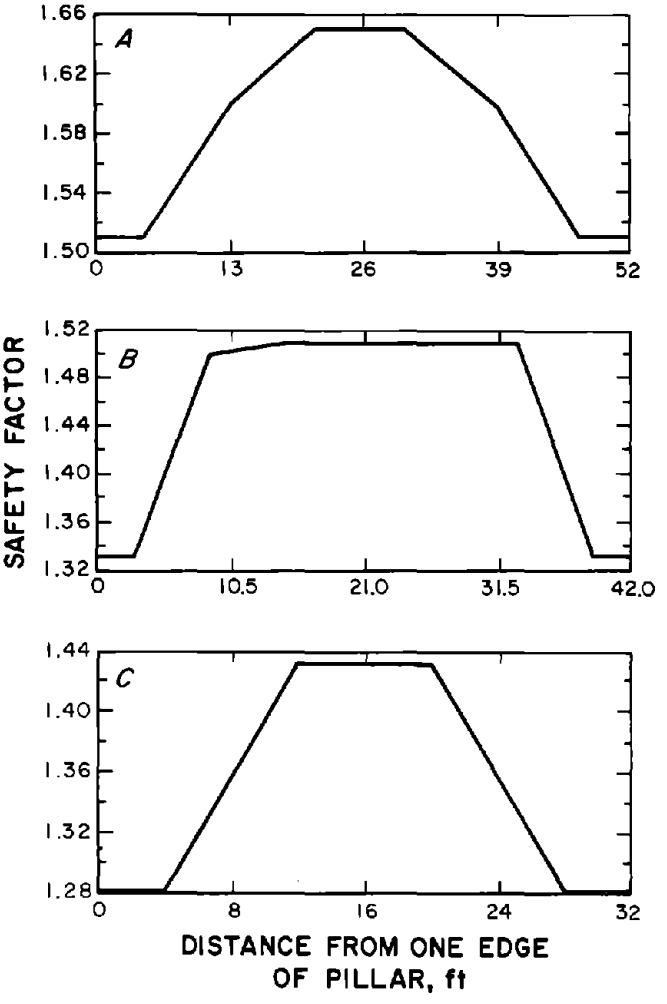

Figure 8.—*A*, Typical distribution of safety factor in 52-ft-wide pillar. *B*, Typical distribution of safety factor in 42-ft-wide pillar. *C*, Typical distribution of safety factor in 32-ft-wide pillar.

At the center of the entry, failure is always tensile in nature rather than shear failure represented by Coulomb failure criterion. So, safety factors are large at the center of entries because of low shear stresses at those regions. Figure 9 is the bar chart of tensile stresses at the center of the entries in sections A, B, C, and D. High-tensile stresses are developed at the center of the entries in section B, where the pillars are 32 ft wide. In sections A, C, and D low-tensile stresses are developed at the center of the entries. Tensile stresses in the center of the entries in sections A, C, and D vary between 62 to 64 psi. In section B, tensile stresses at the center of the entries vary between 81 to 84 psi.

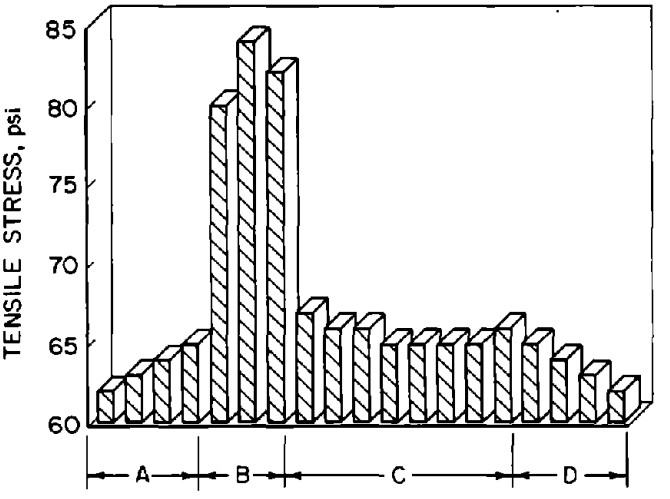

Figure 9.—Tensile stress at center of entries in four sections.

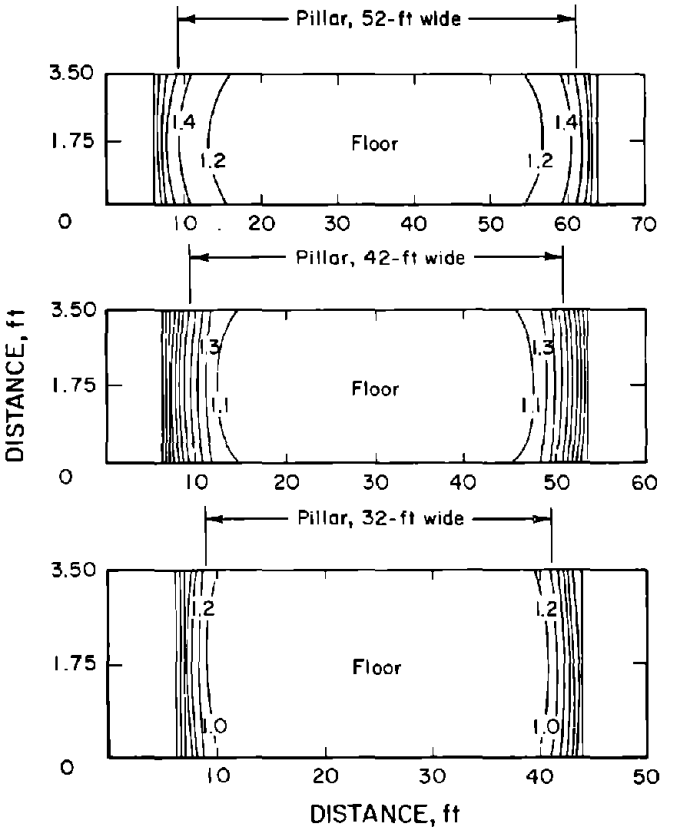

Figure 10.—Contours of floor safety factors beneath three different sizes of pillars.

Figure 10 shows the contours of floor safety factors beneath the pillars of three different sizes. Uniaxial compressive strength of the floor was scaled down to one-fourth from the laboratory determined value reported in table 1. Angle of internal friction for floor rock was taken to be 32°. In figure 10, the three different sizes of pillars are shown in center-to-center distances in feet in the X direction, and in the Y direction a thickness of 3.5 ft of immediate floor is also shown.

From figure 10, it is clear that the floor safety factors beneath the 52-ft and 42-ft-wide pillars are equal to or more than 1.1. On the floor, beneath the core of the pillar, safety factor is the least and it increases towards the edge of the pillars. The safety factor is at least 1.5 near but beneath, and immediate outside, the pillar edges. The floor safety factor beneath the 32-ft-wide pillar is 1. Only at the extreme edges of the 32-ft-wide pillars, 1 ft on each side, floor safety factor increases to 1.2.

From the above results, it is clear that the pillars of all three dimensions are stable. But high-tensile stresses at the center of the entries surrounded by 32-ft-wide pillars can initiate tensile failure at the center of the entries in section B. Once failure initiates at the entry center, the floor beneath the 32-ft-wide pillar can fail in shear resulting in pillar punching into the floor. A combination of tensile failure at the center of the entries in section B and subsequent pillar punching into the floor may cause floor heave, which in turn results in pillar spalling in section B.

CONCLUSION

In pillar design, it is not sufficient to merely consider the coal strength versus overburden weight as suggested by pillar strength formulas. The interaction of roof, coal, and floor must be considered because very often a strong pillar will punch into the floor and cause the floor to heave up and eventually lead to pillar failure. One way to consider the interaction of roof, coal, and pillar is to use finite element structural-modeling technique as demonstrated in this paper by a case study and earlier [Tang and Peng, 1988 (*11*); 1990 (*12*)].

REFERENCES

1. ASTM, D4543-85. Test Method for Elastic Modulus of Intact Rock Core Specimens in Uniaxial Compression. 1991.

2. ASTM, D2938-79. Test method for Unconfined Compressive Strength of Intact Rock Core Specimens. 1991.

3. Bieniawski, Z. T. Improved Design of Room-and-Pillar Coal Mines for U.S. Conditions. Proc. of the 1st Int. Conf. on Stability in Underground Mining. SME-AIME, 1983, pp. 19-51.

4. Gaddy, F. L. A Study of the Ultimate Strength of Coal as Related to the Absolute Size of the Cubical Specimens Tested. Va. Polytech. Inst. Res. Div. Bull., No. 112, 1956, pp. 1-27.

5. Holland, C. T., and F. L. Gaddy. Some Aspects of Permanent Support of Overburden on Coal Beds. Proc. of the West Virginia Coal Mining Institute. 1957, pp. 43-66.

6. Holland, C. T. The Strength of Coal in Mine Pillars. Proc. of the 6th Symp. on Rock Mechanics. Univ. MO, Rolla, MO, 1964, pp. 450-466.

7. Hustrulid, W. A. Review of Coal Strength Formula. Rock Mech., v. 8, 1976, pp. 43-50.

8. MSC/NASTRAN. User's Manual. MacNeal-Schwendler Corp., 1986.

9. Obert, L., and W. I. Duvall. Rock Mechanics and the Design of Structures in Rocks. Wiley, 1967, pp. 236-274.

10. Peng, S. S. Coal Pillars. Ch. 7 in Coal Mine Ground Control. Wiley, 2d ed., 1986, pp. 241-242.

11. Tang, D. H. Y., and S. S. Peng. Structural Analysis of Mine Pillars Using Finite Element Method—A Case Study. Min. Eng., v. 40, No. 9, 1988, pp. 893-897.

12. ____. Mine Pillar Stability Analysis Using FEM Methods—Two Case Studies. Proc. of the 9th Int. Conf. on Ground Control in Mining, ed. by S. S. Peng. WV Univ., Morgantown, WV, 1990, pp. 88-98.

13. Wilson, A. W. Stress and Stability in Coal Ribsides and Pillars. Proc. of the 1st Conf. on Ground Control in Mining, ed. by S. S. Peng. WV Univ., Morgantown, WV, 1981, pp. 1-12.

A PRACTITIONER'S APPROACH TO PILLAR DESIGN

By Vincent A. Scovazzo[1]

INTRODUCTION

Most published pillar design formulas have limitations when practitioners attempt to use them. These drawbacks are attributed to the method of formula development. Most were developed empirically by placing failed, poor performing, and stable pillars on a plot. The axes of this plot are the parameters that the investigator perceives as controlling pillar stability. A line is fitted between failed and stable pillars. This approach, as noted by most developers of these formulas, has pitfalls. Some of these plots included pillars whose poor performance was due to foundation failure. This tends to cause the developed equation to oversize the designed pillars. Equations developed in this manner do not allow the practitioner to separate and understand the floor and pillar instability effects on pillar design. Understanding these effects allows for informed decisions in the design.

When drawing this line for the development of the empirical formula, two options are available: to use a compromising line and place some failed pillars in the stable zone or to use a line that places all failed pillars in the failed zone. From a practitioner's standpoint, this means some equations will, at times, underdesign the pillar while others will overdesign the pillar.

Empirical equations also assume a loading condition that is often not applicable to the conditions at the mine being considered. Finally, these equations are often site specific, not allowing for change in coal strength, floor, or roof stability or in mine observations of pillar behavior.

This paper will suggest another approach to pillar design by developing an equation that will be mine specific. Developing such an equation will require laboratory rock testing and, if possible, in-mine observations. The paper presents two examples for developing a pillar equation, one based on the hyperbola and the other on the ellipse. These equations also may be applied toward other sites that match the assumptions used in their development.

MINE CONDITIONS

In many mines, especially coal mines, the floor's bearing strength is the limiting factor in determining pillar size. In these mines, the pillar's foundation should be analyzed so the anticipated behavior can be included in the pillar design. The roof also should be analyzed to understand roof behavior, which may be used as input into the pillar design. Briefly stated, pillar design is not isolated from the design of the pillar foundation and roof support.

When a pillar is made stronger or stiffer, more load is drawn to that pillar and away from the surrounding pillars. This changes loading criterion on the floor and the stability of the roof. Thus, pillar and opening design is a related and interactive process.

PILLAR MATERIAL STRENGTH PARAMETERS

If the pillar foundation and roof support design have progressed to a point that the pillar design can begin, the first requirement is to establish in-place rock mass strength parameter values. There are only three valid inputs into this development: in situ and laboratory testing and field observations. Since in situ testing is often too time consuming and expensive, it is important to test the pillar material in the laboratory. The intact specimens tested will give an upper bound to the possible strength of the rock mass.

Strength testing should include uniaxial and triaxial compressive and direct shear. Direct shear and triaxial tests are used to develop similar strength parameter values, but in testing the rock in two ways, an understanding of these two failures and rock anisotropy is gained. Also, this allows testing of the pillar material in

[1]Senior engineer, John T. Boyd Co., Pittsburgh, PA.

the anticipated failure modes. For example, if using Wilson's [1972 (*4*)[2]] equation, the preferred testing methods for determining input values are direct shear for shear strength and triaxial compressive for confined compressive strength. The actual number and type of tests are based on in-mine (if possible) behavior of the pillar. Obviously, if pillar failure in a mine involves sliding along a bedding plane, this bed should be tested. Laboratory test reports should discuss how the specimen failed; this will aid in defining intact strengths.

Residual laboratory tests also should be undertaken to establish a possible lower bound for the mass behavior. If the pillar material is not coal, the intact and residual behaviors are plotted against published estimators of the rock mass internal angle of friction and cohesion. These are plotted on a shear strength versus normal stress plot (fig. 1).

Two excellent estimators for noncoal rock mass strength used by this practitioner are Rock Mass Rating system and Hoek and Brown system, both of which are presented in detail by Bieniawski [1989 (*1*)]. This practitioner has experienced little success using these systems for coal. After all this information is plotted, an estimate of the rock mass is made or the failure modes established and the rock mass strength calculated.

Coal and other pillar materials as a rock mass may behave in such a manner that a curve can be fitted to the data. Figure 2 assumes a hyperbola can be fitted to both a compressive strength versus confinement stress and shear strength versus normal stress plots. Here one of the foci of the hyperbola is at the origin of the plot that allows for easy development of the material strength equations.

On occasions, the shear strength plot approaches an ellipse. Figure 3 shows such a plot with the one focus of an ellipse at the origin. The plot for normal stresses greater than x_o is ignored.

On those occasions when the in-place pillar material strength can be estimated by a hyperbola, the formula for the shear strength would be

$$\tau = \{[((\sigma_n+e)/a)^2-1]b^2\}^{0.5} \qquad (1)$$

where τ = shear strength of failure plane,

σ_n = normal stress to failure plane,

$e = (a^2 + b^2)^{0.5}$,

and a and b are constants defining shape of shear strength curve.

[2]Italic numbers in parentheses refer to items in the list of references at the end of this paper.

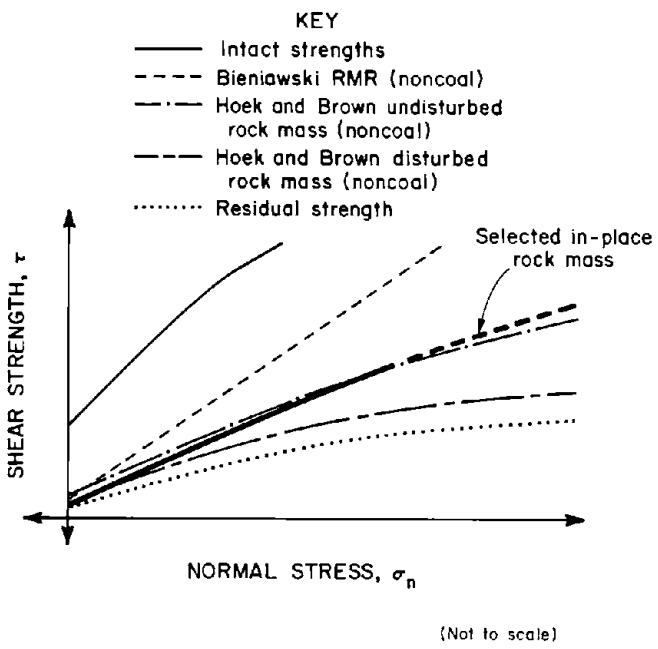

Figure 1.—Schematic showing the possible relationship between failure envelopes for a pillar material.

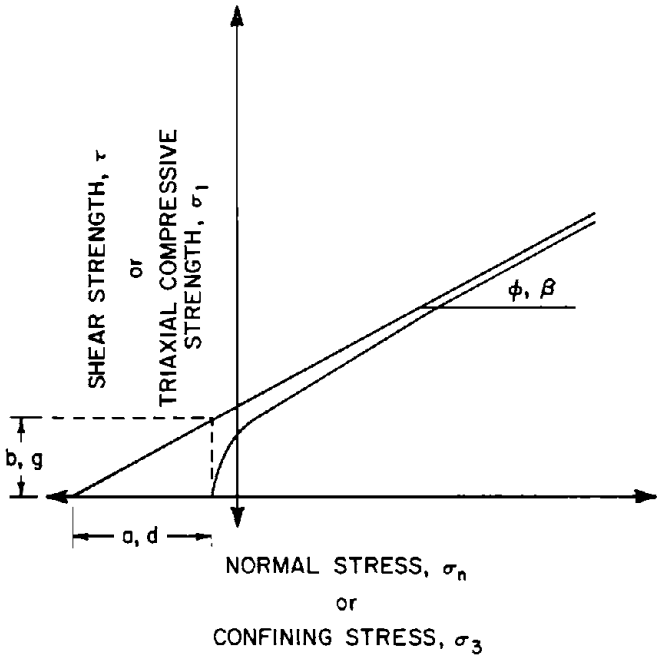

Figure 2.—Failure envelopes using the hyperbola equation.

If the in-place compressive material strength can also be fitted to a hyperbola, then

$$\sigma_1 = \{[((\sigma_3+f)/d)^2-1]g^2\}^{0.5} \qquad (2)$$

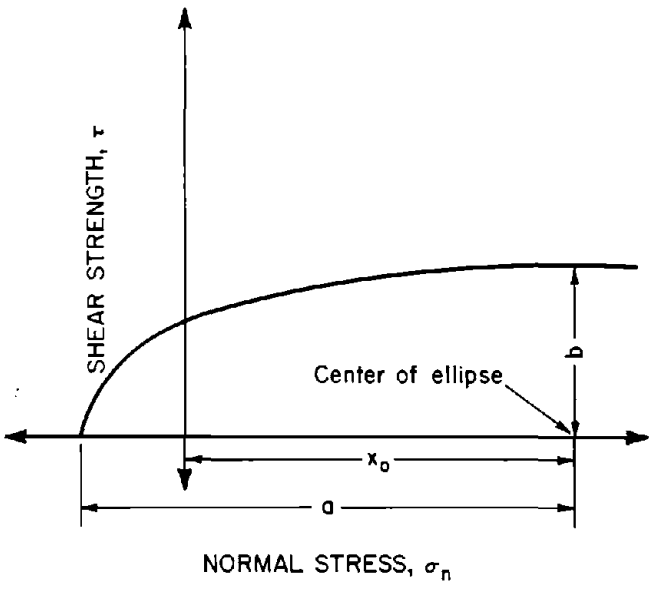

Figure 3.—Failure envelope using the ellipse equation.

$$\sigma_3 = \{[(d\sigma_1)/g]^2+d^2\}-f \quad (3)$$

where σ_1 = triaxial compressive strength,

σ_3 = confining pressure,

$f = (d^2+g^2)^{0.5}$,

and d and g are constants defining shape of compressive strength curve.

When the shear strength and compressive strengths are derived from the same data or the pillar is assumed to be homogeneous (a rare case), the following relationships from mechanics can be used:

$$\tan\beta = (1+\sin\phi)/(1-\sin\phi) \quad (4)$$

where ϕ = angle of internal friction.

If, $$S = 2C(\tan\beta)^{0.5} \quad (5)$$

where S = uniaxial compressive strength

and C = cohesion,

then $$f = 2e\tan\phi(\tan\beta)^{-0.5} \quad (6)$$

where in this equation, ϕ and β are as shown in figure 2.

Shear strength can be expressed as an ellipse. An ellipse may be needed if it can be shown that little strength is gained in the core of a pillar as the pillar width increases. This practitioner has not found an application for this presentation, but the ellipse does represent a lower bound of possible pillar material behavior. The shear strength will then be represented by (fig. 3):

$$\tau = \{[1-((\sigma_n-x_o)/a)^2]b^2\}^{0.5} \quad (7)$$

where x_o, a, and b are constants defining shape of shear strength curve and are defined in figure 3.

When compressive and shear strengths are derived from the same data or the pillar material is considered homogeneous, the compressive strength is best defined as a hyperbola with β equal to 45°. Using this assumption, equations 2 and 3 can be modified using equations 8 and 9,

$$f = 2^{0.5}d \quad (8)$$

$$d = g \quad (9)$$

Of course, other possible, more appropriate equations can also be used.

SITE-SPECIFIC PILLAR EQUATION

Noting Wilson's 1972 presentation and subsequent more developed presentations, this practitioner does not believe the significant portion of these analyses is the final formula, but rather the method of arriving at the formula. This methodology has allowed this practitioner to consider in the design, field observations, pillar behavior, and any strength equation developed. For example, if the floor is softer than the coal or the coal shear strength is not linear with respect to normal stress, these parameters are included as boundary conditions for the pillar design.

To demonstrate this approach, let's assume a stable roof and floor in a mine where it is observed that failure occurs in the coal. These are identical with Wilson's original assumptions, but in this case, it will be assumed the in-place rock mass strength can be fitted to a hyperbola. Using Wilson's 1972 approach and keeping with his presentation (fig. 4) and notation, it can be seen that

$$\sigma_H mp+2\tau p\delta y = (\sigma_H + \delta\sigma_H)mp \quad (10)$$

where parameters are defined in figure 4.

This is a point in the development of a site-specific pillar formula that allows for input of field observations and the various strength formulas. For instance, if there is an observed shear failure along the floor pillar contact, there would be two shear terms in equation 10: one for coal and one for coal-floor contact.

In this case, equation 10 reduces as per Wilson to:

$$2\tau\delta y = m\delta\sigma_H \quad (11)$$

noting $$\sigma_n = \sigma_1 = \sigma_v \quad (12)$$

and $$\sigma_3 = \sigma_H. \quad (13)$$

From equation 3:

$$\delta\sigma_H = (d/g)^2[(d/g)^2+(d/\sigma_v)^2]^{-0.5}\delta\sigma_v \quad (14)$$

and then combining equations 1, 11, 12, 13, and 14,

$$\delta y/\delta\sigma_v = 0.5m(d/g)^2[(d/g)^2 + (d/\sigma_v)^2]^{-0.5}\{[((\sigma_v+e)/a)^2-1]b^2\}^{-0.5} \quad (15)$$

This equation must be integrated between zero and σ_v max. Here again, the designer may wish to input field observations or in situ stress measurements in deciding the actual limits that will be used for the design. This practitioner cannot integrate equations of this type, so the Simpson's rule is used. This rule can be found in any introductory calculus book and can easily be placed on a spreadsheet.

For an in-place rock mass shear strength expressed as an ellipse, this equation would be:

$$\delta y/\delta\sigma_v = 0.5m\{[1-((\sigma_v-x_o)/a)^2]b^2\}^{-0.5}[1+(d/\sigma_v)^2]^{-0.5} \quad (16)$$

Equations 15 and 16, when integrated and solved, provide a distance Y. This Y is the distance from the rib of the pillar to the maximum vertical stress carried by the pillar.

To obtain the strength of a pillar, equation 2 and figure 2 are modified. These modifications are based on the Y distance and the maximum horizontal and maximum vertical stresses in the pillar occurring at the same point. The maximum horizontal stress at the Y distance into the pillar is calculated using equation 3. This is accomplished by inputting the same maximum vertical stress used in equations 15 or 16 as σ_v max. Thus, the distance into the rib for any horizontal stress can be calculated using:

$$y = Y\sigma_H/\sigma_H max = K\sigma_H \quad (17)$$

where y = distance into rib to σ_H,

$\sigma_H$max = maximum horizontal stress in pillar,

and σ_H = horizontal stress in pillar at y distance from the rib.

Using K from equation 17, equation 2 can now be adjusted to:

$$\sigma_v = \{[((y+Kf)/Kd)^2-1]g^2\}^{0.5} \quad (18)$$

Equation 18 is shown graphically in figure 5. The total load, T, that the pillar can carry from rib to Y distance into the rib is:

$$T = \int_0^Y \{[((y+Kf)/Kd)^2-1]g^2\}^{0.5}. \quad (19)$$

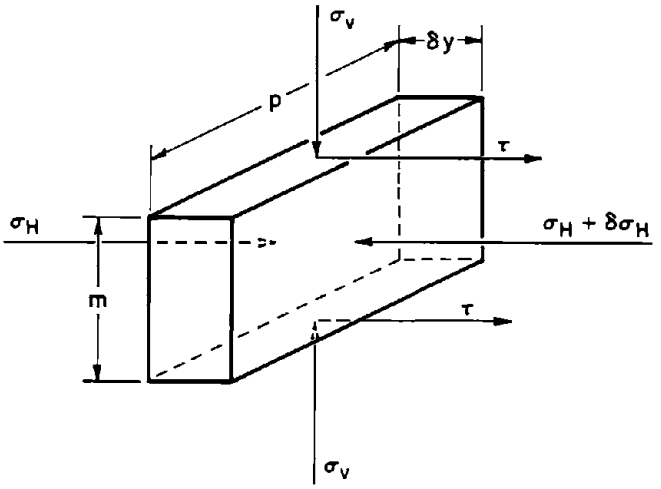

Figure 4.—Free body diagram of pillar slice, after Wilson and Ashwin, 1972.

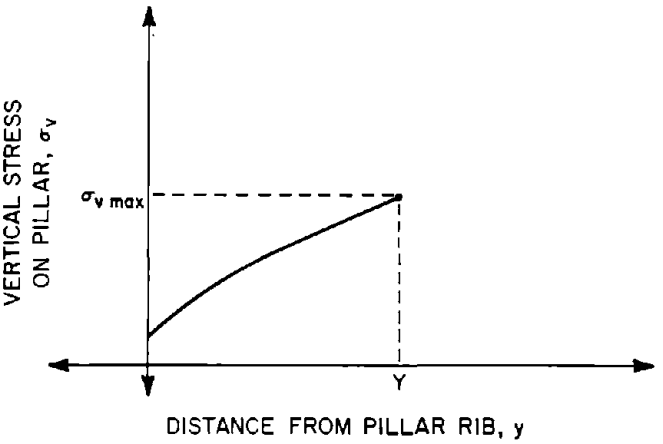

Figure 5.—Relationship between vertical stress on pillar and distance into pillar rib based on compressive strength plot, figure 2.

At this point, the developed pillar equation can be compared with observed conditions. If the conditions are not predicted by the developed pillar equation, the strength equation or the equation's limits or restraints can be adjusted. This adjustment must be made before design begins.

COMPARISON WITH OTHER EQUATIONS

Figure 6 presents a comparison of four pillar equations. These equations are 15 and 16, Wilson's [1972, (*4*)] and Bieniawski's [1984, (*2*)]. Bieniawski's equation is

$$\sigma_p = \sigma_c(0.64+0.36w/h) \qquad (20)$$

where σ_p = pillar strength,

σ_c = in-place rock mass compressive strength,

w = least width of pillar,

and h = pillar height.

The input parameters for these four equations are presented as follows:

INPUT PARAMETERS FOR PILLAR EQUATIONS

For Equation 15	For Equation 16
a = 300 psi	x_o = $1x10^8$ psi
b = 173 psi	a = ($1x10^8$+46) psi
d = 115 psi	b = 69,300 psi
g = 346 psi	d = 346 psi

For Bieniawski's Equation	For Wilson's Equation
Compressive Strength = 693 psi	ϕ = 30° Compressive Strength = 693 psi

This input gives similar low confinement strengths for the pillar material, except equation 16, allowing for comparison of equations for wide pillars. For equation 16, which represents the ellipse, the selected parameters result in higher low confinement strengths than the other equations.

In figure 6, Wilson's equation shows a rapid increase in strength as the width of a pillar is increased. This is due to the linearly elastic nature of the pillar material assumed by Wilson in the development of his equation. This assumption results in this equation acting as an upper limit to pillar strength and often overestimates pillar strength especially for wider pillars. Mark [1990 (*3*)], using field data, shows this conclusion may be true.

Equation 16 is derived from an ellipse, which assumes a pillar material to be ductile. Thus, this equation likely underestimates pillar strength. To date, no coal examined by this practitioner, at expected pillar confinements, has displayed this characteristic. Equation 16 is presented as a lower bound for pillar strength.

Equation 15, which employs the hyperbola, lies between Wilson's equation and equation 16. Equation 15 assumes as elastic-plastic to plastic-ductile material behavior depending on the equation's inputs. Although figure 6 shows this equation predicts pillar strength to be greater than those predicted by Bieniawski, parameters can be chosen that will closely match both equations.

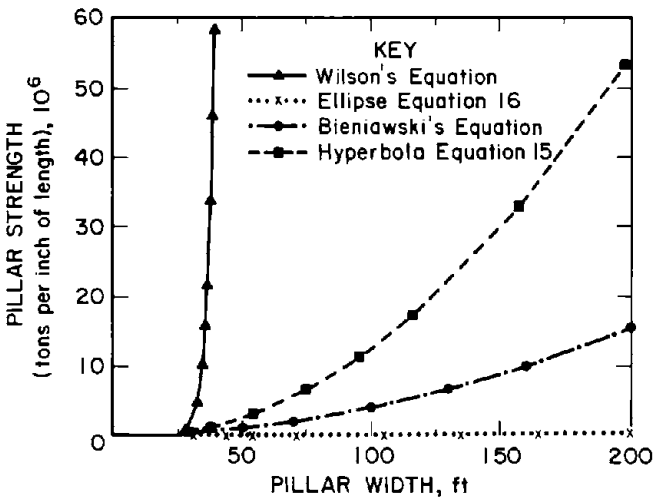

Figure 6.—Comparison of pillar formulas for a long pillar.

CONCLUSIONS

The pillar equations developed in this paper are not for use in all mines. This limitation is due to the structural setting and strength behavior of the pillar assumed during equation development. This paper encourages the development of site-specific equations using similar approaches as presented here.

REFERENCES

1. Bieniawski, Z. T. Engineering Rock Mass Classifications. Wiley, 1989, 251 pp.

2. _____. Rock Mechanics Design In Mining And Tunneling. A. A. Balkema, 1984, 272 pp.

3. Mark, C. Pillar Design Methods for Longwall Mining. BuMines IC 9247, 1990, 53 pp.

4. Wilson, A. H., and D. P. Ashwin. Research Into the Determination of Pillar Size, Part 1, An Hypothesis Concerning Pillar Stability, Min. Eng., No. 141, June 1972, pp. 409-427.

PILLAR DESIGN IN SOUTH AFRICAN COLLIERIES

By H. Wagner[1]

BACKGROUND

Bord-and-pillar mining, which is the South African term for room-and-pillar mining, is the dominant method of coal mining in the Republic of South Africa and accounts for nearly 50 pct of the annual production of 180 million metric tons of coal (fig. 1). With regard to underground mining, bord-and-pillar mining accounts for more than 75 pct of production. Most of the coal produced in bord-and-pillar workings comes from what is locally known as conventional mechanized sections, i.e., sections employing coal cutters, loaders, shuttle cars, and sometimes roof bolters. The uncleated nature of the coal seams and the high compressive strength of the coal have hindered the large-scale introduction of continuous miners. Boom-type road headers are competing successfully with continuous miners under the difficult cutting conditions. Hand-loading, which was the almost exclusive method of coal mining until the 1960's, has virtually disappeared from South African collieries.

The moderately thick horizontal coal seams and favorable strata conditions, together with the relatively shallow depth of most seams, are close to ideal conditions for bord-and-pillar mining (fig. 2). Vertical dolerite intrusions ranging in thickness from a few centimeters to several meters and massive horizontal dolerite sills that are present in the overburden strata of many of the coal seams are the only significant geological disturbances. The massive dolerite sills are a unique feature and have had a major influence on underground coal mining in the Republic of South Africa.

The design of bord-and-pillar workings in South African collieries was influenced by one single event—the sudden collapse of an area of 2.5 km^2 of bord-and-pillar workings, with considerable violence, at Coalbrook Colliery in the Orange Free State coalfield in January 1960, resulting in the loss of 437 lives (*3*).[2] Prior to this mining disaster, rock mechanics considerations played a minor role in the design of bord-and-pillar workings. The design was based on practical experiences and good judgment by the mine operators. Apart from a few isolated pillar collapses, the experience-based approach to pillar design appeared to work very well, with no indication of the possibility of a pillar collapse of the magnitude and nature observed at Coalbrook Colliery.

As a direct consequence of the Coalbrook disaster, the Coal Mining Research Controlling Council (CMRCC) was established in 1961. Under the auspices of this council, the Coal Mining Laboratory of the Research Organization of the Chamber of Mines, headed by M. D. G. Salamon, and the National Mechanical Engineering Research Institute (NMERI) of the Council for Scientific and Industrial Research (CSIR), led by H. G. Denkhaus, were the principal agencies in the search for improved pillar design methods.

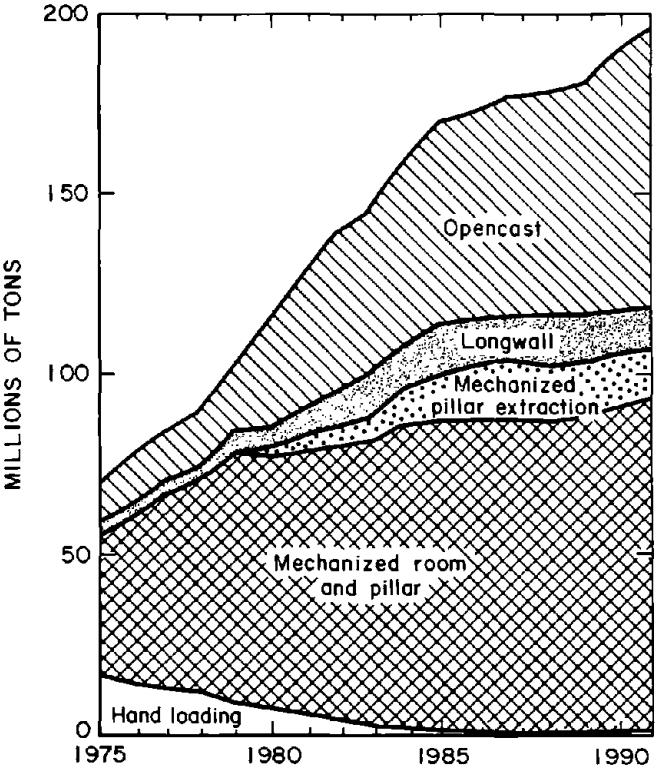

Figure 1.—South African coal production according to mining method.

[1]Senior general manager, Operations, Chamber of Mines of South Africa, Johannesburg, Republic of South Africa.

[2]Italic numbers in parentheses refer to items in the list of references at the end of this paper.

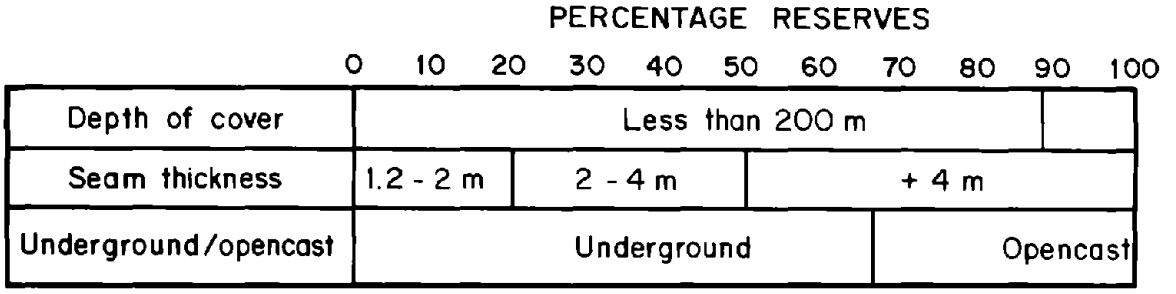

Figure 2.—Distribution of South African coal reserves in terms of depth of cover, seam thickness, and opencast potential.

The two research teams followed radically different approaches. The team led by Salamon followed an empirical design approach, while the NMERI, with its strong experimental orientation, embarked on a program of large-scale in situ pillar testing to determine the strength and deformation properties of coal pillars. As a result of these activities, the understanding of the behavior of coal pillars and the design of bord-and-pillar workings are at a very advanced stage, making the South African coal mining industry a recognized leader in this important field.

The purpose of this paper is to review the design of bord-and-pillar workings and pillar extraction operations in South African collieries from a practical point of view and to provide design guidelines, where appropriate. This will be done under the following main headings:

- Design of permanent bord-and-pillar workings.
- Design of pillar extraction workings.
- Special considerations.

DESIGN OF PERMANENT BORD-AND-PILLAR WORKINGS

STRENGTH OF COAL PILLARS

The design of permanent bord-and-pillar workings in South African collieries is based on the pioneering work by Salamon, who realized in the early 1960's that the industry had a long history of employing the bord-and-pillar system. The industry also had reasonably good records of the incidence of pillar failures and the circumstances surrounding them. For these and several other reasons, Salamon decided to base the development of the pillar design procedure on actual field data involving case histories. A collection of data was initiated with a view to obtaining information relevant to as many case histories as possible. An important feature of the survey was that it was designed to cover both failed and unfailed areas of pillar workings.

The analysis of the pillar design procedure was based on the concept of a safety factor, S, which is defined as:

$$S = \frac{\text{Pillar Strength}}{\text{Pillar Load}}, \qquad (1)$$

where the strength is taken to mean the strength of the pillar and the load as the average pressure acting on the pillar. If the actual strength and load values are substituted into equation 1, it is found that $S<1$ or $S>1$, then these values of S can be taken to indicate that the pillar will fail or remain intact, respectively.

Since in pillar design the load acting on the pillar and the strength are actually not known at the design stage but are predicted in some manner, it will be found that the safety factors calculated for cases where actual failure has taken place will scatter around unity, if the predictions are unbiased. The extent of scatter is a measure of the accuracy of the predictions.

If a large number of pillars are formed according to a particular method of design and tested to destruction, then the observed variation in the critical safety factor can be described by a frequency distribution that gives the relative frequency of occurrence of pillars with critical safety factors in the interval (S, S + ds). Figures 3*A* and 3*B* show the relative frequency, f(s), and cumulative frequency, F(s), distributions of critical safety factors for three imaginary sets of tests. Clearly, curves A, B, and C reflect less and less reliable methods of design (*15*).

Employing these probabilistic concepts of design, Salamon and Munro (*15*) analyzed 27 collapsed and 98 stable bord-and-pillar geometries from collieries of the Transvaal and Orange Free State. The only cases included in the analysis were where bord collapses could be excluded as the cause of failure and where the width of the collapsed area was large compared to the depth of workings. The latter criterion ensured that the tributary area concept could be applied to obtain a realistic estimate of pillar load, p.

$$p = \frac{\rho \cdot g \cdot H \cdot A}{A_p} \qquad (2)$$

where ρ = the density of the overburden, $Kg \cdot m^{-3}$

g = the gravitational acceleration, 9.8 $m \cdot s^{-2}$

H = the depth of mining, m

A = the area supported by the pillar, m^2

and A_p = the area of the pillar, m^2.

The effect of the properties of the coal seam, the size of the pillar, and its shape on the pillar strength were taken into account by Salamon and Munro (*15*) through the following formulation of the pillar strength:

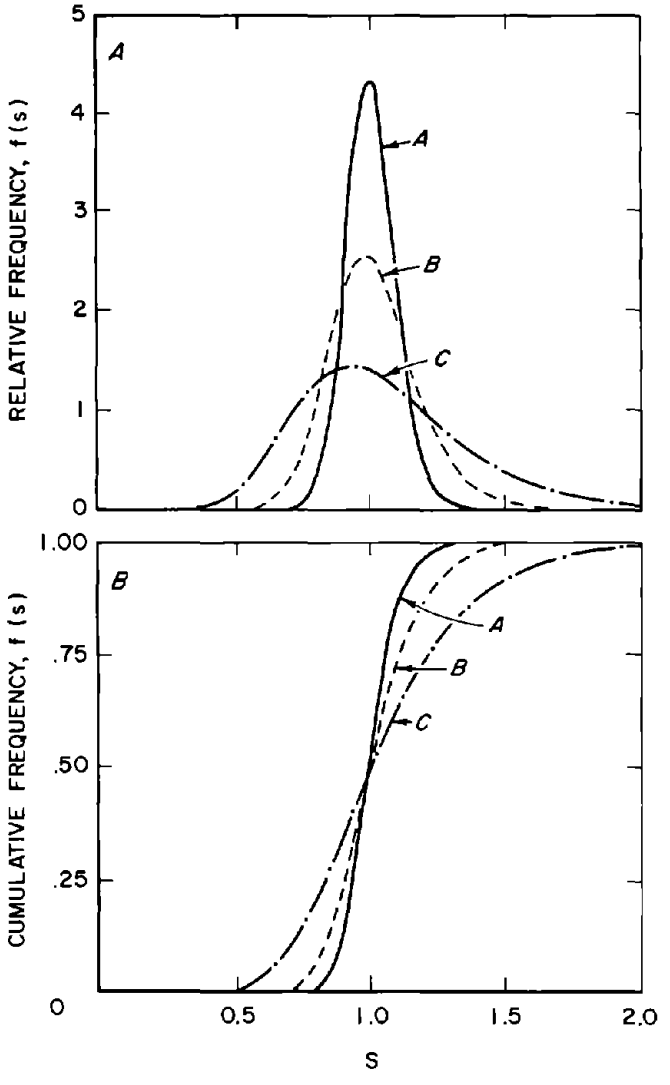

Figure 3.—Examples of relative frequency, f (s), and cumulative frequency, F (S), distribution of critical safety factors. From Salamon and Munro (1967).

$$\text{Strength} = C \cdot h^{\alpha} \cdot w^{\beta}, \qquad (3)$$

where C is the compressive strength of a cube of unit length of pillar material; h and w are the height and width of the pillar, respectively; and α and β are appropriately chosen constants.

Employing the method of maximum likelihood and expressing the pillar dimensions in meters, the following values for the parameters C, α and β were obtained by Salamon and Munro (*15*):

$$C = 7176 \text{ (kPa)}, \quad \alpha = -0.66, \quad \beta = 0.46.$$

Substituting these values into equation 3 yields the well-known pillar strength formula:

$$P = 7200 \cdot \frac{w^{0.46}}{h^{0.66}}. \qquad (4)$$

In a recent reassessment of coal pillar design, Madden (*9*) analyzed the 98 stable cases and 27 failed cases used by Salamon and Munro together with 17 pillar collapses that occurred between 1966 and 1988. Using the same statistical techniques, Madden found the following values for the parameters C, α, and β:

$$C = 5240, \quad \alpha = -0.78, \quad \beta = 0.63.$$

Table 1 gives a comparison of the cases analyzed by Salamon and Munro in 1967 and the additional 17 collapsed cases used by Madden (*9*). The comparison shows that the differences in the range of parameters for the original 27 collapsed cases and the newly added 17 collapses are minor. Not shown in this table, but of importance, is that a larger proportion of recent pillar collapses occurred in the Orange Free State and South Rand coalfields, which are known for a greater prevalence of cleats in the seams.

Table 1.—Comparison of case studies used by Salamon and Munro (1967) and Madden (1991)

Group	Unfailed	Collapsed 1904-65	Collapsed 1966-88
No. of cases in the group	98	27	17
Depth (H), m.	20-220	21-192	22-205
Height (h), m.	1.20-5.0	1.50-5.5	1.35-5.94
Pillar width (w) m.	2.70-21	3.40-16.0	3.50-17.0
Extraction ratio, e.	0.37-0.89	0.45-0.91	0.44-0.88
Width-to-height ratio (w/h).	1.20-8.8	0.90-3.6	1.30-3.7

Figure 4 shows a comparison of the original pillar strength formula published by Salamon and Munro in 1967 and the revised formula by Madden (*9*). In discussing his findings, Madden concluded that in the range of practical interest, i.e., width-to-height ratios of 2 to 6, the differences are sufficiently small to be of no concern.

A critical examination of table 1 shows that the maximum width-to-height ratio at which pillar collapse occurred was less than 4. However, the original pillar strength formula by Salamon and Munro has been applied well outside the range for which it was established. This practice did not result in unsafe situations, but in poor resource utilization since the original formula underestimates the strength of squat coal pillars. It was Salamon (*12*) who recognized this shortcoming and who proposed an extension to the original formula to account for the increase in strength of pillars with large width-to-height ratios.

The original pillar strength formula (equation 4), which is valid for square coal pillars, can be expressed in the following form:

$$P = 7200\,\frac{R^{0.5933}}{V^{0.0667}}, \qquad (5)$$

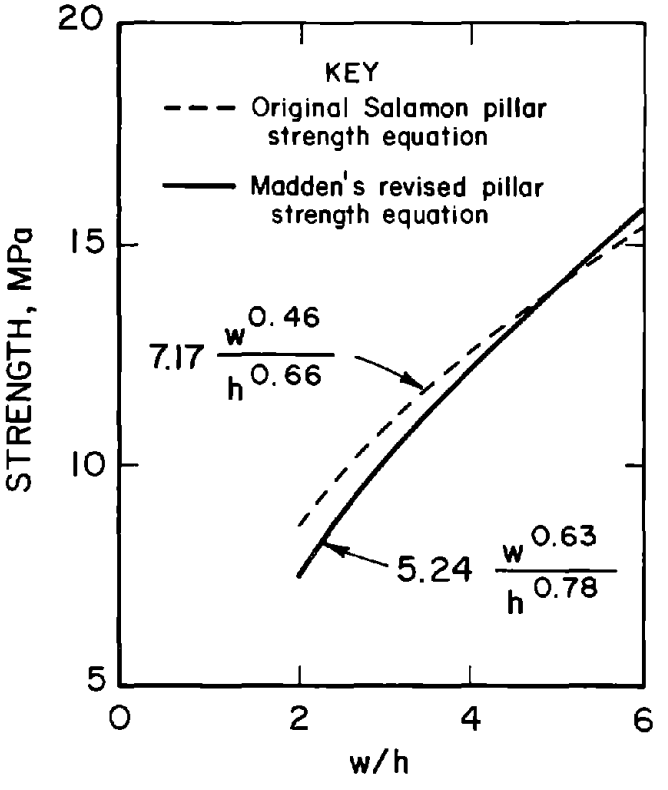

Figure 4.—Comparison of Salamon and Munro pillar strength formula with pillar strength formula by Madden.

where R is the width-to-height ratio and V is the pillar volume, i.e.,

$$R = \frac{w}{h}, \qquad V = w^2 \cdot h.$$

Equation 5 is valid as long as the ratio R is smaller or equal to a critical ratio R_o. On the basis of practical experience, model tests, and theoretical considerations, Salamon (*12*) suggested that when the width-to-height ratio of a pillar is greater than R_o, the strength can be expressed more accurately by the following formula:

$$P_{squat} = 7200\,\frac{R_o^{0.5933}}{V^{0.0667}}\left\{\frac{0,5933}{\epsilon}\left[\left(\frac{R}{R_o}\right)^{\epsilon} - 1\right] + 1\right\}. \qquad (6)$$

This formula has the properties that at $R = R_o$,

$$P = P_{squat}; \quad \frac{\partial P}{\partial R} = \frac{\partial P_{squat}}{\partial R}.$$

According to equation 6, the critical width-to-height ratio, R_o, at which the pillar strength changes and the rate of strength increase, which is given by the parameter ϵ, have to be known to determine the strength of squat coal pillars.

Laboratory tests (*8*) and field trials on three relatively deep South African collieries have shown that a value of 5 was a conservative estimate for R_o. More difficult was the estimation of a realistic value for the parameter ϵ. Model tests on sandstone specimens with width-to-height ratios ranging from R = 1 to R = 8 suggested that a value of 2.5 was a conservative estimate for the parameter ϵ (*8*).

Figure 5 shows that at large width-to-height ratios the differences between the strength predictions based on the original pillar strength formula and the so-called squat pillar formula are significant. As in the case of the original pillar strength formula, care must be taken to apply the squat pillar formula outside the range for which it has been tested. Table 2 gives an indication of the conditions under which the field trials to verify the design of squat pillars have been conducted (*10*).

Table 2.— Summary of field experiments to verify squat pillar design procedure (from Madden and Wagner, 1991)

Colliery	Depth below surface, m	Pillar height, m	Pillar width	R	Percent extraction
Piet Retief ..	550	2.0	28.0	14.0	32.1
Hlobane	180	.8	14.0	17.5	51.0
Longridge ..	252	2.5	32.0	12.8	29.1

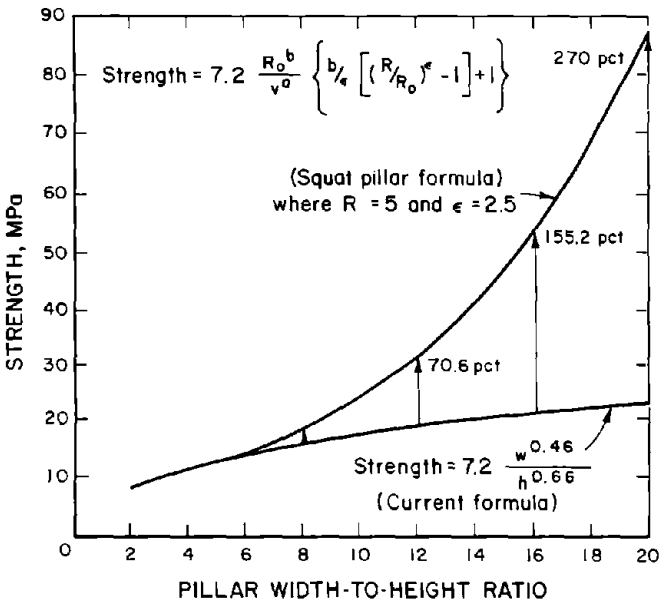

Figure 5.—Comparison of pillar strength formulas for normal and squat coal pillars.

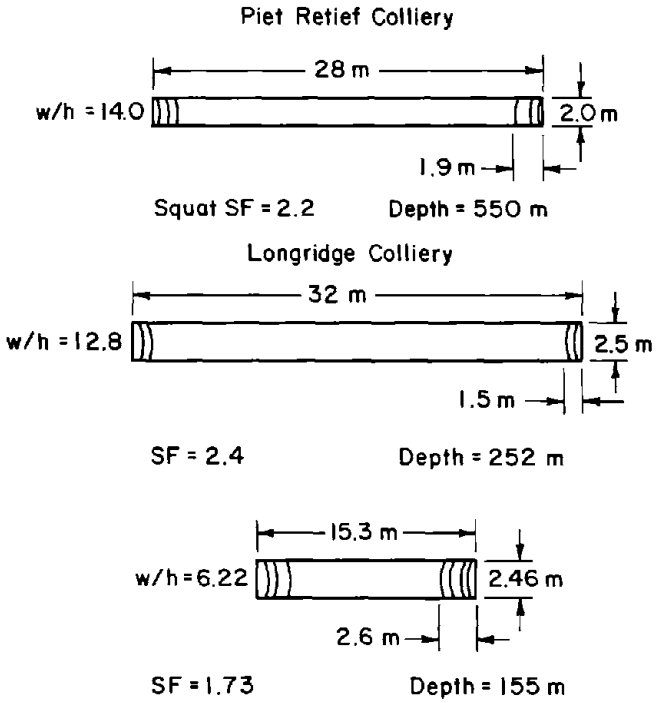

Figure 6.—Extent of sidewall fracturing in squat pillars (Madden, 1991).

An important aspect of squat coal pillars is that as a result of the lateral constraint provided to the central portion of the pillar by the roof-and-floor contacts, the average pillar strength is well in excess of the unconfined strength of the coal. As a result, extensive fracturing can be expected at the pillar circumference. This can give rise to local strata control problems and may require elaborate sidewall support to contain the extent of sidewall fracturing. This aspect was studied in some detail, with measurements of the extent of sidewall fracturing into the pillars taken at each of the collieries listed in table 2. Figure 6 gives details of the results obtained at two of the collieries. A significant aspect of these observations is that fracturing of the pillars is confined to a narrow zone at the circumference of the pillar and that the central portion of the pillar remains essentially unfractured.

Attempts to arrive at statistically significant differences in the strength of individual coal seams have been largely unsuccessful. While there are indications that the coal seams in the Orange Free State and South Rand coalfields are more cleated than those in other coalfields, there are insufficient factual data to treat these coal seams differently.

In discussing the approach to pillar design, it was stated that two distinctly different approaches were adopted, namely:

1. Back analysis of existing bord-and-pillar workings using statistical methods; and

2. Determination of strength and deformation properties of coal pillars with widths ranging from 1 to 2 m.

The results of the statistical approach to pillar design have been discussed in some detail. No mention was made of the in situ tests on coal pillars. These proved to be more difficult than anticipated. The problem was to design a test arrangement that preserved the important end constraints at the contact between the pillar and the surrounding strata (*2*). In an effort to preserve the pillar end constraint as far as possible, Cook et al. (*4*) proposed the test arrangement shown in figure 7. This test configuration was used by Wagner (*19*) to determine the complete load deformation characteristics of in situ coal pillars with a width of up to 2.2 m and a width-to-height ratio of up to 2.6 m. These tests were very successful in determining the postfailure behavior of coal pillars and providing a detailed insight into the mechanism of pillar failure (fig. 8). A shortcoming of the uniform displacement loading arrangement was that the loading jacks at the circumference could not be utilized to their full capacity as it was there where pillar failure initiated. This limited the tests to pillar width-to-height ratios of about 2.5 m. These limitations were overcome to some extent by Van Heerden (*18*), who introduced custom-designed concrete loading platens that simulated the natural end constraints of the pillars. This arrangement enabled Van Heerden to utilize the full-loading capacity of the hydraulic jacks and to extend the range of width-to-height ratio to 3.4. Figure 9 gives a summary of all in situ coal pillar tests. Also shown in this figure is the pillar strength according to Salamon and Munro (*15*).

A comparison of the pillar strength values obtained from pillar tests with the statistically derived pillar strength values shows that, except for the tests at Witbank Colliery, the strength values of the test pillars were significantly higher than those derived from the back analysis of real pillars. With regard to the tests at Witbank Colliery, there is considerable uncertainty as to validity of the loading conditions. The higher strength values obtained in the in situ tests should not be surprising, as the volume of the test pillars was significantly smaller than that of actual coal pillars, and size effects cannot be ruled out, although Salamon and Munro's study of pillar strength showed that these could be rather small. Furthermore, loading of the test pillars took place over a few hours, whereas mine pillars are loaded over very much longer periods. Again, it is a well-known fact that the strength of rock materials at high-loading rates tends to be higher than at very slow loading rates.

In conclusion, it can be said that the tests on relatively small in situ coal pillars have yielded valuable insights into the behavior of highly stressed coal pillars, but have been of limited value from the point of view of the design of bord-and-pillar workings.

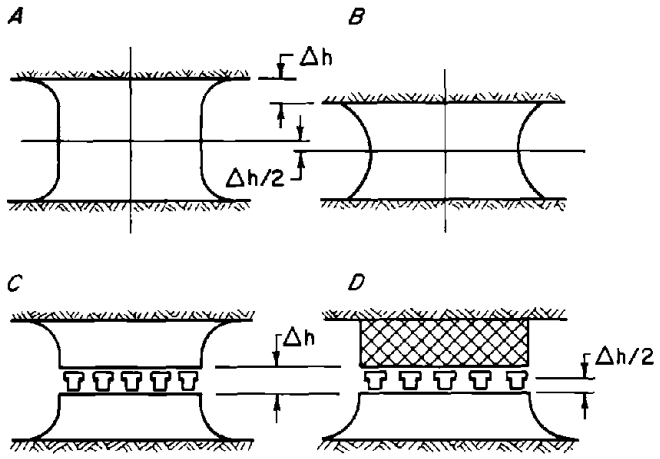

Figure 7.—Principle of coal pillar testing under conditions of uniform deformation.

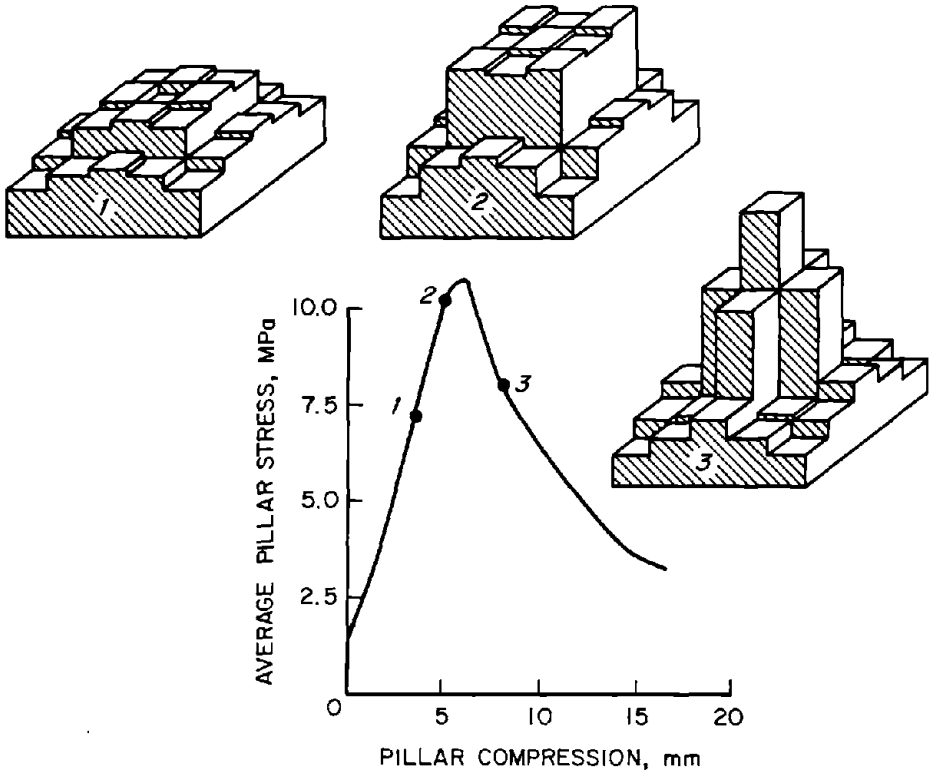

Figure 8.—Complete load deformation behavior of a coal pillar and stress distribution at various stages of pillar loading (after Wagner, 1974).

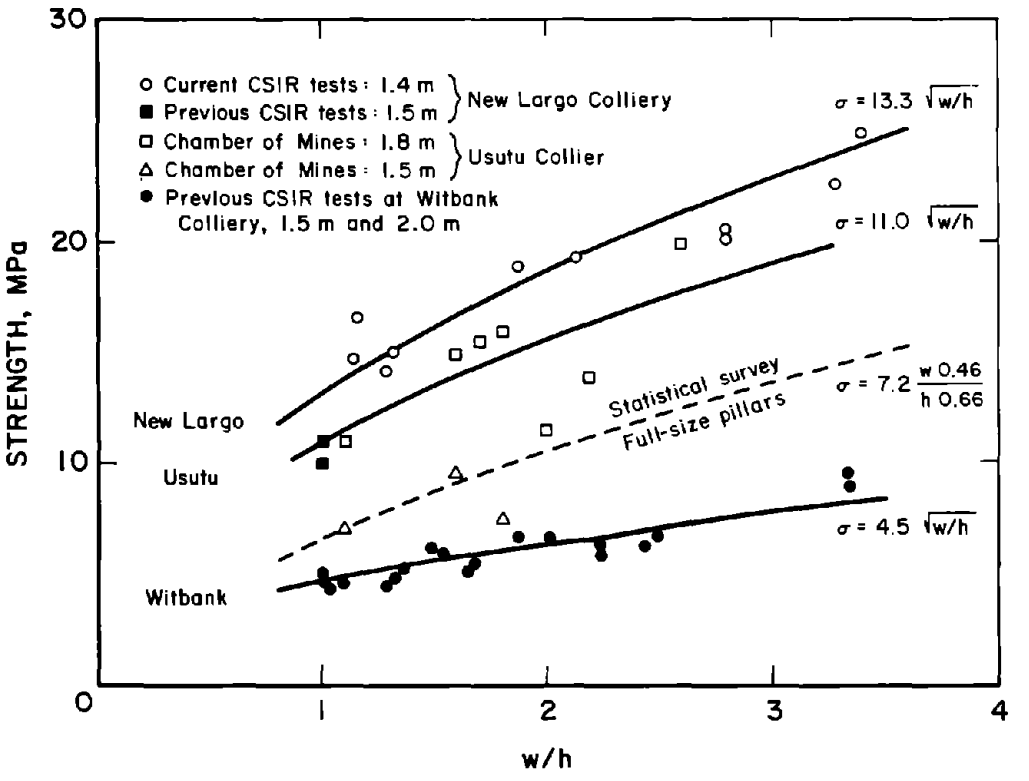

Figure 9.—Comparison of strength results of in situ coal pillar tests in South African coal mines (after Van Heerden, 1975).

DESIGN OF PERMANENT PILLAR WORKINGS

PILLAR DIMENSIONS AND SAFETY FACTORS

The design of permanent bord-and-pillar workings in South African collieries is based on a method that was proposed by Salamon (*11*) and that has been refined over time. The most recent refinement was the introduction of the squat pillar formula. The pillar design method has become mandatory in South African underground collieries.

Salamon's design method is based on the concept of a design safety factor, S. As pointed out above, the design safety factor is defined as:

$$S = \frac{\text{Pillar Strength}}{\text{Pillar Load}}, \qquad (1)$$

where the pillar strength, P, is given by equations 4 and 6 for normal and squat pillars, respectively. The pillar load, p, is given by equation 2. Using appropriate values for the density of the overburden strata and the gravitational acceleration, equation 2 can be simplified to:

$$p = \frac{25 \cdot H \cdot A}{A_p} \quad (\text{kPa}). \qquad (7)$$

In the case of a regular pattern of square coal pillars, the following expression is obtained:

$$p = 25 \cdot H \cdot \left[\frac{w + B}{w}\right]^2, \qquad (8)$$

where w is the pillar width and B is the bord width.

Substituting equations 4 and 8 into equation 1 yields:

$$S = 288 \frac{w^{2.46}}{H \cdot h^{0.66}(w + B)^2}. \qquad (9)$$

This equation contains five variables (S, H, h, w, B). Of these, the depth, H, is given. If the minable seam thickness, h, is small, this variable is also fixed. In the case of thick coal seams, the mining height may be determined by other considerations, such as coal quality

variations through the seam or height constraints resulting from the type of equipment used.

The bord width, B, is determined by the quality of the immediate roof. No general recommendations can be made in this respect, except that a value of 5.5 to 6.5 m appears acceptable in most mining areas in the Transvaal and Orange Free State coalfields. Finally, a suitable safety factor must be selected before the pillar width, w, can be determined.

In terms of Salamon's design safety factor concept, a safety factor of 1 implies that there is a 50 pct probability of a pillar collapse. To safeguard against the possibility of a collapse, it is necessary that a safety factor significantly greater than unity is chosen. Table 3, which was first published by Salamon and Munro (*15*), gives a comparison of observed and predicted probabilities of stable geometry for a range of safety factors. From this table, it will be noted that at a safety factor of 1.5, the predicted probability of a stable geometry is 0.9947. This means that out of 1,000 bord-and-pillar sections designed to a safety factor of 1.5, there is a probability that five sections will collapse. An examination of the performance of bord-and-pillar workings designed according to Salamon's design method has verified the basic validity of the method and has shown surprisingly good agreement between predicted and actual pillar collapses (*21*). These findings were confirmed more recently by a reassessment of coal pillar design carried out by B. J. Madden (*9*). Figure 10 shows the distribution of collapsed pillar workings as a function of the design safety factor. Since Salamon published his pillar design method in 1967, three pillar collapses at design safety factors in excess of 1.5 were observed. All three collapses occurred in very shallow mines and involved coal pillars with width-to-height ratios of less than 2.

Table 3.—Comparison of observed and predicted probabilities of stable pillar geometry (after Salamon and Munro, 1967)

S	Probability of stable geometry	
	Observed	Predicted
1.5 . . .	1.0000	0.9947
1.4 . . .	.9630	.9830
1.3 . . .	.9630	.9508
1.2 . . .	.8148	.8748
1.1 . . .	.5926	.7259
1.0 . . .	.4444	.5000
0.9 . . .	.1852	.2534
0.8 . . .	.1111	.0799
0.7 . . .	0	.0066
0.6 . . .	0	.0006

Over the years, certain design safety factors have been established for the different categories of bord-and-pillar workings. These are summarized in table 4. These guidelines apply to single-seam mining. In the case of multiseam mining operations, the pillar design is complicated by other factors such as the need to superimpose pillars under certain circumstances. In these instances, the pillar design is usually governed by the workings that require the largest pillar to meet the required design safety factor.

Table 4.—Recommended safety factors for different types of bord-and-pillar workings

Type of working	Design safety factor
Main development	SF≥2.0
Secondary development	SF≥1.8
Panel development	SF≥1.6
Top or bottom coaling on retreat	SF≥1.4

INTERPANEL OR BARRIER PILLARS

So far, the discussion of pillar design has concerned itself with the design of panel pillars in single-seam situations. Before considering certain aspects of the design of permanent pillars in multiseam situations, it is necessary to introduce the concept of interpanel pillars.

A feature of bord-and-pillar workings that were designed prior to the Coalbrook disaster was that large areas were extracted on fixed pillar centers. No barrier or interpanel pillars were left between individual extraction panels. One of the first steps taken to prevent a regional pillar collapse of the Coalbrook type was to introduce continuous barrier pillars between individual extraction panels.

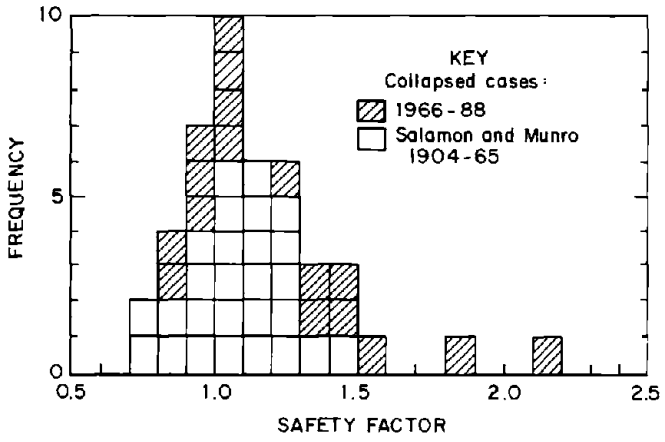

Figure 10.—Frequency of occurrence versus the design safety factor for collapsed pillars (from Madden, 1991).

The main reasons for this practice are to limit a pillar collapse to an individual panel and to facilitate the sealing of panels from a ventilation and water control point of view.

No universally accepted rules exist for the design of interpanel or barrier pillars in South African collieries. Salamon and Oravecz (*16*) in their handbook on pillar design, which has become the design authority for bord-and-pillar workings, give no details of the design of barrier pillars other than stating that a well-designed barrier pillar is a very substantial support and if the width-height ratio of such a pillar is greater than 10, it can support an unlimited load. Recent experiences with some pillar collapses have shown that a continuous barrier pillar of the same width as the panel pillars can act as an effective barrier. An explanation for this observation can be found in Wagner (*20*), who suggested that the effective width of a rectangular pillar is given by the following relationship:

$$w_{eff} = \frac{4 \cdot A_p}{U}, \qquad (10)$$

where A_p is the area of the pillar and U is the pillar circumference.

According to equation 10, the effective width of an infinitely long barrier pillar is twice the actual pillar width. Since the strength of a pillar is strongly dependent on the width-to-height ratio, it follows that the continuous barrier pillar has a very much greater strength than a square panel pillar of the same width.

Figure 11 shows the results of three different methods of determining the effective width of a rectangular pillar on its strength. The approach, which is based on the square root of the pillar area, is valid only for rectangular pillars the length of which is less than twice the actual pillar width. On the other hand, the approach that is based on the actual pillar width is unduly conservative.

From a regional design point of view, the introduction of interpanel or barrier pillars upsets the simple distribution of load on pillars. Because of the greater stiffness of barrier pillars (even continuous barrier pillars of the same width as square panel pillars have a higher stiffness than the panel pillars), the uniform load distribution in the bord-and-pillar workings is disturbed. The extent of this disturbance depends on the difference in stiffness between the barrier pillar and the panel pillars, the span between barrier pillars, and the nature and composition of the overburden strata.

Detailed numerical studies and field observations show that the load acting on the stiffer interpanel or barrier pillars is greater than that calculated from the percentage extraction, whereas the load acting on the pillars inside the panel is smaller than that calculated from the percentage extraction. As the width of the panel is increased, the pillars in the center will carry loads that approach those calculated from the percentage extraction.

MULTISEAM MINING

The general observations concerning interpanel or barrier pillars are of considerable importance in pillar design for multiseam mining. Here, it is strongly recommended that barrier pillars in the various seams are superimposed. Where this is not possible, panel pillars in seams situated above or below a barrier pillar should be designed to a higher safety factor than would otherwise by required to allow for the higher stresses that act on barrier pillars. From a practical design point of view, this is achieved most readily by maintaining the normal pillar width in the panels above or below the barrier pillar and by reducing the mining height. This is one way of increasing the width-to-height ratio of the panel pillar, thereby increasing the pillar strength.

With regard to the design of panel pillars in multiseam situations, the same rules apply as for single-seam operations unless the seams are relatively close. In cases where the parting between two seams is less than 0.75 of the pillar center distance, the superimposition of panel pillars is recommended.

As the parting between seams become thinner, the quality of rock forming the parting becomes more and more important. Mining of neighboring seams with parting thicknesses less than 0.5 to 0.3 of the bord width is considered practical only if the separating strata contain a reasonable proportion of competent sandstone. Furthermore, it is advisable in these instances to design the pillars in the individual seams to a safety factor of not less than 1.8.

Furthermore, the possibility of a failure of the parting between the two seams has to be taken into account if the parting between the seams is less than 1.5 B. In the extreme case, the effect of such a parting failure would be that the effective pillar height would increase to a value equivalent to the combined height of the workings. As in the case with top or bottom coaling (table 4), the recommended design safety factor for this hypothetical pillar should not be less than 1.4.

To assist colliery management and the Mines Inspectorate with the design of bord-and-pillar workings, a number of design aids have been developed. These range from a pillar design nomogram (*11*) to design tables for bord-and-pillar workings (Chamber of Mines 1972 and 1990), to a well-known handbook by Salamon and Oravecz published in 1976.

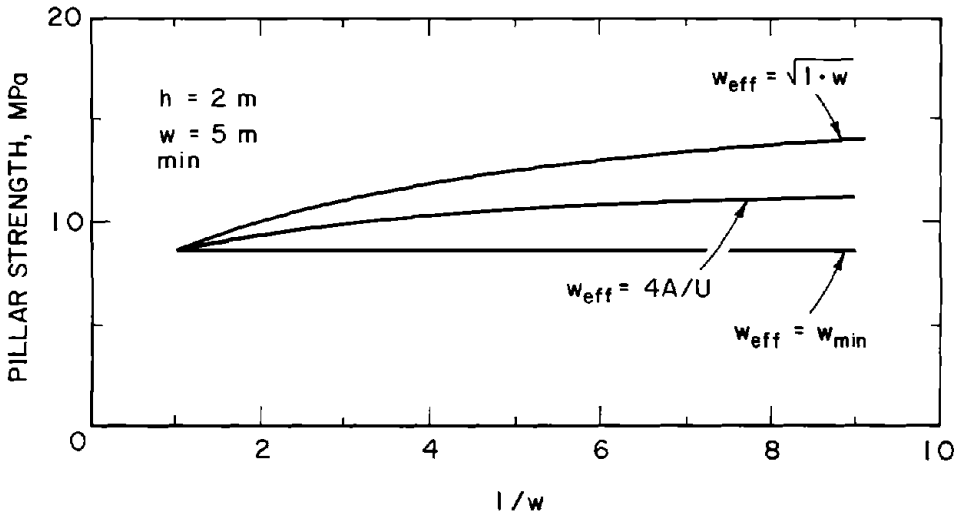

Figure 11.—Effect of length-to-width ratio on strength of rectangular pillars.

DESIGN OF PILLAR EXTRACTION WORKINGS

GENERAL CONSIDERATIONS

In contrast to bord-and-pillar mining, high-percentage extraction methods, such as longwall mining and pillar extraction methods, offer a virtually complete recovery of coal from the mining panels. In the process of longwall mining or pillar extraction, the support for the overburden strata is removed and caving is allowed to take place. The extent of caving depends on the nature of the overburden strata, the panel width, and the depth of mining, as well as the extracted seam height.

Three typical panel widths can be distinguished, namely:

1. subcritical;
2. critical;
3. supercritical.

SUBCRITICAL PANEL

In the case of a subcritical panel, the width is insufficient for extensive caving to take place. Caving is usually confined to the immediate roof strata and arrested by the first competent beds. Surface subsidence above subcritical panels is generally less than 0.1 of the extracted seam height. The upper strata remain intact and tend to behave like an elastic body.

Strata control problems are generally only encountered if a significant number of adjacent subcritical panels have been mined. In these cases, a large area is supported by the pillars that were left intact between the extraction panels. Regional instability cannot be excluded and has to be considered seriously (fig. 12*A*).

Within the South African context, pillar extraction layouts based on subcritical extraction panels are the exception. However, consideration to this concept has been given in situations where the dolerite sill above coal seams has such a thickness that failure of the sill cannot be induced at realistic panel dimensions. The problem of subcritical extraction panels is likely to increase in the future as a result of the very favorable experiences with short longwall installations. One approach that is favored at this stage is shown in figure 12*B*. In this proposal, narrow interpanel pillars are left between two or three of the

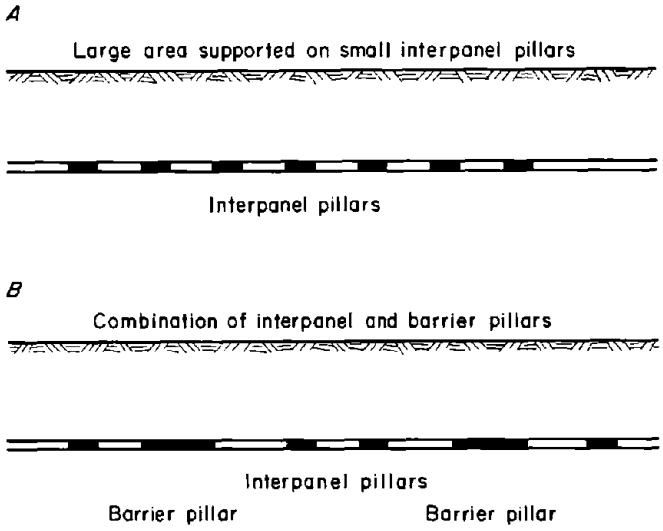

Figure 12.—Regional aspects of mining large areas with subcritical panels.

subcritical panels with the intent that these pillars will ultimately crush and result in the formation of a supercritical panel. The supercritical panels are separated by very substantial barrier pillars. It must be pointed out that this layout is not without dangers, as the formation of the supercritical panel could take place while the last of the subcritical panels in a compartment is being extracted. Apart from the strata control problems caused by high abutment stresses, airblasts, and sudden inflow of methane into the workings are other potential dangers.

CRITICAL PANELS

An extraction panel is termed "critical" when its minimum width is just short of the span required to induce extensive caving of the overburden strata. Features of critical extraction panels are high abutment stresses, severe slabbing of coal from pillars in the extraction zone, floor lift where conditions are favorable for this to occur, and extensive roof falls in the extraction area. Airblasts and inflow of methane from the extracted area are often associated with the regional caving of the upper roof.

The main objective of the design of total extraction panels is to avoid critical panel dimensions and to design the panel width so that extensive caving of the upper strata occurs at the earliest opportunity. In this manner, the difficulties referred to above are confined to a relatively short period in the life of the extraction panel. Furthermore, the total amount of strain energy in the system is minimized, which is an important consideration when dealing with potential instabilities (*14*).

SUPERCRITICAL PANELS

Supercritical extraction panels are those whose span is such that caving of the overburden occurs at the earliest opportunity. A feature of supercritical extraction panels is that the abutment stresses are moderate, strata control problems are well contained, and airblasts and sudden inflow of methane from the goaf are largely avoided. Most strata control problems are confined to the first extensive caving.

Table 5 gives a summary of the features of the three types of extraction panels. From this summary and the earlier discussion, it is evident that extraction panels of critical dimension should be avoided and the choice should be between panels with subcritical and supercritical dimensions. Where feasible, the objective of mine design should be to design supercritical extraction panels, as this design minimizes long-term strata control problems and maximizes overall percentage extraction.

DETERMINATION OF CRITICAL PANEL DIMENSION

From a strata control point of view, the panel width is the critical dimension. Included in the panel width are the two roadways on either side of the extraction panel. The panel width or span required to induce caving of the upper roof strata is a function of the depth of the seam and the strength properties of the overburden strata. In the case of the South African coal mining areas, two typical sets of strata conditions have to be distinguished, namely:

1. a generally weak and incompetent upper roof stratum comprising shale and weak sandstone layers; and
2. a roof stratum that contains one or several thick dolerite sills or massive beds of competent sandstone.

INCOMPETENT ROOF STRATA

In the case of a generally weak and incompetent roof stratum, it was found that the critical mining span, L, at

Table 5.—Classification of extraction panels

	Panel width		
	Subcritical	Critical	Supercritical
Extent of caving	Confined to local roof.	Local roof to base of competent beds.	Most of overburden strata.
Surface subsidence	Minimal.	0.1 to 0.3 m.	0.5 to 0.7 of extracted seam height.
Abutment stresses	Low.	High.	Moderate to high at initial cave, thereafter moderate.
Face conditions	Generally favorable but can deteriorate with large numbers of panels.	Excessive spalling of coal from face roof falls.	Moderate spalling of coal from face periodic weight on face.
Roadways	Roadways show stress when a number of subcritical panels have been extracted.	Severe deterioration of roadway conditions within a distance of 50 to 100 m from abutment.	Average conditions with occasional deterioration.
Regional stability	Potential danger if a large number of subcritical panels has been extracted. Need for regional barrier pillars.	Potential for sudden collapse of a whole panel. Airblast. Methane inflow.	Stability problems confined to first extensive cave. Thereafter, caving takes place at regular intervals.

which caving to the surface occurs, can be estimated by the following simple relationship:

$$L = 2 \cdot H \cdot \cot\beta, \quad (11)$$

where H is the depth of mining below surface and β is the average dip angle of the face-induced fractures (*6*).

Local experience indicates that the angle of face-induced fractures, β, varies from about 60° for competent sandstone beds to about 75° for highly laminated weak shale bands (*22*). The relationship given by equation 11 is illustrated in figure 13. This figure shows that the critical mining spans are relatively small even at mining depths of 200 m. Equation 11 has been verified only for depths of less than 200 m. Care needs to be taken to apply it beyond this range since the stress distribution around deep total extraction panels differs significantly from that around shallow extraction panels (*13*).

COMPETENT ROOF STRATA

A common feature of many of the South African coalfields is the presence of one or several massive dolerite sills in the upper roof strata. The thickness of these sills can vary greatly, but is typically on the order of 30 to 70 m. Vertical, and to a lesser extent horizontal, cooling cracks are a dominant feature of these sills, as is the extremely high compressive strength of the intrusive. Strength values in excess of 300 MPa are not uncommon, but it should be noted that dolerite exposed to the atmosphere weathers readily. A feature of dolerite sills is that they bridge large spans without failing. Furthermore, these sills deform elastically close to the point of failure (fig. 14).

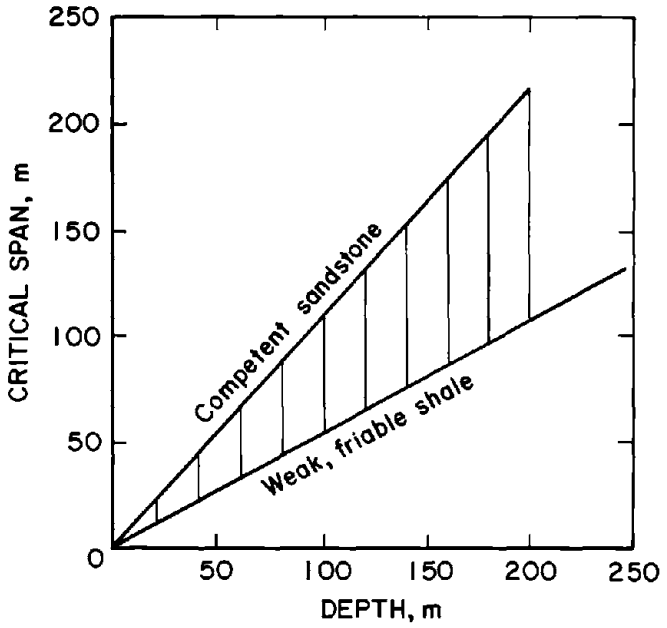

Figure 13.—Relationship between depth of mining, type of roof strata, and critical mining span.

Theoretical studies of the behavior of dolerite sills have shown that the maximum span that can be supported by a sill can be estimated using the simple model of a thick plate (*17*). As more experience became available, the simple plate model was refined to account for the effects of the parting between the coal seam and the dolerite sill, and the effects of the stiffness of the overburden strata on the loading of the sill (*5*). According to the model developed by Galvin, the minimum mining span, L_c, required to induce failure of dolerite sill is

$$L_c = \sqrt{1165t_D - 935\frac{t_D^2}{D_D}} + 2t_p\tan(\beta - 90), \quad (12)$$

where t_D is the thickness of the dolerite sill, D_D is the depth below surface of the base of the sill, t_p is the thickness of parting between the seam and the base of the sill, and β is caving angle measured from a horizontal through the goaf to the face.

Equation 12 has been applied with considerable success in determining the minimum panel dimensions to induce failure of dolerite sills. An important aspect of equation 12 is that it is a two-dimensional model, whereas in reality dolerite sills and other competent strata are three-dimensional structures. Figure 15 shows how the maximum stresses at the base of a dolerite sill develop as a function of the face advance to panel width ratio. The maximum stress value is reached when the plate is infinitely long. Of practical importance is the fact that at a face advance to panel width ratio of 2.5 the stress at the base of the sill has reached a value of 95 pct of the

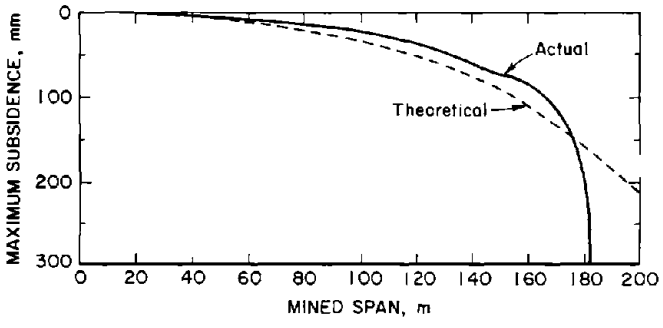

Figure 14.—Comparison of actual and calculated deformation of a dolerite sill. The calculated deformation is based on an "ideal" elastic behavior of the sill (Hardman, 1971).

maximum stress value. Failure of the sill is unlikely to occur after the panel has advanced to a dis-tance of 2.5 times its width. Of course, this assumes that the geological conditions remain unchanged.

DESIGN OF INTERPANEL PILLARS

Interpanel pillars serve three main functions: (1) they act as ventilation and water barriers, (2) they isolate individual extraction panels, and (3) pillars are employed to minimize the effects of high abutment stresses on roadways and ground control in adjacent panels.

Contrary to conventional bord-and-pillar mining, interpanel pillars in total extraction systems are ultimately isolated pillars that are formed behind the longwall face or the pillar extraction line. In most instances, the function of these pillars is not to support the superincumbent roof strata, but to act as water and ventilation barriers. Failure of these pillars behind the retreating faces is, therefore, not necessarily dangerous, but often desirable. An important exception are interpanel pillars that separate extraction panels of subcritical width. In this case, the interpanel pillars must be designed to support the overburden strata. This is particularly important where dolerite is present in the upper strata and when the thickness of the sill is such that it cannot be broken at realistic panel width. In this case, the sill breaches over a number of extraction panels, and the stability of the mining situation depends on the behavior of the interpanel pillars.

In the design of interpanel pillars, two opposing criteria must be considered. First, the interpanel pillar should be as narrow as possible to minimize coal losses and surface irregularities and, second, the interpanel pillar should be as wide as necessary to protect the development roads and panel operations from the effects of high abutment stresses.

The basic principle involved in the design of interpanel pillars is shown in figure 16. The first step in the design procedure is to determine the stress distribution at the edge of the total extraction panel. This can be accomplished with the aid of either finite-element or boundary-element stress analysis programs. When determining the stress distribution, the nature of the upper roof strata, the floor strata, and the seam must be taken into account. Of particular importance is whether or not the upper roof strata in the mined panel has caved and to what extent massive beds overhang.

The second step in the design process is to determine the critical stress level, σ_c, that can be tolerated by the development roads in panels adjacent to total extraction panels. The critical stress level depends mainly on the strength properties of the coal seam, the working height, the nature of the immediate roof and floor strata, the width of the roadways, and the support employed in the roadways. A first estimate of the magnitude of the critical stress level can be obtained from a comparison of the average pillar stresses and pillar conditions in bord-and-pillar workings situated in the same seam. The average pillar stress is given in equation 2.

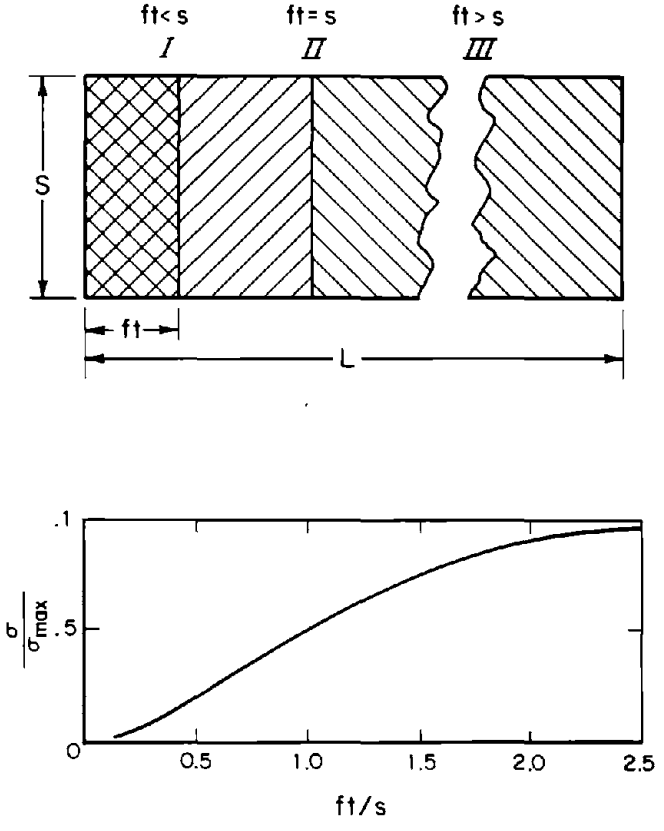

Figure 15.—Effect of panel geometry on value of critical stresses at the base of the dolerite sill. ft = face advance distance; s = panel width.

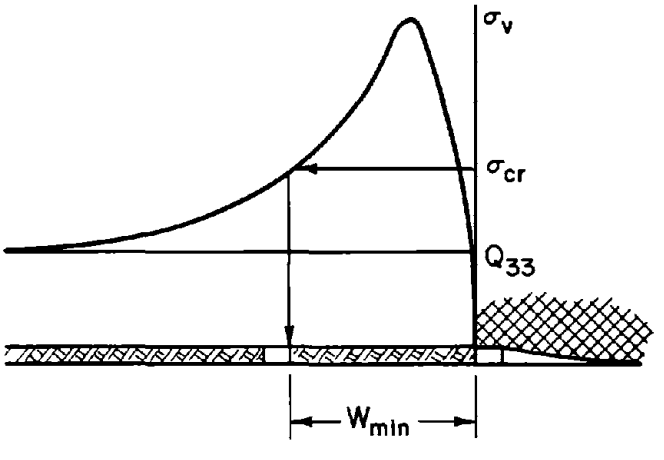

Figure 16.—Design of interpanel pillars.

$$p = \frac{25 \cdot H \cdot A}{A_p}$$

For comparable strata conditions:

$$\sigma_c = \frac{25 \cdot H \cdot A}{A_p}.$$

Once the critical stress level has been determined, the minimum pillar width can be read from diagrams similar to the one shown in figure 17. Because of the uncertainty of the extent of the yield zone, it is important to establish whether the critical stress value, σ_c, falls in the steep or flat portion of the stress profile. In the case of the former, it is advisable to increase the pillar width to ensure that the roadway is situated in an environment of low stress gradient. An important feature of the stress profiles shown in figure 17 is that an increase in pillar width beyond 30 m only yields marginal improvements in terms of stress levels. Given that the in situ uniaxial compressive strength of coal is on the order of 5 to 10 MPa, significant sidewall fracturing of roadways is to be expected at depths in excess of 200 m. This is irrespective of the width of the interpanel pillars. Appropriate support measures will have to be introduced to deal with this problem.

Table 6 gives details of longwall layouts from seven large South African collieries. Apart from localized strata control problems, none of the collieries experienced significant roadway problems. Colliery No. 5 extracted the interpanel pillar on the retreat, while in Colliery No. 6 the interpanel pillar is partially extracted to minimize surface irregularities resulting from differential subsidence above the center of the extraction panel and above interpanel pillars.

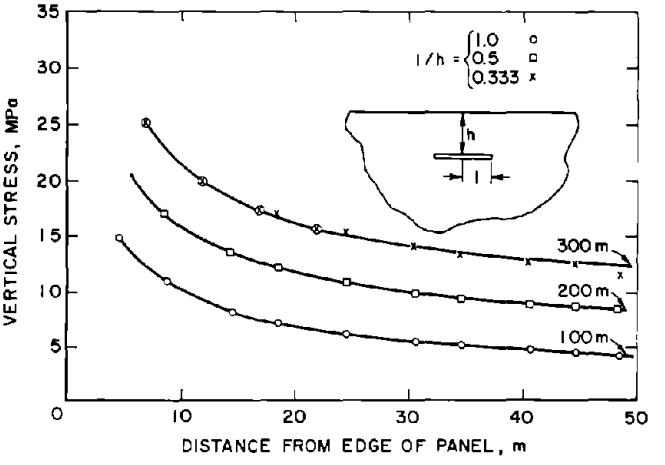

Figure 17.—Distribution of abutment stresses around an isolated 200-m-wide extraction panel situated at depths of 100, 200, and 300 m below surface.

Table 6.—Details of longwall layouts in seven South African collieries

	Mine Identification						
	No. 1	No. 2	No. 3	No. 4	No. 5	No. 6	No. 7
Depth . . . . . m . .	125	130	130	165	48	210	200
Face length . . . . . m . .	212	218	186 to 198	200	165	170 to 205	90 to 195
Mining height . . . . . m . .	3.1	3.2	3.1	2.8	1.9	2.0	1.15
Number of roadways:							
Main gate	3	3/2	3	2	2	3	2
Tail gate	3	2	3	2	2	2/3	2
Piller center distance . . m . .	24	24	20 to 25	28	15 to 18	26 to 46	30
Roadway width . . . . . m . .	5.5	6.2	6.2	6.0	6.5	6.5	4.8
Effective interpanel pillar	42.5	41.8 to 17.8	33.8 to 43.8	22	8.5 to 11.5	45.5 to 8.9	25.2
Dolerite (Yes/No)	Y	N	N	Y	N	Y	Y

PILLAR EXTRACTION METHODS

Two methods of pillar extraction are widely practiced in South African collieries:

1. rib pillar extraction; and
2. extraction of pillars from existing workings using continuous miners.

In addition, a number of older collieries practice various forms of pillar extractions using conventional mechanized mining equipment. Details of the various pillar extraction methods in use in South African collieries are given in a comprehensive report by Beukes (*1*).

RIB PILLAR EXTRACTION

The layout of a typical rib pillar extraction panel is shown in figure 18. The panel is developed using three main development roads that also act as intake and return airways. The central road is utilized by the section conveyor. From the main development, two to three 200-m-long roads are driven to develop the rib pillars. The rib pillars themselves are typically 6 m wide and between 40 and 60 m long. The length of rib pillar is chosen so as to enable the extraction of one complete rib pillar in one production shift. Timber breaker-line supports are used to protect the machine operator. At one of the Secunda Collieries, a fully mechanized breaker-line support has been developed and used successfully.

From a strata control point of view, rib pillar extraction has been highly successful. The only problem has been the extraction of the last one or two cuts from the rib pillar (see cut 5 in fig. 18). During this operation, the support from a relatively large area of roof is suddenly removed, and premature goafing is sometimes experienced.

From a mining point of view, rib pillar extraction has lost some of its initial popularity because of the poor continuous miner efficiencies during the development of the rib pillars.

EXTRACTION OF EXISTING PILLARS USING CONTINUOUS MINERS

A wide variety of methods of extracting existing coal pillars with continuous miners is in use in the Republic of South Africa. In recent years, a method that closely resembles the rib pillar method is finding wide acceptance. Figure 19 shows the overall extraction sequence, which follows the principle of extracting pillars in a straight line.

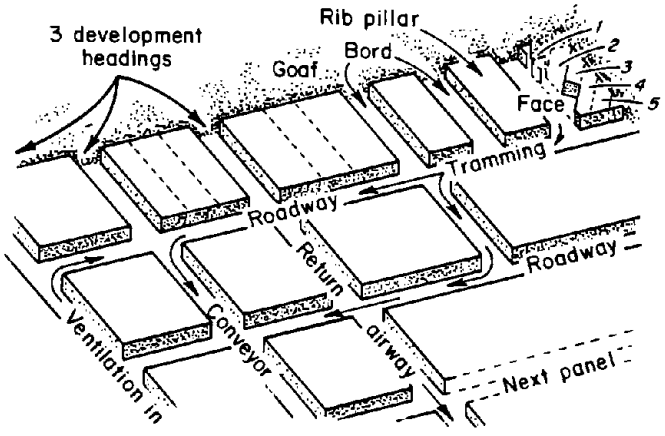

Figure 18.—Diagrammatic view of a rib-pillar panel.

The key to the success of this method is that only one pillar is extracted at any one time. Details of the extraction sequence of the pillar itself are shown in figure 20.

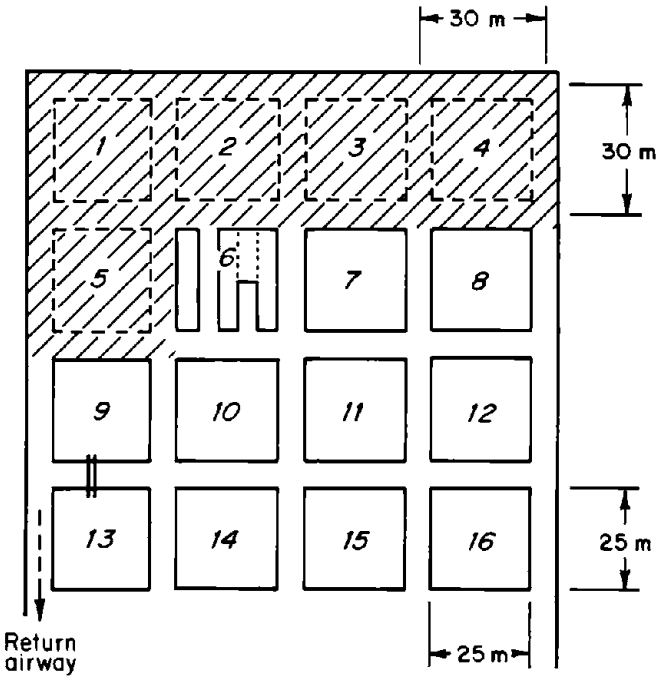

Figure 19.—Pillar extraction sequence using continuous miners.

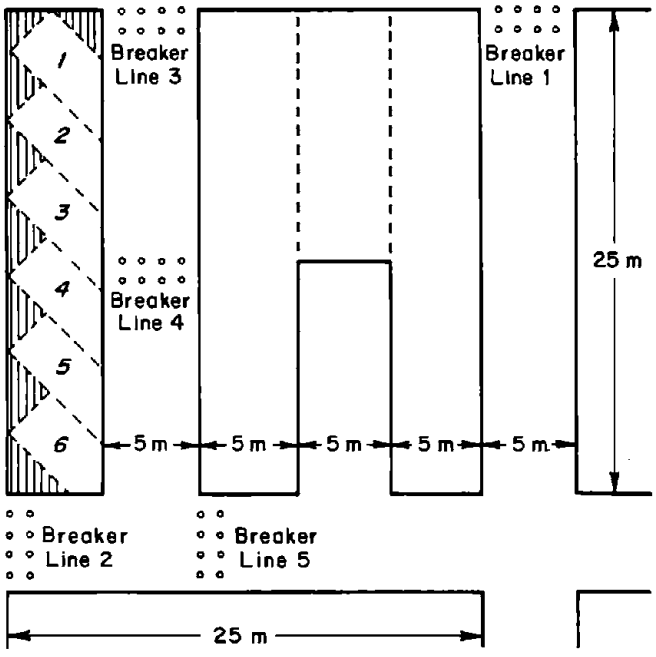

Figure 20.—Details of the extraction sequence of an individual pillar.

A prerequisite for successful pillar extraction is that the original pillars are designed to a high safety factor. In terms of conventional pillar design, the safety factor should be in excess of 2, preferably 2.5, to ensure that the effect of abutment stresses on mining conditions is minimized. Equally important is that the actual extraction method is designed to fully accommodate the requirements of the mining equipment. Furthermore, the fenders should be at least 5 m wide to ensure adequate protection during the extraction process. In the case of extraction heights greater than 3 m, it is wise to err on the safe side and to design fenders with a width-to-height ratio of at least 2.

A factor critical to all pillar extraction methods is the extent to which the method allows all coal to be extracted. Most methods share the common trait that small remnants of coal are left behind to provide short-term local support. If the size of these remnants is excessive, they can prevent regular caving of the intermediate roof strata. This results in the development of a potentially unstable situation wherein several tens of meters of roof strata are supported by undersized pillars. Apart from sudden goaf collapses with airblasts, the failure to allow free caving of the immediate roof strata results in the development of high abutment stresses and a deterioration of strata conditions in the working area. Most of these problems can be avoided through the maintenance of strict discipline and appropriate recording schemes.

SPECIAL CONSIDERATIONS

SUDDEN COLLAPSES

One of the dangers in pillar extraction mining is that large mined-out areas, which are supported by a number of small remnants of coal that are left intact during pillar extraction, suddenly fail. Often this failure is accompanied by considerable violence, and there known instances where roof failure has overrun the pillar extraction line.

The most concise discussion of the stability and instability of bord-and-pillar workings was published by Salamon (*14*). Only some of the very basic aspects of this discussion are considered here. Figure 21*A* shows an idealized situation of a coal pillar that is loaded. The specimen resembles the coal pillar and the spring loading system. Figure 21*B* shows the load deformation curve of the pillar and the loading line of a mining system. A condition of stable equilibrium exists if the slope of the loading line is steeper than the slope of the load deformation curve of the pillar. In this instance, external work has to be done to deform the pillar further. On the other hand, if the postfailure slope of the pillar becomes steeper then the loading line of the system, the energy that is stored in the system becomes available to deform the pillar. This results in an uncontrolled failure of the pillar. The critical point is reached when the loading line of the system becomes tangent to the postfailure slope, λ, of the pillar.

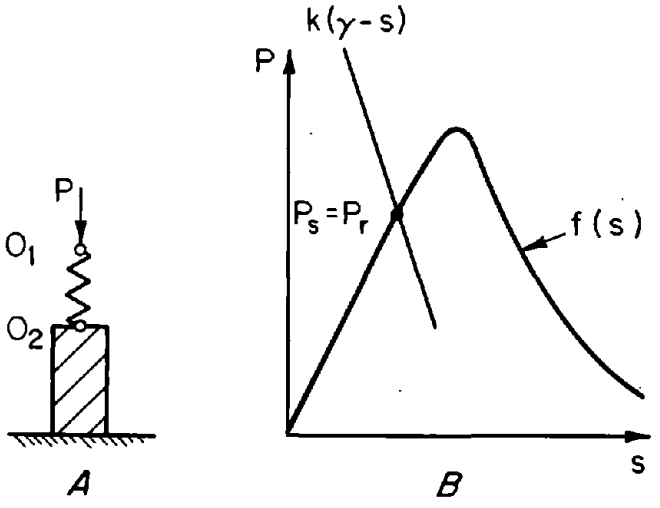

Figure 21.—Idealized model of pillar loading (after Salamon, 1970).

Figure 22*A* and 22*B* give examples of stable (*A*) and unstable (*B*) failures. Because the slope of the loading line of the system is negative, it follows that a condition of instability can only occur if the pillar has been deformed beyond its point of maximum resistance, i.e., the pillar is in the postfailure regime. This condition is most readily reached when pillars are reduced in size during the process of pillar extraction. This is particularly true for remnants of coal pillars that have been left behind in the mined-out area.

From the discussion up until now, it is obvious that the critical parameters determining whether a pillar will fail in a stable or unstable manner are the slope of the loading line, κ, and the postfailure slope, λ, of the pillar. Salamon (*14*) has shown that the slope of the loading line becomes smaller as the number of pillars in a panel increases (fig. 23). He states that it becomes progressively more difficult to satisfy the condition for perfect stability, i.e., $\kappa > \lambda$, as the number of pillars in a panel increases. In fact, it is true in general that as the mined-out area, supported by uniform-sized pillars, becomes very large, $\kappa \rightarrow 0$.

There is another condition that can result in a sudden reduction in the value of κ. This is when the roof stratum, which resembles the loading system, is disrupted by a fault and the fault is exposed as a result of mining.

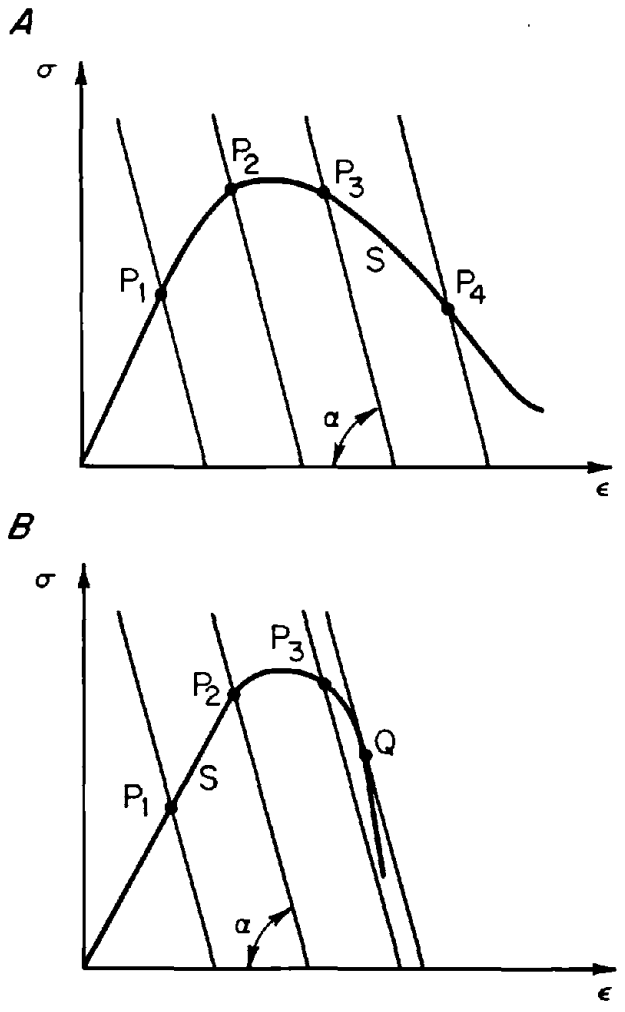

Figure 22.—Example of stable (*A*) and unstable (*B*) failures (after Salamon and Oravecz, 1976).

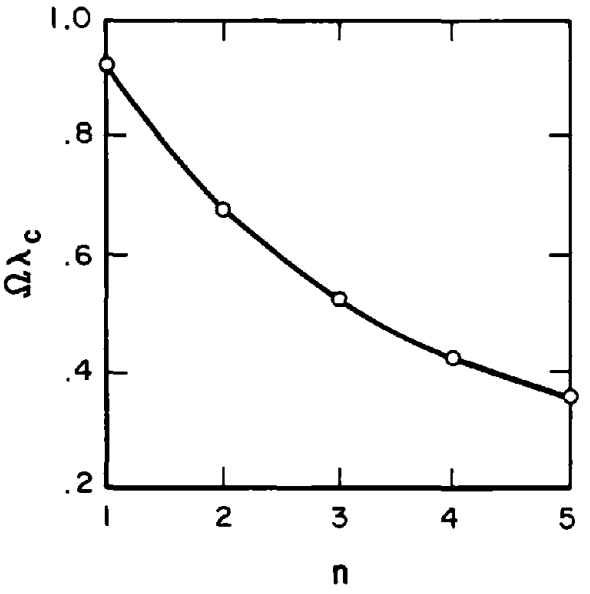

Figure 23.—Effect of number of pillars in a panel on critical stiffness (after Salamon, 1970).

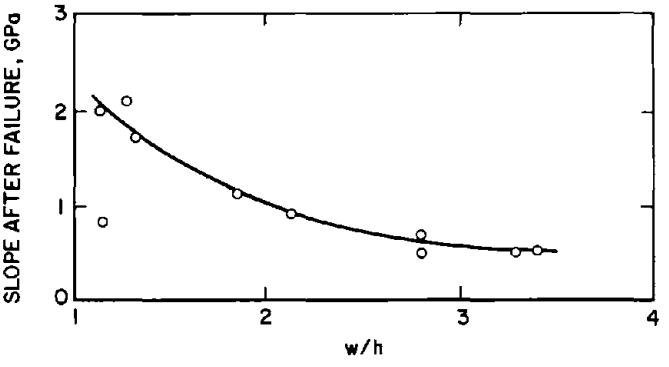

Figure 24.—Slope of coal pillars after failure (Van Heerden, 1975).

Because of the limited ability of fault planes to transmit shear stresses, the elastic continuum is destroyed and the loading system can suddenly change from a displacement-controlled to a load-controlled system. In terms of this discussion, it should be pointed out that the slope of the loading line of a load-controlled system is $\kappa = 0$.

Many of the violent collapses in underdesigned bord-and-pillar workings can be linked to the exposure of steeply dipping fault planes. This aspect requires careful consideration in the planning and operation of pillar extraction sections.

The second major parameter concerns the postfailure slope of coal pillars. Relatively little is known about the load deformation behavior of in situ coal pillars. Probably the most reliable information is that published by Wagner (*19*) and Van Heerden (*18*). Both authors have shown that the slope of coal pillars after failure is strongly influenced by the width-to-height ratio of the coal pillars. Figure 24 shows that for pillars with a width-to-height ratio of 3, the slope after failure or the postfailure modulus is 0.5 GPa, whereas that of pillars with a width-to-height ratio of 1 is about 2 GPa.

From this if follows that small remnants that are left in the mined-out area are more prone to unstable failure than would be the case with larger pillars. Again, this is confirmed by practical observations.

DESIGN OF PILLAR EXPERIMENTS

In a attempt to improve on existing pillar design, mine managers frequently consider the design of experimental panels. Much care has to be taken in finalizing the experimental parameters. Frequently, the design parameters

for these experiments are controlled by practical considerations in order to minimize costs and obtain results as quickly as possible. There are grave dangers in such an approach, as the results obtained in such an experiment may be totally misleading and result in potentially dangerous mine designs when applied on a large scale.

One of the major problems in pillar experiments is to determine the load that acts on a pillar. Stress measurements are time-consuming, costly, but most important of all, very difficult to conduct and unreliable. For this reason, it is important that the experimental panel be sufficiently wide to ensure that the load calculation based on the tributary area theory (equation 2) is meaningful. As a guideline, this implies that the panel width should be about twice the depth of mining. In the case of weak overburden strata, this requirement can be relaxed somewhat, whereas in the case of massive beds it may be necessary to increase the panel width.

Another important reason for wide experimental panels is the influence of the number of pillars in a panel on the loading line of the mining system. This is particularly important in the case of competent beds in the strata above the experimental panel. Cases are known where pillars in narrow experimental panels failed in a stable manner because of the very stiff loading line of the system. This failure is not always evident, and a false security can be created. However, had pillars of the same dimensions been used in a much wider panel, the possibility of a violent pillar collapse could not have been excluded.

These examples demonstrate that the design of pillar experiments should be based on sound rock mechanics considerations. Furthermore, the applications of the results of pillar experiments should be done with great care and, ideally, the first few applications should be treated as pillar experiments on a larger scale. This implies a certain amount of monitoring and strata observations.

CONCLUSIONS

Bord-and-pillar mining can be a very efficient method of mining, provided the conditions are right.

The method of back analysis as the basis for improvements to pillar design is very powerful and deserves preference over purely analytical or experimental methods.

The design of interpanel pillars in total extraction mining systems is controlled by stress rather than strength considerations. From this point of view, it differs greatly from the design of panel pillars.

The design of pillar experiments is a delicate issue and requires detailed rock mechanics investigations to avoid costly and dangerous mistakes.

REFERENCES

1. Beukes, J. S. Pillar and Rib-Pillar Extraction in South African Collieries. Res. Rep. Mar. 1990, Chamber of Mines Res. Organization, Johannesburg, pp. 110.

2. Bieniawski, Z. T. Note on In-Situ Testing of the Strength of Coal Pillars. J. S. Afr. Inst. Min. Metall., v. 68, 1968, pp. 455-465.

3. Bryan, A., J. G. Bryan, and J. Fouche. Some Problems of Strata Control and Support in Pillar Workings. Min. Eng., Feb. 1964, pp. 238-266.

4. Cook, N. G. W., K. Hodgson, and J. P. M. Hojem. 100-MN Jacking System for Testing Coal Pillars Underground. J. S. Afr. Inst. Min. Metall., v. 71, 1971, pp. 215-224.

5. Galvin, J. M. The Mining of South African Thick Coal Seams—Rock Mechanics and Mining Considerations. Ph.D. Thesis, Univ. Witwatersrand, Johannesburg, 1981, pp. 303.

6. Galvin, J. M., J. J. Steijn, and H. Wagner. Rock Mechanics of Total Extraction. In Increased Underground Extraction of Coal. S. Afr. Inst. Min. Metall., Monograph Series No. 4, Johannesburg, 1982, pp. 69-110.

7. Hardman, D. R. Longwall Mining Under Dolerite, Sigma Colliery—Panel No. 4. Res. Rep. No. 9/71. Chamber of Mines of S. Afr., Johannesburg, 1971.

8. Madden, B. J. An Investigation Into the Factors Affecting the Strength of Pillars in South African Coal Mines. Ph.D. Thesis, Univ. Witwatersrand, Johannesburg, 1991, pp. 266.

9. Madden, B. J. A Re-Assessment of Coal Pillar Design. J. S. Afr. Inst. Min. Metall., v. 91, 1991, pp. 27-37.

10. Madden, B. J. and H. Wagner. Development of a Design Programme for Coal Pillars With Large Width to Height Ratios. Proc. 9th Int. Conf. Coal Res., Washington, DC, BuMines Spec. Publ., 1991, pp. 66-76.

11. Salamon, M. D. G. A Method of Designing Bord and Pillar Workings. J. S. Afr. Inst. Min. Metall., v. 68, 1967, pp. 68-78.

12. ____. Notes Arising From Visit to Wankie Colliery, 18 June 1982. Private communication, 1982, available upon request from author.

13. ____. Rock Mechanics of Underground Excavations. Proc. 3d Congr. Int. Soc. Rock Mech., v. 1, Pt. B, 1974, pp. 951-1099.

14. ____. Stability, Instability and Design of Pillar Workings. Int. J. Rock Mech. Min. Sci., v. 7, 1970, pp. 613-631.

15. Salamon, M. D. G., and A. H. Munro. A Study of the Strength of Coal Pillars. J. S. Afr. Inst. Min. Metall., v. 67, 1967, pp. 55-67.

16. Salamon, M. D. G., and K. I. Oravecz. Rock Mechanics in Coal Mining. Chamber of Mines of South Africa, P.R.D. Ser. No. 198, Johannesburg, 1976, pp. 119.

17. Salamon, M. D. G., K. I. Oravecz, and D. R. Hardman. Rock Mechanics Problems Associated With Longwall Trials In South Africa. Proc. Fifth Intern. Strata Control Conf., paper No. 14, 1972, London.

18. Van Heerden, W. L. In Situ Complete Stress-Strain Characteristics of Large Coal Specimen. J. S. Afr. Inst. Min. Metall., v. 75, 1975, pp. 207-217.

19. Wagner, H. Determination of the Complete Load-Deformation Characteristics of Coal Pillars. Proc. 3d Congr. Int. Soc. Rock Mech., Denver, CO, 1974, pp. 1076-1081.

20. ____. Pillar Design in Coal Mines. J. S. Afr. Inst. Min. Metall., v. 80, 1980, pp. 37-45.

21. Wagner, H. and B. J. Madden. Fifteen Years of Experience With the Design of Coal Pillars in Shallow South African Collieries: An Evaluation of the Performance of the Design Procedures and Recent Improvements. In Design and Performance of Underground Excavations. ISRM/BGS Cambridge, 1984, pp. 391-399.

22. Wagner, H., and J. J. Steijn. Effect of Local Strata Conditions on the Support Requirements on Longwall Faces. Int. Soc. Rock Mech., Montreux, 1979. Proc. v. 1, Rotterdam, Balkema, 1979, pp. 557-561.

APPENDIX.—ABBREVIATIONS USED IN THIS REPORT

ADINA	finite element program
ALPS	Analysis of Longwall Pillar Stability
AMIRA	Australian Mineral Industries Research Association
APRS	Analysis of Pillar Retreat Stability
ASTM	American Society for Testing and Materials
BEM	boundary-element method
BPC	borehole pressure cell
BPF	borehole platened flatjack
BPFCAL	borehole platened flatjack calibration
CANMET	Canada Centre for Mineral and Energy Technology
CBCRL	Cape Breton Coal Research Laboratory
CBDC	Cape Breton Development Corporation
CMRA	Coal Mines Regulation Act (Australia)
CMRCC	Coal Mining Research Controlling Council
CMRS	Central Mining Research Station
CSIR	Council for Scientific and Industrial Research
CSIRO	Commonwealth Scientific and Industrial Research Organisation
ECE	Economic Commission for Europe
ERR	energy release rate
FEM	finite element method
FLAC	Fast Lagrangian Analysis of Continua
FSF	floor safety factor
HWM	high-water mark
ISRM	International Standard of Rock Mechanics
JWR	Jim Walter Resources, Inc.
LMS	local mine stiffness
LMSTIFF	experimental program
MESE	MSHA Elastic Stress Equation
MSC/NASTRAN	finite element program
MSHA	Mine Safety and Health Administration
MSHA-ESE	Mine Safety and Health Administration elastic stress equation
MULSIM/NL	boundary element program
N.G.I.	Norwegian Geotechnical Institute
NMERI	National Mechanical Engineering Research Institute
NSW	New South Wales (Australia)
PCD	pillar center distance
R/L	resistance/load ratio
RCS	roof classification system
RMR	rock mass rating
RR	roof rating
SCT	Strata Control Technology
SF	stability factor
SI	International System of Units
TDR	time domain reflectometry
UBC	ultimate bearing capacity
UCS	unconfined compressive strength
USBMDE	U. S. Bureau of Mines discrete element program
VWS	vibrating wire stressmeter

☆ U.S. GOVERNMENT PRINTING OFFICE: 1992-611-321

Bureau of Mines
Information Circular 9315

PROCEEDINGS OF THE WORKSHOP ON COAL PILLAR MECHANICS AND DESIGN

Compiled by Anthony T. Iannacchione, Christopher Mark, Richard Repsher, Robert J. Tuchman, and Caddie C. Jones

---

ERRATA

Page 123:

The note to table 1 should read as follows:

NOTE.—In the case of rectangular pillars, the equivalent square pillar width was obtained from

$$W = \frac{2 w_1 w_2}{w_1 + w_2},$$

where w_1, w_2 are the two sides of a rectangular pillar.

Page 253, column 1, lines 10-11, should read:

σ_{tn} = normalized tensile strength, expressed

$$\frac{1}{2} m - (m^2 + 4 s)^{1/2}.$$

Page 253, column 2, equation 7 should read:

$$\tau_{xy,allowable} = A \sigma_c \left(\frac{\sigma_z}{\sigma_c} + \sigma_{tn} \right)^B \qquad (7)$$

where $\tau_{xy,allowable}$ is allowable shear stress, and σ_z is normal stress in z-axis.

Page 295, figure 15:

On the y-axis of the graph, ".1" should read as "1".